MODERNIZATION AND ENGINEERING DEVELOPMENT OF RESOURCE-SAVING TECHNOLOGIES IN MINERAL MINING AND PROCESSING

Multi-authored monograph

UNIVERSITAS Publishing
Petroșani, 2019

UDC 622.002

Recommended for publication by the Board of Directors of the University of Petroșani, 09.09.2019

Recommended for publication by the Academic Board of the Kryvyi Rih National University, Minutes №1, 30.08.2019

Reviewers: ***Mihaela TODERAS***, Ph.D.Habil.Eng., Professor,
Vice-Dean Faculty of Mines University of Petroșani, Romania

Serik MOLDABAYEV, DSc (Engineering), Professor of the Department of "Mining", Satbayev University**,** Republic of Kazakhstan

***Oleh KRUZHILKO*,** DSc (Engineering), Senior Researcher, Head of Scientific Department, National Scientific and Research Institute of Industrial Safety and Occupational Safety and Health, Ukraine

Modernization and engineering development of resource-saving technologies in mineral mining and processing. Multi-authored monograph. – Petroșani, Romania: UNIVERSITAS Publishing, 2019. - 476 p.

ISBN 978-973-741-645-2

The monograph considers potential technological development of ore mining and processing industries through updating mining machines and technologies

The book is intended for a broad mining audience of scholars, practitioners, postgraduates and students.

UDC 622.002

ISBN 978-973-741-645-2

Table of contents

PREFACE

Multi-authored monograph "Modernization and engineering development of resource-saving technologies in mineral mining and processing" edited by Prof. Vsevolod Kalinichenko and Prof. Ronald Moraru

We are glad to present the multi-authored monograph "Modernization and engineering development of resource-saving technologies in mineral mining and processing".

The monograph contains forecast data on mineral base mining in various regions of the world. The increased demand for raw materials is substantiated and there are required complex steps to satisfy this demand through developing resource-saving technologies of mineral mining and processing.

There are highlighted peculiarities of engineering and technological development of mining industries including modernization of operating enterprises, deposit mining and parameters of development of mining and concentrating enterprises.

The contributors consider the whole range of mining operations including mining enterprise design and raw materials or end products sale.

Co - editors,

Vsevolod KALINICHENKO - Academician of the Academy of Mining Sciences of Ukraine, Doctor of Sciences (Engineering), Professor, Kryvyi Rih National University, Ukraine.

Roland MORARU, Professor, Ph.D.Habil.Eng. Research Vice-Rector University of Petroșani, Romania.

RECENT STUDIES ON RECOVERY OF GALLIUM, GERMANIUM AND INDIUM FROM METALS EXTRACTION WASTE AND WASTEWATER

Panayotov V. T.
Bulgarian Academy of Sciences, Group on Technical Sciences,
D. Sci., Prof., Correspondent member, Bulgaria

Panayotova M. I.
University of Mining and Geology, Dept. of Chemistry,
PhD, Prof., Bulgaria

Abstract
The development of modern society is unthinkable without the availability of high-tech metals, such as gallium, germanium and indium. After a brief review of the use, future necessity and traditional ways of those minor metals production, the opportunity of their recycling from technogenic waste from the ores extraction and processing and from industrial wastewater is discussed. Recent studies are presented. Barriers to Ga, Ge and In recycling from technogenic waste are also briefly discussed.
Keywords: gallium, germanium, indium, recycling, technogenic waste

1. Introduction - gallium, germanium and indium use

Gallium (Ga), germanium (Ge) and indium (In) are minor metals used in advanced technologies needed for the sustainable development of our society and for our everyday comfortable life.

Gallium arsenide (GaAs) is used to manufacture integrated circuits (ICs) and optoelectronic devices (laser diodes, light emitting diodes - LEDs, photodetectors, and solar cells). Gallium nitride (GaN) is applied to produce optoelectronic devices. ICs predominate recently the USA Ga consumption - 68% (2018, 2017), and 60 % (2016). Optoelectronic devices accounted for 30% (2018, 2017), and approximately 40 % (2016), the left to 100 % is used in research and development, medicine, etc. (Jaskula, 2017; Jaskula, 2018; Jaskula, 2019). In Europe the electric and electronic equipment (EEE) sector is the main user of Ga - 95 % of the element is used in the sector (Mathieux et al., 2017).

Electronics and solar applications, fiber-optic systems and infrared optics are the major global end uses for germanium (Ge). Other uses include polymerization catalysts, chemotherapy, and

metallurgy. The Ge end-uses in the USA in 2016 (the recent available data) were estimated to be: fiber optics, 40%; infrared optics, 30%; electronics and solar applications, 20%; and other, 10% (Guberman, 2017). In the European Union the electric and electronic equipment sectors are the major user of Ge (87%) (Mathieux et al, 2017). Germanium use in fiber optics increased substantially in China from 2012 to 2016 and it was the leading Ge consumption growth area. Production of infrared optics and substrates for solar cells also increased (Guberman, 2017; Thomas, 2019).

Indium (In) is used mainly as indium tin oxide (ITO). ITO thin-film coatings are applied for electrical conductive purposes in a variety of flat-panel displays - most commonly liquid crystal displays (LCDs). Production of ITO accounts for most of global In consumption. Other In end uses are: alloys and solders, compounds, semiconductors and electrical components, and research (Anderson, 2019). In the European Union the electric and electronic equipment sectors are the major user of In (81%) (Mathieux et al., 2017).

This chapter describes briefly primary production of Ga, Ge and In, as well as the expected increase in their use. Special attention is paid to the recent studies on enhancing the comprehensive use of ores with the aim to extract Ga, Ge and In as by-products and to the recovery of those metals from metals' extraction waste and wastewater.

2. Gallium, germanium and indium production

2.1. Gallium production

Gallium concentration in the Earth's crust is in the range of 5-15 parts per million (ppm). The metal is not produces from its own ores because this is unfeasible. At present most Ga is produced as a by-product of bauxite processing and the remainder - from the processing of sphalerite ore from three types of deposits (sediment-hosted, Mississippi Valley-type - MVT, and volcanogenic massive sulfide) (Foley at al, 2017; Jaskula, 2019). The repotted Ga content in bauxite is 30-80 ppm (EU, 2015), on average 50 ppm (Jaskula, 2019). Zinc ores bear up to 50 ppm of Ga and could be a significant resource (Jaskula, 2019). Minor concentrations of Ga, on average 10 ppm (Lu et al., 2017) can be found in some coal deposits. Anomalous high Ga content was discover in some coal deposits in China

and Ga production from this coal combustion residues and coal fly ash is considered promising resource (Qin et al., 2015). However, industrial processes for Ga extraction from coal or coal fly ashes with reasonable expenses are not developed yet (Ueberschaar et. al., 2017). Gallium is also recovered as secondary production from recycled Ga bearing, mainly new, scrap.

Gallium contained in world resources of bauxite is estimated to exceed 1 million t, and a considerable quantity could be contained in world zinc (Zn) resources. However, less than 10% of the Ga in bauxite and Zn resources is potentially recoverable (Jaskula, 2018; Jaskula, 2019). Other estimates show somehow different figures. Based on the data on: the reports of the United States Geological Survey (USGS) on the world bauxite reserves of 30 billion t and Zn reserves of 230 million t, the averaged Ga content in those ores, and the Ga recovery rates from those sources, it was estimated that Ga contained in bauxite is 600000 t and additional 2300-23000 t could be contained in the world's zinc resources (Brown et al., 2018).

The Bayer process is the most commonly used process for the alumina production from bauxite. During this process the aluminium (Al) bearing minerals in bauxite are dissolved in sodium hydroxide (NaOH) solution at high temperatures and high pressure. The resulting sodium aluminate solution is cooled and filtered to remove the non dissolved bauxite residue containing iron (Fe), calcium (Ca), silicon (Si) and other elements in small quantities. The separated liquid, known as Bayor liquor (BL), is then seeded in order to crystallize aluminium hydroxide and the liquid remaining after crystallization is recycled. The recycled liquid contains Ga in concentrations 100-300 mg/L (Zhao et al., 2012; Brown et al., 2018). There are different options for Ga recovering from this solution, such as precipitation methods, widely used by the industry, electrochemical method, solvent extraction (Virolainen, 2013). Most methods applied by industry for Ga recovery from BL are proprietary and therefore not disclosed in details.

Another commercial resource of Ga is zinc residue from Zn extraction from sphalerite (ZnS) ore by the roast-leach-electrowinning (RLE) process. During the Zn extraction process, the sphalerite is roasted to zinc oxide (ZnO), the oxide is leached with sulfuric acid (H_2SO_4). Gallium is contained in impurities, which are separated

from the leach solution through the addition of antimony trioxide, Zn dust or proprietary reagents. The Zn leaching residues (ZLR) may contain Ga (0.03-0.4 wt.%). It is estimated that currently, the ZLR accounts for nearly 10% of the annual Ga production worldwide (Lu et al., 2017). According to Frenzel et al. (2016) the concentration of 100 ppm in sphalerite zinc concentrate from MVT deposits, and 250 ppm in sphalerite zinc concentrate from other deposits is feasible for Ga recovery. This corresponds to a cut-off grade in the leach residue of 1000 ppm Ga. From ZLR the Ga is recovered by acid or alkali leaching processes (Fayram and Anderson, 2008). In the acid leach circuit the residue is dissolved in H_2SO_4 under pressure at 80-90 °C. Then the leached Fe is converted from ferric to ferrous and cementation of metals that present in the leachate, such as copper (Cu), cadmium (Cd) along with Fe is carried out. Further, Ga is recovered by a solvent extraction, stripped with acid solutions and crude Ga metal is obtained by electrowinning from the acid solution. The solvent extraction stage can be replaced by ion exchange. The alkaline leaching process includes the following stages: Alkaline leaching using NaOH to form a jarosite residue; Precipitation of Al, Ca, and Zn with calcium hydroxide; Precipitation of germanium (Ge) with magnesium (Mg) hydroxide; Recovery of Ga by electrowinning. The process is not suitable when the ZLR contain lead (Pb) since it was found to interfere with the Ga recovery. Whether from bauxite or from ZLR, the extracted Ga (typically recovered at 99.9 to 99.99 %), often is further purified, applying processes such as electrolytic refining or zone refining.

Data on the recent world production of Ga are presented in Figure 1 and on the world Ga production capacity are shown in Table 1 (Jaskula, 2010; Jaskula, 2011; Jaskula, 2012; Jaskula, 2013; Jaskula, 2014; Jaskula, 2015; Jaskula, 2016; Jaskula, 2017; Jaskula, 2018; Jaskula, 2019). The Figure 1 depicts also the corresponding price of low-grade (99.99%-pure) Ga. The increase in the primary low-grade Ga production lead to a decrease of its price, as it can be seen in the Figure 1. China is the biggest low-grade Ga producer with (93-95 % of the world production recently – 2015-2018). The other producers in recent years are Japan, the Republic of Korea, Russia, and Ukraine. Germany and Kazakhstan ceased their primary production in 2016 and 2013, respectively. China, Japan, Slovakia, the United

Kingdom, and the United States are the principal producers of high-purity refined Ga (Jaskula, 2019). The increase in the primary low-grade Ga production capacity (Table 1) is due mainly to the expansion of the China's primary low-grade Ga production capacity to approximately 600 t per year since 2016 from 140 t per year in 2010 (Jaskula, 2019).

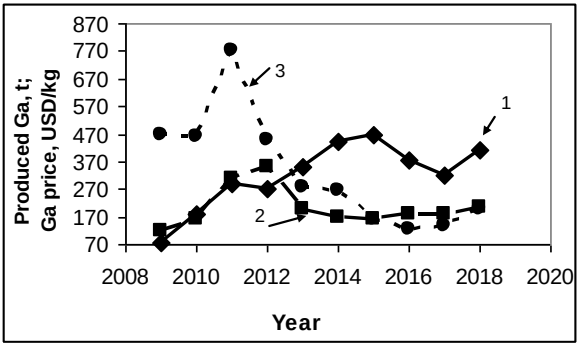

Fig. 1. Recent world production of: primary low-grade Ga (1-♦), primary high-purity refined Ga (2-■); the price of low-grade (99.99%-pure) Ga (3-●)

Table 1

The world gallium production capacity

Production/ year	2009	2010	2011	2012	2013	2014	2015	2016	2017	2018
Primary	184	184	320	474	470	680	730	730	730	730
Refinery	167	177	270	270	300	230	230	320	320	320
Secondary	78	141	198	198	200	200	200	270	270	270

2.2. Germanium production

The abundance of Ge in the continental crust is reported as 1.3-1.5 ppm. Germanite, which occurs in Namibia, is a mineral containing 5-10% Ge, while argyrodite, mined in Germany, contains 1.8-6.9% Ge (Moskalyk, 2004). Germanium is present as a trace element in other minerals, most often in the zinc-sulfide and lead-zinc-sulfide deposits, which contain some tens ppm Ge on average (Frenzelet al., 2014). Coal contains on average about 2 ppm Ge (Ketris and Yudovich, 2009), but there are some coal deposits with a Ge content above 100 ppm, especially in Eastern Asia (Du et al., 2009). Currently Ge

is produced mostly from zinc-smelter residues and coal ashes of coal deposits with high Ge content. The source material can be treated by pyro- or hydrometallurgical methods, or both. The pyrometallurgical treatment results in formation of dusts and fumes, where the Ge is concentrated under the form of oxide (GeO_2) or sulfide (GeS_2). The pyrometallurgical processes are losing importance as a result of the environmental problems created due to the volatility of GeO_2 and GeS_2. Hydrometallurgical processes are favored recently. They are used both to treat products from pyrometallurgical pre-treatment or directly the row Ge-bearing materials. Ge is usually leached in aqueous solutions of H_2SO_4 (most often), oxalic acid ($H_2C_2O_4$), or alkalis. Then, it is recovered from solutions by (i) precipitation with tannic acid, sulphide, catechol-cetyltrimethyl ammonium salts, (ii) solvent extraction, and (iii) ion-exchange techniques (Drzazga, et al. 2018). The products of the different recovery processes that produce a germanium-bearing material are further refined.

Data on the recent world production of Ge are presented in Figure 2 (Guberman, 2010; Guberman, 2011; Guberman, 2012; Guberman, 2013; Guberman, 2014; Guberman, 2015; Guberman, 2016; Guberman, 2017; Thomas, 2018; Thomas, 2019). The Figure 2 depicts also the corresponding price of Ge metal and GeO_2. China is the leading global producer of Ge as it can be seen in Fig. 2. Its Ge production (primary and secondary) was 80, 60 and 75 t in 2016, 2017 and 2018 correspondingly. For the recent 3 years Russia reported Ge production of 6 t per year. Belgium, Canada, Germany, Japan and Ukraine produced together 40, 40 and 35 t in 2016, 2017 and 2018 correspondingly (Guberman, 2017, Thomas, 2018, Thomas, 2019). China's Ge production growth rate decreased since 2015 due to the implementation of stricter environmental standards and restrictions. Worldwide, about 30% of the total Ge consumed is produced from recycled materials - mainly new scrap from the optical devices manufacture. During the manufacture of most optical devices, more than 60% of the Ge metal used is routinely recycled as new scrap (Thomas, 2019).

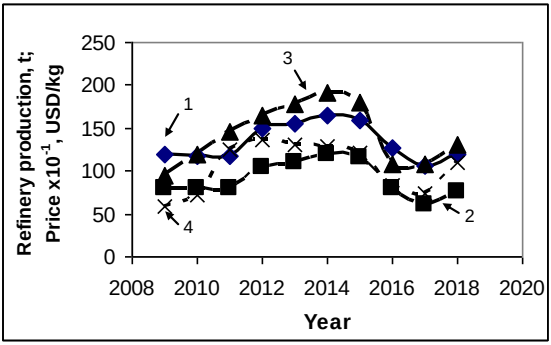

Fig. 2. Recent world production of Ge (1-♦), production of Ge by China (2-■), the price of Ge metal (3-▲), the price of GeO_2 (4-X)

According to some estimates, the world reserve of Ge is only 8600 tons and none of it - in mineable deposits (Chen et al., 2018). Data on the recoverable Ge content of Zn ores are not publicly obtainable. The available resources of Ge are associated mainly with certain zinc and lead-zinc-copper sulfide ores. Based on the analysis of zinc concentrates, for example, the U.S. reserves of Zn are estimated to contain 2500 t Ge. However, on a global scale, as little as 3% of the Ge contained in Zn concentrates is recovered. Significant amounts of Ge are contained in ash and flue dust generated in the combustion of certain coals for power generation (Thomas, 2019).

2.3. Indium production

Indium's abundance in the continental crust is estimated at 0.05 ppm (Tolcin, 2013). Indium is most commonly recovered from the zinc-sulfide ore mineral sphalerite. The In content of zinc deposits from which it is recovered is from less than 1 ppm to 100 ppm. Other base-metal sulfides, such as chalcopyrite and stannite also bare In in trace amounts, however most deposits of these minerals are subeconomic for In extraction. Indium is recovered from the processing of the base metal concentrates. It is produced mainly by leaching with hydrochloric acid (HCl) or H_2SO_4 of dusts, fumes, residues, and slag from the zinc and lead-zinc smelting. The obtained raw In is then further purified by electrolysis and/or solvent extraction. The metal can be refined to purities of 99.9999%. The average In content of zinc concentrates in key Peruvian and Bolivian mines is

estimated to be 187 ppm and 630 ppm respectively (Ad hoc Working Group, 2014).

Data on the recent world production of In, as well as on the In production by China and Republic of Korea (the two biggest producers) are presented in Figure 3 (Tolcin, 2010; Tolcin, 2011; Tolcin, 2012; Tolcin, 2013; Tolcin, 2014; Tolcin, 2015; Tolcin, 2016; Tolcin, 2017; Anderson, 2018; Anderson, 2019). The Figure 3 depicts also the corresponding New York dealer price of In.

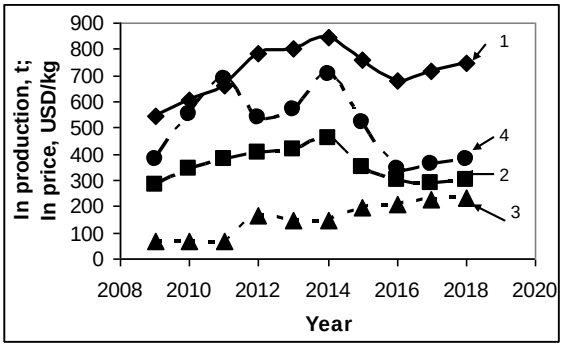

Fig. 3. Recent world production of In (1-♦); Production of In by: China (2-■), Republic of Korea (3-▲); The price of In metal (4-●)

The sharp raise in In production and price in the period 2009 - 2011 is assigned mainly to (i) the increase in the In demand since in December 2008, China began a 4-year, 13% subsidy program in certain agricultural regions to encourage farmers to purchase home appliances, mobile phones, and televisions leading to an increased domestic demand of In for LCD-containing electronics; (ii) increase in indium consumption in Japan (the biggest global consumer of In) by ca. 20% in 2010 from that of 2009 (Tolcin, 2010). China decided to increase its domestic manufacturing of high-end-value electronics rather than sell the raw materials to Japan and buy back the electronic products at high prices. So, the Chinese Government cut the In export quotas (Tolcin, 2011). The global consumption of primary and secondary indium in 2011 was estimated to be more than 1800 t, of which approximately 60% was consumed in Japan. At the same time world production of primary indium was ca. 660 t

(Tolcin, 2012). This led to a sharp raise in the primary production in the next 3 years. Secondary production, which accounted for a greater share of global production than primary, was thought to have increased as well, as many ITO producers were reported to have increased their recycling rates of the new scrap (Tolcin, 2013). In production continued to grow in 2013 due to the increased imports of In by Japan and the Republic of Korea, the two leading consumers of In. In addition to increasing demand for ITO in LCD displays, two leading flat-panel makers announced intentions to replace amorphous Si with indium-gallium-zinc-oxide (IGZO) as the thin-film transistor in displays used in some consumer electronics, including organic light-emitting diode (OLED) televisions, smartphones, and tablets (Tolcin, 2014). The further raise in the In production was related mainly with (i) the work of a Japanese company that was the only world mass producer of CIGS solar cells and consumed about per year at its three CIGS solar cell production plants and the announcements on the construction of a 4th plant that was expected to begin production in 2015; (ii) the fact that in China, two large-scale ITO projects were under development and expected to begin production in 2015 (Tolcin, 2015). At the same time the 2015 prices decreased which was attributed to an absence of investor demand in China coincident with the Fanya Metal Exchange halting In deliveries. Decreasing prices resulted in China large state-owned zinc smelters reducing their In production by at least 10%, small-scale zinc smelters suspending their In production, and stand-alone In producers reducing their output by 30% to 40% (Tolcin, 2016). New production sources and depressed demand after the collapse of the Fanya Metal Exchange Co. Ltd. in 2015 contributed to low prices in 2016. Indium production in China continued to decrease in 2016, owing to a continued decrease in production by small-scale In producers. Indium production at large Pb and Zn smelters was reported to have remained level. The Government of China increased policy support in the years 2016 - 2020 for the development of its minor metals industry and related value-added products, potentially leading to a notable increase in In consumption and production (Tolcin, 2017).

According to the USGS a quantitative estimates of In reserves are not available (Tolcin, 2014). According to the Indium Corporation,

In reserves (proven and probable, measured and indicated, and inferred) worldwide are close to 50000 t within zinc and copper minerals at existing mines (Mikolajczak, 2009). However, a study undertaken by the Indium Corporation showed that only about 30% of the In mined worldwide every year is transformed into refined In metal because of the following reasons: (i) 30% of In-containing base metal concentrates still do not reach "In-capable" smelters and this In is lost in metallurgy waste; (ii) 70% of the In-containing concentrates that do reach In-capable smelters are only extracted at a final average rate of about 50%. The remaining 50% that is not immediately transformed into In metal and remains associated with other elements and impurities in a residue form is accumulated and is available for further treatment and recovery later. Above-ground stocks, for example tailings and residues, were estimated at an additional 15000 t of reserves and another 500 t of In is generated every year in residue form. These In-containing materials are more difficult and thus more expensive to treat. However, they can be treated if demand and price warrants (Mikolajczak, 2009). The production of In is also heavily dependent of the production of Zn. However, even if there is clear opportunity for expansion in the production of In, this is difficult decision for the base-metal producers, since In contributes only a small amount of their profit. Production of indium requires investment in refining technology. In addition, the company has to ensure enough amounts of In-containing zinc concentrates to justify In recovery. Indium Corporation estimates that, to justify its economic recovery, a minimum In content of around 100 ppm is required in the concentrate (Mikolajczak, 2009).

Data on the quantity of secondary In recovered from new scrap are not available (Anderson, 2019). Indium is most commonly recovered from ITO. Sputtering, the process in which ITO is deposited as a thin-film coating onto a substrate, is inefficient. Approximately 30% of an ITO target material is deposited onto the substrate, while the remaining 70% consists of the spent ITO target material, the grinding sludge, and the after-processing residue left on the walls of the sputtering chamber. This new scrap is subjected to recycling. ITO recycling is concentrated in China, Japan, and the Republic of Korea - the countries where ITO production and sputtering take place (Tolcin, 2013). Presently, In is also recovered from CIGS new scrap

in Belgium. This is economically viable due to the high metal concentrations found in these materials and the large quantities of new scrap formed during production, which is recorded to be 50% (Ad hoc Working Group, 2014).

Indium recycling from post consumer scrap is practically non-existing. Only 1% of In from end-of-use LCDs appears to be recovered (Ad hoc Working Group, 2014).

3. Trends in gallium, germanium and indium substitution, use and the expected shortage

3.1. Gallium

Gallium can be substituted in some of its applications but for others, it has no effective substitutes. Organic liquid crystals are used in visual displays as substitutes for LEDs. Silicon-based metal-oxide semiconductor power amplifiers compete with GaAs power amplifiers in 3G cellular handsets. Indium phosphide components can be used instead of GaAs-based infrared laser diodes in some specific-wavelength applications, and helium-neon lasers compete with GaAs in visible laser diode applications. Silicon is the competitor with GaAs in solar-cell applications. GaAs in heterojunction bipolar transistors is being substituted in some applications by silicon-germanium. GaAs-based ICs are used in many defense-related applications where no effective substitutes exist (Jaskula, 2018; Jaskula, 2019). However, In, Ge and Si are also classified as critical materials for EU (EU, 2017) and In and Ge are included in the list of 35 critical minerals (83 FR 23295, 2018) by the U.S. Department of the Interior.

Global demand for GaAs- and GaN-based products has increased recently mainly due to the growth production of 3G and 4G smartphones, which employ up to 10 times the amount of GaAs in standard cellular handsets. The use of GaN-based products in cable television transmission, commercial wireless infrastructure, power electronics, and satellite markets continued to increase. The global LED market has also increased recently - from USD15.3 billion in 2015 to USD18.8 billion in 2018 (Jaskula, 2019). Global demand growth for Ga is expected to be at around 8% per year to 2020, up to around 650 tons. The most rapid growth is anticipated for the LED and solar PV segments of the Ga market, which could grow at 13%

and 22% per year to 2020. For the semiconductors market, a growth of 5% per year is forecast. This strong demand growth may take the market into deficit in coming decades (EU, 2015). In addition, the small market for Ga as a specialty metal creates little incentive for refiners of Zn, Cu, and Al ores to invest in improvements to increase byproduct recovery of Ga. Production of Ga is limited by market factors that influence the production of the principal mineral commodity, whether it is zinc or aluminum (Foley at al, 2017).

Expected problems with Ga supply led to its classification in 2017 as a critical for Europe material (EU, 2017) and as a critical for the USA - in 2018 (83 FR 23295, 2018). The critical materials are defined as materials with high supply risk and above average economic importance compared to other raw materials (Fortier et al, 2019). Even for the leading world producer – China, the forecasts are that the cumulative domestic Ga consumption will overpass reserves before 2050 (Eheliyagoda et al., 2019).

3.2. Germanium

Silicon can be used as a substitute for Ge in certain electronic applications. Zinc selenide and Ge glass substitute for Ge metal in infrared applications systems, but often at the compromise of the performance. Antimony (Sb) and titanium (Ti) are substitutes for use as polymerization catalysts. However Si and Sb are also classified as critical materials (EU, 2017; 83 FR 23295). According to the European Commission (EU, 2017) substitutes of Ge in optical fibers are not really used because of performance losses, but fluorine and phosphorus can be mentioned, with a low probability of industrial use.

Ge demand is expected to grow with a rate of 4.4% per year. The largest increases are expected in infrared and fiber optics (5.6% per year). Ge demand for solar and electronics applications are expected to raise at rates of over 4% per year, the market for catalysts is only expected to be flat. There currently exists a small market surplus of Ge supply. However, it is expected that over the coming decade the supply growth will not keep up with demand growth (Deloitte et al., 2017). Germanium's use in fiber optics, infrared, and photovoltaic products increased in China in 2018 year, which increased the demand for the metal (Thomas, 2019).

Expected problems with Ge supply led to its classification in 2017 in the list of critical for Europe materials (EU, 2017) and in the list of critical for the USA materials - in 2018 (83 FR 23295).

3.3. Indium

Some substitutes of In are already available. Antimony tin oxide coatings are an alternative to ITO coatings in LCDs. Carbon nanotube coatings are an alternative to ITO coatings in flexible displays, solar cells, and touch screens. PEDOT [poly(3,4-ethylene dioxythiophene)] has been developed as a substitute for ITO in flexible displays and organic LEDs. Graphene has been developed for replacing ITO electrodes in solar cells and ITO in flexible touch screens. Zinc oxide nanopowder with good adhesion has been developed to replace ITO in LCDs. Gallium arsenide can substitute for In phosphide in solar cells and in many semiconductor applications. Hafnium (Hf) can replace In in nuclear reactor control rod alloys. However, many of the suggested substitutes (such as Sb, Ga, Hf) are classified as critical materials (EU, 2017; 83 FR 23295, 2018). In addition, the price of carbon nanotubes and graphene is still relatively high.

Indium demand is expected to grow rapidly for LEDs and PV applications. By 2020 these two applications could account for 20% of primary In demand (compared to 7% in 2012). For flat panel displays, indium's largest end-market, demand growth is expected to be around 5.5% per year, driven in particular due to the rise of smart phones and tablets, as well as steady growth in demand for flat screen TVs, laptops and computers (Ad hoc Working Group, 2014). Indium consumption is expected to be supported also by the growth of the emerging IGZO (Indium Gallium Zinc Oxide) display market (Deloitte Sustainability, 2017). On the supply-side, production of virgin In will be driven by zinc refiners' willingness to recover indium. This means that virgin supply probably will grow a more slowly than primary demand, and may push the market into a certain deficit (Ad hoc Working Group, 2014).

Expected problems with In supply led to its classification in 2017 in the list of critical for Europe materials (EU, 2017) and in the list of critical for the USA materials - in 2018 (83 FR 23295).

Increasing the primary production, raising the minor metals recycling from pre- and post-consumer scrap, and enhancing the comprehensive use of ores and the recovery from metals' extraction waste and wastewater can be pointed as measures aimed at mitigation of the expected shortage of Ga, Ge and In. This chapter is devoted to recent studies on enhancing the comprehensive use of ores and the Ga, Ge and In recovery from metals' extraction waste and wastewater.

4. Recent studies on gallium, germanium and indium recovery from mining and metals' extraction waste

Recycling of waste formed during base metals extraction from ores can be a source of Ga, Ge and In. For example, in the EU in extractive waste disposed in situ/in tailings annually 100 t of Ga, and 10 t of In are added, and the stock in tailings for the last 20 years is evaluated correspondingly to 1200 t Ga, and 120 t In (Mathieux et al., 2017).

4.1. Gallium recovery

Studies have shown that from 100 units of Ga, that is present in the bauxite ore, 70-90 % are transferred to the Bayor liquor and the other 10-30 % are deposited in the red mud. On average, 54-77 % of the Ga available in the BL pass to the BL feedstock, the other 23-46 % are lost in alumina and red mud. In the process of the crude Ga recovery from the feedstock other 4-25 % are lost in the waste liquor depending on the technology applied. As a result from the initial 100 Ga units, only 28-67 units (depending on the producer capacity and capability) are extracted as a crude Ga, the other are left as waste (mainly red mud) (Redlinger et al., 2015). This represents a big Ga resource, where the Ga is as rule in higher concentrations compared to the initial bauxite ore. For example, it is estimated that over 150 million t of bauxite residue are produced annually, while more than 2.7 billion t were already stockpiled by 2011 (Ujaczki et. al., 2017). Therefore, recycling strategies for Ga from red mud and other metal extraction residues bear major opportunities to reduce Ga losses and to increase Ga availability.

A method, named acidic-leaching-ion-exchange process (ALIEP), was developed to extract Ga from Bayer red mud (BRM) under nor-

mal atmospheric pressure (Lu et al., 2018). The method involved three main stages: 1) The BRM sample dissolution in HCl acid and removal of the Fe^{3+} from the obtained leachate followed by the purified leachate pre-concentration by re-circulation process; 2) Ion exchange process (with LSD-396) for the Ga recovery; 3) Elution of loaded resin with HCl solution to obtain Ga-rich solution (97.54 mg/L of Ga) suitable for Ga electrowinning. 94.77% of Ga (3.91 mg/L in leachate) was leached under the optimal conditions (HCl 159 g/L, 8 mL/g, 55 °C, 5 h). Nearly complete Fe removal from the leachate was achieved (at 45 °C, resin dosage of 0.6 g/mL, 2 h).

Extraction of Ga from bauxite residue (Ga ~ 106.8±7.3 ppm) by selective acid leaching with $H_2C_2O_4$ has been proposed (Ujaczki et. al. 2017). Under the optimum conditions (2.5 M $H_2C_2O_4$, 21.7 h, 80.0 °C and slurry concentration 10.0 g/L) 80% of the of the aqua regia accessible Ga content was extracted from the residue.

A kind of solid waste called "coal red mud - CRM" is produced during the extraction of Al from Inner Mongolia, China coal fly ash by HCl leaching. It contained 0.305 wt% of Ga_2O_3, where Ga and Fe exist in CRM in the form of $Ga(OH)_3$ and $Fe(OH)_3$, and the $Fe(OH)_3$ coats $Ga(OH)_3$. A hydrothermal alkaline leaching method was developed which converted $Fe(OH)_3$ to Fe_2O_3 (Xue et al., 2019). Since the latter is with small specific surface area, this weakened the coating of $Ga(OH)_3$ and accelerated the leaching reaction between $Ga(OH)_3$ and NaOH. Under the optimal leaching conditions (NaOH 20 wt %, 120 °C, 12 h, 5 mL/g) 91.4% of the Ga present in the CRM were leached and the Ga_2O_3 concentration in leaching solution was 73.44 mg/L. Fe was not detected, the leaching residue was α-Fe_2O_3.

Bioleaching and Ga recovering from Al smelting slag have been studied (Wang et al., 2018) using *Acidithiobacillus thiooxidans*. At 2% pulp density the Ga bioleaching efficiency was nearly 100% in 24 h, the Ga concentration in the pregnant leach solution (PLS) was 505 mg/L. Further, under the optimized experimental conditions, precipitation with lime milk yielded the Ga recovery of 60.6% from the PLS that contained also Al, Fe, Ca and Mg -1360, 101, 505 and 258 mg/L respectively. The lime milk technique proved to be superior to the also tested ion exchange with D113 and D001 (strong cation-exchange resins in hydrogen form).

A method for Ga recovery has been developed, based on sintering and carbonization, for the treatment of electro-filter dust (containing 38 ppm Ga_2O_3 and 89.5% Al_2O_3) of a calcination plant (Gladyshev et al., 2015). A Ga-rich precipitate was produced after a series of alkaline digestions and then two-stage carbonate precipitation procedure. The precipitate found was used for preparation of Ga_2O_3 electrolyte (0.6 g/L) for Ga electrowinning.

Copper tailings were subjected to chlorination roasting with calcium chloride used as the chlorination reagent (Lei et al., 2015). The results showed that increases in roasting temperature, quantity of chlorination agent, and roasting time lead to increased chloridizing volatilization rate of Ga that reached 78.86 % at 900 °C, 40 min roasting, air flow of 0.1 m^3/h, and Ca content of 33.33 wt%.

Mining residues from the exploitation of Fe and polymetallic (Pb-Zn-Ag) ores were studied in order to evaluate the possibility to recover strategic elements, like Ga, In, Ge (Ceniceros-Gómez et al., 2018). The results indicated that the major elements (> 100 ppm) in the samples are Fe, Zn, Pb and Cu. The strategic elements with the greatest recovery potential are Ga from Fe non-oxidized tailings and In, Ge from the Zn refinery hydrometallurgical waste. The results showed that the total concentrations of Ga, Ge and In did not depend importantly on the particle size, thus indicating that a previous concentration is not necessary for their recovery. Further, Ga was recovered from the Fe non-oxidized mine tailings that contained approximately 13 ppm Ga (Macías-Macías et al., 2019). The tailings were leached with 8M HCl for 48 h, achieving total dissolution of the Ga present. Then, up to 98% of Ga were extracted with tributylphosphate (TBP at 10% v/v in benzene, in aqueous : organic phase ratio of 1:1 in a single stage with 3 min of agitation) and less than 35% of the Fe present. In the stripping stage with 0.1M H_2SO_4 up to 100% of the extracted Ga was recovered and less than 2% of the Fe present. A conclusion is drawn that in order to be economic, the method has to be applied to tailings with higher Ga content.

4.2. Germanium recovery

Germanium can be produced from historical metallurgical waste. For example, according to Moskalyk (2004) lead smelting operations

during the period 1963 - 1996 generated furnace slag which was discarded in the nowadays abandoned slag dump at the old Tsumeb mine in Namibia. The abandoned dump (totally about 2.9-million t of slag) contains Zn (9.03%), Pb (2.05%), Ge (0.026%), Ga (~0.02%), and In (~0.017%) with a combined value of over 1-billion USD. Moskalyk gave data from a technical feasibility study, conducted by Korea Zinc that is a recognized leader in slag treatment. High recoveries of Pb (91%) and Zn (75%) were predicted. The recoveries of Ge and Ga were expected to approach 94% and 50% respectively. Tests demonstrated that the residual metals within the discarded slag can be concentrated into an oxide dust by reduction and fuming. The technologies were patented and proprietary.

Limited information about recovery of Ge from slags and tailings is available. The current studies on the Ge recovery are mainly focused on the hydrometallurgical processes to dissolve and extract Ge, followed by a process to separate Ge from the other elements that are available in the leachates. Below are presented some examples.

Copper cake of Çinkur Zinc Plant was characterized and studied with the aim to extract Ge (Kul and Topkaya, 2008). It has been found that the fraction below 147 μm contained 700 ppm Ge. The mineralogical analysis indicated the complex nature of the Cu cake which was mainly composed of metallic and oxidized phases containing Cu, As, Zn, Cd, etc. The H_2SO_4 acid leaching experiments were carried out and optimized for selective and collective leaching. The optimum selective leaching conditions of Ge were: reaction time - half an hour, a solid to liquid ratio 1:4 g/cm^3, 100 g/L H_2SO_4 acid concentration, no chemical oxidant addition or air pumping, and the temperature range of 40 - 60 °C. Under these conditions 78% of the Ge was leached. The dissolution of other metals like Co, Ni, Fe, Cu, Cd and As was insignificant. So, Ge would be separated more selectively at the following stage that comprises precipitation by tannin. The optimum conditions for collective extraction of Ge and other valuable metals were: temperature range of 60-85 °C, reaction time of 1 h, H_2SO_4 acid concentration of 150 g/L, a solid-liquid ratio 1:8, air pumping. Under these conditions, the recovery of Ge was 92.7% while the other metals were leached almost completely. After the optimization of leaching conditions of the Cu cake, the precipitation of Ge from the PLS with tannin was optimized. The precipitation

with tannin was preferred for the Ge recovery since the Ge concentration in the PLS obtained after leaching was <1000 mg/L Ge. Thus, 94% of Ge in PLS could be precipitated selectively. Further, germanium oxide concentrate with ~20% Ge content was produced by atmospheric roasting. The experiments indicated that selective precipitation of Cu and Ge with Zn powder was not possible. So, the proposal was to precipitate initially the Ge by tannin addition. Further Cu can be precipitated from the PLS by Zn powder or steel scrap. Finally, the Zn in the solution can be precipitated or recovered by electrowinning.

4.3. Indium recovery

Indium extraction from lead-smelting dust (LSD) containing percent levels of In has been studied (Sawai et al., 2015). The main difficulty in recovering In from the LSD is the coexisting presence of Pb and Zn. A separation process was designed, combining techniques that involve washing with a chelant, leaching with acid and precipitation as hydroxide. The majority of the Pb in the LSD was selectively separated by chelant-assisted washing with ethylenediamine-disuccinate. The chelant washing step ensures 100 % separation of In from the chelant-treated dust, a decrease in the raw LSD weight by approximately 82% due to the removal of lead and counter-ions such as sulfate. The residual Pb left in the chelant-treated dust was removed through an acid leaching treatment with a mixed solution of H_2SO_4 and HCl. The selective In separation from LSD is complicated by the similar behavior of Zn and In during the acid leaching step. Hydroxide precipitation at pH 5 has been introduced as the final step, ensuring the maintenance of Zn as a soluble species in the supernatant and the selective separation of In (~88%) as a hydroxide precipitate.

Indium separation and extraction from lead smelting hazardous dust (LSHD) was studied (Zhang et al., 2017). The technology included a pressure H_2SO_4 leaching of LSHD, precipitation and enrichment of In, atmosphere H_2SO_4 leaching of In-enriched residues and solvent extraction of In. More than 99% Zn and 95% In were leached from LSHD by two-stage countercurrent pressure H_2SO_4 leaching using the initial H_2SO_4 concentration of 30-50 g/ L in the 1st stage, the initial H_2SO_4 of 120-150 g/L in the 2nd stage, temperature

140-160 °C, total pressure 0.6-1.0 MPa, for 1-1.5 h at L/S ratio 3–5/1. More than 97% indium was precipitated from the 1st pressure H_2SO_4 leaching solution at neutralization to pH 4.0, 70-80 C for 1 h. More than 96% In was re-leached by two-stage countercurrent atmosphere H_2SO_4 leaching from the In-enrichment residues at L/S ratio of 3-5/1 for 0.75-1.5 h. Temperature of the 1st stage was 90-95 C, of the 2nd stage - 70-80 °C, where the initial H_2SO_4 concentration was 40-50 g/L and 90-110 g/L, respectively. More than 98% In was extracted by three-stage solvent extraction using 30% (v/v) di(2-ethylhexyl)phosphoric acid (D2EHPA), phase ratio 1/6, for 1 min at temperature 25 °C.

Goethite residue was leached by addition of 3 M H_2SO_4 for 24 h at 65 °C. The PLS contained, in mg/L: In(III) (53), Fe(III) (10764), Pb(II) (269), Zn(II) (1502), As(III) (480) and Cu(II) (41). Then a process for the separation and purification of In from the Fe-rich matrix solutions has been proposed based on the use of supported ionic liquid phase (SILP) (Roosendael et al., 2019). The SILP was synthesized by impregnating Amberlite XAD-16N with the iodide form of the quaternary ammonium salt Aliquat 336. Adsorption was preceded by the addition of an excess of iodide anions to the solution, to form indium iodide species, which were extracted to the ionic liquid of the SILP. A high selectivity for In over Fe was achieved because iron iodide species are not stable in aqueous medium. A two step stripping procedure with 0.1 M H_2SO_4 solution for 40 min, was found as optimal to recover and concentrate the adsorbed In(III) ions. The SILP system is reusable in multiple cycles without losses of adsorption or stripping efficiencies and without the need to regenerate the SILP adsorbent with a fresh potassium iodide solution. A pure In solution of 49 mg/L was obtained with an indium-over-iron selectivity factor of 5400.

Indium recovery from sphalerite ore and flotation tailings by bioleaching and subsequent precipitation processes has been proposed (Martin et al, 2015). Flotation tailings dump material of the former lead-zinc mine near Freiberg (Germany) contains galena and sphalerite not recovered by flotation. The sphalerite contains, aside from Fe, Cu and Cd, significant amounts of In (up to 0.38% (w/w)) leading to In contents up to 70 ppm in the tailings. Preliminary ther-

modynamic assessment showed a comparatively small Eh–pH-range where In is not hydrolytically precipitated and bioleaching is possible. As inoculum for the experiments was obtained from a leachate sample (pH 2.3) of the Maurliden zinc–lead mine (Sweden, BOLIDEN Group). The inoculum contained uncultured acidophilic ferrous iron-oxidising and sulphur-oxidising species and was enriched in modified basal salts medium. Shake flask bioleaching of original polymetallic sphalerite ore from the Freiberg mining district (400 ppm indium) achieved 97.7% (w/w) of Zn and 75.2% (w/w) of In leaching at pH 1.8, respectively. The column bioleaching tests on tailings material achieved Zn and In yields of 94.6% (w/w) and 79.9% (w/w) respectively. It has been found that the leaching efficiency slowed down with continuous leaching progress and by an additional direct aeration of the substrate in the columns the leaching process could be enhanced. The leaching solutions contained about 20 g/L Zn and 33 mg/L In, that means sufficient quantities of In and Zn for a further recovery from the PLS by hydrometallurgy. Further a bioreactor experiment was conducted at pH 1.8. Leaching of Zn and In reached 81% (w/w) and 87% (w/w), respectively, with a decrease of In after 10 days due to partial precipitation as $InAsO_4$ phases or adsorption to Fe phases. However, also heavy metals could be mobilised as high leaching rates for As and Cd indicate (72% and 88% (w/w), respectively). The PLS of the tailings material contained high concentrations of Fe, Zn and As. For this reason a stepwise precipitation approach was chosen for In separation making use of the fact that $InA_SO_4.2H_2O$ is with lower solubility than $In(OH)_3$. So, whereas indium hydroxide precipitation takes place in a pH range of 2.0-4.0 a shift to a pH range of 1.5-2.0 occurs in the presence of AsO_4^{3-} ions. This allows for separation of In (by PLS neutralisation with 9 M NaOH) from aluminium ions, most of ferric iron as well as the divalent ions (e.g. Zn, Cd, Cu) which are not precipitated at that low pH. The pre-concentrate formed contains ferric iron. It can be redissolved and In can be precipitated after reduction of ferric iron to ferrous iron as $In(OH)_3/InAsO_4$. In this way In rich concentrate is obtained that might be processed by hydro- or pyrometallurgy.

Three secondary raw material resources (zinc processing wastes) have been analysed for their In content, namely a “tailings” sample which is a waste from flotation plant, a “jarosite” sample which is a

waste from a hydrometallurgical plant, and a “ferrite” sample which is a waste from pyro-hydrometallurgical plant (Karumb, 2016). Results from the chemical analysis showed that the In content in the tailings, jarosite, and ferrite samples was 18.3, 246, and 783 ppm, respectively. Indium was mainly present in the matrix of the jarosite mineral which was predominant in the jarosite sample. Investigation on the possibility for In beneficiation via physical separation methods (gravity, magnetic, and electrostatic separation) was conducted on all three samples. The conclusion was that physical separation did not achieved appreciable beneficiation. However, it was found that the sample could be screened at 297 μm to remove a portion of the coarser gangue minerals followed by leaching of the fines fraction. Indium was successfully extracted into solution via a H_2SO_4 leaching for both the jarosite (95% extraction) and the ferrite (90% extraction) fines fraction. It was found that for the jarosite sample higher In extraction was achieved at lower temperature, higher initial acid concentration, and lower pulp density. The highest In extraction from the jarosite sample was achieved at the following conditions: 3M H_2SO_4, 4 hours, 20 % solid, and 80°C. The main contaminants in the PLS were Fe, Zn, Na, and Al. It was found that for the ferrite sample higher In extractions were obtained at 80°C with higher initial acid concentration and lower pulp density. The highest In extraction was achieved at the following conditions: 4M H_2SO_4, 4 hours, 20 % solid, and 80 °C. The main contaminants in the PLS were Fe and Cu. During leaching of the both materials acid consumption increased with higher temperatures, higher initial acid concentration, and lower pulp density. The following treatment was proposed for the PLS obtained from jarosite leaching:

a - In precipitation with NH_4OH solution, conciserable separation of Fe and Zn is achieved;

b - the resuling from the previous stage precipitate hot reductive (with Na_2S) leaching - the obtained PLS contains low Fe and high In amounts;

c - In extraction with D2EPHA;

d - In stripping with H_2SO_4 solution;

e - In precipitation by ZnO addition to obtain In concentrate.

The following treatment was proposed for the PLS obtained from ferrite leaching: *a* - Addition of Fe powder to precipitate and separate Cu;

b - In extraction with D2EPHA - the obtained loaded organics contains low Fe and high In amounts;

c - In stripping with HCl solution;
d - In precipitation by ZnO addition to obtain In concentrate.

4.4. Recovery of two or three of the minor metals

An European patent presented the separation and concentration of Ga and In by jarosite precipitation (Yoshito, 2000). Ferrous, ferric, sulfate ions, monovalent cations and oxidizing agent (air, oxygen, $KMnO_4$) are added to a Ga-In containing solution; the pH is adjusted to 2-4. Jarosite seeds are added to the mixture which is vigorously stirred at temperature 70-100 °C for 10-24 h. Solid liquid separation of the mixture results in a filtrate and jarosite, containing Ga and In. The Ga and In content of jarosite is increased with the increase in ferric ions content and monovalent cation content, with higher Ga incorporation than In. The solid is leached in alkaline media (with NaOH or KOH) to separate Ga and In. 100% Ga and nearly 77% Al are leached with 200 g/L NaOH at 80 °C for 2 hours, iron hydroxide is precipitated, while the In present in the jarosite together with Ga does not dissolve in the solution at higher pH values (about 13). The solution containing Ga is collected, $Ca(OH)_2$ is added to remove Al and Zn; the amount of Al precipitated increased with the temperature increase and $Ca(OH)_2$ addition accompanied however with Ga co-precipitation up to 2.1 %. In the case when Ge is present in the solution, $Mg(OH)_2$ is added for Ge removal as a precipitate; the extent of which increases with an increase in magnesium compound addition. The resulting filtrate is neutralized by the addition of H_2SO_4 which precipitates insoluble sulfates; at pH 6-7, the precipitate had higher Al, Zn, Na, and Fe content, while at pH 1-4 it had higher Ga content. The Ga-containing precipitate is then leached (150 g/L NaOH at 80°C, 1 h, pH 13, pulp density of 200 g/L). The final leached solution contains 55 g/L Ga and is sent to electrowinning.

Germanium and gallium were separated and recovered from zinc refinery residues by a two stage leaching (Liu et al, 2017a). In the first leaching stage with H_2SO_4 solution, 92% of Zn and 94% of Cu (that were present in the material) were leached, resulting in significant Ga and Ge enrichment of the material left - up to ca. 300%. In the 2nd stage $H_2C_2O_4$ solution was used. More than 96% of Ga and 99% of Ge were leached out by using 70 g/L $H_2C_2O_4$ with a L/S ratio of 10 at 90 °C for 2 h. Iron was removed by an ultrasound-assisted

ferrous iron precipitation method in which 96% of Fe(III) was precipitated as $FeC_2O_4 \cdot 2H_2O$ with minor losses of Ga(III) and Ge(IV) (1.4% and 1.3%). After iron removal, Ga(III) and Ge(IV) were extracted from the Fe free solution (Liu et al., 2017b). An organic system, based on tri(octyl-decyl) amine (№235), was used. The extraction equilibriums for both metals were obtained within 10 min at 30 °C. More than 99.0% Ga(III) and 99.8% Ge(IV) were extracted in three-stage counter current extraction using an organic system consisting of 20% (v/v) №235 and 10% (v/v) TBP in 70% (v/v) sulfonated kerosene at an A/O ratio of 3:1 and 30 °C for 10 min. Then, over 99.0% Ga(III) was selectively stripped from the loaded organic solution by three-stage counter current stripping using 2.5 M H_2SO_4 at A/O ratio of 1:2 and 30 °C for 15 min, resulting in a loaded strip liquor containing 3.8 g/L Ga(III). After Ga(III) stripping, 99.8% Ge(IV) was stripped by two-stage counter current stripping using 4 M NaOH at A/O ratio of 1:3 and 40 °C for 15 min, resulting in a final loaded strip liquor containing 8.3 g/L Ge(IV).

Germanium and indium have been recovered from two alloys that are byproducts from refining of crude Zn, produced in the Imperial smelting process - PbSnIn and PbSnCuInGe alloys (Winberg, 2018). The PbSnIn alloy contained 0.23 wt % In while the PbSnCuInGe alloy contained 6.9 mass % Ge and 1.74% In. Both alloys were first treated pyrometallurgically (at 600-700 °C), with the aim to concentrate In and Ge in an oxide dross. The yield of In from the PbSnIn alloy to the dross fraction <0.3 mm was 90%, and the In concentration in the dross was 1.12 %. The yield of In and Ge in the dross obtained by the pyrometallurgical treatment of the PbSnCuInGe alloy to the dross fraction <0.3 mm was 99.4 % In (the In concentration in the obtained InGe dross was 2.19 %) and 100 % Ge (the Ge concentration in the obtained InGe dross was 8.75 %). The oxide dross was further treated hydrometallurgically to produce In and Ge concentrate. The hydrometallurgical treatment of the indium dross started with its leaching with HCl at 75°C for 3 h. During that time a Pb concentrate was formed. The suspension was cooled to room temperature before filtering to separate the Pb concentrate. The filtrate was again heated to 75 °C. Then NaOH was added to the solution until the pH reached 5.0. The suspension was mixed for 3 h, after which flocculant was added and the solids, constituting the In concentrate,

were allowed to sediment for one day. The clear solution was removed and the sediment was pulped with water heated to 55 °C and mixed for one hour. After sedimentation and filtering, the final In concentrate was obtained. The concentrate contained 15.4 % In, the In yield from the dross to the indium concentrate was 54.8 %. The hydrometallurgical treatment of GeIn dross obtained started with leaching with aqueous solution of H_2SO_4 at 80°C. The suspension was mixed for 2 h, during the time of which the lead-tin-copper concentrate was formed. The suspension was filtered. Hydrogen peroxide was added to the filtrate to precipitate tin (Sn). Any excess hydrogen peroxide was decomposed by the suspension heating to 70 °C and mixing for one hour. Flocculant was added and the suspension was left to sediment overnight. The clarified solution was directed to the next (Ge precipitation) stage, while the Sn suspension was redirected to the leaching stage, in order to improve both Ge and In yields. In the Ge precipitation stage NaOH was first added to the solution to adjust the pH of the solution to 2.0. Then the solution was heated to 80 °C and technical grade tannic acid powder was added to the solution. Further, the solution was mixed for 2 h, during the time of which a germanium-tannin concentrate precipitated. Then the suspension was filtered. The concentrate was pulped with water at 70 °C and again filtered. The yield of Ge from the dross to the germanium-tannin concentrate was 80%.

Leaching of the dross containing 28.7% Sn, 18.0 Pb, 10.6% Cu, 8.9% Ge, 8.1% Zn, and 2.7% In in H_2SO_4 and $H_2C_2O_4$ solution was studied (Drzazga et al., 2018). The dross was obtained from thermal oxidation of by-product alloy generated during a New Jersey zinc rectification process. It has been found that Ge leachability in H_2SO_4 strongly depends on acid concentration and S/L ratio, and the highest leaching yield of Ge obtained was 85%. It was achieved at the following conditions: 80 °C, 3 h, 10% H_2SO_4, S/L = 1/10. Leaching in $H_2C_2O_4$ allowed achieving Ge leaching yield of 80% while the leaching yields of In and Sn were below 20%. Indium leachability in H_2SO_4 it strongly depends on process temperature, and reached 80% at 80 °C for 2 h. The addition of an oxidant (sodium hypochlorite) to H_2SO_4 during leaching increased Cu leachability (by up to 69%). However, it did not have a positive impact on Ge, In, and Sn leaching yields. Solutions obtained after leaching contain Ge, In, Zn, and

Sn. In order to selectively recover Ge, precipitation with tannic acid was applied. Then, Sn and In can be precipitated by solution pH increase or solvent extraction techniques may be applied.

Very recently a stepwise leaching has been proposed for selective dissolution of Zn, Ga and Ge from Zn refinery residue, containing Ga 0.15 wt % and Ge 0.47 wt % (Rao, 2019). In the first stage >93% of the Zn content, approximately 100% of the Ga content, and <8% of the Ge content were leached using 2 M H_2SO_4 with a liquid-solid ratio of 10 mL/g at 80 °C for 4 h. In the second stage about 90% of the Ge content and 33% of the lead content were extracted using 1 M NaOH with a liquid-solid ratio of 20 mL/g at 80 °C for 4 h.

A hydrometallurgical approach (named the Jarogain process) has been proposed and tested for treating Zn-containing side-streams and residues, in particular jarosite, goethite and electric arc furnace (EAF) dust (Kangas et al., 2017). The process is based on a sequence of steps, where the feedstock is initially leached in a reducing environment and ferric iron is converted to ferrous iron. The leaching residue contains lead, silver and gold to be recovered as a value-added concentrate. Further In, Ga and Ge are selectively precipitated from the solution as hydroxide concentrates by adjusting the pH to 4.5 with MgO, at 70 °C. The metal contents are subsequently separated as hydroxide and sulfide precipitates. Finally, the remaining Fe is crystallized from the solution. The major products of the Jarogain process are:

a - lead concentrate, that contains silver and gold;

b - mixed indium, gallium and germanium concentrate,

c - zinc concentrate,

d - iron concentrate,

e - H_2SO_4.

The In-Ga-Ge rich precipitate contained, in mg/g:

In - 3, Ga - 0.79, Ge - 0.37. In addition, the material was rich in Fe (161 mg/g), S (257 mg/g), Al (49.8 mg/g), As (46.8 mg/g), Zn (34.9 mg/g), Si (18.1 mg/g), Mg (13.2 mg/g) with other elements present such as Ca, Cd, Cr, Cu, Mn, Na, Sb and Sr in trace amounts. In the leaching experiments with that precipitate, the best In and Ga extraction were achieved with 150 g/L H_2SO_4 at 55 °C and O_2 purging. Then the pH of the solution was adjusted to 2.1 and 250 g/L of ascorbic acid powder was added. After the iron reduction step the

solution contained Ga - 44 mg/L, Ge - 18.2 mg/L and In - 190 mg/L. Further, solvent extraction was carried out (with 20 v-% D2EHPA diluted in Escaid 110, A/O=1:1, contact time 5 min, settling time 15 min, pH of 1.5), resulting in 93% In, 22% Ga, 67% Zn, 1.2% Al and 1.6% Ge extractions. Gallium and Ge are manly left in the aqueous phase from the solvent extraction. Zinc can be scrubbed (96% of the Zn) from the organic phase, then 66% of In was stripped (with 3 M HCl A/O=1:1, contact time 5 min, settling time 15 min). The aqueous phase from the stripping stage contains In (116 mg/L) at relatively high purity and can be subjected to In electrowinning.

5. Recent studies on gallium, germanium and indium recovery from wastewater

The major problem with the economic recovery of minor metals from the industrial wastewater is their low concentration (often less than 100 mg/L) in the wastewater along with larger concentration of other contaminants.

5.1. Gallium recovery

Ion exchangers (Zhao et al., 2012) and conventional solvent-extraction processes (Nusen et al., 2016) have been tested for the Ga recovery but were economically unfeasible. Sorption followed by desorption is a cost-effective technology for removal of contaminants from low concentrated metal wastewaters. An adsorbent has been prepared based on carbonized rice husk using epichlorohydrin as a cross-linker and diethanolamine as a modifier and containing trihydroxy as active sites for adsorption of gallium ions (DEA-EPI-RH) (Xiong et al., 2019). The maximum adsorption capacity achieved from wastewater was to 130.44 mg/g. The DEA-EPI-RH has good adsorption performance for Ga(III) in the binary systems of Ga(III)/Ge(IV) and Ga(III)/As(III).

Siderophores desferrioxamine B (DFOB) and desferrioxamine E (DFOE) in reversed-phase chromatography column have been successfully applied to recover of Ga^{3+} from wastewaters containing Ga in low concentrations and released by the wafer fabrication industry (Jain et al., 2019). DFOB and DFOE formed highly stable complexes with Ga^{3+} through hydroxamate group and were able to successfully complex 100% Ga in the two different process waters from wafer

fabrication industry. To recover the Ga, a high rate of decomplexation (>90%) was achieved by addition of 6 times excess of EDTA at pH of 3.5. More than 95% of Ga-DFOB and Ga-DFOE complex were recovered with purity (% of Ga moles in comparison to total moles of metals) of 69.8 and 92.9%, respectively by use of a C18 reversed-phase chromatography column.

Very recently, graphene oxide polyacrylic acid functionalized composites (PAA/GO) have been applied as adsorbent of Ga (20 mg/L) from acidic wastewater (pH 1-3) in the presence of 200 mg/L of each of Al and Zn (Zhang et al., 2019). The adsorption capacity for Ga achieved at 30 ºC for 24 h was 196.84 mg/g, much higher than that of other commercially available resins (CL-P204, P507), and at the same time the selectivity was relatively good, especially with respect to Zn.

5.2. Germanium recovery

Ion-exchange is a powerful tool for metal recovery. Germanium has been recovered from wastewater from solar panels displays production by using the commercially available N-methylglucamine resin (Takemura et al., 2013). To treat this type of wastewater a method to separate selectively Ge from silicate ion is required. To recover Ge, it is complexed with with catechol, 3-methylcatechol and 4-nitrocatechol in solution. Then the solution with complexes flowed through a membrane or packed-bed column. It has been found that catechol complexes exhibited a high adsorption performance in neutral pH. In a continuous system, the membrane achieved faster adsorption of the germanium complex than a packed-bed column. A Ge solution containing silicate ions was passed through the membrane system, resulting in highly selective recovery of Ge.

Ion exchange recovery of Ge from sulfate solutions was studied with equilibrium experiments and column experiments (Virolainen et al., 2013). It has been found that when the initial pH was 3.0, the N-methylglucamine functional resin (IRA-743) proved to be superior for Ge removal from sulfate solutions containing several base metals compared to other commercial resins containing functional groups with nitrogen donor atoms. However, at a low pH (<1) the aminomethylphosphonium resin (Lewatit TP-260) showed higher adsorption capacity. Based on screening of four commercial resins

by equilibrium experiments, a bifunctional N-methylglucamine resin was selected for dynamic adsorption studies and modeling. Authentic and simulated feed solutions were used to study the effect of competing metals. The feed solutions contained 63–490 mg/L Ge and metal sulfates so that ionic strengths were between 0.58 and 5.82 mol/L. The adsorption of Ge onto the resin depended strongly on pH. The first pKa value of germanic acid, $Ge(OH)_4$, is 9 and its anionic dissociation products (oxoanions) were adsorbed to the nitrogen containing groups by anion exchange mechanism. Since increasing pH does not increase the affinity for competing metals, the selectivity of N-methylglucamine for Ge improves with increasing pH. All germanium species were adsorbed to glucose sites. Other metal ions in the studied multimetal feeds decreased the Ge adsorption directly by competition, and indirectly by acting as buffers by forming hydroxide complexes and thus preventing pH increase to the range in which germanic acid dissociates. Iron was found to have a particularly detrimental effect on the adsorption.

Germanium extraction from waste aqueous effluents by catechol based resins has been studied (Cruz et al, 2018). Selective extraction and separation of Ge was demonstrated in the presence of elements such as Si, Zn and Cu which are likely to be competitive cations in solutions from urban mines or mine deposits.

5.3. Indium recovery

Indium recovery from aqueous solutions using commercially available iminodiacetate resin Lewatit1 TP207 (TP207) was investigated (Lee, et al., 2016). The polymer resin had In adsorption capacity of 55 mgIn/g TP207 at 25 ˚C and desorption efficiency of 99% in pH 0.8 acidic aqueous solution. The TP207 showed efficiency of 99% after four adsorption-desorption cycles. These results offer an effective recovery of In from industrial wastewater.

Alginate-sulfonate-silica (ASS) particles were prepared and studied as adsorbent for the recovery of In(III) from synthetic, dilute, aqueous solutions, both from single-element solutions and a multielement mixture (Roosen, 2017). The adsorption of In(III) by ASS particles was characterized by slow kinetics but a high adsorption capacity. The In(III) adsorption efficiency was about 85% after 4 consecutive adsorption-desorption cycles. In a binary Ga(III)/

In(III) solution and a multielement solution, the highest affinity was observed for In(III). The higher selectivity for In(III) was exploited by gravitational column chromatography to separate In(III) together with Ga(III) from the other elements that present in higher concentrations, in the simulated leachate of a zinc refinery residue.

Indium (III) extraction from HCl solutions (0.1- 6M HCl) by the use of ionic liquid ($A324H^+$)(Cl^-) has been proposed (Alguacil, 2019). The ionic liquid was obtained by a reaction of the tertiary amine Hostarex A324 (triisooctyl amine) dissolved in Solvesso 100 with 1M HCl solution. The results suggested that the In extraction is due to an anionic exchange reaction between the chloride ion of the ionic liquid and the $InCl_4^-$ of the aqueous solution. The system's performance was compared against the extraction of other metals in binary solution (In and accompanying metal). High separation factors were obtained from the binary systems under the following conditions: 6M HCl, In 0.1 - 0.5 g/L, concentration of each other metal 8.7×10^{-4} M, organic phase: 0.12M $A324H^+Cl^-$ in Solvesso 100, 20° C, 15 min, V_{org}/V_{aq} = 1. The separation factors obtained, at In metal extraction over 99 %, are: > 3000 (for In - Ni), 199 (for In - Co), 27 (for In - Cu), 50 (for In - Zn). For In - Sn(IV) separation 0.1M HCl gave better results (the other conditions remained unchanged) with the separation factor of 5. Indium(III) was stripped from metal-loaded organic solutions by the use of diluted HCl, and the precipitation of zero valent In is possible by further addition of sodium borohydride to the In-bearing strip solution.

5.4. Recovery of two or three of the minor metals

The retention of $In_2(SO_4)_3$ and GeO_2 with two different commercially available polymeric nanofiltration (NF) flat sheet membranes (NP010, NF99HF) was investigated between pH 2 and 12 with the main goal to investigate the selective separation of both In and Ge in aqueous sulfate solution (Werner et al, 2018). The experiments were focused on further future membrane application for winning In and Ge from bioleaching solutions. Depending on pH value, ions show different speciation which strongly influences membrane charge and separation performance. The results were ascribed to specific adsorption of In^{3+} on the membrane surface. The nanofiltration experiments revealed that In and Ge are separated successfully within distinct pH

values which is caused by electrostatic interaction of species like In^{3+} and $In(OH)_4^-$ and the charged membrane. The size exclusion plays a distinctive role in the separation of $In(OH)_3^o$ and $Ge(OH)_4^o$. The Ge can successfully be enriched in the permeate.

6. Conclusions

Gallium, germanium and indium recovery from technogenic waste (mining and metallurgy residues and industrial wastewater) can significantly contribute to ensuring the future supply of those minor metals needed for the sustainable development of the society. Some technical barriers are encountered, mainly related with the presence of other metals, such as iron and other basic metals in concentrations much higher than the desired minor metals. The efforts should be directed to the development of viable industrial technologies. Hydrometallurgy is more suitable, compared to pyrometallurgy, to extract the discussed high-tech metals from the above-mentioned secondary resources. After metals' leaching different technologies are applicable to separately recover the Ga, Ge and In from the PLS, such as precipitation, ion-exchange, and extraction. Usually one technology alone cannot solve all the problems because solid wastes are complicated systems. Hence, the optimum combination and integrated technologies should be applied. Additional research appears to be necessary to establish a highly efficient and environmentally friendly processes. Last but not the least, the economic barriers should be overcome, including with some incentives and other legislative measures.

References

1. 83 FR 23295, 2018, Final List of Critical Minerals 2018, the U.S. Department of the Interior, Federal Register 83 (97), 23295-23296.

2. Ad hoc Working Group on defining critical raw materials, 2014, Report on critical raw materials for the EU, Critical raw material profiles, DG Enterprise and Industry, EC.

3. **Alguacil F. J., Escudero E.** 2019, Solvent extraction of indium(III) from HCl solutions by the ionic liquid $(A324H^+)(Cl^-)$ dissolved in Solvesso 100, Hydrometallurgy, 189, 105104.

4. **Anderson C. S**. 2018, Indium.- In: Mineral Commodity Summaries 2018, USGS, 78-9.

5. **Anderson C. S**. 2019, Indium, Mineral Commodity Summaries 2019, USGS, 78–79.

6. **Brown T., Gunn G., Sievers H., Liedtke M., Huy D., Homberg D**. 2018, Challenges of locating, mining and extracting CRM resources, SCRREEN, BGS.

7. **Ceniceros-Gómez A.E., Macías-Macías K.Y., Cruz-Moreno J.E., Gutiérrez-Ruiz M.E.L., Martínez-Jardines G.**, 2018, Characterization of mining tailings in México for the possible recovery of strategic elements, Journal of South American Earth Sciences, 88, 72-9.

8. **Chen W. S., Chang B. C., Chen Y. J.** 2018, Using ion-exchange to recovery of germanium from waste optical fibers by adding citric acid, IOP Conf. Ser.: Earth Environ. Sci., 159 012008.

9. **Cruz C. A., Marie S., Arrachart G., Pellet-Rostaing S.** 2018, Selective extraction and separation of germanium by catechol based resins Separation and Purification Technology, 193, 214–219.

10. Deloitte Sustainability, British Geological Survey, Bureau de Recherches Géologiques et Minières, Netherlands Organization for Applied Scientific Research, 2017, Study on the review of the list of Critical Raw Materials, Critical Raw Materials Factsheets, Luxembourg: Publications Office of the European Union, 130-131.

11. **Drzazga M., Prajsnar R., Chmielarz A., Benke G., Leszczynska-Sejda K., Ciszewski M., Bilewska K., Krawiec G**. 2018, Germanium and indium recovery from zinc metallurgy by-products - dross leaching in sulphuric and oxalic acids, Metals, 8, 1041.

12. **Du G., Zhuang X., Querol X., Izquierdo M., Alastuey A., Moreno T., Font** O. 2009, Ge distribution in the Wulantuga high-germanium coal deposit in the Shengli coalfield, Inner Mongolia, northeastern China, International Journal of Coal Geology, 78(1), 16–26.

13. **Eheliyagoda D., Zeng X., Wang Z., Albalghiti E., Li J**. 2019, Forecasting the temporal stock generation and recycling potential of metals towards a sustainable future - The case of gallium in China, Science of the Total Environment, 689, 332–340.

14. EU, 2015, Report on critical raw materials for the EU critical raw materials profiles, Ref. Ares (2015) 1819595 - 29/04/2015 European Commission.

15. EU, 2017, Communication from the Commission to the European Parliament, the Council, the European Economic and Social Committee and the Committee of the Regions on the 2017 list of Critical Raw Materials for the EU, COM(2017) 490 final.

16. European Commission, 2017, Study on the review of the list of critical raw materials - Critical Raw Materials Factsheets, European Commission.

17. **Fayram T.S., Anderson C.G.** 2008, The development and implementation of industrial hydrometallurgical gallium and germanium recovery, The Journal of The Southern African Institute of Mining and Metallurgy, 108, 261-271.

18. **Foley N.K., Jaskula B.W., Kimball B.E., Schulte R.F**. 2017, Gallium, chap. H of Schulz

19. **K.J., De Young J.H., Seal R.R., Bradley D.C.,** eds., Critical mineral resources of the United States - Economic and environmental geology and prospects for future supply: USGS Professional Paper 1802, H1– H35.

20. **Frenzel M., Ketris M. P., Gutzmer J**. 2014, On the geological availability of germanium, Mineralium Deposita, 49(4), 471–486.

21. **Frenzel M., Ketris M.P., Seifert T., Gutzmer J.** 2016, On the current and future availability of gallium, Resources Policy, 4738–4750.

22. **Gladyshev S.V., Akcil A., Abdulvaliyev R.A., Tastanov E.A., Beisembekova K.O., Temirova S.S., Deveci H**. 2015, Recovery of vanadium and gallium from solid waste by-products of **Bayer process, Minerals Engineering, 74, 91–98.**

23. **Guberman D.E.** 2010, Germanium, Mineral Commodity Summaries 2010, USGS, 64-65.

24. **Guberman D.E.** 2011, Germanium, Mineral Commodity Summaries 2011, USGS, 64-65.

25. **Guberman D.E.** 2012, Germanium, Mineral Commodity Summaries 2012, USGS, 64-65.

26. **Guberman D.E.** 2013, Germanium,Mineral Commodity Summaries 2013, USGS, 64-5.

27. **Guberman D.E.** 2014, Germanium, Mineral Commodity Summaries 2014, USGS, 64-65.

28. **Guberman D.E**. 2015, Germanium, Mineral Commodity Summaries 2015, USGS, 64-65.

29. **Guberman D.E**. 2016, Germanium, Mineral Commodity Summaries 2016, USGS, 70-71.

30. **Guberman D.E.** 2017, Germanium, Mineral Commodity Summaries 2017, USGS, 70-1.

31. **Jain R., Fan S., Kaden P., Tsushima S., Foerstendorf H., Barthen R., Lehmann F., Pollmann K.** 2019, Recovery of gallium from wafer fabrication industry wastewaters by Desferrioxamine B and E using reversed-phase chromatography Approach, Water Research, 158, 203-212.

32. **Jaskula B.W.** 2010, Gallium, Mineral Commodity Summaries 2010, USGS, 58–59.

33. **Jaskula B.W.** 2011, Gallium, Mineral Commodity Summaries 2011, USGS, 58–59.

34. **Jaskula B.W**. 2012, Gallium, Mineral Commodity Summaries 2012, USGS, 58–59.

35. **Jaskula B.W**. 2013, Gallium, Mineral Commodity Summaries 2013, USGS, 58–59.

36. **Jaskula B.W.** 2014, Gallium, Mineral Commodity Summaries 2014, USGS, 58–59.

37. **Jaskula B.W.** 2015, Gallium, Mineral Commodity Summaries 2015, USGS, 58–59.

38. **Jaskula B.W**. 2016, Gallium, Mineral Commodity Summaries 2016, USGS, 64–65.

39. **Jaskula B.W**. 2017, Gallium, Mineral Commodity Summaries 2017, USGS, 64–65.

40. **Jaskula B.W**. 2018, Gallium, Mineral Commodity Summaries 2018, USGS, 62–63.

41. **Jaskula B.W.** 2019, Gallium, Mineral Commodity Summaries 2019, USGS, 62–63.

42. **Kangas P., Nyström M., Orko I., Koukkari P., Saikkonen P., Rastas J**. 2017, The Jarogain Process for Metals Recovery from Jarosite and Electric Arc Furnace Dust, Process Design and Economics, VTT Technical Research Centre of Finland Ltd, Finland.

43. **Karumb E. T.** 2016, The recovery of indium from mining wastes, A thesis submitted to the faculty and the Board of Trustees of the Colorado School of Mines in the partial fulfillment of the requirements for the degree of Master of Science (Metallurgical and Materials Engineering), 158 pp.

44. **Ketris M. P., Yudovich Y. E**. 2009, Estimations of Clarkes for carbonaceous biolithes: World averages for trace element contents in black shales and coals, International Journal of Coal Geology, 78(2), 135–148.

45. **Kul M., Topkaya Y**. 2008, Recovery of germanium and other valuable metals from zinc plant residues, Hydrometallurgy, 92, 87–94.

46. **Lee S. K., Lee U. H**. 2016, Adsorption and desorption property of iminodiacetate resin (Lewatit1 TP207) for indium recovery, Journal of Industrial and Engineering Chemistry 40, 23-25.

47. **Lei C., Chen T., Yan B., Xiao X.M.** 2015, Reaction characteristics and kinetics of gallium in chlorination roasting of copper tailings using calcium chloride, *Rare Metals*, 1-8.

48. **Liu F., Liu Z., Li Y., Wilson B. P., Lundström M.** 2017b, Recovery and separation of gallium(III) and germanium(IV) from zinc refinery residues: Part II: Solvent extraction, Hydrometallurgy, 171, 149–156.

49. **Liu F., Liu Z., Li Y., Wilson B. P., Lundström M**. 2017a, Recovery and separation of gallium(III) and germanium(IV) from zinc refinery residues: Part I: Leaching and iron(III) removal, *Hydrometallurgy*, 169, 564–570.

50. **Lu F., Xiao T., Lin J., Li A., Long Q., Huang F., Xiao L., Li X., Wang J., Xiaob Q., Chen H.** 2018, Recovery of gallium from Bayer red mud through acidic-leaching-ion exchange process under normal atmospheric pressure, *Hydrometallurgy*, 175, 124–132.

51. **Lu F., Xiao T., Lin J., Ning Z., Long Q., Xiao L., Huang F., Wang W., Xiao Q., Lan X., Chen H.** 2017, Resources and extraction of gallium: A review, *Hydrometallurgy*, 174, 105–115.

52. **Macías-Macías K.Y., Ceniceros-Gómez A.E., Gutiérrez-Ruiz M.E., González-Chávez J.L., Martínez-Jardines L.G.** 2019, Extraction and recovery of the strategic element gallium from an iron mine Tailing, Journal of Environmental Chemical Engineering, 7, 102964.

53. **Martin M., Janneck E., Kermer R., Patzi A., Reichel S.** 2015, Recovery of indium from sphalerite ore and flotation tailings by bioleaching and subsequent precipitation processes, Minerals Engineering, 75, 94–99.

54. **Mathieux F., Ardente F., Bobba S., Nuss P., Blengini G., Alves Dias P., Blagoeva D., Torres De Matos C., Wittmer D., Pavel C., Hamor T., Saveyn H., Gawlik B., Orveillon G., Huygens D., Garbarino E., Tzimas E., Bouraoui F., Solar S.** 2017, Critical Raw Materials and the Circular Economy – Background report. JRC Science-for-policy report, Publications Office of the European Union, Luxembourg.

55. **Mikolajczak C**. 2009, Availability of indium and gallium, Indium Corporation, https://www.gps-tec.eu/files/availability_of_indium_and_gallium_01.pdf.

56. **Moskalyk R. R**. 2004. Review of germanium processing worldwide, Minerals Engineering, 17, 393–402.

57. **Nusen S., Chairuangsri T., Zhu Z., Cheng C.Y**. 2016, Recovery of indium and gallium from synthetic leach solution of zinc refinery residues using synergistic solvent extraction with LIX 63 and Versatic 10 acid, Hydrometallurgy, 160, 137-146.

58. **Qin S., Sun Y., Li Y., Wang J., Zhao C., Gao K.** 2015, Coal deposits as promising alternative sources for gallium, Earth-Science Reviews, 150, 95–101.

59. **Rao S., Wang D., Liu Z., Zhang K., Cao H., Tao J**. 2019, Selective extraction of zinc, gallium, and germanium from zinc refinery residue using two stage acid and alkaline leaching, Hydrometallurgy, 183, 38-4.

60. **Redlinger M., Eggert R., Woodhouse M.** 2015, Evaluating the availability of gallium, indium, and tellurium from recycled photovoltaic modules, Solar Energy Materials & Solar Cells, 138, 58-1.

61. **Roosen J., Mullens S., Binnemans K.** 2017, Multifunctional Alginate-ulfonate-ilica Sphere-Shaped Adsorbent Particles for the Recovery of Indium(III) from Secondary

62. Resources, Industrial and Engineering Chemistry Research, 56, 8677-688.

63. **Roosendael S.V., Regadio M., Roosen J., Binnemans Koen**, Selective recovery of indium from iron-rich solutions using an Aliquat 336 iodide supported ionic liquid phase (SILP), Separation and Purification Technology, 212 (2019) 843-5.

64**. Sawai H., Rahman I. M. M., Tsukagoshi Y., Wakabayashi T., Maki T., Mizutani S., Hasegawa H.** 2015, Selective recovery of indium from lead-smelting dust, Chemical Engineering Journal, 277, 219-228.

65. **Takemura H., Morisada S., Ohto K., Kawakita H., Matsuo Y., Fukuda D.** 2013, Germanium recovery by catechol complexation and subsequent flow through membrane and bead‐packed bed column, Journal of chemical technology and Biotechnology, 88 (8), 1468-1472.

66. **Thomas C. L**. 2018, Germanium, Mineral Commodity Summaries 2018, USGS, 68–69.

67. **Thomas C. L.** 2019, Germanium, Mineral Commodity Summaries 2019, USGS, 68–69.

68. **Tolcin A. C.** 2010, Indium, Mineral Commodity Summaries 2010, USGS, 74–75

69. **Tolcin A. C.** 2011, Indium, Mineral Commodity Summaries 2011, USGS, 74–75

70. **Tolcin A. C.** 2013, Indium, Mineral Commodity Summaries 2013, USGS, 74–75,

71. **Tolcin A. C.** 2015, Indium, Mineral Commodity Summaries 2015, USGS, 74–75

72. **Tolcin A. C.** 2016, Indium, Mineral Commodity Summaries 2016, USGS, 80–81

73. **Tolcin A. C.** 2017, Indium, Mineral Commodity Summaries 2017, USGS, 80–81

74. **Tolcin A. C**. 2012, Indium, Mineral Commodity Summaries 2012, USGS, 74–75

75. **Tolcin A. C.** 2014, Indium, Mineral Commodity Summaries 2014, USGS, 74–75

76. **Ueberschaar M., Otto S.J., Rotter V.S.** 2017, Challenges for critical raw material recovery from WEEE – The case study of gallium, Waste Management, 60, 534–545.

77. **Ujaczki É., Cusack P., Clifford S., Curtin T., Courtney R., O'Donoghue L.** 2017, Bauxite residues a source of gallium – an extraction study, Travaux 46, Proceedings of 35th International ICSOBA Conference, Hamburg, 485-490.

78. **Virolainen S.**, 2013, Hydrometallurgical recovery of valuable metals from secondary raw materials, Acta Universitatis Lappeenrantaensis, 554.

79**. Virolainen S., Heinonen J., Paatero E.** 2013. Selective recovery of germanium with N-methylglucamine functional resin from sulfate solutions, Separation and Purification Technology, 104, 193–199.

80. **Wang J., Bao Y., Ma R., Li Y., Gong L., Zhang Y., Niu Z., Xin B**. 2018, Gallium recovery from aluminum smelting slag via a novel combined process of bioleaching and chemical methods, Hydrometallurgy, 177, 140–145.

81. **Werner A., Rieger A., Mosch M., Haseneder R., Repke J. U.** 2018, Nanofiltration of indium and germanium ions in aqueous solutions: Influence of pH and charge on retention and membrane flux, Separation and Purification Technology, 194, 319–328.

82. **Winberg I.** 2018, Techno-economic assessment of the process for recovery of indium, germanium and tin from alloys obtained as byproducts of zinc production, Åbo Akademi University.

83. **Xiong Y., Cui X., Wang D., Wang Y., Lou Z., Shan W., Fan Y.** 2019, Diethanolamine functionalized rice husk for highly efficient recovery of gallium(III) from solution and a mechanism study, Materials Science & Engineering C, 99, 1115–1122.

84. **Xue B., Wei B., Ruan L., Li F., Jiang Y., Tian W., Su B., Zhou L**. 2019, The influencing factor study on the extraction of gallium from red mud, Hydrometallurgy, 186, 91–97.

85. **Yoshito K., Maruyama Y.** 2000, Separation and Concentration Method for Recovering Gallium and Indium from Solutions by Jarosite Precipitation, EP 1 020 537 A1, European Patent Office.

86. **Zhang Y., Jin B., Ma B., Feng X.** 2017, Separation of indium from lead smelting hazardous dust via leaching and solvent extraction, Journal of Environmental Chemical Engineering, 5 (3), 2182-2188.

87. **Zhang Y., Liu X., Wang Y., Lou Z., Shan W., Xiong Y.** 2019, Polyacrylic acid-functionalized graphene oxide for high-performance adsorption of gallium from aqueous solution, Journal of Colloid and Interface Science, 556, 102–110.

88. **Zhao Z., Yang Y., Xiao Y., Fan Y**. 2012, Recovery of gallium from Bayer liquor: A review, Hydrometallurgy, 125-126, 115-124.

INNOVATIVE TECHNOLOGY FOR THE PRODUCTION OF CEEOLITE-SMECTITE TUFFS

Malanchuk Z.R.
National University of Water and Environmental Engineering (NUWEE), Professor, Doctor of Technical Sciences, Professor, Department of Development of Deposits and Mining, Ukraine

Malanchuk E.Z.
National University of Water and Environmental Engineering (NUWEE), Professor, Doctor of Technical Sciences, Professor, Department of Automation and Computer Integrated Systems, Ukraine

Stets S.Ye.
National University of Water and Environmental Engineering (NUWEE), Associate Professor, Ph.D., Associate Professor, Department of Automation and Computer Integrated Systems, Ukraine

Korniyenko V.Ya.
National University of Water and Environmental Engineering (NUWEE), Professor, Doctor of Technical Sciences, Professor, Department of Development of Deposits and Mining, Ukraine

Summary

The essence of the work is to improve the technology of underground mining of zeolite-smectite tuffs by hydro-well method, taking into account all the dominant factors in the process of hydraulic production. The proposed calculation method for self-propelled hydraulic transport is significantly different from the methods proposed earlier. Developed recommendations for the use of well hydrotechnology, depending on the mineral composition of the rock, and the method of selecting equipment parameters for the extraction of zeolite-smectite tuffs on the daily surface make it possible in the process of mining operations to determine the rational limits of application of the method of development in the varieties of tuff production, formation of general principles of complex processing.

Proposals for the design of a site of pre-industrial preparation at the Rafalovka deposit of zeolite-smectite tuffs have been submitted, which take into account the needs of the rational use of mineral resources, nature protection and the environment.

Introduction

Intensive development of mining requires improvement of methods and schemes of working out, technology of processes of extraction, enrichment and processing of tuff raw materials in the direction of increasing the degree of extraction of minerals from the bowels with

minimal energy costs for the process itself. These principles correspond to the development of zeolite-smectite tuff deposits in the Rivne-Volyn region by the method of well hydrotechnology.

To create and use efficient well systems, it is important to identify specific technical solutions that will reduce the cost of development of the field due to the favorable geological conditions of the mountain environment, the improvement of technological methods and technical solutions, optimization of the processes and parameters of the system, high quality, simplicity and interoperability nodes and structural elements of extractive equipment and the ability of zeolite-smectite tuff to absorb water.

A wide range of researchers have been engaged in the issues of development of hydropower technologies, but the difference in the conditions of occurrence and the composition of the minerals did not allow to make universal quantitative conclusions in the research [1-3].

The physical assumptions underlying the analysis must, in order of magnitude, be consistent with natural conditions to give practical meaning to quantitative decisions. Hence the lack, to the extent necessary, of comprehensive research into the selection and comparative evaluation of test and development systems based on scientific methods. In addition, the diversity of mineral deposits, the stages of their industrial development and operating conditions determine the need not only scientific justification for the use of systems, but also the definition of their technical and economic indicators, on the basis of which the choice and comparative assessment [4-7].

Investigation of technological processes of down hole hydraulic production

After establishing the possibility of phase transformation of minerals, it is necessary to solve a complex of scientific, technical and economic problems [8, 9]. The first is the problem of delivery of working agents to the ore body of the deposit, the choice of type of working agents, the method and parameters of their transportation. Second, it is the problem of managing the production process, which involves the spread of working agents in the array. Thirdly, it is a problem of transportation of minerals from the place of occurrence to the surface and its further processing. Fourth, it is a

choice of such systems of development, which would be characterized by high technological efficiency and economic profitability. The main elements in the geotechnological system are wells drilled to the place of occurrence, which open access of the working agents to the deposit, and the minerals to the surface, and the part of the deposit covered by the influence of the working agents.

The basic equipment required for the geotechnological method of extraction can be divided by purpose and placement in the technological scheme into three groups [10]:

1. Equipment for the construction of wells, including drilling rigs, cementing units, equipment for the preparation of wells, tools for the study of minerals and rocks. The type of rig is selected depending on the depth and diameter of the well and the strength of the rocks. Rotary drilling rigs are used for drilling shallow wells in soft and medium strength drills. The diameter of the well determines the type of special mining equipment.

2. The equipment of the working agents, represented by various pumping units for the production of high-pressure water, heating units for the production of hot water and steam, compressor units for the production of compressed air, mixers for the production of solutions of alkali and acids of the required concentration, generator sets for creating alternating electromagnetic fields.

3. Mining equipment includes the following two types of equipment: for separation from the massif and delivery of minerals to the bottom of the well, and for lifting of minerals to the surface. The first type includes columns of perforated pipes, down hole hydromonitors, down hole heaters, vibrators. The second type is equipment include ejectors (airlifts, hydraulic elevators), columns of service pipes and submersible pumps.

To create effective test and development systems, it is important to identify specific technical solutions that reduce the specific costs of facility testing, trial operation, and mining through growth:

- degree of favorable mountain-geological conditions;
- utilization ratio of production reserves;
- the degree of perfection of technological methods and technical means;
- reliability coefficient of equipment, wells and workings that provide the process;

- coefficient of optimality of elements and parameters of systems;
- degree of automation of systems;
- ensuring the high quality and simplicity of the units of the equipment and the variety of interchangeable elements of the design of the working bodies.

The basis for the choice of rational technology of extraction of tuff raw materials is the results of the study of the influence of physical and geological state on the technology and parameters of destruction of tuffs, taking into account their ability to increase in volume when interacting with water up to 60%, as well as the influence of hydraulic and structural parameters of extractive equipment on delivery hydraulic mix and its lifting.

An alternative to the traditional methods of developing a zeolite-smectite tuff deposit is geotechnological methods, among which one of the main and most promising is the well production method.

The development of tuff deposit by the method of well hydrotechnology will allow to simultaneously evaluate the reserves of zeolite-smectite raw materials by improving the geological study of the deposit and to carry out additional studies of their composition and properties.

For the general technical and economic evaluation of the estimated variant of down hole hydraulic production, a general scheme of field drilling is drawn up, maps of drilling and construction of pipelines, placement of pumping and compressor stations, transmission lines and roads, auxiliary structures, staffing are developed. The calculation of the main technical and economic indicators ends the consideration of the basic option.

The following are considered other options for development taking into account the technological and technical capabilities of the extraction equipment, and their calculation is carried out according to the scheme. Comparison of indicators by economic effect or other factors makes the choice of the development system and its parameters. Adjustment of the basic variant of the technology of well production is possible also on separate elements (for example, type of drilling equipment, type of transport on a surface, etc.), thus influence of these factors on the resultant indicators is estimated [11-15].

Technical proposals for creating a technical assignment when designing a section for the industrial development of a zeolite-smectite tuff deposit

Designing a mining enterprise is a system of calculation methods and specific recommendations.

The main task of designing the development of tuff deposits is the choice of a rational development system, in which the reserves will be removed with the least losses and costs. This should take into account the rational use of mineral resources, measures for the protection of nature and the environment.

Designing a well site for the production of zeolite-smectite tuffs is a complex task in which the ore reservoir, mining chamber, well and ground equipment are considered as one.

When designing a well site, an important point is to take into account mining, geological and technological factors, with a specific feature being the ability to adjust the technology parameters during the operation of the field without changing the basic decisions.

The choice of the method of control of mountain pressure during design is allocated to a separate task, the solution of which determines the parameters of the development system and its indicators.

The formation of underground chambers in wells is one of the central processes of technology and completely determines the level of technological losses of minerals. This development project addresses the management and control of the shape and size of cameras.

Designing itself is a closely intertwined multifactorial connection of all sections: geological, technological, mountain, economic.

For the design of water supply systems, hydrogeological characterization of the deposit is required, with the selection and indication of parameters of aquifers, filtration properties of water-saturated rocks. These are groundwater quality, direction of their movement, chemical composition and physical properties. More baseline information is needed on the distribution and characteristics of water resistors in the context of rocks of the roof and sole. These data are presented in the form of capacity maps of aquifers, strato-gypsum roofs, water conductivity of minerals and aquifers.

The physical and mechanical properties of the rocks of the deposit affect the main processes (hydro fracture, stability of the pillars) of production technology. An important indicator is the content of clay minerals in the deposit and in the resulting product.

In order to calculate the fracture performance, research results and practical data on the relationship of the hydro monitor jet to the rock are required, as well as the radius of erosion and resizing over time, the nature of the fracture.

The process of moving the rock in the underground chamber is determined depending on the extraction scheme, the slope of the formation, the size of the chamber, the properties of the destroyed rock. For the design, the results of the study of schemes of transportation of hydraulic mixture in the underground chamber are required.

Initial data include a general flow chart of production, the component processes of technology, ancillary services. The working technological parameters and the permissible range of oscillations for each process are given, recommendations on the procedure of starting production, normal and emergency shutdown.

The mathematical description of processes and equipment is given in a form suitable for practical calculations. It is based on experimental data. Recommendations are also needed on the selection of optimal equipment models [11-13].

Recommendations for the use of down hole hydrotechnology depending on the mineral composition of tuffs

Suitable for physical and mechanical properties for well production are zeolite-smectite tuffs with a content of smectite minerals of more than 50%, which have a swollen crystalline lattice and in most cases high surface energy, which causes the active interaction of minerals with water or water. Minerals thus increase or decrease in volume and become plastic when wet. The recommended smectite for hydraulic production is montmorillonite, which is able to increase 20 times in volume due to the absorption (adsorption) of water. During dehydration, the mineral volume decreases dramatically.

With respect to zeolite tuffs, they are solid inorganic compounds of frame structure that are highly cemented, are not hydro-erodible and are not subject to hydraulic production.

Given the significant dependence of the chemical composition of tuffs on the field and its significant difference within one field, and the lack of detailed studies in this direction, it can be predicted that in the process of mining operations will determine the rational limits of application of the method of development for varieties of tuff raw materials improved methods of its extraction and formulated general principles of integrated processing.

Calculation of parameters of the process of erosion of tuff

In the conditions of well hydrotechnology the effect of known laws of mechanics is expressed, which are expressed in the implementation of the law of balance of work of mountain pressure, the consequences of which are directly proportional to the loss of minerals in the bowels. On this basis, the main task of managing rock pressure is to maximize the proportion of work that goes to secure deformation of the array outside the extraction chambers and minimize it to deformation of the roof and pillars. Specificity of testing and development of deposits by the considered methods is to arrange the production chambers without mounting. Continuous recess from the cameras is rational. In the process of excavation, a unloading zone is created in the roof of the chambers, which perceives only the mass of the direct roof, the pressure of which is mainly transmitted to adjacent arrays and the inundated rocks of the produced space. Using this solution, it is possible to reduce the roof pressure by 2 to 5% and up to 10%.

In the exploration and development of semi-rock deposits, such as zeolite-smectite tuffs, the marginal spans of roofs of mining chambers, installed on the factor of mountain pressure, significantly exceed their linear dimensions due to the processes of erosion and self-flowing hydraulic transport at the bottom.

Because the pressure control factor for such fields is the main one, for systems with different shapes of the extraction chambers, a marginal erosion radius R is set as a function of the marginal roof span. The most rational parameters $R=f(L_{pr})$ are systems with round cameras in which $R<L_{pr}$ is equal to

$$R = \frac{L_{pr}}{2} \tag{1}$$

An increase in $R \rangle L_{pr}$ (diamond-shaped camera systems) leads to a significant increase in losses.

For deposits of zeolite-smectite tuffs, the radius of erosion of the mineral is set taking into account the pressure of the pump minus the loss of pressure in the pipeline

$$R(d_0, H_0) = 0{,}9e^{0{,}064 d_0} + 2{,}5 \cdot H_0 - 2{,}5\ , \qquad (2)$$

where R is the radius of erosion of the mineral; d_0 is the diameter of the nozzle; H_0 - pressure of the working agent in the nozzle.

The following is the axial dynamic pressure of the jet at the distance of the washout radius

$$P_m = H_0 \left(\frac{l_n}{R} \right)^t , \qquad (3)$$

where l_n is the length of the initial section of the jet; t is an indicator that for distances of 5-7 m it is recommended to take 0.25 m.

The erosion performance of zeolite-smectite tuff is by the formula

$$\Pi_p(d_0, H_0) = 0{,}07 H_0 \cdot e^{148 d_0} + 3{,}3 \cdot H_0 - 2{,}8 , \qquad (4)$$

Specific consumption of the working agent and energy intensity in the erosion of the mineral

$$E_и, g = -a d_0^{\,2} + b d_0 - c , \qquad (5)$$

where a, b, c are constant approximations, the values of which are given in Table 1.

Tab. 1

The value of constant approximations

Specific cost	Energy consumption
$E_и = -a d_0^{\,2} + b d_0 - c$	$q = -a d_0^{\,2} + b d_0 - c$
$\begin{cases} a = 3174 \cdot H_0^{\,2} - 11158 \cdot H_0 + 12755 \\ b = 134{,}8 \cdot H_0^{\,2} - 448{,}1 \cdot H_0 + 546{,}1 \\ c = 1{,}09 \cdot H_0^{\,2} - 3{,}465 \cdot H_0 + 3{,}26 \end{cases}$	$\begin{cases} a = -1983 \cdot H_0^{\,2} + 4203 \cdot H_0 + 9209 \\ b = -174{,}2 \cdot H_0^{\,2} + 525{,}3 \cdot H_0 + 192{,}3 \\ c = -2{,}71 \cdot H_0^{\,2} + 10{,}5 \cdot H_0 - 8{,}3 \end{cases}$

The mining time of the mining chamber is set as part of the division of the volume of the mining chamber by the productivity of the erosion of the mineral defined by formula (4).

The mining chamber's working time is compared to that of the roof. If the working time of the camera exceeds the time of collapse, then a correction of the span toward the decrease is made with the

provision of measures to strengthen the pillars at depths of less than 50 m, or the separation of the reservoir power into layers with the subsequent bookmark of the clearing space.

The technique is universal in the range of use, both in terms of mining and geological conditions of objects and fields, and to determine the structural, qualitative and quantitative parameters of systems in which the main element is erosion (for example, in the exploration and development of fields in which the factor of stability plays minor role).

Water supply

One of the advantages of down hole hydroelectric production of zeolite-smectite tuffs is recycled water supply. The extracted rock is deposited on the map of the levee, and after settling; the water flows into the receiving pool and again pumps to the mining units. According to another scheme, when the rock is conveyed by hydrotransport to a processing plant or to another consumer, the water is separated from the ore at the end of the main hydrotransport and returned to the pumps. At the same time, together with the return water, it is possible to supply mortgage material to the waste chambers and to organize underground disposal of the waste of the processing plant.

The total hourly demand for water is determined by the imposition of a predetermined hourly production on the specific consumption of water plus the loss of water for evaporation and filtration. Usually the total water loss is 15-20% of the estimated flow rate. At the same time, when working out the flooded tuff deposits, some of the water along with the ore is fed to the surface and is involved in water supply.

During the development of a specific deposit, the required pressure of the jet from the nozzle for the destruction of the ore is determined on the basis of the exploratory works. They determine the required pump parameters.

The total value of the required pressure will be equal to the sum of the hydraulic losses in the pipeline, the hydraulic monitor and the required water pressure on the nozzle. Local pressure losses (in turns, joints, latches, etc.) take equal to 10% of the total losses along the entire length of the water main.

When designing water supply for a well site, the greatest attention should be paid to the protection of water resources. But because of the return water supply, the drain is practically absent and the possibility of contamination is minimal. Taking additional measures to prevent surface and underground (filtration) losses of water will eliminate any harmful effects on the environment.

Checking the parameters of hydraulic fracturing of a hydraulic monitor installation

By the performance of hydraulic fracturing we mean the volume of rock per unit time of net production, as opposed to the performance of the hydraulic installation, which, in addition to the actual process of destruction, as is known, carry out the operations on the formation, flushing and various technological downtime associated with rewiring moving the tubes of the hydraulic monitor, airlift, etc.

In this case, the destruction performance of P is defined as the ratio of energy consumed by the jet of water E per unit time to the specific energy intensity of the destruction process of zeolite-smectite tuff, *t*/hour

$$P = \frac{E}{e}, \tag{6}$$

where e is the specific energy intensity of the process of destruction of rocks.

Currently, there are no established dependencies of the specific energy intensity of the destruction of rocks on their strength characteristics. Therefore, for specific breeds, the dependence of fracture productivity on pressure and water flow is obtained in a field experiment.

There have been many attempts in recent years to incorporate natural and technological factors into these empirical dependencies. For example, Donugi offers a formula of average performance depending on the angle of incidence, formation capacity, nature of the face, etc.

Specific energy consumption is defined as the ratio of jet power to productivity

$$e = \frac{N}{P}. \tag{7}$$

Specific flow of pressure water

$$q = \frac{Q}{P} = \frac{1{,}22 \cdot 10^4 d_н^2 \sqrt{H_0}}{P}. \quad (8)$$

A more complete idea of the specific flow of water for the destruction of q gives its dependence on the specific dynamic pressure of the jet at the contact with the hole p_v, obtained in practice

$$q = \frac{M'}{p_v^n}, \quad (9)$$

where M 'is the experimental coefficient depending on the conditions of application of hydraulic fracturing in the bottom; n - experimental indicator of the effectiveness of hydraulic fracturing.

Calculation of mining profile

It must be done taking into account the change in the depth of flow and, as a consequence, the cost and speed of the length of transportation. Design features of the development system include the extraction of minerals from the camera to perform a hydromonitor with a specified angle of rotation (and the flow of the agent through the nozzle).

Properly designed profile of the bottom of the extraction chamber is characterized by certain ratios between the slopes of the bottom and the cost of the entire length of transportation. Moreover, changing the design parameters of the systems will change the nature of the profile of the bottom of the camera.

The erosion of minerals by sectors at the mandatory constant flow of time and a single flow that varies in length leads to the need to constantly change the length of the conveying slope, ie to create a profile of the bottom of the camera with such a variable slope, which in combination with the flow of work the specified transport speed.

On this basis, it is proposed to vary the following quantitative parameters in the calculation of self-propelled hydraulic transport: the amount of working agent required for erosion; the amount of minerals transported; sieve analysis of the useful component; roughness factor; sector erosion radius; the angle of the erosion sector.

Depending on the particle size distribution of the minerals and the parameters of the erosion process is determined by the slope of the bottom of the extraction chamber, which provides reliable transportation:

$$i_H = \frac{Q_T - 2{,}2}{0{,}65 \cdot Q} \quad (10)$$

where Q_T is the productivity of the erosion of the minerals or underlying rocks; $Q=P_n\, q_n$; or $Q=R_{pp}\, q_{pp}$ - the flow of water for erosion of minerals and underlying rocks, respectively.

Speed of reliable transportation

$$u_н = c \cdot \sqrt{R_т \cdot i_н} \quad (11)$$

where c is the coefficient of Shazi.

Checking the calculation of the profiled bottom under conditions of transportation of high-density minerals at zero losses

When the size of the minerals +3 mm is a comparison of the specific consumption of the working agent and the slope of the bottom. If the slope of the bottom with the condition of minimum losses exceeds the slope in the speed of reliable transportation, the construction of the profile and working out of the camera is carried out to its maximum value.

The proposed calculation method for self-propelled hydraulic transportation is significantly different from the methods proposed earlier. The amount of working agent going to the hydrotransport, in the proposed method is determined based on the condition of ensuring efficient water erosion. Therefore, the calculation of hydrotransport on the bottom of the camera is conducted not on condition of finding the transport capacity of the flow, as was done by most researchers, but on the basis of a given number of working agent and basic qualitative and quantitative parameters of the systems, according to the criterion - the balance of the working agent for erosion and self-flowing hydrotransport.

Practical recommendations for the design of well equipment

Optimal dynamic characteristics of the jet and its best compactness can be ensured: by providing a smoother contour channel and installing in the nozzle of the hydrometer to quench the almost inevitable turbulence, in particular, for short hydromonitors it is advisable to use the needle in the form of a needle-shaped plant. The best hydrodynamic properties of the jet are ensured by the formation of a stream of water in the barrel of the monitor, equipped with a cell type

caliper with an even number of square cells, provided that the size of the side of the square of each cell is 0.25 diameter of the channel of the barrel.

The ratio of the dimensions of the barrel and the mouthpiece should be within the following limits: the length of the longitudinal plates of the mouthpiece is 2.5-3 diameters of the barrel; the section of the flow channel of the barrel of the monitor between the settler and the nozzle is equal to 3-4 the diameter of the channel of the barrel; the section of the flow channel of the barrel from the swivel hinge to the damper is equal to two diameters of the barrel channel. Then the total length of the trunk of the monitor will be equal to 7.5-9.0 diameters of the trunk channel.

Choosing the type of nozzle hydromonitor should be made in accordance with the following established provisions: nozzles with a rounded inlet have less resistance, that is, a higher coefficient of flow than nozzles with sharp inlet edges; the cone nozzle has a higher flow rate and a smaller jet compression ratio than the cone nozzles. For nozzles of hydraulic monitors of the mine type with a diameter of 20-30 mm for a pressure of 2-10 MPa, the length of the cylindrical section of the nozzle is recommended to be equal to $4d_0$.

Industrial production

For the industrial production of zeolite-smectite tuffs of the Rafaliv deposit, a technological scheme is presented, which is presented in Fig. 1.

It is advisable to open the reservoir with a single-well production pattern with a counter-hole. The deposit is divided into blocks with backfill. In the spent block, dismantling works and work out repayments are carried out, in the work block - extraction of tuffs, and in the preparatory block - drilling and equipment of production wells and laying of block pipelines.

It is advisable to design the site with single cameras with the left interspace. For the conditions of this section, the distance between the wells is taken to be 30-5 m. Water is supplied according to the reverse scheme.

The drained water enters the sump and then pumps 8MS-7X4 and 8MS-7X6 (with a capacity of 280-290 m^3 / h at a pressure of 2.9-3.9 MPa) is fed to the nozzles of hydraulic monitors.

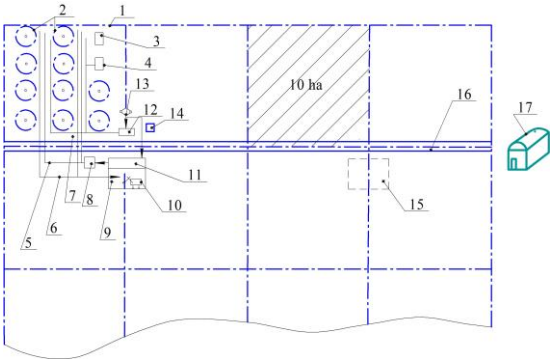

Fig. 1. Flow diagram of wells production of tuffs: *1* - working unit; *2* - production wells; *3* - drilling rig; 4 - mining unit; *5* - water main; *6* - slurry pipeline; *7* - a pneumatic pipeline; *8* - pumping station; *9* - composition of the extracted ore; *10* - bucket excavator; *11* - water intake; *12* - compressor station; *13* - water wells; *14* - power substation; *15* - location of the map of the embankment; *16* - access roads; *17* is a factory

Water losses are replenished from two artesian wells equipped with deep pumps ECV-8-40-65 with a capacity of 40 m^3/h. The hydraulic mix is fed to the map by the 8PS-10 earthquake with a capacity of 342 m^3/h, and then the extracted rock is transported to the receiving hopper of the factory.

Conclusions

1. For down hole hydraulic production, suitable for physical and mechanical properties are zeolite-smectite tuffs containing smectite minerals of more than 50%, which have a swollen crystalline lattice and in most cases high surface energy, which causes active interaction of minerals with water or mineral water. interstitial intervals. The recommended smectite for hydraulic production is montmorillonite, which is able to increase 20 times in volume due to the absorption (adsorption) of water.

2. The total value of the required pressure at which the pumping unit is selected, when the water supply of the production well is equal to the sum of hydraulic losses in the pipeline, the monitor and the required water pressure on the nozzle. Local pressure losses (in

turns, joints, latches, etc.) take equal to 10% of the total losses along the entire length of the water main.

3. Recommendations for calculating the parameters of the processes of rock erosion, displacement and lifting of the hydraulic mixture using well-mining of zeolite-smectite tuffs, the method of determination of indicators of completeness and quality of mineral extraction for systems with round chambers are developed.

4. Proposals for designing a site of pre-industrial preparation at the field of zeolite-smectite tuffs have been developed, taking into account the needs of rational use of mineral resources, nature protection and the environment.

References

1. **Malanchuk Z.R. Malanchuk E.Z. Kornienko V.** Special technologies of mining. Tutorial - Exactly: NSULP, 2017, p. 290.

2. **Malanchuk E.Z.** Efficiency of using magnetic separation for the processing of metal-containing basalt raw materials. Topical issues of resource-saving technologies in mineral mining and processing. Multi-authored monograph. – Petroșani, Romania: UNIVERSITAS Publishing, 2018. – 270 p., 65-89 pp.

3. **Stets S.** Improvement of technological parameter of the technology of production of zeolite-smectite tuffs. Sustainable development of resource-saving technologies in mineral mining and processing. Multi-authored monograph. – Petroșani, Romania: UNIVERSITAS Publishing, 2019. - 400 pp., 244-265 pp.

4**. Naduty V.** Research results proving the dependence of the copper concentrate amount recovered from basalt raw material on the electric separator field intensity.Eastern – European Journal of Enterprise Technologies. Volume 5/5(83),– 2016, p 19-24. ISSN 1729-3774, UDC 622.277 DOI: 10.15587/1729-4061.2016.79524

5. **Malanchuk E.Z.** The analysis of the state of the question on the content of nonferrous metals in basalt raw materials Volyn region of Ukraine. Canadian Journal of Science, Education and Culture. № 2(6), July-December, 2014 «Toronto Press». – P. 361-365

6. **Rokochinskiy A., Gromachenko S.** Engineering Land Reclamation Measures to Minimize Long-term Impacts of Waste on the Environment. Canadian

Journal of Science, Education and Culture. № 2(6), July-December, 2014 «Toronto Press». – P. 366-371

7. **Zagorovsky V.** Experience in the use of products processing of basalt raw material in Ukraine. American Journal of Scientific and Educational Research № 2(5), July-December, 2014. «Columbia Press», New York. 2014. – P. 642-648

8. **Malanchuk Z.** Examining features of the process of heavy metals distribution in technogenic placers at hydraulic mining Восточно-Европейский журнал передовых технологий. - 2017. - № 1(10). - P. 45-51. http://nbuv.gov.ua/UJRN/Vejpte_2017_1(10)__7

9. **Hristuk A., Zagorovsky V.** Simulation of the comminution process to complex processing of metal-bearing basalt raw material. Cambridge Journal of Education and Science. No.2. (14), July-December, 2015. VOLUME VI "Cambridge University Press". – P. 542-549

10. **Malanchuk Z., Stets S., Malanchuk E., Zhomyruk R**., and others. Technology and management of mineral production. NSWGP, 2009. - 480 p.

11. **Korniyenko V.** Modeling of vibro screening at fine classification of metallic basalt [Text] / Theoretical and Practical Solutions of Mineral Resources Mining, 2015. – P. 441–443. doi: 10.1201/b19901-77

12. **Soroka V.** Modeling the formation of high metal concentration zones in man-made deposits. Mining of Mineral Deposits, 12(2), 2018, p.76-84. https://doi.org/10.15407/mining12.02.076

13. **Khrystiuk A.** Mathematical Modeling Of Hydraulic Mining From Placer Deposits Of Minerals. Mining Of Mineral Deposits. V. 10 (2). 2016. Pp.: 18-24. DOI: 10.15407/mining10.02.013

14. **Gromachenko S.** The Results Of Magnetic Separation Use In Ore Processing Of Metalliferous Raw Basalt Of Volyn Region. Mining Of Mineral Deposits. V. 10(3). 2016. Pp. 77-83. DOI: 10.15407/mining10.03.077

15. **Malanchuk Z.R.,** The results of studies of the distribution of native copper in rock mass Volhynia (Ukraine). The 1st International Academic Congress «Fundamental and Applied Studies in the Pacific and Atlantic Oceans Countries». Japan, Tokyo, 25 October 2014. «Tokyo University Press» - P. 322-325

CARBON ACID CORROSION MECHANISMS OF CONSTRUCTION PIPE STEELS FOR OIL AND GAS APPLICATION

Makarenko V.D.
Poltava National Technical Yuri Kondratyuk University
DCs (Engineering), Professor, professor of the Department of Oil and Gas Engineering and Technology, Ukraine

Manhura A.M.
Poltava National Technical Yuri Kondratyuk University
Senior Lecturer, head of the Department of Oil and Gas Engineering and Technology, Ukraine

Syzonenko A.V.
Poltava National Technical Yuri Kondratyuk University
Senior Lecturer, head of the Department of Oil and Gas Engineering and Technology, Ukraine

Lytviak O.L.
Poltava National Technical Yuri Kondratyuk University
Student of the Department of Oil and Gas Engineering and Technology, Ukraine

Absract. Many authors believe that for carbon and low alloy steels from which the oilfield equipment is made, uniform corrosion is the most typical. However, in the last few decades, there have been regular occurrences of pipelines damages caused by localized corrosion. Moreover, localized corrosion starts from the inside and extends, in most cases, to horizontal sections of the pipelines on the outer generating lines of the pipe, mostly in the area of the welded joint. It is established that over the last 30 years, about 50% of all corrosion losses of the pipelines operated at oil and gas fields are because of carbon dioxide corrosion, and therefore it is urgent to study more closely the mechanisms of this corrosion. The state and key directions of carbon dioxide corrosion mechanisms development of oil and gas pipelines exploited in chemical-aggressive media in the fields are considered. The most realistic schemes according to which corrosion damages of pipe walls occur are presented in the article. The most promising corrosion mechanisms that adequately reflect the processes of damage and destruction of long-term operated structures are formulated and substantiated. The rationale for the mechanisms of localized corrosion, which most often causes local (pitting and grooves) corrosion and which is not easy to identify at the beginning of nucleation and growth, is given.

The possibility of increasing the stability of metal structures by reducing the degree of technological media corrosion, which is directly related to the formation water pumped together with oil, is substinated in the article.

Keywords: corrosion, hydrogen, sulfur, corrosion mechanisms, sediments, deposits, chlorides

Problem formulation and task formation. Schematically, the mechanism of localized corrosion damage (ulceration), as well as the processes of sulfur-hydrogen-containing medium formation, in the destruction of pipelines are now sufficiently disclosed, although some of the physicochemical processes of localized corrosion are not fully explained. At the same time, local (pitting and groove) corrosion represent a significant technological and environmental problem in the operation of oil and industrial pipelines and wells (pumping and casing pipes, deep pumping rods, etc.).

Many authors believe that uniform corrosion is the most typical for carbon and low-alloy steels from which petroleum equipment is made. However, in the last few decades, there have been regular occurrences of pipelines damages caused by localized corrosion. Moreover, localized corrosion starts from the inside and extends, in the vast majority of cases, on horizontal sections of pipelines, on the outer generating lines of the pipes, preferably in the area of the welded joint. It has been established that over the last 30 years, about 50% of all corrosion losses of pipelines operated at oil and gas fields are because of carbon dioxide corrosion, that is why it is urgent to study more closely the mechanisms of this type of corrosion.

The purpose of the study is to analyze the literature on the causes and mechanisms of carbon dioxide corrosion of oil and gas pipelines that are used in aggressive media.

The results of the analysis and their discussion. Systematic studies in the field of carbon-acid corrosion of petroleum equipment have been intensively conducted in the last 40 years of the last century [1-43]. In the last 20 years, a series of studies have been conducted on the corrosion process of steel in an oxygen-free, water phase containing dissolved carbon dioxide CO_2, the results of which are of some interest, since the problem of carbonic acid corrosion remains a matter of debate. Let us briefly consider the basic provisions of carbon-acid corrosion in an oxygen-free water media, taking into account changes in the most characteristic parameters of the CO_2 pressure system, temperature and pH of the medium.

1. Conceptual issues of carbon-acid corrosion.

The corrosive risk of CO_2-rich water media is primarily associated with lowering the pH of the medium. It depends on the concentration of carbon dioxide in the water phase and is determined by its partial pressure of PCO_2. Common to all water media in the working range of PCO_2 are the following reactions that take place in the solution:

$$CO_2+H_2O\leftrightarrow H^++HCO_3^-\leftrightarrow H_2CO_{3\ р\text{-}н}, \quad (1)$$

so at the active centers of the steel surface

$$CO_{2р\text{-}н} = CO_{2адс}, \quad (2)$$

$$CO_{2адс} + H_2O \rightarrow H_2CO_{3адс}. \quad (3)$$

As it is known [2,4,5,16-22,25,26,37-43], near the hydroxonium ions, depolarizers in oxygen-free water media can act H_2CO_3, HCO_3^-, $CO_2{\cdot}H_2O$. The total concentration of carbonic acid $C_{CO2}=[CO_2{\cdot}H_2O] + [H_2CO_3]+[HCO_3^-]+[HCO_3^-]+[CO_3^{2-}]$ and the ratios of molecular ($CO_2{\cdot}H_2O$, H_2CO_3) and ionic forms (HCO_3^-, CO_3^{2-}) in the volume of the solution and in the adsorbed state vary, respectively, with changes in the P_{CO2} and pH media.

Using known nomograms [3,39,40] of equilibrium dependencies H_2CO_3, HCO_3^- and CO_3^{2-} on pH it is possible to determine the form (molecular or ionic) of carbonic acid existence in solution. As the pH of the solution changes, the ratio of molecular and ionic forms changes, that is, the concentration of one or another depolarizer potential changes.

In water media with a pH<5, dissolved CO_2 exists in molecular form: 99.5% H_2CO_3 (t=25°C) and the adsorbed carbonic acid mainly acts as a depolarizer, and the cathode process is realized according to the equation

$$H_2CO_{3адс}+e=H_{адс}+HCO_{3адс}^-. \quad (4)$$

According to [37-43], carbonic acid is regenerated simultaneously

$$HCO_{3адс}^-+H_2O^+=H_2CO_{3адс}+H_2O. \quad (5)$$

In this case, hydroxonium ions involved in the cathodic process can be formed both in the volume of the solution and in the adsorbed state as a result of carbonic acid hydrolysis:

$$H_2CO_{3адс}+H_2O= H_3O_{адс}^++HCO_{3адс}^-; \quad (6)$$

$$H_2CO_{3р\text{-}н}+H_2O=H_3O_{р\text{-}н}^+ +HCO_3^-. \quad (7)$$

Probably with increasing concentration of hydroxonium ions in the adsorbed and surface layer, the role of competing reactions in the cathodic process increases

$$H_3O_{s\text{-}n}^{+} + e = H_{ads} + H_2O; \quad (8)$$

$$H_3O_{ads}^{+} + e \leftrightarrow H_{ads} + H_2O. \quad (9)$$

At pH=6.5-6.8, the solution contains ≈30% H_2CO_3 and 70% HCO_3-, so the implementation of the cathode process is possible simultaneously in two directions and also, as in the previous case, by homogeneous and heterogeneous mechanisms (4) and (8, 9)

$$HCO_{s\text{-}n}^{-} + e \rightarrow H_{ads} + CO_3^{2-}; \quad (10)$$

$$HCO_{3ads} + e \rightarrow H_{ads} + CO_3^{2-};$$

$$2H_{ads} \rightarrow H_2\uparrow. \quad (11)$$

It is possibly that with increasing P_{CO2} in the system, the proportion of reaction (9) and (11) in the total cathode process will increase.

At pH>6.8 in water media contains up to 99% HCO_3- [5,10,37-40]. Therefore, depolarization under such conditions is carried out mainly by ions and HCO_3- present in the solution [equation (10)].

At pH>7 together with the reaction (10) in the cathodic process increases the role of the reaction [3,40]

$$2H_2O + 2e \rightarrow H_2\uparrow + 2OH^{-}. \quad (12)$$

When OH ions are accumulated in solution, favorable conditions are created for the formation of CO_3^{2}- ions by reaction:

$$HCO_{3s\text{-}n}^{-} + OH^{-} \rightarrow H_2O + CO_3^{2-}, \quad (13)$$

which ultimately contributes to the formation of $FeCO_3$ and the formation of a protective layer of siderite on the metal surface. However, in this case, the risk of corrosion, primarily local, remains due to the local acidification of the environment in pores, films, deposits, in particular, as a result of reaction (6).

The probability of a depolarizer involvement in the cathode process and the implementation of the latter by a homogeneous or heterogeneous mechanism is determined by the concentration HCO_3, HCO_3^{-} and CO_3^{2-}, pH on a partial pressure system CO_2, temperature and hydrodynamic parameters of the medium. Changes in the pH and partial pressure of CO_2 change the composition of the solution and, as a result, the nature of the corrosion process, including the cathodic and anodic processes.

Considering that the total pressure in the system is the sum of the partial pressures of the present gases (in our conditions, these are CO_2 and H_2, which are formed as a result of the cathodic process), we can assume that the increase in the speed of the cathodic process with an increase in the total and partial pressure of CO_2 in the system will take place only in a certain critical value of CO_2, above which it decreases due to the cathodic evolution of hydrogen.

Analyzing the variety of flow patterns, proposed in the works [37-43], of the anode process, closely related to the cathode), we can note the following. The reaction of anodic dissolution of steel in water oxygen-free media over a wide pH range is

$$Fe+2H_2O \rightarrow Fe(OH)_{2тв}+2H^++2e. \quad (14)$$

In carbonic media with pH<5, a competing reaction is the direct interaction of iron with acid

$$Fe+2H_2CO_3 \rightarrow Fe(HCO_3)_2+H_2\uparrow. \quad (15)$$

Hydrocarbonates formed by the reaction (15) are unstable and eventually decompose in sequence

$$Fe(HCO_3)_2 \rightarrow Fe^{2+}+2HCO_3^-; \quad (16)$$

$$HCO_3^- \rightarrow H^+ + CO_3^{2-}; \quad (17)$$

$$Fe^{2+}+CO_3^{2-} \rightarrow FeCO_{3тв}, \quad (18)$$

which ultimately leads to the formation of a film or layer of siderite on the metal surface and inhibition of cathode and anode processes.

In environments with a pH>6.8, where the HCO_3 content is high, the formation of iron carbonate can occur by the direct interaction of HCO_3- with iron

$$Fe+HCO_3^- \rightarrow FeCO_{3тв}+H^++2e^- \quad (19)$$

and with iron hydroxide, which is formed by the above reaction (14):

$$Fe(OH)_2 + HCO_3^- \rightarrow FeCO_{3тв} + H_2O + OH. \quad (20)$$

Iron carbonate in turn interacts with HCO_3- forming a soluble complex compound

$$FeCO_{3тв}+HCO_3^- \rightarrow [Fe(CO_3)_2]^{2-}+H^+. \quad (21)$$

This explains the known [39,40] fact of dissolution of the siderite hydroxide film in the media with high content of HCO_3 and loss of its protective properties.

It should be noted that during the process of corrosion in water carbonic acid media, the formation of deposits on the metal surface,

which largely depends on the lifetime of the equipment and significantly affects the speed of the cathode and anode processes, is of great importance. During the course of chemical and electrochemical reactions, the composition of the water phase can be changed significantly, affecting the composition and properties of sediments. Therefore, the time factor significantly affects the speed, sequence and the possibility of one or other of the above reactions.

In addition to pH and PCO_2, the second important factor that determines the rate and mechanism of carbon-acid corrosion is the temperature. Unlike acid corrosion, the dependence of carbon-acid corrosion rate is observed only up to 40-60°C, and then its inhibition occurs, which is explained by a change in mechanism. At a temperature of 25-40°C a porous oxide-hydroxide film is formed, through which the penetration of the depolarizer occurs, sometimes with splashes of iron carbonate. The speed of the process is determined by the discharge stage of H_2CO_3 and HCO_3- (equations 4 and 10). At 60°C, the film or deposition of corrosion products becomes more dense, which increases its protective properties. In this case, the composition of the corrosion products changes - instead of oxide-hydroxide, carbonate, hydrocarbonate and purely carbonate films or deposits (with cementite at t> 100 °C) are formed, with the nature of the limiting stage is changing. The solubility and permeability of films or deposits are the main determinants of the corrosion rate, which, in turn, is controlled by the step (10) of dissolution of siderite $FeCO_3$. The solubility of siderite increases with increase in PCO_2 and decrease in pH and temperature [15,18,39-42].

The above idea can explain the following facts concerning carbon-acid corrosion: first, the destructions observed in the industrial conditions of oil fields, far exceeding those which are expected only because of the effect of CO_2 oxidation; second, cases of steel flooding in carbonic acid environments. Hence the probable falseness of the accepted opinion that at pH>7 the risk of corrosion of steel under the action of CO_2 in mineralized environments is practically absent.

The idea of the mechanism of carbon-acid corrosion in different conditions, the influence of various factors on this process makes it

possible to approach this important question - the prediction of the corrosion rate of oilfield equipment. Since the rate of carbon-acid corrosion is largely determined by the partial pressure of CO_2, pH, ambient temperature, then VNIIGAZ proposed classification of gas condensate systems according to corrosion, depending on temperature and partial pressure CO_2 [24,34,37-43]. The lower boundary (P_{CO2}>0.2 MPa), which defines corrosive environments according to this classification coincide with the recommendations of the American Petroleum Institute [25,36].

In the work [3], based on the above ideas about the mechanism of carbon-acid corrosion in oxygen-free water media, changes in the corrosion rate of low carbon steel and the pH of a model 3% NaCl solution with a higher partial pressure of CO_2 in a system with 0.7-1.1 MPa and the temperature in the working range of oilfield equipment 20-80^{o}C were studied. The authors, on the example of a simple model system, considered the possibility of predicting the corrosion rate of a steel by values of the partial pressure of CO_2 and pH.

The results obtained in [37-42] made it possible to draw the following conclusions: 1) with the change of the most significant characteristic parameters of the system - CO_2 pressure, temperature and pH of the medium, the duration of contact of the metal with the water phase, the mechanism of carbon-acid corrosion changes due to the change the sequence and speed of electro-chemical and chemical reactions occurring on the steel surface and in solution; 2) in contrast to the term change of the metal exposure in the corrosive medium and temperature, the change in the partial pressure of CO_2 in the range 0.7-1.1 MPa has little effect on the total corrosion rate and stationary potential of the steel electrode; 3) In oxygen-free mineralized water media in the range of PCO_2=0.7-1.1 MPa with increasing temperature up to 80^{o}C, even at pH10-11, the protective film of siderite on its surface is not formed and the danger of corrosion destruction under the action of dissolved CO_2 remains; 4) experimental values of the corrosion rate of grade 3 steel in 3% CO_2-saturated NaCl solution are much higher than those predicted by mathematical equations, not taking into account the growth of corrosion products on the metal surface, which indicates the complexity of predicting the corrosion rate by the magnitude of

PCO_2 for real systems under prolonged detection of metal in an aggressive environment; 5) for the temperature range of 25-80ºC, the possibility of calculating the pH and the initial corrosion rate of low carbon steel by known partial pressure of CO_2 in water oxygen-free media is shown. There are many other points of view on the mechanism of corrosion of metal in the presence of oxygen, sulfur and hydrogen in the process medium, in particular, for example, energy-enzymatic reaction [3]

$$SO_4^{2-}+4H_2O+8e\rightarrow S^{2-}+8OH^-. \quad (22)$$

Consider in more details the mechanisms of corrosion damage development of the pipe body in the form of pitting at different stages of the process [39].

2. The mechanisms of pipelines localized corrosion.

2.1. The first stage of localized corrosion. According to existing notions [37-42], reaction (22) can promote the electro-chemical corrosion of iron when, for example, electrons released by the anode process are partially used

$$Fe\rightarrow Fe^{2+}+2e, \quad (23)$$

or the formed Fe ions are bound

$$Fe^{2+}+S^{2-}\rightarrow FeS.$$

The reactions are possible here

$$S^{2-}+H_2O\rightarrow HS^-+OH^-,$$
$$HS^-\rightarrow H^++e+S^{2-}.$$

Formed, as a result of the biogenic process, hydrogen sulfide molecules can exert a catalytic effect on the reaction

$H^++H^+\rightarrow H_2$ (hydrogen molization stage);

$$H_2S_{ads}+2e\rightarrow 2H+S^{2-};$$
$$HS^-+H_3O\rightarrow H_2S\uparrow+H_2O.$$

H_2S dissociation takes place in two stages

$$H_2S\rightarrow H^++HS^-;$$
$$HS^-\rightarrow H^++S^{2-}.$$

The interaction of hydrogen sulfide dissolved in a water-oil mixture with the metal surface is carried out by the reactions

$$2H_2+Fe\rightarrow Fe^{2+}+4H;$$
$$Fe^{2+}+S^{2-}\rightarrow FeS\downarrow;$$
$$H+H\rightarrow H_2\uparrow.$$

Further may occur the reactions, which are confirmed by the results of the analysis of the formed phases in the corrosion products [38-40]

$$2FeSO_4+H_2SO_4+0.5O_2\rightarrow Fe_2(SO_4)_3+H_2O;$$
$$Fe(SO_4)_3+2FeS_2\rightarrow 3FeSO_4+4S°;$$
$$S°+2e\rightarrow S;$$
$$S+H_2O+3/2O_2\rightarrow H_2SO_4;$$
$$H_2SO_4\rightarrow 2H^++SO_4^{2-}.$$

As a result of the components interaction of the mixture according to the above reactions, the degree of acidity of the mineralized water medium (pH decreases from 7-8 to 5-6), which will increase its corrosion activity.

Besides, on the pipe surface (in volumes of thin liquid film), adsorbed sulfur and iron ions interact by reactions

$$Fe^{2+}+S_{ads}^{2-}\rightarrow(FeS)_{ads}^{2-}+2e+FeS_{тв.}; \quad (24)$$
$$FeS_{тв.}+2H_3O^-\rightarrow Fe^{2+}+2H_2O+H_2S. \quad (25)$$

From the equations (24) and (25) could be seen, that sulfide ions S_{ads}^{2-} in comparison with OH_{ads}^- - a stronger stimulator of iron dissolution.

Surface ions S_{ads}^{2-} i OH_{ads}^- engage in electro-chemical interaction with iron, ie the anode process of dissolving iron is realized

$$Fe+OH^-\rightarrow FeOH_{ads}^-\rightarrow Fe^{2+}+2e$$
$$\text{or } Fe+n(OH^-)\rightarrow Fe(OH)_{птв}\downarrow+ne^-.$$

According to the results of the analysis of corrosion products [10-13,39,40], sediments or deposits, even with a small amount of oxygen (less than 0.02 mg/l), create, apparently, favorable conditions for the active process of microbiological corrosion in the presence of bacteria, facilitating the reaction

$$Fe^{2+}+SO_4^{2-}+H_2O\rightarrow FeS+Fe(OH)_2+OH^-. \quad (26)$$

The reservoir water raised with oil from wells contains up to 200 mg / l of ferrous iron, which reacts with oxygen in its solution

$$Fe^{2+}+OH^-\rightarrow Fe(OH)_2,$$
$$4Fe(OH)_2+O_2+2H_2O\rightarrow 4Fe(OH)_3. \quad (27)$$

Therefore, reactions (1-27) describe the most probable ways of the sulfur appearance in corrosion products, for example, at the base and on the side walls of nucleated pits resulting from the biological action of bacteria, as well as the initial process of corrosion of the

inner surface of the pipe wall. The absence or negligible presence of sulfur on the walls and bottom of the pit, as well as on the walls of the corrugated corrugated barrel, helps to predict that the subsequent stages of localized corrosion development take place not by biological, but by the electro-chemical mechanism.

2.2. At the second stage, Cl- ions, which are present in large quantities in incidentally extracted water, accelerate the process of iron ionization and intensify the development of localized corrosion in accordance with the reactions [34,37-40,43]

$$Fe^{2+}+Cl^{-}\rightarrow FeCl_2\downarrow; \quad (28)$$

$$FeCl_2+2H_2O\rightarrow 2HCl+Fe(OH)_2\downarrow; \quad (29)$$

$$2FeCl+Fe\rightarrow FeCl_2\downarrow+H_2\uparrow; \quad (30)$$

$$Fe^{3+}+Cl^{-}\rightarrow FeCl_3\downarrow; \quad (31)$$

$$3HCl+Fe\rightarrow FeCl_3\downarrow+3/2H_2. \quad (32)$$

The reaction products (28-32) found in [39,40] confirm the calculated data.

2.3. At the third stage there is an intense destruction of the crystalline structure of the metal with the formation of bulk oxides, carbonates and bicarbonates in the middle of the cracks, which contributes to the additional creation of structural stresses, causing a cracking effect at the mouth of the crack vertices. At this stage the corrosion is stimulated, in our view, present in oil-water mixture in a great amount associated gas CO_2 , which increases the acidity of the medium (lowers pH).

The following are the reactions, according to which most likely a corrosion process occurs [37-40,42,43]

$$Ca^{2+}+CO_3^{2-}\rightarrow CaCO_3\ ;$$

$$Fe^{2+}+CO_3^{2-}\rightarrow FeCO_3\ ;$$

$$Mg^{2+}+CO_3^{2-}\rightarrow MgCO_3\ .$$

Anion CO_3^{2-} is formed as a result of interaction of CO_2 and H_2O according to reaction

$$CO_2+H_2O\rightarrow H_2CO_3\rightarrow H_2CO_3^{-}+H^{+}\rightarrow CO_3^{2-}+2H^{+}.$$

The physico-chemical equilibrium between bicarbonate carbonate and carbon dioxide is expressed by the following reactions [10-13,37-40]

$$Ca(HCO_3)_2\leftrightarrow CaCO_3\downarrow+CO_2\downarrow+H_2O;$$

$$Mg(HCO_3)_2\leftrightarrow MgCO_3\downarrow+CO_2\downarrow+H_2O;$$

$$Fe(HCO_3)_2\leftrightarrow FeCO_3\downarrow+CO_2\downarrow+H_2O.$$

After the formation of carbonate salts deposits, corrosive processes are inhibited, as it serves as a protective insulating layer on the metal surface, the walls of the hole and the fitting bottom. Fusion and deepening of the pit as a result of chloride-carbon corrosion leads to the formation of the canyon at the site of the initial nucleation. The progressive destruction of the pipe wall at the deepest point of the canyon, where chlorides, oxides and carbonates concentrate, ends with its opening in the form of a through hole [5,10-13]. The effect of the chloride-carbon-acid mechanism for the development of pitting corrosion destructions is confirmed by the fact that local pipeline leaks of oil-gathering system pass on the pads, from the wells where the products are being extracted - oil and formation water - contain short-term increased concentrations of chlorine ions (Cl^-), in particular from 8000 to 10000 mg/l and CO_2 from 50 to 200 mg/l [10-13]. From the experience of operating oil-gathering systems it follows that when the content of chlorides and carbon gas is more stable and does not exceed 300-800 mg/l and 5-20 mg/l accordingly, such leaks do not occur.

Conclusions.

1. The state and key directions of carbon dioxide corrosion mechanisms development of oil and gas pipelines that are used in chemical-aggressive media in the fields are considered.

2. The most realistic schemes according to which corrosion damages of pipe walls occur are presented.

3. The most promising corrosion mechanisms that adequately reflect the processes of damage and destruction of long-term operated structures are formulated and substantiated.

4. The rationale for the mechanisms of localized corrosion, which most often causes local (pitting and grooves) corrosion and which are

not easy to identify at the beginning of nucleation and growth, is given.

5. The possibility of increasing the stability of metal structures by reducing the degree of corrosive activity of technological media, which is directly related to the formation water, which is pumped together with oil, is substantiated.

References

1. **Leninskiy B.M., Manakov L.I.** (2007)Fizicheskaya himiya oksidnyih i oksihloridnyih rasplavov. Moskva. Nauka.

2. **Makarenko V.D., Kovenskiy I.M., Prohorov N.N.** i dr.(2000) Korrozionnaya stoykost svarnyih metallokonstruktsiy neftegazovyih ob'ektov. Moskva. OOO «Nedra-Biznestsentr».

3. **Moiseeva L.S.** (2005) Uglekislotnaya korroziya neftegazopromyislovogo oborudovaniya. Zaschita metallov. T.41.1.82-90.

4. **Radkevich O., Chumalo G., Dominyuk I.** ta Insh. (2004)Osnovni zakonomirnosti navodnyuvannya ta poverhnevogo puhirinnya trubnoYi stali v sirkovodnevih seredovischah. Fiz.-him. mexanika materialiv. 4, t. 1. 446-449.

5. **Makarenko V.D., Paliy R.V., Galichenko E.N.** i dr. (2002)Fiziko-mehanicheskie osnovyi serovodorodnogo korrozionnogo razrusheniya promyislovyih truboprovodov. Chelyabinsk. TsNTI.6.Coedited bu R.N.Tuttle , R.D.Cane. (1981) H_2S corrosion in oil qas production. Houston. NASE.

7. **S. Serna, B. Campillo, J .G. Gonzalez-Rodriguez**, et al. (2005) Identifying Sour Environments Conditions for Preventing Hydrogen Embrittlement of Microalloyed Pipeline Steels. Proceedings of the European Corrosion Congress «Eurocorr 2005». Lisbon. Portugal. 594.

8. **W.-Y. Chu, S.-Q. Li, C.-M. Hsiao**, et al. (1981)Effect of Hydrogen on the Apparent Yield Stress - Research on the Cause of Hydrogen-Induced Delayed Plasticity. Corrosion. Vol. 37. **9**. 514-521.

9. **Turn J.C., Wilde B.E., Troianos C.A.** (1983) On the Sulfide Stress Cracking of Line Pipe Steels. Corrosion. Vol. 39. **9**. 364-369.

10. **Makarenko V.D., Muravjev K.A.,Kalyanov A.I.** (2006) Special features of manual ars weldinq of root joints in nonrotatinq welds in pipelines in Westem Siberia. Weldinq International.**10** (5). 64-71.

11. **Makarenko V.D., Shatilo S.P.,Astafev V.I.** (1998). Methods of increasing the corrosion resistance of oil pipelines. Welding Internationa. **12**. 34-39.

12. **Makarenko V.D.,Shatilo S.P.** (1999) Increasing desulphurisation of the metal of welded joints in oil pipelines. Welding International. **12.** 56-61.

13. **Makarenko V.D., Beljaev V.A., Protasov V.N., Shatilo S.P.** (2000) Mathematical model of the mechanism of resistance of welded joints in oil and gas pipelines to static hydrogen fatigue. Welding International.**4**. 83-88.

14. **Kuzmenko Yu**. (2004) Suchasni vimogi do nadiynosti ta bezpeki magistralnih truboprovodiv. Fiz.-xim. mexanika materialiv. 4. t.1. 373-375.

15. **Gareev AG Ivanov IA Abdullin** IGPi dr (1997)Prognozirovanie korrozionno-mehanicheskih razrusheniy truboprovodov. Moskva. IRTs Gazprom.

16. **Radkevich O Chumalo G Dominyuk I I I**n. (2004)Osnovni zakonomirnosti navodnyuvannya ta poverhnevogo puhirinnya trubno'i stali v sirkovodnevih seredovischah. Fiz.-him. mexanika materialiv. 4, t.1. 446-449.

17. **Kuzmenko Yu**. (2001) Sovremennyie trebovaniya k monitoringu tehnicheskogo sostoyaniya magistralnyih truboprovodov. Fiz.-him. mexanika materialiv. 2. t.1. 45-50.

18. **Gutman E.M**. (1981)Mehanohimiya metallov i zashita ot korrozii. Moskva. Metallurgiya.

19. **Karpenko G.V.** (1976) Vliyanie sredyi na prochnost i dolgovechnost metallov. Kiev. Naukova dumka.

20. **Petrov L.N**. (1986) Korroziya pod napryazheniem. Kiev. Vischa shkola.

21. **Dmitrah I.M., Panasyuk V.V**.(1999) Vpliv koroziynih seredovisch na lokalne ruynuvannya metaliv bilya kontsentpatopiv napruzhen. Lviv. Lvivska oblasna knizhkova drukarnya.

22. **W.- У. Chu, S.-Q. Li, .C-M. Hsiao**, et al. (1980) Mechanism of Stress Corrosion Cracking of Steels in H_2S. Corrosion. Vol. 36. **9**. 475-481.

23. **Radkevich O.I., P'yasetskiy O.C., Vasilenko I.I**. (2000) Koroziyno-mehanichna trivkist trubnoYi stali v sirkovodnevomu seredovischi. Fiz.-him. mexanika materialiv. 3. 93-97.

24. **Kolachev B.A**. (1985) Vodorodnaya hrupkost metallov. Moskva. Metallurgiya.

25. **W.-Y. Chu, S.-Q. Li, C.-M. Hsiao**, et al.(1981) Effect of Hydrogen on the Apparent Yield Stress - Research on the Cause of Hydrogen-Induced Delayed Plasticity. Corrosion.Vol. 37. **9.** 514-521.

26. **J. Sojka, P. Vanova, P. Jonsta,** et al. (2005) Role of Microstructure in Sulphide Stress Cracking of Carbon Steels. Proceedings of the European Corrosion Congress «Eurocorr 2005». Lisbon. Portugal. №.156.

27. **Panasyuk V.V., Andreykiv A.E., Harin V.S**. (1987) Model rosta treschin v deformirovannyih metallah pri vozdeystvii vodoroda. Fiz.-him. mexanika materialiv. 2. 3-17.

28. **Petrov L.M.** (2001) Fiziko-himichni aspekti mehaniki koroziynogo ruynuvannya. Fiz.-him. mexanika materialiv. 3. 127-129.

29. **Kasatkin G.N.** (2003) Vodorod v konstruktsionnyih stalyah. Moskva. Intermet Inzhiniring.

30. **Andreykiv O.E., Nikiforchin G.M., Tkachov B.I.** (2001) Mitsnist i ruynuvannya metalichnih materialiv i elementiv konstruktsiy u vodnevomisnih seredovischah. Lviv. Prostir-M. 248-286.

31. **Tkachov B.I.** (2000) Problemi vodnevo'i degradatsiI metaliv. Fiz.-him. mexanika materialiv. 4. 7-14.

32. **Pohmurskiy B.I., Fedorov V.V**. (1998) Vpliv vodnyu na difuziyni protsesi v metalah. Lviv. Eney.

33. **Ovchinnikov I.G., Shein A.A., Denisova A.P.** (1997) Korrozionnaya stoykost i zaschita rezervuarnyih konstruktsiy ot korrozii. Sarat. gos. tehn. un-t. Saratov.

34. **Suhotin A.M., Archakov Yu.I.** (1889) Korrozionnaya stoykost oborudovaniya himicheskih proizvodstv. Leningrad. Himiya.

35. **Nikiforchin G.M., Slobodyan Z.V., Tsirulnik O.T.** I In. (2004) Rol pId tovarnoYi vodi v korozIyno-vodnevIy degradatsIYi stalI magIstralnogo truboprovodu. MaterIali 8-oYi MIzhnarodnoYi nauk.-prakt. Konf. "Nafta I gaz UkraYini-2004". KiYiv. 165-166

36. **Zagorski A., Matysiak H., Tsyrulnuk O.** (2004) Corrosion and stress corrosion cracking of exploited storage tank steei. Фіз.-мех. механіка матеріалів. **3**. 113-117.

37. **Mitina A.P., Goryachev I.G., Horoshilov A.V.** i dr. (1992) Teoreticheskie osnovyi karbonatnoy korrozii stali. Moskva. VNIIEGazprom.

38. **Legezin N.E., Glazov N.P., Kesselman G.S.** (1973) Zaschita ot korrozii neftepromyislovyih sooruzheniy v gazovoy i neftedobyivayuschey promyishlennosti. Moskva. Nedra.

39. **Saakiyan L.S., Efremov A.P.** (1982) Zaschita neftegazopromyislovogo oborudovaniya ot korrozii. Moskva. Nedra.

40. **Rozanova E.P., Kuznetsov S.I.** (1974) Mikroflora neftyanyih mestorozhdeniy. Moskva. Nauka.

41. **Radkevuich A.I., Pohmurskiy O.S.** (2001) Vliyanie serovodoroda na rabotosposobnost materialov oborudovaniya gazodobyivayuschey promyishlennosti. Fiz.-him. mehanika materialov. 2. 137-168.

42. **Gonik A.A.** (1976) Korroziya neftepromyislovogo oborudovaniya i meryi ee preduprezhdeniya. Moskva. Nedra.

43. **Asfandiyarov F.A.** (1983) Metodyi borbyi s sulfatvosstanavlivayuschimi bakteriyami i vyizyivaemoy imi korrozii stali. Moskva. VNII organizatsii, upravleniya i ekonomiki neftegazovoy promyishlennosti.

SAFETY OF WORK OF MINING WORKERS AND ANTI-SAVING PROTECTION OF MINING ENTERPRISE: PROBLEMS AND SOLUTIONS

Ryasnoy V.M.
Candidate of Technical Sciences, Safety laboratory for mining and processing of ores, and mine rescue work,
Scientific Research Institute of Occupational Safety and Ecology in the Mining and Metallurgical Industry of the Kryvyi Rih National University, Ukraine

Shchokin V.P.
Doctor of Technical Sciences, Professor, Acting Director
Scientific Research Institute of Occupational Safety and Ecology in the Mining and Metallurgical Industry of the Kryvyi Rih National University, Ukraine

Chukharev S.M.
Candidate of Technical Sciences, Associate Professor, Kryvyi Rih National University, Ukraine

Underground and open-pit mining of minerals remains a source of a significant number of accidents and emergencies, as well as accidents, which lead to significant material losses and injuries, including fatalities to operating personnel.

Keywords: mining enterprises, labor safety, emergency protection, mine rescue service, special equipment, technical progress.

Introduction

The most potentially dangerous production processes during the mining of minerals is the excavation, ore drawing from the refining units, operation of in-mine (electric and self-propelled non-rail), railway and automobile transport, and electrical installations.

The objects and areas requiring increased attention were and remain vertical and inclined shafts, lifting systems, ventilation of extractions, emergency as well as fire protection, protection of mining enterprises.

In the recent years, the enterprises controlled by the Krivoy Rih State Mining and Industrial Supervision Territorial Administration of Ukraine (Derzhgirpromnaglyad) (currently the State Labor Service of Ukraine) have faced with several resonant accidents. So, on mine named after Frunze PJSC "EVRAZ Sucha Balka" as a result of

breakage of counterweight frame cage-lifting to cage winding plant the cage was stopped in an emergency order, in which there were 35 people. Mine-rescuers took almost 10:00 to evacuate the miners from the cage, and 18 days to eliminate the consequences of the accident itself. At the mine named after Ordzhonikidze “TsGZK”, JSC due to the dumping curve skip sticking there was a rope overlap on the drum of the skip lifting device, as a result of which the dynamic hitch broke it and, as a result, the skip fell into the sump. A large-scale accident due to the skip fall took place also in the shaft of the Oktyabrskaya mine of Kryvbasszhelezrudkom, PJSC.

Fires cause major hazards and significant material damage to the enterprises. Thus at the area conveyor ore transportation (TsPT) of one of the open pits of "PIVNGZK" there occured a fire, which led to the suspension for a long period of the entire production process and economic losses in the amount of several tens of millions of Hryvnias.

As a result of the problems due to the inefficient ventilation of mining workings, several cases of miners' poisoning with harmful explosion products were recorded, two of which were fatal.

Analysis of the reasons of the low state of safety of miners and the emergency protection of mining enterprises

Among the reasons for this state of affairs, first of all, it is necessary to name the insufficient financing of labor protection; operation of machinery, mechanisms and other mining equipment, which has run out its service life; low level of labor mechanization; unsatisfactory functioning of the entire labor protection management system, especially at the enterprise level.

As experience shows, the success of accidents elimination that occur at the mining enterprises largely depends on the technical equipment of the mine rescue brigade. In the recent years, new types of respiratory equipment, communications equipment, fire extinguishing equipment and vehicles have been introduced into service of mine rescue brigade.

But the level of technical equipment of mine rescuers still does not meet the modern requirements of scientific and technical progress, especially due to the constant complication of the mining-geological and mining-technical conditions for the development of mineral deposits.

The lack of many types of special means forces the rescuers to use mining equipment that is not adapted to the specific conditions that are observed during accidents or emergencies. Thus, for example, in the absence of mobile, highly maneuverable vehicles for the delivery of equipment, transportation of victims directly in the mine workings necessitates the use of mining electric locomotive and mine cars. But during the accidents, electricity is basically turned off. On mine retractable lines the traffic block are formed, that considerably complicates, and sometimes completely excludes the possibility of using this technique.

For similar reasons, it is not always possible to use cargo handling machines, scraper-loading hoists and other mining equipment.

Significant problems arise in front of rescuers, when conducting rescue operations in vertical (rising) mining workings.

The existing legal framework allows enterprises owners to violate the requirements of regulatory and legal acts on labor protection and industrial safety almost with impunity. The legal framework itself is very imperfect. More than 75% of the normative acts that have been entered into the state register do not take into account the modern socio-economic relations, changes in the form of ownership, the modern legislative base of Ukraine.

3. Special equipment for improving the labor safety of miners and emergency protection of mining enterprises

Despite the state of science in general in the State, NDIBPG KNU together with co-contractors and production workers managed to solve a number of very important issues necessary for production, to propose new technical solutions in the field of optimization and improvement of safety of production processes, emergency and fire prevention of enterprises.

To prevent injuries from falling pieces of rock mass and collapses, the Institute has developed:

- New patterns of drilling and blasting operations during excavations, the use of which reduces the number of roof flaws by 1.5-1.8 times. These patterns have been tested in the mines of ShU ArcelorMittal Kryvyi Rih, PJSC, Kryvbasszhelezrudkom OJSC, and others;

- New types of roadway supports of sublevel workings with increased rigidity, which ensures their approach to mine face.

To improve the safety of ore production, it has been proposed to blast it in a variety of environments, at which the explosive energy utilization factor is almost doubled, the amount of ore lumps and the number of congestions is reduced. This method of blasting was tested during the development of research blocks in the mines of "Kryvbusszhelezrudkom", PJSC, "TsGOK", PJSC and "ArcelorMittal Kryvyi Rih", PJSC.

A significant amount of works has been carried out by the Institute in the direction of increasing the level of mechanization and miners labor safety during the carrying out of rising mine workings. There were developed the following structures that have passed successful state acceptance tests:

- KP-1 and KP-2 monorail tunneling systems with the specifications of lowering and raising operations from 100 to 160 m, which simultaneously provide 2.5 times increase in labor productivity of the drifters (Fig. 1). Serial production of such systems was mastered by the repair-mechanical plant SE "SkhidGZK" (Zhovti Vody).

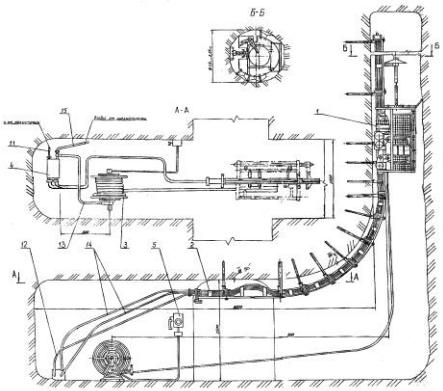

Fig. 1. Schematic diagram of the penetration of drifting of rising mining driftage with the use of monorail tunneling systems "KP-1" and "KP-2"

Fundamentally new complex of equipment for drifting of short (up to 20 m) rising driving of different purpose sinking short films (to a height of up to 20 m) of rising mine workings for various purposes (rock dumping, ventilation, material-travelling) “KOPV-20RVM” (Fig. 2).

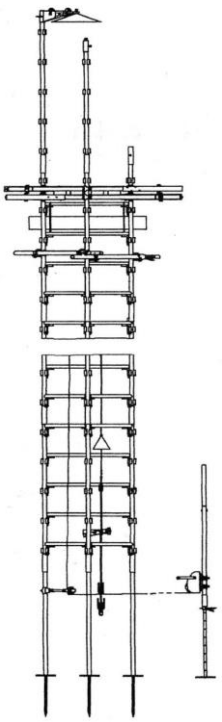

Fig. 2. Complex of equipment for travelling into one section of short-length (to a height of up to 20m) the rising mine workings "KOPV-20RVM"

- Improved version of the device for the remote sampling of air and express analysis of its qualitative composition at the drifter's workplace before starting the works PDKSP-20 / 80RVM (Fig. 3). In the conditions of the existing mines of the Krivoy Rih iron ore basin, the device has undergone extensive industrial testing, including state acceptance testing. The manufacturing company is Tehnotron, LLC (Zhovti Vody).

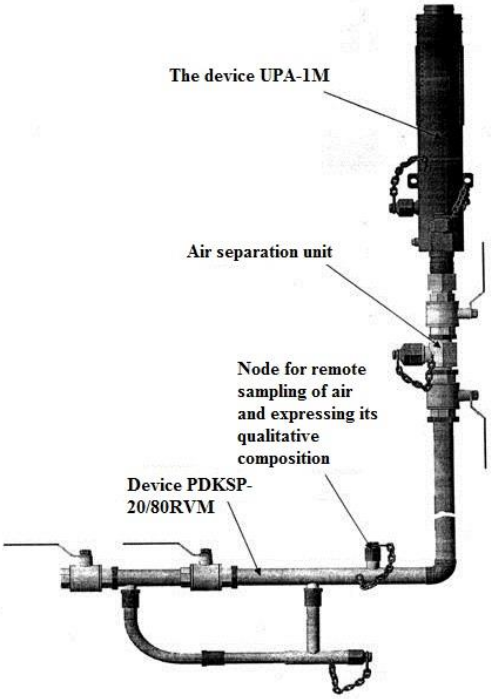

Fig. 3. General view of the device for remote air sampling and express analysis of its qualitative composition PDKSP-20 / 80RVM combined with an apparatus for ventilation and neutralizing of the explosion products UPA-1M

Normalize the sanitary and hygienic working conditions during the drilling and blasting method of mining of various purposes allow the special means for neutralizing dust and harmful gases worked out by the NDIBPG KNU:

- High-pressure ejector foam generator EPG-2PM - for horizontal mine workings;
- Universal device of the ejector type UPA-1M - for rising mine workings.

Derzhgirpromnaglyad, after reviewing the test results and petitions of the most mining enterprises, allowed the constant use of specifications and ventilation schemes of mine workings using this equipment.

To protect the miners' respiratory organs from the unsuitable for breathing atmosphere, which may occur during the fires in mine conditions or entry of natural gases to the mine workings of natural origin, the Institute has developed and implemented, in addition to the previously worked out refuge chamber (KAPP) stationary and mobile miners emergency air supply stations PAPP-2 and PAPP-10.

In order to further improve the efficiency and reliability of actions of mine rescue brigade (VGRS), re-equipping them with modern technical means and equipment, NDIBPG KNU, as the main Institute for emergency rescue service together with DVGRZ DSNS (State Militarized Mine-Rescue (Rescue) Squad) of Ukraine and SE "DPI" Kryvbasproekt have worked out the" Plan of the technical progress of the mountain rescue services for the period up to 2020".

The developed Plan consists of three sections, including 15 research and developmental works (R&D).

The First section, "Preparing mines for emergency response and mines fire protection," provides for four R&D activities related to:

- Development and implementation of a modern system of radio notification of miners about the mine accidents (emergencies);
- Development of automatic fire extinguishing systems for the most fire hazardous facilities served by VGRS and other fire extinguishing equipment.

Today we have developed and successfully implemented:

- Mine radio communication and emergency alert complex "Vesna-Sh1" (manufactured by "Interinkom", OJSC, Dnepropetrovsk);
- ASP Automatic powder-gas fire extinguishing system for oil stations, power substations, cable channels;
- MUP-50 modular automatic powder-gas fire extinguishing system for fire protection of drive stations of conveyor paths located at ground surface (galleries and racks of crushing, crushing and processing plants and other facilities). Energiya LLC (c. Liman) is the ASP and MUP-50 manufacturer.
- Universal mobile (rail-mounted) water-foam-powder fire-fighting unit UPP-600/750 (manufactured by Tekhnomash, LLC (Zhovti Vody).

Figure 4 shows a photo illustration of the field tests of the developed fire extinguishing equipments.

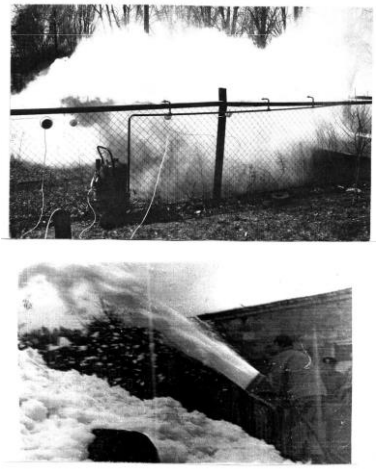

Fig. 4. Photo illustration of the field tests of the fire extinguishing equipments

Under the second section, "Mine-rescue equipment", 11 research and development works are carried out. Today we have successfully worked out:

- Small-sized monorail elevator PGR-350 (Fig. 5), is intended for rescue operations in the rising workings, driven by a mechanical method using complexes of KPP type (manufactured by Tekhnomash, LLC).

- LGRU-100RVM Universal Mine-rescue hoist (Fig. 6) (manufactured by Tekhnomash, LLC).

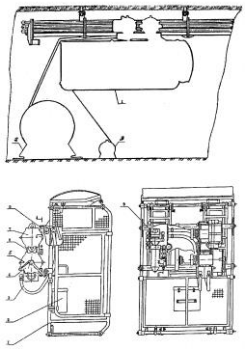

Fig. 5. Structural diagram and design of the PGR-350small-sized monorail emergency rescue hoist cage

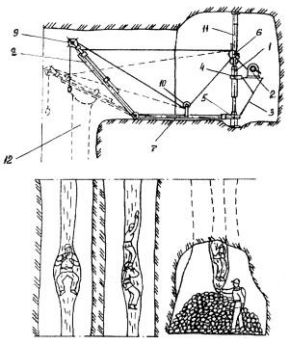

Fig. 6. General view of the LGRU-100RVM Universal Mine-rescue hoist

Demountable metal reinforcement complex for the rapid construction of the travelling channel in vertical workings with a device for miners mass evacuation in emergency situations “Khid-100 RVM” (Fig. 7) (manufactured by Tehnotron, LLC);

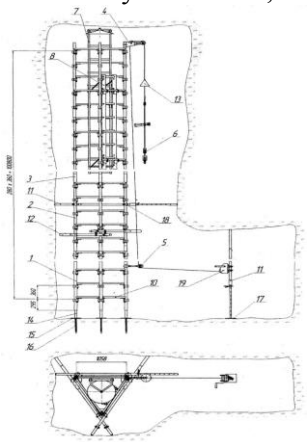

Fig.7 General view of reinforcement complex for construction of the temporary travelling channel in the ascending workings “Khid-100 RVM”

Equipment for non-explosive destruction of oversized rocks, as well as concrete or reinforced concrete building structures (for example, foundations, blocks, etc.).

Currently, NDIBPG KNU, together with DVGRZ DSNS are completing the works related to the development of a universal multi-purpose mountain rescue jumper, as well as a set of means for transporting of equipment (equipment, materials, etc.), as well as evacuating of injured people through the horizontal mine workings (small-sized trucks modular type with a lifting capacity of 50–100 kg, a universal folding cart with a lifting capacity of up to 800 kg, a mountain-rescue trolley with a foot-operated mechanical drive).

Together with the Enterprise-co-contractor “Automation and Mechanical Engineering” (Zhovti Vody) of the National power generating company “Energoatom”, the final works related to the state acceptance tests and the introduction of a MASPO 2.5 / 1500 mobile lifting facility for the accidents elimination and the salvage of people in vertical shafts of mines up to 1,500 m in depth (Fig. 8) and a complex of special equipment for television inspection of mine ventila-

tion shafts that are not equipped with mechanized hoists, MKTS-0.5 / 1500 (Fig. 9) with the possibility of its use in emergency situations are being carried out.

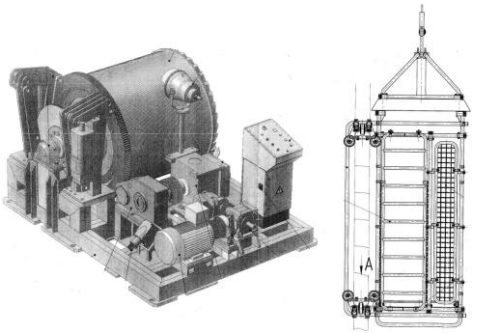

Fig. 8. General view of the hoist and the cage of the MASPO 2.5 / 1500 mobile hoisting plant for emergency response and rescue of people in vertical shafts to a depth of up to 1500 m

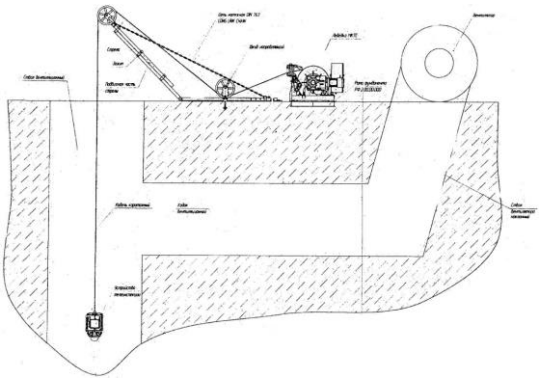

Fig. 9. General view of a special complex of equipment for television inspection of mine ventilation shafts that are not equipped with mechanized hoists, MKTS-0.5 / 1500

The above described developments have gone through all the stages stipulated by the State standards of Ukraine.

The last (third) Section of the “Plan of technical progress ...” is devoted to the development of regulatory and procedural documents. In particular, today we have developed and implemented:

- “Guidelines for the inspection arrangement of the safe state of equipment for vertical shafts and mine hoisting plants”;

- “Guidelines for the inspection arrangement of the safe state of hoisting plants and equipment for inclined shafts of mines and the TsPT (conveyor ore transportation) of mining and processing plants";

- "Guidelines for the design of ore mines ventilation";

- "Instructions for safe execution of works when carrying out rising workings using the drifting complexes";

- "Instructions on labor protection for personnel dealing with inspection, maintenance and repair of equipment for mines hoisting equipment";

- “Methodological guidelines for the design of fire protection of mines and underground facilities of the TsPT of mining and processing plants";

- “Methodological guidelines for the design of fire protection of quarries for the extraction of ore and non-metallic minerals, facilities of the technological cycle and other facilities of mining and processing plants”.

4. Conclusion

The organization of industrial production and the mass introduction of the developed complex of equipment, means of normalizing of working conditions and protection in emergency situations, as well as the full implementation of the VGRS Technical Progress Plan will significantly improve the safety of miners, the efficiency and effectiveness of the mine rescue service, as well as the level of emergency (including fire-extinguishing) protection of mining enterprises.

LINKAGES BETWEEN PHYSICAL AND MECHANICAL CHARACTERISTICS OF COMPACTED SMALL-CONNECTING OVERBURDEN IN QUARRIES OF IRON QUARTZITE DEPOSITS

Vynnykov Yu.L.,
Poltava National Technical Yuri Kondratyuk University
DSc, Professor, professor of the Department
of Oil and Gas Engineering and Technology, Ukraine

Dmytrenko V.I.,
Poltava National Technical Yuri Kondratyuk University
PhD, associated professor, associated professor of the Department of Oil and Gas Engineering and Technology, Ukraine

Lopan R.M.,
Poltava National Technical Yuri Kondratyuk University
PhD, associated professor of the Department of Oil and Gas Engineering and Technology, Ukraine

Drozd I.S.
Poltava National Technical Yuri Kondratyuk University
Student of the Department of Oil and Gas Engineering and Technology, Ukraine

Abstract. The economic and environmental feasibility of using overburden from the quarries of iron quartzite deposits and their mixtures as a material for the construction of massive ground pillows are proved.

On the basis of the theory of mathematical statistics, the conditions for plotting and determining equations for the relationship between the physical and mechanical characteristics of compacted low-bonded overburden are grounded. Based on the theory of mathematical statistics, the conditions for constructing graphs and the determination of the equations of the relationship between the physical and mechanical characteristics of compacted small-connecting overburden are substantiated.

According to laboratory and field studies of the physicomechanical characteristics of compacted small-connecting overburden of iron quartzite quarries and mining and processing industry wastes, graphic and analytical dependencies of the deformation modulus and strength different types of compacted small-connecting overburden of iron quartzite quarries with their physical properties were found (specific skeleton volume soil) taking into account the influence of rolling parameters.

It is proved an important practical conclusion that in any technological

parameters of rolling would not be obtained a certain value of the skeleton density of the rockρ_d, it corresponds to certain the internal friction angle φ, specific cohesion of soil and modulus of soil deformation E for sand of a certain particle size composition.

Keywords: the career, the iron quartzites, small-connecting overburden, compaction, the internal friction angle, the specific cohesion, the modulus of deformation, the link.

Introduction. It is economically and environmentally advisable to use overburden and their mixtures formed during the extraction of minerals as a material for the construction of massive soil pillows [1-7].

Determining the mechanical characteristics of compacted rocks for the pillows in a volume sufficient for their design is associated with significant time and material costs. However, it has been found that correlation or even functional dependencies can be obtained between mechanical properties and physical condition of rocks under certain conditions [4-13].

The imperfection of standards for the design and construction of pillows is the lack of requirements for determining the mechanical properties of compacted rocks. It is possible correlation or functional dependencies between their mechanical and physical properties. These dependencies for small-connecting overburden have hardly been investigated. The effect of rolling technology (parameters and mechanism mode; number of passes per track; initial layer thickness) on the mechanical properties of rocks has not been established [14, 15].

The purpose of this work is to correlate the physical and mechanical characteristics of the compacted overburden of the quarzite deposits in the quarries with the parameters of their rolling.

1. The issue of establishing the linkages between physical and mechanical characteristics of soils in the design of artificial foundations

E. Kuzakhmetov [11] assigns values c and φ for the calculations of the stability of embankments of compacted rocks by the relative coefficients of cohesion k_c and the internal friction angle k_φ at the corresponding fluidity index I_L.

$$k_c = c_i / c_{поч}; \quad (1)$$

$$k_\varphi = \varphi_i / \varphi_{поч}, \quad (2)$$

c_i, φ_i - the specific cohesion and the internal friction angle for a certain the fluidity index; $c_{поч}, \varphi_{поч}$ - the same in the initial condition of the soil (I_L=0).

M. Goldstein [16] recorded a significant increase in the specific cohesion at a constant of internal friction angle with an increase in soil density for compacted loamy loam. According to M. Maslov [12] a decrease in density and increase in soil humidity in the course of incomplete consolidation leads to a decrease in φ and c.

In 1948 M. Gersevanov showed that there is a linear relationship between the porosity coefficient e and the logarithm of the limit shear strength lgτ. This issue is most fully resolved by the scientific school of V. Razoryonov [8, 10, 13, 17-22]: Yu. Velykodnyi, G. Zhornik, V. Zabara, M. Zotsenko, V. Kovalenko, I. Skryl, V. Hilobok, V. Shitov, A. Yakovlev. The dependence for the connected soils with the broken structure in the conditions of their water saturation on the basis of penetration tests is established

$$W_i = W_0 - 1/r_0 \cdot \lg R_i / R_0, \quad (3)$$

W_i і W_0 - the value of the total soil water content corresponding to two values of soil porosity coefficient e_i and e_0; R_i - specific penetration resistivity of water-saturated soil with the porosity coefficient e_i; R_0=1 - for the accepted dimension R_i (кPa, MPa) (based on this prerequisite set the value e_0); $1/r_0$ - angular coefficient of linear dependence in coordinates «W - lg$R$».

The link between physical and mechanical parameters in the three-phase state of clay rocks, taking into account the water saturation factor S_r. The equation of the calculation scheme looks like this

$$W_i \cdot L_0 = W - 1/r_0 \cdot \lg R_i / R_0, \quad (4)$$

L_0 - water saturation function that is equal to

$$L_0 = 1 + (1/S_r - 1) \cdot \frac{1/r_0}{1/r}, \quad (5)$$

$1/r$ - angular coefficient of linear dependence for S_r<1 (with W_i=const).

The relationship design scheme of rocks in terms of natural

structure is similar. When solving the problem of establishing the relationship between the physical and mechanical properties of the three-phase state of the rock of the natural structure, it is necessary to determine the following indications - the free term and two angular coefficients of conditional linear equations. The relationship equation looks like this

$$lg(R/R_0) = W_R \frac{1}{e_0} + \frac{\rho_w}{\rho_s} \cdot \frac{1 - M_{kpf}}{1/e_0} - W \frac{M_{kpf}}{1/e_0} - \frac{\rho_w}{\rho_d} \cdot \frac{M_{kpf}}{1/e_0}, \quad (6)$$

W_R - humidity of water-saturated soil at R_0=1 MPa; $M_{kpf} = 1 - (1/e_0)/(1/e)$; $1/e_0$ and $1/e$ - angular coefficients of linear equations respectively for the case of complete water saturation of the rock and subject to constant humidity.

It was proved [10, 13, 17, 20-22] that the indices of expression (6) are affected by the plasticity number, mineralogical composition of the clay component, particle size distribution and mineralogy of the coarse dispersed component.

The condition for establishing the relationship between the physical (W, e) and the mechanical parameters of the soil (R, φ, c, E) is the accumulation of test data to determine these characteristics with a relatively constant the plasticity number and homogeneous geneticall-ly [10, 13, 17, 20-22].

Determination of the correlation equation coefficients for each array of test data is usually performed by the method of least squares with the calculation of the correlation coefficients, variation, and measurement errors.

Therefore, the following dependencies can be set for each soil

$$lg(R/R_0) = A_R - B_R \cdot e - C_R \cdot W; \quad (7)$$

$$lg(E/E_0) = A_E - B_E \cdot e - C_E \cdot W; \quad (8)$$

$$lg(c/c_0) = A_c - B_c \cdot e - C_c \cdot W; \quad (9)$$

$$lg(tg\varphi/tg\varphi_0) = A_\varphi - B_\varphi \cdot e - C_\varphi \cdot W, \quad (10)$$

R_0, E_0, c_0, $tg\varphi_0$ - values equal to the units of the selected dimension. The coefficients A, B, C are functions of soil indicative features: $1/e_0$, $1/e$, W_R.

From here, it is possible to set the following dependencies for a

particular rock

$$\lg(E/E_0) = A_E - (B_E/B_R)A_R - W(C_E - (B_E/B_R)C_R) - (B_E/B_R)\lg(R/R_o) \quad (11);$$

$$\lg(c/c_0) = A_c - (B_c/B_R)A_R - W(C_c - (B_c/B_R)C_R) - (B_c/B_R)\lg(R/R_o) \quad (12);$$

$$\lg(tg\varphi/tg\varphi_0) = A_\varphi - (B_\varphi/B_R)A_R - W(C_\varphi - (B_\varphi/B_R)C_R) - (B_\varphi/B_R)\lg(R/R_o) \quad (13).$$

By the equations of interconnection determine the physical and mechanical properties of rocks. Having the expressions (7-10) for a particular soil variety, the known values of *e* and *W* uniquely set the corresponding values: *R; E; c; φ*.

Using expressions (7-13) according to the values of *W* and *R*, at any point in the array, they uniquely determine the mechanical properties: *E, c, φ*. The method was applied by M. Zotsenko in the study of compacted zones of foundations and artificial bases and preparation of initial data for modeling their work [22].

The example of method validation is the prediction [18, 19] of the variability of the mechanical characteristics of a mixture (70% of tails and 30% of loam) when changing its physical state over a wide range of humidity and density. Correlation equations of the relationship between the mechanical and physical properties of the mixture were obtained

$$\lg E/E_0 = 7{,}652 - 10{,}792 \cdot W - 7{,}897 \cdot 1/\rho_d, MPa \quad (14)$$

(under the Fisher criterion k_f=1,025 and correlation coefficient r=0,924);

$$lg\, c/c_0 = 9{,}706 - 14{,}662 \cdot W - 9{,}582 \cdot 1/\rho_d, \text{кPa}$$

(at k_f =1,092 and r = 0,949);

$$\lg \varphi/\varphi_0 = 2{,}074 - 1{,}363 \cdot W - 0{,}517 \cdot 1/\rho_d, deg. \quad (15)$$

(at k_f =1,547 and r = 0,801). (16)

The multivariate analysis obtained the equation of the relationship between the number of strokes of the cargo, humidity and specific volume of dry mixture.

$$lg\, n/n_0 = 8{,}467 - 13{,}295W - 8{,}748 \cdot 1/\rho_d, \quad (17)$$

n_0=1 (при k_f=1,107 та r=0,948). Therefore, there is a strong relationship between the number of strokes of the cargo, the humidity and the specific volume of dry soil.

Therefore, the relationship between the physical and mechanical properties of small-connecting overburden (sand of various sizes, including clay impurities) has not been investigated. That is, the designer has no information about the mechanical parameters of these rocks in the compacted state without further research.

Therefore, for the practice of designing sand pillows it is important to investigate the relationship between the physical (granulometric composition, clay impurities, skeletal density ρ_d, humidity w) and mechanical (E; φ; c) characteristics of compacted overburden in the pillow composition. Impact on mechanical properties of compacted rocks of mechanism parameters (parameters and mechanism mode; number of passes per track; initial layer thickness) is important

2. Conditions for constructing graphs and equations for the linkages between the physical and mechanical parameters of compacted small-connecting overburden

Therefore, the condition of the correct link (graphs and equations of the form (8-10) or (14-16)) between the physical (w,ρ_d (e) or $1/\rho_d$) and mechanical properties of the rock (E, φ,c) is the accumulation of a statistically valid data set to determine these characteristics for genetically homogeneous rocks with a relatively constant particle size distribution for sands and plasticity for clay rocks. This condition is fulfilled for quaternary sand of three types: 1) sand is fine, homogeneous; 2) a mixture of fine sand, homogeneous with sandy loam, plastic; 3) sand of medium size, homogeneous. There are correct prerequisites for constructing for several small intervals of humidity in semi-log coordinates of the dependence on the specific volume of the skeleton for each of the sand types $1/\rho_d$:1) the deformation module for four pressure intervals σ=0-0,05; 0,05-0,1; 0,1-0,2; 0,2-0,3 MPa-$\lg E = f\left(1/\rho_d\right)$; 2) the internal friction angle $\lg\varphi = f\left(1/\rho_d\right)$ and the specific cohesion $\lg c = f\left(1/\rho_d\right)$. The experimental points on the charts are classified according to the appropriate types of mechanisms and modes of their operation. The experimental points on the charts are classified according to the appropriate types of mechanisms and their modes of operation to detect the influence of the roller parameters on the mechanical properties of

the rocks. It is rational to perform the determination of the equations coefficients of correlation for each array of test data by the method of least squares with the calculation of the correlation coefficients, variation coefficients, measurement errors etc.

3. Linkages between physical and deformation characteristics of compacted fine sand, homogeneous sand

The dependence graphs of the soil deformation module E on its specific skeleton volume $\lg E=f(1/\rho_d)$ at four intervals of compression pressure: 0-0,05 MPa; 0,05-0,10 MPa; 0,1-0,2 MPa (Fig. 3.1); 0,2-0,3 MPa are shown for fine, homogeneous sand compacted by rolling.

The experimental dependence points $\lg E=f(1/\rho_d)$ are presented within each of these pressure ranges σ for seven small humidity intervals W: 0-5% (the soil characteristics number used to construct the complete experimental complexes was n=19); 5-7,5% (n=40); 7,5-10% (n=97); 10-12,5% (n=77); 12,5-15% (n=22); 15-17,5% (n=35); 17,5-20% (n=24).

From the analysis of the graphs $\lg E=f(1/\rho_d)$ it is clear that as the specific volume of the soil skeleton decreases $1/\rho_d$ (that is, as it grows) the modulus of deformation of compacted sand of small, homogeneous linear increases in all experimental humidity intervals w.

According to the graphs $\lg E=f(1/\rho_d)$, the modulus of deformation of compacted fine homogeneous sand E linear increases in all experimental humidity intervals W with a decrease in the specific volume of the soil skeleton $1/\rho_d$ (that is, as it grows ρ_d).

The general equation of the linear dependence of the soil deformation modulus E on the specific volume of the soil skeleton $1/\rho_d$ is

$$\lg\left(E/E_0\right) = A_E - B_E \cdot \left(1/\rho_d\right), \qquad (3.1)$$

E_0=1 MPa; A_E (free member), B_E (angular coefficient with dimension g/cm^3) – empirical coefficients of the linear link quation.

The dependence in the pressure range σ=0-0,05 MPa is deduced for the soil humidity range 0-5% with the number of complete experimental complexes of soil characteristics n=19. Under these conditions, the equation of the linear dependence of the soil deformation modulus E on the specific volume of the soil skeleton $1/\rho_d$ is ex-

pressed by formula (3.2) at a variation coefficient v=0,220.

$$\lg(E/E_0) = 1{,}490 - 1{,}447 \cdot (1/\rho_d). \quad (3.2)$$

The dependence is deduced at in the pressure range σ=0-0,05 MPa for the soil humidity range 0-5% with the number of complete experimental complexes of soil characteristics n=19. Under these conditions, the equation of the linear dependence of the soil deformation modulus E on the specific volume of the soil skeleton $1/\rho_d$ is expressed by formula (3.2) at a variation coefficient v=0,220.

$$\lg(E/E_0) = 1{,}490 - 1{,}447 \cdot (1/\rho_d). \quad (3.2)$$

Dependence $\lg E=f(1/\rho_d)$ in the pressure range σ=0-0,05 MPa for the soil humidity interval w=5-7,5% is expressed by formula (3.3) at n=40 and v=0,161

$$\lg(E/E_0) = 1{,}109 - 0{,}582 \cdot (1/\rho_d). \quad (3.3)$$

Similarly: in the pressure range σ=0-0,05 MPa for a soil humidity interval w=7,5-10%) at n=97 and v=0,119:

$$\lg(E/E_0) = 1{,}199 - 0{,}697 \cdot (1/\rho_d); \quad (3.4)$$

in the pressure range σ=0-0,05 MPa for a soil humidity interval w=10-12,5% at n=77 and v=0,147.

$$\lg(E/E_0) = 1{,}474 - 0{,}954 \cdot (1/\rho_d); \quad (3.5)$$

in the pressure range σ=0-0,05 MPa for a soil humidity interval w=12,5-15 % at n=22 and v=0,127

$$\lg(E/E_0) = 1{,}933 - 1{,}815 \cdot (1/\rho_d); \quad (3.6)$$

in the pressure range σ=0-0,05 MPa for a soil humidity interval w=15-17,5 % at n=35 and v=0,159

$$\lg(E/E_0) = 1{,}955 - 1{,}913 \cdot (1/\rho_d); \quad (3.7)$$

in the pressure range σ=0-0,05 MPa for a soil humidity interval w=17,5-20 % at n=24 and v=0,178

$$\lg(E/E_0) = 1{,}661 - 1{,}518 \cdot (1/\rho_d). \quad (3.8)$$

Similar dependencies $\lg E=f(1/\rho_d)$ is deduced at σ=0,05-0,10 MPa. The humidity intervals w and the number of complete experimental complexes of soil characteristics remain unchanged, and the magnitude of the variation coefficient is:

for soil humidity interval w=0-5 %, v=0,175

$$\lg(E/E_0) = 1{,}358 - 0{,}951 \cdot (1/\rho_d); \quad (3.9)$$

for *w*=5-7,5 % - *v*=0,164,

$$lg(E/E_0) = 1{,}245 - 0{,}730 \cdot (1/\rho_d); \quad (3.10)$$

for *w*=7,5-10 % -*v*=0,127,

$$\lg(E/E_0) = 1{,}318 - 0{,}830 \cdot (1/\rho_d); \quad (3.11)$$

for *w*=10 - 12,5 % - *v*=0,099,

$$\lg(E/E_0) = 1{,}433 - 0{,}795 \cdot (1/\rho_d); \quad (3.12)$$

for *w*=12,5 - 15 % - *v*=0,148,

$$\lg(E/E_0) = 2{,}247 - 2{,}282 \cdot (1/\rho_d); \quad (3.13)$$

for *w*=15-17,5 % - *v*=0,097,

$$\lg(E/E_0) = 1{,}770 - 1{,}533 \cdot (1/\rho_d); \quad (3.14)$$

for *w*=17,5 – 20 % - *v*=0,140,

$$\lg(E/E_0) = 1{,}502 - 1{,}138 \cdot (1/\rho_d). \quad (3.15)$$

Similar dependencies at 0,10-0,20 MPa are shown in Fig. 3.1. The value of the coefficient of variation of empirical expressions is

for *w*=0-5 % (Fig. 3.1,*a*) - *v*=0,095)

$$\lg(E/E_0) = 1{,}727 - 1{,}184 \cdot (1/\rho_d); \quad (3.16)$$

for *w*=5-7,5 % (Fig. 3.1,*b*) - *v*=0,113,

$$\lg(E/E_0) = 1{,}265 - 0{,}417 \cdot (1/\rho_d); \quad (3.17)$$

for *w*=7,5-10 % (Fig. 3.1,*c*) - *v*=0,102,

$$\lg(E/E_0) = 1{,}629 - 0{,}987 \cdot (1/\rho_d); \quad (3.18)$$

for *w*=10-12,5 % (Fig. 3.1,*d*) -*v*=0,099,

$$\lg(E/E_0) = 1{,}839 - 1{,}124 \cdot (1/\rho_d); \quad (3.19)$$

for *w*=12,5-15 % (Fig. 3.1,*e*) - *v*=0,079,

$$\lg(E/E_0) = 2{,}151 - 1{,}760 \cdot (1/\rho_d); \quad (3.20)$$

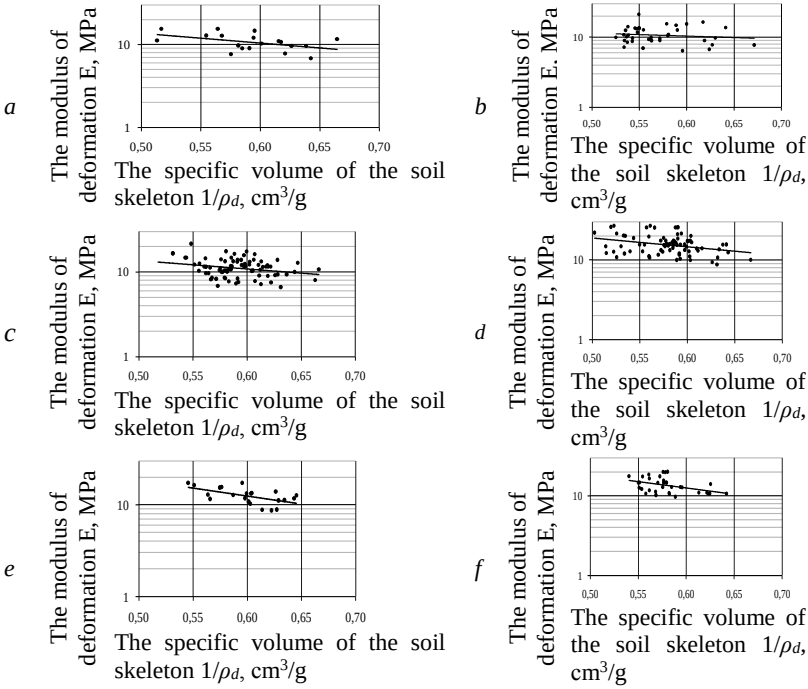

Fig. 3.1. Dependence graphs of the modulus of deformation of fine sand $\lambda gE = f(1/\rho_d)$ on the specific volume of the soil skeleton for pressure intervals σ during compression tests of 0,1-0,2 MPa at different humidity *w*: *a* - 0-5%; *b* - 5-7,5%; *c* - 7,5-10%; *d* – 10-12,5%; *e* - 12,5-15%; *f* - 15-17,5%; *g* - 17,5-20%

for *w*=15-17,5 % (Fig. 3.1, *f*) - *v*=0,081,

$$\lg(E/E_0) = 2{,}040 - 1{,}566 \cdot (1/\rho_d); \qquad (3.21)$$

for *w*=17,5-20 % (Fig. 3.1, *g*) -*v* =0,120,

$$\lg(E/E_0) = 1{,}580 - 0{,}837 \cdot (1/\rho_d). \qquad (3.22)$$

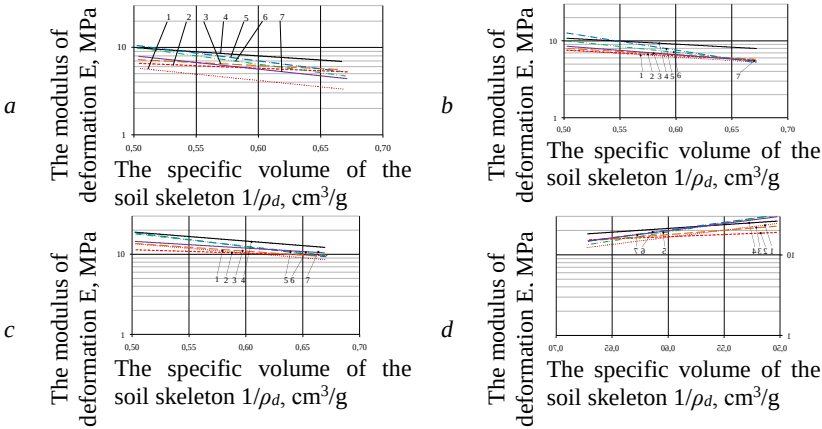

Fig. 3.2. Dependence graphics of the modulus of deformation for fine sand on the specific volume of the soil skeleton lg*E*-*f*(1/ρ_d) for pressure intervals σ during compression tests: *a* - 0-0,05 MPa; *b* - 0,05-0,1 MPa; *c*- 0,1-0,2 MPa; *d* - 0,2-0,3 MPa, at different humidity values *w*: 1 - 0-5%; 2 - 57,5%; 3 - 7,5-10%; 4 - 10-12,5%; 5 - 12,5-15%; 6 -15- 7,5%; 7 - 17,5-20%

Identical dependence lg*E*-*f*(1/ρ_d) is deduced at σ=0,20-0,30 MPa. The value of the variation coefficient of empirical expressions is:

for *w*=0-5 % - *v*=0,081,

$$\lg(E/E_0) = 2{,}282 - 1{,}773 \cdot (1/\rho_d); \quad (3.23)$$

for *w*=5-7,5 % - *v*=0,088,

$$\lg(E/E_0) = 1{,}558 - 0{,}553 \cdot (1/\rho_d); \quad (3.24)$$

for *w*=7,5-10 % - *v*=0,076,

$$\lg(E/E_0) = 1{,}902 - 1{,}084 \cdot (1/\rho_d); \quad (3.25)$$

for *w*=10-12,5 % - *v*=0,075,

$$\lg(E/E_0) = 1{,}893 - 0{,}941 \cdot (1/\rho_d); \quad (3.26)$$

for *w*=12,5-15 % - *v*=0,078

$$\lg(E/E_0) = 2{,}458 - 1{,}917 \cdot (1/\rho_d); \quad (3.27)$$

for *w*=15-17,5 % – *v*=0,078,

$$\lg(E/E_0) = 2{,}591 - 2{,}178 \cdot (1/\rho_d); \quad (3.28)$$

for *w*=17,5-20 % – *v*=0,109,

$$\lg(E/E_0) = 2{,}369 - 1{,}783 \cdot (1/\rho_d). \quad (3.29)$$

Graphic dependences lg$E$-$f(1/\rho_d)$ were also grouped at four pressure intervals during compression tests σ and at seven humidity intervals (Fig. 3.2).

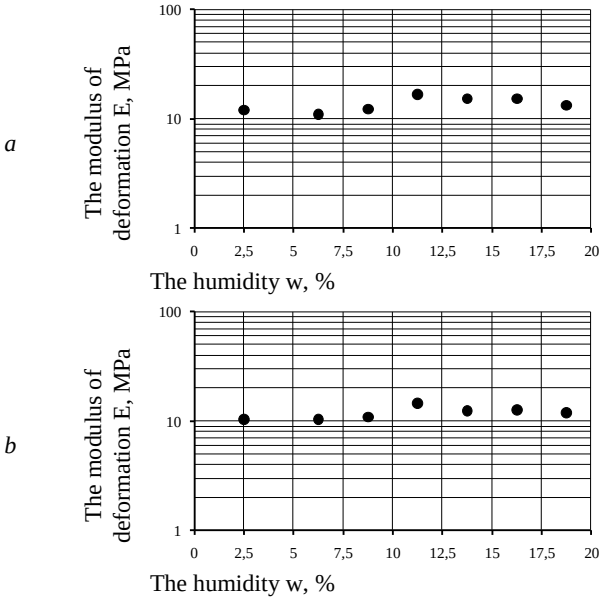

Fig. 3.3. Dependences of the deformation modulus E for fine homogeneous sand on soil humidity w for pressure intervals during compression tests σ=0,1-0,2 MPa for specific volume of soil skeleton a – $1/\rho_d = 0{,}55$; b – $1/\rho_d = 0{,}60$

From the analysis of these graphs and the correlation equations (3.2-3.29), the following generalizations are possible for fine, homogeneous sand compacted by rolling:

- the graphs of the dependence of the deformation modulus E on the specific volume of the soil skeleton lg$E$-$f(1/\rho_d)$ are linearized in semilogarithmic coordinates;

- the size of the deformation modulus of the sand E increases linearly at all experimental humidity intervals w with a decrease in the specific volume of the soil skeleton $1/\rho_d$;

- the value of the soil deformation modulus E increases linearly at a constant value of its humidity, and the linear graphs lg$E$-$f(1/\rho_d)$ at different pressure intervals are close to parallel when increasing the pressure interval during the compression test σ from 0-0,05 to 0,20-0,30 MPa;

- the induced (obtained by rolling) structural strength of the soil p_{str} is fixed for the initial pressure interval of σ=0-0,05 MPa;

- the sand humidity is less significant (this, incidentally, confirms the absence of the humidity parameter or water saturation factor in the reference table B.1 of Appendix B of DBN B.2.1-10-2009) influences the modulus of deformation E (Fig. 3.2-3.3). But it reaches a slightly larger (its maximum) value within each pressure interval at a humidity close to optimal;

- the values of the variation coefficient of all the equations of relation except one (3.2) do not exceed v=0,20, which indicates that the empirical expressions are correct; by the way, with increasing pressure from σ=0-0,05 to σ=0,20-0,30 MPa the variation of the experimental data decreases (at σ=0,20-0,30 MPa the variation coefficient of all equations is v<0,11).

The same results apply for compacted, fine, homogeneous sand with impurity sandy loam sand and medium size, homogeneous sand.

Based on the conclusion that for all types of test sands with increasing compression pressure σ from 0-0,05 to 0,20-0,30 MPa, the deformation modulus increases linearly at constant humidity w (and the sand humidity has little effect on this pattern, Fig. 3.2) and practical parallelism of linear graphs $\lg E$-$f(1/\rho_d)$ at different pressure intervals σ for each type of sand. That is, the variability of the coefficient B_E from the mean values $\overline{B}_E$ within certain limits, it is expedient to reveal the regularities of the change of the coefficient A_E of the equation (3.1) in relation to the pressure $A_E=f(\sigma)$.

Graphs of dependence of the coefficient A_E on the pressure $A_E=f(\sigma)$ for fine, homogeneous sand at different humidity values are deduced.

From them it is easy to see that within the pressure of σ=0-0,30 MPa, under which the experiments were conducted, the dependence $A_E=f(\sigma)$ is quite correct (the values of the variation coefficients for all equations except one do not exceed v=0,20, and the coefficients correlation are greater than r=0,85) approximated by a linear function of the form

$$A_E = A_{E,0} + A_{E.1} \cdot \sigma \cdot \qquad (3.30)$$

$A_{E,0}$ and $A_{E,1}$ (MPa^{-1}) - empirical coefficients to the linear equation (3.30).

In particular, for fine, homogeneous sand the dependence (3.30) has the form:

for w=0-5% at v=0,206 and r=0,930,

$$A_E = 1{,}229 + 3{,}879 \cdot \sigma; \quad (3.31)$$

for w=5-7,5% at v=0,127 and r=0,959,

$$A_E = 1{,}062 + 1{,}851 \cdot \sigma; \quad (3.32)$$

for w=7,5-10% at v=0,182 and r=0,995,

$$A_E = 1{,}109 + 3{,}233 \cdot \sigma; \quad (3.33)$$

for w=10-12,5% at v=0,125 and r=0,902,

$$A_E = 1{,}383 + 2{,}210 \cdot \sigma; \quad (3.34)$$

for w=12,5-15% at v=0,086 and r=0,865,

$$A_E = 1{,}956 + 1{,}926 \cdot \sigma; \quad (3.35)$$

for w=15-17,5% at v=0,146 and r=0,876,

$$A_E = 1{,}693 + 3{,}160 \cdot \sigma; \quad (3.36)$$

for w=17,5-20% at v=0,195 and r=0,805,

$$A_E = 1{,}367 + 3{,}284 \cdot \sigma. \quad (3.37)$$

a

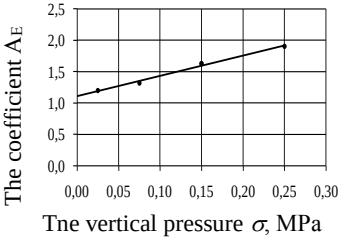

b

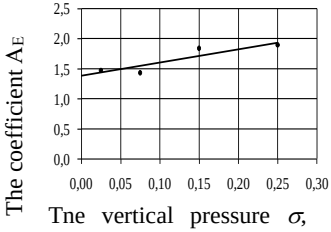

c

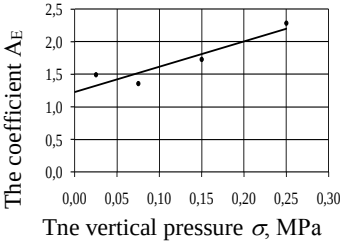

d

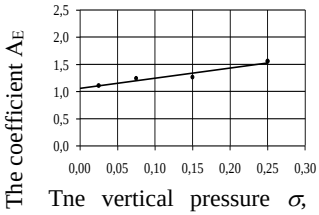

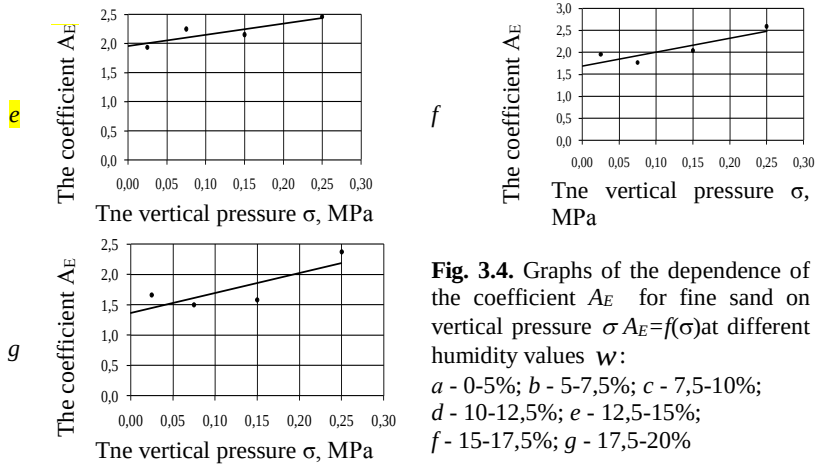

Fig. 3.4. Graphs of the dependence of the coefficient A_E for fine sand on vertical pressure σ $A_E=f(\sigma)$at different humidity values w:
a - 0-5%; *b* - 5-7,5%; *c* - 7,5-10%;
d - 10-12,5%; *e* - 12,5-15%;
f - 15-17,5%; *g* - 17,5-20%

Of course, it is possible to combine expressions (3.1) and (3.30) into one formula

$$\lg(E/E_0) = A_{E,0} + A_{E.1} \cdot \sigma - B_E \cdot (1/\rho_d). \qquad (3.38)$$

Therefore, for the link equations between the specific volume of the soil skeleton $1/\rho_d$ and the deformation modulus compacted by the rolling of each of the three-phase overburden sands, two indicative signs must be defined: the free term A_E and the angular coefficient B_E of the conditional linear equations. The free term for each of the sand types is described by a linear equation depending on the pressure σ_t which the compression tests of the samples were carried out.

4. The influence of the roller operation modes on the linkages between physical and deformation characteristics of compacted overburden sands

Field studies of the influence the technological parameters of rolling of sand pillows layers (static or vibration work mode and roller mass, number of passes in one trace) on regularities of interrelation of physical and deformation properties of compacted overburden, in particular, for fine, homogeneous sand were carried out within such limits:

single drum self-propelled vibrating roller NAMM 3520: 12 passes in vibration mode; 8 passes in vibration mode; 6 - in vibration mode; 5 - in vibration mode; 4 - in static mode;

single drum self-propelled vibrating roller Vibromax VM132: 4 passes in vibration; 4 – in static mode;

single drum self-propelled vibrating roller ATLAS 1140: 8 passes in vibration mode;

trailed pneumatic roller DU-16: 4 passes;

combined rolling: DU-16 roller for 4 passes and NAMM 3520 rollers for 6 passes in vibration mode or Vibromax VM132 for 6 passes in vibration mode.

The possible influence the type and mode of rollers operation on the dependence patterns of the modulus of deformation of the soil on its specific volume of the skeleton lg$E$-f(1/ρ_d) at different pressure intervals σ for each type of sand. That is, the for fine, homogeneous sand, for one of the humidity intervals is investigated in Fig. 4.1 drawing on the graphs of the symbols of each of the above technological modes of rolling the sand pillows layers.

a

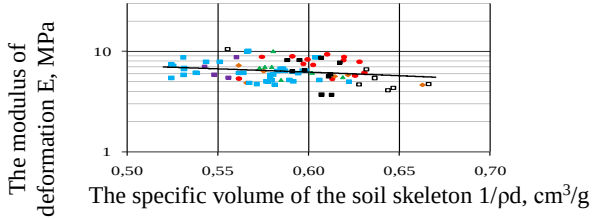

b

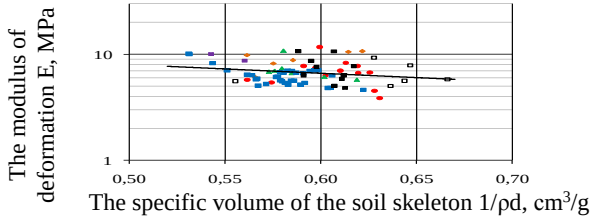

c

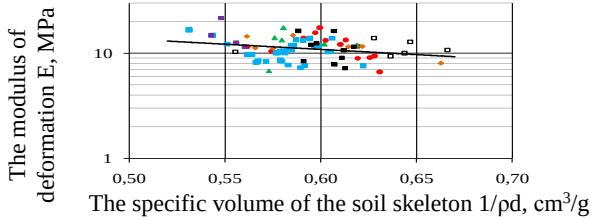

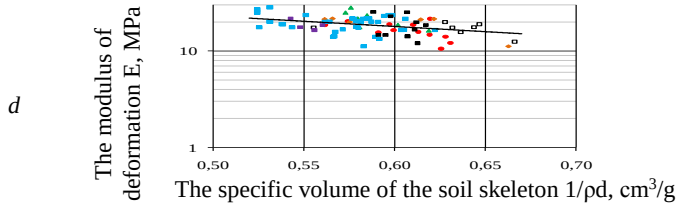

Fig. 4.1. Dependence graphs of the deformation modulus for fine sand on the specific volume of the soil skeleton lg*E*-*f*(1/ρ_d) at different pressure intervals σ for each type of sand. That is, the when rolling with different mechanisms in humidity *w*=7,5-10 % (at compression tests for pressure intervals σ, MPa: *a* - 0-0,05; *b*- 0,05-0,1; *c* - 0,1-0,2; *d* - 0,2-0,3:

Legend: ■ - NAMM 3520 rollers, 8 passes in vibration mode; ■ - NAMM 3520 rollers, 6 passes in vibration mode; ■ - NAMM 3520 rollers, 12 passes in vibration mode; □ - NAMM 3520 rollers, 4 passes; ● - ATLAS 1140 rollers, 8 passes in vibration mode; ▲ - Vibromax VM132 rollers, 4 passes in vibration mode; ◆ - DU-16 rollers, 4 passes

Similar graphs were obtained for fine, homogeneous sand with impurity of sandy loam and medium uniform sand.

From them it is evident that for each type of compacted overburden, regardless of the rollers technological regime and its mass, the deformation modulus *E* increases linearly at the specific volume of the skeleton of the soil decreases 1/ρ_d. That is, under whatever rolling technological parameters, a certain value of the density of the skeleton of the soil ρ_d would not be obtained, for a sand of a certain particle size distribution (and for the same pressure interval in the process of compression testing of specimens) a certain value of the modulus of deformation corresponds.

5. Influence of particle size distribution of compacted overburden sands on the link their physical properties and strength characteristics

Dependent internal friction angles φ and specific cohesion *c* to the specific volume of the soil skeleton lgφ-*f*(1/ρ_d), and $\lg c = f(1/\rho_d)$ like similar graphs, are constructed in semi-logarithmic coordinates for fine, homogeneous sand compacted by rolling. For each type of overburden, these dependencies are defined for four to six small humidity intervals. So for fine, homogeneous sand we have the follow-

ing number of complexes (n) of soil characteristics at different humidity intervals: w=5-7,5% (n=13); w=7,5-10% (n=19); w=10-12,5% (n=22); w=12,5-15% (n=8); w=15 – 17,5% (n=8); w=17,5-20% (n=6).

So in fig. 5.1 shows the dependence graphs of the internal friction angle on the specific volume of the soil skeleton $\lg\varphi$-$f(1/\rho_d)$, and in Fig. 5.2 - specific cohesion dependencies $\lg c$-$f(1/\rho_d)$ for compacted fine homogeneous sand at different humidity intervals. From them it is noticeable that with decrease of the specific volume of the soil skeleton $1/\rho_d$ (as it grows ρ_d), the internal friction angle of the sand increases linearly (though rather slowly, which is generally characteristic of the sands) at all W intervals, and for the specific cohesion of the soil a similar linear increase of its value is much more noticeable. The general equations for the linear dependence of the strength characteristics on the specific volume of the soil skeleton are

$$\lg(\varphi/\varphi_0) = A_\varphi - B_\varphi \cdot (1/\rho_d); \quad (5.1)$$

$$\lg(c/c_0) = A_c - B_c \cdot (1/\rho_d), \quad (5.2)$$

φ_0=1°;c_0=1 кPa; A_φ, B_φ, A_c, B_c – empirical coefficients of equations.

In particular, in Fig. 5.1*a*, the graph of the dependence of the internal friction angle on the specific volume of the soil skeleton $\lg\varphi$-$f(1/\rho_d)$ for fine, homogeneous sand at humidity interval 5-7,5% is presented. The corresponding relation linl (5.1) at n=13 and v=0,047 is expressed by the formula

$$\lg(\varphi/\varphi_0) = 2{,}051 - 0{,}777 \cdot (1/\rho_d); \quad (5.3)$$

for w=7,5-10% (Fig. 5.1, *b*) at n=19 and v=0,040,

$$\lg(\varphi/\varphi_0) = 2{,}209 - 1{,}111 \cdot (1/\rho_d); \quad (5.4)$$

for w=10-12,5% (Fig. 5.1, *c*) at n=22 and v=0,035,

$$\lg(\varphi/\varphi_0) = 1{,}912 - 0{,}607 \cdot (1/\rho_d); \quad (5.5)$$

for w=12,5-15% (Fig. 5.1, *d*) at n=8 and v=0,034,

$$\lg(\varphi/\varphi_0) = 2{,}125 - 0{,}932 \cdot (1/\rho_d); \quad (5.6)$$

for w=15-17,5% (Fig. 5.1, *e*) at n=8 and v=0,025,

$$\lg(\varphi/\varphi_0) = 2{,}458 - 1{,}255 \cdot (1/\rho_d); \quad (5.7)$$

for w=17,5-20% (Fig. 5.1, *f*) at n=6 and v=0,027,

$$\lg(\varphi/\varphi_0) = 2{,}289 - 1{,}200 \cdot (1/\rho_d). \quad (5.8)$$

Dependence graphs of the specific cohesion to the specific volume of the soil skeleton $\lg c = f(1/\rho_d)$ for compacted fine, uniform sand at humidity 5-7,5% is shown in Fig. 5.2, *a*. The correlation equation of the form (5.2) at *n*=19 and $\nu = 0{,}169$ is:

$$\lg(c/c_0) = 3{,}726 - 4{,}406 \cdot (1/\rho_d); \quad (5.9)$$

for *w*=7,5 – 10% (Fig. 5.2, *b*) at *n*=19 and *v*=0,136

$$\lg(c/c_0) = 3{,}356 - 4{,}093 \cdot (1/\rho_d); \quad (5.10)$$

for *w*=10 – 12,5% (Fig. 5.2, *c*) at *n*=22 and *v*=0,181

$$\lg(c/c_0) = 4{,}362 - 5{,}458 \cdot (1/\rho_d); \quad (5.11)$$

for *w*=12,5 – 15% (Fig. 5.2, *d*) at *n*=8 and *v*=0,159

$$\lg(c/c_0) = 4{,}005 - 4{,}781 \cdot (1/\rho_d); \quad (5.12)$$

a

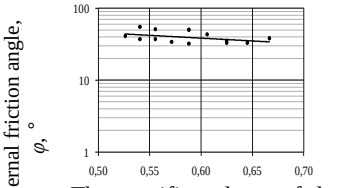

b

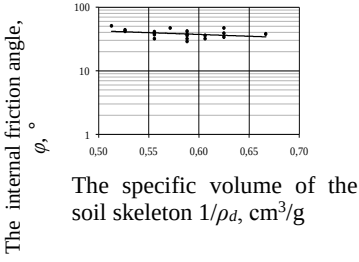

c

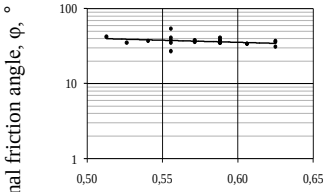

d

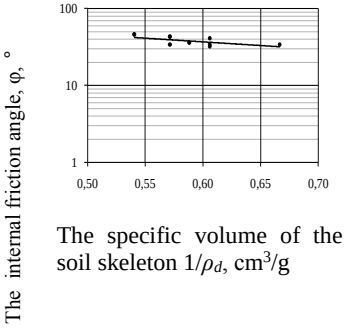

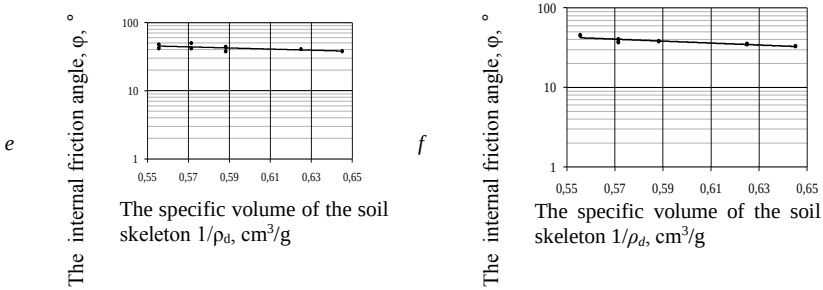

Fig. 5.1. Dependence graphs of the internal friction angle for fine sand on the specific volume of the soil skeleton lgφ-f(1/ρ_d) during tests for single-plane displacement at different humidity w: *a* - 5-7,5%; *b* - 7,5-10%; *c* - 10-12,5%; *d* - 12,5-15%; *e* - 15-17,5%; *f* - 17,5-20%

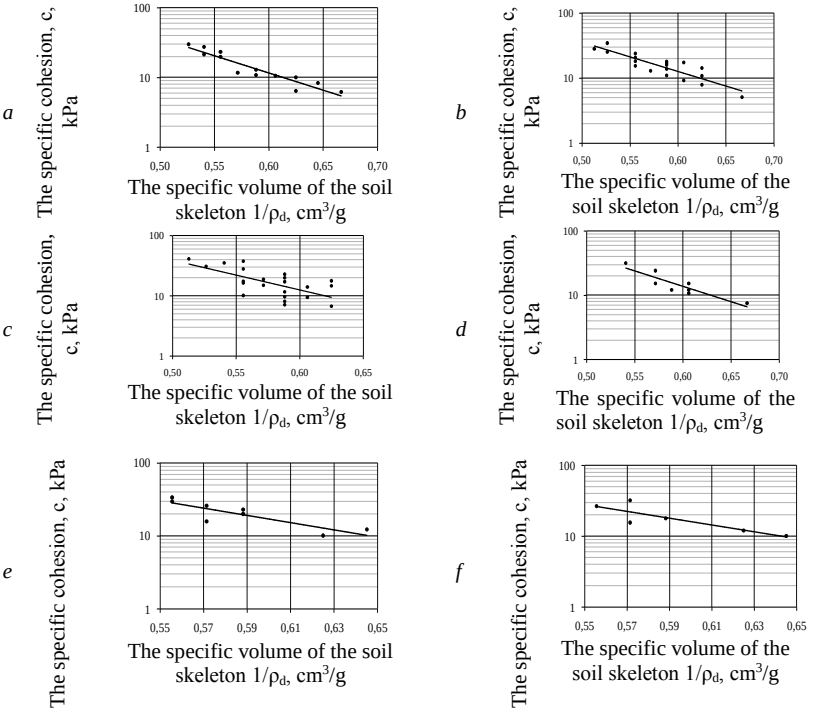

Fig. 5.2. Dependence graphs of the specific cohesion of fine sand on the specific volume of the soil skeleton lg$c$=f(1/ρ_d) when tested for single-plane displacement at different humidity w: *a* - 5-7,5%; *b* - 7,5-10%; *c* - 10-12,5%; *d* - 12,5-15%; *e* - 15-17,5%; *f* - 17,5-20%

for w=15-17,5% (Fig. 5.2, *e*) at n=8 and v=0,133

$$\lg(c/c_0) = 4{,}207 - 4{,}957 \cdot (1/\rho_d); \quad (5.13)$$

for w=17,5-20% (Fig. 5.2, *f*) at n=6 and v=0,143

$$\lg(c/c_0) = 4{,}078 - 4{,}785 \cdot (1/\rho_d). \quad (5.14)$$

Linear graphs $\lg\varphi = f(1/\rho_d)$ and $\lg c = f(1/\rho_d)$ for different humidity intervals w for compacted fine, homogeneous sand are summarized according to fig. 5.3*a* and 5.3*b*. From them it is clear that these graphs are parallel and sufficiently close to each other (especially nomograms $\lg\varphi = f(1/\rho_d)$, and at humidity close to the optimum strength characteristics somewhat larger. The dependences of the internal friction angle and the specific cohesion for fine sand to soil humidity ($\lg\varphi = f(w)$, $\lg c = f(w)$) for different values of the specific volume of the soil skeleton are shown in Figs. 5.4 and 5.5.

a

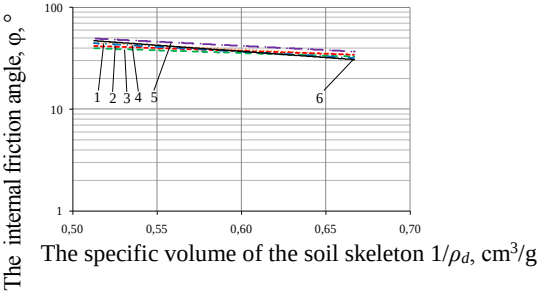

b

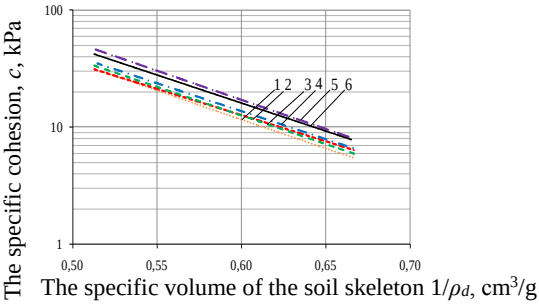

Fig. 5.3. Dependency graphs: *a* - internal friction angle $\lg\varphi = f(1/\rho_d)$; *b* - the specific cohesion $\lg\varphi = f(1/\rho_d)$ for fine sand on the specific volume of the soil skeleton when tested for single-plane displacement at different humidity *w*: 1-5-7,5%; 2-7,5-10%; 3 – 10-12,5%; *4*-12,5-15%; *5*-15-17,5%; *6*-17,5-20%.

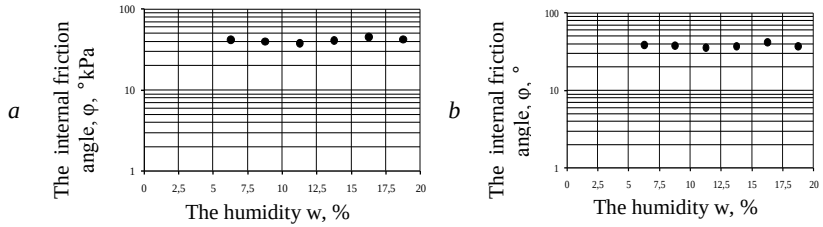

Fig. 5.4 . Dependences of the internal friction angle φ of fine sand on humidity w for the specific volume of soil skeleton: *a* -$1/\rho_d$ =0,55; *b* - $1/\rho_d$ =0,60

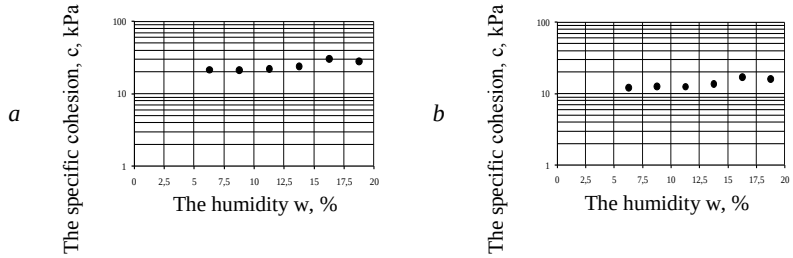

Fig. 5.5. Dependences of specific cohesion c for fine sand on humidity w for specific volume of soil skeleton: *a* -$1/\rho_d$ =0,55; *b* - $1/\rho_d$ =0,60

According to the analysis of graphs and equations of the link strength and specific volume of the skeleton of the soil $\lg\varphi=f(1/\rho_d)$ and $\lg c=f(1/\rho_d)$ the following conclusions can be drawn sand compacted by rolling compacted rolling of all types of exploratory sands:

- dependence graphs of the internal friction angle and the specific cohesion on the specific volume of the soil skeleton are linearized in semilogarithmic coordinates ;
- the internal friction angle and specific cohesion increase linearly at all humidity intervals as the specific volume of the soil skeleton decreases;
- humidity practically does not affect the internal friction angle of sand, and the specific cohesion is slightly higher at humidity close to optimally;
- the variation coefficient for all the link equations (5.1) and (5.2) do not exceed v=0,20, which proves that they are sufficient correctness.

6. Influence of operating roller modes on the link beetwen physical properties and strength characteristics of compacted overburden sands

The possible influence of the technological rolling parameters for the pillow layers on the link regularities beetwen the indices of the strength of the compacted overburden sands and the specific volume of the skeleton $\lg\varphi=f(1/\rho_d)$ and $\lg c=f(1/\rho_d)$ was investigated by the method tested for the soil deformation module.

In particular, after drawing on the corresponding graphs (Fig. 6.1 and 6.2 – for sand of small, homogeneous), the notation of each of the technological modes of rolling of the pillows layers listed in item 4, it is established that the rolling technological parameters does not significantly affect the nature of the set in item 5 dependencies $\lg\varphi=f(1/\rho_d)$ and $\lg c=f(1/\rho_d)$.

That is, (similar to the conclusion to item 4), under which the rolling technological parameters would not obtain a certain value of the density of the skeleton of the soil ρ_d, for the sand of a certain granulometric composition correspond to certain values of the internal friction angle φ and the specific adhesion of the soil c.

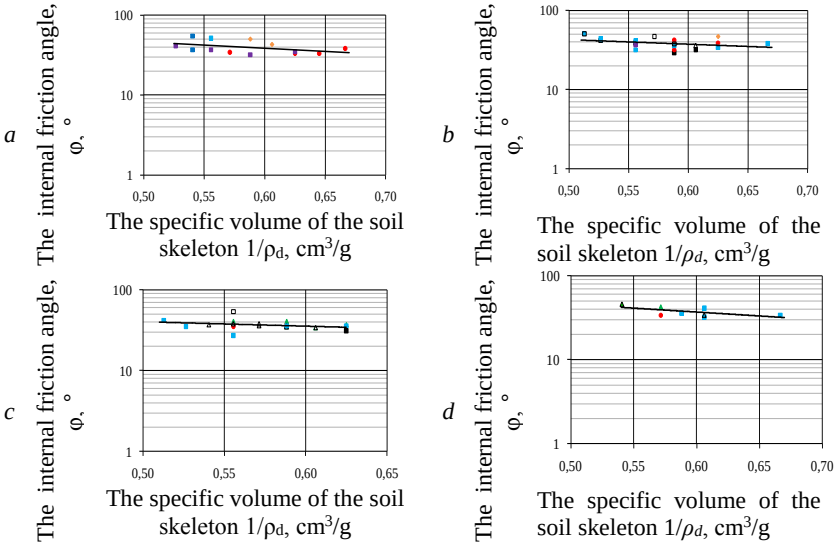

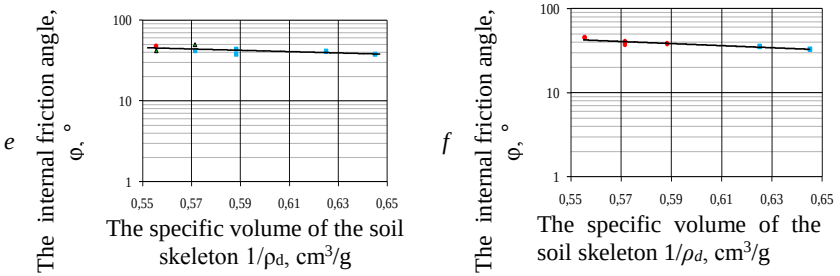

Fig. 6.1. Dependence graphs of the internal friction angle for fine sand on the specific volume of the soil skeleton when rolling with different mechanisms at different humidity *w*: *a* – 5-7,5%; *b* – 7,5-10%; *c* – 10-12,5%; *d* – 12,5-15%; *e* – 15-17,5%; *f* – 17,5-20%

Legend: ■ – NAMM 3520 rollers, 20 passes in vibration mode; ■ – NAMM 3520 rollers, 8 passes in vibration mode; ■ – NAMM 3520 rollers, 6 passes in vibration mode; ■ – NAMM 3520 rollers, 5 passes in vibration mode; □ – NAMM 3520 rollers, four passes; ■ – NAMM 3520 rollers, 6 passes in vibration mode and DU-16, 4 passes; ● – ATLAS 1140 rollers, 8 passes in vibration mode; ▲ – Vibromax VM132 rollers, 4 passes in vibration mode; △ – котюк Vibromax VM132, 4 проходи; ▲ – Vibromax VM132 rollers, 6 passes and DU-16, 4 passes; ◆ – DU-16 rollers, 4 passes

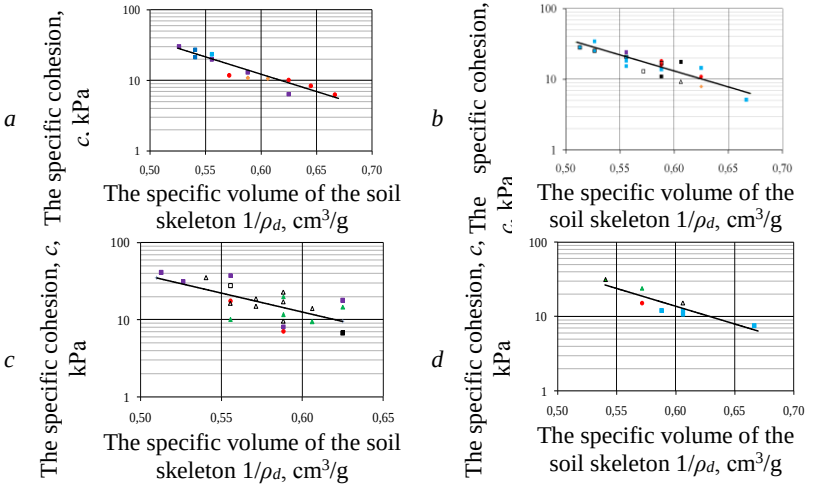

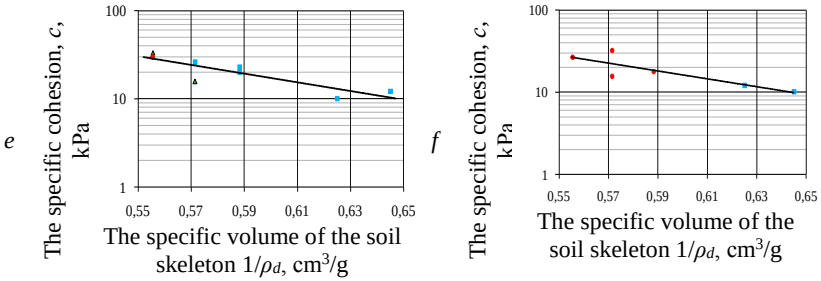

Fig. 6.2. Dependence graphs of the specific cohesion of fine sand on the specific volume of the soil skeleton when rolling with different mechanisms at different humidity w: *a* - 5-7,5%; *b* - 7,5-10%; *c* - 10-12,5%; *d* - 12,5-15%; *e* - 15-17,5%; *f* - 17,5-20%.

Legend:■ – NAMM 3520 rollers, 20 passes in vibration mode; ■ – NAMM 3520 rollers, 8 passes in vibration mode; ■ – NAMM 3520 rollers, 6 passes in vibration mode;■ – NAMM 3520 rollers, 5 passes in vibration mode;□ – NAMM 3520 rollers, four passes;■ – NAMM 3520 rollers, 6 passes in vibration mode and DU-16, 4 passes; ● – ATLAS 1140 rollers, 8 passes in vibration mode; ▲ – Vibromax VM132 rollers, 4 passes in vibration mode; △ – котюк Vibromax VM132, 4 проходи; ▲ – Vibromax VM132 rollers, 6 passes and DU-16, 4 passes; ◆ – DU-16 rollers, 4 passes

Conclusions. According to the results of determining the linkages between the physical and mechanical parameters of compacted overburden in quarries of iron quartzite deposits, taking into account the parameters of their rolling, possible conclusions.

1. The graphical and analytical dependences of the modulus of deformation and the strength characteristics of different types of compacted overburden in quarries of iron quartzite deposits with their physical properties (specific volume of the soil skeleton $1/\rho_d$) are considered taking into account the influence of the rolling parameters.

2. Dependences of the deformation modulus, the internal friction angle and the specific cohesion of all types experimental overburden (sand fine, homogeneous; mixture of sand fine, homogeneous with sandy loam; sand of medium size, homogeneous) on the specific volume of the skeleton of the soil $\lg E=f(1/\rho_d)$, , $\lg c=f(1/\rho_d)$ have the linear character in semilogarithmic coordinates/

3. By increasing the pressure interval in the process of compression tests σ from 0-0,05 to 0,20-0,30 MPa, the value of the modulus of rock deformation increases linearly at the constant humidity, and the linear graphs $\lg E=f(1/\rho_d)$ at different pressure intervals σ – close to parallel for each type of sand.

4. Whatever the technological parameters of rolling, a certain val-

ue of the skeleton density of the rock ρ_d would not be obtained, for the sand of a certain particle size distribution correspond to certain values of the internal friction angle φ, the specific soil cohesion c and the modulus of deformation of the soil E.

5. The values of the variation coefficients of virtually all the correlation equations of physical and mechanical properties of compacted small-connecting overburden rocks do not exceed v=0,20, and the correlation coefficients are greater than r=0,85, which proves that the empirical expressions are correct.

6. To establish the correlation equations between physical (specific volume of the skeleton) and mechanical (modulus of deformation, internal friction angle, specific cohesion) by the properties of the three-phase state of each of the sand types, it is necessary to determine its two indicative features – free member (respectively A_E,A_φ,A_c) and angular coefficient (B_E,B_φ,B_c) in conditional linear equations. The free term A_E for each of the sand types is described by a linear equation depending on the pressure σ at which the compression tests of the samples were carried out.

References

1. **Krutov, V. I., & Tanatarov, N. T.** (1993). Fiziko-mehanicheskie harakteristiki neodnorodnyh uplotnennyh gruntov. Osnovaniya, Fundamenty i Mehanika Gruntov, (3), 2-5.

2. **Vynnykov, Yu. L., Kharchenko, M. O., Lopan, R. M., & Manzhalii, S. M.** (2017).Heotekhnichni vlastyvosti shtuchnykh osnov dlia obiektiv hirnycho-zbahachuvalnoho kompleksu. Poltava: PoltNTU.

3. **Vynnykov, Yu. L., Kharchenko, M. O., Dmytrenko, V. I., & Drozd, I. S**. (2019). Ubstantiation of the use conditions small-connecting quarries overburden of iron quartzite deposits for artificial bases of the mining and concentrating complex objects. In Traditions and innovations of resource-saving technologies in mineral mining and processing (Multi-authored monograph, pp. 248-265). Petroșani, Romania: UNIVERSITAS Publishing.

4. **Ouni, M. R., Bouassida, M., & Das, B. M.** (2009). Vibro compaction improvement of Tunisian liquefiable sands. In Proc. of 17th Intern. Conf. on Soil Mechanics and Geotechnical Engineering (pp. 2366-2369). Olexandria: Amsterdam, Berlin, Tokyo, Washington: JOS Press.

5. **Phoon, K. K.** (2008). Reliability-based design in geotechnical engineering. Computions and applications . New York: Taylor & Francis.

6. **Vaníček, I., & Vaníček, M.** (2006). Embankment of transport infrastructure and waste or recycled materials . In Proc. of the XIIIth Danube-European Conf. on Geotechnical Engineering (Active Geotechnical Design in Infrastructure Development, Vol. 1). Ljubljana.

7. **Briaud, J.-L.** (2013). Geotechnical Engineering: Unsaturated and Saturated Soils . Wiley.

8. **Zotsenko, M. L., Kovalenko, V. I., Yakovliev, A. V., Petrakov, O. O., Shvets, V. B., Shkola, O. V., … Vynnykov, Yu. L.** (2004). Inzhenerna heolohiia. Mekhanika gruntiv, osnovy ta fundamenty (pidruchnyk). Poltava: PoltNTU.

9. **Kazarnovskij, V. D.** (2007). Geotehnicheskie problemy pri vozvedenii nasypej. In Tr. konf. (Rossijskaya geotehnika – shag v XXI vek. , Vol. 2, pp. 105–113). Moskva: NIIOSP.

10. **Kovalenko, V. I., Razorenov, V. F., & Hilobok, V. G.** (1981). Issledovaniya uplotnyaemosti svyaznyh gruntov. Voronezh: VGU.

11. **Kuzahmetova, E. K**. (1997). Osnovy prognoza osadki vysokih nasypej pri ispolzovanii glinistyh gruntov s vlazhnostyu vyshe optimalnoj (dissertation). MADI, Moskva.

12. **Maslov, N. N.** (1982). Osnovy inzhenernoj geologii i mehaniki gruntov . Moskva: Vyssh. shk.

13. **Razorenov, V. F.** (1980). Penetracionnye ispytaniya gruntov: Teoriya i praktika primeneniya . Moskva: Strojizdat.

14. **Van Impe, W. F., & Verastegui Flores , R. D.** (2007). On the design, construction and monitoring of embankments on soft soil in underwater conditions . Saint Petersburg: NPO «Georeconstruction – Fundamentproject».

15. **Pooley, E. J., Laue, J., & Springman, S. M.** (2009). Assessment of the use of dynamic compaction on double porosity clay landfill . In Proc. of 17th Intern. Conf. on Soil Mechanics and Geotechnical Engineering. (pp. 2252–2255). Olexandria: Amsterdam, Berlin, Tokyo, Washington: JOS Press.

16. **Goldshtejn, M**. (1971-1979). Mehanicheskie svojstva gruntov (Vol. I, II, III). Moskvva: Strojizdat.

17. **Velikodnyj, Yu. I**. (1974). Eksperimentalnye issledovaniya osobennostej vyyavleniya vzaimosvyazi mezhdu pokazatelyami fizicheskogo sostoyaniya i prochnostnymi svojstvami svyaznyh gruntov (dissertation). OISI, Odessa.

18. **Iermakova, I.** (2006). Osoblyvosti dynamichnoho ushchilnennia gruntovykh sumishei z vykorystanniam vidkhodiv hirnychoho vyrobnytstva – «khvostiv» (Doctoral dissertation, PDABA, 2006). Dnepropetrovsk.

19. **Zotsenko, M.** (2005). Vykorystannia «khvostiv» Poltavskoho HZK pry vlashtuvanni zemlianykh sporud. Svit heotekhniky, (4), 7-11.

20. **Yakovliev, A. V., Vynnykov, Yu. L., & Yakovliev, V. S.** (2004). Dosvid rehionalnoho normuvannia deformatyvnosti ta mitsnosti hlynystoho gruntu metodamy penetratsi. In Budivelni konstruktsii: Mizhvid. nauk.-tekhn. zb. (Vol. 1, pp. 217–222).

21. **Zotsenko, M., Vynnykov, Y., & Yakovlev, A**. (2010). Modern practice of determination of strength characteristics of cohesive soils by penetration methods . In Proc. of XIVth Danube – European Conf. on Geotechnical Engineering (pp. 245–253). Bratislava: Slovak University of Technology.

22. **Zotsenko, M. L., & Vynnykov, Yu. L.** (2019). Fundamenty, shcho sporudzhuiutsia bez vyimannia gruntu. Poltava: PoltNTU.

PROSPECTS OF GAS OIL PIPELINES RELIABILITY GROWTH BY PIPE STEELS IMPROVEMENT

Makarenko V.D.
Poltava National Technical Yuri Kondratyuk University
DCs (Engineering), Professor, professor of the Department
of Oil and Gas Engineering and Technology, Ukraine

Manhura A.M.
Poltava National Technical Yuri Kondratyuk University
Senior Lecturer, head of the Department of Oil and Gas Engineering
and Technology, Ukraine

Zimin O.L.
Poltava National Technical Yuri Kondratyuk University
Senior Lecturer, head of the Department of Oil and Gas Engineering
and Technology, Ukraine

Nohina A.M.
Poltava National Technical Yuri Kondratyuk University
Student of the Department of Oil and Gas Engineering
and Technology, Ukraine

Abstract. State and main directions for solving problems related to high load carrying capacity and operational reliability of long-running oil and gas pipelines of different capacity are retrospectively considered. It is shown that the solution of problems set to the rolling industry on the basis of ordinary low-alloy normalized steels is no longer possible, and therefore the new approaches are needed to develop the production of low-pearlitic and pearless steels obtained by the method of controlled rolling with a stepped hot working. Thus, high mechanical-corrosion characteristics of such steels are achieved due to minimum alloying (for example, carbonitride elements), due to maximum fragmentation of the structure during rolling and controlled high-speed cooling. Specific working conditions of pipes in high-pressure gas pipelines, which differ sharply from the working conditions of metal in other metal structures, are considered in detail. The requirements for steel and welding joints of pipes depending on the working parameters of the pipelines are presented in order to prevent their destruction. The possibility of the operational reliability increase of the pipelines, depending on strength factors, mechanical properties and quality of the pipes is substantiated. The most promising ways of increasing the residual (accident-free) pipeline resource are formulated, taking into

account the influence of degradation processes caused by the presence of harmful impurities of sulfur, hydrogen, and non-metallic inclusions in the metal.
Keywords: pipeline, welded joint, metal structure, corrosion, alloying, operation.

The oil and gas industry is a basic sector of the Ukrainian economy. Increased production and transportation of oil and gas, a systematic increase in the capacity of oil and gas pipelines under construction, and an increase in their length, determine a large metal intensity of oil and gas industry, which annually consumes hundreds of thousands of tons of steel, mainly in the form of pipes. [1-11,21,22,19,20,23-35]. The need for a stable supply of raw materials and fuels to the industry and rigid requirements to ensure the efficiency of pipelines require not only a high cost of metal for the production of pipes, but also the use for these purposes of steels with too high properties. In this regard, when developing steel for pipes, in addition to the requirements of high reliability in operation, there is a question of ensuring their minimum cost with high durability, toughness and cold resistance, which will allow to minimize the steel intensity of gas pipelines [21,22].

Nowadays, the requirements for pipe steel strength have rised exponentially (from 480-500 to 600-700 MPa), while increasing its viscosity and weldability in field conditions. Pipe metal viscosity requirements of optional 0.5MJ / m^2 on standard round Mesnager specimen increased to 0.8-1.2 MJ / m^2 on V-notch Sharpy specimen [9-16]. All this has led to an intensive development of scientific research in the metallurgical and pipeline industries.

It is no longer possible to solve these problems on the basis of conventional low-alloy normalized steels, since in such production, an increase in the strength of the steel will inevitably lead to a decrease in its viscosity and a deterioration of weldability. [17,19,20].

Over the past 20-25 years, a number of Ukrainian and Russian factories have organized the production of a new type of low-pearlitic steel and non-pearlitic steels obtained by controlled rolling [15,16]. High properties of this type of steel are achieved at minimal alloying (microalloying with carbonitride elements) due to maximum fragmentation of its structure during rolling and controlled cooling. Increasing the plasticity and viscosity of the steel is due to the

formation of a homogeneous structure and substructure, low content of harmful impurities, reducing the level of local internal stresses. The achievement of metallurgists in this area can be illustrated by the reduction of sulfur content in the metal – from 0.04 to 0.002-0.006%, grain size - from 7-8 number to 12-14 [12]. The physical essence of a new type of pipe steel is to form a possibly more homogeneous and dispersed structure. This type of steel can be obtained by using different modes of controlled rolling or thermal improving [19,28-32].

The process of controlled rolling allows to obtain sheet steel, microalloyed with carbonitrides, with the highest complex of properties by giving it a special structure. For this purpose, rolling is carried out according to a specially designed program based on the optimal combination of metal temperature and the amount of elastic deformation (compression) of steel under the conditions of carbonitrid precipitation, which provide the desired structure [21,22].

For the effective controlled rolling, the chemical composition of steel must be selected according to the number of basic alloying elements - carbon, manganese, silicon and microalloying impurities - vanadium, niobium, nickel, molybdenum, etc. Steel must be sufficiently cleaned from harmful impurities, first of all, from sulfur; treated with rare earth elements (eg. cerium) to prevent the formation of elongated strip and needle-like impurities [15,16,30].

In general, controlled rolling by programing the carbonitride phase during hot deformation produces steel with the highest strength, toughness and cold resistance properties with minimal alloying. For further improving the properties of the steel, after the end of the cycle of controlled rolling, in the temperature range from 800-700 to 500-400ºC an accelerated adjustable cooling is carried out in special installations [18]. This operation completes structural transformations in the desired direction, further enhancing the strength properties of the steel, almost without reducing the viscosity and cold resistance characteristics. The combination of a high degree of steel purification from harmful impurities, its microalloying with carbide-forming elements with processes of continuous casting, controlled rolling and accelerated controlled cooling made it possible to obtain a particularly high quality steel for

the production of pipes with minimal consumption of expensive and scarce alloying elements. [18-20].

An increase in the capacity of pipelines and a decrease in the gas transfer temperature necessitated the development of a new pipe designs and a new technology for their production, appeared multilayer pipes from twisted shells, two-layer spiral-welded pipes, seamless pipes from hollow billets obtained by the method of continuous casting of molten steel, etc..

In theoretical terms, the basis for the development of a new steel grades for gas pipelines, proceed from the ability to control the properties of steel by maximum fragmentation of its structure and substructure in the process of controlled rolling, followed by the use of accelerated controlled cooling. In addition, the main focus will be set on improvement and production development of thermally reinforced pipes. The rapid progress made in the production of progressive pipe steels over the past 15-20 years is well illustrated by the following figures. The temporary resistance of the pipe metal increased from 500-540 to 600-650 MPa, the yield strength increased even more. The cold resistance of steel, that is, the temperature of metal transition to the brittle state, decreased from +5÷0 to -15÷-25^{o}C and even to -40 ^{o}C when evaluating it with relation to the main gas pipelines [18,22].

The viscosity of the steel, estimated by Sharpie (KCV), increased from 0.1-0.2 MJ/m^2 at the temperature -15 °C to 0.8-1.2 MJ/m^2 at the same temperature. Pipe steels with a viscosity of 1.5-2 MJ/m^2 and above have been developed [21,22].

Further improvement of the pipe properties and improvement of their economic performance will be achieved when solving complex measures. It can be expected that the focus will be on reducing the cost of alloying impurities and complete eliminating of scarce elements such as molybdenum, with some improvement in the strength of pipe steel, as well as viscosity and cold resistance.

Great advances have been made in improving the properties of pipe steels at low alloying element costs. With the organization of mass production of modern low-pearlitic steels, controlled rolling for the manufacturing of pipes, the interest of consumers to the pipes of a new structures has sharply decreased. Despite the large number of

proposed structures, technical development to the level of industrial testing is made only for two-layer spiral-welded pipes and multilayer pipes made of shells. Apparently, in the future we can not expect the development of new pipe designs, since in fact the operating parameters of gas pipelines are already close to optimal. In addition, the development of pipe production will be determined by the technical and economic indicators of products transportation through pipelines, oil and gas reserves, which are far from endless [21].

In the near future (2020-2030), there will be a need for the construction of powerful gas pipelines, as well as the development of a wide network of small product pipelines, a system of industrial, collecting networks of different diameters and pressures up to high (about 12-35 MPa). Therefore, depending on the operating parameters of gas pipelines and industrial networks, types of pipes that differ in diameter and construction, and, most importantly, in the type of steel, should be produced. The classification of pipes has largely been determined. Here is a rough schematic specification of pipes types and steels for oil pipelines, which will be discussed below:

- for the pipelines with a diameter of 325-530 mm of responsible use at a pressure of 10 MPa and higher at low pumping temperatures, as well as for the pipelines transporting certain types of petroleum products, only seamless tubes of rolled blanks should be used, for example, supplied by TU 24-3-1128-82 for the construction of gas elevators, ie pipelines intended for injection of associated gas into the reservoir at a pressure of 12 MPa and above.

Similar quality seamless pipes were used to construct ammonia pipelines. As a rule, at a diameter of less than 530 mm (depending on the pressure in the pipeline), economical and reliable pipes made of simple carbon steels of grades 10 and 20 (GOST 1050-74), as well as steel grades ВСт3 (GOST 380-71) in hot-rolled or heat-treated state. It should be noted that heat-treated steels are the most competitive with the low alloy steel grade 09G2C.

- for the pipelines with a diameter of less than 500 mm, use seamless and welded tubes of simple carbon hot-rolled and heat-strengthened steels; there is a separate question regarding the pipes of the specified diameter, but which are designed to operate at a pressure of 10-35 MPa;

- for the pipelines of 500-1020 mm use welded pipes of simple low-alloy steels of grade 17G1C in hot-rolled normalized or heat-strengthened state;

- for the pipelines with a diameter of 1020-1420 mm, intended for work under high pressure, use welded pipes made of steels of controlled rolling and low-alloy heat-strengthed steels, as well as pipes of special designs.

Pipes - the main structural element of any pipelines. Their quality, the properties of the metal and the welded joints largely determine the possible failures, stops and crashes in the pipelines, as well as the magnitude and consequences of failures and accidents. Therefore, it is necessary to know the requirements for steel and welding of pipes, depending on the operating parameters of the pipelines in order to prevent their destruction. Specificity of gas pipelines operation is conditioned by fundamentally different requirements for steel pipes of large diameter for high working pressure in comparison with any other steel structures. [12,18,21].

The data about the nature and mechanism of long plasic fracture inhibition are of the most useful practical utility and difficulty. The physical essence of such destruction is as follows. When the pipeline breaks, the compressed gas is sent to the formed discontinuity (crack), while seeking to deploy the pipe in the sheet and its edges, thus contributing to the destruction at high speeds. At the same time, as a result of gas decompression from the pipeline, as the fracture propagates, the pressure acting on the sides of the pipes at the top of the crack is reduced. The action of these two factors and the properties of the pipe metal determine the nature and extent of the fracture. The peculiarity of viscous fracture of gas pipelines is the formation of a wide zone of plastically deformable material along the edge of the fracture. Therefore, the propagation of high-speed long plastic fracture in the pipe is resisted by a large volume of metal working in the elastic-plastic zone. It is known that the physical nature of pipe steel resistance to the plastic fracture in the pipe is determined by its tensile strength under high-speed loading and the volume of deformable metal in the fracture zone. However, the absence of high-speed test machines with loading speeds of 100-300 m/s still prevents the physically correct determination of steel pipes resistance of the gas pipeline destruction, resulting in the use of the

approximate indirect method of evaluating the properties of steel on samples that are tested for impact testing of the pipes prior to destruction, including testing of pipe sections by air or gas. In the pipeline design and construction process, it is necessary to consider in detail the resistance of pipe metal and welding joints to fracture under conditions of oil and gas pipelines operation.

The complexity of accounting for pipelines under cyclic loading is that the resistance of a pipe metal and welding joints is evaluated by the test results of the samples for axial tensile, while the metal in the pipelines operates under conditions of biaxial stress state in the presence of structural and technological concentrators which can significantly reduce the cyclic strength of the pipeline. Therefore, it is important, along with the correct choice of the pipes at the stage of designing to reduce the amplitude of oscillations and the steepness of the pressure waves arising from a complete stop of pumping stations [19-21]. The practice of oil pipelines operating shows that the cyclic loads caused by the dynamic (turbulent) pumping process, in some cases, lead to the formation of fatigue cracks in the concentrators that cause a pipelines breakage.

It is known [21] that existing hydraulic pressure test methods that cause circular stresses at the lower points of the pipelines, equal to or even larger than the nominal pipe metal yield stress, allow to detect sufficiently defective sections of pipelines and thus ensure reliable and practically trouble-free operation of the structure.

Pipeline transportation is considered to be one of the most economical means of delivering liquid and gaseous products over long distances with minimal loss of product in the course of delivery to consumers. Modern pipelines are exceptionally long metal structures with a length exceeding thousands of kilometers.

It is known [17] that the destruction of gas pipelines is too dangerous. The area of environmental impact from the site of destruction ranges from several hundred meters to several kilometers. Particular danger during destruction is associated with the possibility of gas contamination of territories and settlements, the formation of an explosive mixture of gas and air, inflammation of transported products, their possible penetration into large bodies of water. It is known [11], for example, that only 1 tonne of spilled oil creates an 18 km^2 oil film on the surface of water bodies. In such

cases, the complete restoration of the ecological balance requires the implementation of a whole complex of remediation works, which is associated with high material costs.

The working conditions of the pipe metal in a high-pressure gas pipelines are very specific, sharply different from the operating conditions of the metal in other metal structures, which is caused by the following factors [7,8,17,19].

1. Exploitation of metal pipes of the same pipeline due to its large length is carried out in dramatically different natural and climatic conditions - from sub-zero temperatures in the northern regions of the country to plus in the southern. The same conditions determine a wide range of types and mechanical characteristics of the soils in which the pipeline is laid; possibility of plastic deformation of the pipes when crossing various natural obstacles - water obstacles, swamps, mountains, lakes, etc

In underground gas pipelines, the metal works at ground temperature. Fixing of the pipes with a diameter up to 1020 mm with soil is carried out on the area of several tens of meters long. As shown by the results of experimental measurements of elastic axial displacements and stresses taken during the cutting of an emergency underground gas pipeline with a diameter of 425 mm, fixing of the pipes with soil is carried out at a length of 25-50 m. Moving the ends of the pipes at the point of incision reached ≈ 29 mm, and longitudinal stresses a ≈ 200 MPa. In the pipelines with diameters of 1020 mm or more, fixing of the pipeline with soil is not always sufficient; the temperature regime and the magnitude of the longitudinal deformations are largely determined by the conditions of operation of the air cooling apparatus (ACA) and their number. In the case of ACA absence, the temperature of the pipeline may increase along its length, as the soil is no longer able to absorb the heat obtained by gas during compression. Therefore, securing absence of powerful gas pipelines in soils, preventing them from rising or bending in swampy and flooded places is a difficult task that cannot always be reliably solved, so the stability of the pipeline is not always secure.

2. Depending on climatic conditions, the metal of the pipes is operated in a wide temperature range - from 30...40 °C in summer to

-15 ... -20 °C in winter, and in the northern climatic zones in the areas of the above-ground routing the minimum operating temperature can be much lower. Construction and installation works on pipelines is in some cases are carried out only in winter at temperatures up to -40°C.

3. During the amortization cycle (more than 30 years), the pipe metal works almost constantly in a two-axis stress state with different, depending on many factors, ratio of stresses in the circular and longitudinal directions. In addition, metal pipelines are subjected to low-cycle loads, which in some cases can cause stresses that reach a yield strength.

The influence of pipelines scheme stressed state on the plastic properties of the pipes metal is clearly traced by the change in a relative elongation. Thus, when on flat fivefold specimens with a uniaxial tensile elongation is 20-30%, then in the conditions of flat stress state in hydraulic tests before the destruction of full-sized pipes, the plastic elongation of the perimeter reaches only 3-7%, and in high-viscosity plastic pipes of controlled rolling steels - 8-12%.

4. In metal pipelines, as a rule, the inevitable presence of concentrators - burrs, scratches, oriented along the forming pipe. They can be of factory, transport and construction origin. The action of stress concentrators is enhanced by the deflection of the cylindrical pipe due to the oval cross section and the presence of dents.

Experimental studies have allowed to determine the change of circular deformations of the outer surface from the internal pressure in pipes with different ovalities (in section along the small axis of the oval). In particular, as the ovality decreases due to the increase in internal pressure, the value of deformations in the specified cross section increases the faster the greater the ovality in the initial state. At a pressure of 1 MPa, local deformations can reach values corresponding to the yield stress, at a more or less low value of the average stresses in the pipe metal. The maximum value of local deformation is about 0.6% at a pressure of 5.5 MPa, then the increase in deformation ends, which corresponds to the moment of acceptance of the cylindrical shape pipe.

The most dangerous for the pipes work is the connection in one section of the dent and a bullet or the presence of a bullet on the small axis of the oval section of the pipe. An analysis of the circumstances of many pipe fractures along the route shows that the overwhelming number of fractures occurred along the upper or lower generators, that is, the small diameter of the oval cross section of pipes laid in the soil, since this is the only way the pipe section, laid in the trench, is oriented.

5. Gas pipelines accumulate a large amount of elastic energy of a compressed gas, which can result in long-lasting and brittle fractures occurring under high dynamic loads. With high energy intensity of the process of destruction and speed of loading, it is possible to change the characteristics of the metal pipes.

6. High energy capacity of long-distance pipelines, which provide raw materials or energy to large enterprises and entire industrial areas, requires a steady supply of products to the consumer. The metal of gas pipelines is virtually impossible to inspect and carry out preventative repairs. Only major overhaul of pipelines with their termination for a long term is possible in circumstances that justify such a stop. All this necessitates the adoption of a wide range of measures in order to prevent the destruction of the pipelines, and in case of their occurrence - their maximum localization, ensuring the safety of nearby objects and service personnel, creating the conditions for the quick performance of repair and restoration work. Therefore, despite the apparent simplicity of the structure and design scheme, the pipeline is complex, expensive, extremely metal-intensive and responsible construction. This explains a great attention paid to the development of operational reliability of main pipelines in our country and in other countries of the world.

The strength of the main pipeline, its operational reliability is determined, first of all, by power factors, properties and quality of the pipes. For main pipelines, the main stresses are: internal pressure and longitudinal forces caused by the temperature difference in the linear part of the pipeline due to the difference in temperature conditions of construction and operation. Performance requirements of calculation, necessary formulas and the values of the coefficients are adopted in accordance with GNP 2.05.06-85*.

Only circular stresses are sufficiently accurate to calculate, and longitudinal stresses and durability of the pipeline are determined not only by the influence of temperature, but also by the conditions of interaction of the pipeline with a soil, the presence of loads, supports, compensators, etc. The observed fractures of the pipelines were not due to insufficient strength, that is, not caused by the excess of the existing circular stresses over the calculated [18,22]. Most of the destruction was due to insufficient resistance of steel pipes to the origin of cracks, loss of longitudinal stability in temperature actions, transverse fracturing of the pipes in the process of soil subsidence, corrosion damage, deviation of the actual loading conditions from the calculated underwater transitions in the structures.

Therefore, the operational reliability of the pipelines is ensured by damage preventing. Thus, the destruction associated with insufficient resistance to the origin and propagation of cracks, prevent metallurgical methods - improving the mechanical properties, quality of steel and welding joints of pipes, and the destruction associated with the loss of local or general resistance of the pipelines - method of pipelines calculation and design, as well as improving the quality of construction works; in addition, anti-corrosion measures are being developed and improved.

Since 1990, due to the use of cold-resistant pipes, it has become possible to increase the working pressure in gas pipelines to 7.5-8.8 MPa, as well as to reduce a gas pumping temperature to -25 °C without increasing the maximum diameter of the pipes used. In the former USSR, air cooling apparatuses (ACA) were used for technological reasons and to increase the capacity of gas pipelines. At the same time the production of unique refrigeration units for gas industries was started. Moving gas extraction sites to remote northern areas of Siberia, the presence of refrigeration units for gas pipelines has led to an annual increase in the need for steels, pipes from which can be operated at the temperatures of -5÷-15 °C, with a possible decrease of operating temperature to -25 °C [21,22].

When the properties of the pipes do not allow to reduce the gas temperature to -5ºC in the middle climatic zone and to -15 °C in the north, it requires switching off the ACA at the air temperature below -15 and -25 °C in winter, respectively, which are observed in the

specified climatic zones of the country during 2-4 months a year. The pipes made of cold-resistant steels allow pumping up to 1 billion m^3 of gas per year for each gas pipeline with a diameter of 1020 mm, due to the fuller use of natural cold additionally, without capital investment in construction.

It should be noted that in this work the authors did not consider the choice of steel and pipes for the pipelines that transport acidic gases - that is, gases that contain hydrogen sulfide and carbon dioxide, as well as corrosion-active sulfur oils. This is a special issue and is solved comprehensively both by reducing the corrosive activity of the process product (eg injection into wells or pipelines of corrosion inhibitors), by selecting viscous and pure steels, and by reducing the working stresses in pipe metals with the aim of preventing or reducing corrosion rates under the stresses.

Based on the above, it should be noted that in all the considered cases of the pipes use for different pipelines, the authors find it inappropriate to mention a specific grades of steel, as they change or modify too quickly, but the type of steel - carbon, low-alloy, controlled rolling steel - the concept of more stable rolling and provides a sufficient basis for selecting a particular steel grade when pipelines designing and constructing.

Conclusions

1. The status and the main directions of solving problems related to providing high bearing capacity and operational reliability of the long-running oil and gas pipelines of different capacity were retrospectively considered.

2. It is shown that the solution of problems posed to the rolling industry on the basis of ordinary low-alloy normalized steels is no longer possible, and therefore a new approaches are needed to develop the production of low-pearlitic and pearless steels obtained by the method of controlled rolling with step heat treating. Thus, high mechanical-corrosion characteristics of such steels are achieved due to minimum alloying (for example, carbonitride elements), due to the maximum fragmentation of the structure during rolling and controlled high-speed cooling.

3. The specific working conditions of the pipes in high-pressure gas pipelines, which differ sharply from the working conditions of metal in other metal structures, are considered in detail. The requirements for steel

and welding joints of pipes depending on the working parameters of the pipelines are presented in order to prevent their destruction.

4. The possibility of increasing the operational reliability of the pipelines depending on the power factors, mechanical properties and quality of the pipes is substantiated.

5. The most promising ways of increasing the residual (accident-free) pipeline resource are formulated taking into account the influence of degradation processes caused by the presence of harmful impurities of sulfur, hydrogen, and non-metallic inclusions in the metal.

References

1. **Vasilenko I.I., Melehov R.K.** (1977) Korrozionnoe rastreskivanie staley. Kiev. Naukova dumka.

2. **Gertsog E.** (1984)Korroziya staley v serovodorodnoy brede. Moskva. Metallurgiya.

3. **Pohmurskiy V.I.,Melehov R.K., Krutsan G.M.** i dr.(1985) Korrozionno-mehanicheskoe razrushenie svarnyih konstruktsIy. Kiev. Naukova dumka.

4. **Radkevich O.I., Pyasetskiy O.S., Vasilenko I.I.** (2000) Korrozionno-mehanicheskaya dolgovechnost trubnoy stali v serovodorodnoy srede. Fiz.-him. mehanika materialov. 5..93-97.

5. **Saakiyan L.S., Efremov A.P.** (1982)Zaschita neftegazopromyislovogo oborudovaniya ot korrozii. Moskva. Nedra.

6. **Radkevich O.I., Pohmurskiy** V.I.(2001) Vliyanie serovodoroda na rabotosposobnost materialov oborudovaniya gazodobyivayuschey promyishlennosti.Fiz.-him.mehanika materialov.2.157-168.

7. **Makarenko V.D., Grachev S.I., Prohorov N.N.** i dr. (1996) Svarka i korroziya neftegazoprovodov Zapadnoy Sibiri. Kiev. Naukova dumka.

8. **Makarenko V.D.** (2006)Nadezhnost neftegazopromyislovyih sistem. Chelyabinsk. TsNTI.

9. **Moiseev L.S.** (2005) Uglekislotnaya korroziya neftegazopromyislovogo oborudovaniya. Zaschita metallov. T.41. 82-90.

10. **Monoshkov A.N., Pyihov S.I., Pustin I.**A. (1992) Plasticheskaya ustoychivost i ee rol v otsenke prochnosti trub. Moskva. Metallurgiya.

11. **Scheglov B.A.** (1995) Otsenka mehanicheskih svoystv listovyih metallov pri gidravlicheskih ispyitaniyah. Moskva. Metallurgiya.

12. GOST (1989)Trubyi: Metodyi ispyitaniya gidravlicheskim davlenim. Moskva. Izd-vo Standartov.

13. **Kollinz Dzh**. (1984) Povrezhdenie materialov v konstruktsiyah: Analiz, predskazanie, predotvraschenie. Moskva. Mir.

14. **Borodavkin P.P.** (1992) Podzemnyie truboprovodyi: Proektirovanie i stroitelstvo. Moskva. Nedra.

15**. Lyutak V.P., Boychuk I.Ya**. (2002) EkspluatatsIyna nadIynIst naftoprovodIv v umovah NGDU "NadvIrnanaftogaz". Naftova I gazova promislovIst. 2.38-40.

16. **Safonov V.S., Odishariya G.E**. (1996)Teoriya i praktika analiza riska v gazovoy promyishlennosti. Moskva. Nedra.

17. **Gumerov A.G., Yamaleev K.M., Zhuravlev G.V**. i dr. (2001)Treschinostoykost metalla trub nefteprovodov. Moskva. Nedra-Biznestsentr.

18. **Bridu N., Lafrans M., Provu A**. (1986) Razrabotka novyih sortov stali s povyishennyimi harakteristikami dlya transporta kislogo gaza i nefti. Moskva. Yuzichor Ase.

19. **Kaneko T., Okada U., Ikeda** A. (1989) Vliyanie mikrostrukturyi na chuvstvitelnost k SSC nizkolegirovannyih vyisokoprochnyih trubnyih izdeliy dlya neftedobyivayuschih stran. Yaponiya. Sumitomo Ltd.

20. **Anuchkin M.P., Goritskiy V.N.** (1986)Trubyi dlya magistralnyih truboprovodov. Moskva. Nauka.

21. **Makarenko V.D., Kovenskiy I.M., Prohorov N.N**. i dr. (2000) Korrozionnaya stoykost svarnyih konstruktsiy neftegazovyih ob'ektov. Moskva. OOO "Nedra-Biznestsentr".

22. **Makarenko V.D., Paliy R.V., Galichenko E.N.** i dr.(2000) Fiziko-mehanicheskie osnovyi serovodorodnogo korrozionnogo razrusheniya promyislovyih truboprovodov.Chelyabinsk. TsNTI.23.Berkowitz B.J., Heubaum F.H. (1984)Role of Hydrogen in Sulfide Stress Cracking of Low-Alloy Steels. Corrosion. Vol. 40. **5**. 240-244.

24. **Vasilkovsky O., Rivard A**. (2013) The effect of hydrogen sulfide in gruide oil on fatigue ckackgrouth in pipe line steel. Corrosion.V.38.**1**.19-22.

25. **VidemK.,DugstadA**. 1988). Corrosion-NACE. 86.

26. **Yu G.-H., Cheng Y-H., Chen** L. et al. (1997) Hydrogen Accumulation and Hydrogen-Induced Cracking of API C90 Tubular Steel. Corrosion. Vol. 53. 10. 762-769.

27. **Tuttle R.N., Cane R.**D. (1981) H2S corrosion in oil qas production. Houston. NASE .

28. **Chu W.-Y., Li S.-Q., Hsiao C.-M**., et al. (1981) Effect of Hydrogen on the Apparent Yield Stress - Research on the Cause of Hydrogen-Induced Delayed Plasticity. Corrosion. Vol. 37. 9. 514-521.

29. **LunarskaE**. (1985)Hydrogen-induced degradation of low-carbon steel. Park Ridge. Noyes Publ. 5. 763-798.

30**. Lunarska E., Nikiforow K., Pyrza J**. (2005)Monitoring of the hydrogen charging of the industrial installations. Corrosion-2005. 1. 53-58.

31. **Turn J.C., Wilde B.E., Troianos C.A.** (1983) On the Sulfide Stress Cracking of Line Pipe Steels. Corrosion. Vol. 39. 9. 364-369.

32. **Trucbon M.R., Crolet J.I.** (2013) Experimental limits of sourer servise for tubular steels. SSC Simposium. Saint-Cloud.

33. **Makarenko V.D., Prohorov N.N., Paliy R.V**. (2002)Effect of barium on the phosphorus content of deposited metal of welded joints in cold-resistant steel.Weldinq Snternational. **14(**7). 35-40.

34. **Makarenko V.D., Beljaev V.A.,Galichenko E.N., Prohorov N.N**. (2001) Effect of modifying additions on the ductility and plastic properties and the brittle strength of coldresistant, low-alloy steel. Welding International.**15(**1). 62-70.

35. **Makarenko V.D., Beljaev V.A.,Galichenko E.N., Prohorov N.N.** (2001) Effect of modifying microadditions on the corrosion resistance of welded joints in low-alloy steel. Welding International.**15(**2). 78-85.

PROBLEMS OF USE OF VACUUM DRUMS AND ITS PROSPECTS

Molodini Revaz
Candidate of technical Sciences, Mr,
the Construction & Commissioning Engineer,
"WorleyParsons", Georgia

Molodini Noring
Candidate of technical Sciences Mr.,
Associate Professor of Faculty of Mining and Geology,
Department of Mining Technologies

Annotation

The study discusses the improvement of theoretical and practical research of external friction, considering the provisions of the tribulation and its main task is to regulate the friction forces. In our opinion, in the balanced conditions of the waist quality and normal contact troughs in realization of traction forces, modern researches in the friction field, even ignore the necessity of elastic slip. Vacuumed work process, particularly, at the beginning, when the friction is in the hydrostatic mode, is the same as the work of the belt. Therefore, in determining its parameters, using the iterative method, other issues of theory of calculation of the belt bear may be used. In the case of solving lubrication tasks, as in the case of like constructed belt bearings, as well as in the construction with a vacuum drums structure, the fundamental importance is given to the Sommerfeld`s number, which is one of the most important parameters. The work is also presented by a vacuumed motor in the contact with the ring hole of the belt according to the vacuum squares locations and their number of calculating mathematical images of the developed traction of forces and their using methods. According to the physical parameters of vacuum movement models created in the laboratory of the department and for the individual exams of mathematical expressions and totally for the force of the traction were performed the computer calculations and there was presented as a spreadsheet that analyzed the possibility of receiving the maximum of traction forces and based on this, we determined the advantageous layout of vacuum down squares in a ring hole and their numerical data of parameters $S_{escaping} \leq 2p_{groove}$.

Introduction. Analysis of scientific progress clearly shows, that the development of high-quality science is mostly revealed during the practical works. It fully applies to the friction process in the vacuum. The whole world expresses the interest in this field of research over recent years. Creation of new technique and its work in securing the friction processing nodes is an additional reason for such interest

and an issue of its use was on the agenda itself at the beginning of the study. It turned out, that the exhaust bone in the vacuum quickly dissolves in the firmness of the two smooth surfaces. This phenomenon was the basis for improving the high and easily adjustable traction technologies in conveyor motors.

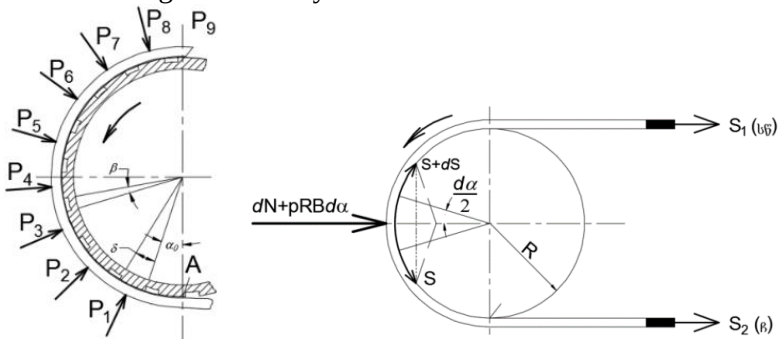

Fig. 1.

The main part. According to classical theories of Leonhard Euler and Petrov-Zhukovsky, issues of transporting large-scale freight cargo with a slight and horizontal long-term conveyor transport (without overload) are still popular. Increasing the tension of the belt (α>270 degree) angle or initial ($S_{escaping}$>pDB) causes undesirable load on the belt or becomes necessary to increase its strength. Regulation of the size of the vacuum and conjugation (μ) on the "relative calmness" and "elastic slide" in the rhythm of the contact surface of the drive resolves this issue, which is sufficiently high and accurate solution based on the data of our and tribal researchers. According to the results obtained based on the literary and patent inquiry, we found out some of the most important issues to build a vacuum drive and the objectives of research for making the vacuum equally distributed in the contact rings.

Conclusions.

1. One of the prospective technological schemes of vacuum formation is the simultaneous recurrence process in the vacuum systems equipped with autonomous vacuum mechanism (AVM) for easy recipients and ring chords; 2. Create effective zone for vacuum (α_{eff}) to obtain “relevantly calm arc“. Depending on the size of the piston $\alpha_{eff} \approx (0{,}05 \div 0{,}2) \cdot \alpha$, and the effective contact area for the traction

forces, the "slippery arc". 3. The vacuum formation and the equilibrium distribution of the vacuum dose should be considered in complex, taking into account the frequency of the circular rotation and the pigmentation rate; 4. The viable condition for creating a vacuum is the adiabatic or hyper adiabatic expansion of the liquid (drip or gas) in the recipients, when the optimum volume is exacerbated $p=(0,9\text{-}0,95)\cdot 10^5$ pa. 5. The structure of the contact surface of the vacuum drive must provide the necessary conditions for the sealing of the ring shell and the mutual independence of AVM. 6. All technical requirements that are set out in the work are considered to be appropriate for any stage to build the vacuum. Research objectives: 1. From the perspective of the constructor, the metal-coating rubber (elastomer) in the friction coupling on the surface of the ring shell is very important to know what conditions are wet (lubrication) or dry friction. Accordingly, we studied the fluid motion in dry, marginal hydrodynamic and elastic hydrodynamic regularity. 2. The mechanism of frictional force generating in the rhythm chute should be considered on the macroscopic level of a completely acceptable macroscopic scale based on a relatively rigid but reliable (convincing) model (the roughness was measured in mm). 3. The methodology has been developed to allow us to calculate the optimal parameters of the vacuum-channel transistor – t, the width of the conduit belt – δ, the width of the groove – β, the perforation diameter – *a*, etc. 4. We have obtained theoretical results and basic parameters with help of laboratory physics and computer model.

Technical requirements for vacuum drives. Vacuum drive friction nodes are presented with various constructions of composite materials. The contact of these nodes with the moving surfaces is made up of channels (recipients) and ring cutting, creating and regulating the vacuum, that is kept for a certain period. There are three main nodes of friction in today`s well-known vacuum systems: 1. Any construction collector. where the vacuum operative recipients are connected to the outer source of vacuum. 2. The ring shell between the drive drum and belt contact surfaces (including our construction long-range grooved circular drum), which are realized by the forces of the traction. 3. Cylinder-piston mechanisms of AVM by which the drum rotation concurring pistons reciprocating motion of a simple

progress through vacuum channel holes, that are formed in the rough rings [1]. Despite significant technical data received by predecessor researchers (K. Vasilev, I.V.Wolchek, VA-Wangkhei, D.Ungmmeister, etc.), vacuummakers needed to improve the construction process, vacuum technological process and further theoretical research, this especially applies to collector vacuum drums with marginal deployment. Their disadvantages and problematic tasks are extensively presented in our work, which is why it is better to refuse to use such a structure. Considering the results of our patent and scientific research analysis, we consider the following technical requirements for the construction and optimal parameters of the vacuum drive:

1. Formation of vacuum movement in the hole of conveyor belt is better to be carried out by autonomous vacuum mechanisms (AVM), which (piston space) is connected with vacuum channels of the surface by means of convenient and simple nodes for operation and repairs; 2. In order to increase the coefficient of driving vacuum coil, it is necessary to create a vacuum in the contact area by ensuring the operation of the AVM hydrodynamic mode; 3. One of the important issues of friction is the nature of mechanical interaction; During the construction process of contact surfaces, the width of chromium of ring shell surfaces (belt – vacuum drum) should ensure the volume of fluid and its rapid, perfect drainage process. 4. The following conditions are necessary to ensure the creation of equally distributed disclosure: a) The speed of vacuum compressor should be appropriate to ensure full fluid drainage (suction) of fluid (dripping, gas) or the efficient pump (S_{eff}) of the object from the spinal cord between the circuit surfaces of the drive. b) Bandwidth of the vacuum source and the drive ring hole connecting with node (it is better to be in a hole and not a complicated labyrinth) (U) should The coefficient of the use of the vacuum creator mechanism (k_t) should be approximately equal to one or $Kk_t=\mathbf{S}_{eff}/\mathbf{S}_t\approx1$ or $Kk_t=\mathbf{U}/(\mathbf{U}+\mathbf{S}_t)\approx1$, which is one of the most important conditions for research and project of the drive. c) Hermitization of the vacuum system of the instant switches (vacuum-mechanical, vacuum-pump collector) of the fluid motion (the drainage, the vacuum pump collector) should be more complete than the sealing of the ring shell, while the parameters of the contact surfaces of the drive must provide minimal absorption of fluid in the envi-

ronmental chalet. d) The speed of effective pump (S_{eff}) and the bandwidth of connected hole (U) should consider the corresponding angular and linear speeds of the drive and cargo. 5. For the processing of long-range conveying equipment, tail and intermediate motions, it is better to consider an anchor smoker (contact surface) drawn from homogeneous elements that will ensure high levels of unification and make it more convenient for the operation and repair process. 6. Construction of the contact surface of the vacuum-drive should provide the necessary conditions for the hermitization of the ring shell: intermodal operation of the ATMs (no liquid absorption from bordering recipients) and the fluid (air) resistance of the shield of the belt. 7. External and internal volume of vacuum recipients of the drive must ensure the vacuum-making mechanisms to work optimally. 8. Selection-calculation of the contact surface geometric parameters should consider the angular speed of the drive (conventional tape). 9. The calculation of the mechanism for the reciprocity-moving motions of the vacuum dock piston pumps (plungers, etc.) should be assessed by the so-called "relative calm arc", in compliance with the limits of the allowable size of specific terms. 10. Formation of vacuum should be completed in all types of vacuum regiments and adjoining contact surfaces by the appropriate vacuum cells of the collector's – $\alpha_{relat.calm}$ (circular, linear) comparable with "calm area". 11. One of the important preconditions for achieving optimization of contact surfaces is to examine the belt drive. Thus, the selected diameter of the central ligand connecting the surface of the dump space of the ADM, must ensure continuous transmission of the fluid flow in vacuum stream recipients - from the external volumes (gates, perforations, etc.) to the vacuum creator mechanism of the contact surface (for example the piston spaces). One of the most important demands for contact surfaces and the complete vacuum structure is the disintegration of the station, the easy access of each node and the component part, compactness, repair, durability etc.

Analysis of vacuum formation in hole. The concept of vacuum, physics and technology is defined as the condition of liquids (gas and drip) of having lower pressure than in atmosphere. Vacuum is quantified by the fluid pressure. The main postulates of vacuum are formulated as follows:

1. Fluids consist of individual molecules.

2. There is a constant supply of fluid molecules according to the speed, i.e. the same number of molecules always have the same speed.

3. In the movement of liquid molecules there is no preferential approach, i.e. the fluid molecule space is isotropic;

4. The fluid temperature is the parameter of the average kinetic energy of its molecules;

5. The fluid molecule will be adsorbed when interacting with the solid surface. It should be considered that the many physical processes in vacuum are significantly dependent on molecular replication walls K_w and molecules of mutual crane K_M in the ratio of $K_{kn}=K_k/K_m$, where K_{kn} is the criteria of dimensionless ratio $K_{nudenss}$, which determines the quality of vacuum: low, medium, high and ultra-high.

During the low vacuum $K_{kn}<<1$, the distance to the molecule recipient wall (L) is significantly less than the rational size of the vacuum cleaner (d_{eff}). The average vacuum is a fluid state where the number of molecules collapses and the number of collisions with the molecules of the recipients is identical, at the same time $L\approx d_{eff}$ and $K_{kn}\approx 1$. High and ultra-high vacuum, or condition when $K_{kn}>>1$ and $L/d_{eff}>>1$ is sufficient for absolute pressure must be no more than 10^9as. Thus, we should assume that the vacuum created in vacuum motors is in low and medium-sized thresholds based on the Knudsen criteria and the velocity of the vertical strength $(0{,}1\text{-}0{,}95)\times 10^5$ may vary within the frames of Pascal. Equal distribution of the vacuum in the conjunction circuit chute in the research of vacuum theories are considered to be a transverse and circular direction. However, some early works have been emphasized on the "elastic binding" of the tape and vacuum compound surfaces, which contradicts the equal distribution condition of the vacuum. Thus, the idea of distributing a vacuum in the above-mentioned works does not include any proven statements, but on the contrary, with "elastic models" more contradictory. Our opinions on this issue fully matches the classical theory of friction and considers the equal distribution of vacuum as necessary condition. We use the criteria of Reynolds, Prandtl and Nusselt in the work of describing the vacuum formation processes in the fringes of the vacuum and fractal contact areas, and in laboratory

experiments, the static regime was measured in the perforations of the vacuum size in the long grabbing and the contact areas; In the dynamics: we demonstrate the friction rate, the size of the piston, and the speed of the tape, with a special passer through the oscilloscope. The results are satisfactory, but with the accuracy of the pacing motion trajectories, it is possible to solve many important problems with the perfection of the current friction process in the motility of the drive, including the reduction of the tape and increase the service term. Research on the location of the vacuum zone due to the abundance of fluid at the expense of the pressure [2]. At the beginning the friction works in hydrostatic mode, the tape is moving towards the piers' periphery, and the process is in progress in the dry strain of the vacuum environment in the arc. The piston software program is implemented by preliminary calculations, the prospective drivers associated with the endorsements. Considering this and analyzing the existing literary sources, we conclude, that the process is manageable and as soon as the pistons start moving towards the periphery, the radius of the fluid involves the activation of the compulsive drainage of the fluid. The working process of vacuum drums, especially at the beginning (when the crank is going into the hydrostatic mode), is the same as the work of the tape mechanism. Therefore, by determining its parameters, we can use the theory of iteration during the calculation process. As for the exact theoretical analysis of the rigid base and the elasticator (e.g., the surface of the drum and the conveyor belt), it does not exist yet. Thus, conventional motions of the conventional conveyor when they have to work with wet friction. In elastic hydrostatic and elastic hydrodynamic regimens, we can calculate it as a powerful tonal bear. In the case of vacuum, the specific parameters of the driving parameters of the drive will be considered as the specific processes (acceleration of the drainage effect, vacuum formation process and mechanical blocking of linear speeds of the drive). We think, that the existence of fluid (any) on the contact surfaces requires the study and processing of friction theory in terms of classical theory of lubrication. The classic theory of lubrication envisages two modes (see fig. 2): hydrodynamics and margin. The main calculation parameter in the lubrication theory is the generalized number of Sommarfeld, which is calculated in ratio with pressure of thick force of the friction

$$S_0 = \frac{\tau L^2}{pL^2} = \frac{\mu U}{pL} = \frac{\mu N}{\overline{P}} \quad (1)$$

where τ is tangential tense; p - normal (force) pressure; n - frequency of rotation; p-average depression; μ - fluid viscosity; U - fluid speed;

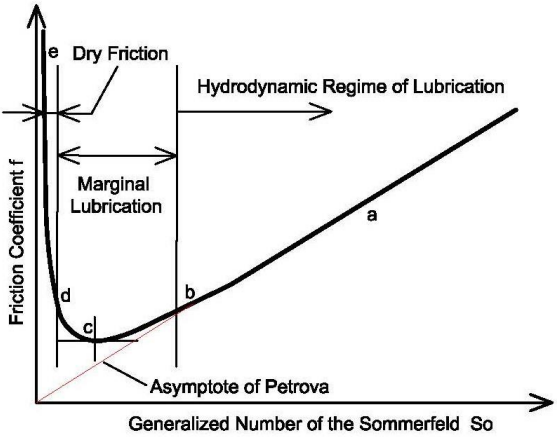

Fig. 2.

The Sommarfeld`s number is fundamental in the solution of the lubrication tasks and is one of the most important parameters in the construction of mechanisms.

As we mentioned, the fluid movement speed in the drum belt will decrease as much as possible (almost to zero) to the droplet point, which corresponds to the change of friction from the liquid (hydrodynamic) to the surface and then to dry friction. This change of friction is caused by the amendment of the general measurable number.

Fig. 2. The maximum value of friction coefficients according to the presented schedule corresponds to: the hydrodynamic regime - maximal value of generalized size, or the dry friction regime - the minimum value of generalized size. In our case, the optimum regime for the type of vacuum-drive is a dry friction regime, while minimizing the generalized size of the Sommarfeld. According to the formula 2, Reduction of the S_0 is caused when μ – fluid viscosity and U – fluid speed, or maybe the both move towards zero.

Fig. 2. The schedule of dependence of F and S_0

$$S_0 = \frac{\mu(U \approx 0)}{pL}$$

or

$$S_0 = \frac{\mu(U \approx 0)}{pL} \approx 0. \qquad (2)$$

In conclusion, we can note that during a full rotation of the vacuum drums, the process of lubricating the surface of the contact surfaces (roughly-elastomer) begins with the hydrodynamic mode, and before the process will go on dry friction, preceded by lubricating process of macro elasto dynamic lining mode. All these modes (except the dry friction regime) obey Reynold`s general equation, which clearly shows that the pressure on the fluid is dependent on the action, stimulating and mucous elements.

$P = pRB$ is the force on contact surface of the vacuum-drive that is obtained by the vacuum on the corresponding arc of the additional pushing force $F_{\max} = pRB\left(e^{\mu\alpha_{\max}} - 1\right) + S_C\left(e^{\mu\alpha} - 1\right)$ complies with A.V. Evnevich's well-known formula.

If the vacuum is in the entire contact surface of vacuum drums and it`s divided into separate vacuum-subzones, we will allow the following theory: a) P size vacuum is created and applied only to the central sub vacuum (see formula 1), and outside its boundaries: b) vacuum is stopped in vacuum-subzone from the drive to the corner of tape deployment point, then we can write a traction force as follows

$$F_{\max} = e^{\mu\alpha_{\max}} pRB\mu \int_{\alpha_0}^{\alpha_0+\delta} e^{-\mu\alpha} d\alpha + S_C\left(e^{\mu\alpha_{\max}} - 1\right);$$

or

$$F = e^{\mu\alpha_{\max}} P\left(e^{-\mu\mu_0} - e^{-\eta(\alpha_0+\delta)} + S_C\left(e^{\mu\alpha_{\max}} - 1\right)\right) \qquad (3)$$

and while forming a vacuum in the working subzones, the formula for traction forces shall be as follows

$$F = e^{\mu\alpha_{\max}} \sum_{k=1}^{n_m} P\left[e^{-\mu[\alpha_0]+(k-1)(\beta+\delta)} - e^{-\mu[\alpha_0+(k-1)(\beta+\delta)+\delta]}\right] + S_C\left(e^{\mu\alpha_{\max}} - 1\right); \qquad (4)$$

where *K* is the number of vacuum subzone.

β is a long-range angle of the arc between the vacuum-subzones.

If we note the angle of vacuum subzones with $t = \beta + \delta$, then we shall have the following formula

$$F = e^{\mu\alpha_{max}} \left(1 - e^{-\mu\delta}\right) \sum_{k=1}^{n_m} Pe^{-\mu[\alpha_0 + t(k-1)]} + S_C \left(e^{\mu\alpha_{max}} - 1\right); \qquad (5)$$

formula allows us to determine the created strength of developed traction in any subset of the vacuum zone.

Analysis of this formula shows that the location of the vacuum vector is important for the entire contact surface of the vacuum compound on the strength of its traction development. In particular, the greater closure of the vacuum isolate from the vacuum drum point (point A, formula 1), increases the effect of traction force.

Conclusions: Thus, if the amount of vacuum subzones are the same on the vacuum surface, depending on where the gap is to the point of pull or the point of view, it gives noticeably different forces. This difference of traction forces can be calculated by the following formula

$$\Delta F = e^{\mu\alpha_{max}} \left(1 - e^{-\mu\delta}\right) P \left[\sum_{k=n}^{n+n_m-1} e^{-\mu[\alpha_0 + t](k-1)} - \sum_{k=\xi}^{\xi-n_m+1} e^{-\mu[\alpha_0 + t(k-1)]} \right]$$

Where ξ is the number of the first working vacuum subzone located in the fastening point of belt of vacuum drums and $\xi = n_s - n + 1$;

n_s - is the amount of vacuum subzones located under tape, of the contact surface.

n - is the first vacuum subzone on the side of the tape running down from the drum.

$n_{adjacent}$ - is the amount of sequentially located vacuum subzones.

Quantitative assessment of this effect allows us to determine the optimal parameters of vacuum drums.

Vacuum drum is characterized by a factor of its own traction, calculated as follows: $\alpha_0 = 0$; $\alpha_{max} = \pi$

$$F'/P = \left(e^{\mu\alpha} \frac{e^{\mu\alpha}}{e^{\mu\delta}} \right) \sum_{K=9}^{1} e^{-\mu[\alpha_0 + (k-1)(\beta+\delta)]} \qquad (6)$$

(15) and (16) equations were solved by computer programs using the following data: laboratory vacuum drum diameter, width, etc. and were chosen according to [3,4] works.

Corner of the conveyor belt of the vacuum drum $\alpha_{max} = \pi$ The coefficient of the belt binding (friction) on the contact surface: $\mu = (0{,}1 - 1{,}2)$;

Angular line of vacuum subzones $t = \beta + \delta = 0{,}33$, radian;

The lagging central angle of vacuum subzones: β=0,11 radian;

The lagging central angle of segment between vacuum subzones $\delta = 0{,}22$ radian;

Additional Stretching of the belt of drum creating vacuum $P=p_{RB}$.

Radius of vacuum drum R=0.18 m.

Width of conveyor belt B=0,50 m.

The calculation was completed between 1 to 9 for separate vacuum subzones, as well as during their joint work, considering the quantity and their allocation in the vacuum zones.

The calculation performed with the formula is available in the experiments spreadsheets and analysis show that traction forces in our case is minimum six times and maximum 14 times beneficial then normal friction drum.

References

1. **Molodini N. Sh**. Privodnoy baraban lentochnogo konveiera. Avt. Cvid. SSSR (USSSR) №543574. Biut. Cvid. Izobreteniy №3, 1977.

2. **Muskhelishvili V.L, Kutateladze A.A., Molodini N. Sh**. Privod lentochnogo konveiera. Avt. Cvid. SSSR (USSSR) №676506. Biut. Cvid. Izobreteniy №28, 1979.

FORECASTING THE QUANTITY OF GRANITE DEMAND IN SELECTED QUARRIES IN EDO, OGUN AND ONDO STATE FOR PRODUCTION PLANNING

Melodi M. M.
PhD (Engineering), Associate Professor,
Department of Mining Engineering The Federal University of Technology, Akure, Nigeria

Oluwafemi V.I.
Master's Student
Department of Mining Engineering The Federal University of Technology, Akure, Nigeria

Abstract

This research forecasted the demand for granite in selected quarries in Edo, Ogun and Ondo state for production planning. This was achieved through the collection and examination of the nature of the sales record of the selected quarries from year 2014 to year 2018; forecast; and estimation of the production rate required to meet up with the forecasted demand. These were achieved through the collection of secondary data and careful review of earlier papers. The demand was forecasted using Linear Regression Supervised Learning and Microsoft Excel was used alongside to estimate the required Production Rate. The forecast reveals that demand will be high in the dry season as high as 33,956 tonnes per month and low in the rainy season as low as 2,464 tonnes in some of the quarries. The estimated production rate are achievable because they are lower to the existing production rate used by all the selected quarries. The forecast is significant and not based on chance because the significant level and P-value for all the locations are less than the α-value of 0.05. In conclusion, the research was able to combine Time Series Model of Centered Moving Average, Associative Model of Linear Regression and Multiplicative Model to forecast sales demand. Ogun 1 will experience the highest demand within 2019 to 2021. It is recommended that the quarries should keep the record of their sales for forecast purposes and that quarry managers should release their sales record for ease of getting data for sales forecast.

Keywords: Forecast, Mining, Granite, Aggregate, and Production.

1. Introduction

Opafunso and Ajaka (2004) stated that quarry project is a capital intensive investment with many uncertainties as a result of geologic condition, reserve estimations, severe problems in forecasting aggregate prices and production costs. All of these factors make it important for the mine manager and mine operator to have a way by

which the quarry product demand can be predicted before the real production. This will help in effective planning and resources allocation.

According to Olasehinde and Bute (2014) stated the following four factors as part of the challenges facing quarrying the challenges include: in the raining seasons the production is lower, the efficiency of machines are low; lack of spare parts and lubricant in the country, it has to be imported which takes a longer time; machine breakdown, in some instances foreign engineer has to come and repair; and the largest consumption of quarry products is in the road construction, as such political situation in the country controls the market.

Olusanya *et al.* (2012) noted that planning is regarded as the most basic of all the management functions that we have. They noted that it involves selection from among alternative future course of action for the organization and every department or section within the organization. The ability of quarries to accurately forecast customers demand is of great importance. Bowersox *et al.* (2002) stated that when there is no forecast business waste resources by either too much (i.e. overstocks) or too little (i.e. stock outs) inventory.

Melodi (2018) noted that many new trends like increase in customer expectation, increase in demand for aggregate and the need to minimize cost of production have led to the delivery of poor services by quarrying industries. There are instances where some quarries have huge stockpiles while in some quarries, customer go back disappointed because there is nothing available for purchase. Nadler and Kros (2007) stated that for this problem to be solved quarry companies need a means to forecast in order to predict customer demand.

Forecasting is a problem that arises in many economic and managerial contexts, many forecasting procedures have been developed over the years, both in and outside of business enterprises. Forecasting can be either quantitatively or qualitatively based. Quantitative forecasting uses historical data to predict the demand for a particular product. Forecasting granite aggregate product demand is important to any quarry. Forecasts of the future granite aggregate demand will predict the quantities that could be purchased, produced, and shipped. Many firms have found that the planning and operation of an effective logistics system requires the use of demand forecasts procedure.

No work on sales forecast for quarry product seems to have been done on the Nigeria quarrying industries. Frederick and Joseph (2014) applied time series analysis to forecast the revenue collection of the Customs, Excise and Preventive Service (CEPS) for the period 2008-2012 to devise a reasonably projection for the individual tax components. This they said will assist in the design of an appropriate expenditure profile as a means of averting any future fiscal deficit in the country. Agyen (2012) also applied time series to model and forecast for petroleum products demand in Ghana. Also, Ezennaya *et al.* (2014) focus on Nigeria electricity demand forecast from 2013-2030 towards vision 2025 using Time Series Analysis on past load demand stating that this is important with increasing dependence of agriculture, industries and day-by-day household comfort upon the continuity of electric supply from PHCN systems in Nigeria.

This study applied the concept of sales forecast to quarrying industries by providing readers and more importantly quarry managers with the understanding of how they can forecast demand with limited access to sophisticated forecasting tools and still have more accurately forecast. This research also combined a time series model and an associative model for accurate demand forecast. This study also estimated the Production Rate required to meet up with the forecasted demand and Forecast Models of the selected states.

The aim of this research is to forecast the quantity of granite that will be demanded in year 2019 to 2021. The specific objectives of this study are to: determine the nature of the sales for the past five years in the quarries; forecast demand for the next three years; and estimate the required Production Rate required to meet up with the demand. The scope of this study is limited to Ogun, Ondo and Edo State Quarries.

This study contributed to knowledge in the following ways: it provides the demand forecast for granite in the selected quarries, and it gives the Production Rate needed to meet up with this demand.

2. Literature review

Nick (2018) noted that over the past five years, the global granite market maintained a strong annual growth rate of 3.3% from US$13.39 billion in 2013. The market growth is mainly driven by the surging construction and renovation activities in developed countries, rapid industrialization and urbanization in developing countries,

changing consumer preference for natural looking home décor, and the growing commercial value of granite products in the global market.

A release by The Nation (2016) noted that the Minister of Solid Minerals Development, Dr. Kayode Fayemi said that Nigeria spends U.S. $4 billion annually on the importation of granite simply reinforces the urgency with which the country must look inwards if is dire economic situation is to improve. The country's loss is the gain of nations like China, Spain, India, Portugal and Italy which are the major exporters of granite to Nigeria. But Melodi and Onipede (2017) stated that apart from the construction usefulness of the granite aggregate, quarry operation had contributed to the economic development in so many areas.

Forecasting is a prediction or an estimation of an actual value in a future time period (Nimai *et al.,* 2017). Ezeliora *et al.* (2014) defined Demand forecasting as the activity of estimating the quantity of a product or service that consumers will purchase. Vladimíra (2010) said that demand forecasting forms the basic keystone for strategic, tactic and operative decision making within the company. Its exploitation rate in planning can have fundamental influence on the effective management of material flow not only within company but within the whole supply chain as well. The production planning cannot be done effectively unless the volume of the demand for the product is known. Accurate forecasts are important for businesses and other organizations in making plans to meet demand for their goods and services (Scott and Kesten, 2017).

Forecasting methods were developed since the 1950s for business forecasting and at the same time for econometric purposes (Vladimira and Michal, 2010). Menezes (2004) admitted that forecast methods are classified as objective/subjective, statistical/judicial, time series/regression/judicial procedure, qualitative time series/causal patterns and qualitative/quantitative. In their work, demand forecast methods are categorized as qualitative and quantitative.

Delphi technique, Market resources, Expert groups' opinion and Sales force mixed are the major method used for qualitative forecasting (Menezes, 2004). Despite handling with abstract and subjective experiences, qualitative techniques are generally concluded with low prediction performances due to bias and tendency (Menezes, 2004).

Quantitative techniques forecasting techniques is used for companies. To use 'quantitative' method, we have to reach quantitative data. The two major method used are Time-Series Models and Associative Models. Time series models look at past patterns of data and attempt to predict the future based upon the underlying patterns contained within those data. While Associative Models which is often called causal models assume that the variable being forecasted is related to other variables in the environment. They try to project based upon those associations.

Artificial Intelligence is a subject taught as a subject in computer science and engineering discipline. It primarily limits itself to the processing of data through computers (Dalvinder, 2014). Hernán (2018) noted that Artificial Intelligence is reshaping how we learn from and utilize data and not just by accessing data, but by actually digging into its importance and to use the data to create personalized customer experiences. Instead of merely accessing the data, AI grants us the opportunity to really dig into the data's implications.

Hernán (2018) continued to say that in terms of forecasting, AI will transform how a company interacts with her own data for and from sales. Jason (2016) said the majority of practical machine learning uses supervised learning. Supervised learning is where you have input variable (x) and an output variable (Y) and you use an algorithm to learn the mapping function from the input to the output.

Gerald (2019) stated that production rate is the ratio of the number of goods produced and the time spent during their production. He also stated that production rates can measure the efficiency of production processes, whether those processes involve manufacturing, software development or food service. He also added that production rates can increase or decrease and that Managers can analyze how production rates can fluctuate, boost parts of the process that contribute to higher rates and address problems that are causing lower rates. Most companies use production rate to set work goals for their workers so that they have a production, or working goals, for the day.

(Gerald 2019). An article by Andrella (2018) noted that each public holiday in Nigeria implies getting an extra day off from job, school, and business. It further stated that Nigeria has three major

types of holidays which includes Public holidays, Observance and Local/seasonal holidays.

3. Materials and method

The study covered a total of four quarries (one quarry in Ondo State, one quarry in Edo State and two quarries in Ogun State) for the research work.

Table 1

Quarry Coordinates

Location	Coordinate
EDO1	6° 58' 0"N, 6° 2' 0" E
OGUN1	6°40′15″N 3°55′15″E
OGUN2	6°35′40″N 3°12′05″E
ONDO1	07° 20' 26.1"*N*, 005° 10' 35.7"E

Data Collection

The past five years data of the quantity of granite aggregate sold by the quarries were acquired by the use of a well-structured questionnaire. The required data was obtained through the use of well-structured questionnaire. Supervised Learning and Microsoft Excel were used to analysis the data for the various objectives.

In time series analysis, the two major aim of a time series data are to observe the nature of movement of the phenomenon over time and Forecast. The time series plot was first plotted. It helps in viewing the time series graphically. More importantly, when the time series exhibits seasonality. Hence, the data was seasonally adjusted so that a trend line can be fitted and long term trends can be predicted. The effect of seasonal adjustment was to smooth away seasonal fluctuation, leaving a clearer view of what might be expected "had seasons not existed". This process involves finding the Seasonal Variation for each month. The steps are highlighted below.

Steps in Seasonally Decomposing a Time Series

a. Moving averages

The time series was seasonally decomposed by first calculating the moving averages.

The first step was to calculate the L step moving average centered at the time period *t*.

Where *L* is the length of the seasonality (since we have a monthly data, then *L*=12). Since the moving average gives the mean of the year's data, the seasonality factor is removed. For even L as in this

case now (L=12), it is a bit difficult to center the moving average on the time period t. For example, the average of the first twelve months of the series will be centered at month 6.5 rather than month 6. To center the moving average at month 7, the moving average centered at 6.5 and 7.5 are computed and the average was gotten. The resulting double average is centered at month 7.

b. Seasonal variation

This is gotten by dividing the actual value by the moving average

c. Compute the seasonal index.

Sum the seasonal variation according to the respective month. Then find the average seasonal estimates

d. Computing the normalization factor

$$Normalization\ Factor = \frac{L}{(Sum\ of\ \ ave.seasonal\ indices\ \ estimates)} \quad (1)$$

e. make final adjustment.

$$New\ seaconal\ \ Index = Seasonal\ \ Index \cdot Normalization\ \ factor \quad (2)$$

f. Calculate the seasonally adjusted series

The seasonally adjusted series was estimated by using this formula

$$\frac{Actual\ \ \ Sales}{Seconal\ \ \ index} \quad (3)$$

Least Square Regression Analysis

Now, to estimate the trend on the seasonally adjusted series the method of least square regression was used. The seasonally adjusted sales was regressed on the time point.

The mathematical model for the simple linear regression of T_t on t is stated below

$$T_t = \alpha + \beta(t) + E \quad (4)$$

"α" is the constant coefficient or intercept is the predicted value for T_t when t = 0,

"β" is the slope, may be interpreted as the change in Y for a unit change in t and

"*E*" is the random error component or error term.

The ANOVA was used to show the various sums of squares and the degrees of freedom associated with each. The most important part of the table is the P-value. The alpha value was set at 0.05. Every P-value less than 0.05 reveals that the forecast is not based on just chance.

To successfully decompose a time series, there is a need to choose between a multiplicative or additive model. Multiplicative model is known most time to conform to economic and business phenomena. Hence, multiplicative model was used. A multiplicative model was used to forecast the monthly sales from 2019 to 2021.

$$Y_{est} = t_{est} \cdot S \tag{5}$$

Y_{est} is the estimated data value;

t_{est} is the projected trend value;

S is the appropriate seasonal variation value.

The selected quarries have a minimum of 250 tonnes/hr. production rate based on their crusher capacity. The minimum production rate to be maintained to be able to meet up with the forecasted demand per hour was determined by using the formula

$$\text{Production Rate} = \frac{F(t+1)}{hnw} \tag{6}$$

F(t+1) is forecast for the month;

h is the number of hours the quarry operates per shift;

n is the number of shift operated by the quarry in a day;

w is the number of working day in a year.

4. Result and discussion

The Nature of the Sales for the Past Five Years

Since the sales data were collected indexed to time, it is a time series data. With this in mind, the first step in time series analysis is to plot the time series, usually known as time series plot which has been done for each of the locations from Figure 1 to Figure 4. This plot enabled to view the time series graphically.

Figure 1 reveals that within year 2014 to year 2018 Edo 1 experienced the highest sales in the month of November year 2016 with a total of 3,989 tonnes granite demanded and the lowest during these

years in the month of August year 2014 with a total of 1,900 tonnes. It was also noted that granite demand falls mostly in the raining season and increases greatly in the dry season.

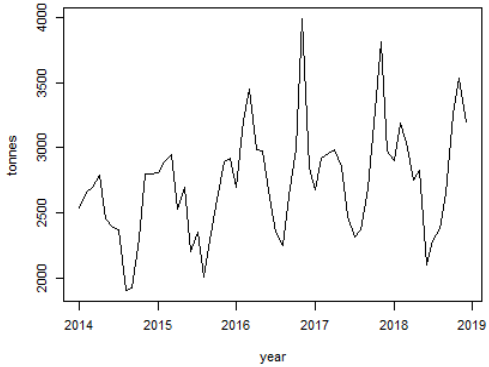

Fig. 1. Sales for Edo 1 from 2014 to 2018

Figure 2 reveals that within year 2014 to year 2018 Ogun 1 experienced the highest sales in the month of December year 2018 with a total of 32,817 tonnes granite demanded and the lowest demand during these period in the month of February year 2014 with a total of 15,489 tonnes.

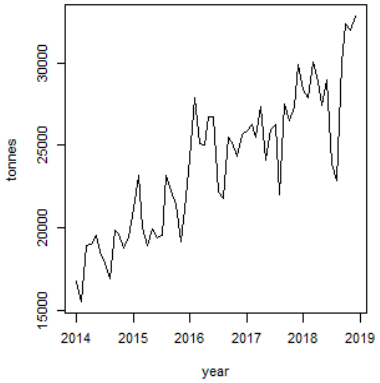

Fig. 2. Sales for Ogun 1 from 2014 to 2018

Figure 3 reveals that within year 2014 to year 2018 Ogun 2 Quarry experienced the highest sales in the month of October year 2017 with a total of 5,509 tonnes granite demanded and the lowest demand

during these period in the month of April year 2014 with a total of 1,894 tonnes.

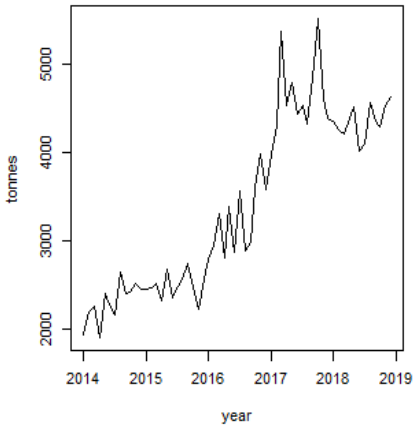

Fig. 3. Sales for Ogun 2 from 2014 to 2018

Figure 4 reveals that within year 2014 to year 2018 Ondo 1 experienced the highest sales in the month of May year 2018 with a total of 12,310 tonnes granite demanded and the lowest demand during these period in the month of September year 2016 with a total of 6,477 tonnes.

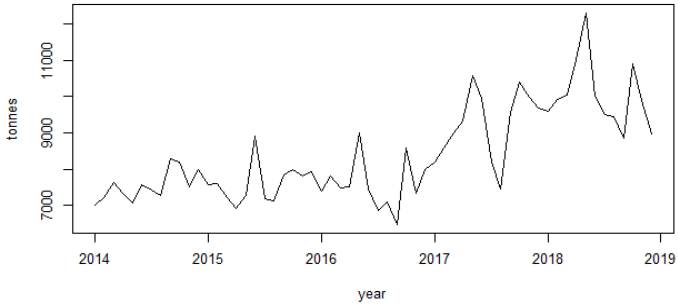

Fig. 4. Sales for Ondo 1 from 2014 to 2018

Demand Forecast for 2019 to 2020

Figure 5 shows that in year 2019 at Edo 1, the largest demand for granite will occur in November with a total of 3757 tonnes of granite to be demanded and the lowest demand will be experienced in the month of August with 2364 tonnes to be demanded. In the year 2020

at Edo 1, the largest demand for granite will occur also in November with a total of 3879 tonnes of granite to be demanded and the lowest demand will be experienced in the month of August with 2441 tonnes to be demanded. In year 2021 at Edo 1, the largest demand for granite will occur also in November with a total of 4001 tonnes of granite to be demanded and the lowest demand will be experienced in the month of August with 2518 tons to be demanded.

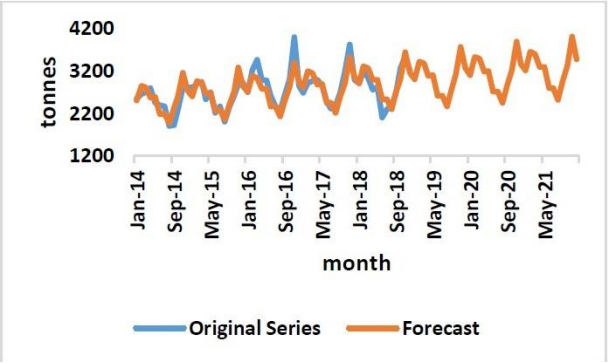

Fig. 5. Demand Forecast for Edo 1

Figure 6 shows that in year 2019, at Ogun 1 the largest demand for granite will occur in the month of February with a total of 33,956 tons of granite to be demanded and the lowest demand will be experienced in the month of August with 28,213 tonnes to be demanded. In year 2020, at Ogun 1 the largest demand for granite will occur in February with a total of 36,866 tonnes of granite to be demanded and the lowest demand will be experienced in the month of August with 30,531 tonnes to be demanded. In the year 2021, at Ogun 1 the highest demand for granite will occur also in February with a total of 39,775 tonnes of granite to be demanded and the lowest demand will be in the month of August with 32,849 tonnes to be demanded.

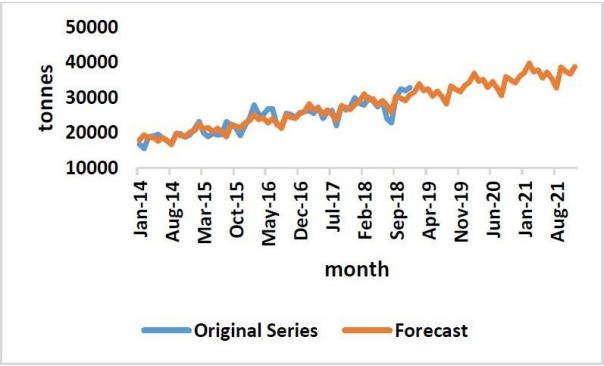

Fig. 6. Demand Forecast for Ogun 1

Figure 7 shows that in year 2019, at Ogun 2 the largest demand for granite will occur in the month of November with a total of 5,635 tonnes of granite to be demanded and the lowest demand will be experienced in the month of June with 4,907 tons to be demanded. In year 2020, at Ogun 2 the largest demand for granite will occur in November with a total of 6,273 tonnes of granite to be demanded and the lowest demand will be experienced in the month of June with 5,491 tonnes to be demanded. In the year 2021, at Ogun 2 the highest demand for granite will occur also in November with a total of 6,911 tonnes of granite to be demanded and the lowest demand will be in the month of June with 6,074 tons to be demanded.

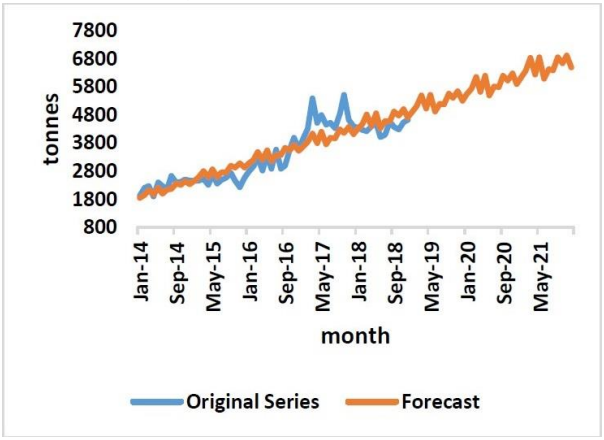

Fig. 7. Demand Forecast for Ogun 2

Figure 8 shows that in year 2019, at Ondo 1 the largest demand for granite will occur in the month of May with a total of 11,932 tonnes of granite to be demanded and the lowest demand will be experienced in the month of July with 9,436 tonnes to be demanded. In year 2020, at Ondo 1 the largest demand for granite will occur in May with a total of 12,677 tonnes of granite to be demanded and the lowest demand will be experienced in the month of July with 10,019 tonnes to be demanded. In the year 2021, at Ondo 1 the highest demand for granite will occur also in May with a total of 13,422 tonnes of granite to be demanded and the lowest demand will be experienced in the month of July with 10,602 tonnes to be demanded.

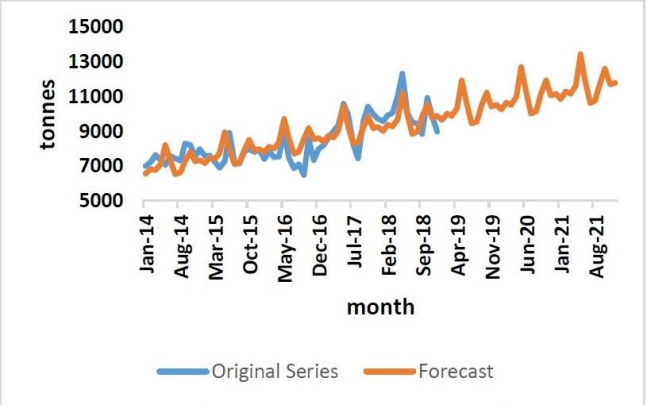

Fig. 8. Demand Forecast for Ondo 1

Production Rate

From the review of literatures the Table 2 was generated by subtracting the holidays and the Sundays from the months.

Table 2

Expected workings days

Year	Jan	Feb	Mar	Apr	May	Jun	Jul	Aug	Sep	Oct	Nov	Dec
2019	26	24	27	25	26	27	27	25	25	26	25	20
2020	26	23	26	25	25	23	27	24	26	26	24	21
2021	25	24	24	25	25	24	27	24	26	25	25	21

Estimated Production Rate for Selected Quarries

Table 3

Estimated Production Rate

	Edo 1 (tonnes/hr)	Ogun 1 (tonnes/hr)	Ogun 2 (tonnes/hr)	Ondo 1 (tonnes/hr)
Jan-19	14.43	151.94	23.65	46.33
Feb-19	17.80	176.86	26.57	52.09
Mar-19	15.58	148.13	25.39	45.79
Apr-19	15.40	162.20	25.08	51.60
May-19	14.85	146.47	26.53	57.37
Jun-19	12.10	147.46	22.72	48.90
Jul-19	12.11	140.06	24.07	43.69
Aug-19	11.82	141.07	25.88	47.79
Sep-19	13.85	165.97	27.78	52.48
Oct-19	14.98	155.51	25.94	53.95
Nov-19	18.79	158.39	28.17	52.12
Dec-19	20.37	209.02	33.12	65.67
Jan-20	14.91	165.05	26.60	49.28
Feb-20	19.19	200.36	31.15	57.80
Mar-20	16.72	166.91	29.60	50.55
Apr-20	15.91	175.91	28.12	54.84
May-20	15.95	165.11	30.90	63.39
Jun-20	14.68	187.53	29.84	60.97
Jul-20	12.51	151.65	26.91	46.38
Aug-20	12.71	159.02	30.10	52.84
Sep-20	13.76	172.61	29.79	53.55
Oct-20	15.47	168.11	28.91	57.24
Nov-20	20.21	178.27	32.67	57.57
Dec-20	20.03	214.98	35.08	66.31
Jan-21	16.00	185.29	30.74	54.33
Feb-21	18.22	198.87	31.82	56.34
Mar-21	18.70	194.99	35.56	58.01
Apr-21	16.42	189.61	31.16	58.08

May-21	16.46	177.89	34.22	67.11
Jun-21	14.51	193.53	31.64	61.84
Jul-21	12.90	163.24	29.74	49.08
Aug-21	13.12	171.09	33.24	55.90
Sep-21	14.19	185.63	32.88	56.63
Oct-21	16.59	187.94	33.15	62.94
Nov-21	20.01	183.89	34.56	58.43
Dec-21	20.65	230.90	38.62	70.08

Table 3 gives the estimated production rate for the selected quarries. Edo 1 operate one shift of eight hours with an existing production rate of 500 tonnes per day. Ogun 1 operates one shift of eight hours with an existing production rate of 1,500 tonnes per day. Ogun 2 operates one shift of eight hours with an existing production rate of 1,000 tonnes per day. Ondo 1 has an existing production rate of 750 tonnes per day.

5. Conclusion and recommendation

5.1 Conclusion

Based on the findings stated above, the following conclusions have been made:

1. The research was combined the Time Series Model of Centered Moving Average, Associative Model of Linear Regression and Multiplicative Model to forecast sales demand.

2. All the selected quarries sales record show that seasonality after their sales.

3. Out of all the quarries used as a case study for this research Quarry B will experience the highest demand within 2019 to 2021.

4. The minimum production rate to be maintained by the quarries are achievable because the selected quarries existing minimum production rate is greater than the estimated minimum production rate.

5.2 Recommendation

The following recommendations are made based on the findings and conclusion of this study:

1. The quarries in general should keep the record of their sales for forecast purposes.

2. It is recommended that quarry managers should release their sales record for ease of getting data for sales forecast.

3. Further study should be done on forecasting the demand for each aggregate size been sold by the quarries.

References

1. **Andrella, T.** (2018). Public holidays in Nigeria in 2019 Retrieved 16/04/2019 from https://www.legit.ng/1209039-public holidays-nigeria-2019.html

2. **Bernard, M.** (2016). What Is the Difference between Artificial Intelligence and Machine Learning? Retrieved on 02/07/2019 https://www.forbes.com/sites/bernardmarr/2016/12/06/what-is-the-difference-between artificial-intelligence-and-machine-learning/#384e0f32742b

3. **Bowersox, D., Closs, D., and Bixby C.** (2002). Supply Chain Logistics Management. New York: McGraw- Hill Irwin.

4. **Dalvinder, S.** (2014). A Critical Conceptual Analysis of Definitions of Artificial Intelligence as Applicable to Computer Engineering IOSR Journal of Computer Engineering (IOSR-JCE) 16(2), pp 09-13

5. **Ezeliora, C., Umeh, M., Mbeledeogu, N., and Okoye, U.P.** (2014). Application of Forecasting Methods for the Estimation of Production Demand International Journal of Science, Engineering and Technology Research (IJSETR), 3(2), pp186.

6. **Gerald, H.** (2019). How to Calculate Production Rates https://bizfluent.com/how 5977077-calculate-production-rates.html accessed 16/04/2019

7. **Jason, B.** (2016). Supervised and Unsupervised Machine Learning Algorithms Retrieved 02/07/2019 from https://machinelearningmastery.com/supervised-and-unsupervised machine-learningalgorithms/

8. Machine Learning with MATLAB. (2016). The MathWorks, Inc Web site. Retrieved 20/04/2019 from https://www.mathworks.com/campaigns/offers/machine-learning-with matlab.html

9. **Melodi, M**. (2018). Challenges and Prospects of Skilled Labour in Quarry Operations in Nigeria Journal of Sustainable Technology, 9(2), pp 78-87.

10. **Melodi, M., and Onipede, T.** (2017). Economic Appraisal of Some Selected Quarries Operation in Ondo State, Nigeria Journal of Engineering and Engineering Technology FUTAJEET 11(2) pp133-138

11. **Menezes, L.** (2004). Review of Principles of Forecasting, J. Scott Armstrong (ed.), Kluwer Academic Publishers, Journal of Forecasting, 23(3), pp 233-235.

12. **Nadler, S., and Kros, J.** (2007). Forecasting with Excel: Suggestions for Managers. Spreadsheets in Education (eJSiE), 2(2) pp 1.

13. **Nick, C.** (2018). Global Granite Market Analysis: Granite Exporters in India Leading in 2018 Retrieved 27/11/2018https://www.bizvibe.com/blog/global-granite-market-analysis/

14. **Nimai, C., Nishanth, D., Chinmaya, C., Gaurav, G., Rajat, G., Teja, S., Lalit, D., Ashutosh**, M. (2017). An Intelligent Approach to Demand Forecasting, Proceedings of the 2nd International Conference on Inventive Computation Technologies IEEE Xplore Compliant

15. **Olasehinde. A., and Bute. S.** (2014). Report on a Feasibility Study: A Case Study of Ratcon Quarry Limited, The Pacific Journal of Science and Technology 15(2), pp 204

16. **Olusanya, S., Awotungase, S., Ohadebere, E.** (2012). Effective Planning and Organizational Productivity (A Case Study of Sterling Bank Nigeria Plc), IOSR Journal of Humanities and Social Science (JHSS) 5(5) pp 31-39

17. **Opafunso, Z., Ajaka, E.** (2004). Application of geographic information system (GIS) to solid mineral resources information management. Pakistan Journal of Science Industrial Research. 47(3) pp 240.

18. **Scott, J., and Kesten, C.** (2017). Demand Forecasting II: Evidence-Based Methods and Checklists Working Paper 89-clean.

19. The Nation (2016). Generating Granite, Nigeria must fast-track local solid minerals development The Nation Web site. Retrieved 27/11/2018 from http://thenationonlineng.net/generating-granite/

20. **Vladimíra, V.** (2010). The Role of Demand Forecasting in Knowledge Society Faculty of Chemical Technology, Department of Economy and Management of Chemical and Food Industries, University of Pardubice, 95, Studentská , Czech Republic.

21. **Vladimira, V., and Michal, P.** (2010). Role of Demand Planning in Business Process Management 6th International Scientific Conference, Vilnius, Lithuania Business and Management.

EFFECT OF CHEMICAL ELEMENTS ON THE PROPERTIES OF PIPE STEEL IN HOT AND NORMALIZED POSITION

Makarenko V.D.
Poltava National Technical Yuri Kondratyuk University
DCs (Engineering), Professor, professor of the Department of Oil and Gas Engineering and Technology, Ukraine

Manhura A.M.
Poltava National Technical Yuri Kondratyuk University
Senior Lecturer, head of the Department of Oil and Gas Engineering and Technology, Ukraine

Rubel V.P.
Poltava National Technical Yuri Kondratyuk University
PhD in Technical Sciences, associated professor, associated professor of the Department of Oil and Gas Engineering and Technology, Ukraine

Melnykov O.L.
Poltava National Technical Yuri Kondratyuk University
Senior Lecturer, head of the Department of Oil and Gas Engineering and Technology, Ukraine

Abstract. The state and key areas of technology development and metallurgical solutions to the problem of increasing the mechanical properties of pipe alloy steels of high-duty particularly for the construction industry and main gas pipelines are considered. Steelmaking practice is presented in this work. The systems of steels alloying, as well as the types of heat treatment in manufacturing process and their advantages and disadvantages are considered in detail. The first part of the review provides brief information on the features of ordinary alloying of steels, and then binary and more complex alloying systems with simultaneous heat treatment in modern metallurgical plants are considered. The most promising, according to the authors, directions of development of metallurgical methods and types of heat treatment of pipe steels for the increase of their bearing capacity and prolongation of operational life are formulated. The substantiation of heat treatment of carbonitride hardening steels with the impurities of vanadium and other alloying elements, as well as ways to significantly reduce the sulfur content, which adversely affects the mechanical properties of steels, causing structure degradation, is given. The

possibility of obtaining pipe steels with a structural condition and viscous-plastic properties satisfying the operational requirements is substantiated. In addition, the paper, in general, gives information about the rffect of individual chemical elements on the properties of steel in hot-rolled and normalized state.
Keywords: normalization, deformation, alloying, modification, structure, phase.

It is known [1-7] that, in addition to the constant impurities – carbon, manganese and silicon, a number of other alloying elements can be introduced into steel composition. Thus, in various alloys, nickel with iron forms a continuous series of solid solutions. The decomposition temperature of austenite nickel-containing steels is lower than that of nickel-free ones, so nickel in the amount of up to 1% helps to obtain a dispersed structure, and in larger quantities – the structure of acicular ferrite. Nickel has little effect on the standard mechanical properties of manganese-containing low-alloy steels. The transformation products that are formed with a nickel content of more than 1.3% increase the transition temperature to a fragile state, while at smaller quantities, this element has a positive effect on this indicator, as well as on the development of cracks.

With the introduction of 0.9% nickel in steel, the ferrite-pearlite structure is retained, and at high concentrations the products of intermediate transformation occur [3,4].

It is believed that one of the factors affecting the properties of nickel containing ferrite is the amount of interaction energy between dislocations and impurity atoms. Nickel reduces the interaction energy between dislocations and impurities – carbon and nitrogen. Increasing the cold resistance of iron in the presence of nickel is a means of reducing the carbon-nitrogen blockage of dislocations.

In ferrigo-pearlitic steels, chromium is mainly in solution. Strengthening of its presence is weaker than that of other elements when its number is not more than 0.7%. In large quantities, the strength increases sharply, and the ductility is significantly reduced. The absolute value of impact toughness decreases, the work of crack development decreases [6,7].

Sulfur, phosphorus, oxygen, hydrogen, nitrogen are harmful impurities that, under certain conditions, increase the brittleness of steel. The removal of these impurities in steelmaking is of fundamental importance.

Vanadium, niobium, titanium, and boron are the most widely used as microalloying elements in modern steels.

When considering the effect of these elements on the properties and structure of low-alloy steels, it is necessary to take into account the degree of their affinity to carbon, nitrogen, oxygen and sulfur (Table 1 [8]).

Table 1

Affinity of micro alloying elements to carbon and a number of other elements

Microalloys	Elements			
	C	N	O	S
Ti	S	VS	VS	AV
Nb	S	AV	W	W
V	S	VS	W	W

Designation: VS - very strong affinity; S - strong; AV - average; W - weak.

In terms of their affinity to nitrogen, titanium and vanadium significantly exceed niobium; to oxygen, sulfur - titanium exceeds niobium and vanadium. Vanadium and niobium form stable carbides and nitrides (carbonitrides) that have a high dissolution temperature in austenite, so they contribute to grain fragmentation. Titanium nitrides are practically insoluble until the melting point.

Vanadium, niobium, and titanium carbides (VC, NbC, and TiC), as well as VN, NbN, and TiN nitrides have a NaCl-type face-lattice. Due to the proximity of the crystal lattice parameters, the carbides and nitrides of each of the elements are soluble in one another indefinitely. Large niobium carbonitrides, which are released during the crystallization of steel, are stored under repeated heating to high temperatures. Small niobium carbonitrides dissolve at temperatures above 1100 ° C and are released when the rolled metal is cooled due to a decrease in the solubility of niobium in austenite and ferrite, located along the grain boundaries. Small niobium carbonitrides inhibit the movement of dislocations, which helps to strengthen the steel. Niobium carbonitride is completely soluble in austenite only when heated to 1250 °C, while vanadium carbide is characterized by a high solubility in austenite. When normalized, this phase goes into a solid solution. At the same time, vanadium nitride has a relatively low solubility in austenite [9,10].

With increasing content of *vanadium* carbonitride in steel increases its strength and toughness. Rolling cooling speed has little

effect on the level of mechanical properties of normalized steel with carbonitride strengthening. This is probably due to the fact that when heated under rolling, almost all of the vanadium carbonitrides pass into a solid solution and with subsequent cooling in the air after rolling is not completely released. Selected coarse nitrides are located mainly along the grain boundaries. When heated under normalization, the isolated vanadium carbonitrides are the centers of austenitic phase origin. They provide fine austenitic grain, then partially dissolve in austenite and under subsequent cooling fall in a dispersed form fairly evenly over the body and grain boundaries.

Aluminum, titanium and zirconium have a higher affinityto nitrogen than vanadium, so when they are introduced into steel in excessive quantities, a part of the nitrogen is spent on the formation of nitrides of these elements, which leads to a deterioration of steel properties with carbonitrid strengthening (strength and viscosity reduction etc.). Therefore, it should be noted that carbonitride strengthened steel containing vanadium and nitrogen should be deoxidized with a minimum of strong nitriding elements or elements having weak nitriding capacity.

Thus, for the effective enhancement of the complex properties of low-alloyed, normalized, manganese-containing steels, microalloying with dispersed nitrides (carbonitrides), first of all vanadium and niobium, is appropriate. The carbonitrides of these elements are relatively easily converted when heated to a solid solution and under cooling are released in austenite (Nb) or preferably in the process of austenite decay in the range of 600 - 700°C (V). The effect of niobium is more evident in the hot-rolled state, while the effect of vanadium carbonitride only after reheating, for example, normalization. The effect of titanium on the properties of steel is manifested depending on its state (in pure form or in the form of compounds). In hot-rolled steel, titanium with a total amount of 0.1% is oxidized in carbides (about 0.055%), nitrides (about 0.025%) and oxides (about 0.002%), as well as in partially solid solution (about 0.02%). After low temperature heating (negative hardening), the amount of titanium solid solution sharply decreases and usually does not exceed 0.003% with the growth of titanium carbides. As a result, the impact toughness increases while reducing strength [11].

It should be noted that minor additives of titanium (0,01-0,03%) are effective in crushing the normal structure of the metal, as formed in liquid steel titanium nitrides serve as centers of crystallization. The size of these particles of titanium nitride is about 0.02 microns. They serve as a barrier to grain growth and facilitate their fragmentation [12].

With small aluminum additives (up to ~0.1%), the critical brittleness temperature decreases, which is a result of the reduced content of dissolved nitrogen. After removal of nitrogen from the solution, the aluminum content practically does not have an effect on this indicator, but with its excessive amount of grain growth occurs, accompanied by an increase in the brittleness temperature.

Nitrogen in the composition of niobium nitrides, vanadium and titanium contributes to the increase of properties, as beforementioned. The presence of free nitrogen in steel causes the phenomenon of deformation aging. The decrease in properties depends largely on the process of cold deformation.

Studies have shown that nitrogen is distributed in the cast ingot fairly evenly, with some predominant release along the grain boundaries.

Studies of the influence of various elements on the properties of normalized low alloy steel type 16G2AF containing vanadium (0.10-0.15%), aluminum (0.02-0.04%) and nitrogen (0.013-0.024%), showed [5-12]:

1. Increase in carbon content from 0.16 to 0.23% strengthens the properties, reduces the toughness at sub-zero temperatures and slightly affects the cold brittleness threshold (T50), which is explained by perlite share increase without changing the size of the ferrite grain.

2. *Manganese* with a content up to 1.7% moderately strengthens the steel, slightly increases the toughness and cold resistance, which is associated with the fragmentation of grain, so it is advisable to alloy steel of this type with manganese to 1.7%.

3. *Silicon* in the amount of 0.45 to 1.5% gradually increases the strength characteristics with a decrease in impact toughness and increased cold resistance, which is associated with some enlargement of the grain, a strong curvature of the crystal lattice and the elimination of this element.

4. *Chromium* up to 1.3% increases the strength, but decreases the yield strength, lowers toughness and increases the cold shortness threshold, which is associated with grain consolidation and increased perlite formation.

5. With an increase in the content of vanadium to 0.28%, there is a slight increase in strength properties with a decrease in impact toughness (when the content is more than 0.15%) and a slight increase of cold shortness threshold. Therefore, steel with carbonitride strengthening is advisable to microalloy vanadium to 0.15%.

6. *Niobium* in the amount up to 0.08% in steel with 0.09% V practically does not affect the mechanical properties, so the use of this element in normalized steel with carbonitride strengthening is impractical.

7. *Nickel* and copper in the amount of 0.5% each slightly increase the strength and impact toughness, but have virtually no effect on the cold shortness threshold, so it is possible to use these elements if necessary to further strengthen the steel with carbidonitride.

8. With increasing nitrogen content, the strength properties increase due to the fragmentation of grain. With a constant content of vanadium, the impact toughness decreases and increases the threshold of cold shortness. However, while increasing the content of vanadium, these indicators are improving, so to obtain optimal properties, it is necessary to ensure the complete binding of nitrogen with vanadium and aluminum.

9. Small *molybdenum* additives have little effect on the properties of such steel. Small titanium additives slightly reduce the yield stress due to the depletion of the metal with nitrogen, which goes into the formation of stable titanium nitride. Joint microalloying with nickel, copper and molybdenum is accompanied by a significant strengthening with the deterioration of cold shortness impact toughness.

In steel with *vanadium and nitrogen* micronutrients, the level of mechanical properties is highly dependent on the content of the nitride (carbonitride) phase. As the content of this phase increases, the yield strength increases monotonically with the increase of impact toughness and reduction of cold shortness threshold.

In steel with *vanadium and nitrogen* micronutrients, the level of mechanical properties is highly dependent on the content of the nitride (carbonitride) phase. With the increase of the content of this phase, the yield strength increases monotonically with the increase of the impact toughness and the decrease of the cold shortness threshold [2,3].

The mechanism of change in the properties of steel with *vanadium carbonitride* depends largely on the content of alloying elements. The optimum content of *vanadium, aluminum and nitrogen* in carbonitride strengthening steels is at 0.08; 0.13% and 0.02% respectively. The upper limit of aluminum content should be 0.05%, to eliminate binding too much nitrogen with a corresponding decrease in strength [3-6]. For hot-rolled pipes, steel 14HGS was developed, which provides the following level of properties in finished pipes after hot straightening, which is equivalent to normalization

$$\sigma_T = 378 H/mm^2 \cdot \sigma_B = 534 N/mm^2 \cdot \delta_5 = 29{,}7\%.$$
$$KCU_{-40} = 59\ J/cm^2.$$

Experimental tests have shown that cold deformation of normalized 14HGS steel (up to 5%) has a relatively small effect on hardness, which remains at a level above 50 J/cm^2. A significant increase in the properties of low-alloy steel, especially plasticity and impact toughness, achieved by normalization, has led to a marked increase in the proportion of sheet steel supplied in the normalized state [5,6].

For less critical pipes with a diameter of 530-820 mm, 17GS steel was developed with slightly less manganese content, which is used in a hot-rolled state. Studies have shown that lowering the temperature of the end of rolling has a positive effect on the toughness of hot-rolled sheets of this steel. The maximum value of this characteristic at -40 °C and the highest number of fibrous components in the fracture of the specimens were noted after rolling with the end of deformation at 850 °C. As the temperature of the end of the rolling decreases, the yield strength and the relative elongation increase.

Rolling in the mass production of gas pipes from 17GS steel confirmed that this steel is technological and belongs to the class of well welded. After adjusting the chemical composition and

increasing the amount of manganese from 0.25% to 1.15-1.55% steel was named 17G1C, with average properties [4,5]

$$\sigma_T = 395 H/mm^2 \cdot \sigma_B = 553 N/mm^2 \cdot \delta_5 = 28{,}8\%.$$
$$KCU_{-40} = 78\ J/cm^2.$$

Studies have shown that normalized 17G1C steel has a good resistance to cracks and tears in rigid plastic deformation, has a low temperature threshold of cold shortness, and sufficiently homogeneous mechanical properties for static stretching along and across the rolling axis. At the same time, anisotropy of impact toughness on longitudinal and transverse samples is observed. The threshold of cold brittle T50 in sheets of steel 17G1C lies in the interval (-20)÷(-40) °C [2].

Despite the use of rolling technology in the longitudinal and transverse scheme, the impact strength on longitudinal samples is ≈ 30% higher than the transverse ones.

The results of the extensive industrial production of 17G1C steel showed that its production does not cause great difficulties, and the properties of finished pipes made of this steel are quite stable. In this regard, steel 17G1C is the main for the manufacture of pipes with a diameter of 1020 and 1220 mm.

Taking into account the need to further increase the viscous properties of 17G1S steel, a limit of sulfur and phosphorus content was adopted: no more than 0.020% and 0.025% respectively. This allowed to significantly increase the impact toughness. 17G1C-U steel began to be used for pipes with diameters of 1020 and 1220 mm, and steel 17G1C used for the production of pipes with diameters of 530-820 mm [1].

A variant of 17GS steel is 12G2C steel, which is designed for the production of hot gas pipelines with a diameter of 530, 720 and 1020 mm (instead of 14HGS steel). The carbon ratio of this steel is 0.35-0.43 with a maximum allowable 0.46 [1.5].

Normalized 12G2C steel is characterized by increased fracture resistance when evaluating impact toughness and fracture fibrillation. The complex of viscous properties at subzero temperatures indicates the fundamental possibility of the use of 12G2S steel for pipes in the northern version. The transition temperature of a semi-brittle fracture

lies in the range (-30)÷(-40) °C, while in steel 14HGS at (10)÷(10)°C [2].

17G1C, 17G1S-U, 17G2SF steels, which are characterized by a strength level from 510 to 540 NU mm^2, are used for common purpose spiral pipes. On the basis of 17G1S steel 17G2SF steel is developed, which contains 0.05-0.1% V and 0.01-0.03% Ti, and which is characterized in the sheets after normalization by the following properties [1,2,5]

$$\sigma_T = 380 - 470 H/mm^2 \cdot \sigma_B = 550 - 650 N/mm^2 \cdot \delta = 28{,}8\%.$$
$$KCU_{-40} = 40 - 65\ J/cm^2.$$

17G2SF steel has high manufacturability in pipe processing (molding, welding by conventional technology). The strength of the welded joint was higher than that of the parent metal. 08G2SFB rolled steel with a temporary resistance of 540 N/mm^2 was developed for a more responsible purpose [1,2].

For spiral pipes intended for operation at high working pressures, a non-perlite 08G2SFT coiled steel is developed, which provides in sheets up to 12 mm a high complex of mechanical properties. Steel has a reduced sulfur impurity content (≤0.008%). After controlled rolling at a temperature of 730-750 °C, the impact toughness can be from 70 to 190 J/cm^2.

For straight pipes, 14G2SFB steel containing 0.045% Nb was tested. The level of temporary resistance in steel after normalization was 550 N / mm^2 in combination with high ductility, toughness and cold resistance. To increase the toughness of this steel, controlled rolling was carried out at a total compression of 40% and a rolling end temperature of 800-850 °C. As a result, were obtained properties that corresponded approximately to the properties of normalized steel.

Pipe steels with vanadium carbonitrides (type 17G2AF, 17G2SAF, 15G2AFY, etc.) have different contents of carbon, silicon, and aluminum. As compulsory micro alloying elements they contain vanadium (0.05-0.12%) and nitrogen (0.015-0.025%). In hot-rolled condition, these steels have high strength (650-700 N/mm^2) and not high impact strength. After heating above Ac_3 temperature with air cooling (normalization), the strength decreases somewhat, but the ductility and

impact toughness increase (by 5-10% and at -40 °C by 30-40 J/cm^2, respectively) [5-8].

Pipes with diameters of 1020-1220 mm were produced from sheet steel (15G2AF, 17G2SAF, 14G2AF-U, 15G2AF, etc.) using hot-straightening method (15G2AF steel) or cold expansion.

To increase the viscous properties, a carbonitride strengthened steel containing about 1% Ni, 0.03% Nb (14NBAF) and a small amount of sulfur was tested. The alloying of steel with nickel and niobium increased the cold resistance to -60 °C.

Conclusions

1. As can be seen from the analysis of the steel grades under consideration, the use of controlled rolling makes it possible to obtain high mechanical properties by using maximum pressures at temperatures close to the recrystallization temperature, which corresponds to the normalization mode. In carbonitride and some microalloyed steels various methods of heat treatment are used to obtain the required mechanical properties.

2. In recent years, the metallurgical industry has mastered the serial and mass production of a number of low-alloy low-permeable steels for gas pipes with a diameter of 10,4-14,4 mm at a pressure of 5,4-7,4 MPa in the northern version, which are subject to controlled rolling on plate reverse machines. In the development of these steels composition at different stages of their development and application different systems of strengthening microalloying were used: joint additives of niobium and vanadium (steel 07G2FB) ; complex microalloying with niobium, vanadium and a small amount of titanium intended for nitrogen binding and grain fragmentation (09G2FB, 10G2FB, 10G2FB-U); carbonitrid strengthening with vanadium and nitrogen (08G2FY); vanadium without special alloying with nitrogen (10G2F), titanium in an amount up to 0.035% (13GS, 13GS-4, 13G1C-U) [1,2-4].

3. Due to the improvement of secondary steelmaking methods, the sulfur content has been significantly reduced. The development of controlled rolling modes with the end of deformations in the middle and lower part of the $\gamma + \alpha$ regions allowed to significantly increase the strength characteristics and resistance to brittle fracture.

References

1. **Bernshteyn M.L., Brunzel Yu.T**., **Golovanenko S.A.** i dr. (1983) Metallovedenie i termicheskaya obrabotka stali: Spravochnik. Moskva. Metallurgizdat. 3.

2. **Matrosov Yu.I., Litvinenko D.A., Golovanenko S.A.** (1989)Stal dlya magistralnyih gazoprovodov. Moskva. Metallurgiya.

3. **Gonik A.A.** (1986)Serovodorodnaya korroziya i meryi ee preduprezhdeniya. Moskva. Nedra.

4. **Grabin V.F., Denisenko A.V.** (1978) Metallovedenie svarki i nizko- i srednelegirovannyih staley. Kiev. Naukova dumka.

5. **Gridnev V.N., Gavrilyuk V.G., Meshkov Yu.Ya.** (1974) Prochnost i plastichnost holodnodeformirovannoy stali. Kiev. Naukova dumka.

6. **Gulyaev B.B.** (1976) Teoriya liteynyih protsessov. Leningrad. Mashinostroenie.

7. **Gumerov A.G., Yamaleev K.M., Zhuravlev G.B.** i dr. (2001) Treschinostoykost metalla trub nefteprovodov. Moskva. OOO "Nedra-Biznestsentr".

8. **Efremov V.A.** (1976) Raskislenie i kristallizatsiya stali. Moskva. Metallurgizdat.

9. **Etskovich G.M.** (1981)Raskislenie stali i modifitsirovanie nemetallicheskih elementov. Moskva. Metallurgiya.

10. **Kalinnikov E.S.** (1976) Hladostoykie nizkolegirovannyie stali. Moskva. Metallurgiya.

11. **Klinov N.Ya.** (1976) Korroziya himicheskoy apparaturyi i korrozionnostoykie materialyi. Moskva. Mashinostroenie.

12. **Kreschanovskiy N.S., Sidorenko M.F.** (1970)Modifitsirovanie stali. Moskva. Metallurgiya.

13. **Kudryashov V.G.** (1978)Vyazkoe i hrupkoe razrushenie. Moskva. Metallovedenie i termicheskaya obrabotka. T.12. 27-85.

14. **Dalskiy A.M., Artyuhova I.A**. i dr. (1985) Tehnologiya konstruktsionnyih materialov. Moskva. Mashinostroenie.

15. **Ermolaev I.F.** (1968) Truboprokatnoe proizvodstvo. Moskva. Gos. nauch.-tehn. izd-vo po chernoy i tsvetnoy metallurgii.16. Makarenko V.D., Prohorov N.N., Paliy R.V. (2002)Effect of barium on the phosphorus content of deposited metal of welded joints in cold-resistant steel.Weldinq Snternational. **14(**7). 35-40.

17. **Makarenko V.D., Beljaev V.A.,Galichenko E.N., Prohorov N.N.** (2001) Effect of modifying additions on the ductility and plastic properties and the brittle strength of coldresistant, low-alloy steel. Welding International.**15**(1). 62-70.

18. **Makarenko V.D., Beljaev V.A.,Galichenko E.N., Prohorov N.N**. (2001) Effect of modifying microadditions on the corrosion resistance of welded joints in low-alloy steel. Welding International.**15(**2). 78-85.

VIRTUAL ASSESSMENT OF THE STATE OF THE OPTIMAL BALL LOAD OF THE MILL GRINDING ORE DRESSING PLANTS

Kondratets V.
Central Ukrainian National Technical University, Doctor of Technical Sciences, Professor, Professor of the Department of Automation of Production Processes, Ukraine

Matsui A.
Central Ukrainian National Technical University, Ph.D., Associate professor, Associate Professor of the Department of Production Process Automation, Ukraine

Abashina A.
Central Ukrainian National Technical University, Student of the KI-17 group, Ukraine

Abstract. The subject of the study is the optimal ball load of the mill grinding ore at the processing plants in closed cycles with a classifier. The optimal ball load of the mill is calculated and refined experimentally. The method is based on the Rittinger crushing law, on the basis of which the dependence of the useful energy spent on the installed mass of the processed ore, the size of the initial ore and the crushed product and the coefficient, which is determined by the strength properties of the material and its density, is obtained. For a certain technological different type of ore, its parameters are unchanged and the amount of usable useful energy is determined with great accuracy. The aim of the work is a virtual assessment of the state of the optimal ball load of the mills grinding ore at the processing plants in a specific field. The state of the optimal ball load is assessed by the average harmonic weighted size of the feed ore, the same size to which the material is ground and the specified amount of ground ore, which approximately corresponds to the operation of the technological unit for one hour. The determined amount of ore being crushed in a separate cycle is determined by conveyor weights with an error of less than 1%. The means for measuring the size of materials are calibrated in units of the average harmonic weighted size. The measurement of ore size does not require sufficiently high accuracy. Measurement results are averaged over the course of determining ball wear. According to the known specific responses of the balls and the lining, according to the specific useful energy expended, the number of balls of different sizes is found, which must be loaded into the technological unit to replace worn ones. Balls must be submitted individually, with the possibility of rounding their residues in cycles to an integer.

Keywords: ball mill, loading, wear and tear, virtual assessment, differently sized load, useful energy

1. Introduction

Due to the fact that deposits of rich iron ores are exhausting their capabilities, from the second half of the last century, deposits of poor iron ores are intensively being developed. From poor iron ores with a content of 20...35% iron, by concentration, the content of the useful component is brought to 65%. Magnetite concentrates have become the raw material base of ferrous metallurgy. In China, the task now is to obtain commercial iron concentrate containing 60.79% from ore, which contains 18.64% of ferrous compounds [1]. The priority areas outlined in [2], this trend is confirmed. Prior to beneficiation, poor iron ores in ore dressing plants are ground in ball mills to reveal impregnations of the useful component. In the first stage of ore grinding, significant overheads of electricity, balls and lining are allowed, resulting in an increase in the cost of iron concentrate, which is a problem for the mining industries.

2. Actuality of the paper

This problem is solved in different ways, among which one of the determining ones is the automation of these technological processes. The importance of this direction was noted in [3]. In [4], the absence of some information tools or their high cost and lack of reliability was noted. In this direction, perhaps, the main thing is to maintain the ball loading of the mill at the required level. It is proved that the highest productivity of the mill is achieved by filling the drum with balls by 50%. Mostly ball mills operate when filling balls with 40-50% [5]. Practice shows that filling the drum of the mill with balls is kept at 40% due to possible overload, losing productivity. It was found that a mixture of balls of different sizes is more productive than the same grinding media. The issues of rational nutrition of mills with balls have been posed for a long time and continue to be posed [6], since it has been proved by practice that mills loaded with balls of four to five sizes provide 10...15% higher productivity compared to technological units with a one-dimensional grinding medium. From the point of view of maximum productivity, there is an optimal characteristic of the size of the ball mixture. The maximum size of the balls and the particle size characteristics of their mixture are specified experimentally [5]. There are selected mixtures of balls for certain working conditions, material and technological units [7, 8, 9]. The developed methods for determining the initial optimal char-

acteristics of the size of the balls, its maintenance in the process by adding new grinding media to replace worn ones [10]. This approach will save billions of monetary units per year in countries with a developed mining industry [11], however, for this it is necessary to control the state of the ball load. To ensure the optimal ball load at a level of about 50% and, as a result, the maximum productivity of the mill, it is necessary to continuously evaluate its condition - or measure the volume in the drum, or the value of the worn ball load. This problem is solved in different ways, mainly starting from the 70s of the last century. One of the first, which is being implemented at the present time, is the principle of interim management. It is more or less effectively used for mills in conditions of stabilization of the output power, when a certain batch of balls is loaded after a given interval of operation (usually after 24 hours) [12]. In conditions of a wider change in the performance of ball mills, the principle of tracking the amount of crushed ore was used [12]. These approaches have poor ball loading accuracy. From time immemorial, a decrease in the load of the drive motor of the mill has been noticed when the grinding medium is worn. Therefore, the loading of balls into the technological unit began to be carried out according to the energy parameters of the drive electric motor [13]. Initially, devices for monitoring the active current of the stator of a ball mill electric motor [14] and active power were developed. At the level of inventions, devices with an acoustic transducer have been proposed, means with controlling the frequency of exit from the mill of unrefined ore pieces, consumption of metal worn from balls and lining, measuring active power and sound signal, determining the correlation between the wear of balls and lining and devices, including changing feed balls and measuring the current weight of the mill and the level of filling the drum with crushed material and grinding media. These proposals were not further developed and were not used in practice. Systems based on measuring the active power of drive motors continued to improve. They were built using the dependence of the signal of the average value of the active power of the mill electric drive on the mass of balls in the drum [5]. Mostly researchers are developing this approach. So, in 2006 M. J. Daniel [15] returned to these same systems, and in 2008 – K.Ya. Ulitenko [16], who proposed a method for evaluating the optimality of ball filling of mills based on monitoring

the unloading of the drum volume during discrete loading of a portion of balls. E.V. Kochura, A.N. Maryuta, and V.I.Dmitriev proposed a method for regulating ball loading with measuring the dispersion of the pulsations of the moment applied to the shaft of the drive motor. Under modern conditions, it was studied in [17] using DEM-modeling. It is noted that the torque signal at ball mills contains sufficient information to uniquely characterize the level of loading of the technological unit. A methodology for estimating the mill fill level based on a spectral analysis of torque is proposed here. So, basically the development is based on measuring the active power of a ball mill drive. The use of torque and DEM-modeling with the use of spectral analysis instead of measuring the active power of the drive does not bring anything new, since the measurement principle remains the same. The very principle of loading a ball mill with grinding bodies cannot be highly accurate, for several reasons. For example, the power formula of a ball mill operating in waterfall mode [9] contains the inner diameter of the drum, which changes when the lining is triggered. The same formula gives overestimated power values, since when the ball load drops, part of its energy is "lost" to the rotation of the mill drum. What part of the total energy of the ball load is this "return" is not exactly established [9]. In addition, the drive motor consumes the total active power, which, along with useful, is spent on overcoming internal losses, losses in gearboxes, own bearings and bearings of the technological unit itself, where they are significant and unstable in time, and the ball load is associated only with its useful share. When the circulating load changes, the resistance moment of the cochlear feeder also significantly increases or decreases, which still introduces a significant additional error. Therefore, it is accepted in practice that the useful power of the mill drive motor is 75...90% of its total value [18]. In these conditions, it is almost impossible to talk about the level of error that will satisfy the process. Moreover, the daily decrease in the mass of the grinding medium in a ball mill is about 4...5% [19]. It should also be borne in mind that a sharp decrease in the active power consumed by the mill most often indicates not a decrease in the ball load, but about its technological overload. Therefore, now there is no alternative to the imperfect temporal principle of controlling the state of ball loading of mills and they are forced to use it [19], signif-

icantly losing productivity, consuming electricity, balls and lining. Despite this, the task of improving control over the state of the optimal ball loading of mills is relevant and requires further research.

3. Unresolved parts of a common problem

It is more efficient to introduce balls into the mill according to the deviation of the consumed active power of the set master action, and in accordance with their wear during ore grinding under specific conditions, which is virtually estimated by the strength properties of the raw material, its size, the size to which it is ground, and the volume of ground material. At the same time, unproductive losses of useful energy during ore grinding are not taken into account and a rather high accuracy of estimating the volume of worn balls is expected, however, no such studies have been carried out.

4. Aim of the research

The aim of the work is a virtual assessment of the state of the optimal ball loading of mills that grind ore at concentration plants in the conditions of specific deposits.

To achieve this goal it is necessary to solve the following tasks:

- evaluate the size of the material crushed in the mill;
- determine the work (energy spent) when grinding ore;
- to prove the possibility of a virtual assessment of the state of the ball load;
- reveal the conditions for virtual assessment of the state of the ball load;
- experimentally test the method in an industrial environment;
- determine the number of balls to be loaded.

5. Method

5.1. Estimation of size of the material crushed in mills

The work of grinding ore in ball mills is expressed in the newly created surface. In such cases, it is customary to use the specific surface area of the bulk material $s_P=S/Q$, where S is the surface Q kg of bulk material. Replace the actual bulk material with an ideal one, consisting of the same sized cubic solid particles. Then the specific surface of the bulk material will be

$$s_P = 6/\delta_T d_C , \quad (1)$$

where δ_T - ore density; d_C - size of a single piece of ore.

Given (1), we argue that the specific surface area of bulk material can serve as a measure of its size.

We apply formula (1) to a selected sample of bulk material of mass m represented by n narrow size classes, where the average size value will be defined as the arithmetic mean $(d_i+d_{i+1})/2$. Let the material in the sample be idealized in which a narrow class is applied cubes with an average value of d_{Ci}. Then the surface of solid particles in each narrow class of size is determined by the dependence

$$S_i = \frac{6 \cdot m_i}{\delta_T d_{Ci}}, \tag{2}$$

where m_i - mass output of narrow size class.

Similarly, we write the dependence for the entire sample of bulk material

$$S_\Sigma = \frac{6 \cdot m}{\delta_T d_C}, \tag{3}$$

where d_C - the average size of the solid in the sample material.

The surface balance for the entire sample of bulk material $S_\Sigma = \Sigma S_i$ can be represented as

$$\frac{6 \cdot m}{\delta_T d_C} = \frac{6 \cdot m_1}{\delta_T d_{C1}} + \frac{6 \cdot m_2}{\delta_T d_{C2}} + \ldots + \frac{6 \cdot m_n}{\delta_T d_{Cn}}$$

or

$$\frac{m}{d_C} = \frac{m_1}{d_{C1}} + \frac{m_2}{d_{C2}} + \ldots + \frac{m_n}{d_{Cn}}. \tag{4}$$

Having submitted the right-hand side of (4) as a sum, we write

$$\frac{m}{d_C} = \sum_{i=1}^{n} \frac{m_i}{d_{Ci}}, \tag{5}$$

where from

$$d_C = \frac{m}{\sum_{i=1}^{n} \frac{m_i}{d_{Ci}}} = d_{CГ}, \tag{6}$$

In dependence (6), d_C is the average solid size calculated as the harmonic mean weighted by the mass yields of fractions. We denote it by $d_{CГ}$. So, dependence (1) can be used to calculate the specific surface area of the actual bulk material, where the solid is represent-

ed by particles of different sizes and shapes, if $d_C=d_{CГ}$, i.e. determined by (6).

When testing technological processes, equipment, the development of instrumentation use the weighted average size of solid in bulk material, which is determined according to the dependence

$$d_{C3} = \frac{d_{C1} \cdot m_1 + d_{C2} \cdot m_2 + ... + d_{Cn} \cdot m_n}{\sum_{i=1}^{n} m_i} = \sum_{i=1}^{n} d_{Ci} \cdot m_i / m, \quad (7)$$

We multiply the left and right sides of expressions (6) and (7), reduce the resulting expression by m, from which we obtain

$$d_{CГ} = \sum_{i=1}^{n} d_{Ci} \cdot m_i \Big/ d_{C3} \sum_{i=1}^{n} \frac{m_i}{d_{Ci}}. \quad (8)$$

Depending on (8), the parameters d_{Ci} and m_i respectively mean the average values of narrow size classes and their mass yield in samples; therefore, there is a relationship between $d_{CГ}$ and d_{C3}. This relationship will not be functional, because, $\sum_{i=1}^{n} d_{Ci} \cdot m_i$ and $\sum_{i=1}^{n} m_i / d_{Ci}$, in addition, are determined by the characteristic size of bulk material. Therefore, this dependence can be applied within a specific bulk material, for example, source ore, sands of the classifier, unloading of a ball mill. For a certain technological different type of ore and technological equipment within a specific product of the technological scheme, this will practically be a functional dependence.

5.2. Work done on grinding ore

It has been experimentally proved that the wear of balls under certain conditions is proportional to the consumption of useful energy [9]. Therefore, we determine the work of crushing ore entering the ball mill.

When crushed, pieces of ore are destroyed in the weakest places, the result of which is the hardening of the material with a decrease in its size. In the process of crushing, external forces first deform pieces in a certain part of their volume, and then, when the tensile strength is exceeded, they are destroyed by a number of fragments. This creates new surfaces in those places where stresses from external forces exceeded the tensile strength. The created surface area during the destruction of a single large piece is always larger compared to the

newly created area during the destruction of an individual small fragment. Therefore, the destruction of a large piece of ore always requires large external forces. When grinding, work is partially spent on deformation of the ore and dissipated into the surrounding space in the form of heat and partially on the creation of new surfaces with conversion to free surface energy of a solid. The work of deformations during fracture is proportional to the deformed volume of a brittle body. The work of creating a new surface during crushing is proportional to its size

$$A_S = \sigma \Delta S , \qquad (9)$$

where σ - proportionality coefficient; ΔS - the value of the newly created surface.

If ΔS=1, then the proportionality coefficient σ represents the work performed to create a surface unit and may have a dimension of kGm/cm^2. When a single piece with a small surface is crushed, and after crushing, a thin product with a large surface is obtained, then when determining the work done in this process, one can neglect the cost of deformation, since they will be small. Then, dependence (9) expresses the Rittinger law, according to which the crushing work is proportional to the value of the new surface created during grinding.

In the process of modeling a different-sized ball load [10], it was found that in the drum of the mill МШР-40×50 along its length it is possible to distinguish ten almost identical sections of almost one-sized balls, the diameters of which increase from the loading to the unloading end. At each of these sites, solid grinding occurs during the movement of the pulp. The analysis shows that the operating conditions of the balls in these areas are such that grinding occurs with almost the same efficiency. Solid, received at the entrance of a separate section, at the exit significantly reduces its size. Therefore, it is possible to consider that this ball mill has 10 grinding stages with a significant degree. Under such conditions, it is possible to apply the Rittinger law.

Suppose that Q tone of the source power is supplied to the input of the ball mill, and it is pieces of various shapes and sizes. To simplify the research, let us give the real bulk material ideal, consisting of particles of the same solid cubic shape with the rib size D_{CT} determined by (6). Then, at the exit from the ball mill, the solid frac-

tions will have a d_{CT} size determined by the same dependence (6). We take the same degree of crushing r in all stages. In this case, the total degree of crushing will be $i=r^{10}$. Considering that $d_{CT}=D_{CT}/i$, the surface area of a small fraction of ore after crushing will be $6(D_{CT}/i)^2$, and its volume – $(D_{CT}/i)^3$. The number of small particles of ore in one piece of its initial size will be D_{CT}^3: $(D_{CT}/i)^3=i^3$. Then the surface of the crushed material will be

$$S_g = 6\left(D_{CT}/i\right)^2 \cdot i^3 = 6D_{CT}^2 i\,. \tag{10}$$

Since the surface of the output ore piece is equal to $S_в=6\ D_{CT}^2$, the value of the newly created surface will be equal to

$$\Delta S = S_g - S_в = 6D_{CT}^2 i - 6D_{CT}^2 = 6D_{CT}^2\left(i-1\right). \tag{11}$$

Based on equations (9) and (11), we determine the crushing work of one large piece of ore, which will be equal to

$$A_S = k_r D_{CT}^2\,, \tag{12}$$

where $k_r=6\sigma(i\text{-}1)$.

The work of crushing the entire ore mass Q kg, presented in the form of cubic particles of size D_{CT}, respectively (12), will be presented in the form

$$A_Q = k_R Q \big/ D_{CT}\,, \tag{13}$$

where $k_R=k_r/\delta=6\sigma(i\text{-}1)/\delta_т$, where $\delta_т$ - density ore.

In a ball mill, grinding will be carried out in approximately 10 stages. The sizes of pieces of ore that go through all stages of crushing create a series whose members contain the average harmonic weighted size D_{CT} and the degree of grinding r. According to (13), it is possible to write down the dependences for the work performed in each stage when grinding Q kg of ore. The total work performed will be equal to the sum of the work in each stage. Having completed a number of mathematical transformations of the general expression of the work performed, we obtain the equation

$$A = k_R\left(\frac{1}{d_{CT}} - \frac{1}{D_{CT}}\right)Q = \frac{6\sigma\left(i-1\right)}{\delta}\left(\frac{1}{d_{CT}} - \frac{1}{D_{CT}}\right)Q\,. \tag{14}$$

Formula (14) expresses the work that needs to be done when grinding Q kilogram of ore with a particle size of D_{CT} to a size of d_{CT}. The dependence is obtained for an idealized material represented

by the same size cubic particles of solid. However, it will be true for real bulk material in which the sizes are found as the harmonic weighted average, since the ore strength does not depend on the form of the solid. According to (14), it is possible to find the work performed in kGm. Work (14) is the equivalent of spent useful energy. Multiplying the left and right sides of (14) by g, we obtain the dependence in Joule. Since 1 kW·h = $3.6 \cdot 10^6$Joule, the work performed or the energy spent in grinding Q kg of ore in kW·h will be, кВт·г

$$A = E = 0{,}2778 \cdot 10^{-6} g k_R \left(\frac{1}{d_{CT}} - \frac{1}{D_{CT}} \right) Q, \qquad (15)$$

where g - acceleration of gravity.

Dependence (15) is obtained on the basis of the Rittinger law, which takes into account only work on the creation of new surfaces. Therefore, it is generally accepted that it can be used only for an approximate determination of the total work. However, if the degree of crushing is high, which applies to ball mills, then this law provides high accuracy in determining the spent useful energy. The problem here is often the unknown and variable value of the proportionality coefficient σ, which characterizes the strength properties of the ore, as well as the density of the ore δ_T. If σ, δ_T, d_{CT}, D_{CT} and Q are known, then, using dependence (15), it is virtually possible to determine the useful energy spent on grinding ore mass Q with high accuracy. This indicator is not affected by the unproductive energy costs of the drive motor of the ball mill, so it is possible to assess the state of its ball load with high accuracy.

5.3. Possibility of virtual assessment of ball load status

First of all, we consider the influence of the coefficient k_R in (15) on the amount of expended energy that is virtually determined. In a ball mill, it is most appropriate to use and maintain optimal ball loading. For example, for a certain technological type of ore, the spherical composition in the mill МШР-40х50 can occupy 50% of the drum volume and contain the resulting rational composition of the grinding medium [10]. The loading of different-sized balls of 90 mm, 75 mm, 65 mm and 50 mm in the specified amount to replace worn ones ensures the invariability of the ball load during operation. Under these conditions, the degree of grinding of ore in the technological unit does not change and the effect on A (15) is not performed.

As the analysis shows, iron ore deposits of poor iron ores contain several technological types of raw materials. These ores are distinguished by their qualitative composition, density and ability to grind, that is, they have different values of the coefficient σ and density δ_T. If these ores are processed for processing in a mixture or if they do not maintain a strict order, the coefficient k_R in (15) will change and a significant error will be introduced in the determination of the consumed energy, since the boundaries of the changes in σ and δ_T in one deposit are quite wide [20]. Currently, scientists and practitioners are increasingly coming to the conclusion that the processing of poor iron ores is much more efficient with separate technological varieties on which a particular ball mill should be adjusted. It has now been proved the feasibility of separate processing of certain types of ores and the possibility of its implementation and recognition of ores in the process of mining [20]. Such a transition is inevitably necessary, because the industries suffer unreasonably large losses, which grow strongly in the face of a decrease in the iron content not only in rich but also in poor iron ores. When switching to the enrichment of individual technological ore types, σ and δ_T will remain unchanged. Therefore, the coefficient k_R in (15) will be constant and will not have a negative impact when virtually determining the amount of useful energy spent on ore grinding.

The size of the spent amount of useful energy during ore grinding is also affected by the size of the solid D_{CI}, which is crushed, the size of the solid d_{CI}, to which the material is crushed, and the mass amount of the crushed material Q, as can be seen from dependence (15). When calculating the spent amount of useful energy according to the formula (15), it is necessary to determine the material at the inlet of the ball mill. It is known that only large-class grains are subject to grinding in the mill, since the finished product is newly created only from grinding such grains [9]. The circulating load mainly plays the role of a carrier. Therefore, the size of solid D_{CI} should be determined without taking into account the circulating load, only by narrow classes of the initial power or by the measured values of its average weighted power. The size of the crushed material is measured directly.

Several approaches have been proposed to determine the weighted average particle size of the initial ore. Perhaps the most

suitable is a method based on the measured cross-sectional area of the flow and the linear load of bulk material on a conveyor belt. The weighted average size of the solid in the discharge of the ball mill can be determined by the device, the main provisions of which are described in [22]. The considered devices measure the weighted average particle size of the crushed material, and the dependence (15) includes the average harmonic weighted particle sizes. Since there is a relationship between them (8), these means of measuring the size of bulk materials can be calibrated in harmonic mean weighted units. It is advisable to determine the mass Q of the crushed material using a conveyor scale, since only large pieces of ore, represented by the flow of the source material, are crushed in a ball mill.

5.4. Virtual ball condition assessment conditions

Three hypotheses are known regarding the speed of operation of balls in a mill - Davis, Mertsel and Prentis, Bond. All three hypotheses were summarized by K.A. Razumov, who suggested that the speed of the balls be determined by the equation [9]

$$\frac{dG}{dt} = -kD^m, \tag{16}$$

where G - ball weight at the moment of starting; t - response time; k - proportionality coefficient; D - ball diameter; m - exponent that varies from 2 to 3.

Knowing the speed of operation of the balls and the time of their operation, it is possible to establish a worn-out mass of balls, however, this cannot be precisely determined, since k and m remain unknown in (16). The flow rate of balls can be determined by the mass of crushed ore. As noted in [23], the consumption of balls per ton of ground ore is not stable, since it is associated with the mill productivity, which depends on the properties of the ore. More stable is the consumption of balls, referred to a unit of energy spent on crushing the material [23], which was established back in 1937. Despite what has been said in the future, their consumption per ton of processed raw materials is widely used as an indicator for triggering balls. Relative to this indicator, a lot of experience and statistics have been accumulated. Indeed, if the grinding conditions of the material change, the stability indices will not differ. Therefore, especially in the processing industry, where the properties of ores and other grind-

ing conditions vary, these indicators are very different and they cannot be used unequivocally. For example, later in [9] they are given for chromium, carbon steel and cast iron during grinding to different values of the final fineness of the product, however, the type of ore and its initial fineness are not considered. The characteristics of the balls are not given. These tasks were studied in more detail in the cement industry, where specific experience was gained. Thus, stable data on the response of balls and armored plates per ton of processed specific raw materials are provided. The statistics on improving the management of the ball economy for many years are given. Attention was also paid to suppliers of balls and armored plates. The indicators relative to the same grinding media in different manufacturers are quite different, especially in one of them the indicators are much higher [24]. This cannot but affect the solution to this problem. That is, both the properties of the crushed ore and the wear resistance of the balls themselves have an effect on the wear of the balls. Togo is not necessary to perform their duties at the festival of singers and fencers. On the approach, we recommend that you reincarnate the transformation of the cul to hardness. To monitor the health of children should not be any problems with the skin. Skin can be processed into solids, solids, and solids [25].

The invariability of the technological variety of ore creates the same conditions for the operation of balls. Balls and lining with constant hardness and durability guarantee the same. However, the operation of the balls and the lining, in addition, can be affected by the dilution of the pulp in the mill, the optimal value of the circulation load and the amount of ore loading, which, with a specific technological type of raw material, can change only with fluctuations in the size of the feed. So, only the change in the size of the initial supply, which occurs when unloading storage bins on a conveyor belt, can affect the deflection response of balls and lining [26]. Therefore, if there are changes during ore grinding under specific conditions, they will be caused by a deviation of the average particle size of the feed from a certain standard value, that is, they will be natural and the response can easily be adjusted with the resulting value of the average particle size of the material, which is controlled. This is possible because under these conditions the balls and the lining will wear out naturally.

In formula (15), the coefficient k_R depends on the grindability of the ore σ, its density δ_T and the degree of grinding of the mill, which are constant for a specific technological type of ore and ball mill. If these parameters are determined and taken into account, then k_R will be constant and an error in finding the expenditure of useful energy or the work performed will not occur. Given that the degree of grinding of the ball mill is large, under these conditions, the Rittinger law will provide accurate results. However, it is possible to determine the quantitative laws of ore grinding only on the basis of experimental data for a particular material, because depending on the physical properties, different materials behave differently during grinding [9]. That is, it is possible to clarify the value of the coefficient k_R in (15) only in an experiment on a specific ore type.

Given the conclusion of D. K. Kryukov [27] that for a certain size and hardness of the crushed material, it is possible to select the size characteristic of the ball mixture, which provides the highest mill performance, it is advisable to use the composition of the ball load [10] only for a specific ore type, however, in each case, the characteristic of the size of the ball load, which provides the greatest productivity, should be clarified experimentally [28]. Since for each technological ore type there are optimal values of gross productivity and circulating load, which ensure the highest mill productivity in the finished product [18], these parameters should be clarified in this experiment, which will facilitate the development and simplify the automatic control system of the grinding process.

Dependence (15) corresponds to the value of the useful energy spent on grinding Q kg of ore of a certain technological variety (k_R) of the average weighted size D_{C3} to the average weighted size d_{C3}, therefore, it most precisely, almost accurately complies with an indicator that cannot be obtained using another approach. The amount of expended energy thus obtained most closely corresponds to the truth, since in addition to the volume of crushed ore Q and its technological variety and the characteristics of the mill, it takes into account both its average input size and the size to which it is milled. With certain characteristics of the ball mill, configured to process a specific technological ore type, the operating conditions of the optimal composition of the balls will not change. In this case, the conditions of wear of the balls will not change and the specific wear of the balls will

exactly correspond to the amount of ore being crushed or the energy expended for its grinding.

Under such conditions, when grinding ore of a certain technological type, it is possible to determine the wear of balls and lining per ton of processed raw materials or per kW·h of energy expended. Such unit costs were precisely set in the cement industry. For example, in the case of using conventional unalloyed materials, specific wear can be equal to 1000 g per ton of cement, including 850 g/t for grinding balls and 150 g/t for lining plates.

When grinding one ton of clinker in shaft furnaces, balls wear out by 700 g, and armored plates by 100 g. Otherwise, when grinding clinker for one kW·h of spent useful energy, 40 g of grinding media and 5 g of lining are consumed [24]. For a specific technological type of ore, it is possible to obtain absolutely accurate data on the operation of balls and lining for one kW•h of usable useful energy. Let the consumption of balls be 60 g, and the lining plates 10 g per kWh of usable useful energy in ore processing. As you can see, quite accurate indicators of the wear of the balls and the lining are formed per unit of spent useful energy. They will be unchanged during the processing of a specific technological type of ore in a ball mill configured to grind it.

This indicator allows you to virtually receive the amount of worn balls and lining, which can be compensated during operation, by the amount of useful energy spent.

5.5. Experimental verification of the method in industrial conditions

Dependence (15) includes the average harmonic weighted sizes of the initial power of a ball mill and solid in its discharge. The size of the same products is measured in average weighted values. Since this relationship has never been tested, such research needs to be done.

The study was carried out at the first stage of grinding the initial ore at the processing plant of one of the mining and processing plants. The studies were carried out by sampling the source ore, sands of a single helical classifier, unloading a ball mill, and draining the classifier.

Sampling and processing of material samples was carried out in accordance with generally accepted methods. Based on the test re-

sults using dependences (7) and (8), the weighted average d_{C3} and the average harmonic weighted $d_{CГ}$ solid sizes were determined at all sampling points. Samples were taken in the steady state operation of a closed cycle of grinding the original ore. Since such studies in industrial conditions are laborious, and the relationship between the found parameters is expected to be almost functional, four experiments were conducted.

Their results are presented in Fig. 1, from which it can be seen that in various products of the technological scheme for grinding the initial ore, an exact correlation is observed, sometimes practically functional, between the studied parameters.

The relatively insignificant deviations in these dependences can be explained by the characteristics of the characteristics of the size of the material, and possibly certain errors in the selection and processing of samples. This is especially possible to note regarding the discharge of a ball mill, where it is rather difficult to take samples from the point of view of matching their characteristics to the entire mass of material.

The results obtained allow us to conclude that theoretical positions are confirmed by experimental verification and the possibility of calibration of measuring devices directly in units of measurement of the average harmonic weighted solid size at individual technological points of the closed grinding cycle of the initial ore.

Measured in units of harmonic weighted mean particle sizes, it is possible to obtain $D_{CГ}$ and $d_{CГ}$ of the initial ore and ball mill unloading.

The mass of the crushed ore determined by the conveyor scales was established with the known k_R, according to dependence (15), it is possible to determine the amount of usable useful energy for this process. Let k_R=0,4886 m^2 for this technological variety of ore. Then dependence (15) takes the form, kWh

$$E = 1{,}33154 \cdot 10^{-6}\left(\frac{1}{d_{CГ}} - \frac{1}{D_{CГ}}\right)Q\,,. \qquad (17)$$

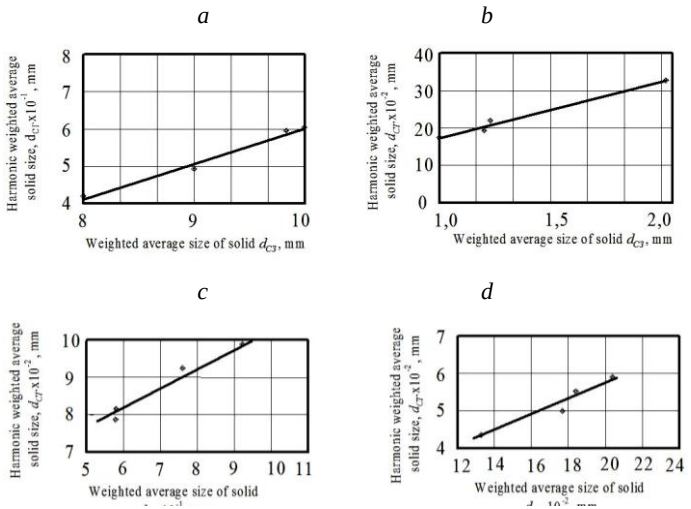

Fig. 1. Dependence of the average harmonic weighted solid size on its weighted average size at various technological points of the closed ore grinding cycle: *a* - source ore; *b* - sands of single spiral classifier; *c* - ball mill unloading; d*г* - single spiral classifier discharge

In dependence (17), d_{CF} is determined by the impregnation of the useful component in the ore and is measured, since there can be certain deviations from the set value in the grinding process. Suppose that d_{CF} is ideally maintained and is equal to 0.09 mm. The average harmonic weighted size of the pieces of ore in the initial feed varies within certain limits and affects the expenditure of useful energy. The effect of the change in D_{CF} on the spent useful energy is seen from Fig. 2. With the growth of the average harmonic weighted particle size of the solid in the initial feed of the ball mill, the spent useful energy for grinding ore increases. In the possible range of changes in D_{CF}, the growth of useful energy can be 12.44%, which is significant. It follows from formula (17) that this growth does not depend on the established volume Q of the crushed ore. An analysis of the curve in Fig. 2 shows that as the size of the solid increases, the relative increase in the usable useful energy for grinding ore increases significantly less. For example, with D_{CF}=0.6 mm, an increase in solid size by 16.7% leads to an increase in the usable useful energy for grinding by only 2.46%, which does not require a sufficiently

high accuracy in measuring D_{CI}. The average harmonic weighted size of the pieces of the initial ore varies over time, therefore, in (17) D_{CI} will not be a constant value. The volume Q of crushed ore is best chosen so that it meets no more than one hour of operation of a ball mill. Take Q=160·10^3 kg. Then, in the process of grinding this amount of ore, it is necessary to continuously determine the D_{CI} and during this time to find its averaged values of D_{CIO}, which should be used to determine the spent useful energy according to (17).

The product of the specific wear of balls defined for a given type of ore and ball mill per kWh of usable energy and the amount of energy expended makes it possible to establish a worn-out mass of balls when grinding a given ore mass (Q=160·10^3 kg). Knowing the ratio of the wear of balls and lining, we find separately the mass of worn lining plates and grinding media. According to the weights of the worn balls and the lining, it is possible to determine the number of balls that need to be loaded into the ball mill to compensate for the worn grinding media and the lining during the measurement cycle. Ball wear and lining cycles are performed continuously.

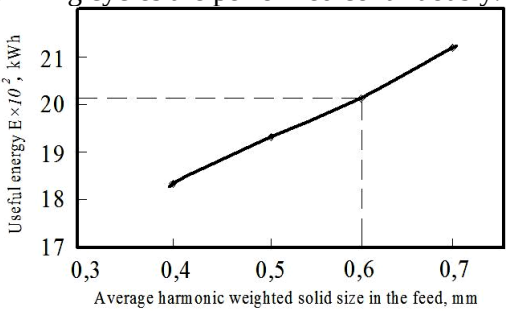

Fig. 2. Dependence of useful energy spent on grinding 160·10^3 kg of ore on its average harmonic weighted size

5.6. Determining the number of balls to load

Let us consider the problem using a specific example of grinding ore in a ball mill МШР-4.0×5.0. We will maintain the mixed ball load [90 mm - 32%, 75 mm - 27%, 65 mm - 23%, 50 mm - 18%] at the level of 50% of the mill drum volume, which is 134.4·10^3 kg. We will make balls after grinding every 160•10^3 kg of ore. Let k_R=0.4886 m^2 for ore to be crushed in technological different types of ore, and

the consumption of balls is 60 g, of the lining plates 10 g per one kWh of usable useful energy.

Suppose that in the experiment when grinding $160 \cdot 10^3$ kg of ore, the measured average harmonic weighted size of the solid in the discharge of the ball mill was 0.09 mm, and the same parameter in the initial ore was 0.58 mm. Then the value of the usable useful energy determined by (17) is E=1999.86 kWh. The consumption of balls was 120 kg. Lining consumption - 20 kg. Given that the density of steel balls is 7800 kg/m^3, we determine the volume of the worn lining V_ϕ=0.002564 m^3. When replacing a worn lining with balls, half of this volume will be filled, that is, V_ϕ=0.001282 m^3. Balls of different sizes have 38% voids. Then 0.00079487 m^3 with a mass of 6.2 kg will be occupied by metal. The total mass of balls will be 126.2 kg.

According to the mass obtained, we determine the number of balls of each size that must be loaded into the mill. The calculation data are given in table 1.

Table 1

The calculation data of the number of balls that must be loaded into the mill after grinding $160 \cdot 10^3$ kg of ore

Diameters of balls, mm	The relative content of the balls in the load,%	The mass of balls in the load, kg	Ball mass, kg	The number of balls of each size, pcs.	The number of loaded balls, pcs.	Remains of balls, pcs.
90	32	40,384	2,9758	13,57	13	0,57
75	27	34,074	1,7221	19,786	19	0,786
65	23	29,026	1,1210	25,893	25	0,893
50	18	22,716	0,5102	44,524	44	0,524

From the data of Table 1 it can be seen that the total mass of worn balls can determine the number of grinding bodies that need to be loaded into the mill after grinding established Q kg of ore. Given the influence of the size of the initial feed on the ore grinding process, the number of balls in individual cycles will vary. According to the obtained values, balls must be supplied to the mill individually. The system for supplying grinding media to the technological unit must have a storage device that will accumulate the remnants of the balls to an integer value with their subsequent loading.

6. Conclusions

It has been established that there is a relationship between the average harmonic weighted and weighted average size within a specific crushed material (initial ore, classifier sands, ball mill unloading, classifier discharge), which is determined by the size characteristic. Based on the Rittinger crushing law, the formula for determining the useful energy in kWh for grinding ore in a ball mill with a grain size D_{CT} weighing Q kg to a size d_{CT}, which includes the coefficient k_R, which depends on the material strength parameter, its density and mill grinding degree, is obtained. If the strength parameter, density, average harmonic weighted size of the initial ore and the size to which grinding is carried out, and the amount of processed ore are known, then it is virtually possible to determine the useful energy spent on this technological operation. This indicator is not affected by the unproductive energy costs of the drive motor of the ball mill, so it is possible to assess the state of its ball load with high accuracy. Since the newly created finished product is obtained only from grinding grains of a large class, and the circulation load plays a role mainly of a transporting agent, the size of the solid that is crushed should be determined by the narrow classes of the feed, i.e., by direct measurement of the weighted average size of the feed of a ball mill. This is best done using a method based on measuring the cross-sectional area of the flow and the linear load of bulk material on a conveyor belt. A tool has also been developed for measuring the weighted average particle size of the discharge of a ball mill. Given the relationship between the average harmonic weighted and weighted average particle size of the crushed material, means for measuring the size of the products can be directly calibrated in the average harmonic weighted values. The mass of crushed ore can be fixed with a conveyor scale. The optimal ball load for a certain technological ore of a different type corresponds to absolutely accurate indicators of wear of the balls and lining per unit of spent useful energy. They will be unchanged during the processing of a specific technological type of ore in a ball mill configured to grind it. This indicator allows you to virtually receive by the amount of useful energy spent the mass of worn balls and lining, which can be compensated in the process. The obtained results of experimental studies in industrial conditions allow

us to conclude that the theoretical positions on the relationship of the average harmonic weighted and weighted average sizes of solid in bulk materials at individual technological points of the closed grinding cycle of the initial ore are confirmed. This relationship is closely correlated, sometimes practically functional. The relatively insignificant deviations in these dependences are mainly explained by the characteristics of the material fineness characteristics. With an increase in the average harmonic weighted particle size of the solid in the initial feed of the ball mill, the useful energy spent on grinding the ore increases. In a possible range of changes in the growth parameter of the spent useful energy can be 12.44%. This growth does not depend on the established volume of crushed ore. Since with an increase in the size of the initial ore by 16.7%, the relative increase in the spent useful energy for grinding ore increases by only 2.46%, the measurement of particle size does not require sufficiently high accuracy. The volume of crushed ore in a separate cycle must be selected within the framework of a ball mill for one hour. Despite the fact that the average harmonic weighted size of the pieces of the original ore varies over time, it is necessary to continuously determine its size and find the averaged value over the established amount of ore grinding, to use it in a virtual assessment of the state of the optimal ball load. By finding the amount of usable useful energy and multiplying it by a known value of the specific wear of the balls by one kWh, a worn-out mass of balls is established in the grinding cycle. Knowing the ratio of the operation of the balls and the lining, separately find the mass of worn lining plates and grinding media. According to these masses, determine the number of balls that must be loaded into a ball mill to compensate for worn grinding media and lining. Considering the inconsistency of the number of balls in individual cycles, they must be supplied individually to the technological unit. The ball feeding system should have a storage device that will accumulate the remnants of the balls of individual sizes to an integer value with their subsequent loading.

The prospect of further development is to ensure optimal ball and ore loading of the mill of the first stage of grinding of raw materials. The basic material for optimal ore loading of a drum mill is the material published in [29].

References

1. **Siqing L., Yang Z., Wanping W., Shuming W.** (2014). Beneficiation of a low-grade, hematite-magnetite ore in China. Minerals & Metallurgical Processing. 31 (2), 136-142.

2. European Commission. Sustainable process industry. Multi-annual roadmap for the contractual PPP under Horizon 2020. (2013), 131. doi: 10.2777/30452.

3. **Azaryan A.A., Krivenko Yu.Yu., Kucher V.G.** (2014). Avtomatizatsiya pervoy stadii izmel'cheniya, klassifikatsii i magnitnoy separatsii – real'nyy put' povysheniya effektivnosti obogashcheniya zheleznykh rud. Visnik Krivoriz'kogo natsional'nogo universitetu. 36, 275-280.

4. **Kupin A.I.** (2008). Intelektual'na identyfikacija ta keruvannja v umovah procesiv zbagachuval'noi' tehnologii'. Vydavnyctvo KTU. Kryvyj Rig, 204.

5. **Pivnyak G.G., Vaysberg L.A., Kirichenko V.I.** (2007). Izmel'chenie. Energetika i tekhnologiya. Izd. dom. «Ruda i Metally». Moskva, 296.

6. **Baatarkhud Zh., Davaatseren G., Bilenko L.F.** (2000). Ob odnom iz putey intensifikatsii protsessa izmel'cheniya v sharovykh mel'nitsakh MShTs-5500kh6500 na kombinate «ERDENET». Obogashchenie rud. 3, 3-5.

7. **Golyshev L.V., Kravets T.Yu.** (2014). Metod formirovaniya sharovoy zagruzki barabannoy mel'nitsy. Nauch.-tekhn.firma «Energoprogress».Energetik. 11, 54-55.

8. **Qingfei X., Huaibin K., Bo L., Chunmei L.** (2014). Optimization study to the ratio of primeval ball loading in φ4.0x6.0m overflow ball mill of Yingerhuang Gold Mine. AASRJ Procedia. 7, 14-19.

9. **Andreev S.E., Perov V.A., Zverevich V.V.** (1980). Droblenie, izmel'chenie i grokhochenie poleznykh iskopaemykh. Moskva, Nedra, 415.

10. **Kondratec' V.O., Reva O.M., Karchevs'ka M.O.** (2008). Teoretychne doslidzhennja ustalenyh i perehidnyh rezhymiv roboty kul' ta futerovky v mlynah. Tehnika v sil's'kogospodars'komu vyrobnyctvi, galuzeve mashynobuduvannja, avtomatyzacija. 21, 187-196.

11. **Yatsenko A.A.** (2011). O povyshenii effektivnosti raboty sharovykh mel'nits na osnove ispol'zovaniya kombinirovannoy melyushchey zagruzki. Obogashchenie rud. 3, 3-5.

12. **Trop A.E., Kozin V.Z., Arshinskiy V.M.** (1970). Avtomatizatsiya obogatitel'nykh fabrik. Nedra. Moskva, 320.

13. **Volotkovskiy S.A., Bun'ko V.A.** (1964). Avtomatizatsiya protsessov na obogatitel'nykh fabrikakh. Nedra. Moskva, 282.

14. **Goncharov Yu.G., Polishchuk A.P., Engel' P.S.** (1972). Povyshenie ekonomichnosti raboty mel'nits pri optimizatsii sharovoy nagruzki. Materialy mezhdunarodnoy konferentsii po sistemam avtomaticheskogo regulirovaniya ARS-72. 19, 1-15.

15. **Daniel M.J.** (2006). Measurement of electrical energy consumption in a Bond ball mill. Proc. Of the XXIII Intern. Mineral Processing Congress, 92-97.

16. **Ulitenko K.Ya.** (2008). Optimizatsiya sharovoy zagruzki barabannykh mel'nits po potreblyaemoy moshchnosti. Obogashchenie rud. 5, 42-44.

17. **Pedrayes F., Norniella J.G., Melero M.G., Menendez-Aguado J.M., del Cor-Diaz J.J.** (2018). Frequency domain characterization of torque in tumbling ball mills level monitoring. Powder Technology. 323, 433-444.

18. **Sergo E.E.** (1975). Droblenie, izmel'chenie i grokhochenie poleznykh iskopaemykh. Vishcha shkola. Kiev, 240.

19. Proizvodstvo kontsentrata na obogatitel'noy fabrike OAO «Poltavskiy GOK». Tekhnologicheskaya instruktsiya TI-3-01-05. (2005). Komsomol'sk-na-Dnepre, 63.

20. **Macuj A.M., Kondratec' V.O.** (2017). Modeljuvannja pidhodiv podribnennja riznotypiv rud konkretnogo rodovyshha u kul'ovyh mlynah zamknenogo cyklu. Matematychne modeljuvannja. 2 (37), 43-49.

21. **Macuj A.M., Kondratec' V.O.** (2017). Modeljuvannja seredn'ozvazhenoi' krupnosti tverdogo v zavantazhenni kul'ovogo mlyna rudoju i piskamy klasyfikatora. Matematychne modeljuvannja. 1 (36), 59-66.

22. **Macuj A.M., Kondratec' V.O.** (2017). Teoretychne i eksperymental'ne doslidzhennja magnitoelektrychnoi' systemy, shho spryjmaje krupnist' piskiv odnospiral'nogo klasyfikatora. Elektrotehnika ta elektroenergetyka. 2, 38-49.

23. **De Vancy E.D., Coghill W.H.** (1937). The relation of ball wear to power in grinding. Mining Eng. Journal. 138, 337-340.

24. **Duda V.** (1981). Tsement. Stroyizdat. Moskva, 464.

25. Normy udel'nogo iznosa i raskhoda sharov dlya uglerazmol'nykh sharovykh barabannykh mel'nits pri razmole antratsita, kamennykh i burykh ugley NR34-70-021-82. (1983). SPO Soyuztekhenergo. Moskva, 8.

26. **Kondratec' V.O., Macuj A.M.** (2015). Modeljuvannja rozpodilu droblenoi' rudy vzdovzh konvejernoi' strichky pry rozvantazhenni bunkeriv. Integrovani tehnologii' ta energozberezhennja. 3, 42-50.

27. **Kryukov D.K.** (1965). Futerovki sharovykh mel'nits. Mashinostroenie. Moskva, 184.

28. **Kasatkin A.G.** (2004). Osnovnye protsessy i apparaty khimicheskoy tekhnologii. OOO TID «Al'yans». Moskva, 753.

29. **Kondratets V., Matsui A., Yatsun V., Lichuk M.** (2019). Identification of energy efficiency of ore grinding and the liner wear by a threephase motion of balls in a mill. Eastern-European Journal of Enterprise Technologies. 3. 5(99), 21-28.

NEW TECHNOLOGY FOR THE INTENSIFICATION OF OIL AND GAS RECOVERY FROM DEPLETED AND MARGINAL WELLS

Bazhaluk Ya. M.
Scientific and Production Firm "INTEX", Ivano-Frankivsk, Ukraine

Karpash O.M.
Ivano-Frankivsk National Technical University of Oil and Gas, Ivano-Frankivsk, Doctor of Technical Sciences, Professor, Ukraine

Voloshyn Yu. D.
Ivano-Frankivsk National Technical University of Oil and Gas, Ivano-Frankivsk, Ukraine

Abstract

The article studies the effect of cyclic loads on the strength characteristics and filtration in a porous medium, fatigue processes in the rock skeleton, and the prospects for developing technologies for active stimulation of formations in order to clean the bottom-hole zone and intensify oil and gas production. The issues of formation and growth of fatigue cracks in the rock under the influence of the pulse generator GKP-1 are also considered.

Analysis of recent researches and publications

The development of wells in low-permeability formations is associated with many difficulties in their construction and completion, as well as in the specifics of the selection of equipment and development of technologies. According to the world practice, in order to increase the initially low filtration and formation properties of the matrix of the formation rock, hydraulic fracturing is mainly used with various options for its implementation (interval, directional, acidic, local, multistage). However, when fracturing, highly permeable sections and systems of fractures are mainly included in the development, since the technology will most likely increase the length and openness of existing fractures rather than creating new ones. Therefore, technologies for active stimulation of the formation are being studied which allow creating, apart from main fractures, a network of fatigue cracks of different sizes and thereby increase the efficiency of field development.

Nowadays, a large number of experimental studies [2,12,17,18,21] confirms the hypothesis that under the influence of cyclic loads of a certain amplitude, the rock is actively destroyed at

stresses, significantly less than the tensile strength of given rock. To the static loads acting constantly on the rock during cyclic action, a dynamic component is added, which is superimposed on them by the principle of superposition. As a result, microcracks can open, grow, or stop their growth depending on the anisotropic properties of the rock and the distribution of local stresses, the scale factor, and nonlinear characteristics of the medium during the waves transmission [4,7,8,9]. That is, damage accumulation processes take place in a rock with a cyclic effect on it. Residual stresses are initiated before stress concentrators in the unloading cycle, and fatigue cracks develop in the direction perpendicular to the load axis [12]. Thus, the evolutionary process of existing microcracks growth and the formation of new ones takes place. This causes a change in the volume of fluid that is filtered through a unit of effective rock area per unit of time. Depending on the type of rock, fatigue during cyclic exposure occurs at loads of 60-80% of the maximum after 10-105 cycles [2,9,18,21]. Moreover, the presence of filtrate in the rock increases this effect [2,4]. According to the authors [5], in some cases, the activation energy of a fracture due to rock saturation with water can decrease by 4 times.

Numerous studies on the effect of alternating load on the rock by recording Kadomtsev A.G. acoustic emission [3,5], Morteza Ghamgosar computed tomography [17], Ko T.Y. video recording [12], Erarslan N. electron microscopy [13] show continuous accumulation of irreversible deformation, energy of dissipation under cyclic loading, growth and coalescence of microcracks into mesocracks and confirm the occurence of fatigue cracks. The studies of X. L. Zhao and J.-C. Roegiers [14], T.B. Celestino [15] and Y. Chen [20] showed that the number of cracks during cyclic loading had increased, along with their length, and the process had a three-stage nature: the first stage was for the growth of existing cracks; the second stage was for the formation of a fracture propagation zone; stage 3 - initiation of new crack growth (Fig. 1).

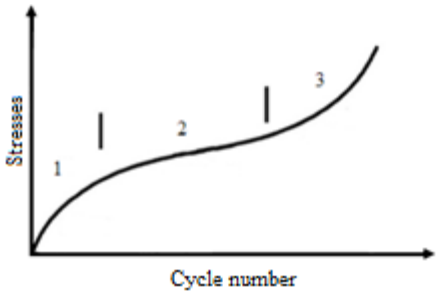

Fig 1. Stages of fatigue damage accumulation

The dislocation of microdestructions in rocks is transcrystalline (intragranular, intergranular) [1,3,11,17]. Such violations form the fracture propagation zone (FPZ) [13,16,17]. This zone consists of microcracks, each of which has its own submicrocrack zones, which turn into mesocracks. Such a hierarchy of structure for fatigue processes plays an important role since a large-scale effect is manifested. However, for shale rocks, as shown by studies with DIC surveys [10], the formation and growth of cracks is different, more complex and unexplored, due to the presence of a large number of layered structures. In [19], when conducting studies on the influence of the hydraulic pulses frequency on acoustic emission and formation characteristics, it was shown that a low frequency causes greater energy release and a greater intensity of crack opening inside test samples compared to a higher frequency. Therefore, studies were carried out within the frequency range of 50-100 Hz.

Research object

In the conducted experimental studies, the main attention was paid to the influence of cyclic loads in combination with surfactants on the strength properties of rock models, as well as on the change in the filtrate volume for artificial and natural core samples.

Research method

The experiment was carried out in two stages. At the first stage of research, we studied the strength characteristics of samples of cement stone with dimensions of 30×30×160 mm by non-destructive testing using an ultrasonic analyzer "Pulsar 1.1" and their change during combined exposure. Samples were formed over 90 days and were saturated with a surfactant solution (solpen) in accordance with the

experimental design. Cyclic loading was carried out on a special installation with a retainer-holder, a loading system and a power control system. The study of the relative strength indices of cement stone samples was carried out in accordance with the Latin plan at five levels for three influential factors: surfactant content *c*, power *I* and time *t* of sample processing. Given the heterogeneity of the samples for strength testing, we studied the relative strength indicators averaged over four facet-ways before sample stimulation started.

To interpret the results of the studies, the relative strength index was used as the ratio of strengths after and before the experiment.

The experimental data were processed using regression analysis methods with the aim of constructing the most adequate model $\hat{\varepsilon}$ in the class *E* of second-order polynomials

$$\sigma_B = a^T b(c,I,t), \tag{1.1}$$

where $b(c,I,t)=(1,c,I,t,cI,ct,cIt,c^2,I^2,t^2)^T$ - vector of basis functions; $a^T = (a_0, a_1, ..., a_\varepsilon)$ - vector of model parameters.

Parameter estimations $\hat{a}$ and models $\hat{\varepsilon}$ ran in class $\varepsilon \in E$ of basic functions arbitrary combinations according to the conditions of the minimum adequacy variance

$$\min\left\{S_s^2 = \frac{1}{n-r_s}\sum_{i=1}^{n}\left[a_s^T b(c_i,I,t_i) - \sigma_{Bi}\right]^2\right\} \Rightarrow \{\hat{a},\hat{\varepsilon}\}, \varepsilon \in E, \tag{1.2}$$

where r_s - the number of estimated models' parameters.

The most adequate model $\hat{\varepsilon}$ dispersion efficacy $S_s^2 = 2{,}25 \cdot 10^{-4}$ and vector of basis function $b(c,I,t)=(1,c,I,t,cI,ct,cIt,c^2,I^2,t^2)^T$ with parameters' estimations

$$a^T = (1{,}015;\ 0{,}030;\ 8{,}898 \cdot 10^{-5};\ -6{,}471 \cdot 10^{-4};\ -2{,}26 \cdot 10^{-3};\ 1{,}385 \cdot 10^{-6})$$

According to the results of the experiment, the presence of the influence trend of the cyclic load intensity (correlation coefficient *r*=-0.400) and the duration of the treatment (correlation coefficient *r*=-0.664 on the relative strength index and the absence of surfactant concentration influence (correlation coefficient *r*=0.004) is confirmed. A graphical interpretation of the processing parameters influence of the rock model on the relative strength indices is shown in the dependences $\sigma_B(c,I) = idem$, as well as $\sigma_B(I,t) = idem$ (Fig. 2).

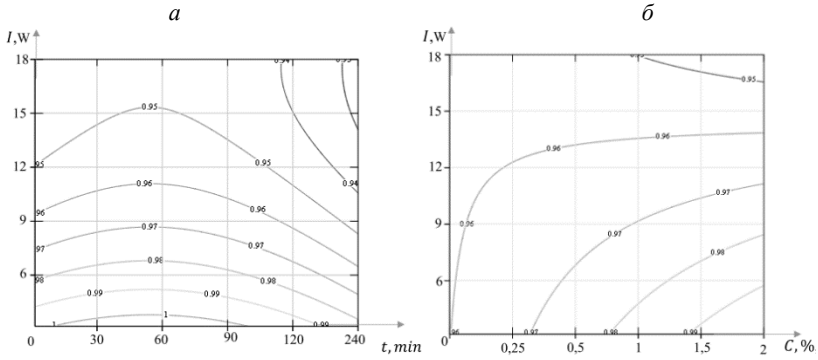

Fig. 2. Influence isolines of processing time (*a*) and surfactant concentration (*b*) change on samples strength

According to the results of the first stage, it was determined that for the experimental conditions there were areas of influential factors combinations that reduce the strength indices of rock models, as well as processing parameters and the necessary oscillation intensity for the technology to increase the FES [24] were selected.

At the second stage, we studied the filtration processes in a porous medium during the action of cyclic loads with different frequencies and amplitudes. To obtain reliable results in the absence of oscillation interference (which are present when using installations for studying the permeability of core samples of the UIPK type), in IFNTUOG, together with the scientific and production company INTEX, a facility was developed for studying the permeability of a porous medium in the process of hydraulic impulse loads on the core UDC-2 (Fig. 3).

Using the installation, when filtering the working fluid through the core 2 in the liquid medium 3, periodic pressure hydraulic pulses were created and transmitted to the core and cause its cyclic loading. As the working fluid, it is possible to use distilled water, produced water, flushing and other process fluids or mixtures. The pressure draw-down across the core during filtration is supported by a pump 10, manufactured with incorporated structural elements of a deadweight pressure-gauge tester, which allows maintaining a predetermined pressure value with high accuracy. Using a piezosensor 8 and a personal computer 14, the stability of the pressure pulses am-

plitude in a liquid medium is controlled. For periodic measurements of cyclic stress parameters on the core, a 795 M107V vibrometer is used. Measurement of oscillation parameters is carried out by inserting the probe of the vibrometer into the fitting 12 before contact with the core.

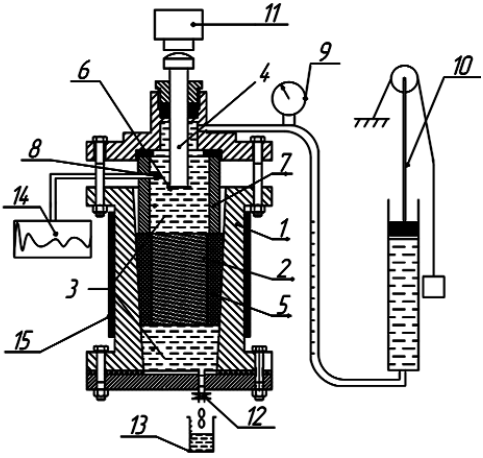

Fig. 3. Installation for studying the permeability of the pore medium in the process of pulsed core loads UDK-2: *1* – casing; *2* – core; *3* – working fluid; *4* - power plunger; *5*- rubber plug; *6* - ram tester; *7* - sealing plug; *8* - piezoelectric transducer; *9* - pressure gauge; *10* - pump; *11* - pressure pulse generator; *12* - fitting; *13* - measuring container; *14* - computer

Installation technical parameters

pressure draw-down on the core, MPa до 3;
lateral pressing, MPa до30;
pressure pulse repetition rate, HZ 50,100;
amplitude range, MPa 0.5-2;
duration of the pressure pulses leading edge, no more, ms 2;
operating temperature range, °C 20-70.

The volume of the filtrate, which is filtered through the core over time, directly indicates the state of spatial permeability, which varies depending on the conditions under which the filtration occurs. Since, during filtration and simultaneous cyclic influence, the fluid moves in the pores and microcracks of the core, changes in its rheological properties, the movement of uncemented particles (pollutant or par-

ent rock) [6], electrokinetic processes, opening, closing, development of new microcracks, the amount of filtrate per unit time can vary within certain limits. In this case, it is necessary to investigate what kind of the filtrate volume will be before, during, and after the treatment with pressure hydroimpulses, and evaluate the changes in comparison with the initial results. It is also necessary to determine the characteristics of materials removed during core filtration by applying the methods of lithological-petrographic analysis.

In this regard, a set of experimental studies was determined on the effect of cyclic loads on core material in order to establish patterns of change in the volume of fluid that is filtered under given conditions depending on the amplitude and number of load cycles

For research purpose, we used an artificial core made on the basis of a sand-cement mixture according to the methodology [22], as well as a natural core made of sandstone for research according to the standard method of UkrNDPI PJSC Ukrnafta. The core was saturated with formation water during its evacuation. Mineralization of produced water was 50 g/l.

The amplitude of the hydraulic pulses was chosen at the level of 2 MPa based on the capabilities of the hydraulic pulse generator GKP-1 of the INTEX company. The indicated amplitude did not exceed the fatigue strength limit for sandstone [11]. The value of the pressure amplitude was determined by measuring the vibration acceleration on the core surface using a 795 M107V vibrometer. The number of load cycles was taken equal to 105, taking into account the repetition rate of hydro pressure pulses of 50 Hz and the processing time of 30 minutes

Lateral pressure on the core was maintained equal to 20 MPa. The pressure draw-down across the core was maintained at 1.3 MPa. The operating temperature of the installation was within 20±1 °C. Measurements of the filtrate volume were carried out after 30 min in a measuring container 13 during filtration without core cyclic loads, during loads, and also after loads. The effect of processing was determined by the ratio of volumes during and after processing to the volume of the filtrate without treatment. To assess changes in the inner surface of the pore space due to fatigue fracture of the rock, a fluid analysis was carried out, for which, fluid samples with removed particles of rock were taken into special ceramic cups before and af-

ter loads. Samples with object glasses inserted into the cups were dried, after which they were subjected to lithological and petrographic analysis under a microscope with a magnification of 1000^x. For each core, the initial parameters were determined by pumping 8 pore volumes, the first 5 of which were not taken into account, and the average value was taken from the last three. Such a sequence of actions makes it possible to minimize the influence of electrokinetic processes and processes occurring on interfaces at the beginning of filtration in a pore medium and to obtain statistically reliable information. After determining the initial values for the cores, a series of 10 experiments were carried out during the treatment with hydraulic pulses and 10 experiments after treatment. To build the dependencies, the average value of each indicator was taken.

Research results

As it is seen from Figure 4, the processing of natural and artificial core mainly caused an increase in the filtrate volume during filtration for the same period of time. The highest growth was observed for artificial cores 2,4 during processing and is equal to 36-38%. After processing, this figure drops to 30-32%. However, for artificial cores 7,11,15, despite the increase in the filtrate volume during processing by 24%, 19.8% and 7%, respectively, when the effect is removed, it decreases to the initial and even lower. For other artificial cores the filtrate volume increases on average by 20% during processing, and after processing this figure decreases by about 4 times. For sample 1, there was a slight increase in the filtrate volume by 6% during processing, and a further increase of the rate to 29.5% under filtration conditions after treatment. Only for sample 18, treatment with pressure hydroimpulses did not give statistically significant results, since the change in volume was only 1-2%. Dispersion for the obtained results is in the range of 8-15%, depending on the specific core. The situation is similar for natural cores. The maximum increase in filtrate volume was observed for cores 2,12,16 by 30-32% during processing and 17-42% after processing respectively. For natural cores 5,10,14 negative results were obtained - the filtrate volume decreased by 8-26%.

The analysis of fluid samples showed that, when filtering without core cyclic loads, the samples mainly show the presence of lumpy oxidized clay mass, as well as dusty clay particles and very small

grains of quartz are present in an insignificant amount. Hydropressure pulses during filtration caused a significant increase in the samples of brownish clay mass and quartz grains coated with a clay film, and with further filtration without the action of hydraulic pulses, a gradual increase in rock cement particles is observed compared to the number of particles removed from the core before processing (by an average of 50%). The change in the filtrate volume for an artificial core is in the range of 5-30%, and natural 10-42%. The indicated indicates the appearance of additional fracturing of the rock. As for a natural core, processing is effective due to the presence of microfailures and microcracks in the samples that are not present in the artificial core, which is confirmed by the results of lithological and petrographic analysis. During filtration under the conditions of hydroimpulse exposure, core clay material, quartz particles are removed, and, consequently, the internal specific surface of the porous medium changes.

Based on the results of experimental studies, technologies and equipment have been developed for active impact on the productive horizon in conditions of repression or depression on the formation [23].

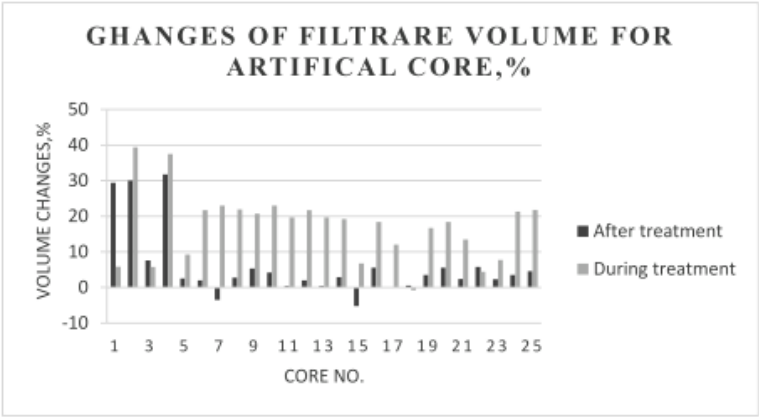

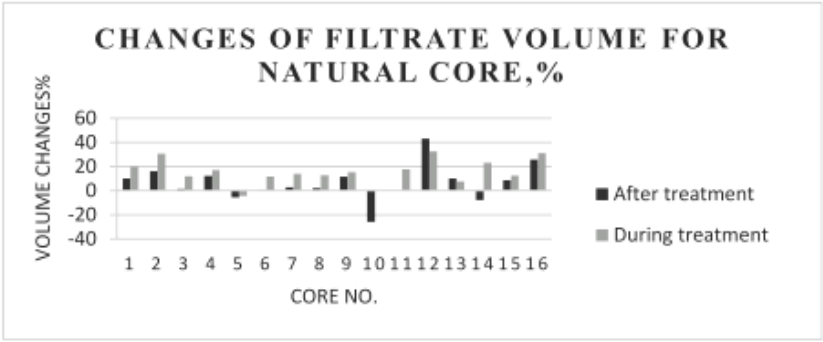

Fig. 4. Changes of filtrate volume during processing of natural and artificial core

The technology of hydroimpulse effects on the reservoir during depression.

The following equipment is used to implement the technology:

1. Multifunctional jet pump UEOS-4 with incorporated hydropulse generator GKP-1.
2. Coiled tubing installation;
3. Mechanical packer PMKV;
4. Depth pressure gauge;
5. Three-section calibrated container of 12-15 m^3.

The technology allows the following operations in wells:

1. Decreasing the bottomhole pressure only in the sub-packer space of the well and causing inflow from the reservoir. This eliminates the possibility of oil emissions and collapse of the casing string.

2. Hydropulse effect on the formation using a hydro-pulse generator and a jet pump with the subsequent generation of controlled depression in order to clean completely the bottom-hole formation zone (PZP) from the mud.

3. Injection of acid or other chemical reagents during repression and simultaneous hydro-pulse treatment of the formation.

4. Selecting of reaction products from the formation at the time required by the technology with controlled depression and simultaneous hydroimpulse effects on the formation.

5. Hydrodynamic investigation of wells in order to assess the initial and final state of the near-bottomhole zone of the formation by recording and decoding the pressure recovery curve of the HPC. The

recording and comparison of hydrodynamic parameters can be carried out with various depressions on the reservoir.

When performing technological operations, the working fluid is supplied to the nozzle of the jet pump through tubing pipes, and to the hydraulic pulse generator through a flexible pipe.

The fluid pumped out from the reservoir moves to the surface along the annular space.

The operations (Fig. 5) are performed as follows:1) the body of the jet pump (2) and the mechanical packer (3) are lowered into the well to the calculated depth at the tubing (1);

the packer is installed, as well as the pressure testing of the tubing and the packer is performed by using special inserts;

after the packing operation, a hydro-pulse generator (5) is descended into the sub-packer zone on the flexible pipe (4).

The generator is lowered with a sealing unit (6), which is fixed in the landing seat of the jet pump housing.

Later, a set of technological operations is carried out to affect the BFZ in accordance with the work plan.

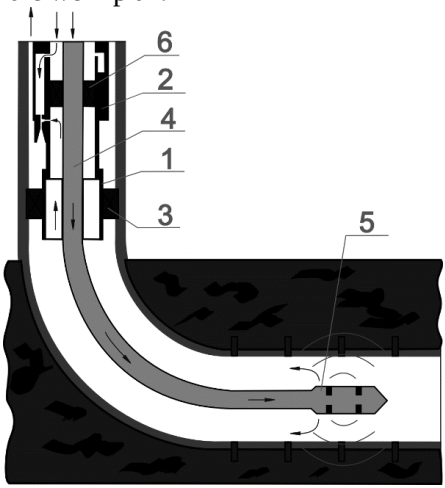

Fig 5. Schematic illustration of equipment for formation stimulation
1-tubing pipe; *2*-jet pump UEOS-4 (UEOS-4B); *3*-packer PMKV; *4*-flexible pipe; *5*-pulse generator GKP-1; *6*-sealing unit

The technology of impact on the colmatage reservoir with hydraulic pressure pulses of adjustable amplitude.

The effect of pressure pulses with a leading edge duration of up to 5 ms and an amplitude of up to 6 MPa on the BFZ makes it possible to create alternating pressure gradients up to 1.5 MPa/m in the formation, resulting in fatigue cracks in the rock as well as a decrease in the viscosity of the colloidal-dispersed structure in the BFZ. After such BFZ processing, the final stage of well development is carried out using a jet pump.

Calculation of parameters for elastic oscillations and generator acoustic power, necessary for the arising of fatigue cracks in the sandstone formation.

To simplify the calculations, the generator operation in the horizontal part of the wellbore is considered and a number of assumptions is adopted:

- a cylindrical wave is propagated in the formation;
- the direction of wave propagation in the horizontal part of the wellbore is perpendicular to the rock layers;
- the thickness of the layers is constant;
- to assess the fatigue strength of the rock, the cyclic loads of the formation with alternating pressure were taken into account;
- strength (strength limit σ_p) and acoustic (density ρ, longitudinal wave propagation velocity in the reservoir c_n, absorption coefficient k of elastic oscillations in a given frequency range f) rock characteristics were constant and consisted of:

rock tensile stress limits σ_p=1÷3 MPa (it was assumed in calculations: σ_p=2,4 MPa);

rock density ρ= 2200÷2600 kg/m^3;

longitudinal wave propagation velocity in the rock c_n=3000 m/s;

absorption coefficient of elastic oscillations in the frequency range 1-100 Гц –k=10^{-4} м$^{-1}$.

Elastic oscillations in the rock arise due to the action of hydraulic pressure pulses in the borehole space. The oscillation generator in this case is an acoustic system consisting of one or more generators of pressure pulses, the fluid of the well and part of the perforated casing. Such a system emits cylindrical elastic waves (Fig. 6).

Hydraulic pressure pulses create elastic oscillation packets in the reservoir medium. The duration period of the elastic oscillations at the point $x_1$is the shortest and, and in the first approximation it is determined according to the expression: $T_{x_1} = 4\tau_{\phi}$, where τ_{Φ} is the leading edge duration of the hydraulic pressure pulse in the well media. The first quarter of fluctuations period in the package is the forced oscillation of the borehole medium, which is arisen in the reservoir during the action of the hydraulic pressure pulse. Depending on the acoustic characteristics of the formation, the frequency of elastic oscillations, when propagating in the formation, will decrease due to the absorption of high-frequency components of the oscillations package (Fig. 7). The high-frequency components of the oscillation packets during propagation in rocks damp at small distances from the generator. At distances of about 20-100 m, oscillations in the frequency range 30-80 Hz are dominant for low-permeable rocks.

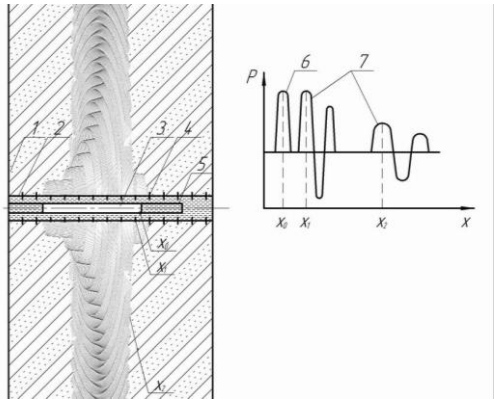

Fig 6. Schematic representation of a borehole emitter of a cylindrical wave and packets of elastic oscillations in the formation: *1* - formation; *2* - perforated casing; *3* - pressure pulse generator; *4* - working fluid; *5* - column tubing; *6* - hydraulic pressure pulse; *7* - packages of elastic vibrations in the formation

For further calculations, the frequency of elastic oscillations in the reservoir was taken up as $f_{x_2} = 50$ Hz. The limit of the rock fatigue strength σ_B was taken up at the level of 0.5 from the limit of its tensile strength. Then σ_B=1.2 MPa. Based on the conditions of fatigue cracks formation in the reservoir, when the amplitude of the

alternating pressure P_{x_2}) exceeds the fatigue strength limit, it was taken up that $P_{x_2} = 1{,}2$ MPa. It should be noted that the expansion of the rock during the wave propagation would be carried out in the phase of pressure decreasing, which with the appropriate number of oscillation cycles would cause the occurence of fatigue cracks in the rock. In the pressure increasing phase, the rock will undergo compression, in which the rock strength is much higher and, accordingly, there is no fatigue cracking. The intensity of the fluctuations necessary to create the amplitude of alternating pressure P_{x_2} in the reservoir, is determines by the expression

$$P_{x_2} = \sqrt{2\rho c_n I_{x_2}},$$

where I_{x_2} - distance of oscillations intensity x_2 meters from well generator, when $I_{x_2} = I_{x_2}^2 / 2\rho c_n$. After calculations, it is received: I_{x_2}=10,435 W/cm². To evaluate the intensity fluctuations I_{x_0} on the emitter surface, necessary to get the intensity I_{x_2} in the formation, so the expression to determine the change in the intensity of the cylindrical wave depending on the distance to the generator can be applied

$$I_{x_2} = \frac{I_{x_0}}{x_2} e^{-2kx_2},$$

where x_2 - distance from the generator to the point of the reservoir, taken up equal to 2 m

After calculations it is receives: I_{x_0}=21 W/cm². For an intensity of 21 W/cm², with an average radiation area of the pressure pulse generator 300 cm², the acoustic power of the generator should be at least 6.3 kW. The hydraulic power of such a generator based on its acoustic power of 6.3 kW is to be determined. As a fact, the power created by hydraulic downhole devices can be determined by the values of the pressure draw-down across the device and the amount of working fluid passing through the device per unit of time according to the expression

$$N = \frac{Q \cdot \Delta P}{600} \cdot \eta ,$$

where N - hydrogenerator power, kW ΔP- pressure draw-down across the generator, bar; Q - fluid flow through a hydrogenerator, l/min; η - device efficiency.

The maximum pressure draw-down across the hydrogenerator type Intex GKP-1 is 7 MPa at a flow rate of 900 l/min. Thus, the hydraulic power generated by the generator is 94.5 kW. Taking up the coefficient of hydraulic energy conversion into acoustic energy equal to 0.3, the acoustic power of the generator is obtained equal to 28.35 kW. On the radiation area, in the zone of maximum oscillation intensity equal to 300 cm², the intensity of the oscillations in the well is 94.5 W / cm². Given the loss of acoustic energy during the transition from the liquid medium of the well into the formation, the transmission coefficient of acoustic energy is taken up as 0.8. Then the intensity of oscillations at the entrance to the formation (on the surface of the cylindrical emitter) will be 75.6 W/cm².

These calculations confirm the possibility of alternating pressure occurrence with an amplitude of more than 1.2 MPa in the reservoir at a distance of 2 m from the downhole hydrogenerator. The time required for processing the reservoir is to be determined. The recycling frequency of the hydraulic pressure pulses of the GKP-56M generator is in the range of 20-70 Hz. For the value of the recycling rate of 50 Hz and the number of rock loading cycles N=106, the obtained treatment time of the formation is equal to 2 hours 47 minutes. The effect of surface-active substances (SAS) on the processes of crack formation in rocks under cyclic loads, in particular the Rebinder effect, is not taken into account in the above written issues.

Conclusions

Industrial testing of technologies that took place in the oil wells of Ukraine and Dagestan [24], showed their effectiveness and promising for exposing the depleted and marginal wells on the bottom-hole zone. So in most cases, cleaning of the bottom hole from the mud was performed and restoration of well productivity lasted for a period of 6-18 months. Well productivity was restored in some cases by 200-300% of the initial values.

This result makes it relevant to develop new technologies for exposing the formation used in the development of oil and gas wells, intensifying the production of shale gas and oil, coal beds degassing and before hydraulic fracture operations.

Further development and improvement of technologies for wells stimulation with low permeable or colmatage formations will occur in the direction of combining cyclic hydro-pulse wave action and hydraulic fracturing, as phased components of a basic technology for intensifying oil and gas recovery.

References

1. **V.I. Vettegren, V.S. Kuksenko, I.P. Scherbakov**. Dinamika mikrotreschin i vremennyie zavisimosti deformatsii po-verhnosti geterogennogo tela (granita) pri udare, Fizika tverdogo tela, 2012, tom 54, vyip. 7, S. 1342-1346.[In Russian]

2. **A. I. Beron, E.S. Vatolin, M.I, Koifman**, i dr. Svoystva gornyih porod pri raznyih vidah i rezhimah nagruzheniya, M., Nedra, 1984.

3. **V.I. Vettegren, V.S. Kuksenko, I.P. Scherbakov, R.I**. Ma-malimov. Transformatsiya strukturyi kvartsa pod vliyaniem udarnoy volnyi, Fizika tverdogo tela, 2015, tom 57, vyip. 12[In Russian]

4. **G.G. Karkashadze**. Mehanicheskoe razrushenie gornyih po-rod: Ucheb. posobie dlya vuzov. – M.: Izdatelstvo Moskovskogo gosudarstvennogo gornogo universiteta, 2004. [In Russian]

5. **A.G. Kadomtsev, E.E. Damaskinskaya, V.S. Kuksenko**. Oso-bennosti razrusheniya granita pri razlichnyih usloviyah de-formirovaniya, Fizika tverdogo tela, 2011, tom 53, vyip. 9[In Russian]

6. **R. F. Ganiev, L. E. Ukrainskiy**. Nelineynaya volnovaya mehanika i tehnologii. Volnovyie i kolebatelnyie yavleniya v osnove vyisokih tehnologiy. - Izd. 2-e, dopoln. - M.: In-stitut kompyuternyih issledovaniy; Nauchno-izdatelskiy tsentr «Regulyarnaya i haoticheskaya dinamika», 2011. [In Russian]

7. **M.E. Pevener , M.A. Iofis, V.N. Popov**. Geomehanika: Uchebnik dlya vuzov. - 2-e izd., ster. - M.: Izdatelstvo Moskovskogo gosudarstvennogo gornogo universiteta, 2008. [In Russian]

8. **V. N. Nikolaevskiy**. Sobranie trudov. Geomehanika. Tom 2. Zemnaya kora. Nelineynaya Seysmika. Vihri i uraganyi. - M. - Izhevsk: NITs «Regulyarnaya i haoticheskaya dinamika», Institut kompyuternyih issledovaniy, 2010. [In Russian]

9. **Ya.O. Kutkin, A.S. Voznesenskiy, M.N. Krasilov, M.N. Tavostin, Yu.V. Osipov.** Otsenka vliyaniya masshtabnogo fak-tora na vzaimosvyaz akusticheskoy dobrotnosti i prochnosti gornyih porod, Uchenyie zapiski fizicheskogofakulteta 6, 146313 (2014) [In Russian]

10. **Alan T. Zehnder, Jay Carroll, Kavan Hazeli, Ryan B. Berke, Garrett Pataky, Matthew Cavalli, Alison M. Beese, Shuman Xia.** Fracture, Fatigue, Failure and Damage Evolution, Volume 8 Proceedings of the 2016 Annual Conference on Experimental and Applied Mechanics

11. **Yu.O. Kuzmin, V.S Zhukov**. Sovremennaya geodnamika i variatsii fizicheskih svoystv gornyih porod. t 2-e izd., ster. - M.: Izdatelstvo «Gornaya kniga», 2012. [In Russian]

12. **Ko, T. Y., Einstein, H.H., Kemeny, J.** Crack Coalescence in Brittle Material under Cyclic Loading, ARMA/USRMS 06-930, 2006.

13. **N. Erarslan, D.J. Williams**, Investigating the Effect of Fatigue on Fracturing Resistance of Rocks Subjected to Cyclic Loading, ARMA 11-464, 2011

14. **X. L. Zhao& J.-C. Roegiers** Creep crack grow thin shale Rock Mechanic, Daemen & Schultz 1995 Balkema, Rotterdam, ARMA-95-0135

15. **T. B. Celestino, A.A., Bortolucci, C.A. Nobreg**. Determination of rock fracture toughness under creep and fatigue, Rock Mechanics, Daemen&Schultz (eds), 1995 Balkema, Rotterda, ARMA-95-0147

16. **Le, J.-L., Manning, J. and Labuz, J. F**. Scaling of Fatigue Crack Kinetics of Sandstone, ARMA 14-7622, 2014

17. **Morteza Ghamgosar, Penny Stewart** Investigation the Effect of Cyclic Loading on Fracture Propagation in Rocks by Using Computed Tomography (CT) Techniques, ARMA 15-488, 2015

18. **Zhuang, L. and Kim, K.Y., Jung, S.G. and Diaz, M.B., K.-B. and Park, S., A., Stephansson, O., Zimmerman, G., Yoon, J.S**. Laboratory study on cyclic hydraulic fracturing of Pocheon granite in Korea, ARMA 16-163, 2016

19. **Wu, J., Zhang, SH. and Cao H., Kemeny, J.** The effect of pulse frequency on the acoustic emission characteristics in coal bed hydraulic fracturing, ARMA 16-756, 2016

20. **Y. Chen, A. Yamazaki, H. Kusuda, E. Kusaka & M**. Mabuchi Harmonising Rock Engineering and the Environment – Qian & Zhou (eds) © 2012 Taylor & Francis Group, London

21. **Mohamed Shafik Khaled** and **Eissa M Shokir**, Cairo University, Effect of Drillstring Vibration Cyclic Loads on Wellbore Stability, SPE-183983-MS, 2017

22. **K.M. Tagirov, E.V. Devyatov, A.I. Nitsenko** Sposob izgo-tovleniya modeley porod-kollektorov. Stavropol: SevKav-NIPIgaz, 1990. [In Russian]

23. **I.M. Bazhaluk, O.M Karpash** European patent application, EP 3 098 378 A1, E21B 28/00 (2006.01) E21B 43/00 (2006.01), Bulletin 2016/48.

24. **Ya. M. Bazhaluk, O. M. Karpash, O. I. Hutak, M. V. Khudin, Yu. D. Voloshyn** Application of pulse-wave technology for oil well completion, Scientific Bulletin of National Mining University. 2016, Issue 5, p16-20.

CURRENT STATE OF EXTRACTION OF STONE BLOCKS USING A PUNCTURE METHOD

Tkachuk K.
National Technical University of Ukraine "Igor Sikorsky Kyiv Polytechnic Institute", Doctor of Technical Sciences, Professor, Head of the Department of Engineering Ecology, Ukraine

Hrebeniuk T.
National Technical University of Ukraine "Igor Sikorsky Kyiv Polytechnic Institute", Candidate of Technical Sciences, Associate Professor of the Department of Engineering Ecology, Ukraine

Prokopenko V.
National Technical University of Ukraine "Igor Sikorsky Kyiv Polytechnic Institute", Candidate of Technical Sciences, Associate Professor of the Department of Power Supply, Ukraine

Zakladnyi O.
National Technical University of Ukraine "Igor Sikorsky Kyiv Polytechnic Institute", Candidate of Technical Sciences, Associate Professor of the Department of Power Supply, Ukraine

Abstract. The paper deals with the choice of effective technology of drilling operations, provides an overview of modern technologies of stone blocks production, their disadvantages and advantages. The main features were developed and developed at the National Technical University of Ukraine " Igor Sikorsky Kyiv Polytechnical Institute", a complex technology of stone blocks extraction, which provides for the preliminary creation in the rock of directed static force action, followed by its combination with dynamic. Complex technology gives the correct qualitative assessment reciprocal force fields and allows you to get such positive results: the creation of a pre-stressed state in certain areas of the rock before the explosion, which made it possible to improve the quality of block splitting and to reduce technological losses of granite; due to the use in this technology of a weaker dynamic force pulse (explosion) significantly reduces the formation of microcracks in the area of the holes of the explosive , which also reduces the technological loss of production during the subsequent processing of blocks. Application of the results of the developed complex technology allow to raise the economic indicators of production.

Introduction. Contouring or cautious blasting intended for the extraction of stone blocks should, where possible, ensure a regular and even surface separation of rocks and reduce the degree of disturbance of the contour massif. In this method, the array adjacent to

the monofilament is minimally cracked, and the explosion-separated blocks do not lose their strength characteristics.

The main condition for ensuring the effectiveness of different purpose contouring methods is to reduce the mass of charges in the holes or wells, the approximation of charges in the system located on the projected plane of separation. To reduce the destructive action of the explosion, explosives with a reduced detonation velocity are used, which determines the initial pressure of the detonation products in the charging chamber.

Particular attention is paid to the controllability of the process and the quality of splitting, as well as to the minimal disturbance of the array, when developing block stone. The low workload of the high-explosive rock blasting method maintains an interest in this method, even though significant losses or poor quality products are lost. Therefore, the improvement of the blasting methods of separation of monoliths by direct split with the help of a boom is still not relevant and requires further scientific research.

Regarding the controllability of the formation of a continuous crack along the line of charges, there are corresponding requirements for the magnitude of deviations of the real plane of separation between charges from the plane of charges, which for borehole contour charges should not exceed 15 cm.

It is clear that the above tolerance is unacceptable for block stone mining. In this case, considerable attention, especially in the development of containing quartz rocks, pay attention to the regularity of the formation of rock-forming minerals. The direction of cleavage under the action of the predominant in the slit-forming process of the tensil principal stresses is chosen according to the plane of the anisotropic separation of the stone, namely, by the correct location of the extraction holes.

Overview of existing technologies. There are various technical solutions regarding the direction of crack development [1]. Of these, a sufficiently transparent and effective solution is the formation of a so-called embryonic crack or a guide hole, or a cut in the form of a disk at the bottom of the hole in its diameter and the subsequent detonation of the explosive charge (EC) in the hole. The formation of a germinal hub or sulcus is performed in a plane in which it is neces-

sary to obtain a crack in an array by a mechanical cutter of a special design.

Today, various types of blasting technologies have been developed and are being used, namely: blasting of blocks using smoky powder; use of plastic and low-density EC; use of brilliant EC; use of hydro-impulse equipment; extraction of blocks by means of a detonating cord; cleavage of a stone by directional charges; use of electric impulse explosion. The cumulative charges of various structures have been widely used to create contour cracks and block finishes [2, 3]. To use them, the line of holes in the line of planned splitting is drilled.

Explosive technology of stone blocks production differs from mining by mechanical means, first of all, by lower labor and energy costs, as well as by the possibility to receive significant pulse energy for a small mass of EC. That is why explosive technology has become widespread in stone quarries, especially for the extraction of high-strength varieties of stone.

Meanwhile, the explosion most violates the solidity of the rock, which leads to a decrease in the output of finished products from $1m^3$ blocks, especially thin and ultra-thin plates. To date, the question of choosing an effective technology of drilling operations in the production of block stone, which provides the required quality of commodity blocks, has not been fully resolved. In some cases, this leads to unnecessarily high costs for extractive work, and in others to improperly reduce the quality of final products. Therefore, improving the explosive deflection of stone monoliths using directional puncturing does not lose its relevance. This is especially true of the periodic problems of the interaction of cylindrical charges, which are located in the holes along the planned cleavage line.

Despite the positive aspects of the blasting of blocks, the share of stone extraction technologies using mechanical means is increasing, which is caused by the mentioned disadvantages of blasting technology.

Over the past 20 years continually evolved the technology of non-explosive destroying compounds (NDCs) for the extraction of stone blocks. Today, this technology has become widely used in the mining industry [4-11, 12-16, 17-19, 20].

NDCs are capable of developing holes in pressures up to 40-50 MPa and are used to separate the monolith from the array and to split the monolith into blocks. In general, as shown by practice, the use of NDCs for the extraction of blocks can be quite effective.

An analysis of the experience of using NDCs has also identified some of the problems of this technology, namely:

- the limited shelf life of NDCs and the need to follow the preparation rules exactly;
- problematic filling of NDCs with horizontal holes as well as vertical holes with water;
- the time of development of maximum pressure in the holes strongly depends on the weather conditions and can fluctuate in the range of 24-48 hours;
- the use of NDCs is limited by the temperature of the array in the range 0-25 °C;
- at a temperature of -5°C, the destruction of the rock occurs only after 3-4 days, and at lower temperatures the NDCs action ceases altogether;
- at temperatures above +25°C and intense reaction occur “shots” of the mixture of holes, which can be the cause of workers' injuries [21, 22];
- if the mixture is not working, re-use of holes with hardened NDCs is not possible;
- after the NDCs is triggered and the initial narrow crack of the cavity filled with the hardened NDCs, the holes cannot be used to further repel the monolith from the massif in order to widen the cracks and use the hoisting machines (this is not a disadvantage if hydraulic units are used).

The National Technical University of Ukraine "Igor Sikorsky Kyiv Polytechnic Institute" has developed a complex technology of stone blocks extraction, which involves the preliminary creation of a directional static force in the rock, followed by its combination with dynamic [23]. In most cases, NDCs were used to create static force action and to obtain the required stress-strain state in the desired rock zones. Theoretical studies of stress distribution around the hole contour were performed using the superposition principle in the interaction of force fields for the entire hole line. Since plastic zones occur

around the holes in the NDCs, the principle of superposition is misused, and nonlinear periodic problems must be solved that take into account the interaction of the holes. The same can be said about the interaction of dynamic force fields created by the use of EC.

Despite this, the above complex technology gave the correct qualitative assessment of the interaction of force fields and allowed to obtain the following positive results:

- pre-stressed rock formation in certain areas of the rock, which made it possible to improve the quality of block splitting and to reduce technological losses of granite;

- due to the use of a weaker dynamic force impulse (explosion) in this technology, the formation of microcracks in the zone of EC holes is significantly reduced, which also reduces the technological loss of production during the subsequent processing of blocks.

Application of the results of the developed complex technology allow to raise the economic indicators of production.

Currently, this technology has limited application, which is explained, first of all, by the complexity of determining the optimal ratio between the static and dynamic components of the technological process in an industrial environment.

One of the newest technologies, which is designed to separate the monolith from the array due to the force action, is the use of a chemical pressure generator "Litokol" [24].

At the rate of loading of the rock, this agent occupies an intermediate position between dynamic and static force action, that is, between the powder and the NDCs. There is no effect of combustion of a two-component mixture in the high-speed combustion mode on the formation of unplanned cracks and micro-cracks in both the split and the solid monolith.

If, during the operation of the NDCs, the crack between the array and the monolith has a width of only 2-5 mm, then when using "Litokol", this crack has a width of an order of magnitude, which eliminates additional technological operation to repel the monolith from the array for the purpose of further use of hoisting and transport machines for moving it.

Aircraft has proven itself well on granite quarries with ledges one to six feet high when using a vertical drill bit, sole, or two-plane

cracks. The most efficient technology works in combination with a rope saw.

There is some danger associated with the use of an electrical network to ignite the mixture in the holes. At present, this new technological development for the splitting of monoliths from the massif for some reasons is not widely used in granite quarries of Ukraine.

A similar technology was developed in russian by Kontech. This technology is based on the use of borehole pressure generators. It is important enough that the resulting block blanks (which are subsequently used for the manufacture of slabs, window sills, monuments, etc.) result in the opening of open cracks that have fused. However, in the zones of contact of the stone with the generator does not form the induced microcracks and gaps characteristic of many of the explosive materials that are currently used. Thus, the operation of the gas generator was started on the principles of action of the gas-dynamic wedge, and, unlike the use of explosives, rocks and concrete structures are split not by the shock wave, but by pressure.

The practice of creating solid cracks by drilling holes shows that this method is effective, but too laborious, in terms of the loss of stone. Quantitative losses are a part of a stone that is lost in the process of drilling a crack, and qualitative - a part that is spoiled by openings (the so-called "comb zone") and irregularities of chipping of the face surfaces. If the quantitative loss from drilling decreases as the diameter of the drill decreases, then the volume of the drilled stone is increased, which is explained by the more likely deviation of the drilling tool from a given drilling plane due to the greater resistance of the drilling rocks and the inaccuracy of setting the tool in that plane. Deviation of the storm (rod) from a given direction not only leads to the destruction of the stone, but also does not allow to obtain a solid crack, which then requires additional splitting of the undeveloped areas, thereby increasing the quality losses on the roughness of the chipping.

Common technologies for extraction of granite blocks, which are based on static force action on the walls of the hole, are technologies that involve the use of hand wedges, NDCs and hydraulic units.

In practice, hand wedges of different designs have been used, namely: simple, with auxiliary cheeks, complex. Usually the length of the wedges is in the range from 120 to 250 mm, which provides

splitting of granite in the area from 1 to 2 m^2. The sharpening angle of the hand wedges is 10-12.5° [25,26].

The use of hand wedges for domestic quarries with small stone extraction will save money on the purchase of expensive machines and mechanisms and will provide the required quality of the blocks. The technology of separating the stone from the array by means of wedges involves the drilling of the line of holes where the wedges are inserted. The tensile force arises either when striking a wedge - a hand wedge, or, more effectively, by the pressure created by the hydraulic system - a hydrocline. Wedges are placed in round holes, sometimes oval, drilled with a special device.

When extracting blocks of facing stone from high-strength rocks, characterized by high viscosity (labradorite, porphyry granites, etc.), it is necessary to perform a large volume of drilling holes.

Increasing the distance between the holes almost twice and thus reducing the amount of drilling allows cutting of the concentrator holes in the holes in the form of profile recesses located in the plane of the intended split.

Parameters of works at separation of a stone of different genetic type essentially differ among themselves. For example, in the case of separation of marble blocks with a height of more than 1000 mm, when drilling slabs up to 150 mm thick and splitting slanted stone, the holes are drilled through, regardless of the height of the monolith.

Despite the high complexity thy method with the use of manual wedges, it is still the main for a number of domestic careers, especially small in productivity, because it does not require expensive machines and mechanisms and provides the required quality of blocks.

In recent years, hydro cline installations have been widely used for block stone extraction. They facilitate working conditions of workers, allow to improve quality of blocks and to increase productivity of extraction works.

Nowadays foreign and domestic installations are used on the quarries of Ukraine. Domestic industry hydro cline are produced in small batches. The technical characteristics of hydro clines for splitting rocks of different strengths are significantly different. Hydro cline plants of foreign production are used in large volumes on Ukrainian quarries. Of these, the most widespread were hydrocline

installations "Darda" company "Porffeld" (Germany). Of the three modifications of the unit, the hydraulic unit of which is equipped with an electric, diesel and pneumatic engine, the most widely used are installations with a pneumatic engine, which is due to the presence on the quarries of compressors.

The first generation of Dard hydro cline units had C1 indexation (splitting force - 1780 kN and weight 11 kg), the latest generation D5 hydro cline rigs had splitting force - 2550 kN and weight 37 kg.

Improving the efficiency of stone extraction by hydro clines is possible by optimizing the parameters of the work (the step of installing hydro cline, optimal cleavage area per wedge, etc.) extraction based on the study of the mechanism and determine the magnitude of the fracture stresses at cleavage.

Many years of experimental studies conducted on a number of Ukrainian quarries have found that the resistance of erupting rocks at cleavage is less than the tensile strength of elongation by 3-7 times (Table [5]).

Table

The magnitude and ratio of the strength of the stone in different types of impact on it

Deposit	Rock	Tensile strength			$\frac{\sigma_c}{\sigma_s}$	$\frac{\sigma_c}{\sigma_{sp}}$
		when compressed σ_c, MPa	when stretching, σ_s, MPa	when splitting σ_{sp} MPa		
Golovinsky	Labradorite	130,5	52,8	15,2	2,5	8,6
Zhezhelivske	Granite	170,0	51,6	13,0	3,3	13,8
Corniche	Granite	153,5	47,2	13,2	3,2	11,6
Yemelyanivske	Granite	116,6	27,6	5,7	4,2	20,4
Leznikovskoe	Granite	161,2	33,4	6,6	4,9	24,4
Korostyshivske	Granite	181,9	37,3	5,8	4,8	31,3
Boguslavske	Granite	136,2	31,3	5,1	4,3	26,7
Slipchiske	Gabro-Lights	152,0	32,8	4,7	4,8	32,3

The small magnitude of the breaking strength of the rocks indicates that the mortgage wedge does not affect the entire surface to be split but only the area near the hole where the stress concentration becomes critical. wedges (in synchronous action on cleavage). The

efficiency of the wedge application increases as the area of cleavage area with the empty holes increases.

The quality and productivity of the stone cleavage works by hydro clines is determined by the ratio of the following factors: the cleavage area per wedge; hydro cline installation steps; texture, strength and anisotropic properties of stone; the specific magnitude of attenuation of the cleavage plane by additional (blank) holes, as well as the scheme of their placement relative to this plane.

When using powerful hydro clines, the inter-hole distances can be increased by 30-50%, which reduces drilling operations. If the height of the monolith separated from the massif exceeds 1 m, the even holes drill the entire height of the ledge, and the odd holes drill at a height of 0.4-0.8 m, which also allows to reduce the volume of drilling operations.

It should be noted that the small magnitude of the strength of the rocks for cleavage indicates the prospect of development and improvement of the wedge method of stone cleavage. In the monograph [5], when using the wedge method, only blank spaces are considered. It is of practical interest to study the combination of the wedge method with the static loading of additional holes.

Hydro Rock Splitter (HRS) - units for static directional destruction of strong rocks are also recently developed hydraulic units for splitting of monolithic blocks. The design of such units involves the use of an elastic chamber, inside which the working fluid under pressure is injected.

Hydropliters have the following advantages over hydroclines: they do not require a reverse system; the ratio of the breaking force to the mass of the unit (the so-called index, which characterizes the perfection of the unit design) in hydroxplitters about 4-6 times more than in the common German hydroclines "Dard" and Japanese "Hirado"; the weight of the HRS is about an order of magnitude lower than that of hydrocline, which allows it to be transported manually under quarry conditions.

A significant drawback of the use of HRS equipment is that in the case of unreasonably selected technological parameters (the distance between the holes and the depth of the holes), the deformation of the housing of the unit with the transition of a circular section into an ellipsoidal one. In such cases, there is a jamming of the units in the

holes, which does not allow to obtain the main crack in the desired direction and requires additional costs for the release of units with deformed housing from the cavity of the holes [27].

Attempts to simplify the construction of the unit described above have initiated the development of the unit at the Kiev Polytechnic Institute with the impact on the hole wall directly elastic chamber.

The production of a test batch of such units and the conduct of industrial testing revealed their major drawback. This disadvantage is the movement of the elastic chamber in the hole formed in the hole. This movement is due primarily to the presence of high pressure inside the elastic chamber and the mechanical properties of the material from which it is made.

Repeated movement of the elastic chamber inside the slit with sharp edges significantly reduces its durability and leads to insufficient reliability of the entire unit as a whole.

Recent experiments at the Kiev Polytechnic Institute have made it possible to outline another variant of a hydraulic unit for splitting monoliths into blocks.

This unit affects the wall of the borehole directly with the working fluid (water) under high pressure. Such units should be distinguished by a simple technological design and a correspondingly low price, which will make it possible to manufacture them in the conditions of a mechanical workshop directly in the quarry.

In addition to the above portable hydraulic unit for splitting monolithic hydraulic fracturing objects, a second version of a portable piston unit for stone blocks production was developed, which differs from the first version developed in 1991-1992 [23,28], by a much smaller mass. and a larger fracture force in the hole. This unit, together with the unit for splitting of monolithic hydraulic fracturing objects, can in the future be used for the further development of technologies of application of hydraulic equipment for mining of granite blocks.

To date, such units are little used in practice, due to the complexity of creating sealing units, which can reliably seal the cavity of the hole and create high pressures in it. The complexity of the issue lies in the large range of gap oscillation between the wall of the hole and the seal, which disrupts the work of seals, which at high pressure are squeezed into the existing gaps.

Formulation of tasks and methods of their solution

An analysis of the above modern methods and methods of mining stone blocks suggests that the most common for these methods is to use a number of holes to create the planned cleavage gap. Typically, the cross-section of these holes has a circular outline. Thus, anisotropy is artificially created in the array from which the block stones are broken or the block is split. Often the blocks have the shape of rectangular parallelepipeds, and the holes are placed in a plane parallel to one of the faces of the parallelepiped. In practice, the most widespread sizes of diameters of holes are in the range of 0.02-0.04 m. Such sizes of holes are much greater than the size of natural microcracks. For the separation of monoliths with the help of holes, the rock is destroyed in the required direction by the splitting voltage (displacement). The destruction occurs on the planes of the cleavage of minerals, and the destruction of the minerals themselves is insignificant and can not be taken into account, considering the array homogeneous.

Since in this work will study the stress-deformed state around the holes at the separation of homogeneous stone monoliths, or splitting them into blocks of the desired size (passivation), we can assume that their material is homogeneous and in theoretical studies use the model of isotropic body for rock.

The scheme, which involves the use of a split unit of uniform static pressure acting inside the system of the holes, requires the solution of periodic problems that take into account the interaction of the force fields from each hole. This is also required by the study of the interaction of dynamic fields from the simultaneous impulse load of a number of holes in the line of planned splitting. In this direction, works are known [26,29,30,31,32], where the problems of elastic wave diffraction in an infinite array with two identical circular cylindrical holes loaded with harmonic pressure are theoretically and experimentally investigated. It is shown that when bursting of charge charges generates shortwave loads, the nature of stress distribution in the zone of influence of interacting charges differs significantly from static. Radial stresses become preferred in magnitude, with maxima being reached at the point between charge centers. The stress level increases sharply, with both radial and tangential reaching the highest value at the point between the charge centers. As can be seen

from the results of the mathematical modeling, phenomena resembling resonance are observed in the interaction of a whole number of waves from elongated charges [26,29,30]. The analysis of the results of experimental studies using piezomaterials showed that with the proper selection of dynamic loads on the contours of adjacent circular holes in an organic glass plate, it is possible to achieve destructive stresses in the middle of the jumper between the holes due to the superposition of the waves initiated by circular piezoceram [31].

Summarizing the current state of development of the use of harmonic pressure on the walls of cylindrical holes, we can conclude that the problems of diffraction of elastic waves in an infinite array with two identical cylindrical holes loaded with harmonic pressure, studied theoretically and theoretically needs further development.

It is necessary to generalize and refine the analysis of the effect of drilling errors on the nature of artificial anisotropy and the cost of splitting blocks just as it was done for the wedge method.

Because in almost all cases the diameters of the holes are much smaller than their length, the split stone block is in a state of flat deformation with uniform static or dynamic loading of the walls of the holes.

The scheme [5] of stress distribution in the cross section to the axes of the holes from the action of the laid hydrocline indicates the possibility for the theoretical and experimental study to apply the theory of flat stress state.

The prospecting and design work undertaken at the Kiev Polytechnic Institute to build effective portable pressure units based on portable technologies based on the use of known hydraulic units and NDCs should continue.

In order to successfully resolve this issue, it is necessary to investigate such important technological parameters as the pressure or the specific force of cracking inside the hole (depending on the load scheme), the ratio of the power parameters at the initial cracking and the further development of the already obtained crack, the distance between the holes is required.

It should be noted that in the known empirical and analytical expressions given in [27,33], to determine the required distance between holes that do not have stress concentrators, the argument is the pressure acting in the cavity of the hole. If to put in these expressions

the underestimated value of such pressure that is less than the pressure of cracking, then the process of splitting of granite theoretically simply does not happen. If, in these expressions, an excess value of pressure exceeding the pressure of cracking is substituted, then such pressure cannot be realized. This is due to the fact that the pressure of crack formation is the maximum pressure that can be created in the cavity of the hole, because the further development of the resulting crack requires less effort.

Therefore, the fracture pressure in the hole is an important technological parameter that characterizes the stress-strain state of the rock as a monolithic medium at the initial moment of destruction. The first stage of the technological process (cracking) is the most responsible in comparison with the second stage - the development of already finished crack, and allows to formulate requirements for the potential capabilities of technological equipment.

It should be noted that in these works there are no methods of calculating the pressure of fracture formation in specific rocks as a monolithic environment, and therefore the development of such a technique is an important step in the creation of technology for the use of small aggregates - pressure sources.

It is important to note that for some time the Ukrainian industry does not release portable pressure units for separation of granite blocks. This segment of the mining equipment market is complete with expensive imported hydraulic equipment.

Conclusion

The development of granite block extraction technology based on the joint use of dynamic and static loading of the borehole walls requires further improvement. This is especially true for non-stationary loads, perturbations from which interact with the fields of static loads and create favorable conditions for the origin and propagation of cracks in the desired direction. Simple devices for the formation of directional cracks in wells, the production of which does not require sophisticated metalworking equipment, allows to make them not only in the conditions of domestic enterprises, but also in the mechanical workshops of quarries for the extraction of stone blocks, which will reduce the dependence on expensive imports equipment and significantly increase the economic performance of production.

The complex variables method can be used to solve the problems of static and dynamics of rock masses and stone blocks. The spatial (three-dimensional) and flat (two-dimensional) problems of elasticity theory are considered, with preference given, if possible, to flat problems that allow the investigation of more multi-parameter systems. In this paper, holes of considerable length and relatively small diameter are considered, so it can be assumed that their end parts practically do not affect the middle part of the block and for it the conditions of flat deformation are realized. In this case, for each perpendicular to the axis of the intersection, we will have the same stress distribution around the contour of the hole (Fig. 1.5, [5]). Therefore, the calculation area for determining the stress distribution around the holes can be selected as a single thickness plate perpendicular to the axes of the holes, and a corresponding load is applied to the walls of the holes. To determine the stress distribution around the hole, we can use the problem of flat stress state [34,35,36,37].

The equations for the case of flat deformation and for flat stress state differ only by a constant factor. This important circumstance allows theoretical and experimental studies for spatial problems of separation of monoliths to be reduced to flat problems of elasticity theory.

In [5,38,33], the substantiation of the form of stress concentrators in the extraction of stone blocks is presented, but in addition to the creation of concentrators in the rock mass, it is also necessary to investigate the effect of the concentration of loads on individual links of the hole contour, which will reduce the total load for splitting the block due to redistribution it along the contour of the hole [40].

Introduction of the developed complex technology will allow to raise economic indicators of production.

At present, this technology has limited application, which is due, first of all, to some complexity in the industrial environment to determine the optimal relationship between the static and dynamic components of the technological process.

References

1. **Mikhaluk A.V.** Rocks at Uneven Dynamic Loads / A.V. Mikhaluk. - Kiev: Sciences. opinion, 1980. - 154 p.

2. **Yurko O.O.** Charge of a rectangular cross-section with two-way cumulative recess / O.O. Yurko // Problems of creation of new machines and technologies. Science. of the KSPU. No. 6/2002 (17). - Kremenchuk: KSPU, 2002.- P. 56-59.

3. **Yurko O.O.** Cylindrical cumulative charge with a cumulative recess of a triangular shape in cross section / OO Yurko // Problems of creation of new machines and technologies. Science. of the KSPU. No. 6/2002 (17). - Kremenchuk: KSPU, 2002.- P. 45 - 48.

4. **Bakka M.T**. Natural stone extraction: [textbook] guide for students of higher education. teach. Baklka MT, Kuzmenko O.Kh., Sachkov LS - K .: KPI, ISDO, 1993. - 352s.

5. **Karasev Yu.G**. Natural stone. Extraction of block and wall stone: [textbook. Higher student allowance. training. trans.] / Karasev Yu.G., Bakka NT - St. Petersburg Mining Institute St. Petersburg, 1997. - 428s.

6. **Karasev Yu.G**. Technology of mining operations on the quarries of facing stone / Karasyov Yu.G. - M.: Nedra, 1995. - 296s.

7. **Tkachuk K.K.** Destruction of rocks by non-explosive destructive substances / Tkachuk K.K. // Development. ore. - K .: Republic. Bear. scientific tech. Sat. - 1986. - Issue. 42. - P. 41-44.

8. **Tkachuk K.K**. Development of effective and safe methods of application of LDCs for separation of blocks of rock from the massif on quarries / Tkachuk K.K., Kichigin A.F., Kozlov S.S. - No. 01870047547, 1987. - P. 51-55.

9. Device for explosive destruction of rock / [**Ushakov AE, Milgunov VG, Rastov VI, Orlov NY**]. Mountain Journal - 1989. - №4. - P. 21-22.

10. **Tkachuk K.K**. Development of non-explosive method of destruction of rocks / **Tkachuk KK, Fomenko IA** // Problems of geotechnology and engineering ecology: scientific conference, March 17-18, 1992: abstracts of reports. - Kiev: 1992. - P. 96.

11. **Tkachuk K.K.** Increasing the efficiency of extraction of granite blocks / **Tkachuk KK, Fomenko IA** - K .: Building Materials and Structures, 1991. - №2. - P. 28-29.

12. Non-invasive destructive agent LDC-1 / VNIISTROM them. Budnikova - M .: PIK VINITI, 1984. - P. 4.

13. **Fazilov S.S.** Application of LDCs for extraction of granite blocks on the quarries of Uzbekistan / S.S. Fazilov // Express information. Series "Industry of nonmetallic and nonmetallic materials" // - 1989. - Iss. 1, pp. 16-21.

14. **Nikolaev M.M.** New material for effective destruction of strong fragile objects / M.M. Nikolaev, Zakharov GV - M. Mountain Journal - No. 6, -1989 - P. 14-17.

15. **Bakka H.T.** Features of extraction of blocks of stone by means of LDCs / NT. Bakka, V.S. Redchitz // - Express information. Series "Industry of nonmetallic and nonmetallic materials" // - 1991. - Issue. 1, pp. 14-28.

16. **A.F. Nizhichenko** Tests of LDC-1 in granite mining / AF Nizhichenko - // M .: VNIIESM, - 1985 - Issue. 2, pp. 8-10.

17. **Tkachuk K.N.** Methods of improving the quality of granite blocks / KN. Tkachuk, IO Fomenko, K.K. Tkachuk, OI Fomenko, TV Grebenyuk // Bulletin of "NTUU KPI". Mining Series K. 2012. Iss. No. 21, pp. 103 - 107.

18. **Kosolapov A.I.** Choosing a method for processing stone deposits. Extraction, processing, application of natural stone / A.I. Kosolapov, EV Bezverkha - Magnitogorsk: Sat. scientific Proceedings of the Moscow State Technical University, 2000. - P. 65-77.

19. **Trubetskoy K.N**. Complexes of mobile equipment in open mining / Trubetskoy KN, Leonov ER, Pankevich Yu.V. - M .: Nedra, 1990. - 250 p.

20. *Tkachuk K.K*. Stress-strain state of rocks during fracture by static loads / Tkachuk K.K. // - Development of ore deposits: Republic. between scientific-technical Sat. - 1994, no. 55. P. 45-52.

21. **Pershin G.D.** Method for assessing the performance of NDCs / GD. Pershin, E.G. Wheat. - M., Empire of stone. - 2002. №1, pp. 30-31.

22. **Kosolapov A.I.** Determination of parameters of technology of extraction of blocks of marble by non-explosive destructive means / A.I. Kosolapov, N.I. Volchenko. - M .: Building Materials No. 1, 1990 - P. 12-14.

23. **Fomenko O.I.** Increasing the efficiency of the technological process of splitting granite blocks / O.I. Fomenko, K.K. Tkachuk // Collection of scientific works of NTUU "KPI". Mining series. K .: - 2009. - №18. - with. 56-61.

24. Chemical generator of "Litokol" chemical agent against LDCs and gunpowder. Stone. Bulletin of masonry. - K .: 2005. - №9 - P.29-31.

25. **Iskov S.S.** Peculiarities of development of ornamental stone deposits and the value of geometrization of their basic properties for the improvement of block mining technology / S.S. Iskov // Bulletin of the Zhytomyr Technological University. - 2004. - №3 (30).

26. **Kravets V.G**. Dynamics of the formation of a single crack by an explosion in a mountain massif / V.G. Kravets, P.Z. Lugovoi, A.L. Gan, Z. Baranovsky // Bulletin of NTUU "KPI". Mining series. - 2006. - Vyp. 13. - P. 18–23.

27. **Blumelfeld V.M.** A rational method of mining granite blocks / V.M. Blumelfeld // Mountain Journal, 1996. - No. 6.

28. **Fomenko O.I.** Comparative analysis of granite block passivation technologies / OI Fomenko, K.K.Tkachuk, K.N. Tkachuk // Collection of scientific works of NTUU "KPI". Mining series. - K .: 2010. - VIP. №19. - p.97-101.

29. **Kravets V.G.** Experimental modeling of the superposition of explosive waves under the action of adjacent charges / V.G. Kravets, P.Z. Lugovoi, A.L. Gan

// Physics and technology of high-energy materials processing. Collection of scientific works. - 2007. Dnepropetrovsk. - P. 274-281.

30. **Kravets, VG**, Dynamics of the formation of a single crack in an explosive rock massif / **VG Kravets, A. L. Gan, and P. Z. Lugovoi** // Miedzynarodowa Konferencja VII Szkola Geomechaniki, Gliwice - Uston 13-16 wrzesnia 2005, S 107-121.

31. **M. Chudek**, Experimental modeling of the superposition of elastic waves from the action of adjacent cylindrical hole charges / M.Chudek, Z.Baranowski, P.Z.Lugovoi, V.G.Kravets // Miedzynarodowa Konferencja "VIII Szkola Geomechaniki 2007". Материалы Naukowe. Glinwice Ustron, 16-19 pazdziernika 2007. p.p. 263-274.

32. **Kravets V.G**. Experimental modeling of the superposition of explosive waves under the action of adjacent charges / V.G. Kravets, P.Z. Lugovoi, A.L. Gan // Physics and technology of high-energy materials processing. Collection of scientific works. - 2007. Dnepropetrovsk. - P. 274-281.

33. **Smirnov A.G**. Extraction and processing of natural stone: Directory / AG. Smirnov, NT Bakka, Birzhiskis - M .: Nedra, 1990. - P. 445.

34. **Mushelishvili N.I.** Some basic problems of the mathematical theory of elasticity / Mushelishvili N.I. - M., Science, 1966. - 707 p.

35. **Savin G.N**. Distribution of stresses near holes / **G.N. Savin**. - K .: Scientific Thought, 1968. - 887 p.

36. **Sazhin V.S**. Elastic-plastic distribution of stresses near mining of different outlines / V.S. Sazhin-M .: Science, 1968. 94 p.

37. **Luchko I.A**. Hydrodynamic calculation of the explosion of a plane horizontally submerged charge in a three-layer medium with the least durable intermediate layer / **I.A. Luchko, V.M. Bulavatsky** // The action of explosion in soils and rocks. Mater, All-Union. scientific Conf. - Kiev: Science, opinion. 1982 - P. 43-47.

38. **Tkachuk K.K**. Control of fracture formation at non-invasive destruction of rocks / **K.K. Tkachuk** // - Development of ore deposits: Republic. between scientific-technical Sat. - 1994, no. 55. P. 52-59.

39. **Tkachuk K.K**. Substantiation of the form of stress concentrators in the extraction of granite blocks / **K.K. Tkachuk, IO Fomenko** // Problems of geotechnology and engineering ecology: Scientific conference, March 17-18, 1992: abstracts of reports. - Kiev: 1992. - p.46-48.

40. Identification of loads during impulse deformation of bodies. Monograph. In 2 parts. Part II. / **E.G. Yanyutin, A.V. Voropai, Povalyaev, I.V. Yanchevsky**. - Kharkov: KhNADU Publishing House, 2010.-121 p.

CLEANING TUBING TECHNOLOGY FROM ASPHALTENE-RESIN-PARAFFIN DEPOSITS

Makarenko V.D.
Poltava National Technical Yuri Kondratyuk University
DSc, Professor, professor of the Chair of Oil
and Gas Engineering and Technology, Ukraine

Zezekalo I.G.
Poltava National Technical Yuri Kondratyuk University
DSc, Professor, Honored Scientist of Ukraine, Academician
of Petroleum and Ukrainian Academy of Science, professor of the
Chair of Oil and Gas Engineering and Technology, Ukraine

Petruniak M.V.
Poltava National Technical Yuri Kondratyuk University
PdD, Assosiate professor, Assosiate professor of the Chair of Oil and
Gas Engineering and Technology, Ukraine

Liashenko A.V.
Poltava National Technical Yuri Kondratyuk University
Senior lecture of the Chair of Oil and Gas Engineering
and Technology, Poltava National Technical Yuri Kondratyuk
University, Ukraine

Abstract. Currently, chemical methods and mechanical brushes are used to clean the internal cavities of tubing at the oil fields of Ukraine, but due to mechanical wear, they quickly fail and do not produce the desired result. Chemical reagents that dissolve hydrate and asphaltene-resin-paraffin deposits are also found to be ineffective for these purposes due to the high local corrosion of the tubing walls and their depressurization. Therefore, the authors have proposed advanced equipment for cleaning internal cavities from deposits. The results of bench and industrial research, as well as design and technological developments have been implemented in the improved regulatory documents governing the inspection, cleaning, repair and control of tubing tubes during their operation.

Keywords: milling tools, hydrate and asphaltene-resin-paraffin deposits, corrosion, depressurization, chemical reagents.

Introduction

As many years of observations show, during the oil production process there is a regular deposition of paraffinized oils and mineral salts on the inner walls of the tubing, which leads to a decrease in the

cross section of the pipe. This causes malfunctioning of deep pumps and pumping rods, which negatively affects the performance of the downhole equipment and ultimately leads to a decrease in oil production [1-3].

For this reason, annual oil production (by experts) is reduced by 10-15%. Currently, chemical methods and mechanical brushes are being used to clean the internal cavities of tubing at the fields of Ukraine, but due to mechanical wear, they quickly fail and do not produce the desired result. Many practitioners have found it ineffective to use for this purpose chemical reagents that dissolve paraffin and other deposits, due to the high local corrosion of the walls of tubes tubing and depressurization.

There are cases where after the use of chemical reagents corrosion damaged the walls of tubing with the formation of through fistulas within 2-3 months, which led to significant material costs and severe environmental consequences.

Therefore, in recent years, oil companies have been paying close attention to this problem due to its relevance and importance [4-7].

To clean the internal cavities of tubing tubes from deposits, the authors proposed advanced equipment (Fig. 1). The design and technical features of the equipment and the cleaning technology are described below.

Design features of the equipment The device includes a bearing housing 2, in which is mounted and secured cantilever mill 1, made in the form of a cut cone.

The other end of the housing 2 is fastened to the link 3, on which the shaft is mounted a back cutter 4 on the sliding bearing 9. The link 3, in turn, is connected to the control rod 5 and locking pin 11 to prevent unscrewing.

At the end of the control rod 5 is mounted a rotorseal 8, which is attached to the rod by means of a strap 6 to the axis 7.

A rope is attached to the rotorseal 8, on which the device goes down the tubing.

The principle of the device operation (model SKF-03) for cleaning internal pipe cavities from paraffin and other deposits is as follows.

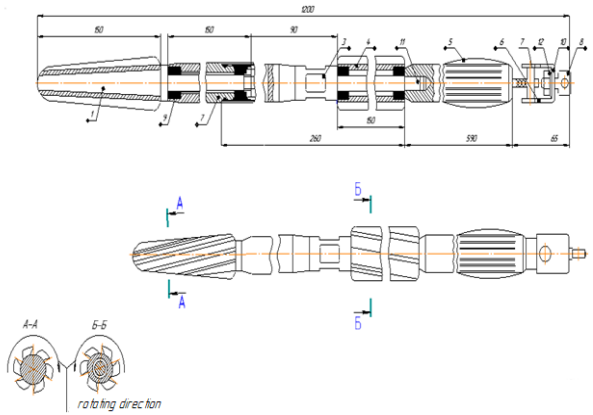

Fig 1. Design of the cleaning device SKF-03 model: *1* - cantilever mill; *2* - bearing housing; *3* - link; *4* - back cutter; *5* - control rod; *6* - strap; *7* - axis; 8 - rotorseal; 9 - sliding bearing; 10 - plain washer; 11 - locking pin; 12 - screw

When the buffer latch is closed, the device is placed in a sealed lubricator. After opening the buffer latch with the help of the traction body, the device is lowered into the tubing tubing before contact with the liquid. The upwardly moving liquid begins to rotate the cantilever mill to the right, and the back mill thus rotates to the left, as they have opposite-directed elements. Thus, the process of cutting off the oil deposits. The destroyed sediments are picked up by the well flow and are brought to the surface. The presence of a cantilever mill 1, made structurally in the form of a cut cone, allows to increase the speed of rotation (up to 900 rpm) and the speed of movement of the device in the operating mode, and therefore, to increase the productivity with high quality of cleaning. The work of the console 1 and the back 4 cutters simultaneously prevents the occurrence of torque on the control rod 5.

The length of the cutting edge of the cutter H is expressed by the ratio

$$H=d/2tg\alpha ,$$

where d – is the diameter of the cantilever mill, α – is the angle of attack of the involute cutter element.

A distinctive feature of the new device SKF-03 from domestic (Fig. 2) and foreign (Fig. 3) analogues is the following. In the first case (Fig. 2) there is no cone on the small milling cutter, which

causes additional braking force when inserting the milling cutter into the paraffin layer and does not create that extra axial force which increases the cleaning performance. In the second case (Fig. 3), the absence of the back cutter creates a twisting moment on the lowering mechanism of the cutter, which, as a rule, leads to twisting of the rope and breakage of the cutter. In this case, the quality of cleaning is significantly reduced and the productivity of the cleaning works is reduced.

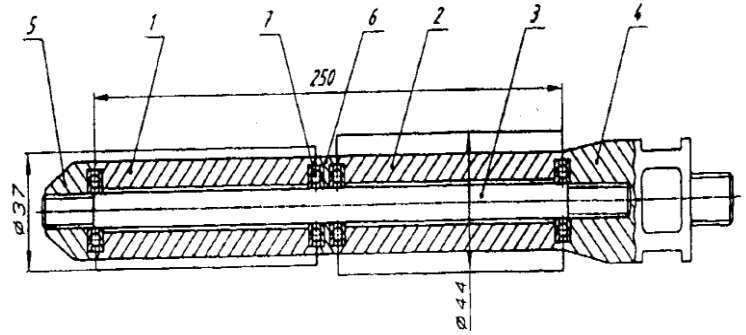

Fig. 2. Design of domestic treatment device: *1* – small mill; *2* – mill; *3* – axis; *4* – shank; *5* – screw; *6* – spacer ring; *7* – support bearing.

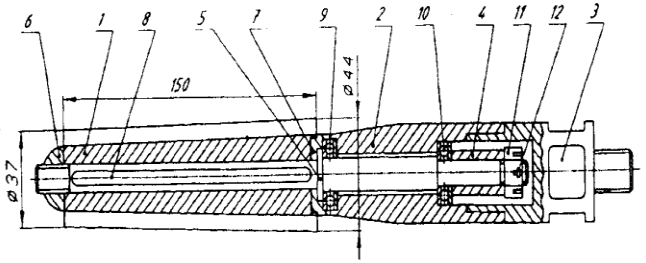

Fig. 3. The design of the foreign cleaning device: *1* - conical mill; *2* - housing; *3* - shank; *4* - bushing; *5* - axis; *6* - screw; *7* - ring; *8* - key; *9* and *10* - bearings; *11* - screw; *12* - pin

The kinetic calculations of equipment

The kinetic calculations of the movement of the cleaning mill in the tubing under the action of hydraulic forces are as follows.

By lowering the treatment device into the mouth of the tubing, it under the action of gravity G begins to move down (towards the oil-

bearing reservoir). At this point, the hydraulic milling force of the liquid mixture, which is lifted by the deep pump up the tubing of the oil reservoir, is acting on the milling cutter. Moving up the channels between the teeth of the working cleaning mill, the liquid simultaneously performs a rotational motion together with the mill (Fig. 4). First, consider the scheme when the cutter *I* (Fig. 4) is stationary, and the liquid mixture moves through the channels between the teeth at the same relative speed as during the rotation of the cutter. The absolute velocities of fluid motion at the inlet of the cutter C_1 and at the outlet of the cutter C_2 are each the geometric sum of the relative and rotational speeds, so they can be decomposed (Fig. 5) into relative components ω_1 and ω_2 (directed along the teeth) and rotational components U_1 and U_2 respectively (directed tangential to the circle of rotation).

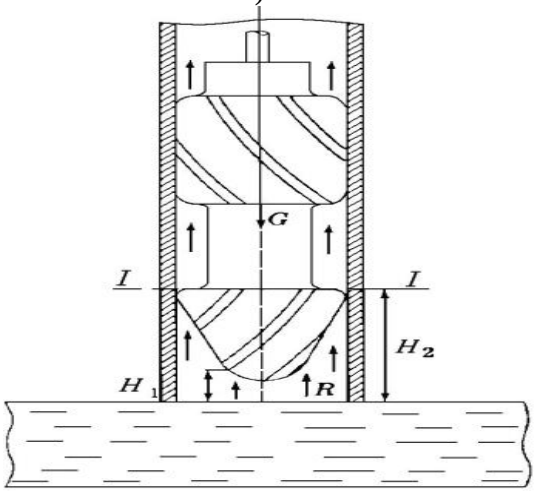

Fig. 4. The scheme of movement of the milling cutter in the tubing tubing:
G - is the weight of the cleaning column, *R* - is the hydraulic resistance of the liquid mixture

Applying to the plane of comparison (*I-I*) the plane of the upper surface of the end face of the milling cutter 1 (Fig. 4), we make the balance of the energy of the liquid as it passes through the milling cutter according to the Bernoulli equation ($z_1 = z_2$):

$$\frac{P_1}{\rho g}+\frac{\omega_1^2}{2g}=\frac{P_2}{\rho g}+\frac{\omega_2^2}{2g}, \qquad (1)$$

where P_1 and P_2 - are the fluid pressure at the tooth at the inlet and outlet of the cutter respectively, ρ - the density of the liquid mixture, g - is the acceleration of free fall.

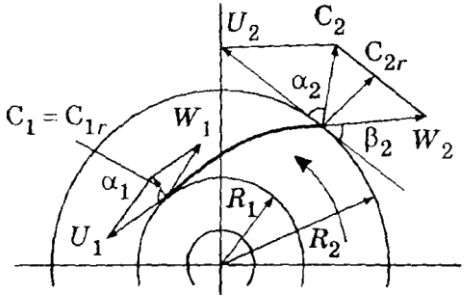

Fig. 5. Kinematic characteristics of the moving fluid particle between the teeth of the working cleaning mill

During rotation of the mill, the liquid at the outlet acquires additional energy E equal to the work of the centrifugal force on a path of length R_2 - R_1. Then

$$\frac{P_1}{\rho g}+\frac{\omega_1^2}{2g}=\frac{P_2}{\rho g}+\frac{\omega_2^2}{2g}-E. \qquad (2)$$

If the working mill rotates at an angular velocity ω, the centrifugal force $F_ц$ acting on a fluid particle of mass m is equal to

$$F_ц = m\,\omega^2\, r = \frac{P}{\rho}\,\omega^2\, r$$

where P - is the weight of the fluid particle, r - is the current radius of rotation of the particle.

The work of the A_P, carried out by centrifugal force when moving the same particle on the path R_2 - R_1, is

$$A_P=\int_{R_1}^{R_2}\frac{P}{g}\omega^2 r dr=\frac{P\omega^2}{2g}(R_2^2-R_1^2).$$

The expression of the angular velocity ω in the radius of rotation R is equal to the rotational velocity U, so

$$\omega^2 R_2^2 = U_2^2 \text{ and } \omega^2 R_1^2 = U_1^2$$

Work A_p is expressed by the equation

$$A_P = \frac{P_1}{g}\left(\frac{U_2^2 - U_1^2}{2}\right).$$

The specific work related to the unit of weight of the fluid is equal to the specific energy obtained by the fluid with the cutter

$$E = \frac{U_2^2 - U_1^2}{2g}$$

Substituting this expression into equation (2), we obtain

$$\frac{P_1}{\rho g} + \frac{\omega_1^2}{2g} = \frac{P_2}{\rho g} + \frac{\omega_2^2}{2g} - \frac{U_2^2 - U_1^2}{2g}$$

where

$$\frac{P_2 - P_1}{\rho g} = \frac{\omega_1^2 - \omega_2^2}{2g} + \frac{U_2^2 - U_1^2}{2g}. \quad (3)$$

According to the Bernoulli equation, the fluid head at the inlet of the rotary cutter H_1 and at the outlet of it H_2 will be

$$H_1 = \frac{P_1}{\rho g} + \frac{C_1^2}{2g},$$

$$H_2 = \frac{P_2}{\rho g} + \frac{C_2^2}{2g}.$$

The theoretical pressure H_T on the cutter is equal to the difference in pressure at the inlet and outlet of the cutter

$$H_T = H_2 - H_1 = \frac{P_2 - P_1}{\rho g} + \frac{C_2^2 - C_1^2}{2g}. \quad (4)$$

Substituting the expression for $(P_2\text{-}P_1)/\rho g$ from equation (3), we obtain

$$H_T = \frac{\omega_1^2 - \omega_2^2}{2g} + \frac{U_2^2 - U_1^2}{2g} + \frac{C_2^2 - C_1^2}{2g}. \quad (5)$$

From the parallelogram of velocities at the inlet and outlet of the cutter (Fig. 5), it follows that

$$\omega_1^2 = U_1^2 + C_1^2 - 2U_1C_1\cos\alpha_1,$$
$$\omega_2^2 = U_2^2 + C_2^2 - 2U_2C_2\cos\alpha_2.$$

Then, after the corresponding transformations, equation (5) is written in the form

$$H_T = \frac{U_2C_2\cos\alpha_2 - U_1C_1\cos\alpha_1}{g}. \quad (6)$$

This expression is the basic equation of motion of the milling cutter in tubes of tubing under the action of hydraulic forces. It correctly expresses the kinematics of the movement of the treatment device in the tubing in the case when all the particles of fluid move in the channels of the milling cutter along similar trajectories. This is possible only if the working mill has an infinitely large number of teeth and the channel cross-section (space between the teeth) for the passage of fluid is small. Typically, the liquid, getting on the mill, moves on it in the radial direction. In this case, the angle between the absolute value of the fluid velocity at the inlet of the milling cutter and the rotational speed $\alpha_1 = 90°$ (which corresponds to the condition of smooth injection of fluid into the milling cutter). Then equation (6) is simplified

$$H_T = \frac{U_2C_2\cos\alpha_2}{g}.$$

From the parallelogram of velocities at the exit of the mill (Fig. 5) we find

$$H_T = \frac{U_2^2}{g}\left(1 - \frac{\omega_2}{U_2}\cos\beta_2\right). \quad (7)$$

Equation (7) shows that the pressure on the milling cutter is proportional to the square of the number of rotations of the milling cutter (since $U_2 = \pi D_2 n$, where D_2 – is the outer diameter of the milling cutter in the section considered, n – is the number of rotations of the milling cutter) and depends on the structural shape of the teeth.

There are three possible cases:

1 - the teeth are tilted in the direction of rotation of the mill:

β_2>90°cos β_2>0 cos β_2<00 и $H_T > U_2^2 / g$;

2 - the teeth are tilted in the direction opposite to the direction of rotation of the cutter:

β_2<90°cos β_2>0° и $H_T < U_2^2 / g$;

3 - the teeth have no inclination:

β_2=90°cos β_2=0 и $H_T = U_2^2 / g$;

It follows that, theoretically, the greatest pressure is achieved on the cutter with the teeth tilted in the direction of rotation of the cutter, the smallest - in the opposite. Therefore, in the development of the design features of the forms of the treatment device, we made the decision to manufacture working mills with small angles (β_2<90°) of inclination of the teeth, as with the increase β_2 hydraulic losses and decreases the hydraulic efficiency of cleaning the column as a whole. We also calculated the actual pressure on the milling cutter, which is less than the theoretical, since some of the fluid energy is spent to overcome the hydraulic resistance between the milling teeth and the fluid in this case does not move along similar (as was calculated) trajectories. Then the real head is

$$H_Д = H_E \eta_Г \xi,$$

where $\eta_Г$ - hydraulic efficiency of the milling cutter (equal to 0.7-0.8), ξ - coefficient taking into account the number of teeth of the milling cutter (equal to 0.8-0.9). The values of the coefficients $\eta_Г$ and ξ obtained from the field tests of treatment facilities in oil wells of Kharkivtsivs′ke oil and gas condensate field of Poltava region. It should be noted that the obtained equations can be used in the calculations of treatment devices for tubing of different diameters. This follows from the fact that, provided that the similarity of the trajectories of the motion of the fluid particles is maintained, the parallelograms of velocities at any similar points of flows will be geometrically similar in the case of different tubing diameters and, accordingly, the sizes of the cleaning mills (Fig. 6). This can be explained by the fact that as the tubing diameter changes, the tubing will change in inverse proportion to the number of rotations of the working mills. Based on the obtained equations, we calculated the sizes and shapes of working (main) and additional (reverse) mills,

the masses and strength characteristics of structural elements (pins, traverse, cable, bolt connections, etc.) provided in the process of design development. the required rigidity and reliability of the entire treatment plant. Industrial tests of the developed structure on oil and gas complexes showed significant advantages in comparison with domestic and foreign analogues.

On the basis of industrial tests, we note the following advantages of the proposed design of the treatment device:

- simplicity in manufacturing and assembly of the structure;
- high maneuverability and flexibility (can be used both in vertical and vertically inclined wells);
- complete (90-100%) cleaning of the inner surface of tubes of tubing from deposits of paraffinized oil;
- high qualification of workers for underground well repair is not required;
- high handling and reliability during operation.

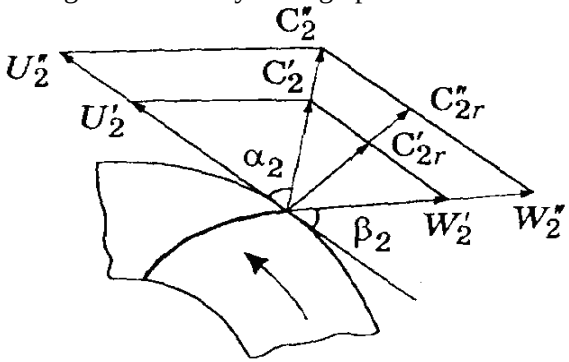

Fig. 6. Typicality of velocity parallelograms when changing the speed of the cutter from n_1 до n_2 for different tubing diameters.

Conclusions

High wear resistance of the milling material makes it possible to use them for a long time (for example, two units of treatment plants in the new design made it possible to clear about 50 tubing tubes at the Kharkivtsivs′ke oil and gas condensate field of Poltava region for 3 years, which made it possible to increase oil production by 15-20%). Nowadays, it is important to establish the production and

repair of treatment plants in new structures at the oil and gas enterprises. The results of bench and industrial research, as well as design and technological developments have been implemented in the improved regulatory documents governing the inspection, cleaning, repair and control of tubing tubes during their operation.

Improved design of the device for cleaning the inner surface of the oil well tubing. The kinetic calculations of the movement of the milling cutter in the tubes of tubing under the action of hydraulic forces were performed. Based on the obtained equations, in the process of design development, the sizes and shapes of working (basic) and additional (reverse) mills were calculated, the masses and strength characteristics of the structural elements (pins, traverse, cable, bolt connections, etc.) were provided the necessary rigidity and reliability of the entire treatment plant. The flushing tests developed on the facilities of the oil and gas industry have shown significant advantages over domestic and foreign analogues.

References

[1]. **Tronov V.P.** Mehanyzm obrazovaniya smoloparafynovyh otlozhenyj i borba s nimy.- M.: Nedra. 1970.- 220.

[2]. **Babalyan G.A.** Fyzyko-xymycheskye processy v dobuche nefti.- M.: Nedra, 1974.- 200.

[3]. **Kolesnyk Y.O., Lukashevych Y.P., Susanyna O.G.** Issledovanie prylypaemosti parafinistyh otlozhenij k stalnoj povernosti / RNTS «Transport i hranenie nefti i nefteproduktov i uglevodorodnogo syr`ya», # 5.- M.: CzNIITNeftehim, 1972.

[4]. **Mazepa B.A.** Zashhita neftepromyslovogo oborudovaniya ot parafinovyh otlozhenij.- M.: Nedra, 1972.—117.

[5]. **Malyshev A.G., Cheremysyn N.A., Shevchenko G.V**. Vybor optimalnyh sposobov borby s parafinogidratoobrazovaniem // Neftyanoe hozyajstvo.- 1997.- # 9.- 62-69.

[6]. **Maganov R., Vahitov G., Vafina N.** Optimal`naya texnologiya borby s gidratoparafinovymi otlozheniyami // Neft` Rossii.- 2000.- # 3.- 96-99.

[7]. **Sizaya V.V.** Himicheskie metody borby s otlozheniyami parafina.— M.: VNIIOENG, 1977.- 41.

STABILITY ASSESSMENT OF ROCK MASS UNDER SHORT DRIFT AND PILLARS BETWEEN DRIFTS EXPLOITATION WITH CAVING, BASED ON THE ANALYTICAL AND NUMERICAL SOLUTIONS TO GUARANTEE THE ROCK MASS STABILITY AND SURFACE BUILDINGS PROTECTION

Krzysztof TOMICZEK

Ph.D. Eng. Krzysztof Tomiczek, Department of Geomechanics and Underground Building, Faculty of Mining, Safety Engineering and Industrial Automation, Silesian University of Technology, Gliwice, Poland

Summary

Underground mining of useful mineral deposits causes changes in the virgin rock mass stress state and may affects on ground buildings and mining excavations damages. The pillar mining system prevents adverse effects. On the basis of analytical solutions, combined functions based on the results of measurements and simplified numerical simulations, dimensions and arrangement of unmined coal pillars were proposed for mining with a caving at a depth of -350m.

Keywords: shallow mining, pillar mining system, pillar stability, pillar dimensions, strength factor, numerical modelling, *Phase2*, stability of rock mass, stresses and displacements in rock mass, surface protection

Introduction

Underground mining of useful mineral deposits causes changes in the virgin stress state. Exploitation of underground minerals creates voids in the rock mass. The caving of the roof layers plus the rocks displacement to the excavations cause as well displacement as also deformation of the rock mass and the surface. The phenomena effects are often damages to above-ground buildings and mining excavations.

Sometimes it is also necessary to excavate the residual coal seam parts.

In both cases, the use of longwall mining systems is impossible due to negative effects, e.g. the forming stress concentration zones or large rock mass displacement.

Therefore, often the only solution of this problem is partial exploitation of coal seam using the pillar system. Of course, dividing the mining field into pillars while leaving the unexploited coal belts is less economically viable. However, the effects of safety level, rock mass stability, surface protection and the possibility of mechanization are encouraging.

For mining exploitation with long drift and pillars left between these drifts the main problem is to determine width of the excavating coal belts as well as of remaining pillars.

Most often, this problem is solved by calculating the pillars material effort. The width of pillars is determined then by comparing the strength of the pillars with the stress value.

Exemplary of the effort criterion are, i.e.: Safety Factor coefficient by Salamon and Munro (1967), loads of pillars with rectangular cross-section by Hoek and Brown (1980), Hedley and Grant (1972), Whittaker and Singh (1979) and Pariseau (1982).

Strength and deformation properties of the pillar depends on its geometry, i.e. the shape and dimensions of the pillar.

Similarly as for testing cuboid rock samples, the pillar strength is influenced by the geometrically effects: Power Shape Effect (*PSEF*), Size Effect (*SEF*) and Linear Shape Effect (*LSEF*).

These effects, describing the relationship between the width, height and length of the pillar have been studied, including but not limited to, by Bunting (1911), Greenwald et al. (1939), Morrison, Cortell and Rice (1956), Sałustowicz (1961), Obert and Duvall (1967), van Heerden (1974), Bieniawski (1975), Belesky (1980), Salamon and Wagner (1985), Sheorey and al. (1987), Madden and Wagner (1991).

The mentioned aspects of pillar stability analysis have already been presented in Polish publications (e.g. Tajduś et al., 2012). The chapter presents the solution for a specific problem of exploitation with short drift with caving and pillars system.

For the preliminary assessment to the selection of the pillar dimensions, the results of tests and measurements carried out in Polish, European and Chinese underground coal mines were used (Chudek and Dehai, 2000). Based on selected formulas and nomograms prepared on the basis of measurement results, the widths of the pillars and mined coal belts were determined.

Adding simple numerical simulations using a program based on the finite element method *Phase2* by Rocscience Inc. To analytical solutions, various variants of the location and width of the mined coal belts and pillars were modelled and tested.

Geomechanical conditions determining the width of mined coal belts and pillars defined by an analytical solution

The planned mining is to be carried out at a depth of up to -300m. For exploitation in conditions of easily breaking roof layers and 1st class of roof stability, the exploitation with caving can be used and the pillars will provide sufficient support for the higher rock layers.

For system of pillars-belts exploitation, as for the dog headings, a pressure arch surrounding the internal caving space is created (Budryk, 1964). The caving shapes as in an arch (Fig. 2.1).

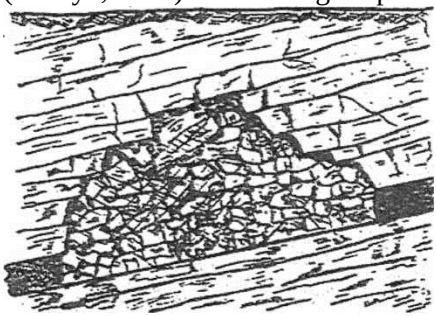

Fig 2.1. Pressure (and caving) arch for the caving system of exploitation (Budryk, 1964)

Cracked and disintegrated rocks have a larger volume than solid, therefore volume of the void between caving and the arch is smaller than the excavated volume. The caving propagates to form a new arch. Range of cracked rocks increases. Finally, volume of cracked and disintegrated rock is same as the volume of the arch together with the mined part of seam.

The greatest bending of the rock roof layers is within the immediate range of the caving. Weber cracks and voids occur. Each next roof layer undergoes less bending, and the cracks and voids above are getting smaller. At a certain distance above the caving no more cracks or voids are formed. The layers decline uniformly. The coal pillars support the overlying rock layers and guarantee an uniformly declination of the rock mass and the surface.

Mining exploitation with pillars and caving will be carried out with regressing of exploitation front in several belts and mine regions (Fig. 2.2).

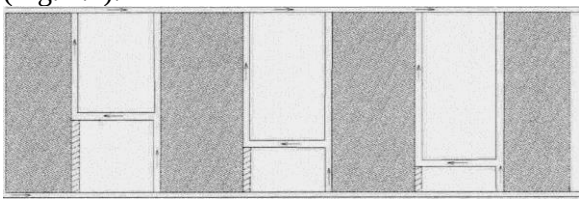

Fig. 2.2. Mining with pillars and caving with regressing of exploitation front (GIG, 1968)

2.1. Brief description of the rock mass and its geomechanical properties

The rock mass in the planned mining area at the level of -300m is mainly recognized by boreholes from the surface and shafts during their driving.

In situ and laboratory tests put the base for determining basic rock and coal properties (Table 2.1).

Table 2.1

Parameters of rocks and coal

№	Rock types	R_c MPa	R_r MPa	E_0 GPa	E_s GPa
1	Conglomerates	0.6-1.1	0.1-0.8	~1.3	~2.6
2	Mudstones	~3.2	~0.1		
3	Sandstones	6.4-9.5	0.2-0.4	0.8-2.4	1.9-3.7
4	Claystones	10.4-12.6	0.1-0.8		
5	Coals	15.8-21.3	0.2	0.7-1.2	1.4-1.6

where

R_c - uniaxial compression strength [MPa],

R_r - tension strength [MPa],

E_0 - deformability modulus [MPa],

E_s - elasticity (Young's) modulus [MPa].

2.2. Defining the width of exploited belts and left pillars based on chosen analytical solutions

Pillars - coal belts exploitation system is one of methods to minimize the influence of underground mining on the surface. In shallow - focus, the pillars exploitation it is often the only option of coal seam mining.

Exploitation of the seam with pillars requires defining the width of exploited and left pillars and coal belts. The width depends on mining and geological conditions. Mainly depends on stress stability of the pillars after exploitation.

According to Knothe (1984), the average width of the mined coal belts should be around 0.25*H*, where *H* is the depth of the coal seam. Degree of deposit exploitation is usually of 50% for *H* depths greater than -400m and slightly greater for *H* depths less than -200 m.

Chudek and Dehai (2000) analysed method of determining the width of coal belts considering experiences of Polish, European and

Chinese underground coal mines for the exploitation of pillar – coal belts mined to a depth of -916m.

They presented relations to determine the width of exploited coal belts and coal pillars:

Width of exploited coal belt S

$$S=(0,10\div 0,25)H$$

Width of unmined coal (pillar) C

$$C=\frac{Sp}{1-p}$$

where: p - deposit exploitation degree

Width of unmined coal (pillar; after Wilson, 1980)

$$C\geq 2y+b$$

where

y - width of loosen part of the pillar with damaged structure, m; $y=0,005gH$.

where g - seam thickness, m; b - the width of the part of the pillar with undamaged structure,

$$b=8,4g$$

Maximum unmined coal pillar load $P_{\max}$

$$P_{\max}=40\gamma H(C-4,92gH10^{-2})$$

Real unmined coal pillar load P_r

$$P_r=10\gamma\left[HC+\frac{S}{2}\left(2H-\frac{S}{0,5}\right)\right]$$

where H - depth of coal seam, m; γ - average bulk density of overlayed rock mass, kN/m^3; g - thickness of the mined seam, m.

The rock mass stability criterion of unmined coal pillars with width C and with the width of mined coal belts S

$$\frac{P_{\max}}{P_r}\geq 1,5$$

Width of unmined coal pillars C (after Guaging, 1991), gH

$$C=\frac{S}{3}-\frac{S^2}{3,6\cdot H}+6,56\cdot 10^{-2}$$

Equilibrium force criterion for rock mass (after Chudek and Stefański, 1989)

$$\sigma_f < R_{cw}$$

R_{cw} - uniaxial compression strength of coal, MPa; σ_f - compression stress in unmined coal pillars, MPa.

where

$$\sigma_f = \frac{L_{\min p_z}}{C}$$

where L_{min} - length of the rigid roof layer supported by unmined coal pillars, above the exploited space.

$$L_{\min} = 3{,}75 h_r \sqrt{R_r / p_z}$$

where R_r - average tensile strength of rocks above the mined seam, MPa; h_r - thickness of the rigid roof layer, m.

$$C = 2C_n$$

$$C_n \geq \frac{L_{\min} p_z}{R_{cw}}$$

Using the above formulas and taking into consideration geological and geomechanical conditions of rock mass, calculations were made for the planned exploitation at the level of -300m (e.g. Table 2.2).

Where, in Table 2.2 are:

1. Depth of mining.
2. Deposit exploitation degree.
3. Degree of unmined coal pillar *C* loosing.
4. Rock mass stability criterion of unmined coal pillars with width *C* and with the width of mined coal *S* seams.
5. Empirical Guaging's criterion.
6. Equilibrium force criterion for rock mass.

Based on the calculations, it was determined that the width of mined coal belts *S* and pillars *C* should equals to 30 m.

Tab. 2.2

Examples of calculations

Obliczenie szerokości pasów S i calizny C c 203/3
część PlnZach O.G.

h=250-270m
g=1.50-1.80m
Rcw=20.66MPa

1. Ze względu na głębokość eksploatacji

H m	S m	C m	p %
>400	0,1 H	0,1 H	50
200-400	30	30	50
100-200	20-25	20	50-55
70-100	12-15	8-10	60

2. Ze względu na stopień wybrania złoża

C= 30 m
S= 30 m

3. Ze względu na zruszenie pasa y

C> 19.98 m

4. Ze względu na wytężenie P_{max}/P_{rz}

P_{max}= 715.62 MN/m
P_{rz}= 370.80 MN/m
warunek $(P_{max}/P_{rz})>1,5$
zalecane $(P_{max}/P_{rz})\approx2,0$

dla S= 30 m
C= 30 m

(P_{max}/P_{rz})= 1.93

5. Ze względu na warunek empiryczny

C> 12.26 m

6. Ze względu na warunek równowagi sił w górotworze

C> 8.66 m

7. Ze względu na dotychczasowe doświadczenia w kopalniach

S= 30 m
C= 30 m

Zalecana szerokość pasów

S= 30 m
C= 30 m

Obliczenie szerokości pasów S i calizny C c 203/3
część PlnZach O.G.

h=250-270m
g=1.50-1.80m
Rcw=20.66MPa

1. Ze względu na głębokość eksploatacji

H m	S m	C m	p %
>400	0,1 H	0,1 H	50
200-400	30	30	50
100-200	20-25	20	50-55
70-100	12-15	8-10	60

2. Ze względu na stopień wybrania złoża

C= 30 m
S= 30 m

3. Ze względu na zruszenie pasa y

C> 19.98 m

4. Ze względu na wytężenie P_{max}/P_{rz}

P_{max}= 715.62 MN/m
P_{rz}= 370.80 MN/m
warunek $(P_{max}/P_{rz})>1,5$
zalecane $(P_{max}/P_{rz})\approx2,0$

dla S= 30 m
C= 30 m

(P_{max}/P_{rz})= 1.93

5. Ze względu na warunek empiryczny

C> 12.26 m

6. Ze względu na warunek równowagi sił w górotworze

C> 8.66 m

7. Ze względu na dotychczasowe doświadczenia w kopalniach

S= 30 m
C= 30 m

Zalecana szerokość pasów

S= 30 m
C= 30 m

Estimation of required width of unmined coal belts *S* and pillars *C* based on combined functions including experiences of Poland and the world

On the basis of data from underground coal mines in Poland, Europe and China exploited with caving, and also taking into account simple functions describing the relations between depth of exploitation *H*, width of unmined coal belts *S* and pillars *C* and thickness of

coal seams *g*, simple functions describing the relations between these quantities were founded (Figs. 3.1-3.4).

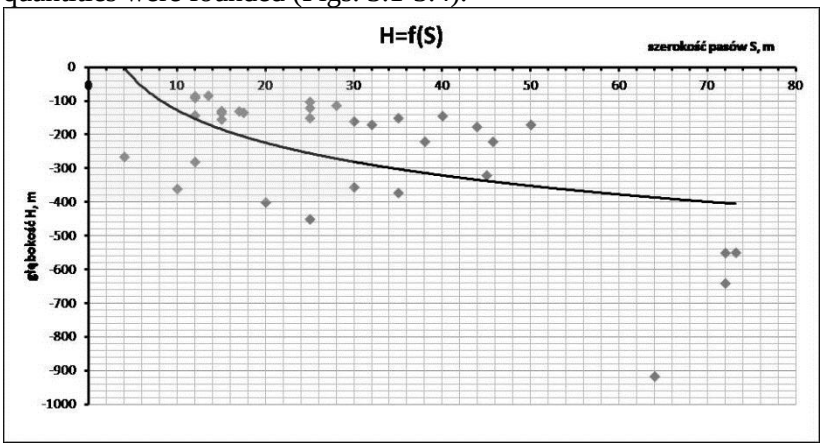

Fig. 3.1 Relation between the depth of mining *H* and the width of the mined coal belts *S*. For the depth *H*=-300 m, the width of the belts *S*≈30 m

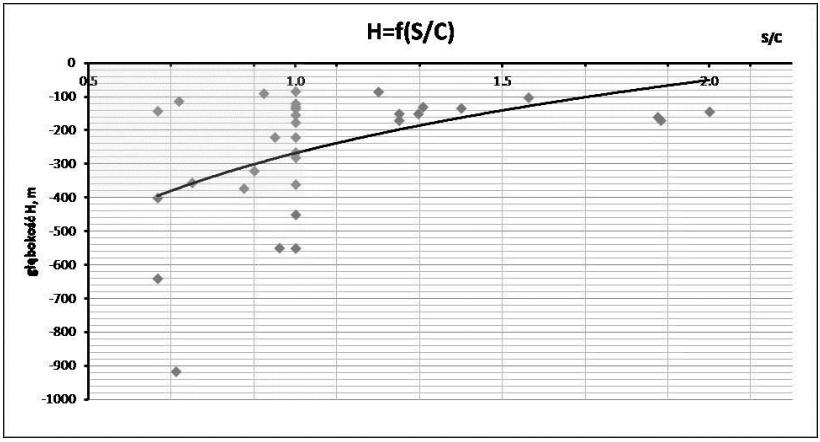

Fig. 3.2 Relation between the depth of mining *H* and the *S*/*C* ratio. For the depth *H*=-300 m, the *S*/*C*≤1; *C* - width of the unmined coal pillars

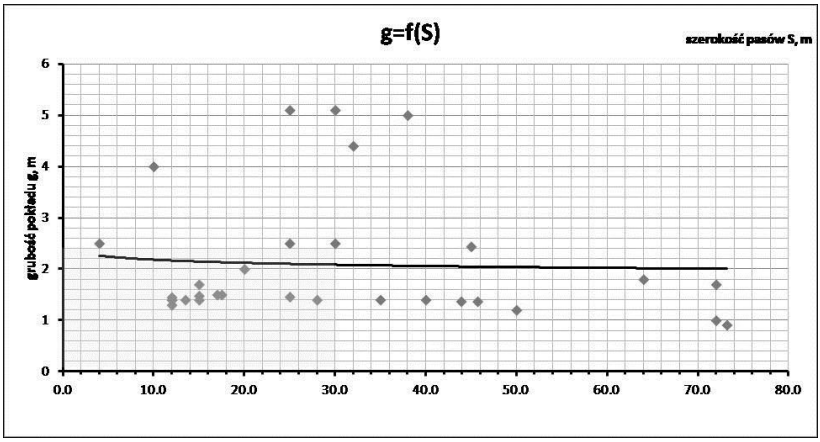

Fig. 3.3. Relation between the thickness of the coal seam *g* and the width of the mined coal belts *S*. For thickness $g \leq 2.4$m, the belts width *S* was usually less than- or equal to 30 m

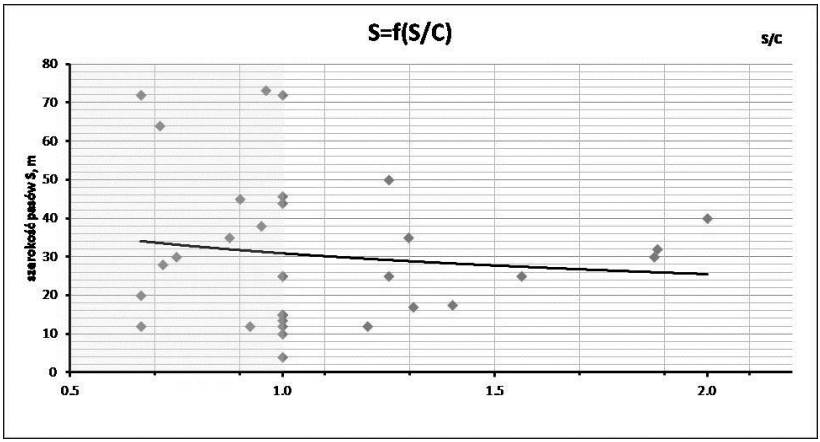

Fig. 2.6. Relation between the width of the mined coal belts *S* and the ratio *S*/*C*. For the width of the belts *S*=30m in the most cases the ratio *S*/*C*=1

Considering relations between quantities (1 to 4) described below, that were defined on the basis of previous experience in underground mines in Poland and over the world:

1. Depth of mining *H* and width of mined coal belts *S* (*S*=*f*(*H*)).
2. Depth of mining *H* and the ratio *S*/*C* (*S*/*C*=f(*H*)).

3. Coal seam thickness g and width of mined coal belts S ($S=f(g)$).

4. Width of mined coal belts S and the ratio S/C (S/C=f(S)) the width of mined coal belts S should equal to 30m and the ratio S/C should equal to 1.

Numerical analysis of effort and vertical stress distribution in the pillars

For determining the effort and vertical stress distribution in the vicinity of the unmined coal belts and pillars, a rock mass 2D model was built and it followed principles as below (1 to 10):

1. 2D flat model was built, and it represented a longitudinal section of the rock mass.

2. It has been assumed that 3 coal seams were mined simultaneously.

3. The coal seams were mined from top seam 200/2 to the 208/3.

4. An extreme case was assumed, i.e. all coal seams were mined successively, i.e. 200/2, 206/1, 206/2, 208/1 and 208/3.

5. The width of the mined coal belts S=30m and the width of the unmined coal pillars C=30m were assumed.

6. Rocks were described by a modified Coulomb-Mohr criterion.

7. Missing values of material constants, i.e. uniaxial compression strength R_c, tension strength R_r, Young's modulus E, Poisson's ratio ν, cohesion c and angle of internal friction φ were determined on the basis of literature studies and own laboratory tests.

8. The depth of the coal seams H and the surface level were determined on the basis of geological cross-sections.

9. Assuming that rocks building rock mass were in a pre-critical state elastic-isotropic materials, the solution given by Wardle and Gerrard was applied. Values of elastic constants of several thin rock layers were treated as of one layer. One layer was modelled as an equivalent monotropic medium. This assumption allowed, among others, for modelling layers with unknown values of material constants.

10. Models were built for the most characteristic systems of mined coal belts S and pillars C.

Three characteristic localisations of unmined coal belts S and – coal pillars C were analysed (Fig. 4.1):

1. Both belts *S* - and pillars *C* lie one below the other (Fig. 4.1a) - "vertical system".

2. Belts *S* and pillars *C* lie alternately below each other (Fig. 4.1b) - "alternate system".

3. Belts *S* are shifted relative to the underlying pillars *C* by 0.5 width, i.e. by 15m - "shifted system" (Fig. 4.1c).

Simulations of other variants of mined belts *S* relative to pillars *C* shifting allowed to determine that the influence on the distribution and magnitude of stress is not significant.

Analysed were as follows (Fig. 4.2-4.10):

1. Distributions and values of the vertical stress component p_z.

2. Stress coefficient σ_{Ft} describing the relationship between tensile strength R_r and the magnitude of tensile stress for a given rock mass R_{rm}. The value of $\sigma_{Ft}>1$ means the rock material failure due to exceeding its tensile strength R_r.

3. Ubiquitous joints coefficient D_{UJ}. A value of $D_{UJ}<1$ means damage the rock material continuity.

a

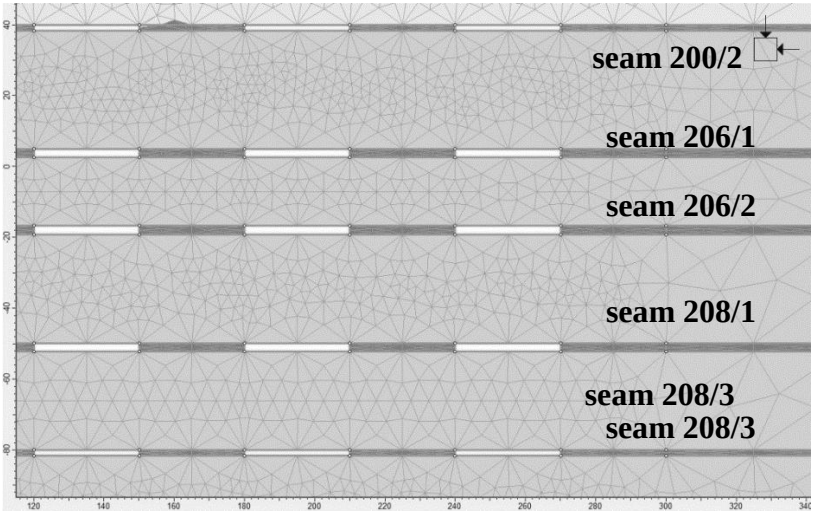

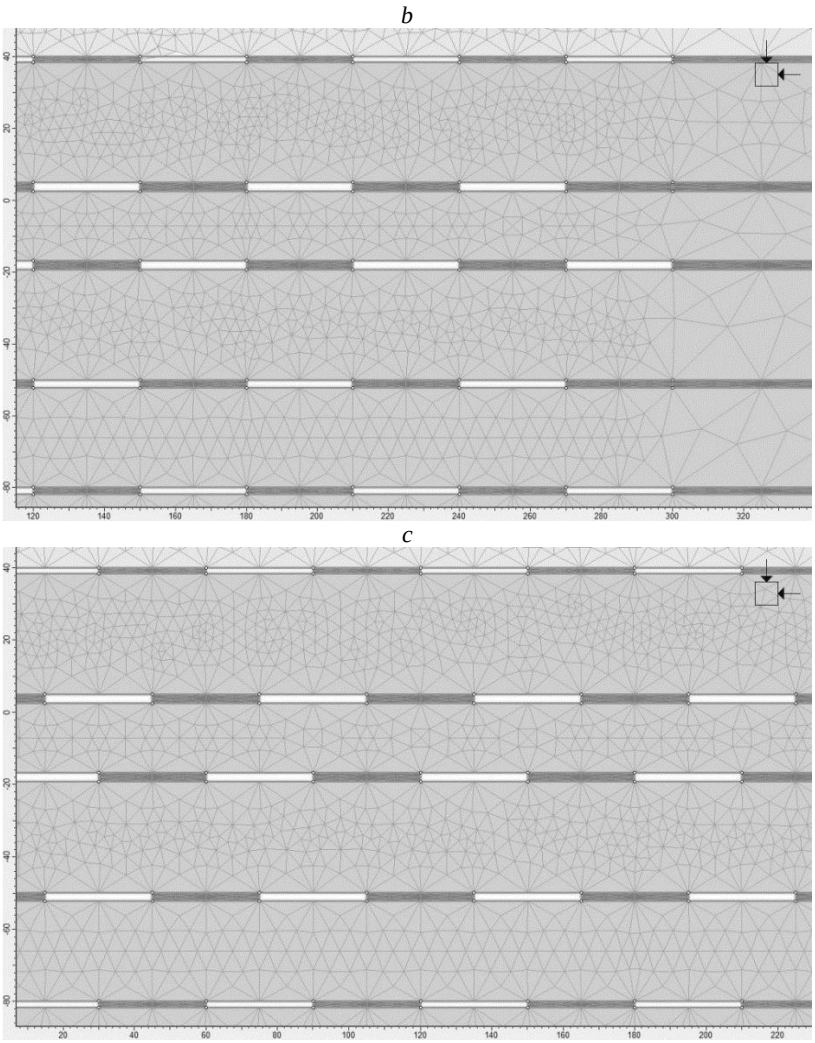

Fig. 4.1. Position of unmined coal belts *S* and coal pillars *C* for three different variants: a - unmined belts *S* are located one above the other, b - belts *S* are located above pillars *C*, c - belts *S* are shifted to pillars *C*

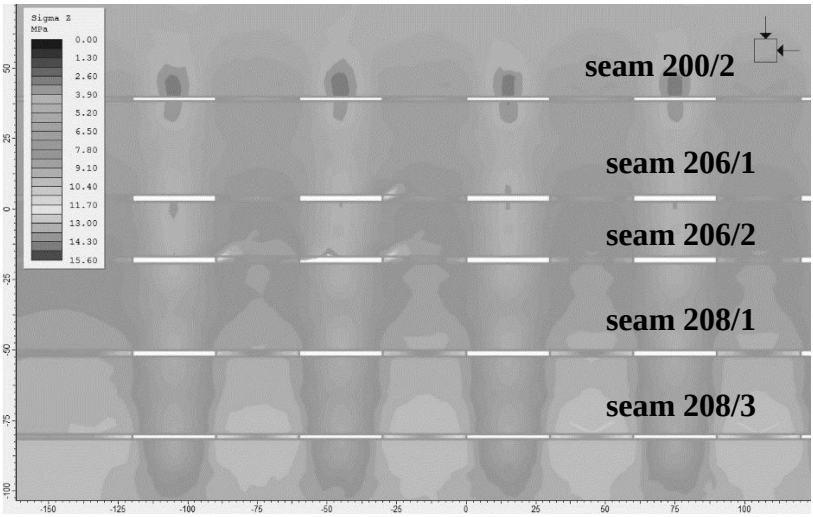

Fig. 4.2. Distributions and values of the vertical stress component p_z in the vicinity of mined coal belts *S* and coal pillars *C* for the "vertical system"

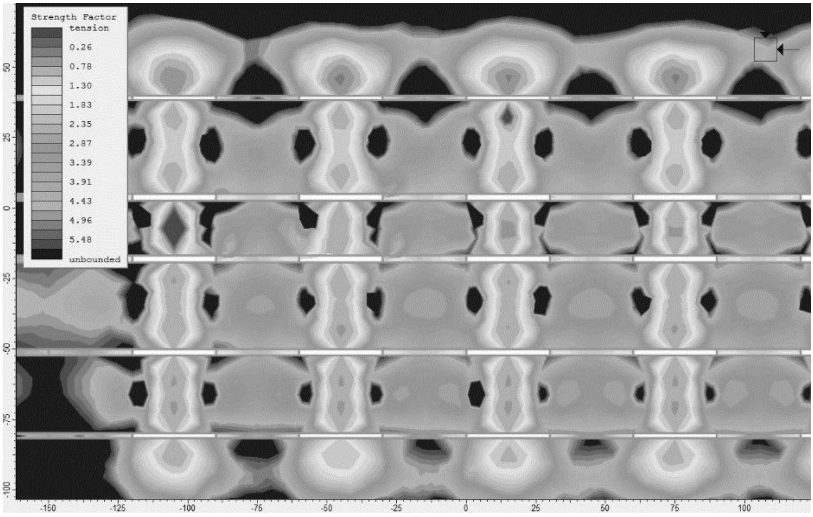

Fig. 4.3. Distributions and values of the stress coefficient σ_{Ft} in the vicinity of mined coal belts *S* and coal pillars *C* for the "vertical system". Values σ_{Ft} less than 1.0 (σ_{Ft}<1.0) indicate the damage of rocks as a result of exceeding their tensile strength R_r.

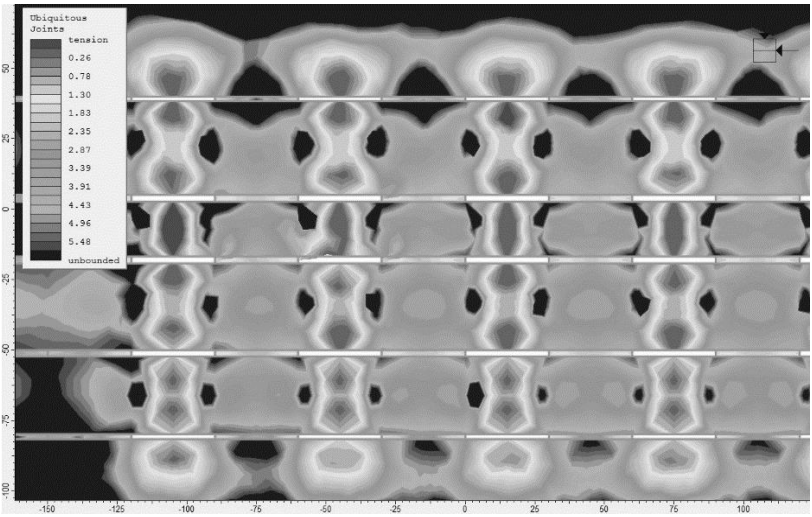

Fig. 4.4. Ubiquitous joints coefficient D_{UJ} in the vicinity of mined coal belts *S* and coal pillars *C* for the "vertical system". A value of $D_{UJ}<1$ means damage of the rock material continuity

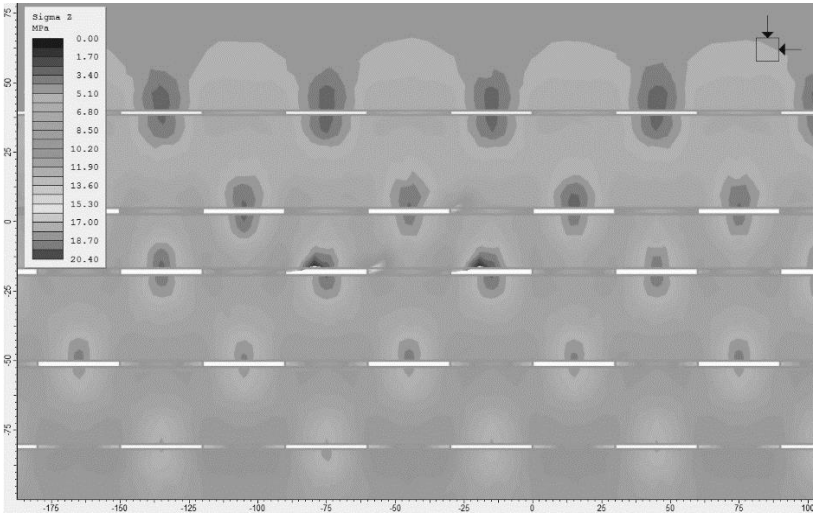

Fig. 4.5. Distributions and values of the vertical stress component p_z in the vicinity of mined coal belts *S* and coal pillars *C* for the "alternate system"

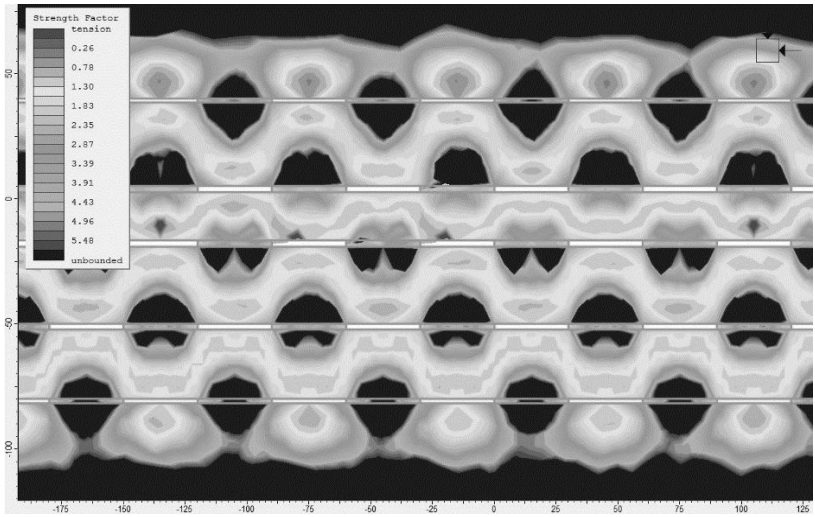

Fig. 4.6. Distributions and values of the stress coefficient σ_{Ft} in the vicinity of mined coal belts *S* and coal pillars *C* for the "alternate system". Values σ_{Ft} less than 1.0 (σ_{Ft}<1.0) indicate the damage of rocks as a result of exceeding their tensile strength R_r

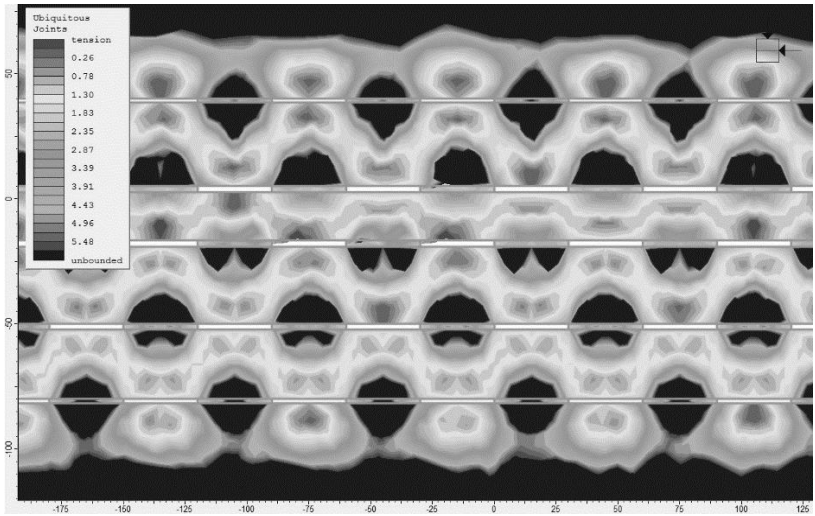

Fig. 4.7. Ubiquitous joints coefficient D_{UJ} in the vicinity of mined coal belts *S* and coal pillars *C* for the "alternate system". A value of D_{UJ}<1 means damage of the rock material continuity

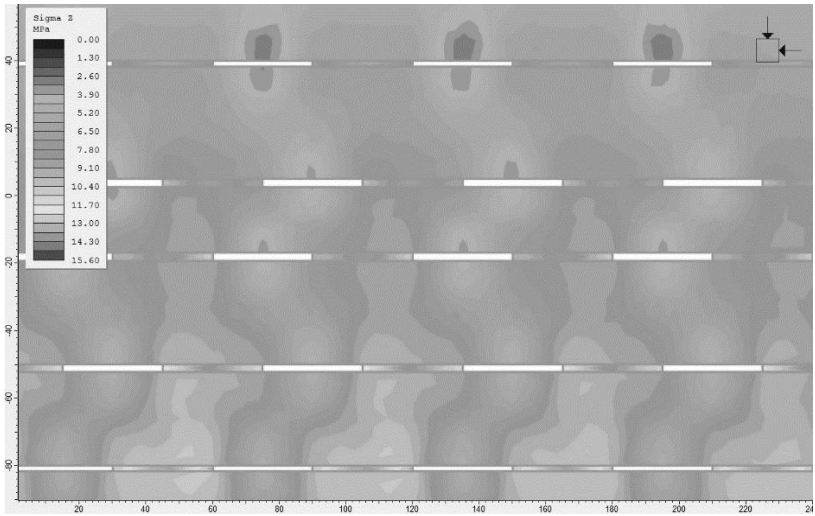

Fig. 4.8. Distributions and values of the vertical stress component p_z in the vicinity of mined coal belts *S* and coal pillars *C* for the "shifted system"

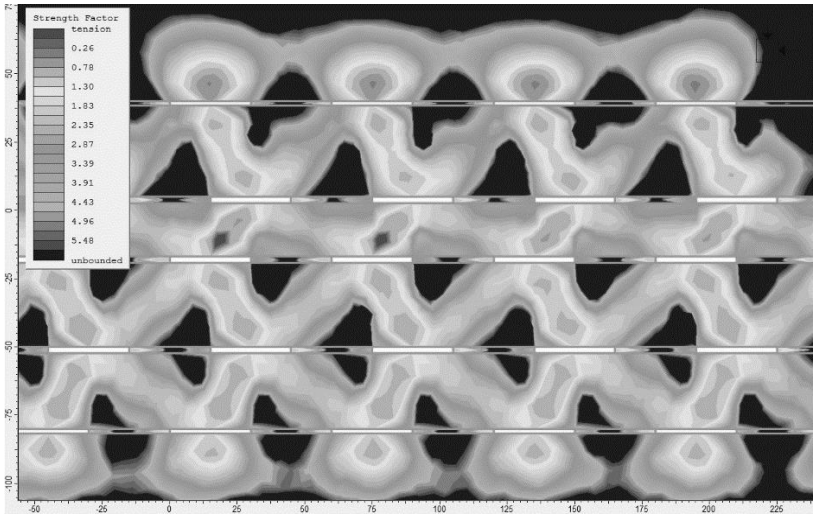

Fig. 4.9. Distributions and values of the stress coefficient σ_{Ft} in the vicinity of mined coal belts *S* and coal pillars *C* for the "shifted system". Values σ_{Ft} less than 1.0 (σ_{Ft}<1.0) indicate the damage of rocks as a result of exceeding their tensile strength R_r

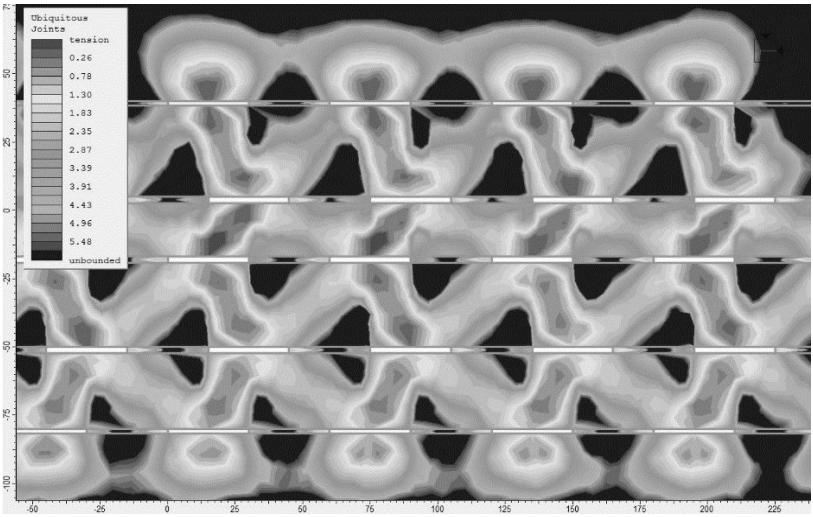

Fig. 4.10. Ubiquitous joints coefficient D_{UJ} in the vicinity of mined coal belts *S* and coal pillars *C* for the "shifted system". A value of D_{UJ}<1 means damage of the rock material continuity

Vertical stresses p_z

For the virgin rock mass, stresses p_z are a function of gravity g, volume density ρ and depth H. For a depth of approx. -350m they are equal to approx. 9.1 MPa (Fig. 4.2, 4.5 and 4.8). Above the mined coal belts *S*, semi-elliptical zones of much smaller stresses p_z appear.

For the "vertical system" (Fig. 4.1*a*), the maximum stresses p_z in the unmined zones at the 208/3 seam level reach 9.8 MPa. In the semi-elliptical unstressed zones over mined coal belts S, the p_z values are lower and reach 2.6 MPa for the 200/2 seam, and 5.2 MPa for the 208/3. Unstressed zones also appear under the floors of mined belts. However the range and size of unstressed zones are smaller, and p_z values equal to 3.9-5.9 MPa. The stress concentration occurs in the left pillars, especially in their side walls. For seams 200/2, 206/1 and 206/2, the p_z values reach 7.8-8.45MPa, while for 208/1 and 208/3 seams these values reach 10.40-12.35 MPa.

Stress concentration zones also appear in the floor and floor layers above and below the left pillars. Stresses reach 6.5 MPa for the 200/2 seam, 8.5 MPa for the 206/2 and 10.4 MPa for the 208/3.

For the “alternating system” (Fig. 4.1*b*), the vertical stress distribution p_z is like different from previous system (Fig. 4.5).

Maximum values of stress p_z in a non-disturbed zone at the 208/3 seam level reach about 9.5 MPa. In unstressed like half-ellipses zones shaped above mined coal belts S, stresses p_z are lower and reach: for the 200/2 seam 2.6 MPa, for the 206/1 and 206/2 seams 3.4 MPa, and for the 208/1 and 208/3 seams about 4.3 MPa and 5.1 MPa. Uncompressed zones also appear under the floors of mined belts, however their ranges and sizes are smaller, and p_z values - from 3.4-4.3 MPa. The stress concentration zones occur in the left unmined pillars, especially in their side walls. In turn, for the 200/2, 206/1, 206/2, 208/1 and 208/3 seams, the stresses p_z are equal to 9.4, 11.1, 11.9, 12.1 and 13.6MPa.

Stress concentration zones also appear in the floor layers above and below the left coal pillars. They reach 6.8MPa for the 200/2 seam, 7.7 MPa for the 206/2 and 9.4 MPa - for the 208/3.

For the “shifted system” (Fig. 4.1*c*, 4.8), the maximum values of stress p_z in the unmined rock mass zone at the 208/3 seam level reach about 9.7MPa. In the semi-elliptical zones under mined coal belts *S*, p_z values are lower and reach: for the 200/2 seam - 2.60 MPa, for the 206/1 and 206/2 seams 3.3 MPa, and for the 208/1 and 208/3 seams - about 4.3 MPa and 5.2 MPa. Unstressed zones also appear under the floors of mined belts, however their ranges and sizes are smaller, and p_z values - from 3.9-5.0 MPa. As in previous variants, stress concentration zones also occur in the left pillars, especially in their side walls. In turn, for the 200/2, 206/1, 206/2, 208/1 and 208/3 seams, the maximum stresses p_z in the side walls of the coal pillars are equal to 7.8, 9.1, 10.4, 11.5 and 12.4MPa .

Stress concentration zones also appear in the above floor layers and below the pillars. They reach 6.8 MPa for the 200/2 seam, 7.7 MPa for the 206/2 and 9.4 MPa for the 208/3.

To sum up, the adverse conditions will occur in situations where the mined coal belts *S* are located above the coal pillars *C*. Generally, for all three belts and pillar systems, the vertical stresses p_z will be greater than that characteristic of the virgin rock mass at a depth *H* by about 40%.

Stress coefficient σ_{Ft}

The stress coefficient σ_{Ft} describes the relationship between tensile strength R_r and the tensile stress in the rock mass R_{rm}. If σ_{Ft} is less than 1.0 (Fig. 4.3, 4.6 and 4.9), it means that the rocks are failured as a result of exceeding their tensile strength.

For the case of the "vertical system" of pillar mined (Fig. 4.3), the rocks will be failure in the roofs of the all mined coal belts in all seams, i.e. 200/2, 202/1, 202/2, 208/1 and 208/3. The failure zones in the roofs of the lower lying seams joint with the failure zones arising in the floors of higher lying mined belts. The coal pillars themselves should not be failure; σ_{Ft} is greater than 1.0 and equal to approximately 1.3.

For the case of the "alternating system" (Fig. 4.6), the rocks will be failured in the roofs of all mined coal belts in all seams, i.e. 200/2, 206/1, 206/2, 208/1 and 208/3. The failured zones in the roofs of the lower lying seams do not joint with the failure zones arising in the floors of mined higher coal belts. The coal pillars themselves should not be failure; σ_{Ft} is greater than 1.0 and equal to approximately 1.3 too.

For the case of the "shifted system" (Fig. 4.9), the rocks will be failured in the roofs of all mined coal belts in all seams, i.e. 200/2, 206/1, 206/2, 208/1 and 208/3. The failured zones in the roofs of the lower lying seams can joint with the failure zones arising in the floors of mined higher coal belts. The coal pillars themselves should not be failure; σ_{Ft} is greater than 1.0 and equal to approximately 1.2.

Ubiquitous joints coefficient D_{UJ}

The ubiquitous joints coefficient D_{UJ}<1 indicates the possibility of discontinuity in the rock material. It means that the rock material will be damaged as a result of loss of its continuity (Fig. 4.4, 4.7 and 4.10).

For the case of the "vertical system" (Fig. 4.1a), the rocks will be damaged in the roofs of all selected mined belts in all seams, i.e. 200/2, 206/1, 206/2, 208/1 and 208/3. The damage zones in the roofs of the lower lying seams joint with the damage zones propagating in the floors of mined higher lying belts. The coal pillars themselves should not be failured. D_{UJ} values are greater than 1.0 and equal to about 1.30-1.35.

For the case of the "alternating system" (Fig. 4.1*b*), the rocks will be damaged in the roofs of all mined belts in all seams, i.e. 200/2, 200/1, 206/2, 208/1 and 208/3. The damage zones in the roofs of the lower lying

seams do not joint with the damage zones in the floors of mined higher belts. The coal pillars themselves should not be failured. D_{UJ} values are greater than 1.0 and equal to approximately 1.3.

For the case of the "shifted system" (Fig. 4.1*c*), the rocks will be damaged in the roofs of all selected mined belts in all seams, i.e. 200/2, 206/1, 206/2, 208/1 and 208/3. The damage zones in the roofs of the lower lying seams joint with the damage zones in the floors of mined higher lying belts. The coal pillars themselves should not be failured. D_{UJ} values are slightly greater than 1.0 and equal to about 1.3.

Summary and final remarks

Underground pillar mining system is often the only mining method that ensures rock mass stability and protection of surface structures and building.

There are various methods for determining the width of mined belts, left coal pillars and calculating the effort in the pillars.

The chapter presents the solution based on observations carried out in underground coal mines in Poland, Europe and China. Simple 2D-numerical simulations of pillar system mining with caving were also carried out. The widths of mined coal belts *S* and left coal pillars *C* pillars were determine.

Values of effort/stress coefficients σ_{Ft} and joint damages D_{UJ} indicate the emergence of extensive damage zones in the roofs of mined coal belts *S*. The damage zones in the roofs of the seams below can connect with the damage zones in the lower layers of the seams above. Values of stress coefficient σ_{Ft} and ubiquitous joints coefficient D_{UJ} indicate the pillars themselves should not be failure and the rock mass stability will be cooled.

Sources (selected)

1. **Belesky R.M**. An in Situ Assessment of Deformability and Strength of Coal Pillar. Master of Science Thesis. Pennsylvania State Univ., 1980

2. **Bieniawski Z.T. and van Heerden W.L.** The significance of in-situ tests on large rock specimens. Int. Soc. Rock Mech. Min. Sci. & Geomech. Abstr., Vol. 12, pp. 101-113, 1975

3. **Borecki M. i Kwaśniewski M**. Metody analityczne obliczania ciśnienia deformacyjnego oraz przemieszczeń lepkosprężystego górotworu izotropowego w sąsiedztwie wyrobisk korytarzowych na dużych głębokościach. Analytical methods for determining deformation stress and viscoelastic-isotropic rock mass displace-

ment in the vicinity of headings at height depths. W: Metody i środki eksploatacji na dużych głębokościach. Wybrane zagadnienia. Wyd. Pol. Śl., str. 195-221, Gliwice 1982

4. **Bunting D.** Chamber-pillars in deep anthracite mines. Trans. AIME, Vol. 42, pp. 739-48, 1911

5. **Chudek M. i Dehai L.** Prognozowanie wpływów eksploatacji pokładu węgla pasami na powierzchnię terenu w warunkach płytkiego zalegania złoża. Forecasting of the influence of coal seam excavation with belts on the surface in a shallow bedding conditions of the deposit. Wiadomości Górnicze, Vol. 51, No 10, str. 433-438, Katowice 2000

6. **Dehai L.** Prognozowanie wpływów eksploatacji pasami na powierzchnię terenu w warunkach płytkiego zalegania złoża węgla w Chińskim Zagłębiu Xi Yu. Forecasting the Influence of Underground Belt Mining on the Surface in Shallow Coal Deposits in the Xi Yu China Coalfield. Praca doktorska, Politechnika Śląska, Gliwice 1999

7. Główny Instytut Górnictwa. Systemy eksploatacji węgla kamiennego. Hard Coal Mining Systems. Monografia polskiego górnictwa węglowego. Wydawnictwo „Śląsk", Katowice 1968

8. **Greenwald H.P., Howath H.C. and Hartman I**. Experiments on the strength of small pillars of coal in the Pittsburgh bed. US Bureau of Mines, Technical Paper, Vol. 605, 1939

9. **Guoging H**. Podstawy prowadzenia eksploatacji pasowej pod obiektami chronionymi. Basic Principles of Belt Mining under Protected Objects. Polskie tłumaczenie za wydawnictwem Xuzhou, Chiny 1994

10. **Hedley D.G.F. Gant F.** Slope and pillar design for the Elliot Lake uranium mines. Can. Inst. Min. Metall. Bull., Vol. 65, pp. 37-44, 1972

11. **Heerden van W.L.** In-situ determination of complete stress-strain characteristics of 1.4 m. square specimens with width to high ratios up to 3.4. CSIR Research Rept, ME 1265, 1974

12. **Hoek E. and Brown E.T**. Underground Excavations in Rock. Institution of Mining and Metallurgy, London 1980

13. **Knothe S.** Prognozowanie wpływów eksploatacji górniczej. Predicting the Influence of Underground Mining. Wydawnictwo „Śląsk", Katowice 1984

14. **Kwaśniewski M.** Badania nad mechanicznymi własnościami skał karbońskich dla potrzeb projektowania wyrobisk górniczych oraz prognozowania deformacyjnych i dynamicznych przejawów ciśnienia górotworu. Research on the mechanical properties of Carboniferous rocks for the design of mining excavations and predicting the deformational and dynamic manifestations of rock mass behaviour. W: "Metody i środki eksploatacji na dużych głębokościach. Wybrane zagadnienia." Proj. Resort. Min. Górn. i Energ. Nr 119 (1981-1985), Politechnika

Śląska, Wydział Górniczy, Instytut Projektowania, Budowy Kopalń i Ochrony Powierzchni, str. 63-72, Gliwice 1987

15. **Madden B.J. and Wagner H.** Development of a design programs for coal pillars with large width to height ratios. 9 th Coal Conference, Washington DC, USA 1991

16. **Morrison R.G.K., Corlett A.V. and Rice H.R**. Report of the special committee on mining practices. Pt. 11, Bull., Vol. 155, Ont. Dept. of Mines, 1961

17. **Obert L., Duvall W.I.** Rock Mechanics and Design of Structure in Rock. Wiley, New York 1967

18. **Pariseau W.G**. Shear stability of mine pillars in dipping seams. In: "Issues in rock mechanics", Proc. 23th U.S. Symp. Rock Mech., pp. 1077-90, 1982

19. **Salamon M.D.G. and Munro A.H.** A Study of the strength of coal pillars. J. of South Afr. Inst. Min. & Metall., pp. 56-67, 1967

20. **Salamon M.D.G. and Wagner H.** Practical experience in design of coal pillars. In: Proc. 21th Int. Conf. of Safety in Mines Research Institutes, pp. 3-10, Australia, Sydney1985

21. **Salustowicz A**. Wyznaczenie szerokości filarów oporowych. Determination of the width of pillars. Archiwum Górnictwa, t. VI, z. 3, s. 177-185, Kraków, 1961

22. **Sheorey P.R., Das M.N., Barat D., Prasad R.K. and Singh B**. Coal pillar strength estimation form failed and stable cases. Int. J. Rock Mech. Sci. & Geomech. Abstr., Vol. 24, pp. 347-55, 1987

23. **Tajduś K., Misa R. i Sroka A**. Eksploatacja częściowa pokładów węgla ze szczególnym uwzględnieniem stabilności filarów i ochrony powierzchni. Partial exploitation of coal seams with particular emphasis on the stability of coal pillars and surface protection. Wydawnictwo Pol. Śl., s. „Górnictwo i Geologia", t.7, z.1, str. 211-226, Gliwice 2012

24. **Tomiczek K**. O różnicach w zachowaniu się skał w warunkach jednoosiowego rozciągania i ściskania. On differences in the properties of rocks under uniaxial tension and compression conditions. W: „Górnictwo i Geoinżynieria", Wydawnictwo AGH, R. 31, z. 3/1, str. 543-554, Kraków 2007

25. **Tomiczek K**. Krótka numeryczna analiza podbierania pokładu z zawałem stropu. Simple numerical analysis on the problem of undermining seams with caving. Zesz. Nauk. Pol. Śl., s. Górnictwo, z. 283, str. 301-312, Gliwice 2008

26. **Whittaker B.N. and Singh R.N**. Design and stability of pillars in longwall mining. Min. Engr., Vol. 138, pp. 59-73, 1979

27. **Wu L.X. and Wang J**. Teoria i doświadczenia eksploatacji pasami pod obiektami. Theory and experience of mining with belts and pillars under structures and buildings. Polskie tłumaczenie za wydawnictwem Xuzhou, Chiny 1994

TECHNOLOGICAL AND METHODOLOGICAL ASPECTS OF THE EXPRESS METHOD FOR RESEARCHING HIGH-YIELD WELLS AND DETERMINING THEIR POTENTIAL PRODUCTION CAPABILITIES

Roy M.M.
Poltava National Technical Yuri Kondratyuk University; Candidate of Technical Sciences, Associate Professor, Ukraine

Akulshin O.O.
Ukrainian Oil and Gas Institute (PJSC "UKRNGI"), Doctor of Technical Sciences, Deputy Chairman of the Board for Scientific Work, Ukraine

Solovyov V.V.
Poltava National Technical Yuri Kondratyuk University; Doctor of Physical and Chemical Sciences, Professor, Head of Physics Department, Ukraine

Usenko D.V.
Poltava National Technical Yuri Kondratyuk University; PhD student, Ukraine

The problem of researching high-yield wells has not yet been solved. Methods for solving this problem in the domestic and world research literature are not covered. Also, a methodology for interpreting the results of the study was not developed. Therefore, the task was set to create a technological approach to the study of such complex wells. And if such a technology is created, then there must be a technique to service it. Therefore, this publication discusses a new technological solution to the problem of researching high-performance gas wells for the case of non-stationary gas filtration to the bottom of the well. The above also developed a methodology for interpreting the research evidence obtained as a result of the new technology. The technique is characterized by complexity through the use of the differential method of Yu.P. Borisov. Therefore, it is described in a step-by-step algorithm. Thanks to this, the user can apply the software product. The effectiveness of the new research method is many times greater than the effectiveness of the known traditional methods of researching gas wells in the case of stationary

filtration. It is important that the new research method does not require the development of several research modes. One actually worked out mode is enough. A particular achievement of the new technological approach is the ability to preliminarily estimate the initial gas reserves at the research stage.

The methodologically set tasks were solved by studying previously developed the material, theoretical generalizations and checking their correctness at an industrial facility.

As a result, confirmation of the correctness of the selected technological solution was obtained.

The introduction of technology into production will provide a significant amount of geological information on the gas-hydrodynamic parameters of high-productivity formations and their use in calculating underground gas reserves and preparing a field development project.

Introduction. Currently, traditional methods for researching gas wells are known. They are used in accordance with the geological and technological conditions of specific wells for the case of a stationary regime of gas filtration. All of them are aimed at obtaining a sufficient range of initial data on the well-reservoir system. These data provide the basis for deciding the future development strategy of the deposit in the future. It is important that the data obtained is as objective as possible. After all, their accuracy directly affects the near future of each well. They require several (at least 5 - 8) study modes. These include: the method of constant sampling, the method of isochronism, accelerated isochronous, monotonous step, express method. Therefore, the task was to develop new research methods. They should be distinguished by the efficiency of the process, the simplification of its practical implementation, a new interpretation technique, high information content and accuracy.

For non-stationary flow regimes in the case of gas well exploration in several modes, there is also an express research method that significantly speeds up the work cycle. It is known that the isochronous method is a modification of the constant selection method. Its essence is that when exploring wells for equal periods of time with different flow rates (in different modes), an indicator curve will be obtained that characterizes the operation of the well for a given period of time. In this case, it is mandatory after each mode of operation

of the well to stop it until the pressure is completely equalized throughout the formation. If the reservoir pressure does not have time to completely equalize between the modes and the well operating time is equal to the shutdown time between the modes, then the obtained indicator curve also allows you to accurately determine the parameters of the formation. The basic principle of the isochronous method is that the radius of the drained area does not depend on flow rate, but on dimensionless time. The accepted condition means the drainage of the same zone of the well for the same period of time, regardless of flow rate. In addition, the study is carried out necessarily with the restoration of pressure between the modes. But these conditions become an obstacle to the application of the method for low permeability reservoirs. For formations with insignificant reservoir properties, pressure recovery after each regime requires from several hours to tens of hours. That is, the study will last several days. Replacing the isochronous method with an accelerated isochron method reduces the duration of the study. But it still takes considerable time. For example, if the duration of the processes of complete stabilization of pressure and flow rate and complete recovery after each mode is 10 hours, then with 6 modes of well study using the isochronous method, the total duration of the study will be 60 hours. When exploring the same well using the accelerated-isochronous method, the total duration of the study will be about 30 hours. When exploring the wells, and not connected to the gas collection and treatment system that takes place on prospecting and exploration areas, a long research time is unacceptable. The same situation is with the initial study of test wells with the release of gas into the atmosphere. This requirement is especially categorical when hydrogen sulfide is present in the gas. In such cases, the express research method is used in 5-8 modes. The technology of the express method is as follows. Before the start of the study, formation pressure is measured or determined by known static pressure. Further, the well is launched with a certain flow rate into operation for a period of 1200 - 1800 s. After that, annular and buffer pressure, pressure and temperature are measured on a diaphragm meter for critical gas flow (DMCGF) or differential pressure gauge, the pressure drop on the differential pressure gauge. Estimated previously by a calculated method, the rate of flow. Then the well is put into operation in the second mode at the same

time. At the end of the second mode, the annulus and buffer pressure, pressure and temperature on the DMCGF, or pressure, differential pressure and temperature on the differential pressure gauge are recorded. Then close the well for recovery at the same time. Similar actions are performed in the following modes. The results are processed and receive some parameters of the reservoir. The advantage of the express method is to minimize the duration of the research process.

But all these methods are less effective from the method of researching high-yield wells in only one actually worked out mode. That is, they all have certain disadvantages.

The disadvantages of these methods include:

- a relatively large amount of time for research;
- insufficient amount of information obtained during interpretation (less than ten parameters of the reservoir)
- the inability to interpret the research results in one cycle using a software product;
- the inability to make a preliminary calculation of the initial gas reserves in the studied object.

All these disadvantages are eliminated by the developed express method.

The technological basis of the express method. The express method for researching high-yield wells is that well surveys are carried out only in one mode as follows. After purging the well with gas and restoring the bottomhole pressure to the reservoir pressure, it immediately opens and fulfills one mode of its operation. In this case, the change in pressure and temperature at the depth of the bottom and along the wellbore is measured in high-speed mode until a steady state of high tide is reached. After that, the well is closed to monitor the restoration of pressure in the well. Measure pressure and temperature at the bottom of the bottom and along the wellbore. At this, the study is stopped. All gas-hydrodynamic parameters of the reservoir are calculated in one cycle according to the results of mathematical processing of the inflow curve and the pressure recovery curve (PRC).

In fig. 1 in coordinates (pressure P_{bot}, time t) shows the change in the bottomhole pressure P_{bot} at all stages of the well study in one unsteady mode, starting from the instantaneous stimulation of the in-

flow, purge and instantaneous shutdown of the well to record the PRC until a static state is reached in the well, which completes the study.

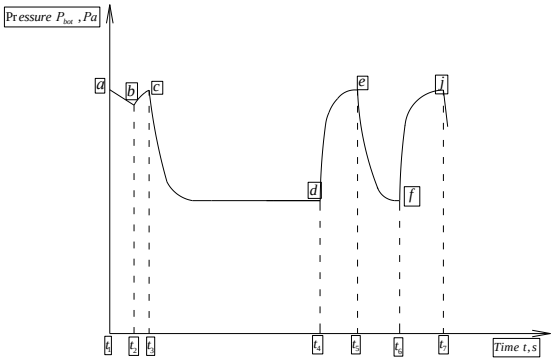

Fig. 1. Graph of pressure changes at the bottom during the study of the well

The change in the pressure at the bottom of the well during the stimulation of the inflow is shown by the line *a*,*b* (time changes from t_1 to t_2), where point *a* corresponds to the beginning of the excitation of gas from the reservoir, and the point *b* corresponds to the moment of complete displacement of the fluid from the well and closing the valve to restore the bottomhole pressure to the reservoir P_{res}. The line *b*,*c* (time from t_2 to t_3) shows the change in the bottomhole pressure in the process of its recovery to a value P_{res}, the point *b* corresponding to the beginning of the pressure recovery, and the point *c* to the moment of complete restoration of pressure at the bottom to the reservoir value.

After measuring the reservoir pressure P_{res} and temperature T_{res}, the well is blown with gas in accordance with the current instructions for the study of wells in order to clean the bottom-hole zone of the formation - line *c*,*d* (respectively, time from t_3 to t_4).

After completion of the purge of the well, it is closed to fully restore the pressure at the bottom to the formation pressure - the line *d*,*e* (time interval from t_4 to t_5), after which one non-stationary mode of operation of the well is worked out - the line *e*,*f*. After the instantaneous closure of the well at the moment t_6, complete pressure recovery is achieved until a static state in the well is reached (time t_7).

This completes the technological steps of the express method for the study of high-yield wells.

Methodology for the interpretation of research results. Next, we have to solve the problem of the methodological plan. All gas-hydrodynamic parameters of the studied formation and, if necessary, a larger number of well operation modes are calculated analytically with one cycle of the software product.

In this case, the pressure recovery curve is processed by the method of Yu.P. Borisov [3].

The final section of PRC is treated according to [4].

The value of reservoir pressure P_{res} is obtained as a result of processing the inflow curve by the universal method Chekalyuk.

According to the results of processing the reservoir pressure recovery curve by Yu.P. Borisov is determined by the gas conductivity of the near-deep $(kh/\mu)_1$ and remote zones $(kh/\mu)_2$: where k is the permeability coefficient of the formation m^2; h - effective thickness of the reservoir, m; μ - dynamic viscosity of gas or gas condensate in reservoir conditions $Pa \cdot s$. Find the coefficient of bottomhole plugging of the reservoir $\Pi_3 = \frac{(kh/\mu)_2}{(kh/\mu)_1}$. The complex parameters of the piezoconductivity are calculated $\frac{æ}{r_p^2}$ (due to the processing of PRC by the method of E.B. Chekalyuk) and $\frac{æ}{R_k^2}$ (due to the processing of PRC in the coordinates $\ln\left[P_{res}{}^2 - P_{bot}{}^2(t)\right]$ from t), where æ is the piezoelectricity of the formation, r_n is the combined radius of the well, R_k is the radius of the drainage circuit.

Using them, is determined the value of the linear resistance coefficient A of the inflow equation by the formula $A = \frac{\ln \frac{R_k}{r_n}}{2(kh/\mu)_2}$, and therefore the coefficient B, by solving the inflow equation with re-

spect to *B*. Thus, an equation of formation fluid inflow to the bottom of the well is obtained $\frac{P_{res}^2 - P_{bot}^2}{2P_{atm}} = AQ + BQ^2$.

Find the summary radius of the well $r_n = \sqrt[П_з]{e^n}$, where $n = П_з \ln r_c - (П_з - 1)\ln\left(\frac{R_к}{r_n}\right)$, r_c - is the radius of the well by bit.

The piezoconductivity coefficient is determined by substituting in the formula for the complex parameter of the piezoconductivity $\frac{æ}{r_n^2}$ the value of the combined radius. The formula $\psi = \frac{k}{m} = \frac{æ \cdot \mu_{пл}}{P_{пл}}$ determines the ratio of permeability to porosity, where $\mu_{пл}$ is the dynamic viscosity of the gas in the reservoir, *m* is the porosity, *k* is the permeability coefficient, P_{res} is the reservoir pressure. The complex parameter *kh* of the formation conductivity is determined by multiplying the complex parameter of the gas conductivity of the remote zone of the formation kh/μ by dynamic viscosity μ. From the known porosity coefficient *m*, the permeability coefficient *k* is found by multiplying the complex parameter ψ by porosity *m*. Calculate the complex parameter - layer capacity: $mh=(kh/\psi)$. Dividing the reservoir capacity *mh* by the value of the coefficient of porosity *m*, is calculated the effective power of the reservoir *h*.

The skin effect is determined by its definition: $S=(r_c/r_n)$ where *S* is the skin effect.

The average pore diameter of a productive formation is calculated by the formula $d_{cp} = \sqrt{32\psi}$, it also makes it possible to calculate the macro-porosity parameter $l = 1/\beta^*$, moreover $\beta^* = \frac{63 \cdot 10^6}{(k/m)^{\frac{3}{2}}}$, it is a structural coefficient of tortuosity and intermittent intersection of pore channels *m* - porosity coefficient of a productive formation, fraction of unity, $63 \cdot 10^6$ - A.I Shirkovsky's correlation [5].

Thus, as a result of an express study of a gas well in an unsteady mode of filtration, consisting of the previous purge and two main unsteady processes: recording HPC after shutting down the well and recording changes in flow rate and pressure after putting the well into operation as a result of a one-cycle mathematical interpretation of the data obtained , less than 24 parameters of the reservoir are determined.

These include:

1. Reservoir pressure P_{res} (by measurement or analytically)

2. The reservoir temperature at the depth of the study T_{res} (by measurement)

3. Gas piping of the remote formation zone (analytically)

4. Gas-bearing in the near-deep zone of the formation (analytically)

5. The coefficient of bottomhole plugging of the reservoir Π_p (analytically)

6. Bottomhole pressure for a given P_{boot} (analytically)

7. Linear drag coefficient flow equation A (analytically)

8. Inertial drag coefficient, flow equation B (analytically)

9. Inflow equation $\frac{P_{res}^{\ 2} - P_{bot}^{\ 2}}{2P_{atm}} = AQ + BQ^2$ (analytically)

10. The parameter of the conductivity of the reservoir kh (analytically)

11. The coefficient of the piezoconductivity formations æ (analytically)

12. Well radius summary r_n (analytically)

13. The radius of the well drainage circuit R_c (analytically)

14. The coefficient of productivity of the reservoir $K_n=(1/A)$ (analytically)

15. The reservoir quality index S (skin effect) (analytically)

16. A complex parameter is the ratio of the permeability of the formation to its porosity $\psi=k/m$ (analytically)

17. The porosity of the reservoir m (laboratory method)

18. The permeability coefficient k of the reservoir (analytically)

19. Formation capacity mh (analytically)

20. Effective reservoir power h (analytically)

21. The ratio of the volume of fluid in atmospheric conditions to the volume of the same mass in reservoir conditions V_{atm}/V_{res} (analytically)

22. The average pore diameter of the reservoir $d_{cp} = \sqrt{32\psi}$ (analytically)

23. The coefficient of macroscale $l = \frac{1}{\beta^*}$ (analytically)

24. The preliminary value of the initial gas reserves V_{atm} (analytically).

All of the listed gas-hydrodynamic parameters, which are determined analytically, when using a single-cycle software product are calculated almost simultaneously.

Calculation of initial gas reserves. Based on the physical quantities obtained as a result of the study:

- the value of the selected gas volume during the purge of the well ΔV_{atm} before the start of the study and its operation on the mode;

- pressure before the start of the study P_{res} and after its completion P_{res1};

- gas compressibility coefficient in reservoir conditions for the study and after completion of the study z_{res}, z_{res1}, dimensionless

- thermodynamic temperature to the study and after completion of the study T_{res}, T_{res1}, K;

it is possible to carry out a preliminary assessment of the initial gas reserves [6]. Its value is calculated by the formula

$$V_{atm} = \Delta V_{atm} \frac{P_{res}\ z_{res1} T_{res1}}{P_{res} z_{res1} T_{res1} - P_{res1} z_{res} T_{res}}$$

In contrast to existing methods for calculating production stocks in the reservoir, this method is characterized by a minimum of initial data.

All are available for measurement or determination.

Conclusions

What gives the use of the express method?

Technologically, the research process occurs due to the registration of the natural speed of real processes in the well when taking the flow curve and the pressure recovery curve in real-time. In this case, the full cycle of only one study mode is being worked out.

In methodological terms, the results of the research process can increase several times the volume of the calculated gas-hydrodynamic parameters. In addition, it is possible to use a single-cycle software product that will significantly speed up the time of interpretation of the research results. The attractiveness of the software product is not only in the speed of calculations, but also in the greater accessibility of complex mathematical calculations for a wider range of users.

And finally, the ability to analytically calculate on the basis of the data obtained the previous value of the initial gas reserves undoubtedly solves the very important task of not only research, but also the task of preliminary estimation of reserves.

Thanks to the application of the proposed calculation methodology, it became possible to simplify and reduce the volume of calculations, reduce the number of source data and increase their availability, since preliminary geophysical studies are not necessary to obtain them.

It is enough to conduct a study of a gas object only in a single stationary or non-stationary mode and fix all the necessary indicators of physical quantities, which are the initial data for applying the technique.

The software product is not complicated. Enough programmer engineering skills. Therefore, it is proposed in this publication. But it, of course, is one of the elements of optimizing the calculation of gas reserves in the studied gas facility.

The prospectivity of the proposed methodology for calculating gas reserves is that it is quite simple and can be used in an industrial environment for quick preliminary estimation of the initial gas reserves.

A new method of research, methods for interpreting the parameters of highly depleted formations studied in one mode, a method of

calculating the initial gas reserves are characterized by novelty and a high level of performance.

They are protected by patents of Ukraine and can be the basis for optimizing research processes in gas wells of any productivity.

And, like all express methods, technologically, environmentally and economically they are very favorably different from previously developed traditional methods and techniques.

They have not only theoretical, but also practical significance.

This provides the basis for a positive assessment and their further application in industrial practice.

References

1. Pat. 51729 Ukraine, MPK3 E21B 47/06. A research method of gas wells / **Matus B.A., Kuriljuk L.V., Slavin B.I., Gorlacheva L.F., Tokarev V.P., Klimenko U.O**.; decl. and hold. Matus B.A. – № U 200601237; decl. 01.04.99; publ. 16.12.02, Bul. №12. (In Ukrainian).

2. Pat. 121860 Ukraine MPK(2017.01) E 21B 47/00. A research method of highly productive gas and gas-condensate wells in at the non-stationary filtration mode/**Roy M. M**., decl. 09.02.2017, publ. 26.12.2017, Bul. № 24. (In Ukrainian).

3. Guidance on wells research / [**Gritsenko A.I., Aliev Z.C., Ermilov O.M.,** and oth.] . – M.: Nauka. - 1995. – 523 p. (in Russian).

4. Instruction on complex research of and gas-condensate layers and wells. – M.: Nedra. - 1971. – 208 p. (in Russian). :[und. edt. **G.A. Zotova, Z.C. Alieva**]. – M.: Nedra. - 1980. – 301 p. (in Russian).

5. Kotyachov F.I. Physicist of oil and gas collectors / F.I. Kotyachov – M.: Nedra. – 1977. – 287 p. (in Russian).

6. Pat. Ukraine №110657. Method of preliminary estimate of openings gas stocks size. **Roy N.N**., decl. 04.03.2016; publ. 25.10.2016, Byul. №20.

RESOURCE-SAVING WAY OF EXPLOSIVE DESTRUCTION GRANITES COMBINED EXPLOSIVE CHARGES

Khomenko E.M.
PhD, associate prof., Cherkassy State Technological University, Ukraine

Ponomarenko I.A.
Graduate stud., Cherkassy State Technological University, Ukraine

Ishchenko K.S.
PhD., Senior Research Fellow, Institute of Geotechnical Mechanics by N.S. Polyakov NAS of Ukraine, Ukraine,

Kratkovsky I.L.
PhD., Senior Research Fellow, Institute of Geotechnical Mechanics by N.S. Polyakov NAS of Ukraine, Ukraine

Abstract

This article presents the results of laboratory and industrial tests of a new resource-saving method for the destruction of granites with combined explosive charges, based on the use of elongated vertical borehole charges in the form of triangular and quadrangular prisms. The proposed charges can significantly reduce the irreplaceable loss of minerals – granite, developed for the production of crushed stone, by reducing the contact area of the explosive with destructible rock. The formation of micron-sized fine dust fractions (regrinding) at the explosive-rock contact, as is well known, is inevitable when emulsion explosives with a high detonation velocity are used for the destruction of strong rocks (granites) by continuous cylindrical charges. Application to reduce the volumes of overgrowth of granites of explosive charges in polyethylene shells with an annular gap between explosives and rock being destroyed is not effective, since it is not ensured constant clearance due to *S*-shaped bending of the elastic sheath. Use of elongated borehole explosive charges in the form of triangular or quadrangular prisms make it possible to more effectively solve the problem of granite overgrinding at the explosive contact with the rock due to gaps in the form of segments, as well as by creating a different-gradient stress field in the destructible medium, in which shear stresses dominate.

The aim of the work is the presentation of a new resource-saving method for the destruction of complex structural granites by an explosion in the open development of deposits of building materials.

Research methods. In creating the resource-saving method of explosive destruction of granites, modern methods have been widely used to study the structure of rocks and its influence on the nature of dynamic destruction by explosives, such as simulation, laboratory and industrial experiment, particle size analysis.

Introduction

Analysis of the results of industrial and experimental studies performed by the authors of [1] revealed that the process of destruction of rocks by the explosion is characterized mainly by one type of destruction - separation under the action of tensile stresses.

In this case, the energy of explosive transformation consists of the energy of waves of stresses and pressure of gaseous products of detonation. The role of stress wave energy is that when they propagate, the mass fractures through natural fracture systems up to 75% of the total fracture volume, and at the subsequent expansion of the detonation products, its by their own pressure expand the created cracks to the complete destruction of the rock. Therefore, when modelling explosive action on the process of destruction of rocks, it is necessary to consider not only the participation of gaseous detonation products, but also the tense state of the massif.

Simulation modelling. Solving the problem of the distribution of stress field in the massif of blast an explosive charge different cross-sectional shape is to develop methods of simulation taking into account the stress-strain state of the rock mass, the permeability of the medium and the non-stationary motion of gaseous detonation products (GPD) of explosivies in the excited array, which is described by the system of equations

$$\sigma_{ij,j} + X_i(t) + Y_i(t) + T_i(t) + P(t) = \rho_n \left(\frac{\partial^2 u_i}{\partial t^2} \right), \; i, j = x, y;$$

$$\mu_e \frac{\partial p}{\partial t} + \frac{\partial}{\partial x}\left(k \frac{\partial p}{\partial x} \right) + \frac{\partial}{\partial y}\left(k \frac{\partial p}{\partial y} \right) + q(t) = 0;$$

$$k = f(\sigma_{ij}, t),$$

where $\sigma_{ij.j}$ - the output of the stress tensor component by x,y; t - time; $X_i(t)$ - projections of external forces acting per unit volume of solid; $Y_i(t)$ - projections of the forces from the action of the explosion are calculated by empirical dependencies *V.* Borovikova and *I.* Vaniahina; $T_i(t)$ - projections of forces caused by internal friction acting on a unit of body volume$T_i(t)$=-$c_g \partial u_i / \partial t$; c_g - the coefficient damping factor; u_i - moving; $P(t)$ - the projection of the forces caused by the gas pressure in the fracture-pore space; ρ_n - rock density; μ_e - viscosity

GPD; p - pressure GPD; $q(t)$- intensity of selection GPD; k - coefficient of permeability.

For the mathematical description of the process of transition of rocks to disturbed state, the Coulona-Mora strength criterion is used.

Initial and boundary conditions

$$\sigma_{yy}\big|_{t=0} = \gamma h; \qquad p\big|_{\Omega_1(t)} = p_0;$$

$$\sigma_{xx}\big|_{t=0} = \lambda\gamma h; \qquad p\big|_{\Omega_2} = 0{,}1\,МПа;$$

$$p\big|_{t=0} = p_0; \qquad u_x\big|_{\Omega_3} = 0;$$

$$p\big|_{t=t_{взр},\, x=x_{взр},\, y=y_{взр}} = \frac{p_d}{2};\; u_y\big|_{\Omega_4} = 0;$$

where γ - the average density of the rocks above; h - depth of development; λ - side expansion coefficient; p_0 - the initial gas pressure in the fractured pore space; t_{expl} - the moment of the explosion; x_{expl}, y_{expl} - coordinates of charge nodes; p_d - detonation pressure; $\Omega_1(t)$ - the boundary of the filter that changes over time; Ω_2 - free surface; Ω_3 - right vertical border of the outer contour; Ω_4 - horizontal border of the outer contour. The calculations are performed using the finite element method (FEM).

The design diagram of a section of an massif of rocks with a free surface and charge of an explosive, for example, a square cross-sectional shape, is shown in Fig. 1*a*, and fragments of finite element grid for charges of different shapes - in Fig. 1*b*.

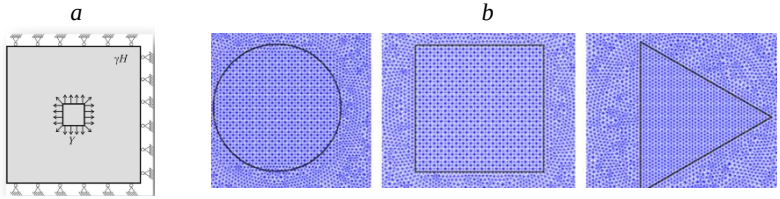

Fig. 1. Calculation scheme and fragments of finite element grid for explosives charges of different cross-sectional shape: cylindrical and triangular

As a result of the calculations, the distribution of the values of the geomechanical parameter $Q=(\sigma_1-\sigma_2)/\gamma H$ is obtained, which characterizes the different component of the stress field at certain moments (time iterations) in Fig. 2 and changes in the maximum component of the principal stress tensor presented σ_1/γH in the direction of the axis - Fig. 3, Fig. 4 [2].

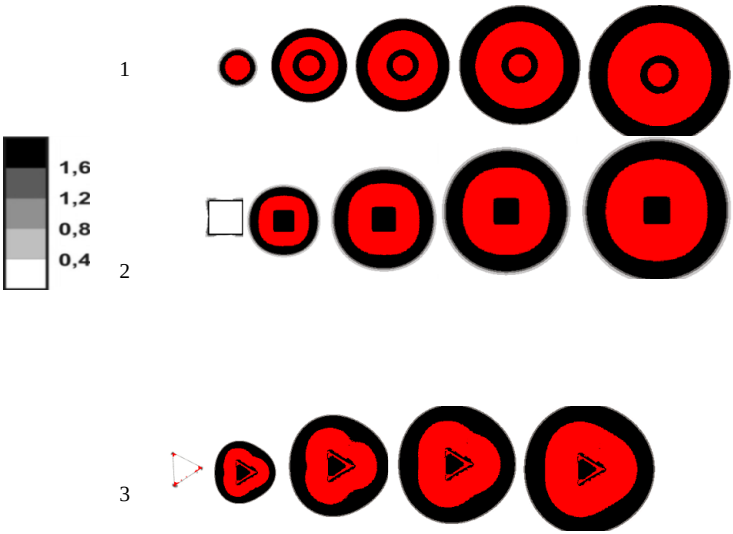

Fig. 2. Distribution of values of parameter *Q* for charges of different cross-sectional shape: *1* - cylindrical; 2 - square; 3 - triangular with changing time frames

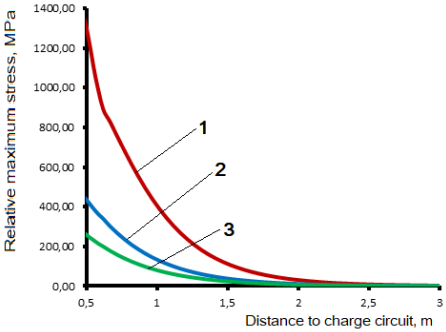

Fig. 3. Changes in the maximum component of the principal stress tensor presented $\sigma_1/\gamma H$ in the direction of the axis, passing through the center of the charge, time iterations *i*=3: *1* - cylindrical; *2* - square; *3* - triangular with changing time frames

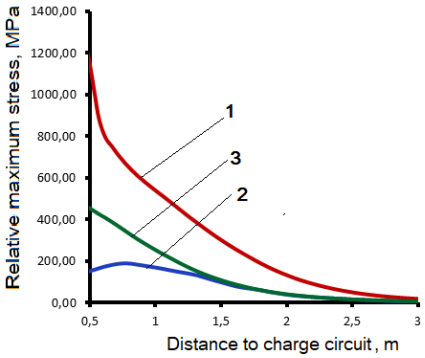

Fig. 4. Changes in the maximum component of the principal stress tensor presented $\sigma_1/\gamma H$ in the direction of the axis, passing through the center of the charge, time iterations i=5: *1* - cylindrical; *2* - square; *3* - triangular with changing time frames

It can be seen from Figure 2, Figure 3, Figure 4, that the deformation zones around the charges practically repeat the charge contour with smoothed angles, eventually becoming a circle.

Experimental investigations into the nature of the destruction of solids by explosive charges of various cross-sectional shapes

In order to study the peculiarities of the mechanism of explosive destruction of the massif by explosives of different designs with variable cross-section shape, as well as to study the process of occurrence, propagation of stress waves and the nature of cracks, it is necessary to know a qualitative picture of the process of destruction of the environment.

Data on fracture solid medium on the wave action phase explosion obtained during experimental research on the optically active material - organic glass sheet constant thickness of 0.015 and 0.035 with a stable strength, mechanical and optical constants.

For this purpose, 0.2×0.2 and 0.15×0.2 m models were manufactured in the laboratory. A cylindrical explosive cavity was formed in the center of the model with dimensions 0.2×0.2×0.015 m with a drill diameter 4.5-5.0 mm for the entire thickness of the model, and in other models with dimensions 0,15×0,2×0,035 m in the center of the face narrow face – cavities with a diameter of 5-6 mm with a length of 110 mm.

Then the cylindrical cavity was provided with a square and triangular shape with an edge of 4-5 mm. In the prepared explosive cavity, a high-explosive explosive substance, 150 mg in weight with the initiator, was placed, the mouth was sealed and blown.

The experimental blasts on organic glass models kept the charge cross-sectional area constant, its mass, the location of the initiation point, and the type of explosive used. Basic requirements for the model environment are the ability to register and subsequently study the process of cracking and displacement over time, as well as the absence of detachment phenomena along the contour of the model during the explosion of explosive charge using a high-speed photographic recording installation.

The appearance of charge structures is shown in Fig. 5.

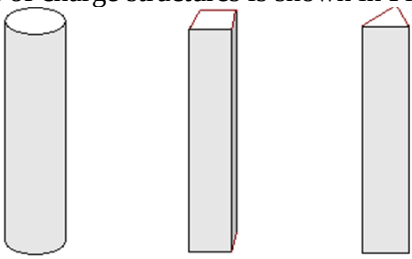

Fig. 5. Construction of blasthole charges of different shapes

During the experiments it was found that the optimal parameters of speed photographic analysis of the process is environment from explosion of the explosive charge consists 15000-30000 frames/sec. According to the results of the process is filming models focused and continuous explosive charge different shapes made frames that represented in Fig. 6, and in Fig. 7 - the appearance of the destroyed models by charges of different shapes.

a

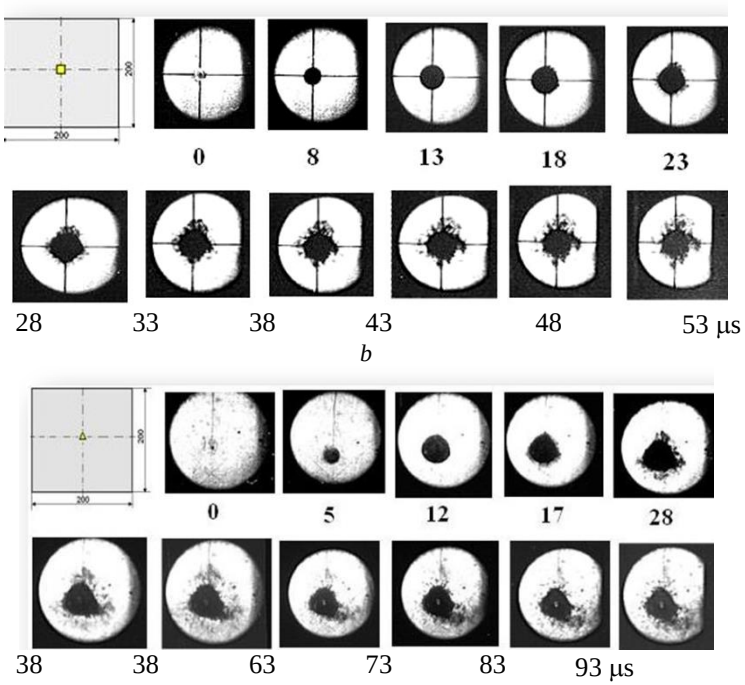

Fig. 6. Motion picture of the process of destruction of models by concentrated charges of explosive material of different cross-sectional shape: *a* - square, *b* - triangular

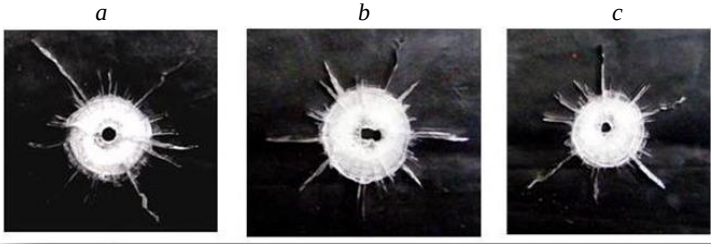

Fig. 7. Photo of a flat model destroyed by concentrated charges of cylindrical (*a*), square (*b*) and triangular (*c*) cross-sectional charges

As can be seen from the motion pictures (see Fig. 6*a*,*b*), explosions of concentrated charges of different shapes, in the first frames of the process registration, in the range of 0-18 μs after detonation of the charge, the wave front propagating in front, and its configuration

is characteristic, for both square and triangular shapes. And already from 23-28 microseconds, the shock waves reflected from the surface of the charging cavity and acting on the destructive medium create stress waves, the maximum values of the voltages of which in the charges of triangular and square cross-sections are concentrated in the corners of the charge circuit, contributing to the development of systems cracks in the model. The next step, by the time of 30-40 μs, stress waves form a network of developing cracks perpendicular to the faces of the charging cavity. The following frames of a motion blast of concentrated charges of different cross-sectional shapes show the alignment of the stress wave front and the crack formation that is characteristic of round-section charges. There is an uneven distribution of different types of deformations around the charge cavity, the nature of which depends on the shape of the charge cross section. In the circular form (see Fig. 6, *a*), there is an extensive network of radial cracks extending to the boundaries of the model. The main cracks spread evenly from the charge in all directions. When exploding a charge having a triangular cross-section (see Fig. 6, *b*), the pattern of the model's destruction is somewhat different from that of a continuous cylindrical charge. While assessing fracture models can highlight the following characteristics of this form of charge. n this case, the distribution of crack has a distinct asymmetry. At the vertices of the triangle the maximum stresses are concentrated which contribute to the formation of a denser crack network in these zones. The analysis of the maximum crack length showed that the vector of the maximum explosive energy flux density of such a structure was directed perpendicular to the faces of the prism, creating an intense crack network around the charge cavity with a radius of 5-10 R_{ch} (R_{ch} is the charge radius). The multifaceted stress field generated in the model creates a branched mesh of cracks oriented perpendicular to the faces of the charge cavity in the form of a triangular prism. When a plane model is destroyed by a square-shaped charge, the radial cracks created during an explosion are also characterized by a clearly pronounced orientation. The maximum length with maximum opening to the limits of the model is observed at places of maximum stress concentration – in the corners of the model. The main crack network is also formed perpendicular to the side surface of the charger cavity in the form of a square prism. In

this case, the zone of plastic deformation is insignificant and is equal to 2-3 R_{ch}, and the crushing zone is 3-5 R_{ch}.

Analyzing the configuration fracture zone charge with a square cross-section, it can be noted the coincidence of the shape of the zone of destruction by the explosion of a cylindrical charge.

Thus, with the same mass and increased length, the destructive medium occurs the redistribution of explosive energy and the formation of a multifaceted stress field that is shifted in time and space during environmental destruction.

This leads to a decrease in the radius of the crushing zone by 20-30% and an increase in the zone of plastic deformation due to the increase in the influence of shear and tensile stresses.

Experimental study of wave and damaging effects of the explosion of charges of different shape cross-section.

The studies were carried out in the landfill conditions of the Syvach granite quarry of UkrAgroBuyprom PJSC. On prepared sand-cement models weighing 6.3 kg cubic shape, it was planned to carry out two series of experimental studies, namely:

- destruction of solid media by charges of different cross-sectional shape under different conditions of energy transfer;
- destruction of solid media by charges of different cross-sectional shapes in cylindrical, square and triangular prisms formed in models of explosive cavities.

The processing of the particle size distribution determined the total mass of the model destroyed by the explosion, the content of small fractions, the content of large fractions, and the area of the newly formed surface and the diameter of the middle piece.

The results of processing the experimental data are given in table. 1.

According to the results of the sieve analysis and processing of the obtained data of the particle size distribution, histograms of the distribution of the fractional composition of the products of the model destruction by the explosion were constructed (Fig. 6).

Table 1

The results of the destruction of sand-cement models by the action of explosion charges explosives of different cross-sectional shape under different conditions of transfer of explosive energy

Charge design	The diameter of a middle piece	The fraction content (%) destroyed by the model explosion	
		d_i<20 mm	d_i>50 mm
The charge round	41,83	27,00	53,00
The cross-sectional charge of a square prism in a cylindrical cavity with an air gap	35,8	31,0	45,0
The charge in cross section of a triangular prism located in a cylindrical cavity with an air gap	49,0	20,0	60,00

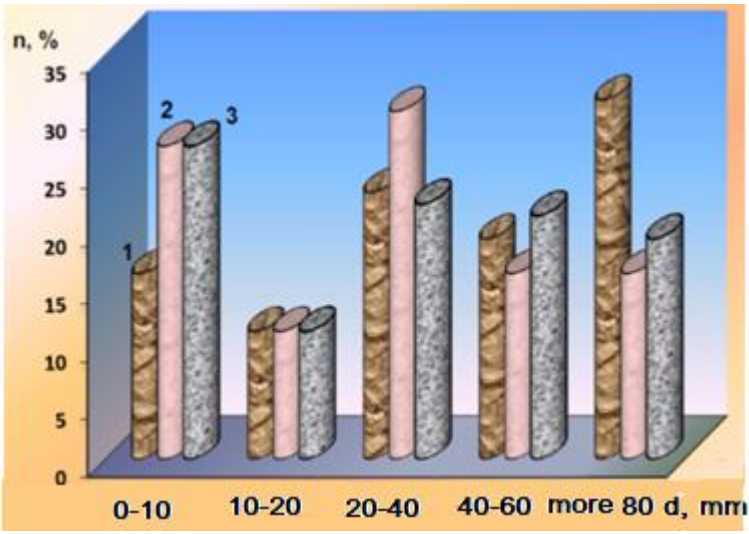

Fig. 8. Histogram of distribution of fractional composition of products of destruction n from their size d destroyed explosion of models with explosives charges of different cross-sectional shape during the transfer of explosive energy through an intermediate medium - air: where 1, 2 and 3 are round-section explosive charges; in section is a triangular prism; in cross section square prism

Experimental and analytical study designs elongated explosive charges of various forms section on the conditions of transfer of energy environment explosion that destroyed

To substantiate and further predict the particle size distribution of products of solid medium destruction, depending on the design of the explosive charge and the conditions of explosion energy transfer on sand-cement models of 150 mm cubic shape, experimental studies were conducted in the polygonal conditions for granulometry particle prediction using the explosion energy [3].

One part of the models was made of sand-cement mixture with closed water at their ratio of 1:1:0.5. M400 cement was used, and fine river sand was the aggregate. The second part of the models was made of aggregate – fine river sand + granite screening with a diameter of fractions 5-10 mm and cement M400 + water at a ratio of components 1:1:1:0,5. Charging cavities were formed in the center of each model in the manufacturing process by placing inserts with a diameter of 16 mm to a depth of 80 mm. After obtaining 30% of the strength of the models, they were removed from the mold and kept in the air until maximum strength was obtained according to current standards.

18 models of 3 pieces were manufactured for the experiments. for each experiment series.

For the destruction of prepared samples of models and 6-series experimental research designs were made for an explosive charge in the form of various forms of cardboard sleeves triangular, square and round shape in cross-section. In the prepared sleeves placed explosive mass of 4 g.

The formed structures of explosive charges were placed in charge cavities of models with different physical and mechanical properties. The space around the sleeves of triangular and square charges was filled with air, water and sand and circular shape in direct contact with the surface of the charging cavity. The prepared models were placed in the explosion chamber, the inner surface of which was lined with vacuum rubber and detonated.

For the particle size analysis of the destroyed model, a set of laboratory sieves with a mesh size of 0.25 to 80.0 mm was used.

According to the obtained indicators, histograms of the distribution of fractions of crushing models were constructed using different

designs of explosive charges (Fig. 9).

Analysis of experimental results revealed that the extended use of explosives section of various shapes – triangular, square in different load conditions (air, water, sand) achieved uniformity crushing destroying the environment compared with charge round. This is especially evident in the destruction of the flooded environment. This shows that it is changing mechanism of explosive loading due to overwhelming shear and tensile forces.

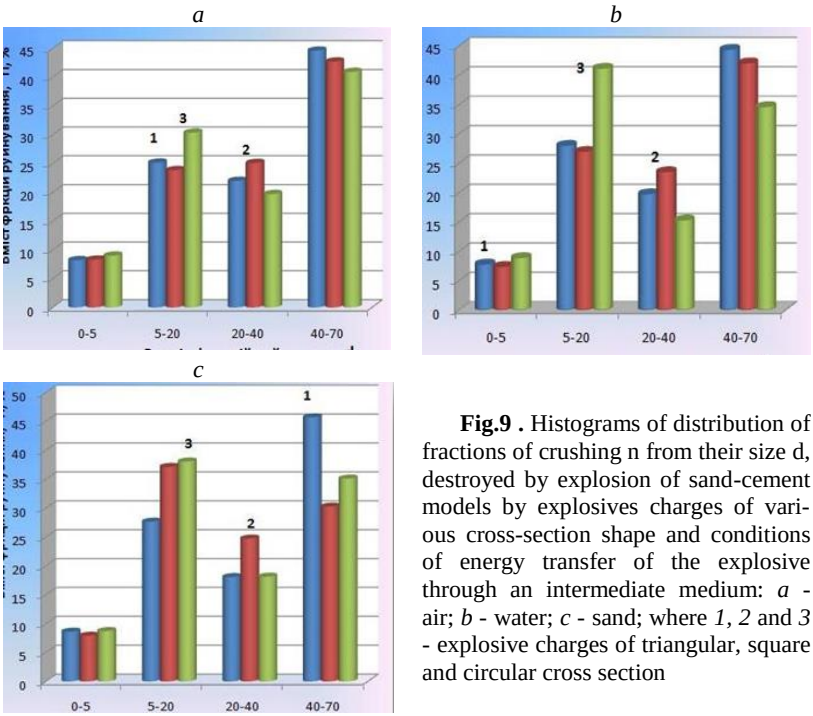

Fig.9 . Histograms of distribution of fractions of crushing n from their size d, destroyed by explosion of sand-cement models by explosives charges of various cross-section shape and conditions of energy transfer of the explosive through an intermediate medium: *a* - air; *b* - water; *c* - sand; where *1, 2* and *3* - explosive charges of triangular, square and circular cross section

Mathematical modeling and forecasting product particle size control fracture rigid environment of explosives of different shapes intersection and conditions of transfer of energy blast

To solve this problem, a mathematical model of the process of solid fracture was developed environment based on the use of normative vector prediction of the results of physical experiments and the

algorithm of simplified linear programming by the method of group accounting of arguments.

The solution to this problem was to take into account the factors affecting the destruction of the solid medium, and to construct comparative graphs with the original and predicted particle size distribution of the results of the solid medium crushing explosion.

According to the results of mathematical modelling, the dependences at each point of the selected distribution range of the particle size distribution on a separate fraction are obtained, which are shown in Fig. 10 and Fig.11.

Mathematical modelling of the prediction of the results of experimental studies in polygon conditions confirmed the high adequacy of the selected model of studies with a permissible error not exceeding 5-6%.

Application of forming hole charges combined with controlled explosion energy by changing the contact area with the surface of the explosive borehole and specific explosive energy transmitted through the rock unit lateral surface charge gives a real economic impact by crushing rock uniformity, lower volume crushed fractions and costs for explosive materials.

Results of analytical and experimental investigations of the effect of a cross section of a explosive borehole charge on the destruction of solid media, namely: mathematical modelling of the fields of stress in a solid environment during the explosion of charges of different section forms and experimental investigations of the character of the destruction of solid environments on optically active materials indicate that elongated charges of different cross-sectional shapes in the zone 2-3 of the charge radius generate a gradient field of stresses with a predominance of tensile and shear forces. This contributes to the uniformity of the crushing environment of the explosion.

Resource-saving method of explosive destruction of granites by combined explosive charges

At destruction granites explosion high quality of the rock mass, reducing irreversible losses during production and processing of metallic and non-metallic minerals can be achieved through the use of rational parameters blasting (reduction of specific explosives flow, applying a rational design of borehole charges grid geometry borehole charges and the direction of breaking) and taking into account

the features of both the microstructure and macrostructure of rocks, as well as the structural features of the massif.

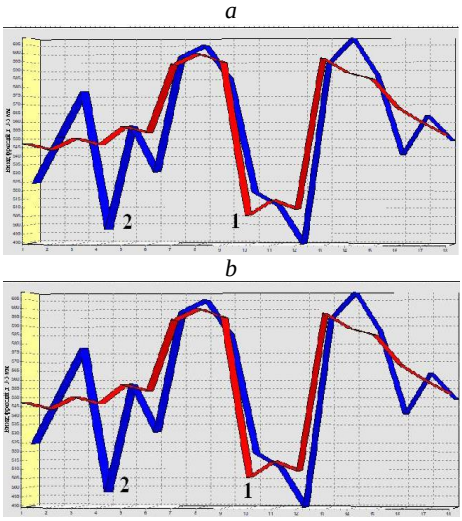

Fig. 10. Graph of distribution of grand composition for the selected range of the studied fraction: *a* - 0-5 mm; *b* - 5-20 mm; where *1* - experimental data; *2* - predicted data

In this regard, a new method of explosive destruction of locally fractured anisotropic rocks was developed (Pat. No. 105730, Ukraine [4]).

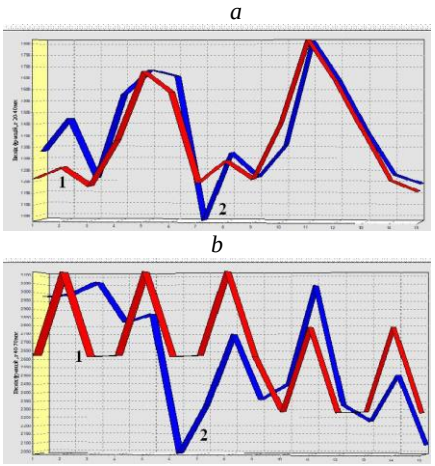

Fig. 11. Graph of distribution of particle size distribution for the selected range of the studied fraction: 20-40 mm (*a*); 40-70 mm (*b*); where *1* is the experimental data; *2* – estimated data

The method is based on taking into account the fractured structure of granites established by stereo photographing the frontal plane of the rock block being destroyed, identifying characteristic zones that differ in intensity and morphology of macrocracks, and placing vertical combined boreholes charges of special designs (Fig. 12).

Charges commute into diagonal circuits and explode with deceleration, starting with the cut charges located on the flank of the destructible block opposite its end.

At the control site, combined borehole charges of a continuous structure were formed, according to the approved standard passport for drilling and blasting operations for a mass explosion for a given block.

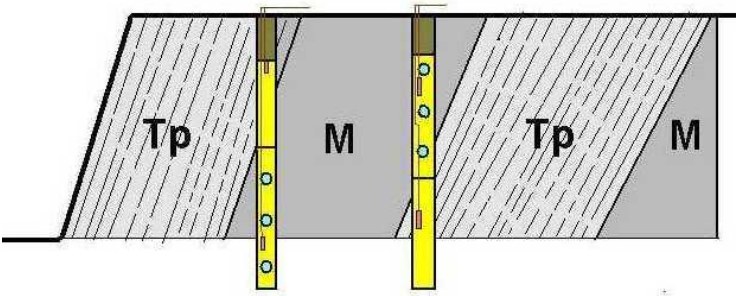

Fig. 12. Scheme of placement of combined explosive charges on the block taking into account the fracture of the granite mass *TP* - zone of fractured rocks; *M* - zone of monolithic rocks

To do this, 2.0-2.4 m was left in the boreholes for stemming, and the rest of the boreholes were divided into two equal sections.

In the lower part of the wells was placed a mixed explosive of TNT (UG+granular ammonia 65/35 proportion of nitrate) or Anemix type emulsion explosive, intermediate detonators of two T-400 TNT checkers connected by a waveguide with a detonator capsule of a non-electric initiation system of the NONEL type were installed. n the experimental section, the upper part of the well was filled with a conversion explosive (ballistic checkers - 3 or 4 pieces to give the charge the shape of a trihedral or tetrahedral prism) and the upper intermediate detonator. The space between the boreholes DKRP-4 walled sections filled mixed explosives -TNT UG+AN. The wellhead was sealed with a stem from a 3-5 mm granite screening (Fig. 13).

Analysis of industrial experiments showed that the use of the modified parameters blasting using the combined charge of variable section structure reduces by 30% the diameter of the middle piece and the consumption of industrial explosives by 10-40 %. The yield of a conditioned piece (201-600 mm) is increased by 10%, and the yield of dust fractions is reduced by 25-30 %.

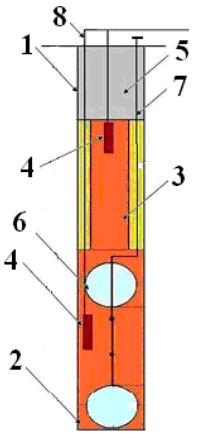

Fig.13. Design of combined borehole charge *1* – hole of type Anemix; *2* – charge of explosion from a mixture of TNT UG+AN or emulsion explosive type Anemix; *3* – charge of explosive (triangular or quadrangular prism); *4* – intermediate initiator; *5* – stemming; *6* – spherical insertion; *7* – twine for connecting spherical inserts; *8* – NONEL

Conclusions

By way of simulation using the finite element method designed inelastic deformation zone around the charge, calculated to contact "explosive-environment", almost the same shape charge to smooth angles, transforming as far as distance from the center of charge in a circle.

Constructed change depending on the maximum ten-components of the stress along the main axis is always the center of charge, and for triangular and square - perpendicular to its flat surface at various time iterating.

It is established that charges of square and triangular shape allow us to form a multifaceted field stresses, which increases the efficiency of the destruction of solid media by overriding the role of shear and tensile stresses.

On models of optically active material, the nature of the destruction of a solid medium by charges of different cross-sectional shapes has been studied.

According to the research found that the explosion of charges cylindrical column height in tension compression waves below (0.14 GPa) than the tension of the explosion of the charges in the plane for square and triangular section with short-pope everywhere intermediate environment – air (0.17 GPa and 10.2 GPa respectively). This

probably indicates that now of explosion of explosive charges in the corners of the prisms the maximum amplitude values of the stresses in the compression wave are concentrated and formed diverse gradient force field. At the same time, the yield of relatively large fractions of di> 50 mm size increases, the area of the newly formed surface and the diameter of the middle piece increase.

Otherwise, the destruction of the models occurs when the charges of different cross-section shapes formed directly in the model with direct contact of the charging cavity with the destructive medium are eroded. The mechanism of action of the explosion energy on the destructive medium has changed, that is, it prevails shear forces over the clamping. Also observed is the uniformity of model crushing by the explosion, reducing the diameter of the middle piece by 5-10% and increase the area of the newly formed surface 1.5-2.0 times for charges in the cross section of square and triangular prisms.

References

1. **Efremov, E.I.** Explosive destruction of outburst hazardous rocks in deep mines / **E.I. Efremov, V.N. Kharitonov, I.A. Semen**

yuk. – M .: Nedra, 1979.– 253 p.

2. Experimental studies of geomechanical processes in an massif of hard rocks during the explosion of explosive charges of various cross-sectional shapes / **C.V. Konoval, I.L. Kratkovsky, V.V. Krukovskaya, A.P. Krukovsky, K.S. Ischenko**.– Field Development 2014: Annual Scientific and Technical Field Collection of National Mining University – D.: Lizunov Press, 2014. – P.373-380.

3. Konoval, S.V. Peculiarities of destruction of solids by explosive charges of different cross-sectional shape / **S.V. Konoval, V.V. Krukovskaya, A.P. Krukovsky, I.L. Kratkovsky** and [others] // Izvestiya Vuzov. Mountain Journal – 2015. – No 5. – PP.35-41.

4. Patent No. 105730 Ukraine, E21 C 37/00, F42 D 3/00 Method of explosive destruction of locally fractured anisotropic rocks / **K.S. Ishchenko, I.L. Kratkovskyi; V.M. Konoval, S.V. Konoval**; applicant and owner of the patent – IGTM of the NAS of Ukraine. – Claim No. a201307372 dated 11.06.2013; Printed 10.06.2014. – Bul. No. 11.

ASSESSMENT OF RESOURCE-SAVING TECHNOLOGY FOR PROCESSING WASTE ROCK DUMPS OF THE MINING INDUSTRY

Mnukhin A.G.
Doctor of engineering Science, Professor
Engineering Institute
Zaporizhzhya National University, Ukraine

Kuris Y.V.
Doctor of engineering Science, Professor
Institute of Technical Thermophysics
National Academy of Sciences of Ukraine, Ukraine

Matyasheva O.B.
Teacher Zaporizhzhya Metallurgical College
Zaporizhzhya National University, Ukraine

Hituliar A.A.
Postgraduate Engineering Institute
Zaporizhzhya National University, Ukraine

Summary. In the industrial waste of our country's production there are almost all kinds of mineral resources, the reserves of which on the planet either are exhausted or difficult to extractin in the coming years. However, the development of existing and the opening of new fields traditionally requires huge financial placements and the use of modern technologies, which Ukraine does not often possess. In addition, it may take several years from the deposit discovery to the beginning of its operation, and thus new projects may simply lose their profitability due to changing external conditions. In developed industrialized countries, the level of industrial waste utilization is 70-80%, for example, in the US industrial waste is 20% aluminum, 33% iron, 50% lead and zinc, 44% copper, and so on. Therefore, for our country where more than 10 billion tons of mineral resources are extracted, from which up to 90% of the waste of rock mass goes to dumps, the problem use of industrial waste as raw material for the industry is becoming increasingly important [1]. Problems can be solved by diversification and modernization of domestic production, more efficient use of existing production capacities and increase of

their technological level, significant improvement of the regulatory environment for doing business, introduction of a mechanism to stimulate resource saving and innovative development, directing investment resources of the state to the introduction of new samples of resources energy efficient technology and technology.

Introduction. The problem of waste in Ukraine is of particular magnitude and importance both as a result of the domination of resource-intensive multi-waste technologies in the national economy, and due to the lack of adequate response to its challenges for a long time. The considerable scale of resource using and energy-raw material specialization of the national economy as well as the outdated technological base have determined and continue to determine high indicators of waste generation and accumulation [2].

Such circumstances result in the deepening of the ecological crisis and exacerbating the socio-economic situation in society and necessitates reform and development taking into account the national and world experience of the whole legal and economic system managing the use of natural resources in general and waste management in particular. The problem of waste is one of the key environmental issues and more significant in terms of resources.

Technological waste from coal, metallurgical and energy companies may become the most suitable alternative source of rare earth metals production in the near future.

The waste generated in the process of extraction, enrichment, chemical-metallurgical processing, transportation and storage of minerals is the secondary raw material reserve of industry and energy.

The high level of waste generation and the low rates of their utilization as secondary raw materials have resulted in the accumulation of significant amounts of solid waste in Ukraine both in industry and the utility sector each year, in addition to above only a small part of that waste is used as secondary material resources, and the rest fall into landfills.

Solving this problem is a key in decision of the of energy and resource independence issues of the state, saving natural material and energy resources, and an urgent strategic task (priority) of public policy.

Analysis of debris. During the centuries-old history of mining and metallurgical production in the country, billions of tons of ore extraction and enrichment wastes, cruciform rocks, low-grade ores, the use of which was economically or technologically inappropriate at the time of their storage have been accumulated in the country. Today, waste heap slages occupy thousands of hectares of fertile land near mines, factories and ore-dressing factories, causing enormous environmental damage to the Ukrainian economy.

For many years, the debris raised from the inerior of the earth and stored on the surface is a typical element of Ukraine's natural landscape. It is characterized by a high content of heavy metals, far exceeding the clark and background indicators for a particular locality as well as the MPC. Physico-chemical transformations in the composition of debris, which are mostly related to the oxidation of sulfide minerals, result in intensive soil contamination by heavy metals and radionuclides, changes in the physical and mechanical properties of the soil and acid-base balance. The stacked debris is a source of gas and dust pollution of the surrounding air. The content of rock dust in the air, even at a distance greater than the designated sanitary protection zone, exceeds the maximum permissible concentration (MPC). This problem is particularly acute when burning the dumps, which results in the release of sulfur dioxide, carbon monoxide and other harmful substances into the atmosphere. It is the reclamation of waste heap slags which is now considered to be the most common method of combating their harmful effects on the environment. According to our estimates, only the content of rare earth metals in the waste heap slags (slags) is on average about 230-260 grams per tonne (not to mention other useful raw material for production) [3]. We carried out a chemical analysis of the debris for the content of individual elements using the method of atomic emission spectroscopy. The analysis showed that in the composition of all samples of the debris there is an increased content of non-ferrous, rare earth and scattered metals. The results of the spectral analysis of the debris which are typical of mines in Eastern Ukraine are shown in Table 1. These data were compared with the clusters of chemical elements in the earth's crust and with minimal industrial concentrations of metals.

Table 1

The results of the spectral analysis of the debris

Place of sampling	Element	Clark, %	Content, mg/kg	Element	Clark, %	Content, mg/kg
The dump of the mine named after S. Frunze (Anthracite)	P	0,12	700	Ba	0,047	-
	Pb	$2 \cdot 10^{-3}$	15	Be	0,001	2
	Cu	0,01	30	Nb	-	20
	Ti	0,58	3000	Mo	$n \cdot 10^{-4}$	2
	V	0,016	70	Sn	$n \cdot 10^{-4}$	5
	Mn	0,08	500	Li	0,004	30
	Ga	$n \cdot 10^{-9}$	10	Zr	0,023	150
	W	$5 \cdot 10^{-3}$	3	Ag	$n \cdot 10^{-6}$	0,03
	Ni	0,018	50	La	-	10
	Cr	0,033	70	Zn	0,004	100
	Ge	$n \cdot 10^{-9}$	2	Sc	$n \cdot 10^{-5}$	10
	Co	0,01	10	Y	-	10
	Bi	$n \cdot 10^{-6}$	2	Ce	-	-
The dump of the mine Lugansk (Lugansk)	P	0,12	-	Ba	0,047	70
	Pb	$2 \cdot 10^{-3}$	5	Be	0,001	-
	Cu	0,01	10	Nb	-	-
	Ti	0,58	300	Mo	$n \cdot 10^{-4}$	2
	V	0,016	20	Sn	$n \cdot 10^{-4}$	1
	Mn	0,08	500	Li	0,004	-
	Ga	$n \cdot 10^{-9}$	2	Zr	0,023	30
	W	$5 \cdot 10^{-3}$	-	Ag	$n \cdot 10^{-6}$	-
	Ni	0,018	7	La	-	10
	Cr	0,033	20	Zn	0,004	-
	Ge	$n \cdot 10^{-9}$	-	Sc	$n \cdot 10^{-5}$	-
	Co	0,01	-	Y	-	10
	Bi	$n \cdot 10^{-6}$	1	Ce	-	-

It was determined that for all four investigated dumps in the rock specimens, there was a significant excess of clark indices and minimum industrial concentrations for gallium and germanium (Table 2).

Table 2

Content of germanium and gallium in debris

Place of selection of the dump rock	dumps content, mg / kg	
	Ge	Ga
Mine named after M.Y. Sverdlov (Sverdlovsk)	0,002	0,01
Mine named after S. Frunze (Anthracite)	2	10
Mine Lugansk (Lugansk)	-	2
Matroska Mine (Lisichansk)	0,015	0,0015

Therefore, it can be concluded that these elements can potentially be considered as having industrial value as a raw material for metallurgy, and additionally they can be removed as associated components during pile leaching and flotation enrichment of the debris [3]. Today technologies for processing man-made deposits have been developed in Ukraine, but all of them are not implemented. No matter what direction the government chooses to reduce the dependence on the import of rare earth metals, one thing is clear: they all require significant government support and serious investment.

Methods of treatment of mountain dumps. In the treatment of rock mass extracted from the dums, the first thing to do is to exclude all iron compounds, with the concentration of germanium and rare-earth materials in the residue increasing accordingly. Since the distribution of rare-earth materials in the initial mass (approximately 260 g/t) requires further refinement by performing special analyzes (Odessa, Donetsk), when compiling this description the unconditional presence of germanium in some dumps up to 40-55 g/t as well as the presence of alumina Al_2O_3 in an amount up to 14,9% was taken into account. The presence of iron-containing components (Fe_2O_3 and FeO) in an amount up to about 20%, and CaO and SiO_2 is not significant for the development of the final process cycle.

Extraction of germanium or, in fact, its compounds, is carried out by extracting the required product from the raw material of alkali, and in some cases by a solution of hydrochloric or sulfuric acids. Moreover, only increasing the acidity of the solution is not a clear condition for increasing the efficiency of the process. Increasing the rate of transition to solution, both germanium and its associated gallium, usually occurs with a significant heating of the object of work, but there are new unconventional methods of electro-hydraulic action on the object of processing, which increase the efficiency of extraction of these materials, ie, the explosion, which is accompanied by a significant increase in the pressure discharge zone (up to 15,000 atm) and temperature (up to 20000°C).

It is known that almost all world production of germanium, apart from other CIS countries, is based on the concomitant extraction of it from sulphide, zinc, lead-zinc and less copper-zinc ores. In the hydrometallurgical method of zinc production, germanium remains in the residual zinc cakes that occur during the leaching process. The

amount of germanium contained in zinc ores currently mined worldwide is 300 tonnes per year.

For the concomitant extraction of germanium in our country, attempts were made to use above-ground waters of coking plants (the initial content of germanium in them is not more than 3 g/t), so the use for the specified purpose of raw materials (dumps) with a content of germanium up to 55 g/t, is very promising in economic terms. Thus, the extraction of germanium from the raw material containing it can be done in one of three ways. The first the simplest one is the processing of raw materials into solution, followed by the use of oak concentrate (tannin complex). However, the verification of this method performed at a coke plant with many years of experience in such technology, in relation to this process did not allow to obtain a sufficiently significant increase in the concentration of germanium in the processed product, if the specified process is used as the main.

The second way to ensure simultaneous apart from germanium extraction other rare-earth elements is the use of electrostatic separation, that was developed by Ukrainian specialists. Electrostatic separation allows the separation of particles that differ in magnitude of charge or different rate of change of charge. The peculiarity of this technological process is that the main physical parameter by which the separation is carried out depends on the method of electrization of the substance to be treated and, in addition, and the physical parameter is a variable value. That is, the magnitude of the charge changes over time. This method was implemented at a pilot special enterprise located in the Dnipropetrovsk region. According to available information, the total number of rare earth elements extracted there was at least six.

In the process of magnetic separation the removal of Fe_2O_3 and FeO (not less than 68,5% of the existing) occurs, the actual percentage of elements will be much higher, about 95-98% (needs further experimental refinement). It is also possible to use powerful cryomagnetic separators. At the same time there is the enrichment of the remaining part by germanium by 10,5%, ie from 55 to 60,8 g/t. However, 6,93 g of germanium is lost from each tonne of raw material, which makes it necessary to further compare the options for extracting iron-containing compounds before and after germanium re-

moval. The technology of all of the above processes is now fully refined and no further sophisticated research will be required.

Electric explosive technology. From the foregoing, it is obvious that the most promising, both in terms of simplicity of implementation and cost, not to mention ecological cleanliness, is a new way of processing rock mass, developed by us together with SPE "Electrohydraulics" on the basis of new electric explosive technologies. This ensures the low cost, chemical and environmental purity of the manufacturing products. For this purpose an electro-hydraulic crusher-separator of special design is created. In this case the crushing process occurs at a pressure of $15 \cdot 10^3$ atm and at a temperature of 20000^0C [4].

Nowadays, in a number of industries such as the processing of waste from the coal and energy industries (dumps and ash dump heaps of thermal power plants) there is a problem of simultaneous crushing and separation of complex mineral resources. It is characteristic that the former technical solutions and technologies in the form of separately functioning crushers and separators for the gradual solution of these tasks are not always sufficiently effective. Devices whose operating principle is based on the use of the described above electro-hydraulic effect for crushing materials generally does not have disadvantages mentioned.

Thus, pulp processed in the laboratory in a flow mode in a special electrohydraulic crusher and using slurry pumps, enters the centrifuge, for example, type PVH - 80 productivity up to 100 t/h. The separated aqueous or acidic germanium solution in this case undergoes standard tannin treatment (tannin complex). The extraction of gallium can also be efficiently effected from the aluminum feedstock by the use of cation exchanger. If appropriate, before the separation of germanium (depending on the saturation of the solution), the solution can be reused for processing the raw material and so several times. The feasibility of implementing such a "repeat" cycle can only be determined experimentally.

As mentioned earlier dumps are a source of valuable raw material. Thus, in separate waste heap slages at an average volume of up to $1{,}8 \cdot 10^6$ m^3 and a mass of $2{,}1 \cdot 10^6$ t there may be contained up to

$0{,}43 \cdot 10^6$ t of iron, up to $1{,}1 \cdot 10^5$ kg of germanium oxide, as well as rare earth elements weighing $5{,}2 \cdot 10^5$ kg. Dumps are a source of alumina that is widely used for the production of aluminum and silumin. Alumina reserves in individual rock dumps reach 15%. One of the consumers of alumina may be Zaporozhye aluminum mill. The demand for silumin products is being tested by the oil, chemical and gas industries. The unconditional demand for iron is caused by the presence of powerful metallurgical enterprises in the country (Azovstal and others). Germany has a steady demand in the world market and its rare earth elements.

Electro-hydraulic effect on the processing facility. The complex for processing of dumps of coal mines should be completed with both standard and new equipment specially created for the purpose.

The development and implementation of new methods of processing dumps, regardless of the nature of production, also requires the development of modern high-performance complexes for the implementation of relevant industrial operations, implemented on the basis of advanced technological machines of the new generation. One of these technological units is an electrohydraulic crusher - separator, which will be implemented for the first time in the industry in general and at the specified technical direction in particular (Fig. 1) [5].

The crusher specified includes as one of the main elements a corresponding discharge chamber. Performing a discharge chamber with intervals over its entire height allows separating not only the homogeneous material, but also non-uniform one, since the latter during the discharge is distributed over the height of the discharge chamber according to its density, and then the stream will be thrown on the appropriate working tray.

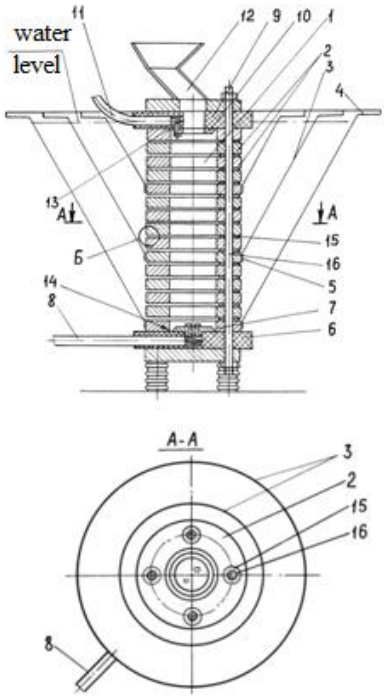

Fig. 1. Electro-hydraulic crusher-separator for processing dumps of coal mines: 1 - a discharge chamber; 2 - flanges; 3 - sump trays; 4 - horizontal annular surface; 5 - a cylindrical sleeve; 6, 9 - disc; 7 - positive electrode; 8, 11 - energy source; 10 - a negative electrode; 12 - boot device; 13, 14 - bit intervals

The use of circular electrodes allows the discharge gap to move in a circle which, firstly, makes it possible to burn the electrodes evenly, and secondly, to improve the material redistribution by density, since the point of occurrence of the shock wave is constantly moving.

The side surface of the discharge chamber is made at intervals. In addition, to improve the separation process the upper end of each flange is made at an angle α relative to the lower end of the previous flange. This is necessary to prevent the crushed material from closing the flanges.

Shock waves in the fluid of the material to be crushed and, at the same time by hydropower corresponding small fraction is made

through the intervals between the flanges in the tray-tanks, along which it rises with the same flow on the horizontal annular surfaces of the trays. During the period between the discharges the crushed material remaining in the chamber is distributed by the specific gravity at different levels of the chamber, and at subsequent discharges, each of the trays enters a crushed fraction of essentially the same density. Thus, the material is crushed and separated simultaneously.

In addition, when crushing the surface of the particles in contact with water sharply increases. As a result soluble compounds pass into water, and due to that fact water repeatedly washes the newly formed particles, the concentration of the compounds increases. The fraction trapped on the trays is separated by any of the known methods for further processing, and the saturated solution is subjected to processing, for example, with the help of tannin complex, to extract the desired product.

The further development of the idea of realization of electrohydraulic processes for crushing of the wastes was obtained while developing the following simplified design. The proposed solution relates to devices that provide technological processes of crushing and separation of mineral raw materials [6].

The disadvantages of this design are the following. This system is intended for crushing only homogeneous material and has low throughput. In addition, the electrode built into the bottom of the housing must be changed frequently as it burns quickly. It should be noted here, that such replacement especially in production conditions is a very time-consuming operation.

Therefore, we solved the problem of creating such an electrohydraulic crusher, in which changing the design of the loading device allows to simultaneously change the intensity of crushing of the starting material and to obtain the finished material of the required fraction without stopping the crushing process. This problem is solved due to the fact that the electro-hydraulic crusher has electrodes built into the hollow cylindrical housing, the upper part of which is provided with a loading device, and the lower one is provided with a hopper, the inner cylindrical part of the housing is equipped with an insulating glass, the electrodes are installed on the side surface of the housing, and the device is equipped with "blinds"

mounted on its side surface with the possibility of changing the angle of inclination (Fig. 2).

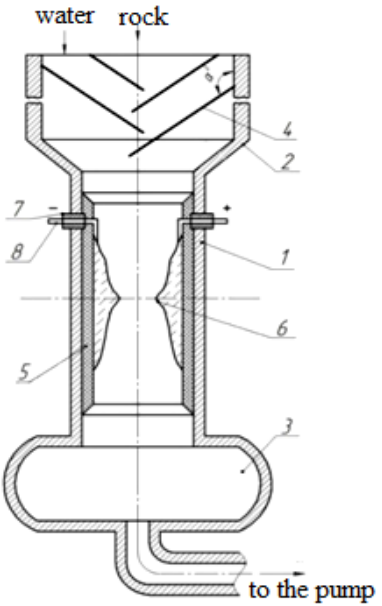

Fig. 2. Cross section of electrohydraulic crusher: 1 - cylindrical housing; 2 - boot device; 3 - hopper; 4 - fixed adjustable blinds; 5 - a glass; 6 - bit electrodes; 7 - insulators; 8 - conductors

The magnitude that characterizes the size of the elements obtained, for example, gravel, depends on the speed of downloading the starting material from the "blinds", the frequency of discharges on the electrodes, the magnitude of the discharge current, the angle of inclination of the "blind" to the axis of its attachment, the intensity, ie the speed of injection of the pulp.

The larger the angle α, the smaller the size of the product. Adjustment of an inclined shutter can be made by means of the appropriate actuator.

The crushing process can be described by a formula that determines the size of the elements of the resulting product:

$$A = K \cdot \left(\frac{V}{\alpha} \cdot f \cdot I \right) \quad (1)$$

where is K - proportionality factor;

f - frequency of discharges;

α- the angle of inclination of the "blind";

I - current;

V - the speed of injection of the pulp.

From the above formula it follows that by adjusting the slope of each "shutter" the loading intensity, current and discharge frequency at the outlet, one can change the intensity of crushing, ie the quality of the product without stopping the process.

This is a positive distinguishing feature of the electro-hydraulic crusher developed.

Working body for electro-hydraulic installation, which contains positive and negative electrodes connected to the pulse generator are separated by an insulating element, characterized in that it is provided with additional electrodes attached to the insulating element and separated discharge intervals (Fig. 3) [7].

The voltage from the generator is supplied to the working body. In this case at the ends of the electrodes located in a liquid medium in the casing a powerful electric arc occurs which is an underwater electric explosion.

The water instantly evaporates and, thus a high pressure zone occurs. It destroys the casing and affects the working organ of the environment, thus doing a useful job.

Since the working fluid is constantly around the electrodes, the entire product may operate in a porous medium, where otherwise a liquid would leak out, that would make the electro-hydraulic process impossible.

The second variant of realization of the developed device is possible, in that the solution of potassium nitrate KNO_3 is used as the working fluid. In this embodiment at an electric arc temperature of $20 \cdot 10^{-3}$°C nitrate ignition occurs.

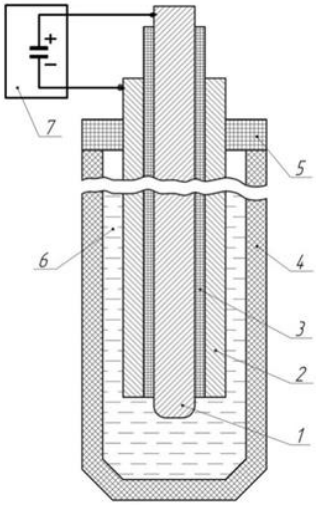

Fig. 3. Working body for electro-hydraulic action: 1 - Central positive electrode; 2 - external negative electrode; 3 - heat-resistant insulation; 4 - fusible insulation; 6 - a liquid medium

The ignition is accompanied by a powerful additional explosive action, whereby, it should be noted that, without the action of high temperature KNO_3 it is absolutely harmless and safe. The proposed technical solution relates to devices that convert the energy stored in the electrical capacitors of the electro-hydraulic installation into the energy of an arc discharge capable of performing useful work such as the destruction of dumps (waste heap slags) of coal mines, ash heaps, source materials.

Conclusions. In spite of the difficulties and risks, the relevance and prospects of using dumps of coal mines is obvious, as their disposal will avoid many health and environmental concerns in the future. It will minimize the social and economic consequences of the current situation and protect the environment and resources from physical and chemical destruction.

Thanks to the laboratory developed devices for dismantling and processing of dumps minding the future prospect of their implementation in industrial conditions, it will be possible to prevent the spread of parts of the treated object, strong sound and other negative influences that were previously present in the blasting with the use of explosives using explosives and outdated high-risk handling equipment and ensure safe dismantling and recycling of the waste heap slags.

References

1. **Kuris Y.V, Matyasheva O.B, Vorobyov O.F.** Investigation of the use of fuel and energy resources and improvement of their rational use in the metallurgical and energy complex. Energy and electrification. 2016. №5. Pp. 38-42.

2. **Kuris Y.V., Pogrebnyak Y.V., Matyasheva O.B.** Investigation of the harmful effect of landfills of solid household waste on the environment. Energy and electrification. 2017. №12. Pp. 28-32.

3. **Mnukhin A.G., Bryukhanov A.M., Goroshko I.P.** About complex processing of waste heaps of mines of Donetsk region: materials II Internar. Symposium "Safety of Life in the 21st Century", January 2002. Dnepropetrovsk: Technopolis. 2002. S. 52-54

4. **Mnukhin A.G., Mnukhina N.O., Hituliar A.A.** Complex processing of dumps of the mining industry: a collection of materials of the conference "Innovative development of the mining industry", Krivoy Rog: 2018. P. 198-200.

5. Electrohydraulic separator: US Pat. 81828 Ukraine: IPC (2006) B 03C5 / 00; claimed 27.02.06; publ. 02/11/08, Bul. №3.

6. **Mnukhin AG, Mnukhina NO, Guitar AA** Analysis of methods of extraction of ferrous and non-ferrous metals by processing of dumps. Metallurgy. 2017. No. 37 (1). Pp. 50-55

7. Working body for electrohydraulic effect on porous medium. Pat.120332 Ukraine: Appl. 22/05/2017; publ. 10/25/17, Bul. №20.

8. **Kachinsky A.B.** Ukraine's environmental safety: a systematic analysis of prospects for improvement. Kyiv: NISD, 2001. 312 p.

TECHNOLOGY OF WASTE DISPOSAL OF THE OIL AND GAS COMPLEX

Zotsenko M.L.
Doctor of Technical Sciences, Professor, Professor
of the Department of Building Technology
Poltava National Technical Yuriy Kondratyuk University, Ukraine

Mykhailovska O.V.
Ph.D., Senior Researcher, Associate Professor
of the Department of Building Technology
Poltava National Technical Yuriy Kondratyuk University, Ukraine

Abstract. The article proposes technological solution of sludge storage with vertical anti-filtration wall of soil-cement. It is proposed to produce soil-cement elements by blending technology without removing the soil in the type of "wall in soil". After hardening of soil-cement elements along the perimeter of the waste, up to 60% of the soil mass is recessed. The choice of technology of soil-cement elements is made in accordance with the feasibility study. The dimensions of the soil-cement elements and the dimensions of the bottom waterproofing are determined at the design stage. The dimensions of the soil-cement elements depend on the particular site of construction, taking into account the soil category, the depth of groundwater. After filling the waste deposit, it is recommended to arrange the soil-cement coating. The coatings are laid on a drilling mud thickened to a rigid-plastic consistency with the addition of soil to the construction site. After the soil cement has hardened, the sludge coatings are covered with a layer of soil. The advantages are the low cost of production by using a waterproof soil layer as the bottom of the structure. The optimal humidity of a mixture of drilling mud and soil in the ratio of 60:40 is investigated. The modulus of deformation of the compacted mixture is determined. It is sufficient for laying on the compacted surface of a flooring from a soil cement at arrangement of a sludge deposit.

1. Introduction

Concentrated solutions of acids, inhibitors, surfactants are used in the drilling and operation of wells and for the intensification of extraction of hydrocarbon raw materials. Most often, waste disposal is used to eliminate drilling waste. Waste disposal of the oil and gas industry is carried out in specially designated places, deep underground storage facilities in the territory of works. To prevent the entry into the soil and surface groundwater of toxic drilling waste a precautionary measure is the construction within the drilling site of underground storage which toxic waste is collected. The dimensions

of the barns are determined by the project and should correspond to the volume of drilling waste. The conditions of construction of slurry barns and their construction depend on the engineering-geological conditions of the area allocated for the construction of the well and the characteristics of soils of this area [1].

2. Basic investigation

2.1 Overview of known recycling technologies

Important when arranging waste is to provide waterproofing the bottom and walls. For this purpose, filtration screens (concrete, geomembranes [2], materials based on synthetic cloth, etc.) are used [3,4]. However, the screens of these materials are not durable enough and damage to them upon contact with chemicals will result in negative environmental effects.

Kachala T.A. (2019) proposes to use composite material based on synthetic fabric (cloth) modified on both sides by polymer-bitumen binder with high thermoplastic and waterproofing properties in the construction underground storage walls [5].

Fig. 1. General view of the storage of waste [6]

Timofeyeva K.A. (2016) propose a soil-cement waste storage. In this case, use the technology of making soil-cement elements by blending technology without removing the soil [3,4]. Wells are being drilled along the perimeter of the underground storage facility. These wells are filled with soil cement, which is a protective screen against groundwater. Then a pit is dug, the bottom of which is waterproofed by such technology [7]. Also known is the method of

fixing the bottom of the pit made of soil cement. Soil-cement which is mixed separately in a concrete mixer and poured with a continuous layer on the bottom [7]. Such storage of drilling waste is arranged open. It has at least 0.5 m height and mineral wire hedges along the perimeter of the mineral soil. This method is time consuming and the main disadvantage of this solution is that the storage is open.

It is also possible to arrange a repository of drilling waste with an anti-filtration veil of the "wall in soil" type. An anti-filtration curtain of the "wall in soil" type of soil-cement elements is immersed in a water-resistant layer of soil. This makes it possible not to arrange an anti-filtration screen of the bottom of the drilling waste storage, the function of which will be performed by a water-resistant layer of soil [4]. This design of the bottom will be more economical. The downside of this design is that the repository is designed to be open. In this case, the possibility of evaporation of harmful substances is not excluded. Thus, there is a need to arrange coverage of the drilling waste storage facility.

Thus, the task is to develop a constructive solution for an efficient, economical and safe storage of drilling waste with a soil cement screen and to arrange its coverage.

2.2. Lifetime waste storage technology

Soil-cement is a mixture of clay soil, cement and water. The main factor in the conversion of soil properties is cement, which is a polydisperse and polymeric system that, after the addition of water, forms a rocky material. Known studies on the effect of aggressive components of drilling waste on soil-cement have shown that over time. The strength of soil cement increases over time (from W4 to W6). This demonstrates the stability of soil cement to aggressive components of drilling waste [7].

Therefore, the authors propose to dig the walls of the pit of the drilling waste storage with a vertical anti-filtration veil of soil cement. The soil-cement elements should be made by blending technology without removing the soil by the «wall-in-soil» type. The walls of the storage deposit into the waterproof layer of soil. The store should be closed.

The choice of technology of soil-cement elements is made in accordance with the feasibility study [7]. The sizes of soil-cement elements and the dimensions of the waterproofing of the bottom are determined at the stage of working design in relation to a specific site of construction, taking into account the soil category, the depth of ground water.

The construction of a lifelong waste storage facility is as follows. For the perimeter of the planned sludge storage, a monolithic vertical anti-filtration wall of the type “wall in soil” is constructed of soil cement elements (Fig. 2). The distance between the centers of adjacent elements should be 0.8d (d - diameter of soil cement elements).

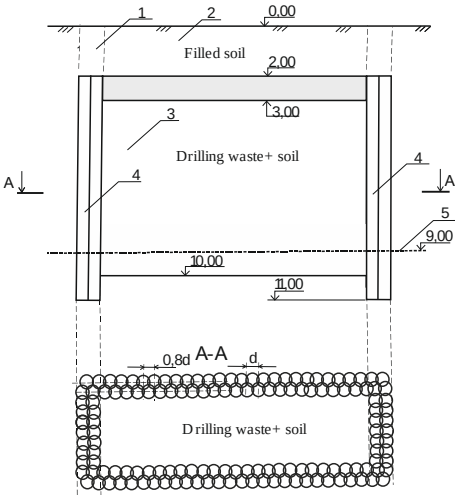

Fig. 2. Drilling waste storage

The soil-cement elements are produced by the blending method. This method is to use the special equipment to loosen the soil without removing it. At the same time a slurry is pumped into the loose soil. The soil-cement mixture is then mixed and compacted.

Thus, we obtain cylindrical soil cement elements with a diameter of 0.3-0.8 m and a length of up to 30 m [3]. The wall-to-soil anti-filtration curtain of soil-cement elements is immersed in a water-resistant layer of soil to a depth of at least 1 m in order to ensure no filtration. An important factor in the design of the repository is the

choice of the location of the repository, provided there is a waterproof layer at the optimum depth from the surface (8-20 m).

After hardening of soil-cement elements along the perimeter of the storage, up to 60% of the soil mass is recessed [3]. Filling of life storage with drilling waste is carried out after soil cement hardening.

The period of wetting in the moistened state lasts 28 days. Over time, the strength and water resistance of soil cement increase.

As the storage of the drilling waste is filled, the soil and drilling waste are mixed in the storage to a tight consistency. Stirring is carried out in order to thicken the waste and to arrange the topsoil cover. The soil cement coatings are laid directly on the drilling waste, which is thickened to a tight consistency.

The soil cement is produced at the construction site in a horizontal concrete mixer of continuous action from soil (loam, sandy loam), Portland cement grade M400 in the amount of 20% by weight of dry soil and water. With the help of mortar pump the soil cement is laid on thickened drilling waste with a uniform layer with a thickness of not less than 0.8 m.

The size of the drilling rig and its volume, profile and depth are determined at the design stage. The design of the repository is different for each site of construction, depending on the soil category, depth of groundwater, and other characteristics.

2.3. Investigation of waste mixture parameters

Investigation of soil characteristics and determination of optimum humidity was performed with drilling waste of Yablunovka oil and gas condensate field well No. 355. The drilling mud had a density of 1.49 g/cm^3, sediment volume of 1.5 ml, solids content was 3%, hydrogen pH value. 6.71.

For the research, the loam was refractory from a depth of 2 m. The average humidity of the soil samples was about W=0.2.

According to the results of laboratorys research, it was determined that the drilling mud had an average humidity of soil samples W=0.50. Its humidity at the yield point W_L=0.36, the moisture at the rolling point W_p =0.21 (Table 1).

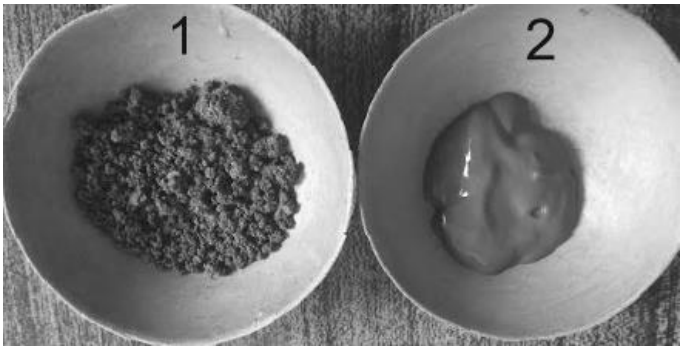

Fig. 3. General view of the components of the mixture: *1* - rigid loam; *2*- drilling mud

It was determined that this drilling mud belongs to the loam of the fluid. The research was performed according to standard laboratory methods of soil research according to DSTU B B.2.1-17: 2009 [8].

Table 1

Indicative characteristics of components of drilling waste mixture and loam loaded at variation coefficient, υ

Objects of research	Moisture, W/υ	Plasticity limit,	The boundary is fluid, W_L/υ	Quantity of plasticity, I_L/υ
Drilling waste	1,01/0,012	0,21/0,06	0,36/0,14	0,15/0,1
Loam	0,20/0,08	0,25/0,07	0,37/0,12	0,12/0,11

The composition of the soil under equal conditions, has a significant impact on the intensity of the compaction process and its final results. An increase in the amount of free, non-sticky water that allows the soil particles to move relative to one another, which results in a decrease in the resistance of the particles to move under external loading. With the same humidity, the amount of free water depends on the composition of the soil.

At constant values of initial soil moisture and specific volume of the soil skeleton, a higher compaction intensity corresponds to soil mixtures having more free water.

The mineral composition of the clay fraction also determines the properties of the soil skeleton when interacting with water. Clay

minerals with a mobile crystalline lattice have the greatest surface activity and hydrophilicity, which are capable of holding water not only on the surface but also between the packet space of the crystal lattice. Therefore, with the same percentage content of clay fraction, the highest values of optimum humidity will have soils with montmorillonite foliage component, and ultra-low - kaolinite. The drilling mud has a significant amount of montmorillonite clay component so optimum humidity in this case was 0.25.

The optimum soil moisture can be theoretically determined.

L.D. Bohoslovsky proposes to determine the optimal humidity by the formula

$$W_{opt} = W_p + (0,1 \div 0,3)\,\mathrm{I}_p . \qquad (1)$$

$W_{opt.}$ - optimum humidity of the mixture (soil); I_p - plasticity number; $W_{p.}$ - plasticity limit; W_L -strength limit.

According to the experiments conducted by V.I. Krutov, optimal humidity was assumed to be 3% more moisture at the limit of plasticity, according to the instructions of DORNDI $W_{onm} = W_p$.

M.Y. Telegin, CA Hohentogler, E.M. Kupriyanov is also recommended. $W_{onm} = W_p$ V.I. Birulya proposes to determine the optimum humidity depending on the soil yield point: $W_{opt} = 0,62W_L$ (2)

Research done by O.K. Birulya, N.F. Sasko, A.F. Kotivitsky, aimed to establish the relationship between the optimal humidity standard compaction and the upper boundaries of plasticity of the respective soils with the help of transient coefficients. As a result of data processing on 572 samples of soils of different origin and particle size distribution the formula was obtained

$$W_{opt} = 1,5(0,5W_L - 0.25I_p - 0,01) . \qquad (3)$$

The characteristics of the soil mixture were determined under laboratory conditions. The loam was mixed in a state of natural humidity. The average humidity of the soil samples was thus 50%.

The values of the optimum humidity were determined for the ratio of the mixture of drilling mud and loam 60:40. The smallest value of optimum humidity can be obtained by calculations according to the method of O.K. Birulya - 0.25. The values of optimal humidity

were obtained according to the formula of Birulya V.I. and according to the method of O.K.Birulya, N.F. Sasko are close and differ in size by up to 3%. The value of optimal humidity determined by V.I. Krutov - 0.41, for L.D. Bohoslovsky - 0.3. The theoretical values of optimal humidity vary over a wide range.

Therefore, for the mixture under consideration, the values of optimal humidity and optimal skeletal density were determined in accordance with the standard soil compaction technique using a stationary mechanized soil compactor MSU-1 (Fig. 4)

The design of the device MSU-1 consists of a base plate and a gearbox, an electric motor, a rack with brackets, the rod on which the weights move. The drive design is made of two pivotally connected rods. This design maintains a constant drop height of the weight in the process of sealing the sample. A variable form is attached to the plate.

For the experiment, 6 samples of the appropriate size were made. Dynamic compaction of the mixture of soil and drilling waste is performed by the following procedure. A certain amount of water is added to the soil sample at initial humidity to obtain samples of optimum humidity. A sample of the soil mixture was applied with a thin layer at the bottom of the tank and moistened evenly with a laboratory burette. With this method, moisture in the soil was distributed evenly. The mixture was thoroughly stirred and poured into a pre-assembled and oiled glass of the instrument MDU-1 (Figure 3) [9,10]. The stirred and moistened mixture was kept in the hydrator for about 2 hours in order to distribute moisture evenly. The mixture was poured into a glass from a height of about 10 cm.

The height was the same for all samples. Prior to sealing, the specimen was compressed for several minutes with a static load of 10 kg. This was done to reduce macro pores and air voids. The initial humidity of the samples was more than half the humidity at the boundary of plasticity. Since the humidity of the samples is less than this value, the sealing of the samples will be less effective. Experiments on dynamic compaction of the samples were carried out at equality of initial height of the samples.

Therefore, before compaction with a depth gauge, the soil level in the glass was checked. After the soil compaction is completed, the mass of the glass with soil is determined to the nearest 1 gram and two samples are taken to determine the humidity. Then a steel beaker

with a prepared soil sample was mounted on the base plate of the device MDU-1. The deformation of the soil in the course of the experiment on the instrument MDU-1 is measured with a depth gauge from the top of the glass after each stroke with the number of strokes up to 10.

The experiment was stopped if the deformation difference during the last 5-10 strokes would be less than 0.5 mm.

The average value of the optimum humidity of the mixture when the ratio of drilling mud to soil 60:40 was 0.27. That is, the closest value to the experimental obtained theoretically using the method of O.K. Birulya, N.F. Sasko.

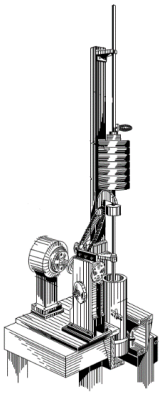

Fig. 4. MDU-1 appliance

Further, samples of the compacted mixture were made according to the ratio of drilling mud and loam 60:40. Next, the compressibility of the mixture in the K-1 compression device was evaluated. According to the results of compression tests, the modulus of deformation at optimum humidity W=0,27 and ρ_d=1,65 g/cm^3 was E=27 MPa. Such considerable compressibility of the mixture is not necessary for the site of disposal of drilling waste. Therefore, it may be considered sufficient to cover the overburden of the cement-based drilling waste on such a compacted basis.

3. Conclusions

1. The aforementioned method of creating a technological solution for the arrangement of a drilling waste storage facility can be used in any territory. An important factor in the design of the repository is the choice of location, provided there is a waterproof layer at the optimum depth from the surface (8 – 20 m).

2. The advantages of the construction of a storage facility with a soil cement coating, which is embedded on a drilling mud thickened to a rigid plastic consistency with the addition of soil to the construction site, is the low cost of production due to the use of a waterproof soil layer as the bottom of the structure. After hardening of the soil

cement, the coverings of the storage are covered with a layer of fertile soil. Thus the solution of the problem of utilization of the soil storage facility extracted during construction is possible.

3. It is proposed to fill the storage of drilling waste with a mixture of drilling mud and ground soil (in the conditions of the Poltava region - loam-tight loam) in the ratio 60:40. At this ratio of the mixture, the modulus of deformation of the mixture was 27 MPa. Which is sufficient to arrange the coating of soil cement storage.

References

1. **Timofeeva, KA** (2016) Soil-cement storage facilities for toxic waste drilling and oil and gas wells operation Cand. Tech. Sciences: 05.23.02, Poltava, 2016

2. **Zotsenko, N. L. and Tymofieieva, K. A.** (2014) Sludge barns for drilling and oil well drilling from soil-cement antifiltration wall. Bulletin of the National University of Water and Environmental Sciences Issue 2 (66). pp. 337-345.

3. **Zotsenko, M.L., Timofeeva, K.A.** (2011). Patent for utility model 71256 Kyiv: State Patent Office of Ukraine

4. **Timofeeva, K.A.** (2013) Patent for utility model 87868 Kyiv: State Patent Office of Ukraine

5. **Kachala, T.** (2019) A method of creating an ecological modification of oil sludge storage [Kindle Version]. Retrieved from: https://studfiles.net/preview/8183270/

6. Construction of drill cuttings storage facilities (2019). [Kindle Version]. Retrieved from: http://izolyaciya.com/stati/sooruzhenie-shlamovyx-ambarov/

7. **Zotsenko, M.L., Vinnikov, Yu.L., Zotsenko, V.M.** (2016). Soil-cement piles by drilling-mixing technology: Monograph - Kharkiv: Madrid Printing House.

8. DSTU B B.2.1-17: 2009. Foundations and foundations of buildings and structures. Soils. Methods of laboratory determination of physical properties. Adopted: 02/08/2018 Date: 01/01/2019 - 36 p.

9. **Zotsenko, N.L., Vinnikov, Y.** (2016), Long-Term Settlement of Buildings Erected on Driven Cast-In-Situ Piles in Loess Soil L // Soil Mechanics and Foundation Engineering, Vol. 53, No. 3, 189 - 195. doi 10.1007/s11204-016-9384-6

10. **Yermakova, I A.** (2005) Features of dynamic compaction of soil mixtures using mining waste - "tails" : Cand. Tech. Sciences: 05.23.02, Poltava, 2005.

METHODS AND SYSTEM FOR NON-SEPARATIONAL EVALUATION OF HYDROCARBON FLOW COMPOSITION

Raiter P.
Doctor of Engineering Sciences, Professor
Ivano-Frankivsk National Technical University of Oil and Gas, ,
Head of the Department of energy management
and technical diagnostics, Ukraine

Karpash O.
Doctor of Engineering Sciences, Professor
Ivano-Frankivsk National Technical University of Oil and Gas,
Professor at the Department of energy management
and technical diagnostics, Ukraine

Yavorskyi A.
Candidate of Engineering Sciences, Associate Professor
Ivano-Frankivsk National Technical University of Oil and Gas,
Associate Professor at the Department of energy management
and technical diagnostics, Ukraine

Rybitskyi I.
Candidate of Engineering Sciences, Associate Professor
Ivano-Frankivsk National Technical University of Oil and Gas,
Associate Professor at the Department of energy management
and technical diagnostics, Ukraine

Abstract

The investigation is devoted to solve the actual scientific and applied problem – providing the ongoing monitoring of the phase composition of the multiphase flows with high gas factor value by way of new methods and resources of nonseparation structure control and determination the phase composition of the gas-liquid multicomponent flows of the on-stream oil and gas condensate wells development.

It is shown that the solved problem is very important for Ukraine. For its solving the current nonseparation testing methods of the structure and phase composition are developed and improved, and also the information and measuring system that implements the specified methods is developed. For the flow structure determining the methods for the flow structure identifying based on symbolization, wavelet decomposition of hydrodynamic and acoustic flow fluctuation signals, and algorithms of artificial neural networks are developed. The method that combines the hydrostatic, cross-correlation acoustic and impedance testing methods for the ongoing determining of the phase composition of gas-water-condensate flow is developed. The im-

pedance testing method that is contained in using the specially developed impedance sensor construction, and frequency locus diagram of the impedance signals like image of the flow water fraction is improved for the flow water fraction definition. The velocities of individual flow phases are determined as a result of flow acoustic signals processing by the methods of wavelet and cross-correlation analysis. The information and measuring control system is developed and tested for the ongoing control of the flow phase composition of the individual well and for hydrocarbon production optimization amid of oil-and-gas industries. The results of the ongoing impedance testing method of the water fraction of the gas-liquid flow well survey for the corrosion phenomena predicting are adjusted.

Keywords: multiphase flow, high gas fraction, flow regime, impedance transducer, water fraction, wavelet decomposition, flow phase velocity, neural network.

Introduction The development and operation of oil and gas and gas condensate fields requires optimization of the production process - maximum extraction of the hydrocarbon mixture with minimal economic costs. The increase in hydrocarbon production volumes in the offshore oil and gas and gas condensate fields of Ukraine in the current economic conditions is mainly realized through the commissioning of plugged and abandoned wells, as well as existing low-producing wells, for which a series of measures to intensify production are carried out.

The solution to this problem is impossible without operational control, management of operating conditions and the composition of the hydrocarbon flows of gas condensate and oil and gas wells, which in many cases are at the final stage of operation. The difficulty in solving this problem is due to the fact that the output of the wells is a time-varying mixture of gas, produced water and condensate or oil. The concentration of the components of the mixture is variable over time, which leads to instability of the structure, physical properties and flow regimes of the multiphase flow. In addition, the mixture may contain a certain amount of solid hydrocarbons, mineral particles and other mechanical impurities.

Traditional methods and information-measuring systems for monitoring well productivity, based on the previous separation of free gas and liquid components, do not correspond to the current needs of the industry and the current level of information-measuring technologies development. The applied separation group metering units have significant weight and size parameters, do not provide complete separation of the gas phase, especially at a high gas flow,

which leads to a significant decrease in the measuring reliability of the well productivity. A significant drawback of such installations is in the selective control for the phase composition of individual wells and the discreteness of indications, due to the accumulation of the separated phase in the separation tank. As a result, the volume and reliability of the information received is insufficient to develop optimal and economically feasible technical solutions for operating modes and terms of structures repair at the gas condensate well. The lack of constant information results in wells downtime , premature wear of equipment and sets the prerequisites for emergency situations.

The problem of evaluation the composition of multiphase flows has been fruitfully worked by national and foreign specialists, in particular: S.M.Stetsiuk, P.P.Kremlevskyi, M.M. Huzhov, S.S. Kutateladze, V. A. Mamaiev, V.F. Medvediev, M.I. Merdukh, , D. Barnea, Y. Teitel, A.K. Dukler, N.Petalas, K.Aziz, G.F. Hewitt, G.Falcone, Alimonti C., R.C.Baker, C.E. Brennen, Crowe C.T., Gudmundsson J.S, M. J. da Silva, W.H. Ahmed, B.Azzopardi, Elkow K.J., Oddie G [1- 20] . A number of researchers tried to apply classical methods and devices for measuring the flow rate of single-phase flows, however, in operating conditions, such measuring systems showed insufficient reliability. Non-separation multiphase flow meters, in which, along with others, methods of transmission through the flow of ionizing radiation, are most famous. However, the operation of such measuring systems is accompanied by difficulties associated with the need to carefully comply with the requirements and rules of radiation safety in force in Ukraine. A common drawback of these types of systems at present is in the low reliability of their readings when controlling phase-shifting multiphase flows with a gas fraction of flow of 95% by volume or more.

Therefore, the problem of developing new methods and technical means of gas phase condensate flow control systems, in particular at high gas factors, without the use of separation devices, is quite acute for field owners and researchers. In the oil and gas industry of Ukraine, the need arose to create affordable, simple and reliable systems and software tools that ensure the determination of the flow regime of wells in the field and devices for continuous monitoring of

the operating parameters of wells, and, above all, the flow characteristics of the components of the gas condensate stream.

The goal and objectives of the research are to solve the urgent scientific and applied problem - providing current monitoring of the phase composition of multiphase flows with high gas factors by developing new methods and means of non-separating control of the structure and determining the phases flow rate of gas-liquid multicomponent flows of production oil and gas and gas condensate wells.

To achieve this goal, the following tasks were set in the work:

to analyze the current state and development trends of means and technologies for controlling the phase composition of multiphase flows for oil and gas production conditions with the aim of formulating a methodology for the development of new methods and means of monitoring the flow phase composition with its high gas fraction;

to develop a method for the rapid identification of the structure of a multiphase flow of a well based on the processing of information signals from a control system to a phase shifter, which will correctly select a method for determining the phase composition and the moment of hydrates or liquid plugs formationin the flow of well loop pipelines;

to develop methods for the non-separation current determination of volume fractions and velocities of the gas and liquid phases in gas-liquid well flows in the presence of high gas fraction and static pressure, which will allow real-time recording of the phase composition and individual phase flow-rate of a controlled flow;

to develop a method for determining the volumetric fraction of water in the liquid phase of a well flow with high gas fractions, which will provide operational current monitoring of water fraction in well gas-liquid flows in the presence of differences in the physical and chemical parameters of the water phase of the various wells flows;

to develop and manufacture an information-measuring system for monitoring the flow phase composition for the current determination of the structure and flow phase-shift, which provides control of the composition under conditions of high static pressures and gas fraction in the flow;

For the effective selection of control methods that are optimal in specific technological conditions of production, a systematization and analysis of known methods and means for measuring the characteristics of mobile gas-liquid multicomponent media has been performed. It is proposed to classify the methods according to the type of measured physical quantity, which results in their dividing into mechanical (static and dynamic) methods and methods based on measuring the field characteristics, modified by the flow: electromagnetic, optical, nuclear-physical and thermal. The directly measured parameter is the intensity or frequency, functionally related to the flow phase composition.

Based on the analysis held, it was found that:

currently existing systems for monitoring the hydrocarbon mixtures do not provide adequate reliability of information on phase composition and structure (PhC&S) flow at high gas factor values, which specifies the development of methods and systems for this type of flows, an example of which is for gas condensate flows of production wells;

considering the value of information about the flow structure for: determination of its phase composition, preventing fluid accumulation in the loop pipe and well operation interrupting, setting the energy-saving mode of boreholes operation, it is recommended further improving of analytical methods for predicting the flow structure, algorithmizing methods for identifying the flow structure based on existing empirical relationships and development of real-time flow structure identification methods;

reliable information in real time on the flow phase composition according to different flow rates of wells allows you make rapid decisions about: changing the mode of their operation to prevent premature flooding of the reservoir and well, increasing the uncompressed period of their operation and ensuring a high degree of hydrocarbon recovery from the fiels. Considering that existing systems do not provide reliable information on the amount of water fraction in conditions of high gas fraction of a flow, the problem of developing methods and means needs to be solved implementing the control of this type of flows;

production well pipelines should be considered as engineering objects, they are inevitably subjected to technogenic action from both

rocks and fluids produced, therefore, the problem of assessing and predicting corrosion and erosion processes in the pipeline needs to be solves due to the influence of the nature of the PhC&S of gas-water-hydrocarbon flows moving in the pipelines;

the operational management pecularity of the field's operation (which is at the final stage of development) is that the production wells operate in self-regulation mode, that is, their flow rate is determined by the pressure at the inlet unit of the gas treatment installation. Performance of the targets for gas production during the well operation in the specified mode does not allow changing their flow rate and requires ensuring the maximum coefficient of well operation. The production well interruption under such conditions occurs as a result of accumulation of formation fluid, which causes a back pressure on the reservoir. Therefore, it is required to development of a control system providing continuous monitoring of the phase composition to identify potential closures in the production system (hydrates, asphaltenes, paraffins, sand, solid sediments on the pipe walls). Here, the trend is more important than providing values with absolute accuracy.

Based on the analysis of the multiphase flow of the well as an object of control, and modern means of monitoring flow phase composition, the requirements for the development of new methods and devices that are optimal for use in the oil and gas industry are formed:

to provide fraction determination of each flow phase;

to provide structure determination of the flow mixture;

to ensure the determination of the actual volumetric fraction of the dispersed phase in the continuous phase;

to provide non-intrusive control;

to have a wide range of applications in relation to the types of liquids flow, flow rates, pipe sizes, temperatures, pressures;

to ensure the implementation of ongoing non-separation control.

In order to identify the structure of the well hydrocarbon flow, a technique is proposed for symbolizing information signals of pressure pulsations and acoustic signals of sensors installed on a pipeline with a multiphase flow from a borehole. Information signals of acoustic sensors and sensors of hydrodynamic pulsations of flow pressure are of essentially stochastic nature. Therefore, in the process

of sensor signals' preliminary processing, their structuring and symbolizing of the signals are occured. After amplification, normalization, analog-to-digital conversion (ADC) of the sensor signals, a value in the range from 0 to 1023 (for a ten-digit ADC) is obtained, that is proportional to the values of the normalized signals. The result of the A/D signal conversion - the number - is perceived by the processor as the address of the cell that needs to be incremented. This operation is performed fast enough, therefore, the speed of signal symbolization is practically determined only by the speed of the ADC module. In memory cells, an estimate of the distribution density function of the information signal sample is formed. By dividing the value in each of these memory cells by the total number of ADC signals during the observation period, in the memory we obtain a symbol-sequential histogram of the information signal energy distribution (Fig. 1).

The indicated histogram is used to: determine the type of distribution and estimate the stationarity interval of the sensor signal; obtain an information signal characteristic image of a particular two-phase flow mode in order to identify the flow structure; obtain the sensor information signal image, which after some time should come from the second sensor, remote from the first one at a given distance. The above given repetition time will determine the flow rate of a multiphase mixture.

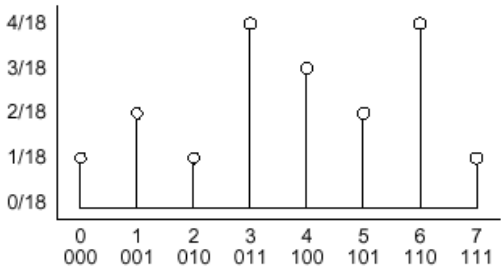

Fig. 1. An example of a symbol-sequence histogram for a symbol series at eight levels of separation of the signal range (1-bit ADC)

For quantitative estimation, the modified Shannon entropy, the Euclidean norm (T statistics), and the modified χ^2 statistics were used.

The modified Shannon statistics is determined as follow:

$$H_S = -\frac{1}{log_2(N_{obs})}\sum_{i=0}^{N_{obs}} p_i \cdot log_2(p_i), \qquad (1)$$

where, p_i - probability (normalized occurrence rate) of i binary character sequence; N_{obs} - the number of binary code sequences that actually appear in the dataset. The Euclidean norm and modified χ^2 statistics are applied for comparing two different histograms. The Euclidean norm is determined as follow

$$T_{XY} = \sqrt{\sum_i (X_i - Y_i)^2}\,, \qquad (2)$$

and modified χ^2 statistics is determined as follow

$$\chi_{XY}^{\ 2} = \sum_i \frac{(X_i - Y_i)^2}{(X_i + Y_i)}, \qquad (3)$$

where X_i and Y_i - the individual sequences of the two information signals for the i sequence in histograms X and Y based on these signals.

Evaluation and practical verification of the given methodology for information signals symbolizing was carried out on the implementation of the signals received in the experimental section of the pipeline with gas condensate flow. The sensor information signal was turned into a proportional electric one, and subsequently it was used as an information signal on the nature of the hydrodynamic pulsations of the two-phase flow inside the pipeline. The oscillations frequency range was 3-6400 Hz. Histograms of the signal range from -10 to +10 V with a step of a sampling interval of 76 mV for signals received from a multiphase well flow are shown in Fig.2.

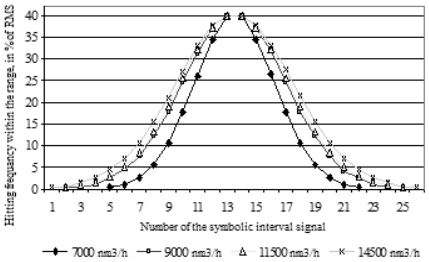

Fig. 2. Histogram of information signal symbolic conversion

Analysis of data from Fig. 2 and Tab. 1 shows that: a change in the flow rate of the well result in a change of the phase composition of the multiphase flow, numerically it causes a change in the Shannon statistics; when using 26 sequences of the signal measuring range symbolization, there is a direct proportionality between the value of the Shannon statistics and the phase fraction of the multiphase mixture; when 86 intervals are used to increase well production, Shannon statistics also grows, but its change is more significantly affected by a change in the fraction of the liquid phase (condensate) than a change in the fraction of the gas phase. This is due to the difference in the densities of the flow phases . An additional factor is the flow static pressure.

Table 1

Estimated values of Shannon statistics for signal histograms

№пп.	Shannon statistics Hs	Gas consumption reduced to n.u., thousand m^3/h	Condensate consumption, m^3/h
1	0,3064	7	30
2	0,3275	9	32
3	0,3320	11,5	36,5
4	0,3379	14,5	38
5	0,3925	13	16,8
6	0,4155	15,5	42
7	0,4062	16,5	30
8	0,3947	22,5	35

The results obtained make it possible to justify the possibility of using symbolic values of the hitting frequencies into individual intervals of the information signal range, as inputs to an artificial neural network, implemented as a programm in a digital signal processor of the information processing unit at the flow structure control system. The use of such neural network information processing algorithms makes it possible to provide identification of the flow structure based on the training of the developed system directly on site of the multiphase flow measurement.

To implement flow structure identification algorithms based on the processed signal of pressure pulsation sensors, a TMS320F2812 digital signal processor (DSP) is used in devices of a two-phase flow structure. During the wavelet transformation, a set of coefficient

values is obtained that reflects both the signal frequency composition and the intensity distribution of these frequency components over time. The resulting set of coefficients is a set of vectors, each of which represents the energy distribution over the same time intervals on the scale (or frequency) of the information signal. The obtained vectors are used as input in the development and training of an artificial neural network, which is implemented by the DSP, which also carries out wavelet transformations. Processing algorithms contain two processes: networks self-excitation and error minimization. In the first process, the network structure is determined by applying wavelet analysis. The network is gradually recovering hidden nodes to cover effectively and completely the time-frequency area taken by this set of information signals realization. At the same time, network parameters are adapted in order to preserve the network topology and take advantage over further process. In the second process, approximations of fluid error values are minimized using adaptation methods based on least-mean-square algorithms (LMS). The initialized network parameters are adapted using the steepest gradient-descent method of minimization. Each hidden node has a square window in a time-frequency representation. We assume that the network initial dependence satisfies the permissible conditions and the network sufficiently approximates the type of flow structure according to the nature of the input signals (pressure pulsation), that is, the time-frequency area is effectively covered by K windows. The approximated signal (of one flow component) of the $\hat{y}(t)$ network is written as follow

$$\hat{y} = u(t)\sum_{k=1}^{K} w_k \cdot h_{a_k,b_k}(t), \tag{4}$$

where K – number of window wavelets, w_k – weighting factors.

Neural network parameters, w_k, a_k and b_k , are optimized by the least-mean-squares method by minimizing the objective function or energy function, E throughout the period of time, t.

$$e(t) = y(t) - \hat{y}(t), \tag{5}$$

where $y(t)$ are the real values of the objective function (the value of the flow structure type). The energy function can be defined as

$$E = \frac{1}{2}\sum_{t=1}^{T} e^2(t). \quad (6)$$

For E minimization the method of steepest descent is applies that requires gradient adaptation $\frac{dE}{dw_k}, \frac{dE}{da_k}, \frac{dE}{db_k}$ by incrementally changing each of the parameters w_k,a_k *i* b_k . For the parent Morlaix wavelet gradients are

$$\frac{\partial E}{\partial w_k} = -\sum_{t=1}^{T} e(t)\cdot h(\tau)\cdot u(t), \quad (7)$$

$$\frac{\partial E}{\partial b_k} = -\sum_{t=1}^{T} e(t)\cdot u(\tau)\cdot w_k \frac{\partial h(\tau)}{\partial b_k}, \quad (8)$$

$$\frac{\partial E}{\partial a_k} = -\sum_{t=1}^{T} e(t)\cdot u(\tau)\cdot w_k \tau \frac{\partial h(\tau)}{\partial b_k} = \tau \frac{\partial E}{\partial b_k}, \quad (9)$$

where $\tau = \frac{t - b_k}{a_k}$.

Incremental changes in each factor are negative gradients

$$\Delta w = -\frac{\partial E}{\partial w}, \Delta b = -\frac{\partial E}{\partial b}, \Delta a = -\frac{\partial E}{\partial a} \quad (10)$$

for each coeficient *w, b, a* of the network the adaptation is performes according to the rule

$$w(n+1) = w(n) + \mu_w \Delta w, b(n+1) = b(n) + \mu_b \Delta b,$$
$$a(n+1) = a(n) + \mu_a \Delta a \quad (11)$$

where μ is *a* fixed significant parameter in neural network training.

The implementation of the specified algorithm for the primary processing of information signals, the structure formation and adaptation of the neural network algorithm for generating information on the structure of the gas-liquid flow based on a digital signal processor with an electric reprogrammed (flash) memory allows to provide technical implementation of both training and optimization of the neural network as well as refinement in the

process of setting up the device parameters of wavelet transformation.

For the non-separation flow rates determination of wells' gas-liquid flow phases, methods for determining the liquid and gas phases fraction in a three-component gas-liquid flow were developed and improved. When measuring the flow rate of a multiphase flow Q, which is a gas-liquid three-component flow of gas, condensate (or oil) and water, the equations of the liquid phases velocity are presented

$$Q = A \cdot \left(U_G \cdot \left(1 - \left(\varphi_C + \varphi_W\right)\right) + U_L \cdot \left(\varphi_C + \varphi_W\right)\right) \quad (12)$$

where U_G,U_L, - velocity of relevant gas mixture or flow condensate and water phases mixture; A,– the cross-sectional area of the pipe.

The volumetric fraction of the flow phase is defined as the ratio of the volume taken by a certain phase of the flow to the internal control volume of the pipeline. An analysis of the equation shows that in order to determine the phase composition of a multiphase (three-component) flow in real time, it is necessary to determine simultaneously four parameters in this mode: gas phase velocity U_G, liquid phase velocity U_L, condensate (liquid) phase volumetric fraction φ_C and water phase volumetric fraction φ_W.

The gas phase is characterized by significant compressibility, therefore, to determine the normal gas flow rate, it is necessary to find the values of pressure P and temperature T at the place of measurement. The water fraction of the liquid phase is defined as the ratio of the volumetric fraction of the liquid phase to the volumetric fraction of the liquid phase in the flow $C_W = \varphi_W / \varphi_L$, then the dependence for determining the volume of liquid in the control volume of the cross-section of the pipeline in the presence of information about the water fraction of the flow (determined by using an in-line moisture meter) will take the form

$$Q_L = \rho_L \cdot \varphi_L = \rho_C \cdot (\varphi_L - C_W \cdot \varphi_L) + \rho_W \cdot C_W \cdot \varphi_L. \quad (13)$$

The main difference between the gas and liquid phases of the flow, which is proposed to be taken as the basis for determining the phase composition, is the specific gravity. Liquid (condensate, oil, water) under normal conditions has a density three times above that

of the gas phase of the flow. Therefore, if an imaginary cylinder of a pipeline section with a length of H=1 cm is considered, then the weight of the gas phase of the flow within this volume is significantly less related to the same volume weight of the flow liquid phase , even with an increase in pressure to 8 MPa, when the gas density increases. This makes it possible to propose the implementation of a hydrostatic method for determining the phase composition of a flow in a pipeline section (Fig. 3)

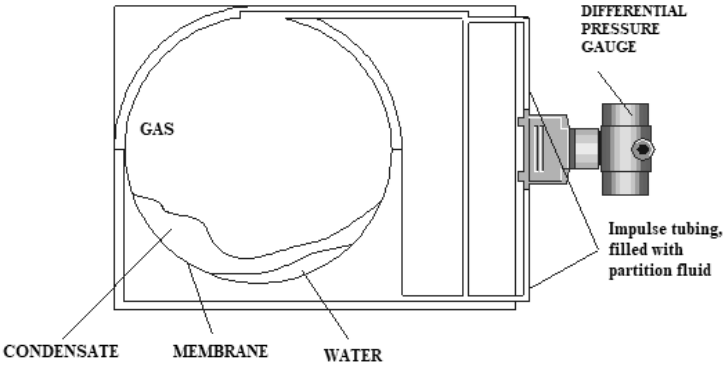

Fig. 3. Schematic representation of the design of the tube insert for measuring phase particles of gas-liquid flow

When weighing of such a selected volume is carried out at a high frequency and the known values of such a sample volume and the density of condensate and water are taken into account , the phase fractions of the flow are determined on the basis of geometric calculations and based on the measurement of hydrostatic pressure in the section of the pipeline. The equivalent height of the liquid level h_L in the pipeline is determined by measuring the differential pressure P_{dif} between the upper and lower points in the cross section of the horizontal pipeline with flow

$$h_L = \frac{P_{dif}}{(\rho_L \cdot g)} \tag{14}$$

and considering gas phase and water fraction weight:

$$h_L = \frac{P_{dif} - g\rho_g D_{vn}}{g\left(\rho_w C_w + \rho_0 (1 - C_w) - \rho_g\right)} \quad (15)$$

The cross-sectional area of the pipe taken by the liquid phase of the flow:

$$A_L = \frac{\left(s_L \cdot \left(\frac{D_{vn}}{2}\right) - S_{GL} \cdot \left(\frac{D_{vn}}{2} - h_L\right)\right)}{2} \quad (16)$$

The cross-sectional area of the pipe taken by the gas, water and oil phases of the flow:

$$A_G = A - A_L, \quad A_W = C_W \times A_L, \quad A_C = A_L - A_W \quad (17)$$

For the purpose of pre-filtering and processing information signals of the primary transducer, wavelet filtering algorithms and information processing algorithms based on artificial neural networks are applied.

In the process of increasing the flow velocity, the difference in the densities of the gas and liquid phases of the flow results in an increase in the difference in the flow phases velocities and the occurrence of the so-called "slip" of the flow phases. As the gas and liquid phases of the flow move at different velocities, this always results in a vortex at the phase boundaries, since there is a velocity gradient at individual points of the boundary volumes of the flow and the liquid medium under the action of external flow forces changes its shape. The multiphase flow is characterized by the generation of flow vortices and, as a consequence, the coherent formations take place characterized by gas-hydrodynamic pulsations and acoustic noise in the flow. Despite the stochastic nature of the flow turbulence, the above coherent formation signals have been used as reference points of the moving flow. The vortices, formed in a stream, are transferred at an average flow velocity. Then, by measuring the velocity of the vortices, the velocity of the flow is measured too. For this purpose, two acoustic sensors in the protective acoustic chambers are installed in/or on the pipeline of two-phase flow at a fixed distance *L*. Pressure fluctuations and acoustic noise generated by the moving vortex of the flow are sequentially recorded at first by the first acoustic sensor, and after a period of time *t*, by the second sen-

sor, mounted coaxially with the first one. By dividing L by t, the velocity value of the medium is obtained. There is a problem in determining the parameter t as the maximum of the correlation function of two sensors signals in a flow. By taking into account stochastic nature of the hydrodynamic pulsations and acoustic noise in the flow, this task requires preliminary processingof the sensors' signals before their correlation functions definitions.

It is proposed to perform the appropriate processing after multilevel decomposition of information signals realization by means of wavelet transformations of the sensors' signals. In the decomposition process, one A_{n+1} dataset will contain the features of the signal on a larger scale than the original set, and the second D_{n+1} set will reflect the differences between the An and A_{n+1} sets, which typically look like the high-frequency components of the sensor input A_n data set. For the decomposition operation at the next level, the data set A_{n+1} is taken as the initial set, and as a result of decomposition, respectively, the sets A_{n+2} and D_{n+2} with a larger signal scale and greater signal refinement are obtained . For each decomposition level, an intercorrelation function is defined between the reciprocal sets of two sensor signals. Function maximums indicate the level of signals compliance at different levels of decomposition. The cross-correlation function argument at its maximum value is numerically equal to the required time t.

To evaluate the cross-correlation function of the decomposition result at the level n (approximation component), the correlogram is defined:

$$C_m^{An} \equiv C^{An}(\Delta t \cdot m) = \frac{1}{N-m} \sum_{k=0}^{N-m-1} a1_k^n \cdot a2_{k+m}^n , \qquad (18)$$

where, Δt - sampling time of the sensor signal; m=0, 1,…,(N-1) - the number of deviations between the two signals indication (equivalent τ for continuous cross-correlation function); k - the indication number of the signal in the sample; N – sample size; $a1^n$ and $a2^n$ - coeficients values of decomposition results (aproximations) at signals' level n of the first and second sensors respectively.

The correlogram, as an estimate of the inter-correlation function of the decomposition result at the level n (component of detail), is calculated similarly to the formula

$$C_m^{Dn} \equiv C^{Dn}(\Delta t \cdot m) = \frac{1}{N-m} \sum_{k=0}^{N-m-1} d1_k^n \cdot d2_{k+m}^n , \quad (19)$$

where $d1^n$ and $d2^n$ - values of decomposition results (detalizations) at n level of the first and second sensors' signals respectively.

The task of t_G and t_L values determination for the gas and liquid phases velocity is solved according to two stages. Initially, small sets of experimental data are used for determination of the maximum value from the set of above-written correlograms of all N/2 decomposition levels

$$t_G = \max_{n=1}^{N/2}\left(C_m^{Dn}\right), \qquad t_L = \max_{n=1}^{N/2}\left(C_m^{An}\right) \quad (20)$$

If the experimental data size increases, the software-based algorithm of artificial neural three-layer network is used in the second stage. The inputs of the network are the values of correlograms at different levels of decomposition while synchronizing the mvalues. The outputs are t_G and t_L values**.**

The impedance method for the current measurement of water fraction in a gas-liquid flow with high gas fraction has been improved. The physical basis of impedance flow control method is considered. The impedance sensor is specifically adapted for the measurement of water volume ratio (water fraction) in oil and gas or gas condensate flows with high gas fraction and static pressure. The measurement principle is founded on the position that the difference in conductivity of the various components or phases flowing between the two capacitor plates (electrodes) makes the capacitance and conductivity between them dependent on the ratio of components or phases concentrations in the flow. The relationship between the ratio of concentration and both the conductivity and the capacity of the mixture is non-linear and depends on the spatial arrangement of the components or phases in the mixture (flow mode). Studies have shown that, despite the significant dependence of impedance methods on the flow mode, provided improvements in the measurement technique and design of the primary transducer, these methods can be used to measure concentrations if the various components are homogeneously mixed [21,23].

The results of an 8-tier wavelet decomposition implementation (8192 points, at a sampling rate of 44 kHz, a duration of approximately 186 ms) of the gas condensate flow acoustic sensor by using Debeshi db4 discrete wavelets are shown as the exsample in Fig.4. At the refining levels of d6 and above there are specific modulation beats of the signal characterizing the presence of a vortex around the moving particles of the flow gas phase. At the last eighth level of the 8-sensor signal approximation,a virtually smooth signal was obtained, the singularities of which are similar for the two sensors, and therefore simplify the function form of their mutual correlation to determine the velocity of the flow liquid phase.

Fig. 5 depict a graphical representation of one of two synchronously recorded acoustic signals samples from sensors mounted on a multiphase pipeline. These signals smoothing with the help of simple nonlinear trend algorithms, embeded into Excel package, indicates that the signal on one of the sensors is preceded by the analog signal on the second sensor. A more detailed analysis of these signals by wavelet decomposition methods allows to obtain information about the delays between its individual components. Based on this information, the conclusion is made about of the gas and liquid phase velocities.

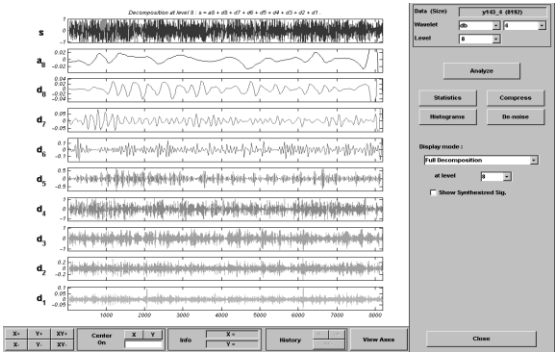

Fig. 4. Eight-tier wavelet decomposition of the implementation of the flow acoustic sensorsignal for gascondensate flow with the help of Debeshi discrete wavelets db4

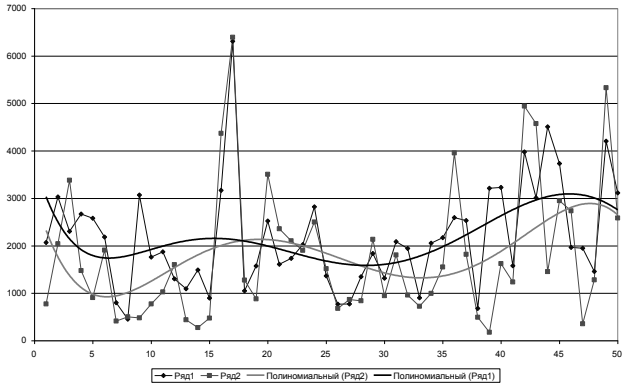

Fig. 5. The nature of the change in the acoustic signals of two sensors spaced 1 m along the pipeline with flow (with a power approximation)

Analysis of gas condensate wells' technological parameters, physical properties of well fluids, data of industrial measurements, mathematical modeling and experimental studies in the laboratory allowed developing a structural diagram (Fig. 6) and the design of individual units of the gas-liquid flow control device.

To determine the velocity of the flow gas phase, two groups of acoustic sensors, separated by a fixed distance on the pipeline, were used.

Consistently registering these signals by two groups of sensors and defining their cross-correlation function, the velocity of the gas phase flow is determined. The cross-correlation function of two differential pressure sensors is used to determine the velocity of the liquid phase flow.

Given that the specific gravity of the liquid phase is higher than the specific gravity of the gas at the in situ pressure, a change in the differential pressure perpendicular to the axis of the pipeline measured at two points makes it possible to measure the liquid phase flow velocity.

The basic parameter for the stratified flow structure is the fluid level that allows determining the fluid fraction in the flow.

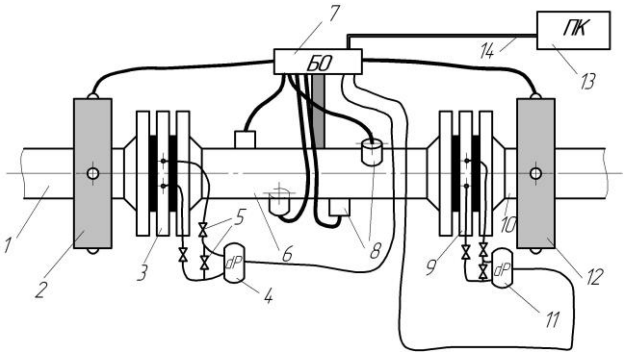

Fig. 6. Structural chart of the control device:

1- Inlet of the pipeline; *2,12* - first and second mounts of acoustic sensors; *3*, 9 - the press and the second insertion of the signals diversion for differential pressure sensors; *4, 11* - first and second differential pressure gauges; *5*- cranes assembly of pressure sensors; *6* - area of the water control sensor; *7* - block for gathering and primary processing of sensors information; *8* - electrodes' outputs of the water fraction sensor; *10* - outlet of the pipeline; *13* - personal computer

The design was developed and materials were selected which allowed to seal the sensor section at a pressure oup to 16.0 MPa.

According to its functions the device for controlling the flow structure and phase composition contains three blocks:

1) a block of primary converters;

2) a secondary unit of the device;

3) personal computer. The secondary unit of the control device is installed directly next to the unit of the primary converters of the measuring section, which is cut into the experimental line of the fishery. The analog and discrete signals from the sensors of the primary converter unit via armored cables are fed into the secondary unit of the device.

The results of the initial processing of information signals are transmitted through a four-wire cable line along the fishery cable trawl to a personal computer that is installed in the fishery operator's office.

Given that the length of the specified cable is about 100 m, the information interface RS-485 is selected. The connection via a standard Ethernet LAN connection to connect the PC to the top-level network was performed.

Conclusions

1. As result of complex analysis of studies of multiphase flows, the laws of signals' formation characterizing the phase composition and structure of gas-liquid flows of high-gas production wells are established, and scientific bases of new methods and means of controlling the flow phase composition in real time are developed:

the principles for increasing the information value of non-separable online methods for evaluation the phase composition of the well gas-liquid flow are formulated, which consist in combining a group of sensors of different physical nature of information signals' generation and complex algorithms of information processing;

a methodology for scientifically justified synthesis of methods for predicting and controlling the PhS&C of gas-liquid flow is proposed by a combination of hydrostatic, capacitive and acoustic methods, which provide the highest control accuracy for flows with high void fraction (>95% by volume). The methodology is focused on obtaining information on the structure and individual flow phase rates at high values of gas fraction and flow overpressure of the production wells in order to optimize production and provide flow monitoring for each well in real time.

2. As a result of experimental studies of gas-liquid flow motion, for the first time, a method of current flow separation into phases by placing the sensor - the coaxial-type capacitor in the extended part of the pipeline, was developed to determine the water fraction of the high gas fraction flows. This provided a significant increase in the sensitivity of the impedance method for determining the water fraction of the liquid phase due to the fact that the gas phase is moved inside the inner capacitor coatings and the liquid phase - outside, between the coatings and the inner surface of the pipe, which is also a component of the capacitive sensor.

3. As a result of experimental studies the gas-liquid flows movement, a methodology and procedures for identifying the structure of a gas-liquid flow in real time were developed based on the symbolization of measuring signals implementation and the subsequent recognition of symbolized images of the flow structure by using artificial neural networks. In contrast to existing methods, this makes it possible to adapt the methodology for determining the flow phase composition correctly to the actual flow conditions

existing in the pipeline

4. In accordance with the proposed methodology, original methods for obtaining data on the phase composition of multiphase flows with high gas fraction were developed. By their information value, these methods exceed the known or make it possible to obtain information about the phase composition and flow structure previously unavailable:

the method was developed, based on the determination of gas and liquid phase velocities taking into account the results correlation processing for wavelet decomposition acoustic signals realizations, generated by the flow. This makes it possible, in the presence of phase information in the pipeline section, to provide a current non-separable determination of the flow rates of the either flow liquid or gas phases;

the current hydrostatic method of controlling the structure and volume fraction of the gas-liquid flow phases is improved, which differs from the existing hydrostatic methods in that the measurements are made without changing the flow regime by measuring pressure differential component that is perpendicular to the flow in the pipeline cross-section. This allows real-time determination of phase fraction in a horizontally oriented pipeline without preliminary flow separation;

References

1. **Hall, A.R.W**. (1992). Multiphase flow of oil, water and gas in horizontal pipes: Dissertation PhD Thesis: **Hall A.R.W**,.- Imperial College, London, UK..

2. **Kremlevskyi P.P.** (1989). Raskhodomery y schetchyky kolychestva: Spravochnyk. /**P.P.Kremlevskyi** – L.:Mashynostroenye.- 701 s.

3. **Malinowsky** (1975). M.S. An experimental study of oil-water and air-oil-water flowing mixtures in horizontal pipes./**Malinowsky, M.S**.// Dissertation: MS Thesis, The University of Tulusa, US.

4. **Mamaiev V.A.** (1969) Hydrodynamyka hazozhydkostnыkh smesei v trubakh. /**V.A.Mamaev, H.Э.Odysharyia, N.Y.Semenov** y dr.- M.: Nedra,- 208s.

5. **S.M.Stetsiuk**, (2009) Prohramnyi kompleks GAZSTRUM yak vitchyzniana alternatyva inzhenernoho metodu rozrakhunku dvofaznykh potokiv /**S.M.Stetsiuk, I.I.Kaptsov, O.V.Bobruk, V.V.Sobol** // Zb. Nauk. prats. Pytannia rozvytku hazovoi promyslovosti Ukrainy. Vyp.XXXVII, 2009 – P.280-287.

6. **Andreussi P, Di Donfrancesco A, Messia M,** (1988) An impedance method for the measurement of liquid holdup in two-phase flow Int. J. Multiphase Flow 14 777

7. **Mehdizadeh, P., Ghaempanah and S.L.Scot**t: “Impact of Data Quality on Production Allocation and Reserves Forecasting”, paper presented at the SPE ATCE, San Antonio (Sept. 24-27, 2006)

8. **Falcone G.** (2009). Multiphase Flow Metering: Principles and Applications / **G. Falcone G., G. F. Hewitt, C. Alimonti**. - London: Elsevier Science.: (Developments in Petroleum Science, 54). - : 978-0-444-52991-6.

9. **E.S. Johansen, A.R.Hall, J.H.Unalmis, D.J.Rodriguez, A.Vera, V.Ramakrishnan**, (2007). A prototype wet-gas and multiphase flowmeter: Weatherford Intl., BP Exploration&Production // 25-th International North Sea Flow Measurement Workshop, 16th-19th October 2007. - Glasgo, 2007. - P.1-16.

10. **Falcone, G.** (2006). Modelling of flows in vertical pipes and its application to multiphase flow metering at high gas content and to the prediction of well performance: [Текст] Ph.D. thesis in Chemical Engineering / Gloria Falcone; Imperial College. - London.

11. **Hewitt, G.F.** (2005). Three-phase gas–liquid–liquid flows in the steady and transient states / **G.F. Hewitt** // Nuclear Engineering and Design. - 2005. - 235. - P.1303–1316.

12. **Xie,** (2006). Measurement of multiphase flow water fraction and water-cut / **Xie, Cheng-Gang** // Proc. 5th Int. Symp. on Measurement Techniques for Multiphase Flows (5th ISMTMF), Dec. 11-14: - Macau, China, 2006. - vol. 914. - P.232-239.

13. **Gudmundsson J.S**. (1999). Gas-liquid metering using pressure-pulse technology: SPE Annual Technical Conference and Exhibition, Houston, Texas, Oct. 3-6, 1999 / J.S.Gudmundsson; Norwegian University of Science and Technology, Trondheim. - Houston, Texas, 1999. - SPE 56584. - 10p.

14. **Corneliussen, S., Couput, J., Dahl, E., Dykesteen, E., Frøysa, K., Malde, E., Moestue, H., Moksnes, P.O., Scheers, L., Tunheim, H**., (2005). Handbook of Multiphase Flow Metering, Revision 2, The Norwegian Society for Oil and Gas Measurement and The Norwegian Society of Chartered Technical and Scientific Professionals, March 2005.

15. **Vilagines, R., Hall, A.R.W.,** (2003). Comparative Behaviour of Multiphase Flowmeter Test Facility, // Oil and Gas Science and Technology, Rev. IFP, Vol. 58 (2003), No. 6, pp. 647-657

16. **Haojiang Wu,** (2001). Intelligent identification system of flow regime of oil-gas-water multiphase flow / **Haojiang Wu, Fangde Zhou, Yuyuan Wu** // International Journal of Multiphase Flow - Vol. 27. – 2001.- P.459-475.

17. **Teniou S.,** (2011). Multiphase Flow Meters Principles and Applications: A Review / **Samir Teniou**, Mahmoud Meribout //Canadian Journal on Scientific and

Industrial Research. -Vol. 2, No. 8. - November 2011. P.290-293.

18. **Whitaker T. S.,** (2005). A review of multiphase flowmeters and future development potential. / **T. S. Whitaker** - Proc. 6th Int. Conf. FLOMEKO, Seoul, Korea, Oct. 2005 - P. 628–634.

19. **Chaoki J.,** (2006). Non-Invasive Monitoring of Multiphase Flows. / **J. Chaoki, L. Larachi, and M. P. Dudokovi**c. - Amsterdam, The Netherlands: Elsevier.

20. **Bom V. R.,** (2001) Accuracy aspects in multiphase flow metering / **V. R. Bom, M. C. Clarijs, C. W. E. van Eijk, Z. I. Kolar, J. Frieling, L. A. Scheers, and G. J. Miller** //IEEE Trans. Nucl. Sci.. - vol. 48, no. 6. - Dec. 2001. -P. 2335–2339.

21. **Raiter P.M.** (2009). Metody ta zasoby obroblennia informatsii dlia kontroliu struktury ta vytraty faz hazoridynnykh potokiv: [Tekst]: monohrafiia / P.M.Raiter, O.M.**Karpash**; Ivano-Frankiv. nats. tekhn. un-t nafty i hazu. - Ivano-Frankivsk: Vydavnytstvo IFNTUNH, 2009. - 262s.- ISBN 978-966-694-114-8.

22. **Raiter P.M.** (2009). Vyznachennia shvydkostei faz hazoridynnoho potoku sverdlovyny na osnovi koreliatsiinoho analizu veivlet peretvoren datchykiv akustychnykh syhnaliv potoku: [Tekst] // Neruinivnyi kontrol materialiv i konstruktsii: Zb. nauk. prats. - Lviv: Fizyko-mekhanichnyi instytut im. H.V. Karpenka NAN Ukrainy, 2009. - vyp.14. - S.13-21 – (Seriia "Fizychni metody ta zasoby kontroliu seredovyshch materialiv ta vyrobiv" ; vyp.14).

23**. Raiter P.N**. (2010).Ydentyfykatsyia strukturы y opredelenye raskhoda faz hazovodoneftianoho potoka skvazhynы: [Elektronnyi re¬surs] // Neftehazovoe delo: Elektronnyi nauchnyi zhurnal. – Ufa: 2010. - №2 (1010). - S.1-15. - http://www.ogbus.ru/authors/Raiter/Raiter_1.pdf .

24. **Raiter P.M.** Vykorystannia veivlet-peretvorenn syhnaliv fluktuatsii tysku hazoridynnoho potoku pry realizatsi neiromerezhevykh prystroiv kontroliu yoho struktury: //Elektromahnitni ta akustychni metody neruinivnoho kontroliu materialiv ta vyrobiv: Zb. nauk. prats. - Lviv: Fizyko-mekhanichnyi instytut im. H.V. Karpenka NAN Ukrainy, 2004. - S.101-107.: (Seriia "Fizychni metody ta zasoby kontroliu seredovyshch materialiv ta vyrobiv" : vyp.9).

CONTROL AND REGULATION OF THE NATURAL-SPATIAL LOCATION OF THE VARIABILITY OF THE CONTENT OF QUALITATIVE AND TECHNOLOGICAL INDICATORS OF MINERALS IN THE ARRAY AND LOOSE IRON ORE MASS

Sholokh M.V.
PhD (Engineering), Associate Professor,
Kryvyi Rih National University, Ukraine

Summary

Object of research. The estimation of mean value of the naturally-spatial placing of changeability of content of quality indexes in the bowels of the earth is based on research of changeability of description of signs, analysis of ore-mining geometrical parameters of blocks, areas of ore body and bed of deposit of ferrous quartzites and network of reconnaissance mining holes. For the regular networks of assay of the naturally-spatial placing of changeability of content of quality indexes of minerals in the array of balance-industrial supplies the calculations of coefficients are conducted in good time for the most tyFigal configurations of mutual location of block and tests that participate in an estimation.

Methodology of researches. This estimation of annual and perspective plans of development of mountain works taking into account the dynamics of changeability of qualitatively-technological descriptions of signs of the naturally-spatial placing of changeability of content of qualitatively-technological indexes of minerals in an array and loosening iron-ore mass at moving of mountain works both on reaching and on the depth of quarry.

Purpose and research problems. The brought main stages over of research of determination of volume of block of balance-industrial supplies of different after configuration of taking blocks from the angle of slope of planning position of cuts and distance between them.

Devices are considered for the operative assay of the naturally-spatial placing of changeability of content of qualitatively-technological indexes of minerals in an array and loosening iron-ore mass at implementation of mountain works in the mode of average of content of qualitatively-technological indexes of minerals in iron-ore mass on ore mining and processing combines of Krivbass.

Keywords: ferrous quartzites, content of qualitatively technological indexes, mountain works.

Introduction

At development of annual and perspective plans of development of mountain works the dynamics of the naturally-spatial placing of changeability of content of qualitatively-technological indexes of min-

erals is taken into account in an array and loosening iron-ore mass at moving of mountain works on reaching and on the depth of quarry.

Within the framework of general conception of management of the prepared products qualitatively technological indexes from positions of approach of the systems construction of the system of surveyor-geological management naturally-spatial placing of changeability of content of qualitatively-technological indexes of minerals in an array and loosening iron-ore mass is based on principles [1-4]:

- to the management unbreak naturally-spatial placing of changeability of content of qualitatively-technological indexes of minerals in an array and loosening iron-ore mass and by volume of producing of the prepared products;
- to the management complexity on functions, tasks and informative providing;
- to unity of management process on all cycle of forming of the naturally-spatial placing of changeability of content of qualitatively-technological indexes of minerals in an array and loosening iron-ore mass from planning to the consumption;
- standardizations of the naturally-spatial placing of changeability of content of qualitatively-technological indexes of minerals in an array and loosening iron-ore mass as to the means of management.

Establishment of conformities to law of changeability of content of qualitatively-technological indexes of minerals in iron-ore mass and determination of limits of oscillation on the different areas of ore body and bed of iron-ore deposit on a career will allow clearly and reasonably to plan direction of development of mountain works, stabilize content of qualitatively-technological indexes of minerals in iron-ore mass and improve the technical-economical indexes of work of ore mining and processing combine [5-7].

Coming from the requirements of mountain production and functions of surveyor-geological departments on the content management of qualitatively-technological indexes of minerals in iron-ore mass embrace practically all complex of tasks, have connection with planning and planning of mountain works, directly with the booty of balance-industrial supplies in the process of development of areas of ore body and bed of iron-ore deposit up to shipping of commodity iron-ore mass on an ore mining and processing factory [8-10].

1. Determination of influence of different configurations of figures of blocks of balance-industrial supplies on exactness of count of volumes taking into account the angle of slope of cuts and distance between them

Successful increase of rates of booty of balance-industrial supplies from the areas of ore body and bed of iron-ore deposit by open, underground or combined methods, the use of the newest measuring devices, high-performance equipment and computer providing on the ore-mining enterprises of Ukraine begins to dictate certain requirements and to change out-of-date methodologies. Availability and development to the proper level of the computer providing it is allowed to use them in a sufficient amount by every worker in a surveyor department. It gave possibility to automatize workaday tasks that is executed by the workers of surveyor department at cameral treatment of the field measuring. Among main problems that must be decided there is a question of count and account of volumes of mountain works balance-industrial supplies subject to condition the use of the geographic information systems, namely, what methods of count to use for providing of necessary exactness, comfort of the use and reduction to time on implementation of works.

In the method of parallel vertical cuts, that was chosen as base for modernization as most suitable for this aim and besides sufficiently widespread there are a few problem questions on a production. Among that it is necessary to pay attention to impossibility to count up volumes at the difficult after configuration excavation blocks of balance-industrial supplies. It is impossible optimally to dispose a line athwart to that build cuts, not in contempt of here condition of parallelism, as an optimal liking of fragments of line is for separate parts of block balance-industrial supplies does not lie on one line. From other side of the use of one line, subject to condition presently actual distances between cuts results in the increase of errors at a count.

Known is a situation, when on occasion projects position of line for cuts clearly set. After such location of cuts it comfortably to count a few figures with possibility them permanent accumulation or implementation of different variants of count of balance-industrial supplies, for example for the different intervals of time. However due to it a possible origin of variants is with the considerable loss of exactness.

Mainly an error arises up in the cases when the blocks of balance-industrial supplies or their part are located not athwart to the cuts, but along or under a corner near to it. As here between cuts ponder able changeabilities of configuration of contours of block of balance-industrial, a supply that is counted up are possible, and the general volume of part of block of balance-industrial supplies between nearby cuts is calculated with an impermissible error.

One of decisions in this situation there is addition of intermediate cuts diminishing distance the same between cuts and due to it error of count balance-industrial supplies diminishes [13].

Being base on these cases will pull out supposition about the use of one arbitrary direction of location of cuts in the method of parallel vertical cuts at reduction to the necessary level of distance between nearby cuts. If to define optimal distance between cuts, at the use of that oscillation of volumes of balance-industrial supplies will be insignificant at any direction of location of cuts.

The stage of being of optimal location of direction of cuts can be dropped for be what count within the limits of booty of balance-industrial supplies from the area of ore body and bed of iron-ore deposit for be what ore-mining enterprises. Simplification of process of count and account of volumes of mountain works will take place thus.

To the lacks of it is possible to take plenty of cuts got as a result. At the hand working does this method impossible at the use in practice. However with the use of his in the geographic information systems on modern computer technologies this defect disappears.

For research of behavior of size of volume of block of balance-industrial supplies from two factors of angle of slope of planning position of cuts and size of distance between them an experimental block was modeled [23]. Through the centre of gravity of block in plane *X*; *Y* and in parallel there was the conducted line the landmark of *Y* athwart to that cuts were separately built through 20 meters. The calculation of volume of block of balance-industrial supplies, that consisted of forming of report, was conducted, with calculations (table 1) and the built cuts in a corresponding scale (Fige 1), for possibility of hand verification of the got results [24]. A next step is calculate the same block of balance-industrial supplies with distances between cuts 20 м. Line athwart to that begin to build cuts is situated in parallel to the landmark of *X*.

Table 1

Calculation of volumes by the method of parallel vertical cuts with distance between them a 20 m

Number of the first cut	Area of the first cut, м^2.	Number of the second cut	Area of the second cut, м^2	Distance between cuts, м	Volume, м^3
1	0,00	2	201,77	16,87	1134,39
2	201,77	3	247,67	20,00	4486,61
3	247,67	4	223,37	20,00	4708,27
4	223,37	5	237,70	20,00	4609,96
5	237,70	6	256,99	20,00	4945,66
6	256,99	7	279,48	20,00	5363,07
7	279,48	8	256,65	20,00	5359,62
8	256,65	9	266,57	20,00	5231,91
9	266,57	10	236,68	20,00	5029,62
10	236,68	11	40,71	20,00	2503,68
11	40,71	12	0,00	6,82	92,51
General volume:					43465,31

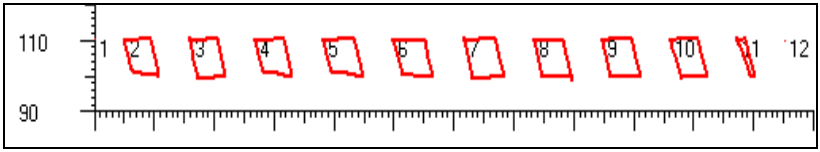

Fig. 1. Calculation of volume of block of balance-industrial supplies by the method of parallel vertical cuts at distance between them 20 м

Got from a report after described before by a template results will be compared to previous. The volume of block is calculated where the corner of planning position of cuts equals middle from two previous.

Analyzing the results of previous calculations the turn of line of cuts proceeds in a plan thus, that a line in relation to the centre of gravity returned after motion of hour-hand on one degree. Calculations recurred while a line was not returned on 180°. All possible variants of count of volumes of block of balance-industrial supplies were taken into account the same. At first the sizes of volumes of block of balance-industrial supplies were calculated at distance between cuts 20 м. Farther for verification of the higher described supposition diminished to distance between cuts to 10; 5; 2 and a 1 m [24].

Further reduction of distances did not give a substantial difference at these sizes of volumes of block of balance-industrial supplies. Re-

search of dependence is completed by the calculation of volume of block of balance-industrial supplies at distances between cuts 1 m.

For every count of volume of block a report that contains a table with data of numbers of cuts of areas and volume of block of balance supplies of areas between two cuts was formed.

From these data the graphic arts of dependences, that specifies on that the angle of slope of cuts loses a substantial role at reduction of distances between cuts to the optimal value, are built.

For example for the chosen block of balance-industrial supplies it is expedient to use distance between cuts, that 1 м. equals Making sure is herein possible even by sight considering the compatible chart of dependence of size of volume of block of balance-industrial supplies, that is counted up from the corner of line of reaching of cuts at the different values of distance between cuts. Line that equals a 20 m has most error of size of volume of block of balance-industrial supplies and impermissible for the use of arbitrary corner. Impermissible and next lines that answer distances 10; 5 and 2 m.

Comparing them there is a tendency to straightening of line on the mark of faithful volume of balance-industrial supplies. Lines do not almost differ one from other, and have an identical value of volume of block of balance-industrial supplies at all variants of angle of slope that confirms our supposition. A line has the least deviation from the real volume of block of balance-industrial supplies and that is why distance between cuts in a 1 m used for the arbitrary planning corner of location of cuts.

For determination of influence of different configurations of figures of blocks of balance-industrial supplies on exactness of count of volumes on the career of ПрАТ «Inhuletskyi ГЗК», three varieties of taking blocks were chosen on different horizons: the event is prolate, with the rounded configuration and the combined variant (Fig. 2) [24]. The volume of different configurations of blocks of balance-industrial supplies was determined at the different values of distance between cuts and anything of corner of line of reaching of cuts [3]. The results of direct configuration of block with authority did not differ from the results of the volume of block of balance-industrial supplies created for research of size from influence of planning location of cuts and distances between them. For the taking block of balance-industrial supplies of round configuration, after before they got results are

erected the described methodology in a table. By the aim of comparison of data and statistical analysis for determination and estimation of exactness undertaken studies. Analogical actions are created for the block of balance-industrial supplies with protuberant configuration.

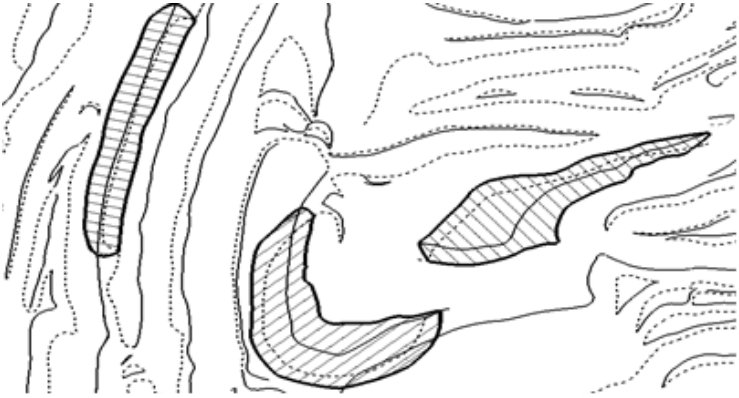

Fig. 2. Configurations of taking blocks of balance-industrial supplies are with crossing for the count of volumes

Comparison of results of the taking blocks of balance-industrial supplies got after different configurations took place after ore-mining geometrical graphic arts. From the analysis of charts come to the conclusion about the use of arbitrary direction of location of cuts in a plan.

Possibility of the use of methodology of count of volumes of balance-industrial supplies is confirmed for different configurations of blocks. Researches wer executed and for the terms of other quarries of Ukraine, that confirmed previous results.

Thus, at reduction to distance between cuts to the optimal value it is possible to use arbitrary direction of planning location of cuts. For comfort of the use and choice of only direction, and for the removal of misunderstanding at the choice of different directions it is recommended to use a northward.

2. Control and adjusting of the naturally-spatial placing of changeability of content of qualitatively-technological indexes of minerals are in an array and loosening iron-ore mass

Increase of qualitatively-technological indexes of the prepared products - one of basic problems of modern science, technique and

all national economy. The increase of level of qualitatively-technological indexes of the prepared products assists the increase of volume of realization of the prepared products and increase of profitability of production. The quality indexes of the prepared products are mortgaged at planning and provided in a production and supported in exploitation. Within the framework of general conception of management of the prepared products quality indexes from positions of approach of the systems construction of the system of the surveyor providing of works for a management naturally-spatial placing of changeability of content of qualitatively-technological indexes of minerals in an array and loosening iron-ore mass is based on next principles [3]:

- to the management unbreak naturally-spatial placing of changeability of content of qualitatively-technological indexes of minerals in an array, loosening iron-ore mass and by volume of producing of the prepared products;
- standardizations of the naturally-spatial placing of changeability of content of qualitatively-technological indexes of minerals in an array and loosening iron-ore mass as to the means of the management;
- to unity of management process on all cycle of forming of content of qualitatively-technological indexes of minerals in iron-ore mass from planning to the consumption;
- to the complexity of the surveyor providing of works for a management on functions, tasks and informative providing.

Control of technological processes of booty and magnetic separation of minerals in iron-ore mass is one of important measures, by means of that support of rhythm of processes is arrived at the maximally possible productivity and set qualitatively-technological indexes of magnetic separation. In order that the checking system was effective, information about content of qualitatively-technological indexes of minerals in iron-ore mass must be clear, objective, operative and exhaustive.

Concentration of production and continuous increase of volumes of booty of balance-industrial supplies and exception of content of qualitatively-technological indexes useful to the component, related to magnetite in iron-ore mass on an ore mining and processing combine, stipulates, necessity of development of new and perfection of existent

methods and technical equipments of assay and control of content of qualitatively-technological indexes of minerals for iron-ore mass.

On Inguletc, Central, North and other ore mining and processing combines the physical methods of assay and control of the naturally-spatial placing of changeability of content of qualitatively-technological indexes of minerals are inculcated in an array and loosening iron-ore mass at operating secret service and geological providing of booty of balance-industrial supplies (Fig. 3) [3].

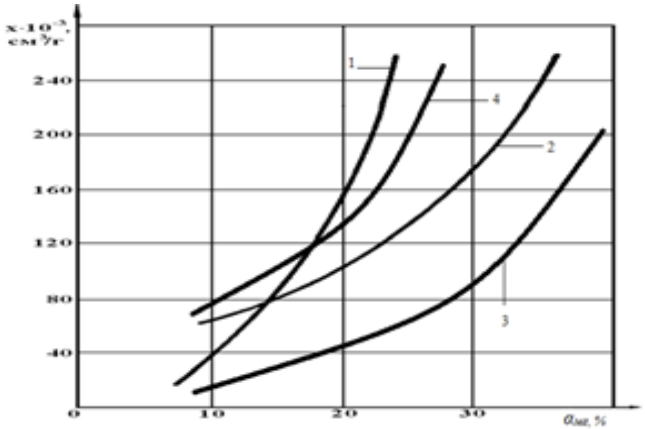

Fig. 3. Dependence of magnetic perception of the naturally-spatial placing of changeability of content of quality indexes of minerals in loosening iron-ore mass from content of quality indexes useful to the component, related to magnetite, on the deposits of Krivbass: *1* - Inhuletskyi; *2* - Skelewativske; *3* - Large Gleuwatka; *4* – Gannivske

Works, from introduction of geophysical methods of assay of content of qualitatively-technological indexes of minerals in iron-ore mass, on ΠpAT «Inhuletskyi ГЗК» conducted on a career on extractive coalfaces. By means of apparatus of *PCP*-3 and *МФ*-2 determination of content of qualitatively-technological indexes is executed useful to the component, related to magnetite in iron-ore mass (general and magnetite). Measuring in a coalface comes true for the networks of supervisions a 1^x1 m at the double measuring in points. Error of assay of content of qualitatively-technological indexes useful to the component, related to magnetite not exceeds 1 %. In the chemical laboratory of ore mining and processing combine for determina-

tion of content of losses of content of qualitatively-technological indexes useful to the component, related to magnetite the device of construction of institute of *НДІАЧермет* is used in the tails of magnetic separation, and for determination of content of qualitatively-technological indexes useful to the component, related to magnetite in loosening iron-ore mass - *АЖР*-1 [3].

On Hleiuvatskyi career of ПрАТ «Central ГЗК» with the use of apparatus of *КМВ*-3 logging of буровибухових mining holes is executed. Error of determination of content of qualitatively-technological indexes useful to the component, related to magnetite in boring sludge's that is got a magnetometer method, in comparing to the error of chemical analysis folds ±1 % [3].

The assay of loosening mountain mass comes true with the use of apparatus of *РИМВ*-1 (for the unoxidized minerals) and to the complex of devices of *РСР*-3 and *МФ*-2 (for simultaneous determination general and useful of magnetite to the component). For express-analyze of the powder-like masses, in laboratory terms, worked out and magnetometer scales are successfully used.

On Hannivskyi and Pershotravnevnyi careers of ПрАТ «Pivnichnyi ГЗК» logging of blast holes, comes true with the use of device of *КМВ*-3, point determinations of the naturally-spatial placing of changeability of content of qualitatively-technological indexes of minerals in an array are executed through a 50 cm on the depth of mining hole. Testimony to the device, translated in content of qualitatively-technological indexes useful to the component, related to magnetite after the chart of cross-correlation dependence (r=0,956) [3].

Assay naturally-spatial placing of changeability of content of qualitatively-technological indexes of minerals in an array on blast holes on Pershotravnevnyi quarry of ПрАТ «Pivnichnyi ГЗК» comes true by geophysical methods.

Divergences in determination of content of qualitatively-technological indexes useful to the component, related to magnetite, by means of logging, with the results of control chemical analyses of boring sludge's does not exceed 1-1,5 %.

For determination of content of qualitatively-technological indexes of minerals in loosening iron-ore mass, in laboratory terms, on ПрАТ «Pivnichnyi ГЗК» the apparatus of *АЖР*-1 is used (Fig. 4.) [3].

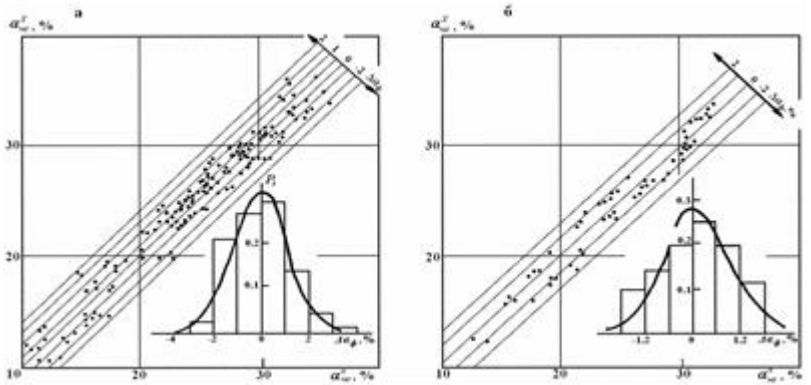

Fig. 4. Comparison of results of assay of the naturally-spatial placing of changeability of content of quality indexes of minerals in an array and loosening iron-ore mass by magnetometer and chemical methods on careers: *a* - ПрАТ «Inhuletskyi ГЗК», *b* - ПрАТ «South ГЗК»

Thus, there are devices that allow operatively with an error that fully satisfies to the requirements of production, to determine content of qualitatively-technological indexes useful to the component, related to magnetite in iron-ore mass. Use of different technical equipments for the receipt of operative information about content of qualitatively-technological indexes useful to the component, related to magnetite in iron-ore mass, does not decide a task forming and surveyor providing of works for a management content of qualitatively-technological indexes useful to the component, related to magnetite in iron-ore mass in the process of booty of balance-industrial supplies and exception of content of qualitatively-technological indexes useful to the component, related to magnetite in iron-ore mass.

Necessary development and introduction on the ore mining and processing combines of the system of the surveyor providing of works for control and management the naturally-spatial placing of changeability of content of qualitatively-technological indexes of minerals are in an array and loosening iron-ore mass.

On the base of modern methods of analysis and technical equipments, in time reliable information turns out about content of qualitatively-technological indexes of minerals in loosening iron-ore mass. On this basis to forecast, operatively to regulate and influence on quality of productive processes of booty of balance-industrial sup-

plies and exception of content of qualitatively-technological indexes useful to the component, related to magnetite in iron-ore mass.

The inalienable constituent of the system are effective methods of economic stimulation of increase of qualitatively-technological indexes of the prepared products. On ore mining and processing combines the scientifically reasonable structures of service and norms of quantity of technical and engineering employees, that carry out control and management naturally-spatial placing of changeability of content of qualitatively-technological indexes of minerals in an array and loosening iron-ore mass in the process of booty of balance-industrial supplies and exception of content of qualitatively-technological indexes useful to the component, related to magnetite in iron-ore mass, are absent. To Volume, these questions, in different there are degrees force to occupy technical and engineering employees of different productive subdivisions. Worked out Automated control system of the surveyor providing of works for a management a quarry, organization of management naturally-spatial placing of changeability of content of qualitatively-technological indexes of minerals in an array and loosening iron-ore mass comes true by such method. Planning of ore-mining technological works is on a career, taking into account descriptions of the naturally-spatial placing of changeability of content of qualitatively-technological indexes of minerals in an array and loosening iron-ore mass [3].

Adjustment of the separate stages of planning, conducted with the use of computer technologies. The analysis of productive situation is preceded the process of correction for the past stage of planning of content of qualitatively-technological indexes of minerals in loosening iron-ore mass. Results of analysis, determine a necessity and size of adjustment of the level of planning of content of qualitatively-technological indexes of minerals marked below for loosening iron-ore mass. Initial information that is needed for drafting of the productive program of *i*-ro level of planning of content of qualitatively-technological indexes of minerals in loosening iron-ore mass comes on the computer center of combine. The results of decision are passed in a technical department, where a rightness and acceptability of the got results are checked up.

For the increase of efficiency of magnetic separation the operative surveyor providing of works comes true for a management content of

qualitatively-technological indexes of minerals in loosening iron-ore mass during a change. It is explained that in the process of work of quarry, arise up different family indignations, that is expressed in changeabilities of mining-and-geological and mining-and-technical terms, that violates plan of change on content of qualitatively-technological indexes of minerals in iron-ore mass.

For support in the set limits of the productivity and content of qualitatively-technological indexes of minerals in iron-ore mass of total stream from a quarry, operative intervention is needed in work of extractive and transport equipment during a change.

At creation of the technical system checking and surveyor providing of works for a management technological processes in a career with the use of facilities of the computing engineering next functions are executed [3]:

- operative control and communication of data come true in control system about content of qualitatively-technological indexes of minerals in loosening iron-ore mass on the coalfaces of booty of balance-industrial supplies and sections of composition of averegenation of content of qualitatively-technological indexes of minerals in iron-ore mass;

- the state of extractive power-shovels is controlled during a change (free, worker, accident);

- control comes true and follows work of power-shovels and motor transport, id est the route of motion empty to autotipper is determined;

- mass of the transported minerals in iron-ore mass, t;

- content of qualitatively-technological indexes of the transported minerals in loosening iron-ore mass %;

- productivity of each autotipper, t·kilometre;

- productivity of every power-shovel, т/hour;

- an unloading (crush factory, composition of averegenation of content of qualitatively-technological indexes of minerals in loosening iron-ore mass) place is appointed;

- content of qualitatively-technological indexes of minerals is controlled in loosening iron-ore mass (%) that comes on an ore mining and processing factory.

Except technical equipments, considered chart of Automated control system of management a quarry, that has the specialized compu-

ting device that intended for the decision of task of the operative planning and corrections volumes of booty of balance-industrial supplies on coalfaces taking into account content of qualitatively-technological indexes of minerals in loosening iron-ore mass, and also, for a management work of transport [3].

Inwardly a variable management a transport and extractive equipment is executed on the basis of results of the operative variable planning of content of qualitatively-technological indexes of minerals in iron-ore mass. After it, time of change, broken up on j of even intervals of management for t minutes each.

Coming from distribution of variable volumes of minerals in iron-ore mass on extractive coalfaces, in the calculation of volumes of qualitatively-technological indexes of minerals in loosening iron-ore mass, that must be shipped from every power-shovel at the t minutes of management, is executed the specialized computing device.

The results of decision are added to block-memory of machine during a change. They are planovimi indexes for every interval of the surveyor providing of works for a management naturally-spatial placing of changeability of content of qualitatively-technological indexes of minerals in an array and loosening iron-ore mass.

3. Management a transport and extractive equipment, with an aim, in iron-ore mass comes stabilizing of content of qualitatively-technological indexes of minerals true by such method

At an entrance in a quarry empty autotipper by means of transmission device reports his number in a transmitter-receiver that is located under linen of way that passes him in block-memory of the specialized computing device. To information that came from the device of the periodic questioning of power-shovels specifies where a free power-shovel and his number are is illuminated on a light board. In accordance with it to the number, driver of autotipper chooses the route of motion.

For control and account of work of mine transport complex fixing of numbers of autotipper and power-shovel to that he is sent is executed in block memory of machine. At departure from a quarry loaded autotipper passes a device that determines the weight and transmitter-receivers, where weighing of mountain mass that are transported, and fixing of number of autotipper is conducted.

They got information is passed in the specialized computing device, where on the number of autotipper to block memory of the specialized computing device the number of extractive power-shovel that executed loading and content of qualitatively-technological indexes of minerals is determined in the shipped iron-ore mass, is added.

After it, on a light board the place of unloading of machine (a crush corps or composition of averegenation of content of qualitatively-technological indexes of minerals is in loosening iron-ore mass) is specified.

For every interval of management in verification of implementation of plan tasks is conducted the specialized computing device on content of qualitatively-technological indexes of minerals in iron-ore mass and volumes of booty of balance-industrial supplies.

If quality indexes and volume of minerals in iron-ore mass in a total stream in j management interval answer plan indexes, all autotipper in (*j*-1) the th interval of management head for unloading in a crush corps.

In case of changeability of productive situation in a career (abrupt end of one or a few power-shovels, salutatory changeabilities of content of qualitatively-technological indexes of minerals in iron-ore mass in i-ohm coalfaces) in the redistribution of volumes of booty of balance-industrial supplies is conducted the specialized computing device on power-shovels. Thus, one or a few sections of composition of averegenation of content of qualitatively-technological indexes of minerals in iron-ore mass (depending on his volume) are accepted as additional extractive coalfaces.

For determination of actual content of qualitatively-technological indexes of minerals in iron-ore mass that comes on an ore mining and processing factory, on a conveyer ribbon the sensor of continuous determination of percent exception of content of qualitatively-technological indexes is set useful to the component, related to magnetite in commodity iron-ore mass. Given about content of qualitatively-technological indexes of minerals in loosening iron-ore mass in the process of change come on controller's point.

Thus, Automated control system over of the surveyor providing of works is brought for a management on a career, allows to do the optimal forming and management naturally-spatial placing of changeability of content of qualitatively-technological indexes of

minerals in an array and loosening iron-ore mass on all stages of planning of mountain production and his management on a career. The further forming of content of qualitatively-technological indexes of minerals in iron-ore mass takes place on an ore mining and processing factory.

In accordance with the technological indexes of magnetic separation, at every level of planning, requirements are set to content of qualitatively-technological indexes of minerals in commodity iron-ore mass on the next stage of planning of mountain works. This same, a feed-back comes true between the process of magnetic separation and mining production.

Practical possibility to do, allows operative control and assay of the naturally-spatial placing of changeability of content of qualitatively-technological indexes of minerals in an array and loosening iron-ore mass and foods of magnetic separation physical methods [3]:

- to give up the out-of-date form of control and pass to more progressive systems checking and surveyor providing of works for a management the naturally-spatial placing of changeability of content of qualitatively-technological indexes of minerals in an array and loosening iron-ore mass;

- to simplify technology inwardly quarry averegenation due to the rational working off power-shovel blocks with the account of even and proportional distribution to the booty of high-quality technological and balanced on maintenance qualitatively-technological indexes minerals of supplies during the planned period;

- as a result of increase of operation ability of receipt of information to bring down in the process of booty the losses of balance-industrial supplies and obstructions of content of qualitatively-technological indexes of minerals in loosening iron-ore mass;

- to promote authenticity, evidentness and operation ability of information about the naturally-spatial placing of changeability of content of qualitatively-technological indexes of minerals in an array and loosening iron-ore mass that allows to intensify introduction of automated systems of the surveyor providing of works for a management mining works on a career.

For the construction of more flexible system of the surveyor providing of works for a management naturally-spatial placing of changeability of content of qualitatively-technological indexes of

minerals in an array and loosening iron-ore mass, expediently, on enterprises to distinguish independent productive subdivision, that is responsible for planning, forming and control of content of qualitatively-technological indexes of minerals in iron-ore mass.

Conclusion

1. The model of the naturally-spatial placing of changeability of content of qualitatively-technological indexes of minerals built after this algorithm in the array of areas of ore body and bed of iron-ore deposit is used for the count of balance and industrial supplies, optimal planning of mining enterprise, and also corporate strategic and medium-term planning of mountain works on an operating enterprise.

2. The brought main stages over of research of determination of volume of block of balance-industrial supplies of different after configuration takeout blocks from the angle of slope of planning position of cuts and distance between them. Reduction to distance between cuts to the optimal value is used arbitrary direction of planning location of cuts. For comfort of the use and choice of only direction, and for the removal of misunderstanding at the choice of different directions it is recommended to use a northward.

3. Automated control system of management is on a career, allows to do the optimal forming and management naturally-spatial placing of changeability of content of qualitatively-technological indexes of minerals in an array and loosening iron-ore mass on all stages of planning of mountain production and his management in a career.

4. Perspective devices that are intended for the operative assay of the naturally-spatial placing of changeability of content of qualitatively-technological indexes of minerals in an array and loosening iron-ore mass at implementation of mountain works in the mode of averegemant of content of qualitatively-technological indexes of minerals on the ore mining and processing combines of Kryvbas are considered.

References

1. Uniform rules for the protection of mineral resources in the development of solid mineral deposits. (1987). M., Nedra.

2. Collection of guidelines on the protection of mineral resources (1973). - M., Nedra.

3. **Adigamov Y.M., Mining C.Z. (**1987). Rationing of loss of minerals in the extraction of ores. M., Nedra.

4. **Sholokh M.V.** (2016). Methods of assigning i normuvvnya to the side of the alleged shows of copalin at industrial and balance reserves - Kryvyi Rig: DVNZ «KNU» Vidavnichy center. - 160 p. Іл.

5. **Sholokh M.V.** (2018). Determination and research of norms of the ferrous quartzites prepared to booty. – pp. 25–52. / Development of scientific foundations of resource-saving technologies of mineral mining and processing. Multi-authored monograph. – Sofia: Publishing House «St. Ivan Rilski». – 264 p. ISBN 978-954-353-355-8.

6**. Sholokh M.V.** (2018). Estimation of content of quality indexes of minerals in array of rogitinums of magnetite and in stream of iron-ore mass. – pp. 180–208. / Resources and resource-saving technologies in mineral mining and processing. Multi-authored monograph. – Petroşani. Romania: UNIVERSITAS Rublishing, 2018. – 363 p. ISBN 978-973-741-592-9.

7. **Sholokh M.V.** (2018). Optimization of preparedness for extraction of balance industrial mineral reserves. – pp. 133–165. / To Figal issues of resource-saving technologies in mineral mining and processing. Multi-authored monograph. – Petrosani, Romania: UNIVERSITAS Publishing. – 270 p. ISBN 978-973-741-585-1.

8. **Sholokh M.V**. (2018). Planning of development of mountain works in the process of exploitation of balance-industrial supplies. – pp. 50–53. / International Scientific and Technical Internet Conference «Innovative Development of Resource-Saving Technologies of Mineral Mining and Processing». Book of Abstracts. – Petroşani, Romania: UNIVERSITAS Publishing. – 221 p. ISBN 978-973-741-615-5.

9**. Sholokh M.V., Sergieieva M.P.** (2019). Mine surveying support of controlling losses of balance industrial reserves. – pp. 343–363. / Sustainable development of resource-saving technologies in mineral mining and processing. Multi-authored monograph. – Petroşani, Romania: UNIVERSITAS Publishing. – 400 p. ISBN 978-973-741-622-3.

10. **Sholokh M.V., Sholokh S.M., Sergieieva M.P.** (2018). An analysis of surveyor control of losses of balance-industrial supplies is at mastering of bowels of the Earth. – pp. 415–438. / Innovative development of resource-saving technologies for mining. Multi-authored monograph. – Sofia: Publishing House «St. Ivan Rilski». – 439 p.

11. **Sidorenko V.D., Sholokh M.V., Sergieieva M.P.** (2015). The exactness of the assignment to both blocs at the pondrachunu of the reserves of the rudisc at the birth of ancestors / Coll. scientific papers «Mining and Metallurgical Industry». – Dnepropetrovsk. - Vol. 1 (272). - pp. 108–112.

12. **Sholokh M.V.** (2018). Having drawn into the balance of the commercial reserves and the reserves of the alleged showers in the procession averaging / Zb. Naukovich prats DVNZ «KNU» «Girnichny Visnik»: – Kryvyi Rig. - Vip. 103. - pp. 50–55.

13. **Sholokh M.V.** (2018). Marksheiderske prediction and forecast management with demonstrators in the development of important ancestors. - pp. 160–168. / Forum girnikiv - 2018: Materiali mizhnar. Conf., 10–13 Zhovtnya 2018 p. - Dnipro: Serednyak T.K. - 307 p. ISBN 978-617-7696-55-0.

14. **Sholokh M.V., Sergieieva M.P.** (2018). Simulation of characteristics of volumetric-qualitative parameters of flows of iron ore in quarries and mines / Zb. scientific works of the State University «KNU» «Mining Bulletin» Scientific and Technical Collection: Kryvyi Rih, 2018. - Vip. 103. - pp. 17-22.

15. **Sholokh M.V., Topchiy O.L., Sergieieva M.P.** (2012). Methods of creating mathematical models of ancestry of quartzite quartz for geometrization of new reserves / Pb. Naukovich Prats «Bulletin of KNU». - Kryvyi Rig. - Vip. 30. - pp. 38–42.

16. **Sholokh N.V**. (2002). Optimal algorithms and programs for automating the construction of mining and geometric graphs. / Development of ore deposits. - Issue number 78. - Krivoy Rog. - pp. 179-182.

17. **Sholokh N.V.** (2005). Prediction of indicators of the geochemical field deposits of ferriginous hornfelses Krivbass. / Development of ore deposits. - Issue number 89. - Krivoy Rog. - pp. 144–147.

18. **Sholokh N.V.** (2007). Optimization of the discovered ore reserves and the direction of mining in the quarry. / Bulletin KTU, - Vipusk number 16. - Kryvyi Rig. - KTU. - pp. 42–44.

19. **Sholokh N.V., Serkin V.N.** (2007). Calculation of mining volumes for different configurations of excavation blocks in a digital quarry model / Sci. Tech. compilation «Developed mines deposits». - Krivoy Rog. - Vol. 91. - pp. 106–109.

20. **Sholokh N.V., Serkin V.N.** (2007). Effective method of calculating the volume of mining in the digital model of the quarry on the example of Poltava GOK / Zb. naukovih prats «Visnik KTU». - Kryvyi Rig. - Vip. 17. - pp. 54–58.

21. **Sholokh M.V.** (2015). Modeluvuvnya processes in the formation of dough and cinnamon from the ore sirovini ore flow / Naukovo-tech. Zbirnik «Girnichiy Visnik» DVNZ «KNU». - Kryvyi Rig. - Vip. 100. - pp. 111–116.

22. **Sholokh M.V.** (2018). Having drawn into the balance of the commercial reserves and the reserves of the alleged showers in the procession averaging / Zb. Naukovich prats DVNZ «KNU» «Girnichny Visnik» Naukovo-technical zbirnik: Kryvyi Rig, - Vip. 103. - pp. 50–55.

23. **Sholokh M.V.** (2018). Models and Criteria of Optimized Identity Indicators in the Magnetitic Horn back Vidobutka. - pp. 65–78. / The 6th International conference Science and society - (August 3, 2018) Accent Graphics Communications & Publishing, Hamilton, Canada. 2018. 250 p. ISBN 978-1-77192-360-6.

24. **Sholokh M.V.** (2018). A model of forecasting predictions for the world of allegedly shown cops. pp. 274–287. / The 3rd International Youth Conference - Perspectives of Science and Education - (July 6, 2018) SLOVO \ WORD, New York, USA. 2018. 524 p. ISBN 978-1-77192-403-0.

25. **Sholokh M.V.** (2018). The normuvannya balance of industrial reserves of saline quartz on the level prepared to the sight of a bottle. - pp. 742–761. / The Second International scientific congress of Europe. - East – West Proceedings of the II International Scientific Forum of Scientists (May 10–11, 2018). Premier Publishing s. r. o. Vienna. - 822 p.

RIGIDITY OF ELASTIC SHELL OF RUBBER-CABLE TRACTIVE ELEMENT DURING MUTUAL SHEAR DISPLACEMENT OF CABLES

Kolosov D.L.
Dnipro University of Technology, Dnipro, Dr. Sc. (Tech.), Associate Professor, Head of Department of Structural, Theoretical and Applied Mechanics, Ukraine

Samusia V.I.
Dnipro University of Technology, Dnipro, Dr. Sc. (Tech.), Professor, Head of Department of Mining Mechanics, Ukraine

Bilous O.I.
Dniprovsk State Technical University, Kamianske, Ph. D. (Tech.), Associate Professor, Associate Professor of Department of Mechanical Engineering, Ukraine

Tantsura H.I.
Dniprovsk State Technical University, Kamianske, Ph. D. (Tech), Associate Professor, Associate Professor of Department of Theoretical and Applied Mechanics, Ukraine

Abstract

Analytical dependencies for determination of rigidity and parameters of a stress-strain state of a layer of rubber located between the mutually sheared cables of a tractive element are established in a closed form. A method of determining the dispersion of deviation of calculated displacements from the given ones is developed. Obtained results allow considering the shape of an elastic layer, and estimate the level of reliability of results when calculating a stress-strain state of rubber-cable tractive elements in which mutual shear displacement of cables along the tractive element occurs due to operating conditions. Possibility to determine a stress-strain state of a layer of elastic material caused by mutual shear displacement of cables, which occurs in a tractive element with cable breakages, in their butt-joints, in elements of attachment of a tractive element to structural elements of a hoisting machine and a possibility of formulating a condition of strength of a rubber-cable tractive element in which shear stresses occur between its cables, allows reasonable consideration of influence of design of a butt-joint in which the shape of rubber between cables is altered on the strength of a rubber layer with a certain level of reliability. This improves the safety of usage of rubber-cable belts and ropes and helps extending their life cycle.

Introduction

Rubber-cable belts and ropes are used as transporting and tractive executing elements of lifting machines, powerful conveyors in vari-

ous branches. They are loaded with tensile forces on lifting machines, and mainly by such forces on the conveyors. Forces are directed along the cables. Belts and ropes have a system of parallel cables of the same type located in one plane. The cables are packed into a shell of elastic material with a constant spacing. Both rubber and polyurethane are used as an elastic material. By choosing the size and diameters of cables, their amount, spacing, it is possible to obtain belts and ropes with quite different mechanical parameters. The essential difference between such belts and ropes is geometric shape of the elastic shell and the material from which it is made.

Due to parallel arrangement of cables of the same type in a rope and belt loaded with tensile forces, the loads are distributed evenly among them. Cross-sections are flat before deformation and remain flat after it. Stresses that occur in elastic shell material are of little importance because the modulus of elasticity of this material is much smaller than the modulus of elasticity of the material of cables.

The elastic shell holds the cables, provides them with a specified placement and performs a function of protecting the cables from their interaction with the environment and elements of machines. The exclusion of this interaction protects rope and belt cables from corrosion and mechanical wear, increases their life cycle.

The character of interaction of a rope, belt with connecting devices, pulleys, drums can lead to a disturbance of even distribution of forces between cables. Cross-sections of cables are curving. Such consequences also occur at breakages of cables. The curvature of sections is accompanied by a shear deformation of some cables relatively to others. The mutual shear displacement of cables leads to deformation of an elastic shell and occurrence of considerable shear stresses in it. Reaching the stress level of tensile strength can lead to destruction of an elastic shell, including its detachment from the surface of cables, and their interaction with the environment.

State of Question and Research Problem

Conveyor belts have a closed shape. They can be made of several parts. In order to form a closed shape parts of a belt, its ends are joined by butt-joints. Butt-joints of various designs are used. The analysis of structures, conditions of use, and the maximum possible strength related to belt strength and a dependency of tangent load distributed along the length is presented in [1] and is determined by

the method of electrical modeling [2]. Designs of individual joints don't assume a change in a cable placement spacing. The strength of such connections is less than 50% of the rope strength. Butt-joints in which all or individual cables of one belt are located between the cables of another have greater tensile strength.

It should also be kept in mind that cables of one part of the belt are not mechanically connected to the cables of the other part in a butt-joint. The transfer of tensile forces from one part to the other is due to the action of shear stresses occurring in the elastic shell. Durability of joints depends on a stress state of shell material. Elastic shell destruction leads to a rupture in a belt integrity, and a loss of its basic property - the transmission of tractive force, and to emergency. The shell destruction is facilitated by an uneven distribution of stresses in the elastic shell.

Shear stresses in rubber-cable belts and ropes occur when one or more cables are broken. Such stresses can occur under the influence of structural elements of machines in which they are used. Thus, they occur in a case of interaction with the drum (pulley) of machines having a curved generatrix. Shear stresses may also occur as a result of deviation of shaft guides from a designed straight line. They affect the technical condition of a belt, rope over their life cycle. The stress distribution depends essentially on a shape of shell material located between cables and its shear rigidity. Determining the character of influence of geometric parameters on shear rigidity and stress distribution in a layer of elastic shell located between cables in a rubber-cable tractive-transporting executive element is an actual scientific and technical problem.

Durability of butt-joints is investigated in [3, 4]. In paper [5] the expediency of timely detection of damage to a conveyor belt is pointed out. Some methods and techniques for real-time monitoring serious faults of steel-cord belt conveyor, such as splice breaking, longitudinal rip, fire and tension super-threshold etc, were analyzed in [6-11]. In [12], a stress-strain state of a conveyor belt is investigated by the finite element method. As in [1] it is shown that a butt-joint is its weakest link. The dissertation [13] is devoted to increase of durability of butt-joints of conveyor belts. The influence of breakages of belt reinforcement elements is analyzed in paper [14]. Their influence on reducing the life of joints was proved. In [15], a technique for deter-

mining the amount of safe loading of a belt with breakages is justified. It is based on empirical dependencies. Mechanical characteristics of composite materials reinforced by a system of circular cross-section elements are investigated in paper [16].

The issue of redistribution of forces between cables in rubber-cable belts with damage is investigated in papers [17-21]. In [22], a stress state of a rubber-cable tractive element is investigated. It is proved that the disturbance of integrity of an extreme cable has a greater effect on redistribution of forces between cables. Scientific-research recommendations aiming at development of rating of methods of forcing factors in spires of multilayer rubber-rope cable of bobbin hoist is given in [23, 24]. Dissertation [25] is devoted to increase of reliability of conveyors with a rubber-fabric belt.

Well-known studies of a condition of rubber-cable belts don't allow considering the influence of a shape of an elastic shell on its stress state from a mutual shift of cables. Use the methods of theory of elasticity. Determine the stress distribution in the elastic shell of a belt in a case of mutual shear displacement of cables.

Methods

Construction of a model, determination of a stressed state of the elastic material of a deformed shape located between the cables during their mutual shear displacement by methods of linear theory of elasticity. Establishment of analytical dependencies of rigidity and parameters of a stress-strain state of a layer of rubber located between mutually sheared cables of a tractive element in a closed form.

Presentation of Main Research

Belts, ropes operate within the boundaries of a linear Hooke's law. Assume the linear dependency of stresses on deformations. Rigidity of the elastic component in a belt is much less than rigidity of cables. Deformation of cable cross-sections is neglected. Elastic shell material is considered isotropic. The conveyor belt is intended for transportation of material. External layers of the belt may be affected by loads due to the mass of material, forces of interaction of a belt with elements of a conveyor structure. Neglect these forces. Assume that elastic material only perceives shear deformation. Shear deformations in planes normal to cables are small. Neglect them as well. Consider the deformed state of an elastic shell as uniaxial. Determine the distribution of stresses in an elastic shell of a sample of a belt of

two cables mutually sheared in a direction of cables (Fig. 1).

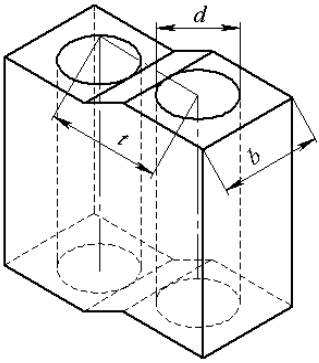

Fig. 1. Element of rope of two cables

Single out a part of elastic inter-cable shell. Supplement it with a conditional additional part. Indicate contours of a conditional additional part of a shell with thin lines in Fig. 2.

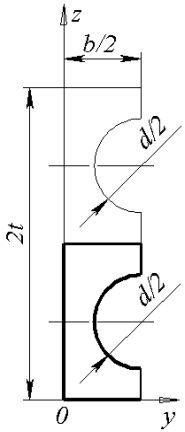

Fig. 2. Computational model of an elastic shell located between cables

Formulate the conditions for moving the boundaries of a sample of elastic material. Coordinate z=0 corresponds to the plane of symmetry of a sample shown in Fig. 1. In a case of mutual reciprocal shear displacement of cables, the movement of sample parts has opposite signs. Movement of the material of a conditional part of the elastic shell with coordinates z=2t is considered absent. Write down the indicated in a form of the following condition

$$\text{when } z=0 \text{ or } z=2t,\ u=0. \qquad (1)$$

The symmetry of a conditional sample ensures the fulfillment of the condition of absence of tangential stresses on a surface $z=t$.

On a surface with coordinates $y=b/2$ and $y=0$ external tangential loads do not act. Formulate the indicated with two following conditions

$$\text{when } y=\frac{b}{2} \quad \frac{du}{dy}=0, \tag{2}$$

$$\text{when } y=0 \quad \frac{du}{dy}=0. \tag{3}$$

The surface of interaction of elastic shell material with a cable is considered to be displaced by one unit, therefore

$$\text{when } \left\{\begin{array}{l}\left(z-\frac{t}{4}\right)^2+\left(y-\frac{b}{2}\right)^2=\left(\frac{d}{2}\right)^2\\ \left(z-\frac{3t}{4}\right)^2+\left(y-\frac{b}{2}\right)^2=\left(\frac{d}{2}\right)^2\end{array}\right\} u=1. \tag{4}$$

Surfaces of the sample $y=\frac{b}{2}\wedge 0\le z\le\frac{t-d}{2}$ and $y=\frac{b}{2}\wedge t-\frac{t-d}{2}\le z\le t$ are the symmetry lines. Tangential stresses do not act along these surfaces

$$\text{when } y=\frac{b}{2}\wedge 0\le z\le\frac{t-d}{2} \quad \frac{du}{dy}=0, \tag{5}$$

$$\text{when } y=\frac{b}{2}\wedge t-\frac{t-d}{2}\le z\le t+\frac{t-d}{2} \quad \frac{du}{dy}=0, \tag{6}$$

$$\text{when } y=\frac{b}{2}\wedge 2t-\frac{t-d}{2}\le z\le 2t \quad \frac{du}{dy}=0. \tag{7}$$

A surface with $z=t$ is a plane of symmetry of deformation of the sample (Fig. 2).

Differential equations of equilibrium of a continuous isotropic material during shear in a plane are determined by Laplace's equation

$$\frac{\partial^2 u}{\partial z^2}+\frac{\partial^2 u}{\partial y^2}=0. \tag{8}$$

The solution of (8) is sought in a form of a product of hyperbolic and trigonometric functions considering the conditions (1) and (3)

$$u(z,y)=\cos h(y)\sin(z). \tag{9}$$

Consider the assumed form of solution. In order to obtain a solution in a general form, assume $2t$=1. Assume values *b*, *d* and *u* related to $2t$. As a result, we have limits of coordinate change $(-1\le z\le 1)$. Write down the functions that specify the boundary conditions by three functions. Define boundary conditions along the surface *y b/2* by the first function $s(z)$

$$s(z)=\left\{\begin{array}{ll}\dfrac{4zt}{t-2d} & \left(0\le z\le\dfrac{t-2d}{4t}\right)\\ 1 & \left(\dfrac{t-2d}{4t}\le z\le 1-\dfrac{t-2d}{4t}\right)\\ \dfrac{(1-z)}{t-2d}4t & \left(1-\dfrac{t-2d}{4t}\le z\le 1\right)\\ \dfrac{4z}{t-2d} & \left(0\ge z\ge -\dfrac{t-2d}{4t}\right)\\ -1 & \left(-\dfrac{t-2d}{4t}\ge z\ge -1+\dfrac{t-2d}{4t}\right)\\ \dfrac{(z-1)}{t-2d}4t & \left(-1+\dfrac{t-2d}{4t}\ge z\ge -1\right)\end{array}\right\}. \tag{10}$$

According to the first function, elastic material has the same displacements on the surface *y=b/2* as the surface of cables. In a general case, the surface between cables, with exception of points that interact with cables, can have different displacements. These displacements should be symmetrical to a surface that separates the real and

the conditional part of the elastic shell. Considering the above-mentioned, define the function $w(z)$, which ensures material displacement between cables in accordance to the sinusoid

$$w(z)=\begin{cases} \dfrac{4z}{t-2d} & \left(0\le z\le \dfrac{1}{2}-\dfrac{t-2d}{4}\right) \\ -\sin\left(\dfrac{z-\dfrac{1}{2}+\dfrac{t-2d}{4t}}{t-2d}2t\pi\right) & \left(\dfrac{1}{2}-\dfrac{t-2d}{4}\le z\le \dfrac{1}{2}+\dfrac{t-2d}{4}\right) \\ 0 & \left(\dfrac{1}{2}+\dfrac{t-2d}{4}\ge z\ge -\dfrac{t-2d}{4}\right) \\ \sin\left(\dfrac{z+\dfrac{1}{2}-\dfrac{t-2d}{4t}}{t-2d}2t\pi\right) & \left(-\dfrac{t-2d}{4}\ge z\ge \dfrac{t-2d}{4}-1\right) \\ 0 & \left(\dfrac{t-2d}{4}-1\ge z\ge -1\right) \end{cases}. \quad (11)$$

Consider the dependency of displacements of elastic material along the surface, which corresponds to surfaces of cables by the third function $v(z)$. Volumes of the elastic shell material must move along with cables. Consider that the first function (10) defines the unit displacement of points corresponding to cable surfaces when $y=b/2$. Also consider the assumed form of solution (9). Define displacements by inverse displacements defined by (9) and referred to displacements in a case $y=b/2$. Reduce them by one

$$v(z)=\begin{cases} 0 & \left(0\le z\le \dfrac{t-2d}{4}\right) \\ \dfrac{\cosh\left(\dfrac{b}{2}\right)}{\cosh\left(\dfrac{b}{2}-\sqrt{\left(\dfrac{d}{2}\right)^2-\left(z-\dfrac{1}{4}\right)^2}\right)\sin(z\pi)}-1 & \left(\dfrac{t-2d}{4}\le z\le \dfrac{1}{2}-\dfrac{t-2d}{4}\right) \\ 0 & \left(\dfrac{1}{2}-\dfrac{t-2d}{4}\le z\le \dfrac{1}{2}+\dfrac{t-2d}{4}\right) \\ \dfrac{\cosh\left(\dfrac{b}{2}\right)}{\cosh\left(\dfrac{b}{2}-\sqrt{\left(\dfrac{d}{2}\right)^2-\left(z-\dfrac{1}{4}\right)^2}\right)\sin(z\pi)}-1 & \left(\dfrac{1}{2}+\dfrac{t-2d}{4}\le z\le 1-\dfrac{t-2d}{4}\right) \\ 0 & \left(1-\dfrac{t-2d}{4}\le z\le 1\right) \\ 0 & \left(0\ge z\ge \dfrac{t-2d}{4}\right) \\ \dfrac{\cosh\left(\dfrac{b}{2}\right)}{\cosh\left(\dfrac{b}{2}-\sqrt{\left(\dfrac{d}{2}\right)^2-\left(z-\dfrac{1}{4}\right)^2}\right)\sin(z\pi)}+1 & \left(-\dfrac{t-2d}{4}\ge z\ge -\dfrac{1}{2}+\dfrac{t-2d}{4}\right) \\ 0 & \left(-\dfrac{1}{2}+\dfrac{t-2d}{4}\ge z\ge -\dfrac{1}{2}-\dfrac{t-2d}{4}\right) \\ \dfrac{\cosh\left(\dfrac{b}{2}\right)}{\cosh\left(\dfrac{b}{2}-\sqrt{\left(\dfrac{d}{2}\right)^2-\left(z-\dfrac{1}{4}\right)^2}\right)\sin(z\pi)}+1 & \left(-\dfrac{1}{2}-\dfrac{t-2d}{4}\ge z\ge \dfrac{t-2d}{4}-1\right) \\ 0 & \left(\dfrac{t-2d}{4}-1\ge z\ge -1\right) \end{cases}. \quad (12)$$

The latter functions set displacement on the surface $y=b/2$. They approximately reproduce the displacement of elastic shell material of a rubber-cable belt. The level of proximity can be determined further by comparing the calculated material displacements with the accepted - unit.

Develop functions in expressions (10-12) in the Fourier series by the sines. Write the solution of (9) in a following form

$$u(y,z)=\sum_{m=1}^{M}\left(BS_m+CW_m+DV_m\right)\frac{\cosh(q_m y)}{\cosh\left(q_m\frac{b}{2}\right)}\sin(q_m z), \quad (13)$$

where B,C,D - constant coefficients; S_m,W_m,V_m - coefficients of development of functions $s(z)$, $w(z)$, $v(z)$ in Fourier series; $q_m=\pi_m$;

M - number of members in each Fourier series.

Find the values of coefficients from several conditions. One of conditions would assume a unit displacement of a point of a cable nearest to the surface $y=0$. Perform conditions (5-7) integrally on the specified surfaces. Also, consider the symmetry of their location. This allows reducing the number of conditions to two. Thus, there is a sufficient amount of conditions for determination of three constant coefficients from the system of algebraic equations written in canonical form

$$\begin{bmatrix}\alpha_{1,1} & \alpha_{1,2} & \alpha_{1,3}\\ \alpha_{2,1} & \alpha_{2,2} & \alpha_{2,3}\\ \alpha_{3,1} & \alpha_{3,2} & \alpha_{3,3}\end{bmatrix}=\begin{bmatrix}1\\0\\0\end{bmatrix}, \quad (14)$$

where

$$\alpha_{1,1}=\sum_{m=1}^{M}s_m\frac{\cosh\left(\frac{b-d}{2b}\right)}{\cosh\left(\frac{b}{2t}\right)}\sin\left(\frac{q_m}{4}\right);$$

$$\alpha_{1,2} = \sum_{m=1}^{M} w_m \frac{\cosh\left(\frac{b-d}{2b}\right)}{\cosh\left(\frac{b}{2t}\right)} \sin\left(\frac{q_m}{4}\right);$$

$$\alpha_{1,3} = \sum_{m=1}^{M} v_m \frac{\cosh\left(\frac{b-d}{2b}\right)}{\cosh\left(\frac{b}{2t}\right)} \sin\left(\frac{q_m}{4}\right);$$

$$\alpha_{2,1} = \sum_{m=1}^{M} s_m \frac{\sinh\left(\frac{b}{2t}\right)}{\cosh\left(\frac{b}{2t}\right)} \left(\cos\left(\frac{q_m(t-2d)}{4t}\right)-1\right);$$

$$\alpha_{2,2} = \sum_{m=1}^{M} w_m \frac{\sinh\left(\frac{b}{2t}\right)}{\cosh\left(\frac{b}{2t}\right)} \left(\cos\left(\frac{q_m(t-2d)}{4t}\right)-1\right);$$

$$\alpha_{2,3} = \sum_{m=1}^{M} v_m \frac{\sinh\left(\frac{b}{2t}\right)}{\cosh\left(\frac{b}{2t}\right)} \left(\cos\left(\frac{q_m(t-2d)}{4t}\right)-1\right);$$

$$\alpha_{3,1} = \sum_{m=1}^{M} s_m \frac{\sinh\left(\frac{b}{2t}\right)}{\cosh\left(\frac{b}{2t}\right)} \left(\cos\left(\frac{q_m}{2}\right)-\cos\left(q_m\left(\frac{1}{2}-\frac{t-2d}{4t}\right)\right)\right);$$

$$\alpha_{3,2} = \sum_{m=1}^{M} w_m \frac{\sinh\left(\frac{b}{2t}\right)}{\cosh\left(\frac{b}{2t}\right)} \left(\cos\left(\frac{q_m}{2}\right)-\cos\left(q_m\left(\frac{1}{2}-\frac{t-2d}{4t}\right)\right)\right);$$

$$\alpha_{3,3} = \sum_{m=1}^{M} v_m \frac{\sinh\left(\frac{b}{2t}\right)}{\cosh\left(\frac{b}{2t}\right)}\left(\cos\left(\frac{q_m}{2}\right) - \cos\left(q_m\left(\frac{1}{2} - \frac{t-2d}{4t}\right)\right)\right).$$

As a result of solving the system of Eq. 14, the values of unknown constants are obtained

$$D = \frac{\alpha_{2,1}\alpha_{3,2} - \alpha_{3,1}\alpha_{2,2}}{\alpha_{3,3}\left(\alpha_{2,2}\alpha_{1,1} - \alpha_{2,1}\alpha_{1,2}\right) + \alpha_{2,3}\left(\alpha_{3,1}\alpha_{1,2} - \alpha_{3,2}\alpha_{1,1}\right) + \alpha_{1,3}\left(\alpha_{3,2}\alpha_{2,1} - \alpha_{3,1}\alpha_{2,2}\right)},$$

$$C = \frac{\alpha_{2,1} + D\left(\alpha_{1,3}\alpha_{1,1} - \alpha_{3,1}\alpha_{2,1}\right)}{\alpha_{1,2}\alpha_{2,1} - \alpha_{2,2}\alpha_{1,1}}, \quad B = \frac{1 - C\alpha_{1,3} - D\alpha_{2,1}}{\alpha_{1,1}}.$$

With the use of determined unknown constants, distributions of deformations and tangential stresses are obtained. The results are given below for relative displacements (unit), the dimensions of an elastic belt shell. Fig. 3 shows a definite form of an elastic shell in a case of displacement of a cable by one unit.

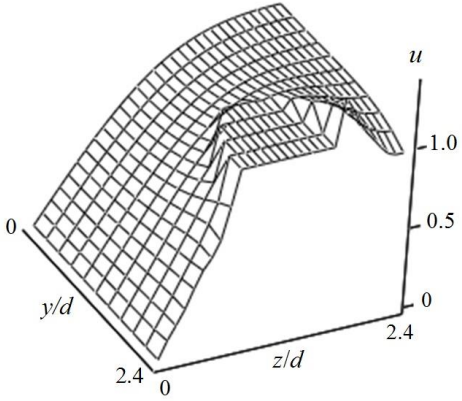

Fig. 3. The shape of an elastic shell part acquired as a result of axial displacement of a cable by one unit

Note that in the figure, a part of the formed shape within the boundaries corresponding to a cable cross-section is conditionally given equal to one. Overall, the indicated deformed shape of elastic material cross-section correspond to the idea of a character of its deformation. Divide half of the circle, which outlines the contour of a

half of cross-section of a cable, into *M* equal parts. Determine the calculated displacements for every point on a circle according to formula (13). Determine the deviation dispersion of these values from a unit. Results for various values of a relative belt thickness and cable placement spacing in it are shown in Fig. 4.

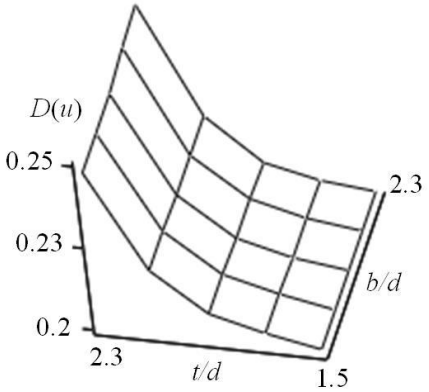

Fig. 4. Dependency of the dispersion of displacements of points of an elastic shell located on an arc with a radius of a cable (*d*/2)

According to the figure value of dispersion increases with increasing relative values of a spacing (*b/d*) and belt thickness (*t/d*). In practice, lifting rubber-cable ropes with minimum ratios of rope thickness and cable placement spacing to their diameters are used. Relative thickness and cable placement spacing in rubber-cable ropes, as a rule, do not exceed 2.3. The indicated shows the possibility of calculating the deformed and, accordingly, stress state of rubber-cable ropes and belts with a certain level of reliability of obtained results.

Stress state, in accordance with Hooke's linear law, are proportional to the shear modulus and the shear angle tangent. The first depends on the material, the second on the mutual displacement of the material volume. Determine the characteristics of the mutual displacement. Differentiate the expression (13) by *dz* and *dy*. Consider that they are constructed for a unit of relative displacement and relative dimensions of the elastic shell of a belt

$$\frac{u(y,z)}{dy} = \sum_{m=1}^{M} \left(BS_m + CW_m + DV_m\right) \frac{\Delta \sinh\left(q_m y\right)}{2\cosh\left(q_m \frac{b}{2}\right) t} \sin\left(q_m z\right) q_m, \quad (15)$$

$$\frac{u(y,z)}{dz} = -\sum_{m=1}^{M} \left(BS_m + CW_m + DV_m\right) \frac{\Delta \cosh\left(q_m y\right)}{2\cosh\left(q_m \frac{b}{2}\right) t} \cos\left(q_m z\right) q_m, \quad (16)$$

where Δ - cable displacement during a mutual shear of cables.

Determine the tangents of shear angles for the boundary z=0 - plane of symmetry of a location of mutually sheared cables

$$\frac{u(y,z=0)}{dz} = -\sum_{m=1}^{M} \left(BS_m + CW_m + DV_m\right) \frac{\Delta \cosh\left(q_m y\right)}{2\cosh\left(q_m \frac{b}{2}\right) t} q_m. \quad (17)$$

Find a definite integral from tangential stresses by *dy* of expression (17) between a zero and *b*/2. By using Hooke's law, determine the force required to mutually displace the rope cables by the value 2Δ

$$T = G \frac{\Delta}{2t} \sum_{m=1}^{M} \left(BS_m + CW_m + DV_m\right) \frac{\sinh\left(q_m \frac{b}{2}\right)}{\cosh\left(q_m \frac{b}{2}\right)}. \quad (18)$$

The obtained value of a force to displace one cable by the value Δ=1/2 is the value of shear rigidity of an elastic shell.

The quantity inverse to shear force, considering the condition of mutual shear displacement of cables by a unit, is defined by a dependency - each cable performs a half of mutual shear displacement

$$c = \frac{t}{G} \left[\sum_{m=1}^{M} \left(BS_m + CW_m + DV_m\right) \frac{\sinh\left(q_m \frac{b}{2}\right)}{\cosh\left(q_m \frac{b}{2}\right)} \right]^{-1}.$$

By using expression (18), a value of a force is determined, that ensures mutual shear displacement of cables on geometric parame-

ters of a belt. In order to obtain the results in a general form, a relative force is determined

$$T_r = \frac{Tt}{2G}.$$

The results of a calculation of forces are shown in the following figure.

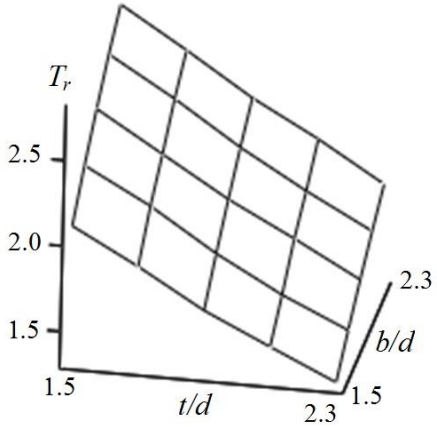

Fig. 5. Dependency of relative shear displacement force of cables (T_r) on belt thickness and placement spacing of cables related to their diameter in a belt

According to Fig. 5, an increase of a relative thickness of a belt leads to a decrease in a force of deformation. At the same time, the growth of a placements spacing of cables leads to an increase of indicated force. Changes in the latter are smaller. This is a consequence of the influence of two factors on a stress state of an elastic material. The first factor is a growth of sample sizes, which reduces its rigidity. Action mechanism of this factor is the same for both cases. The second factor in a mechanism of influence of a sample size on its rigidity is the uneven distribution of deformations, and respectively, of stresses, in a direction of placement of cables. Fig. 6 indicates a dependency of average values of shear stresses (τ_m) on relative dimensions of a cross-section of a rubber-cable belt.

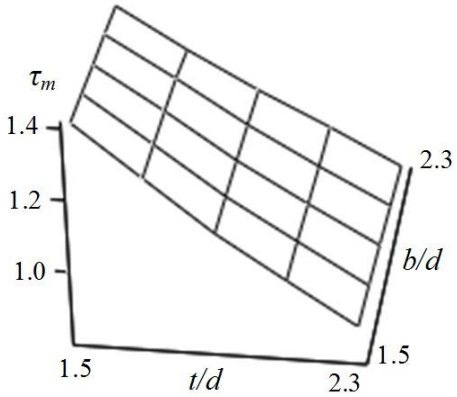

Fig. 6. Dependency of average values of shear stresses (τ_m) on belt thickness and cable placement spacing related to their diameter in a belt

General character of distribution of average stresses coincides with distribution of shear forces. The stress state depends on its distribution in material. The main characteristic of stress distribution is coefficient of their concentration. The Fig. 7 indicates a dependency of shear stress concentration coefficient (K) on belt thickness and cable placement spacing related to their diameter in a belt.

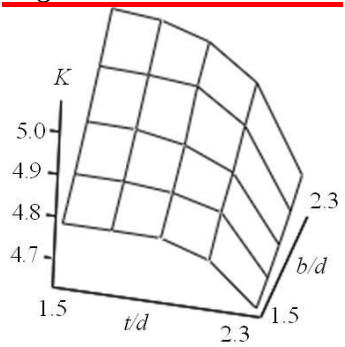

Fig. 7. Dependency of shear stress concentration coefficient (K) on belt thickness and cable placement spacing related to their diameter in a belt

Analysis of distributions of stress concentration coefficients indicates their qualitative coincidence with a dependency of mutual shear force of cables on geometric parameters of belt cross-section.

Conclusions

A research on establishment of a character of influence of geo-

metric parameters on shear rigidity, determination of maximum stresses in a layer of elastic shell located between the cables in a rubber-cable tractive-transporting executing element is carried out and an algorithm for its determination is developed in the paper.

Deformed state of an elastic shell of a flat rubber-cable tractive element caused by mutual shear displacement of adjacent cables is defined by a sum of three states. The first state is presented as constant. Two others consider the features of deformation along the surface that interacts with a cable and the outer surface of the shell that is not loaded. The level of reliability of the model is estimated by determining the dispersion of deviation of model shear along the arc of interaction of shell material and a cable from one unit.

Analysis of rigidity and a stress state of an elastic shell indicated that they depend on geometrical parameters of a cross-section of a rubber-cable belt and rope. Growth of relative thickness of a belt leads to a decrease in rigidity. At the same time, an increase of cable placement spacing leads to its growth.

A model of the deformed state of an elastic shell of a flat rubber-cable tractive element caused by the mutual shear displacement of adjacent cables is constructed and its stress state is determined by the methods of linear theory of elasticity. Analytical dependencies of rigidity, parameters of a stress-strain state of a layer of elastic shell material are obtained in a closed form, and can be used in mathematical models of equilibrium of cables in rubber-cable conveyor belts and flat ropes and in determining the condition of strength, what increases the safety of usage of belts and ropes, analysis of their technical condition during operation to increase their life cycle.

Dependencies for determining the rigidity and parameters of a stress-strain state of a layer of rubber located between the mutually sheared cables of a tractive element, a method for determining the dispersion of deviation of calculated displacements from the given ones, allows reasonable considering the shape of the elastic layer, and estimating the level of reliability of results of calculations of a stress-strain state of rubber-cable tractive elements in which there are mutual shear displacements of cables along the tractive element due to operating conditions.

References

1. **Bel'mas I.V.** (1993). Osnovy teorii i rascheta rezinotrosovoy lenty konvejera s uchetom ego prostranstvennoy formy: Sc.D. IGM.

2. **Kolosov, L.V., Bel'mas, I.V.** (1981). Use of electrical models for investigating composites. Mechanics of Composite Materials, 17(1), 115-119.

3. **Marasová, D., Ambriško, Ľ., Andrejiová, M., Grinčová, A.** (2017). Examination of the process of damaging the top covering layer of a conveyor belt applying the FEM. Journal of the International Measurement Confederation, (112). 47-52. DOI: 10.1016/j.measurement.2017.08.016

4. **Hardygora, M., Komander, H., Blazej, R., Jurdziak, L.** (2012). Method of predicting the fatigue strength in multiplies splices of belt conveyors. Eksploatacja i Niezawodnosc – Maintenance and Reliability 2012, 14 (2), 171-175.

5. **Blazej, R., Jurdziak, L., Burduk, R., Kirjanow, A., Kozlowski, T.** (2017). Analysis of core failure distribution in steel cord belts on the cross-section. International Multidisciplinary Scientific GeoConference Surveying Geology and Mining Ecology Management, 17(13), 987-994. DOI: 10.5593/sgem2017/13/S03.125

6. **Huang, M, Gu Y.-H., Wei, R.-Z.** (2002). Research on method for monitoring longitudinal rip of steel-cord belt. Zhongguo Kuangye Daxue Xuebao/Journal of China University of Mining & Technology, 31(1), 49-52.

7. **Zaremba, D., Heitzmann, P., Overmeyer, L., Hillerns, L., Hassel, T.** (2017). Automatable splicing method for steel cord conveyor belts – evaluation of water jetting as a preparation process. Strojniški vestnik - Journal of Mechanical Engineering 63(10), 590-596. DOI:10.5545/sv-jme.2017.4363

8. **Huang, M.** (2011). Research on the working condition monitoring and protecting system for mine belt conveyor. Applied Mechanics and Materials, (58-60), 518-523. https://doi.org/10.4028/www.scientific.net/AMM.58-60.518

9. **Błażej, R., Jurdziak, L., Kirjanów, A., Kozłowski, T.** (2015). Evaluation of the quality of steel cord belt splices based on belt condition examination using magnetic techniques. Diagnostyka, 16(3), 59-64.

10. **Hardygora, M., Bajda, M., Blazej, R.** (2014). Evaluation of the Effectiveness of an eco-friendly technology for splicing steel cord conveyor belts. Applied Mechanics and Materials, (683), 125-129. DOI:.4028/www.scientific.net/AMM.683.125

11. **Fedorko, G., Molnár, V., Ferková, Ž., Peterka, P., Krešák, J., Tomašková, M.** (2016). Possibilities of failure analysis for steel cord conveyor belts using knowledge obtained from non-destructive testing of steel ropes. Engineering Failure Analysis, (67), 33-45.

12. **Song, W., Shang, W., Li, X.** (2009). Finite element analysis of steel cord conveyor belt splice. ET Conference Publications, 2009(556). DOI: 10.1049/cp.2009.1415

13. **Levchenya, Zh.B.** (2004). Povyshenie nadezhnosti stykovykh soedineniy konveyernykh lent na gornodobyvayushchikh predpriyatiyakh: Na primere RUP

"PO "Belaruskaliy": Ph.D. MGOU

14. **Tantsura H.I.** (2010). Gnuchki tyagovi organy. Stikovi zyednannya konveyernykh strichok. Dniprodzerzhins'k: DDTU

15. **Volokhovskiy V.Yu., Radin V.P., Rudyak M.B.** (2010). Kontsentratsiya usiliy v trosakh i nesushchaya sposobnost' rezinotrosovykh konveyernykh lent s povrezhdeniyami. MEI Bulletin, (5), 5-12

16. **Dariya Zade S.** (2013). Chislennaya metodika opredeleniya effektivnykh kharakteristik odnonapravleno armirovannykh kompozitov. Bulletin NTU "KhPI", (58), 71-77

17. **Kolosov, D., Dolgov, O., Bilous, O., Kolosov, A.** (2015). The stress-strain state of the belt in the operating changes of the burdening conveyor parameters. New Developments in Mining Engineering 2015: Theoretical and Practical Solutions of Mineral Resources Mining, 585-590.

18. **Kolosov, D., Bilous, O., Tantsura H., Onyshchenko, S.** (2018). Stress-strain state of a flat tractive-bearing element of a lifting and transporting machine at operational changes of its parameters. Solid State Phenomena, (277), 188-201.

19. **Belmas, I., Kolosov, D.** (2011). The stress-strain state of the stepped rubber-rope cable in bobbin of winding. Technical and Geoinformational Systems in Mining: School of Underground Mining 2011, 211-214

20. **Belmas, I.V., Kolosov, D.L., Kolosov, A.L., Onyshchenko, S.V.** (2018). Stress-strain state of rubber-cable tractive element of tubular shape. Naukovyi Visnyk Natsionalnoho Hirnychoho Universytetu, (2), 60-69.

21. **Kolosov, D., Dolgov, O., Kolosov, A.** (2014). Analytical determination of stress-strain state of rope caused by the transmission of the drive drum traction. Progressive Technologies of Coal, Coalbed Methane, and Ores Mining, 499-504

22. **Bel'mas, I.V.** (1993). Stress state of rubber-rope tapes during their random damages. Problemy Prochnosti i Nadezhnos'ti Mashin, (6), 45-48

23. **Zabolotny, K., Panchenko, Y.** (2010). Definition of rating loading in spires of multilayer winding of rubber-rope cable. New Techniques and technologies in Mining, 223-229.

24. **Zabolotny, K.S., Panchenko, E.V., Zhupiev, A.L.** (2011). Teoriya mnogosloynoy namotki rezinotrosovogo kanata. Dnipropetrovs`k: NGU

25. **Ischenko R.V.** (2013). Povyishenie nadezhnosti byistroiznashivayuschihsya detaley lentochnyih konveyerov v vozdushno-solyanoy srede: Ph.D. MGOU im. V.S. Chernomyirdina.

ANALYSIS OF MINING ROCKS DISINTEGRATION CONDITIONS IN CRUSHERS HAVING THE WAVE PROFILE OF ROLLS

Tytov O.O.
Associate Professor, Associate Professor in Department
of Engineering and Design in Machinery Industry
Dnipro University of Technology, Dnipro, Ph. D. (Tech), Ukraine

Abstract

The subject of research is the parameters of operational part of roll crusher with the wave profile of rolls. The goal of work is estimation of relative efficiency of the wave profile of rolls by its comparison to the smooth profile by such parameters, as the grab angle, the maximum size of pulled-in piece and the coefficient of equivalent destruction stress increase. Real pieces of mining rock are simulated by pieces of the pincushion shape, having changeable ratio of dimensions. They are used to simulate the cuboid, the needle-shaped and the lamellar pieces. Estimation of the grab angle and the maximum size of pulled-in pieces has made by analysis of the force balance for the piece being clamped between the ledge of one roll and the neighbouring hollow of the another roll.The rise of the grab angle up to 8% as a dependence of the wave profile taper angle is shown. It is set, that the size of the pulled-in pieces is increased up to 11% for the isometric-shaped pieces. Also, the size is decreased up to 27% for pieces of any another shape. The cases of large pieces destruction by the shear and the bend are considered. The values of the equivalent destruction stress for the smooth and the wave profiles, dependent on the piece shape and the profile taper angle, are determined based on the known criterion of mining rock destruction in multi-axial stress. It is set, that the wave profile allows to decrease the acting destruction forces for the pieces of non-isometric shape from 2 to 6 times.The results of research can be used for designing of crusher rolls of the wave profile, in order to lower the energy consumption during crushing of mining rocks.

Introduction

Today, the crushing of mining rocks is made by such types of crushers, as jaw, cone, roll and impact ones [1, 2]. The roll crushers favourably differ by simplicity and reliability of design, and also by relatively small dimensions and values of productivity. It allows to use them at the enterprises of small and average capacity.

The design of roll crusher may be featured by smooth or toothed rolls. The crushers with smooth rolls are mainly used for fine crushing and coarse grinding of hard and average fortress mining rocks. The crushers with toothed rolls cannot treat such rocks, so they are acceptable for rather weak mining rocks, otherwise, the wear of their

sharp teeth rises sufficiently.

But, the shortcoming of smooth rolls is high energy consumption of disintegration in consequence of disadvantageous compression load action, and also relatively small size of the pieces being pulled in the crusher.

State of Question and Research Problem

The design of wave profiled rolls (Fig. 1), developed with participation of the author, allows to improve the conditions of material pieces pulling in the working zone, and also to reduce sufficiently the energy consumption of disintegration process [3].

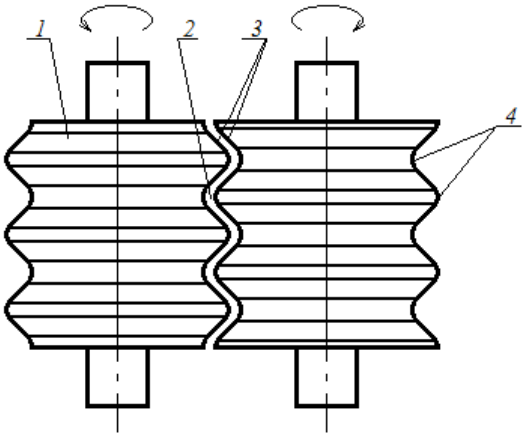

Fig. 1. The scheme of wave profiled rolls: 1 - bandage; *2* -constant gap; *3* - conic sites; *4* -radiuses

The large pieces can be destructed efficiently by bending loading, when getting between the ledges and the hollows *4* of neighbouring rolls. The smaller pieces, in turn, are crushed between the neighbouring conic sites *3* of rolls by combination of compression and shear forces being more efficient than linear compression. The constant value of the gap *2* between rolls guarantees not large dispersion on product size.

It is necessary to solve problems of the analytical substantiation of the geometry of modernized operational part influence on conditions of the material grab and destruction by the crusher. It will help to make a conscious choice of new crusher parameters.

The grab angle is an important parameter influencing the ratio of

the roll diameter and the size of piece pulled in the crusher.

There is a ratio for the limit grab angle of crushers in the work [4]. It is also correct for smooth rolls

$$\alpha = 2arctg(f), \tag{1}$$

where f is the friction coefficient of the piece against the roll.

In such a case, the maximum diameter of spherical-shaped piece pulled in crusher can be calculated by expression

$$d = \frac{D + b_0}{\cos(\alpha / 2)} - D, \tag{2}$$

or

$$d = (D + b_0)\sqrt{1 + f^2} - D, \tag{3}$$

where D is the roll diameter; b_0 is the gap between rolls.

The analysis of the last formula shows, that the size of pulled-in piece rises together with growth of all the input parameters. Usually, the maximum size of pieces doesn't exceed 5-6% of the roll diameter [4].

The maximum size of piece for the toothed-roll crusher is much more and approximately 40-50% of the roll diameter by teeth tops. It is explained by availability of sharp corners and edges penetrating the piece and pulling it into the crusher. But, the analytical substantiation for this issue is absent in literature, and all the data are obtained in the empirical way.

Thus, it is necessary to set the analytical dependence of the gap angle and the size of pulled-in piece on the rolls geometrical parameters, for the crusher presented in Fig. 1.

Only the most common cases of the regular-shaped pieces loading are given in literature, for example [5], as to the forces influencing the material piece in roll crusher. In particular, the ultimate destruction force of compression is determined for cubic-shaped pieces of certain size and for strictly normal direction of loading application to the opposite sides of piece as follows

$$P = R_c F, \tag{4}$$

where R_c is the ultimate compressive strength; F is the end face surface area.

The problem here is that the real piece has non-regular shape and is destructed by shear and bending stresses, but not by compressive

stress.

The "Brazilian test" is closer to reality, because it deals with resistance to stretching stress [6]. In this case, the ultimate compressive force along the diameter of cylindrical sample can be calculated so

$$P = R_t \frac{\pi d L}{2}, \quad (5)$$

where R_t is the ultimate linear stretching strength; d is the cylinder diameter; L is the cylinder length.

The various techniques to determine the ultimate shear strength [6] give such a value for the ultimate destruction force

$$P = \tau_s F_s, \quad (6)$$

where τ_s is the ultimate shear strength; F_s is the shear surface area.

The ultimate strength values for different types of loading are related to each other by the expression[7]

$$\tau_s = \frac{1}{2}\sqrt{R_c R_t}, \quad (7)$$

and also [8]

$$R_t = \psi R_c, \quad (8)$$

where ψ is the coefficient characterizing the rock plasticity.

It should be noted, that there are no special research works on the analytical simulation of irregular-shaped pieces in the roll (and another types of) crushers. So, the development of corresponding technique is relevant. It will allow to take into consideration the influence of rolls geometry on value of the crushing force decrease, depending on the direction of force application and the piece shape.

Substantiation of Piece Shape and Grab Angle

The material piece shape influences strongly the stresses distribution in volume, that follows from the fundamentals of the theory of elastic strength and the resistance of materials theory.

The real pieces of mining rocks in crushers have different shapes: cuboid, pyramidal, flat, needle etc. In any case, the surface of a piece has numerous big and small deviations from flat, cylindrical, spherical and other regular shape. So, substantiation of the piece settlement geometry and its deviation from the real shape is relevant.

The settlement geometry must correspond to such criteria:

to reflect the ratio of the piece length, width and thickness;

to display the surface curvature, influencing the distribution of applied forces;

to provide the similarity of ratio of stress conditions parameters for different types of pieces loadings, such as compression, shear and stretching;

to be available for analysis.

The pincushion shape of piece, formed by cuboid with rounded edges and described in the work [9], is the most preferable from our point of view. Here, the radiuses are half of the cuboid thickness. Further, it will be showed, that such a shape allows to set the conditions of a piece pulling in the gap between rolls, to use checked in practice destruction models for calculation of stress condition, and also it approaches equally well for both isometric and flat pieces.

Let's set previously the main geometrical parameters of rolls. The roll profiles are showed in Fig. 2 in plane of the maximum rapprochement passing through their axes.

Here, the conic sites have the taper angle β, and radiuses values correspond to the formula

$$r_2 = r_1 + b_0. \tag{9}$$

The schemes for calculation of grab angle by crusher rolls are presented in Fig. 3 and Fig. 4. The grab means such a forces ratio, when the friction forces pulling the piece into crusher exceed the components of pushing out forces.

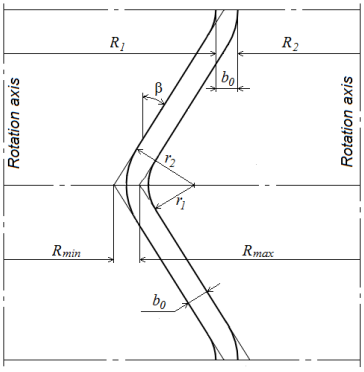

Fig. 2. Geometry of wave profiled rolls

The material piece of pincushion shape, being pulled in the gap between rolls on its shortest side of thickness $a=2r$, with its longest

side along the rolls axes, is shown in Fig. 3. It is the most probable position of the piece during pulling in crusher. The piece contacts with roll ledge of radius R_1 on the right side. Also, it contacts on the other side with roll hollow in two points located at distance R_c from the rotation axis (Fig. 4).

Forces P_1 and P_2 act along normal lines to contact surfaces. The force of dry friction, correspondingly, ($f_1 P_1$) and combination of $F_{fr,z}$ and $F_{fr,xy}$, act in tangential directions.

Here, such ratios have to be carried out by conditions of no slip

$$f_1 \le f \; ; \tag{10}$$

$$f_2 = \frac{\sqrt{F_{fr,z}{}^2 + F_{fr,xy}{}^2}}{P_2} \le f \; . \tag{11}$$

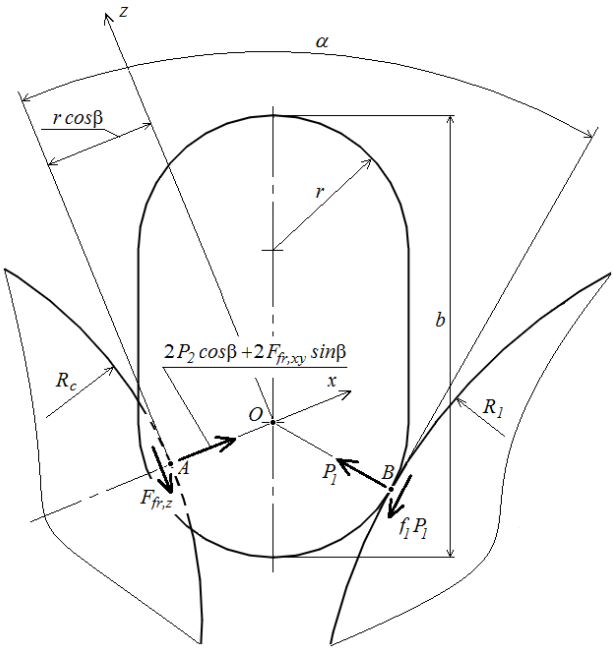

Fig. 3. Scheme for determination of grab angle (*x*-*z* plane)

Let's compose the equations of the piece balance:

- forces along *x* axis (Fig. 4):

$$P_1(\cos\alpha + f_1 \cdot \sin\alpha) = 2P_2 \cos\beta + 2F_{fr,xy} \sin\beta; \quad (12)$$

- forces along *z* axis (Fig. 3):

$$P_1(\sin\alpha - f_1 \cdot \cos\alpha) = 2F_{fr,z}; \quad (13)$$

- moments of forces relative to the point *A* in *x*-*z* plane (Fig. 3)

$$P_1 r \cos\beta \sin\alpha = f_1 P_1 r(1 + \cos\beta\cos\alpha). \quad (14)$$

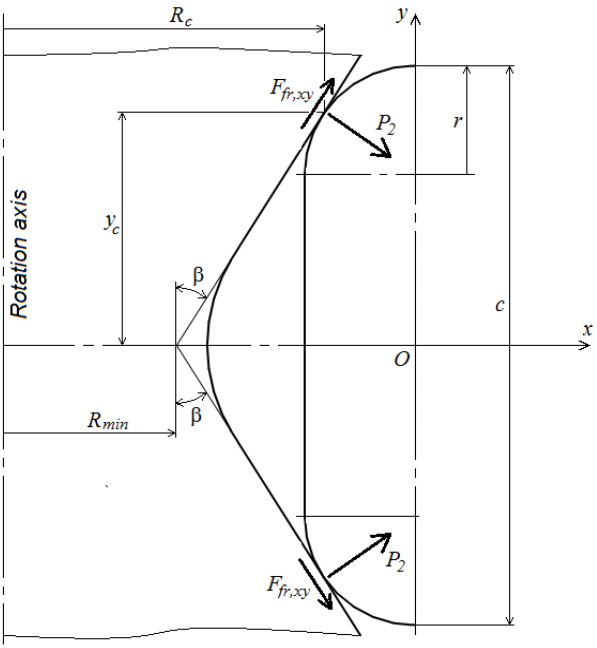

Fig. 4. Scheme for determination of grab angle (*x*-*y* plane)

It should be noted, that it is possible to set $F_{fr,xy}$=0, because the piece movement into the roll hollow (along *x* axis) is blocked. And we will have f_1=f_2=f while simultaneous reaching the extreme balance condition on both the rolls.

So, we will get the following ratio from Eq.(14):

$$f = \frac{\cos(\beta)\sin(\alpha)}{\cos(\beta)\cos(\alpha)+1}. \quad (15)$$

Also, we will have from Eq. (11)-(13):

$$P_2 = P_1 \frac{2\cos\beta}{\cos\alpha + f\sin\alpha}; \quad (16)$$

$$F_{fr,z} = \frac{P_1}{2}(\sin\alpha - f\cos\alpha) = fP_2. \quad (17)$$

The Eq. (15) coincides with Eq. (1) when β=0. The grab angle α increases together with the taper angle β. Thus, when f=0,3 and β=10º, 20º and 30º, relative rise of the grab angle values makes, correspondently, 0.8%, 3.3% and 8.0%.

Substantiation of maximum size of piece

The relative positioning of the piece and the rolls in *x*-*z* plane is shown in Fig. 5. Here, the corresponding distances values are the following: $O_1A=R_c$; $O_2B=R_1$; $AO\text{-}r\cos\beta$; $OB=r$. Also we have (see Fig. 2)

$$O_1O_2 = R_1 + R_2 + b_0. \quad (18)$$

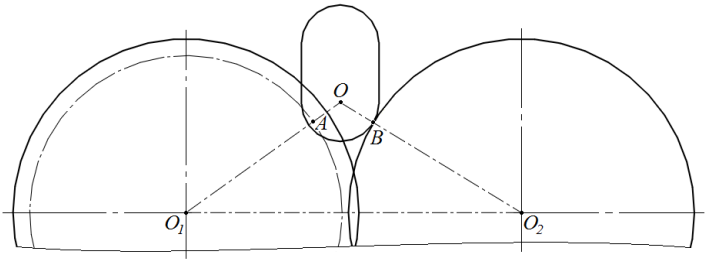

Fig. 5. Scheme to determine relative positioning of piece and rolls

Then, we can compose the following equation based on the cosine law for O_1O_2O triangle

$$(R_1 + R_2 + b_0)^2 = (R_c + r\cdot\cos\beta)^2 + (R_1 + r)^2 - \\ -2(R_c + r\cdot\cos\beta)(R_1 + r)\cos(\pi - \alpha), \quad (19)$$

where $\angle O_1OO_2=(\pi\text{-}\alpha)$.

The equations of interrelations between the characteristic radiuses of the roll profile can be written as follows (see Fig. 2 and 4)

$$R_{\max} = R_1 + r_1\frac{1-\cos\beta}{\cos\beta}; \quad (20)$$

$$R_{\min} = R_2 - (r_1 + b_0)\frac{1-\cos\beta}{\cos\beta}; \quad (21)$$

$$R_c = R_{\min} + r\tan\beta\left(\frac{c}{a} - 1 + \sin\beta\right). \quad (22)$$

Let's determine such parameters:

- average diameter of profile:

$$D = R_{\max} + R_{\min}; \quad (23)$$

- coefficient of profile depth:

$$k_h = \frac{2\left(R_{\max} - R_{\min}\right)}{D}; \quad (24)$$

- coefficient of piece size:

$$k_s = b/D; \quad (25)$$

- coefficient of piece thickness:

$$k_a = \frac{b}{a} = \frac{b}{2r}; \quad (26)$$

- coefficient of piece length:

$$k_c = c/b/D, \quad (27)$$

here $a \le b \le c$.

The dependence for the coefficient of piece size k_s on the taper angle β and the coefficients of piece shape k_a and k_c can be obtained from Eq. (15) and (19)-(27), setting such profile parameters as $R_{\max}$, $R_{\min}$ and r_1. The analytical dependence conclusion is possible, but it will be so complicated, that it doesn't make sence.

The results of calculation for input data k_h=0,16, k_{r1}=0,021 and k_h=0,011 are given in Table 1. Here, the width b is taken as the size of piece, because exactly the width determines if the piece goes through control sieve or not. Left column of the Table (β=0°) corresponds to the case of smooth rolls, and the size of piece also equals to $d=b$.

Table 1

Calculation values of coefficient of piece size k_S

β	0º	10º	20º	30º
k_a=1, k_c=1	0.055	0.055	0.057	0.061
k_a=1.32, k_c =1.32	0.072	0.069	0.067	0.067
k_a=1, k_c=3	0.055	0.047	0.043	0.04
k_a=1,73, k_c=1,73	0.095	0.082	0.074	0.069
k_a=3, k_c=1	0.16	0.14	0.13	0.12

The analysis of results shows, that the rise of β angle leads to the increase of pulled-in piece size up to 11% for isometric pieces (k_a=1, k_c=1).

As to the piece of average cuboid shape (k_a=1.32, k_c=1.32), the increasing of β angle reduces the pulled-in piece size up to 7%.

The rise of β leads to decreasing of the maximum piece size up to 27% for the pieces of needle shape [10] having (k_a=1, k_c=3) values of shape coefficients.

The size of pieces of lamellar shape [10] with parameters (k_a=1,73, k_c=1,73) and (k_a=3, k_c=1) is also reduced up to 27% while β angle increases.

Analysis of Efficiency of Large Pieces Destruction

We will carry out the analysis of the piece stress condition in terms of a flat model, corresponding to central section of the piece in longitudinal plane. The grab of piece is equal to the one considered in Fig. 4.

Here, we assume the following:

settlement forces are applied in the piece plane of symmetry x_2-y_2 (Fig. 6);

we neglect the local stresses in contact areas and the dimensions of such areas.

In such a case, we are interested not in absolute values of crushing stresses and forces, influencing the piece of real irregular shape, but in ratios of stresses and forces for the simulated pieces with different ratio values of dimensions, being destructed by rolls with smooth or wave profile.

The settlement concentrated forces, influencing the piece, are approximately determined by formulas

$$P_{1,c} = P_1.\left[\cos(\alpha/2) + f\sin(\alpha/2)\right]; \tag{28}$$

$$P_{2,c} = \frac{P_{1,c}}{2\cos\beta}. \tag{29}$$

The components of $P_{2,c}$ force along x_2 and y_2 axes are so

$$Q_2 = P_{2,c}\cos\beta = \frac{P_{1,c}}{2}; \tag{30}$$

$$N_2 = P_{2,c} \sin\beta = \frac{P_{1,c}}{2} \tan\beta . \qquad (31)$$

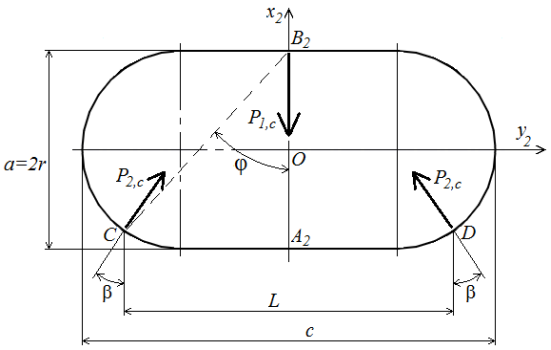

Fig. 6. Calculation scheme of piece loading

We assume, that the most probable ways of the piece destruction are the following:

shear on the line close to B_2C (or B_2D), caused by $P_{1,c}$ force;

destruction on the line close to A_2B_2 by stretching stress of bending in point A_2, caused by forces $P_{1,c}$ and $P_{2,c}$.

Here, the tangential stress values are taken average on the shear planes. As to point A_2, we will take into consideration only the stretching stress along y_2 axis, because the normal stress along x_2 axis and the tangential stresses along x_2 and y_2 axes are equal to zero.

In the first settlement case, average values of stress components, acting along B_2C shear line, are determined by formulas:

- normal compressive stress:

$$\sigma_{c1} = \frac{P_{1,c} \sin\varphi}{F_s}; \qquad (32)$$

- tangential stress:

$$\tau_1 = \frac{P_{1,c} \cos\varphi}{F_s}, \qquad (33)$$

where $F_s = f\left(r, k_a, k_c, \beta\right)$ is the shear surface area; φ is the angle of acting force deviation from the shear plane

$$\varphi = \operatorname{atan}\left(\frac{c/a - 1 + \sin\beta}{1 + \cos\beta}\right). \qquad (34)$$

The main stresses acting at the shear site are calculated from the expression

$$\sigma_{1,3} = \frac{1}{2}\left(\sigma_{c1} \pm \sqrt{{\sigma_{c1}}^2 + 4{\tau_1}^2} \right). \quad (35)$$

The equivalent destruction stress for a piece in multi-axial stress condition is determined according to [6]

$$\sigma_{e1} = \frac{(\psi - 1)(\sigma_1 + \sigma_3) + \sqrt{(1-\psi)^2(\sigma_1 + \sigma_3)^2 + 4\psi(\sigma_1 - \sigma_3)^2}}{2\psi}. \quad (36)$$

The first settlement case is relevant for small values of φ angle, for close to isometric piece shape.

The value of stretching stress in A_2 point along y_2 axis is calculated in the second settlement case as follows

$$\sigma_{f2} = \frac{0.5Q_2L - N_2 r\cos\beta}{W_{y2}} - \frac{N_2}{F_{y2}}, \quad (37)$$

where L is the rated length of bending part (see. Fig. 6)

$$L = 2r(k_a k_c - 1 + \sin\beta); \quad (38)$$

W_{y2} is the axial bending section modulus of the piece

$$W_{y2} = r^3\left[\frac{\pi}{4} + \frac{4}{3}(k_a - 1)\right]; \quad (39)$$

F_{y2} is the piece cross-section area:

$$F_{y2} = r^2[\pi + 4(k_a - 1)]. \quad (40)$$

The value of equivalent destruction stress in A_2 point according to Eq. (8) is given by expression

$$\sigma_{e2} = \frac{\sigma_{f2}}{\psi}. \quad (41)$$

The second settlement case is relevant for pieces of needle and lamellar shapes.

The coefficient of equivalent destruction stress increase is used for estimation of efficiency of the wave profiled roll crusher in comparison with the smooth roll crusher

$$k_\sigma = \frac{\sigma_e}{\sigma_{e0}}, \quad (42)$$

where σ_{e0} is the basic equivalent stress, which is created in the

same-shaped piece in the crusher with smooth rolls of the same dimensions.

Here, it goes about the piece being clamped in A_2 and B_2 points and cut along the trajectory close to this line by $P_{1,c}$ force. In this case, taking into consideration Eq. (7) and (8), we obtain the following

$$\sigma_{e0} = \frac{2}{\sqrt{\psi}} \frac{P_{1,c}}{F_{y2}}. \qquad (43)$$

The calculated values of the coefficient of equivalent destruction stress increase are given in Table 2 for the crusher with wave profiled rolls. The values in numerator are for the shear case, the values in denominator are for the bending case.

Table 2

Calculated values of k_σ coefficient

β	10º	20º	30º
k_a=1, k_c=1	1,0 -	0,93 -	0,85 -
k_a=1.32, k_c =1.32	0,65 2,0	0,59 1,9	0,52 1,7
k_a=1, k_c=3	- 6,2	- 6,0	- 5,9
k_a=1,73, k_c=1,73	- 5,3	- 5,1	- 5,0
k_a=3, k_c=1	- 5,0	- 4,8	- 4,6

The analysis of results proves, that only destruction of ideally isometric pieces gives 15% increase of acting force during destruction in the crusher with wave profiled rolls in comparison to smooth rolls. Here, we mean linear dependence of the force on the equivalent destruction stress.

In any other cases, the wave profile of rolls is more efficient than the smooth one approximately from 2 to 6 times. The more the piece differs from isometric shape, the stronger is this effect.

Conclusions

The crushers with wave profile of rolls are more efficient than ones with smooth rolls mainly due to the usage of bending instead of shear deformations for the destruction of large rock pieces.

The usage of the wave profile increases the angle of material grab up to 8% compared to smooth rolls.

The maximum size of pulled-in piece is up to 11% more for the isometric shape, but from 7 to 27% less while the shape declines from isometric one.

The usage of wave profile is resulted in reducing of acting forces for crushing of pieces of non-isometric shape from 2 to 6 times compared to smooth profile of rolls.

Further, the work results will be used for designing of operational part for the crushers with wave profiled rolls, in order to decrease sufficiently the energy consumption of mining rocks crushing.

References

[1] Spravochnik po obogashcheniiu rud (1982). Pod red. O.S. Bogdanova. Vol. 1. Podgotovitelnye protsessy. Nedra, Moskva, 367 p.

[2] **Avdokhin, V.M**. (2006). Osnovy obogashcheniia poleznykh iskopaemykh. Uchebnik dlia vuzov. Vol. 1. Obogatitelnye protsessy. Izd-vo MGGU, Moskva, 417 p.

[3] **Nadutiy, V.P. and Tytov, O.O**, National Technical University «Dnipro Polytechnic» (2019), Valkova drobarka [Roll crusher], Dnipro, UA, Pat. № 132083.

[4] **Andreev, E.E., Bilenko, L.F. and Perov, V.A**. (1990). Drobleniye, izmelcheniye i grokhochenie poleznykh iskopaemykh. Nedra, Moskva, 301 p.

[5] **Kartashov, Yu.M., Matveev, B.V., Makeev, G.V. and Fadeev, A.B.** (1979). Prochnost i deformiruemost gornykh porod. Nedra, Moskva, 269 p.

[6] **Shashenko, O.M., Pustovoitenko, V.P. and Sdvizhkova, O.O.** (2016). Heomekhanika: Pidruchnyk dlia VUZiv. Novyi druk, Kyiv, 528 p.

[7] **Shashenko, A.N., Surgay, N,S, and Parchevskiy, L.Ya.** (1994). Metody teorii veroiatnostey v geomekhanike. Tekhnika, Kiev, 216 p.

[8] **Baklashov, I.V.** (1988). Deformirovanie i razrushenie porodnykh massivov. Nedra, Moskva, 270 p.

[9] **Yelishevich, A.T**. (1989). Briketirovanie poleznykh iskopaemykh. Ucheb. dlia vuzov. Nedra, Moskva, 300 p.

[10] DSTU B V.2.7-75-98 (1999), Shchebin i hravii pryrodni dlia budivelnykh materialiv, vyrobiv, konstruktsii i robit. Tekhnichni umovy, Uved. 25.08.1998, Derzhavnyi komitet budivnytstva, arkhitektury i zhytlovoi polityky Ukrainy, Kyiv.

OBJECTIVE-ORIENTED APPROACH TO IMPROVING ENVIRONMENTAL SECURITY OF PRODUCTION TECHNOLOGIES AND PROCESSING OF MINING

Bredun V.I.
PhD, associate professor
Poltava National Technical Yuri Kondratyuk University, Ukraine

Stepova O.V.
associate professor PhD
Poltava National Technical Yuri Kondratyuk University, Ukraine

Maksiuta N.S.
assistant PhD
Poltava National Technical Yuri Kondratyuk University, Ukraine

Abstract

The paper considers the prerequisites and principles of modernization of object-oriented technologies of environmental safety management of oil and gas and mining enterprises as an element of ensuring the rational and energy-efficient use of natural resources and preserving the ecosystems of the regions.

In the course of the research, the concept of environmental safety management of mining enterprises was developed based on the analysis of the interaction of objects of natural-technogenic systems of the mining industry territorial-industrial complexes. The theoretical aspects of the formation of ecologaical hazards by the objects of the mining industry have been established. The scheme and mechanism of formation of the ecological hazard in regions under the influence of technogenic factors are determined. Internal and external sources of generation of ecologically hazardous factors in relation to technological objects of oil and gas production and transportation have been established. The expediency of at least a two-stage study of the ecological hazard formation of mining complex objects and transport systems is substantiated. The structure of formation of ecological hazard of the region by technogenic factors is developed in a general form and the system of ecological safety management of technologic loaded regions, that is built on the basis of the principles of correlation of object and regional levels, which is the basis of an object-oriented approach to ecological safety management. A characteristic feature of the system is that the development of specific technical solutions is based on the results of research of different ways to reduce the impact of anthropogenic factors on the environment and human, as well as the possibility of their implementation in the specific region.

Keywords: mining enterprises, environmental safety, management system, factor, hazard formation.

Introduction

Mining is an important component of economic development in many countries. For many countries, oil and gas production in today's economic and geopolitical context is becoming an important strategic direction for ensuring economic stability and energy independence. However, mankind is well aware of the negative environmental consequences of the activities of mining companies, which in the conditions of modern technogenic load on the natural environment is extremely unacceptable. Therefore, the issue of ensuring the environmental safety of hydrocarbon and mineral production facilities must be an integral element of the philosophy of nature using any modern mining company and the state as a whole.

Environmental aspects of exploitation of mining enterprises can be analyzed in terms of impact on the atmosphere, surface and groundwater, soils and landscapes, biodiversity. Traditionally, the environmental impact of hydrocarbon transportation systems has been attributed to the contamination of soil and water, the emission of gas flares, etc. into the atmosphere. Many scientists in the world are devoted to solving these questions. Both individual factors and their complex interaction were investigated. However, the existing environmental management systems of the mining industry only allow for a certain parity between the intensification of production processes and the environmental impact. Therefore, the modernization of technologies for managing the environmental safety of oil and gas and mining enterprises as an element of ensuring the rational and energy-efficient use of natural resources and preserving the ecosystems of the regions is an urgent task.

Therefore, the purpose of the research is to develop the concept of environmental safety management of mining enterprises based on the analysis of the interaction of objects of natural-technogenic systems of territorial-industrial complexes of the mining industry. For this purpose, using the methods of factor and structural-genetic analysis and synthesis, the mechanism of formation of ecological hazard of regions under the influence of technogenic factors, peculiarities of research of the process of formation of ecological hazard will be found out, and the structure of the system of ecological safety management of the region under conditions of technogenic loading will be developed.

1. Theoretical bases of ecological hazard formation by extractive industry objects

Functional load on the environment in the process of ecological hazard formation in oil and gas and mining regions is multifactorial. For example, the geological environment is at the same time an environment of technologic mechanical impact and a zone of the generation of technogenic seismic fields, a tool for transferring seismic energy to ecologically hazardous technogenic systems, the object of possible contamination by hydrocarbons and by their migration into groundwater.

The mechanism of formation of a specific state of the environment is essentially a set of interrelated events, processes that occur with particular elements of the environment by known or unknown laws. Of course, some random factors determine the choice of standardized algorithms for the situation.

Most negative environmental factors can affect a person in two ways: directly and indirectly. It is advisable to consider the direct influences path if the impact parameters exceed the sanitary norms. Then the environmental factor is a direct factor in the formation of the ecological safety of the territory by sanitary indicators.

Consider the indirect way of formation of ecological hazards (Fig. 1).

This scheme is generalized. In industries related to mining, including oil and gas, most of the negative environmental factors are closely related to the geological environment. It is both the place of origin, the medium of distribution, and the object of influence of these factors. Explain this with an example of technogenic seismicity.

As a result of technological processes, mechanical oscillations occur in the sources of technogenic seismicity, which generate technogenic seismic waves (TSW) in the geological environment. Distributing in a geological environment, TSW reach the location of a particular seismically affected object. There is a process of transfer of TSW energy to the object. Under the influence of this energy, the structural elements of the object make vibrational motions, which can cause mechanical connections between the individual structural elements as well as the internal structure of the elements. As a result, the engineering condition of the object changes. Any natural or artificial object has its level of potential ecological hazard, as well as

the degree of risk of realization of the potential hazard. Changes in the status of an object cause a change in its hazard levels. As any material object cannot exist separately from a specific territorial structure, the level of environmental security of the object's location changes as a result. The described sequence is a channel of formation of ecological safety of a region by the influence of sources of the TS on anthropogenic objects.

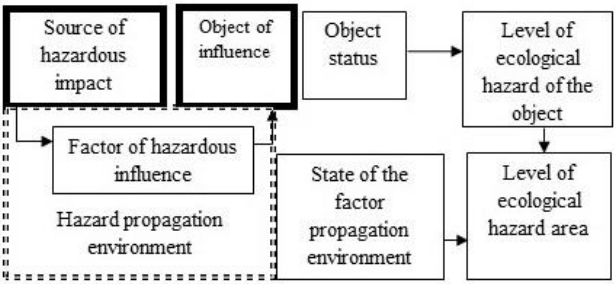

Fig. 1. Simplified scheme of ecological hazard formation under the influence of technogenic environmental factors on abiotic objects

If we consider the geological environment not only as a distribution medium but also as an object of TSW impact, then a channel of formation of environmental safety of the region due to the effect of human-made seismic sources on natural abiotic objects emerges.

The mechanism of formation of ecological hazard of the industrial region under the influence of technogenic factors in the general form is a set of elements of the environment, processes, and states (Fig. 2).It should be noted that the nature and level of the hazards that create different sources of hazard is determined by their type and characteristics. This makes it possible to influence the state of environmental safety by changing its structural and technological features.

The role of the impact propagation environment in the process under study and the mechanisms of formation of the influence fields of various factors are mostly well known. It is proved that the process of propagation of one or another factor (chemical pollution, technogenic seismicity, etc.) in the geological environment depends on its structure and physical characteristics. Therefore, these parameters can be used to control the environmental impact of TS.

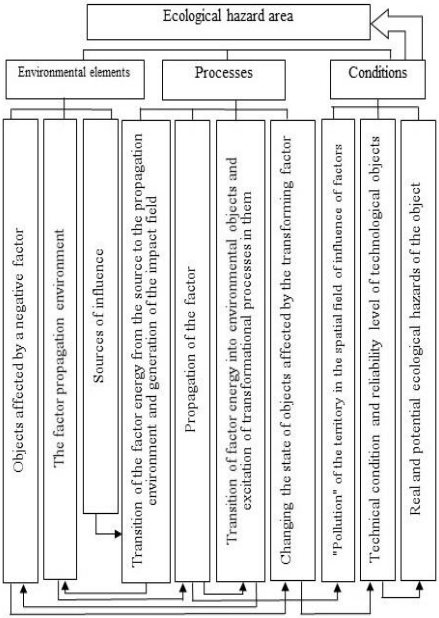

Fig. 2. The mechanism of formation of ecological hazard regions under the influence of anthropogenic factors

The processes of the transition of the energy of the factor from the source to the propagation medium and the object of influence are the boundary processes occurring at the intersection of the two environments. The main method of regulating the flow of this process is to apply specific technical solutions in the energy transition zone to absorb or redirect energy flows.

Changing the engineering state of an object is a complex process with a significant period (seconds to years) [1]. The intensity of its flow and the results depend to a large extent on the parameters of the influence factor (concentration, intensity, etc.), structural features and characteristics of the objects, as well as, for example, technogenic seismicity, the ratio of the amplitude-frequency characteristics of the waves and objects. Changing such parameters, that is possible to influence the result of the processes of environmental transformation, which is the level of engineering reliability of technological objects of oil and gas or mining complex,

as well as other natural and anthropogenic objects located in the field of influence of a hazardous human-made environmental factor.

Each engineering object has its structural degree of strength (whether seismic or corrosion resistance) and ecological hazard class [2]. Over time, under the influence of internal and external factors, the technical reliability of engineering facilities declines, and the risk of accidents (manifestations of hazard) increases. The magnitude of the potential hazard may remain at the basic level. However, the ecological hazard level of the object, as a function of the reliability of a hazard, will increase.

The ecological hazard of the mining region is determined by a complex function, the components of which, among other things, are the levels of hazards of individual human-made objects [3]. Thus, the impact on the level of hazard of a particular object changes the level of ecological hazard of the region. And the combination of various natural and human-made objects in the region determines the species composition and nature of the hazards. This leads to the legitimacy of an object-oriented approach to the processes of ecological hazard formation in technogenically loaded regions, which can be attributed to any territory with developed oil and gas or mining industries.

Sources of the generation of ecologically hazardous factors about technological objects of oil and gas production and transportation can be divided into internal and external (Fig. 3).

Internal sources of ecological hazards include the technological equipment of oil and gas production and transportation facilities (mainly drilling rigs, powerful pumping and compressor stations). Thus, internal sources are sources of the ecological hazard of anthropogenic genesis, which form fields of chemical or physical pollution of the geological environment (oil and process fluids entering groundwater and soil, human-made seismicity). The objects of their influence are the natural and anthropogenic elements of the environment and the technological objects of the deposit.

External sources of ecological hazards include natural processes and anthropogenic objects that may adversely affect the technological equipment of the drilling and transport networks.

It is expedient to carry out research into the formation of ecological hazard of objects of oil and gas complex and transport systems in several stages.

In the early stages of exploitation of the fields, the following can be attributed to the inland: drilling equipment, pumping and compressor stations, oil and gas pipelines. External - natural geophysical and hydrological processes in the area of extraction and transportation, as well as third-party man-made objects. In the late stage of the field operation, a factor of influence on the technological objects of the results of the transformation of the environment by internal factors is added. For example, natural, anthropogenic earthquakes may occur with or without subsidence [4].

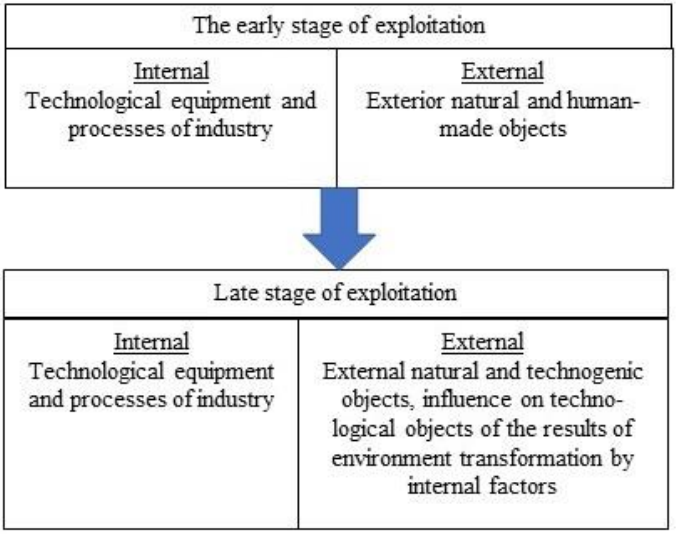

Fig. 3. Sources of ecological hazard formation by seismic factors at different stages of oil and gas field exploitation

It should be noted that in each case the structure of the hazard and its level would be determined by regional conditions (the presence of a neighborhood of potentially hazardous natural or human-made objects, their nature and degree of hazard, the conditions for the spread of the hazard).

As an example of the interaction of internal and external factors that accompany the entire life cycle of oil and gas facilities, let us consider the process of formation of ecological hazards of technological objects of the oil and gas transportation system by the factors of corrosion wear of equipment. An internal factor is the

emergence of electrostatic potentials along the pipeline from the movement of oil or gas and the state of waterproofing of the pipeline. The external factor is the corrosive activity of soils in the area of the pipeline.

2. Object and region - elements of the chain of formation of ecological hazards.

As can be seen from the previous material, as well as other sources [5, 6], in the theory of ecological hazard formation and management of ecological safety of territorial-industrial complexes of oil and mining industries, the object and the region are elements of one chain "natural resources - human-made object - environment - region - ecological safety".

In Fig. 4 shows, in general, the structure of formation of the ecological hazard of the region by human-made factors.

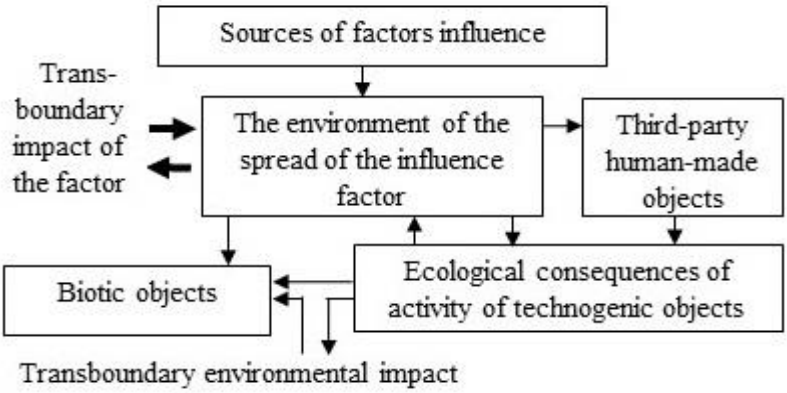

Fig. 4. Dynamic structure of ecological hazard of techno natural geosystem

This block diagram can be adapted to any human-made factor. In addition, the structure may have parallel branches — for example, chemical pollution in the area of the pipeline in the event of an emergency. Depending on the conditions of the particular terrain, the topsoil (geological) surface and surface water, bodies (rivers, lakes, etc.) may be the objects of pollution and, at the same time, the field of influence of this factor.

Characteristic of the extractive industries is the presence of two

paths of transboundary impact. The first is caused by a primary hazardous factor (for example blasting of quarries → technogenic seismicity → change of geological structure outside the field → change of hydrological regime of territories, etc.). The second is caused by secondary environmental factors, which are the consequences of the activity of both primary and third party human-made objects.

3. Environmental safety management system for mining facilities

Environmental safety management is a complex process that is based on common principles and is primarily determined by regional characteristics. There are different theories, methodologies, systems of environmental safety management: synergistic approach [7], management using probabilistic structural modeling [8], economical approach [9], complex hierarchical regional system of technical and technological management [10], and others.

In Fig. 5 presents the environmental management subsystems of the technogenically-loaded regions, built based on the above principles of the ratio of the object and regional levels, which is the basis of an object-oriented approach to environmental safety management.

The management process consists of five steps: 1) exploring the ecological factor in the facility and the region (identifying sources and objects of the float, investigating the environment of the impact field); 2) assessment of the current state of environmental safety; 3) determination of methods of regulation of anthropogenic load, formed by each factor, on the basis of the analysis of the mechanism of formation of hazard and development of specific technical and organizational solutions; 4) implementation of decisions; 5) analysis of the results obtained.

The basic procedure of the first stage (1 in Fig. 5) is to monitor sources and objects that are affected by a specific factor. The purpose of monitoring the sources is to determine their location, zones of influence of factors and environmental objects located in these zones, to determine the types of emerging hazards, conditions of their distribution, the maximum size of the zones of formation of hazards with seasonal changes.

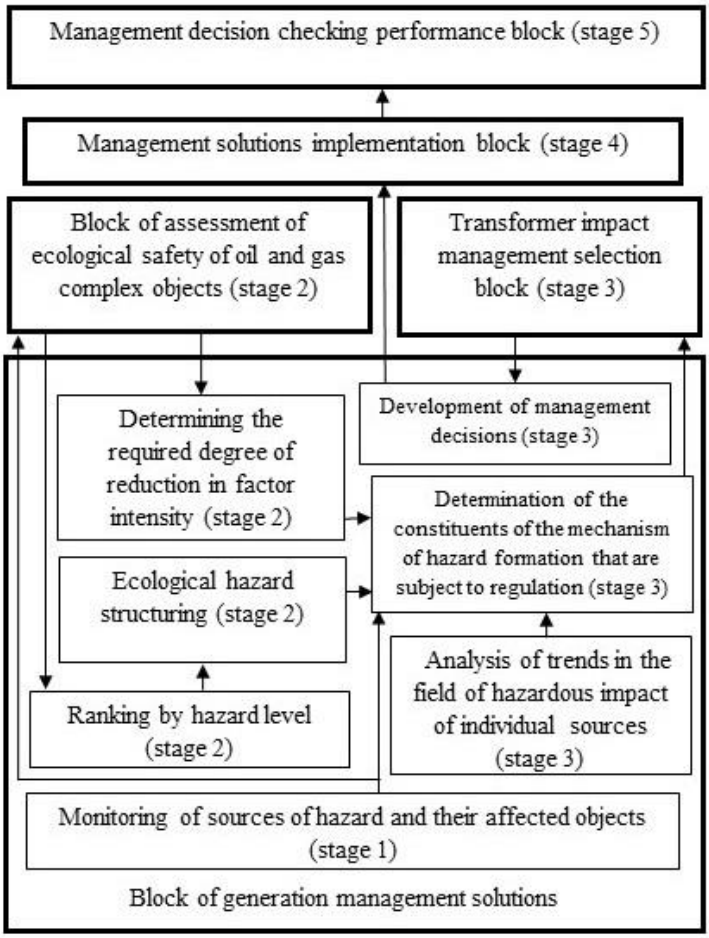

Fig. 5. The system of management of ecological safety of the region in the conditions of technogenic loading (in brackets the stages of the management process, during which certain elements of the system are implemented) are specified

The dimensions of the zone of possible spread of ecological hazards in case of disturbance of the object, which is adversely affected by a factor (such as technogenic seismicity), may exceed the size of the zone of distribution of the primary hazardous factor from a specific source (eg seismic influence of a hazardous level of a specific source). The potential source area of the primary source will

then be determined by the area of potential ecological hazard of the affected object.

In the case of overlapping of the zones of action of several sources, dominant sources (such as generating a factor of the maximum level, such as oil contamination of the soil) are determined, as well as the imposition of the same elements from other separate sources.

In the course of the monitoring of the affected objects, their type, resistance to the action of a specific factor, the characteristics of the object that can enhance or diminish the effect of the factor, the physical condition, nature, and extent of the potential hazard are established.

As a result of the works of the first stage, potentially hazardous combinations are identified, the "object of hazard is a source of impact" and a regional structure of ecological hazard is formed, formed by all factors generated and distributed by all technological and natural objects on the territory of the research. At this stage, to fully understand the hazards, it is essential to have a comprehensive analysis of all-natural and human-made objects that are in the area of real and potential impact of the exploration enterprise.

In the second stage (2 in Fig. 5), depending on the scale of possible ecological consequences and the degree of risk of realization of the hazards, the ranking is performed most probable potential, highest potential hazard and hazard profile of the territory is determined. The basis of this step is the procedure for assessing the environmental safety of individual object and the region as a whole.

The result of the implementation of the work of this stage is to determine the priority areas for environmental measures and the necessary value of reducing the intensity of technogenic factors, which is a task for the next stages.

The third stage identifies the elements of the mechanism of formation of hazard, the correction of which achieves the solution of the tasks set in the second stage. For each specific situation, based on the principles of development of complexly organized systems [7], the own trends of development are forecasted. For example, the plan for the development of the field laid the gradual removal of the front of blasting from the settlement. In this case, there will be a gradual

self-organized decline in the impact of the quarry on the rural area within the programmed development of "quarry - city". Using systems of measures to establish safe operating conditions of structures in man-made earthquakes [10], taking into account the trends of self-development, one or more elements for regulation (parameters of the source, propagation environment or object affected by human-made seismic waves) are determined according to which specific methods of safety management are selected (block of choice of methods of management of technogenic seismic influence in Fig. 5):

- positioning in the space and time of sources of anthropogenic seismicity and objects affected by anthropogenic seismic waves (for example, organizing the movement of multi-tonnage transport outside the settlement, conducting explosions at the quarries of the region on different days);
- engineering arrangement of the zone of transition of energy of oscillations and contact zones of sources and objects (installation between the soil and the foundation of the building of the vibration absorbing layer);
- creating conditions for increasing the degree of attenuation of techno-waves in the geological environment (loosening of soils);
- antigenic phasing of simultaneously operating sources of technogenic seismic waves;
- rational design of structural and technological parameters of sources and objects affected by technogenic seismic waves (preventing the occurrence of resonant vibrations);
- elimination of sources.

The final procedure at this stage is the development of appropriate management decisions, the essence of which is to create new and improve the efficiency of existing technical means and organizational measures that ensure the achievement of acceptable environmental safety in the region of extraction, transportation or processing of minerals.

The development of specific technical solutions is based on the results of experimental studies of ways to reduce the impact of technogenic factors on the environment and man, as well as the possibility of their implementation in the specific region.

During the implementation of the fourth stage (4 in Fig. 5), practical application is carried out in the conditions of the studied region, developed for each solutions: carrying out certain organizational measures, engineering equipment of the territory, the use of technical devices and systems.

The fifth stage (5 in Fig. 5) is an analysis of the effectiveness of the implementation of management decisions. Its result is the conclusions about improving the environmental safety of the industrial site and the region.

The sequence and content of the steps describing the scheme of fig. 5 is, in essence, an object-oriented heuristic algorithm for managing the ecological safety of human-made territories, which can be specified under the specific features of the socio-man-made structure of any industrial region.

Conclusions: The introduction of object-oriented technologies for managing the environmental safety of oil and gas and mining enterprises is an essential element in ensuring the rational and energy-efficient use of natural resources and preserving the ecosystems of the regions. The mechanism of formation of the ecological hazard of regions under the influence of technogenic factors includes both internal and external sources of generation of ecologically hazardous factors concerning technological objects.

This is advisable to conduct at least two stages of investigating the ecological hazards of mining complexes and transport systems. This will create an effective environmental management system throughout the life cycle of the industrial site.

The ecological security management system of the technogenically-loaded regions is based on the principles of the correlation between the objective and the regional levels, which is the basis of an object-oriented approach of environmental safety. The main principle of system construction is the development of specific technical solutions based on the analysis of research results of ways to reduce the impact of human-made factors on the environment and

humans, as well as the possibility of implementation.

References

1. **Perelmuter A.V.** (1999) Selected problems of reliability and safety of building structures. Kyiv: Ukrniiproektstalkonstruktsiya.

2. Criteria for the distribution of economic entities by the degree of risk of conducting economic activities for the safety of life and health of the population, the environment and the frequency of implementation of state surveillance (control) measures: approved by the Cabinet of Ministers of Ukraine of May 28, 2008 No. 493.

3. **Kachynskyi A.B.** (1997) Environmental safety of Ukraine: analysis, evaluation and state policy. **Kyiv: NISD.**

4. Bredun V.I. (2017) Formation of ecological hazard of objects of oil and gas industry of Poltava region by factors of technogenic seismicity. Ecological safety, 2/2017 (22), 21-26.

5. **Bredun V.I.** (2017) The natural resource potential of the region as a factor in the formation of ecological hazards. Theses of the 69th scientific conference of professors, teachers, researchers, graduate students and students of the PoltNTU. Volume 1, 291-293.

6. **Bredun V.I**. (2017) Geotechnical aspects of formation of ecological hazard of oil and gas complex objects. Environmental safety issues: abstract of the 15th International Scientific and Practical Conference, 19.

7. **Muravych A.I.** (2004) A synergistic approach to environmental safety management. Law and security, №3 (12). Retrieved from http://dpr.ru/pravo/pravo_9 _26.htm.

8. **Begun V.V**. (2007) Development of technogenic city safety management methods based on probabilistic structural and logical models of production hazards. (PhD dissertation abstract).

9. **Luc`ko V.S.** (2001) Improvement of the economic mechanism of regulation of ecological safety. (PhD dissertation abstract).

10. **Shmandiy V.M**. (2003) Environmental management at the regional level (theoretical and practical aspects). (Doctoral dissertation).

STUDY OF THE CONDITIONS FOR BLAST WAVES EXCITATION AND DAMPING

Zaikina D.P.
PhD seeker ((Engineering), associated professor of the Department of General Engineering Disciplines and Equipment,
Donetsk National University
of Economics and Trade named after Mykhailo Tugan-Baranovsky,
Ukraina

The studies were carried out on the basis of a search and analysis of publications on the work subject, the analysis of the research subject was used to mathematically formulate the problem and justify the boundary conditions and parameters of numerical modeling. To justify rational configurations, an analytical assessment of the interaction of the wave front and the working wall was performed. By numerical simulation, the physical processes of waves propagation control are studied.

Analysis of the physical processes occurring during the suppression of blast waves by taking into account the influence of mechanical parameters on the structure and configuration of the blast wave made it possible to identify a number of qualitative and quantitative laws of motion of the wave front at the interface.

The considered parameters ($\Delta P+$, t_0, d_t+) make it possible to generate accurate theoretical information about the blast wave, which subsequently will help us to develop effective techniques and methods of damping the blast wave and increase the efficiency of personnel protection from the action of waves in long structures of mining facilities. Classifications of configurations and areas of existence of their different varieties are analyzed: type 1, type 2, type 3, type 4. It is determined that the most problematic issues are significant underestimation of low pressures, overestimates of excess pressures and inaccuracies in phase duration on different sides.

1 Introduction.

Anticipating the effects of the blast wave generated from explosive material is undoubtedly the main task in the design of techniques and methods for blast wave exciting and damping, and for protection or mitigating the consequences of an accident. From this point of view it is necessary to take into account that the waves of combustion and detonation propagating through the mine openings are characterized by the following features [1-2]:

huge ranges of implemented parameters per speeds, pressures, time, and the like;

significant heterogeneity of the parameters in space, especially strongly affecting the kinetics of dust and gas mixtures in mine openings;

the heterogeneous nature of the air – dust system in mine openings;

the effect of the generated pressure pulse and the induced pulse on the design and configuration of the blast wave;

the initial form of explosive material, which are the most important and determining for the shape of the blast wave.

2 Literature review and problem statement.

Due to the high peak overpressure and a sharp rise time, the blast wave has a devastating effect on the environment, personnel and process equipment. This issue has been the subject of a lot of studies [ ].

Authors Benselama et al. studied the principle of the action of a blast wave in tunnel structures of a quadrangular section; a series of parametric analyzes were performed to study the effect of the relative initial position of the explosive and the cross-sectional area of the tunnel on the development of the blast wave.

In the work of Larcher et al. complex numerical model was developed for analyzing the effect of ventilation on the evolution of pressure and momentum after detonation of explosives. It has been determined that zone ventilation has a strong impact on the effects of an explosion (including injury levels).

Clutter and Stahl pay attention to various scenarios with complex configurations and geometries. Scientists have proposed a new interpretation of the term "explosive source." To study the relevance of geometric detalization during complex media and blast waves modeling, the scientists applied the definition of enthalpy, which was subsequently confirmed by several experiments with a shock tube, which served as an extension of the experimental model.

Vanderstraeten et al. studied the relationship between the configuration after detonation and the form before detonation of an explosive material. Based on the study, Lefrancois et al., Mespoulet et al. developed a numerical model.

Wojciech Mamrak examines an approach for comparing analytical and numerical wave propagation methods; compares the results by using various numerical codes - Computational Fluid Dynamics (which is part of the Air3D software) and Coupled

Eulerian Lagrangian (Abaqus software). Subsequently, a simplified model was adopted (in Python script), which makes it possible to simulate the environment, interference, etc. inside it. Thus, the scientists performed 29 simulations and studied three tasks (determination of the specific energy of TNT (3.68 MJ/kg); blast wave flow; shielding phenomenon). Wojciech Mamrak revealed that one of the two main phenomena associated with the propagation of waves is shielding. The influence of the second one is directed energy transfer.

Based on the foregoing, the following conclusions were obtained:

The internal peak pressure is about 25% of the external reflected pressure;

The results obtained using the Abaqus software tool are useful for accurate and simple, as well as for more complex geometries (CFD codes are more reliable).

However, the study did not take into account the phenomenon of absorption of the wave and its energy by obstacles, their deformation, or damage criteria.

Various methods for estimating peak pressure were collected in the works of T. Ngo, P. Mendis, A. Gupta, J. Ramsay.

Eriksson, Keenan, Wager, Vretblad, Joachim, Lunderman, Chabin, Pitiot, Absil et al. conducted series of experiments to study the mitigation of the blast wave effects through a water shield. It was found that storing water near an explosive atmosphere significantly reduces the maximum peak pressure and momentum. According to the tests, crushed small droplets upon impact can achieve a pressure reduction of up to 90%. However, recent studies have shown only a small effect of water mitigation in the KLOTZ-Club tunnel. In addition, it was determined that in some cases, water enhances the effect of the blast wave.

However, progress has an impact on the development of many aspects of technology and science, including the appearance of numerical codes, which makes it possible to simulate situations. Numerical simulation is an alternative to expensive testing.

Shin et al. conducted numerical studies on the softening effect of a blast wave with water using the multimaterial Euler finite element method.

Chong, Cheng et al. conducted a series of three-dimensional numerical calculations on DYTRAN software. Birnbaum et al. simulated tests inside the chamber using the AUTODYN software.

Based on a critical analysis of scientific papers on blast wave damping means and methods design, it is established that modern research is focused on the analysis and study of peak pressures, arrival time, and blast wave impulse. The exception is that in the above studies, the shape of the initial blast wave is assumed to be spherical.

3 The aim and objectives of the study.

This article discusses the conditions for the excitation and suppression of a blast wave by taking into account the influence of a number of parameters on the structure and configuration of the blast wave.

4 Materials and methods used in studying.

A blast wave is a special type of perturbation generated by a chemical reaction zone (flame front), and is a region of medium compression with a sharp jump in pressure, density and temperature, moving at a supersonic speed. In this case, the dynamic action of the explosion is usually estimated by the basic parameters of the wave, i.e. according to wave energy, its momentum, maximum pressure, etc. The parameters of the wave or equivalent to this explosion parameters, as is known, depend on the combustion process. When burning any combustible mixture, two stages are distinguished, namely: ignition, combustion itself, which can proceed at different speeds, depending on a number of internal natural properties of the fuel, oxidizer, and external environmental conditions. The phenomenon of wave interaction is very complex and significantly different from linear wave phenomena, since the usual laws of superposition, reflection, and refraction become inapplicable. The nature of wave reflection substantially depends on its intensity and angle of incidence on the reflected surface. At sufficiently large angles between the wave front and the wall, the resulting reflected wave propagates faster than the point of intersection of the incident wave from the surface of the working wall. Thus, we consider the following configuration modeling options performed using the MM-ALE technique implemented on the commercial FEM code LS-DYNA v. R7.

1. Free field configuration.

Qualitatively, the modeling tool correctly displays all the phenomena present during the interaction of a wave with an obstacle.

The configurations studied on a small scale are designed to analyze several physical phenomena (reflection, relaxation, and recombination of waves), as well as the protective effect of the protective barrier, depending on its geometry. An unobstructed configuration (free field) makes it possible to characterize the evolution of various mechanical parameters of the blast wave ($\Delta P+$, t_0, d_t+) for a gaseous charge (propane-oxygen) as a function of the distance traveled by the wave (m/MJ$^{1/3}$).

The free field corresponds to the configuration without the use of obstacles, that is, a blast wave develops in a spherical diverging way without interacting with the structure.

Studying the evolution of the maximum overpressure and positive momentum in the propagation time of an air wave for detonation of a gas charge (propane-oxygen), it is necessary to perform non-linear regression, which will allow us to formulate the evolution of these two mechanical indicators depending on the reduced distance.

Figure 1 shows the placement of the reference sensor at a distance of 0.10 m from the load center (Trélat (2006)) [1].

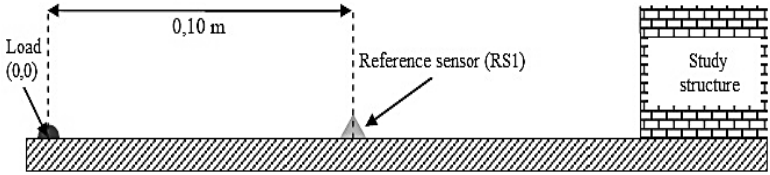

Fig. 1. Representation of the reference sensor

This measurement point allows you to check the accuracy of experiments and analyze the differences between experimental data and theoretical information, which are built from numerous measurements in a free field.

The decrease in overpressure from the peak value can be estimated using the Friedland equation. To take into account the influence of physical phenomena of diffraction and expansion of the

shock wave on the reduction of overpressure, measurements in areas subject to strong attenuation are converted to digital form.

The measurement grid is laid out to study three-dimensional geometry in order to ensure compatibility of the simulation case with the calculation tools.

The cell size is 1.77 mm, that is, 10.8 mm/MJ$^{1/3}$ during the passage of the shock front and during the duration of the positive phase.

This leads to a numerical discrepancy, that is, to an underestimation of the results by about 20%.

Processing the experimental point (CR1) by modeling is preferable in 2D axisymmetric «fine» geometry, rather than in «rough» 3D geometry.

The study of a number of parameters focuses on three configurations (Trélat (2006)) with two forms of obstacles: parallelepipedal and cylindrical structures, Fig. 2.

Regarding the element (block) of the obstacle, in the configuration, it faces the load in accordance with its greatest length, and in another configuration - in accordance with its shorter length[1].

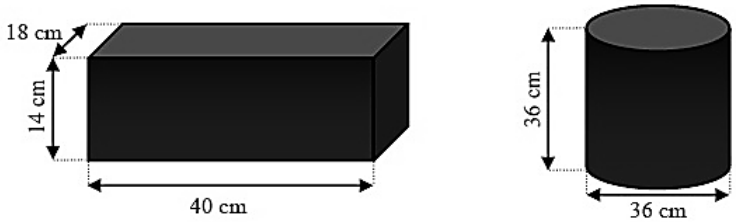

Fig. 2. Presentation of the element (block) of obstacles

The experimental configurations are modeled here by numerical simulation using the calculation protocol in 2D axisymmetric geometry and in 3D geometry in the case of a box and a cylinder.

The studied configurations are shown in Fig. 3 and are described in table one[1].

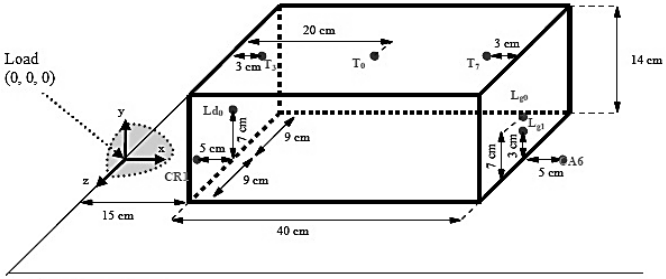

a) configuration 2

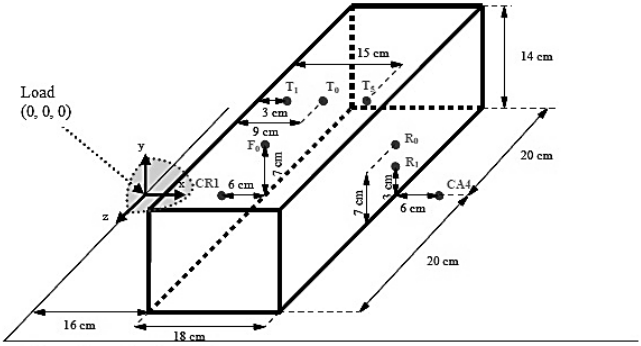

b) configuration 3

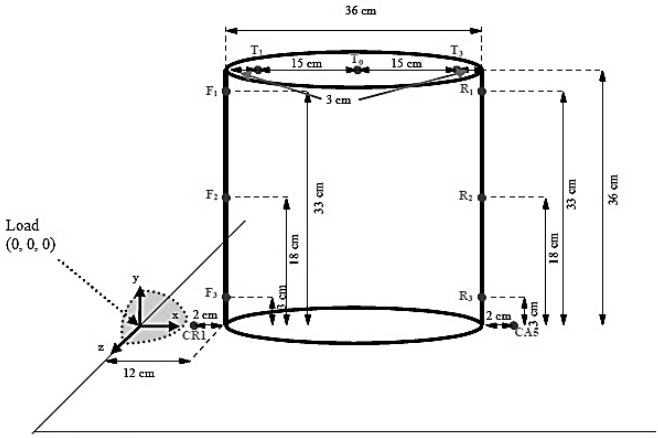

c) configuration 4

Fig. 3. Schematic diagram of the studied configurations

Table 1

Configurations studied by Trelat (2006)

Studied configurations	The radius of the load (in m)	The distance between the load center and the edges of the obstacles (in m)	The height of the obstacle (m)	Width of obstacle (m)	The length of the obstacle in the explosion (m)
1 - reference sensor (RS1)	Free field				
2 - panel 1	0,041 (*E*=4,4 kJ)	0,15	0,14	0,40	0,18
3 - panel 2	0,041 (*E*=4,4 kJ)	0,16	0,14	0,18	0,40
4 - cylinder	0,041 (*E*=4,4 kJ)	0,12	0,36	0,36	0,57

Table 2 shows the cell sizes used in the study of configurations (Fig. 3).

Table 2

Configurations studied by Trelat (2006)

Studied configurations	Energy charge (in MJ)	Mesh type	
		«end» edges of the mesh 0.13 mm (standard - 0.80 mm/MJ$^{1/3}$)	«coarse [*b*]», mesh edges 1.77 mm (or 10.8 mm/MJ$^{1/3}$)
1 - reference sensor (RS1)	$4{,}4 \cdot 10^{-3}$	2D axisymmetric geometry «fine»	3D geometry «coarse [b]»
2 - panel 1		2D axisymmetric geometry «fine»	2D axisymmetric geometry and 3D geometry «coarse [*b*]»
3 - panel 2		2D axisymmetric geometry «fine»	
4 - cylinder		2D axisymmetric geometry «fine»	3D geometry «coarse [*b*]»

Numerical modeling in the «fine» 2D axisymmetric geometry corresponds to the previously defined calculation standard (0.13 mm, that is 0.8 mm/MJ$^{1/3}$). This grid implementation allows placement in the conditions of satisfactory digital convergence. The study of bypass waves around a cylinder and parallelepiped requires a three-dimensional geometry approach. For this three-dimensional geometric approach, the size of the cell edges is fixed at 1.77 mm when passing the front of the impact (i.e. 10.8 mm/MJ$^{1/3}$). This grid size («coarse [b]») is smaller than the previously determined size limit, and is indicated by «coarse [a]» grid [1].

2. Configuration with 3D cube.

With configurations 2 and 3 (Fig. 3), the same obstacle shape is used - 3D cube. The phenomenologies present during the interaction of the wave with this type of structure are of the same type for these two configurations (reflection, diffraction, and relaxation). However, their evolution and their predominance are different due to different orientations: the larger parallelepiped length is opposite or not equal to the explosive charge. A study of 2D axisymmetric geometry on the load axis is carried out with the aim of studying the possible effects of bypassing the first interactions of the incident wave with an obstacle: reflection on the front face, diffraction and relaxation to the top and bottom of the structure, Fig. 4.

The overpressure profiles of the reference sensors highlight the first difference between the two configurations.

In configuration 2, the box is slightly closer to the explosive charge than in configuration 3 (d_3>d_2, 7%). This difference is clearly visible in the simulation results during the passage of the wave reflected from the obstacle at the control sensor. A time offset of 0.045 ms is indeed observed between the two configurations, as well as a difference in overpressure of about -9% in configuration 2 [1].

According to the geometric design, the reflection mode on the front surface is identical for the two studied configurations, namely for regular reflection. In his work, Trélat (2006) established several empirical formulas for estimating the characteristics of a reflected shock wave as a function of the reduced distance between the center of load and the point of impact.

The reflected pressure can be estimated by two parameters: the angle of incidence (β) and the maximum of the incident overpressure ($\Delta P+$). Depending on the value and evolution of these two parameters, the maximum of the reflected overpressure ($\Delta Pr+$) can be estimated.

The maximum overpressure can be estimated as a function of the reduced distance, but the angle of incidence (β) depends on the shape of the obstacle and the distance between the load center and the structure.

If we consider only a vertical surface (α=90°) for a diverging spherical incident wave, three parameters are taken into account (β,d and λ) [1].

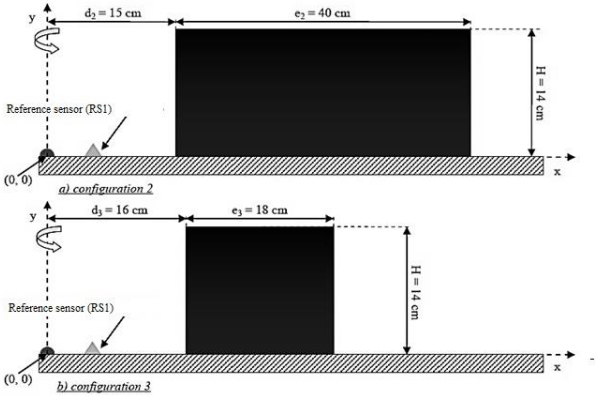

Fig. 4. Schematic representations of areas studied in 2D axisymmetric geometry

For this configuration of obstacles, the incidence angle (β) depends on the reduced distance and the distance between the load center and the structure (d), Fig. 5 [1].

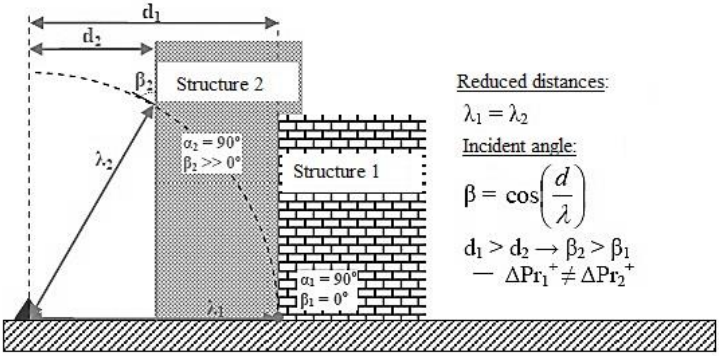

Fig. 5. Reflection on the vertical wall with and without the influence of the angle of incidence (β)

After the first relaxation along the top of the parallelepiped, the incident wave will be scattered along the back wall of the obstacle («relaxation in two stages»). Wave scattering leads to a further decrease in overpressure compared to the free field, which provides a protective effect. Subsequently, this protective effect decreases when reflected on the surface of the wave. Then regular reflection and scattering are formed on the surface lower in the direction from the obstacle, Fig. 6 [1].

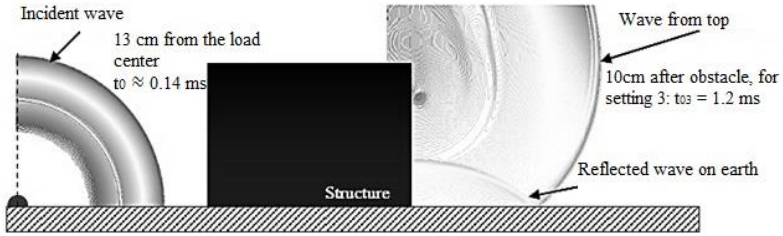

Fig. 6. Schematic representation of relaxation and reflection on the ground after configuration 3 obstacle

This statement is valid only if the intensity of the bypass waves can be neglected with respect to the wave emanating from the top. This is the case when the distance that the bypass waves (*C*) must travel to recombine downstream is significantly greater than the distance traveled by the wave passing through peak (*S*) (*C*>>*S*). This

interpretation applies to configuration 3, where *C*=0.58 m, i.e. 3.54 m/MJ$^{1/3}$, and S=0.46 m, i.e. 2.81 m/MJ$^{1/3}$, fig. 7 [1].

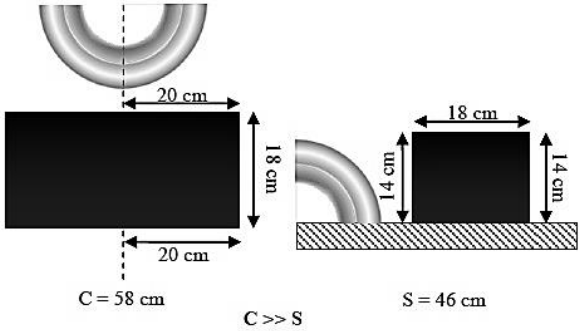

Fig. 7. Schematic representation of distances around an obstacle for configuration 3

For configuration 2, the length of the explosion obstacle is lower (*L*=0.18 m, i.e. 1.1 m/MJ$^{1/3}$) than for configuration 3. Bypass waves are not insignificant (*S*>*C* with *C*=0.58 m, i.e., 3.54 m/MJ$^{1/3}$, and S=0.68 m, i.e., 4.15 m/MJ$^{1/3}$, Fig. 8).

Therefore, this configuration is three-dimensional with possible recombination of blast waves downstream of the site [1].

Therefore, after the parallelepiped, wave recombination is possible, which makes it possible to increase the excess pressure more than a simple reflection based on the wave emanating from the top, Fig. 9.

To test this hypothesis, it is necessary to complete the study of configuration 2, simulating in three-dimensional geometry. The conditions for controlling the mesh sizes are presented in Table 2.

Therefore, the simulation is performed on a «coarse [b]» grid, so that the numerical convergence will be less only for modeling in a 2D axisymmetric «fine» geometry, which has been performed so far for this configurations.

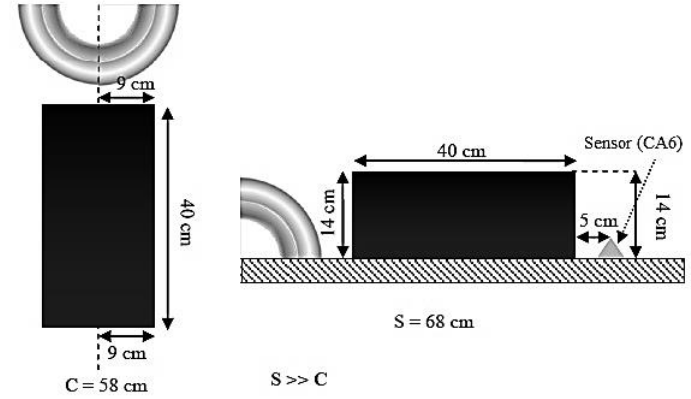

Fig. 8. Schematic representation of distances around an obstacle for configuration 2

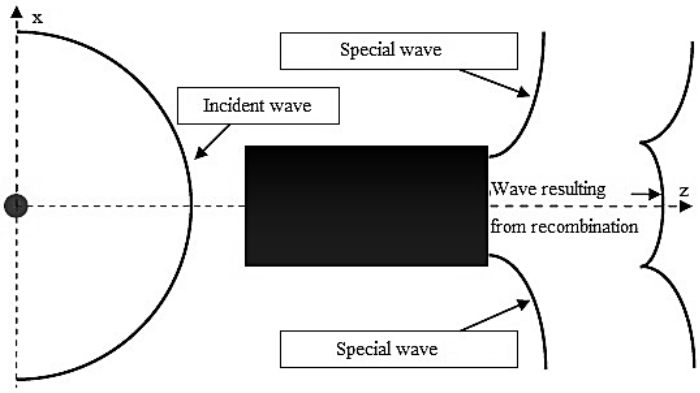

Fig. 9. Schematic representation of the wave path for configuration 2, top view

3. Configuration with the cylinder.

A study in 2D axisymmetric geometry makes it possible to study the reflection mode and the level of gauge pressure along the cylinder front (μ=0°). Then, the study of this configuration is completed by modeling in three-dimensional geometry on a «coarse [b]» grid to take into account the phenomenon of reflection around a cylindrical

surface ($0° \leq \mu \leq 90°$), as well as the effects of wave propagation, even if the pressure levels predicted by the simulation can be underestimated 20% due to a lower level of digital convergence than the «fine» grid (Fig. 10).

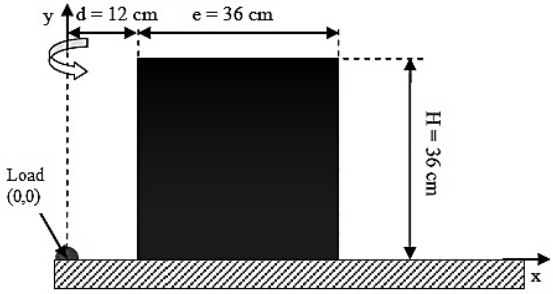

a) research in 2D-axisymmetric geometry (toric cylinder)

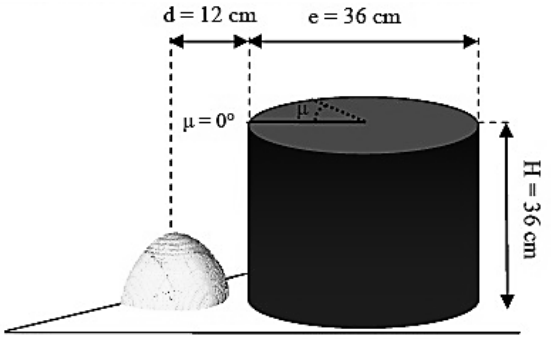

b) research in 3D geometry (the shape of the obstacle is observed)

Fig. 10. Schematic representation of two geometries studied for configuration 4

The results of numerical modeling in 2D axisymmetric geometry approach theoretical data with a difference of +/- 15%. 3D calculations that are not numerically convergent are qualitatively correct. However, this does not allow quantifying the decrease in the maximum amount of positive pressure reflected on the front of the cylinder (Fig. 11). Only modeling from the "end" of the grid allows this to be achieved (calculations in 2D axisymmetric geometry). The experimental data from Trélat (2006) present deviations that can be extremely important as theoretical data.

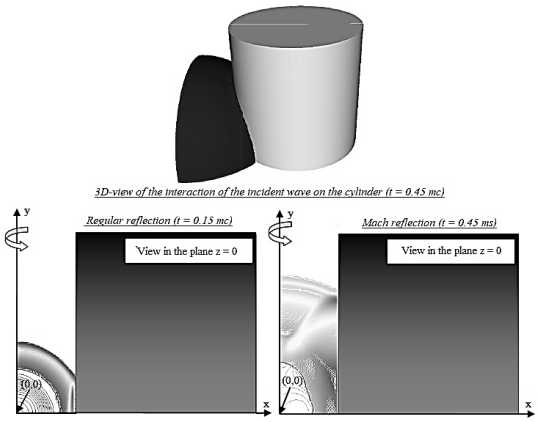

Fig. 11. Reflection on the front surface of the cylinder at μ=0°

When a wave interacts with a cylinder, a reflection is formed along the wall at μ=0°.

Along the rear surface of the obstacle for 90°≤μ≤270°, depending on the nature of the wave, several phenomenologies are visible: a wave from above or bypass waves. As a result, only a qualitative analysis of the simulation results is proposed [1].

A wave coming from the top of an obstacle is a wave passing through a cylinder. The rear of the cylinder undergoes relaxation before recombination with the waves. The waves correspond to the waves that propagate around the cylinder (convex surface). After passing the obstacle, bypass waves will be focused at the rear of the cylinder, along the generator μ=180°, taking into account the symmetry of the geometry.

The cylindrical structure of configuration 4 requires the study of three-dimensional geometry in order to take into account the influence of waves above and around this obstacle, the propagation of a wave resulting from an explosion of a gas charge. In addition, this configuration of obstacles is more complex than the simple interaction of a shock wave with a flat wall due to the convex nature of the surface. Therefore, this type of experiment represents a very strong limitation of the computational chain due to complex physical phenomena.

For experimental configurations, it was shown that if the embankment is at least 4-6 times longer than its height, the influence of bypass waves is negligible. These types of embankments are then assimilated with obstacles of the required length. In the case of a protective barrier called a “short embankment”, to evaluate the protective effect it is necessary to take into account bypass effects and three-dimensional recombinations. That is limited geometries with complex three-dimensional phenomenology, and therefore they are especially demanding from the point of view of restoration during numerical modeling in three-dimensional geometry. Therefore, the calculated geometry will necessarily be modeled in a three-dimensional configuration. This geometric approach requires significant computational resources and, therefore, represents significant material costs, human costs [1].

For this type of geometry, there are several quick methods for assessing the evolution of the mechanical characteristics of a wave in a neighborhood of a structure. One possible approach is to assess the evolution of wave characteristics from geometric and empirical relationships. In the literature, this methodology is limited to elementary configurations using a two-dimensional approach (Hyde, Needham). One possible approach is to assess the evolution of wave characteristics from geometric and empirical relationships. In the literature, this methodology is limited to elementary configurations using a two-dimensional approach (Hyde, Needham).

Their application to three-dimensional geometry does not satisfactorily evaluate the evolution of the maximum overpressure; moreover, they are limited by parallelepiped structures (Miller) [1].

The following evaluation method extends to trapezoidal cross-sections of the barrier for three-dimensional geometry (Eveillard). The results obtained using this quick estimation method will be compared with the experimental data and the results of numerical simulation for two configurations of the «short barrier» associated with detonation of a gaseous charge.

5 Conclusions.

According to the results of the study, previously completed scientific approaches, principles, etc. lead us to the following conclusions:

a description of the configurations is possible with the MM-ALE technique, implemented on the commercial FEM code LS-DYNA v. *R7*;

the structural and dynamic effects of reflected pressure pulses should be taken into account, since they are much higher in reflected areas (zones) than when scattering a blast wave on the walls of a mine, which is relevant for closed circuits, where the number of reflections is significant;

perpendicular to the propagation of the blast wave, the parameter of the exciting pulse is the initial region of the explosive atmosphere.

References

1. **Trélat, S.** (2006). Impact de fortes explosions sur les bâtiments représentatifs d'une installation industrielle. *Thèse de doctorat* . Orléans [France].

2. **Ballereau, P**. et al. (2012). Méthode de raffinement adaptatif de maillage et modèles avancés de programmation pour le calcul haute performance. *Chocs, 41*, 81-87 [France].

ANALYSIS OF THE RESULTS OF A COMPUTATIONAL EXPERIMENT TO DETERMINE OPERATIONAL PARAMETERS FOR PARTIAL BACKFILLING OF THE WORKED-OUT AREA

Fomichov V.V.
Doctor of Technical Sciences, Professor at Department of the Mining Department, Dnipro University of Technology, Dnipro, Ukraine
Sotskov V.O.
Candidate of Technical Sciences, Associate Professor of the Mining Department, Dnipro University of Technology, Dnipro, Ukraine
Dereviahina N.I.
Candidate of Technical Sciences, Associate Professor at Department of Hydrogeology and Engineering Geology, Dnipro University of Technology, Dnipro, Ukraine
Leonenko O.V.
Senior Lecturer at Department of Project Management, Buildings and Building Materials, Dnipro National University of Railway Transport named after Academician V.Lazaryan, Dnipro, Ukraine

Abstract

The computational experiment is intended to determine ranges of mechanical characteristics of the disturbed rock mass making it possible to select the structural features of the applied powered support while providing optimum operating performance of a geomechanical system. Objective of the system analysis of a state of a roof of a stope as well as load distribution within the structural components of the powered support is to identify a system of selection of optimum configuration of the support section within a stope basing upon a forecast of qualitative indices of deformation of boundary rock layers. The performed calculations of a state of geomechanical system of a stope-mine working conjugations have made it possible to identify typical areas of the disturbed rock mass determining mechanism of a stope roof caving progress taking into consideration backfilling parameters. The analysis of a stress-strain state of the geomechanical system within a stope roof, carried out according to the selected cross sections, has helped determine interaction conditions of the rock layers resulted in the roof fault on packs. Parameters of the disturbed rock mass effecton the structural components of the powered support section have been identified. The regularities of changes in the stress-strain state of a geomechanical system of a stope, obtaine dunder different conditions of partial backfilling, have helped define the mechanism to select a stope advance velocity, type of the packs, being erected, and their geometry. The above enables to provide minimization of expenditures, connected with internal logistic of the production unit; to reduce prime cost of

mining; and to improve safety of the stope miners. The developed methods helps select optimum conditions for the stope functioning at a design stage with no extra geological survey involvement.

Introduction. Mining and geological conditions of stope operation in Ukrainian mines needs solving complicated technological problems providing an opportunity of mineral mining [1 - 3]. Analysis of deformation features of geomechanical system of mine workings has revealed the two dominating alternatives of deformation development within the rock mass: deformations being oriented close to a vertical axis, and deformation, being oriented close to a horizontal one [1, 4]. It is obvious that nonhomogeneity of mechanical characteristics of rocks is the basic factor determining directions of the dominating deformations if only the mine workings were driven in the undisturbed rock mass.Mutual effect of the mine workings varies shaping conditions of a deformation field of the geomechanical system which results in the necessity of extra protective measures. In this context, the rocks, being cut in the process of selective coal mining and left within a production unit, may be used to erect protective structures providing satisfactory deformation mode of geomechanical system of a stope-mine working conjugation.

Efficiency of various structures of the powered support legs depends directly upon mining and geological conditions as well as upon technological conditions of a specific production unit. For instance, in terms of *Samarskaia* mine [1, 2] the powered support was reinforced with the help of pit props providing immediate roof holding within the operating area of a shearer. Hence, design characteristics of the powered support in the context of backfilling technique implementation have been determined for two alternatives – rigid alternative, and flexible one.

Analysis of load distribution nature during coal seam mining with backfilling to compare with roof control by means of complete roof caving has shown that there are fundamental differences in the process of immediate roof caving of a stope [3 – 6]. The stated ideas, concerning hypothesis and mechanism of deformations of rock layers, surrounding a stope, and roof rock-support interaction may become a basis for the development of a number of analytical models which should involve both elements of the process kinematics and

mechanical characteristics describing nonelastic state of elements of the geomechanical system.

Selective coal mining helps solve a number of problems arising in the process of extraction performed within the coal seams which thickness is less than a meter. However, considerable volume of rock, being cut, which had to be transported to the surface initially, is the basic major problem of the procedure. Nevertheless, the development of a method to backfill the mined area by means of the cut rock has helped solve the problem. Boundaries of the technology to protect mine workings as well as its efficiency determine volume of rock available for backfilling. To be more accurate, empty volume of the mined out area-volume of rock being cut ratio is meant.

The ratio defines option of two backfilling alternatives, i.e. complete backfilling or backfilling with the help of packs. Complete backfilling is possible if only height values of the rocks, being cut, are significant when no less than 0.8 of rock volume is extracted while mining of one coal volume. In the context of the packs, the restriction is senseless since their formation involves option of distance between them. The geometrical factor is not the only one effecting backfilling format.In some cases, mechanical characteristics of rocks need backfilling method optimization. That is connected with the aim to provide operational requirements for the conjugated stope and mine working. The backfilling parameters may become the determinative factor effecting performance of supports of mine workings and progress of deformation of their boundaries.

Statement of the problem. To carry out comparative analysis of the efficiency of different structural features of the powered support, a model of rock mass, corresponding to actual operation conditions, has been developed. Structure of the enclosing rock mass and coal seam as well as their mechanical characteristics is based upon “A project of a mining site of longwall 4205 of C_4^2 of a block 3”, and the detailed design “Opening and preparation of blocks 2 and 3 of *Samarskaia* mine” performed by *Dneprogiproshakht* Institute in accordance with “Safety Rules in Coal Mines НПАОП 10.0-1.01-10”, “ПТЭСОУ10.1-00185790-002-2005”, and “Manual for roof and support control within a stope on coal seam with up to 35^0 inclination slope”КД.12.01.01.503-2001.

Longwall 4205 of C_4^2seam is equipped with the powered complex

КД-80, coal shearer КА-200, conveyor СП-251.14. The longwall length is 180 m. Ventilation scheme of the longwall is direct-flow 3-В-Н-г-пт.

Table 1.1

Basic mining indices of the working area

Indicators	Indicator values
Period of the area mining, months	10
Seam thickness, m:	
Geological thickness	0.66-0.83
Extracting thickness	1.03
Seam inclination, degrees:	
Along the longwall	1°
In the direction of mining	1-5°
Longwall length, m	180
Extraction pillar length, m	1666
Mining technique	Pillarless
Longwall mining direction	To the rise
Stope direction	Backward
Stope advance, m	
mining cycle	0.8
per day	7.4
per month	228.2

Longwall 4205 will be mined in block 3 of a mine field along coal seam C_4^2 with cutting of the seam immediate roof rocks.

Mining area, being modeled during the research, involves characteristics of mining and geological conditions determining the use of decreasing and compensating correction coefficients to perform the calculations [4,7].

Strength characteristics of the rocks are decreased according to the longwall watering connected with the availability of coal shed, sandstone within the main roof and immediate roof, and covering deposits. The forecasted water inflow is up to 10 m³/h (however, it may achieve 25 m³/h, which was registered while driving a haulage drift of C_4^2 seam).

Initial fault of the main roof is expected to be over 20-30 m, further fault of the main roof is expected to be over 20-35 m (by analogy with longwalls 4203, 4201, 4204 and 4202, and above mined longwalls a parting is 11.2-12.8 m).

Convergence of wall rocks within the mined-out area is inconvertible result of a stope advance as well as gradual compression and densification of backfill material up to the steady density (i.e. rock density within a pillar). Hence, to represent a real situation with the rock mass behavior, the model should involve appropriate mechanical characteristics of backfilling material demonstrating its state under the compressive loading.

The backfilling material, being simulated, consists of the broken rock resulting from selective mining. The carried-out research [5] of the selective mining shows that up to 55% of all the cut rocks, broken by means of an auger end organ, are of 25-120 mm fineness.

A process of the back filling material compression is divided into the two stages – initial compression and a final one. Stage one is filling up of cavities between the material particles in the context of up toσ_z= 2.0 MPa vertical compressive stresses corresponding to ε= 0.18 relative deformation. Stage two (i.e. final stage) is exponential increase in the deformation along with the stress increase. The material particles brake into smaller ones and experience more compact redistribution while increasing rigidity of the filling mass. In terms ofσ=8.0 MPa, i.e. at 160 - 320 m depths, relative deformation ε of the filling mass will be 0.26.

Relyinguponthеanalysisofdeformationcharacteristicsofthefilling-mass, its following mechanical characteristics, corresponding to a compressive loading period, have been taken up. Thus, at stage one (i.e. a stage of initial compression), deformation characteristics of a rock pack are as follows: elasticity modulus is E_1=11 MPa, and Poisson ratio isμ_1=0.4. At stage two they correspond to deformation characteristics after the filling material compaction, i.e. E_1=30 MPa, and μ_1=0.3.

In the context of a complete backfilling for the cut rocks we take up relying upon experimental data represented in [1-3]. Naturally, the taken values of elasticity modulus E=50 MPa and degree of fragmentation K_p=1.45 are not absolute ones since the degree of fragmentation of the rock, being cut, depends upon its mechanical strength, and coal mining technique. In turn, residual deformation characteristics of rock, used for backfilling, are determined basing upon its softening geometry. Hence, the selected parameters of the cut rocks are average parameters; moreover, they are typical for the

considered coal mining method as well as mechanical characteristics of Western Donbas rocks.

Three alternatives of the cut rock height (i.e. 0.5 m, 0.6 m, and 0.7 m) will be applied while considering the efficiency of different back fillings cenarios. Each of the alternatives should involve calculation of rock volume after its softening. Perform the calculation relying upon the formula

$$V_p = K_p \cdot V, \quad (1)$$

where V_p is cut rock volume resulting from its softening; and V is volume of the rock, being cut, before its extraction from rock mass.

Consequently, in terms of the selected technological values, equivalent of line a dimensions throughout the height of the rocks, being cut, before softening and after it will be: 0.73 m for 0.5 m; 0.87 m for 0.6 m; and 1.02 m for 0.7 m. Further, the obtained values are used for computational experiment intended to determine stress-strain state of geomechanical system of a stope-mine working conjugation.

Select following values of elasticity modulus and degree of fragmentation for packs: E=500 MPa and K_p =1.2. Apply expression (1) again and obtain the equivalent of line a dimensions throughout the height of the rocks, being cut, before softening and after it taking into consideration pneumatic compaction: 0.6 m for 0.5 m; 0.72 m for 0.6 m; and 0.84 m for 0.7 m.

Relying upon the data, determine operation parameters of the packs depending upon different heights of the rocks, being cut. Select the expression to calculate stage one

$$V_b = b \cdot h \cdot l, \quad (2)$$

where V_p is volume of the mined out area per a shearer pass; b and l are height of a stope and its length respectively; and h is web width of end organ of the shearer for b=1 m, l=250 m, and h=0.8 m values we obtain

for b =1 m, l=250 m , and h= 0.8 m values we obtain, m^3

$$V_b = 1 \cdot 0.8 \cdot 250 = 200\, m^3. \quad (3)$$

If the equivalent dimensions, obtained for the loose rocks, are used as *b* values, then we get the volumes which can be used to backfill a stope.

Now, taking into consideration the fact that 0.8 m^3 of the mined-out volume fall on a running meter of a shearer advance, we obtain total length of the unpacked area within the stope under study: 100 m for $V_{0,5e}$; 70 m for $V_{0,6e}$; and 40 m for $V_{0,7e}$ Consequently, pack width is 7.5 m for $V_{0,5e}$ and distance between neighbouring packs is 5 m; pack width is 9 m for $V_{0,6e}$, and distance between neighbouring packs is 3.5 m; and pack width is 10.5 m, and distance between neighbouring packs is 2 m.

Hence, the basic operational parameters have been formed determining both extent and possibility to implement different backfilling types depending upon mechanical characteristics of rock as well as stope-mine working conjugation. The described backfilling parameters provide optimum selection of geometry of packs in terms of a coal mining method, stope length, and height of rocks being cut.

Primary analysis of the state of the powered support sections. In the context of a traditional method, consoles from rock layers of the main roof, hanging over a longwall, form an area of unstable rocks bearing basic pressure on the support in a mine working. Fig. 1 explains stress distribution within a section of the powered support when a traditional technique is applied. The selected projection of 3-D model of the powered support helps analyze loading degree of certain support parts contacting with rock mass.

The curve shows that the pressure, putting on the support section from the broken-down rocks, is close to a boundary one being comparable with the force taken by the hydraulic system components. In this context, pressure of roof and floor of the stope is 1.8-2.1 times less. It is possible to conclude that lack of sufficient flexibility of the support components from the mined-out area results in the increased loading of hydraulic cylinders. Moreover, load vector is shifted relative to a longitudinal axis of the cylinder, which should involve 5-7% increase in the internal pressure of the hydraulic system depending upon the stope advance velocity.

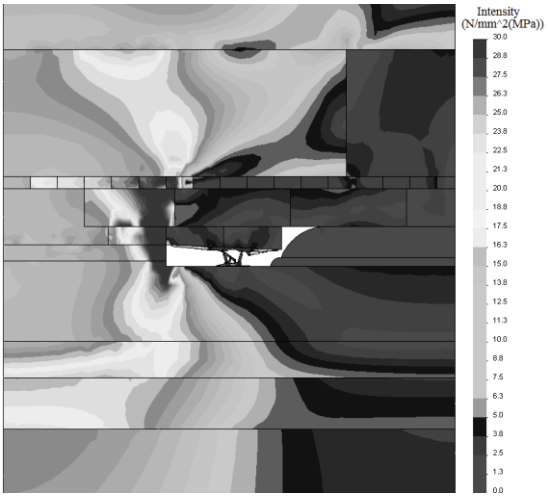

Fig. 1. Stress intensity within rock mass in the process of partial backfilling

Arrangement of the support section within the rock mass model reflexes completely its actual operational conditions under which excess pressure, bearing on the reversed console of rock support of the immediate roof, is not available owing to partial backfilling. As a result, the support body experiences uniform loading with concentration of internal forces within the contact areas of certain structural elements. As a whole, stress level corresponds to the values obtained for the traditional support (see Fig. 1); in this context, load of all cylinders of the hydraulic system is 1.3-1.5 times less. The support model distributes regularly roof and floor load towards the stope advance. Hence, functioning condition for the design option of the support section under the considered mining and geological conditions is optimal one since it provides minor wear and tear of the equipment [9].

Analysis of a state of the disturbed rock mass. The identified discontinuities and areas of rock softening have been analyzed as for their interaction and integral effect on a stope support. As a consequence, 3-D model of the layered rock mass has been developed involving maximally each feature of strengthening characteristics and deformation characteristics of the rock and coal seam.

A curve of stress intensity distribution within the structure of the rock mass under study, represented in Fig. 2, makes it possible to

determine the nodes where the main fissures, forming rock blocks, are developed. The process involves three rock layers composing the immediate roof of the stope.

Stage one is the longitudinal stratification of a rock block, neighbouring the coal seam. The process takes place at the expense of the effect of a high-stress closed area occurring within the rock mass at the depth of 4-7 m down from the stope face. Stage two is the process when the forming blocks of layer one develops excessive pressure bearing on the lower plane of layer two from the top of the rock layer. Through a minor height of the layer, critical concentration of the deformation energy forms a plane of the block separation with 2.5-4.5 m intervals henceforth forming chain of plastic hinges providing smooth lowering of coal lumps. Stage three of rock block formation takes place owing to grouping of stress concentration areas being shaped within the upper boundary and lower boundary of a rock layer located as the third one from above the coal seam. Therefore, through different types of the geomechanical processes, formation of a block structure takes place within a stope roof. Parameters of the block structure are determined unmistakably in the process of the computational experiment which will provide in future adequate research as for the efficiency of the powered support sections with different designs.

Block caving of rock layers of immediate roof of a stope effects mainly horizontal stresses as follows: absolute stress values decrease down to 17 %; the blocks, arranged above the powered support, are influenced by compressive internal forces, and tensile ones; and pressure of the immediate roof rock block provokes pack material displacement towards the stope. All that agrees completely with theoretical studies and experiments [10] as well as with the findings of previous computational experiments carried for Western Donbas mines [11].

Determining optimum structural characteristics of the powered support section. As it has been mentioned, the most advantageous design of the powered support section should be selected for the available mining and geological conditions. The analysis considered the three structural alternatives of the sections: traditional alternative; alternative being applied in the context of partial backfilling;

and alternative being designed with the reinforced reversal console for partial backfilling.

It is expedient to start analyzing findings of the computational experiment from the study of characteristics of horizontal stresses of the geomechanical system.

The obtained data point to the dominating direction of expansion of horizontal stresses oriented across the stope face. Comparative analysis should involve separation of the four groups of structural components of the powered support section, namely: group one – basic expansion cylinders of the hydraulic system; group two - base plate of the section; group three – upper plate of the support section; and group four - design of reverse console of the support.

In the context of traditional mining method, horizontal stresses concentrate within the bodies of the hydraulic cylinders, within the central part of the base plate, and within the structural components of the reverse console. In other words, as for the design, high horizontal stresses result from a wall pressure of the immediate roof rocks caved behind the section.

Within the support section under design, load on the hydraulic cylinders is 23% less and structural components of the reversal console bear a load which value is equal to the previous result. In the context of the calculation results as for the designed and applied section of the powered support, distribution of horizontal stresses shows that when selective mining is used, in terms of any design of the power support section, the loads, taken up by lower base plate are 1.5-1.7 times less than those taken up by the upper base plate.

The fact is the fundamental dissimilarity from the results obtained for a model of a support section used in the context of traditional coal mining.

Strength reserve approximates zero in terms of general level of strength reserve conservation within different components of the section; in terms of partial backfilling (0.08-0.12); and within stress concentration areas being less than 3% of the support design volume.

The above means that in the context of the mining and geological conditions under consideration only the last support alternative operates as far as possible.

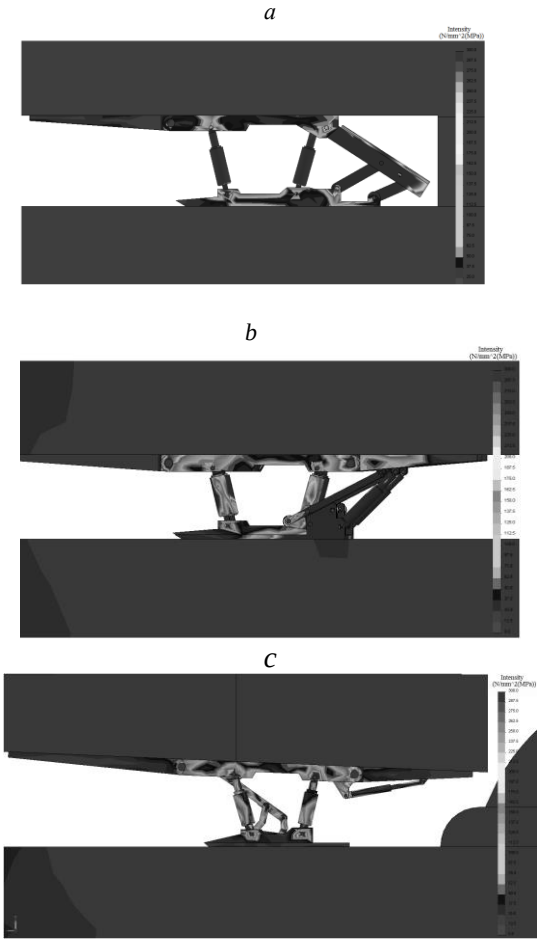

Fig.2 . Stress intensity within the powered support section: *a* - traditional; *b* - being designed; and *c* - in the context of partial backfilling

Evaluate features of stress concentration within structural components of the powered support section relying upon the analysis of stress intensity variation (see Fig. 3).

Since materials of leg components of the powered support are closely spaced as for their mechanical characteristics, there is no necessity to apply differential analysis of structural strength.

Concerning the alternatives, represented in Fig.2*a* and Fig. 2*b*, stress intensity is of ultimate value within movable components of the support transmitting loads between base plates.

Additionally, in case one the high stresses are distributed uniformly between hydraulic cylinders and nondeformable punch props; in case two, 20-42 MPa increase in ultimate stresses is observed within components supporting the section reverse console relative to the system of hydraulic cylinders resulting in 12-17 MPa increase of pressure on the stope floor from the mined out area.

Absolute stress concentration values for the support, applied in the process of partial backfilling (see Fig. 2*c*), are not higher than the absolute values, obtained for the two previous alternatives, but have two critical features.

First, ultimate stress intensity is observed within the contact assemblies of certain components of the support pointing to non-coordination of deformation of the support components which may result in the structure damage with bearing-capacity failure.

Hence, both sections of the powered support (i.e. the section, being designed, and the section being applied in the process of partial backfilling) complement each other technologically providing mining operations within the whole range of complex mining and geological conditions typical for Western Donbas mines at 400-1000 m depths.

Analyzing condition of geomechanical system of stop-mine working conjugation in terms of different backfilling parameters.

Analysis of curves of stress intensity distribution within the rock mass determines zones of ultimate principal stresses which will help form optimum conditions for the limit equilibrium of a mine working arch after backfilling operations.

Consider stress intensity curves within a plane being equal to a plane of a working face located at the 10 km distance towards the mined-out area in terms of packs and complete backfilling.

The increased pack width decreases stress concentration value for 0.7 m height option of rocks being cut as well and both the first rock

layer and packs experience closely spaced stresses. In other words, the mine working roof and packs resist the deformation consistently which prevents from origination of the main fissures up to the progress of the rock mass deformation under the effect of rheology [6-9].

When the complete backfilling takes place (see Fig. 3), ultimate concentration of stress intensity is observed from the undisturbed rock mass. If the height of rocks being cut is 0.5 m (see Fig. 3*a*) then the stress concentrations are comparable with the values obtained for a mine working packing; if the heights are greater (see Fig. 3*b,c*) then stress intensity maximum experiences 30-36% increase. Increase in the height of the rocks being cut is followed by the number of rock layers with high intensity stresses. In this context, distance of the mine working effect on the stress distribution is 34 km lengthwise the stope face.

To compare with packing, stress intensity maximums within a stope roof increase along with the increase of the height of rocks being cut. The increase happens in accordance with nonlinear law with a falling gradient, i.e. in the process of complete backfilling, height of rocks being cut is the key parameter determining condition of a mine working roof under the conditions of static equilibrium of analytical model.

Hence, while comparing stress distribution for complete backfilling (Fig. 2*a*) and for packs (Fig. 1), we obtain the following: under the selected mining and geological conditions, engineering solution two is less effective than engineering solution one.

Moreover, it provokes “fast” breaking of the mine working roof deteriorating operation of the powered support throughout the length of the stope.

Comparative analysis of curves, represented in Fig. 3, has shown that increase in the height of rocks being cut results in the decrease of ultimate stress intensity values as well as in their oscillatory range.

However, if stress intensity peaks in Graph b (see Fig. 4) are of the same value along the whole stope length, in Graph a the peaks decreases to the center, and experience their increase in Graph c

demonstrating changes in the behavior of loading of the powered support section depending upon a pack width.

a

b

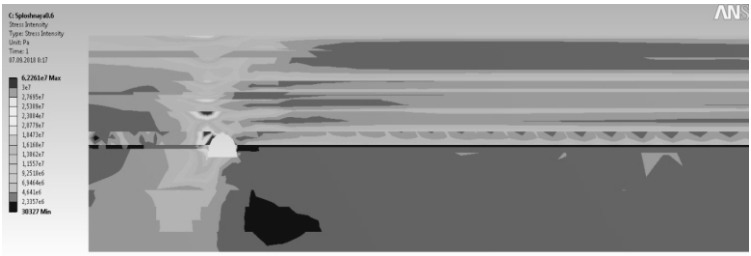

c

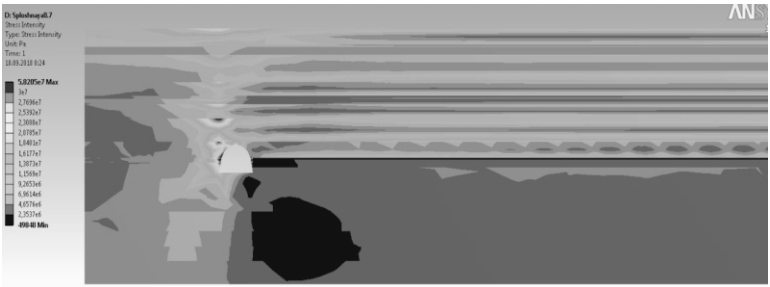

Fig. 3. Deformation intensity of the rock mass in front of a stope face in the process of complete backfilling in terms of following heights of rocks being cut: *a* - 0.5 m; *b* - 0.6 m; and *c* - 0.7 m

In the context of the method, being studied, the value also determines geometrical parameters of an empty area of the worked-out area of the stope, i.e. it effects the characteristics of pressure taken up by walls of packs in the backfilling process. In terms of a dynamic equilibrium, a wall of a pack is in an unstable stability which parameters depend naturally upon the pack height as well as upon the dis-

tance between neighbouring packs. Changes in the first roof rock layer are caused by the fact that height increase of the rocks being cut results in the decreased distance between packs factoring into the changes in the nature of stress intensity distribution.

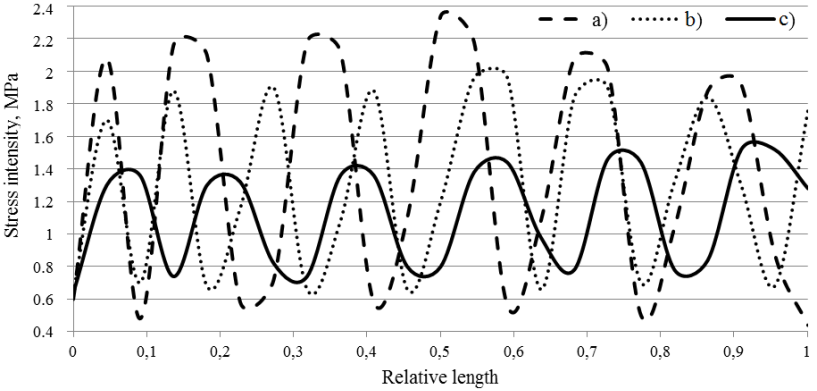

Fig 4. Changes in stress intensity within the first rock layer of the stope roof in terms of packing for following heights of rocks being cut: *a* - 0.5 m; *b* - 0.6 m; and *c* - 0.7 m

To describe stability state of wall packs, introduce correlation coefficients K_{max} and K_{min} making it possible to evaluate vibration degree of stress intensity maximums above the pack and above the empty worked-out area of a stope.

Hence, relying upon the graphs of changes in stress intensity values (Fig. 4), and according to the performed analysis of the state of geomechanical system of a stope, obtain a condition of satisfactory state of the pack walls in the form of

$$\left| \frac{\sigma_{max} - \sigma_{min}}{\sigma_{max}} \cdot \frac{h}{b} - \frac{K_{max}}{K_{min}} \right| \langle 4.08, \qquad (4)$$

where σ_{max} and σ_{min} are maximum and minimum of stress intensity vibrations along the stope length; h is pack width taken up during design; and b is height of rocks being cut.

Analysis of rock mass deformation development in terms of different backfilling methods.

Taking into consideration the computational experiment parameters, distribution of deformations within the rock mass is analyzed

only from the viewpoint of qualitative evaluation if continuity of each component of the analytical model is preserved which excludes naturally origination of considerable rock mass deformations directed lengthwise stratification plane.

Figures 5 and 6 represent fragments of 3-D analytical model of geomechanical model of a stope-mine working conjugation in the process of use of packs and complete backfilling respectively.

The obtained images of distribution of total deformations within the rock mass show that the nature of a stope roof fault cannot depend upon the selected backfilling method; however, deformation values of roof rocks are 19% higher in terms of complete backfilling (see Fig. 5). That points to the decrease in the potential deformation energy in terms of complete backfilling resulted from the decreased structural strength of the crushed stone used for complete backfilling relative to the conditions of the packs formation.

Fig. 6 represents distribution of deformations within a plane, selected in the process of stress pattern, shown in Fig. 4. The curves demonstrate that increase in height of the rocks being cut results in the decreased deformation value of roof rocks of a stope according to a law being close to linear one. Rock mass deformation in the neighbourhood of a mine working for the calculations, performed for partial backfilling, is of similar value and pattern. However, if calculations are made for 0.7 m height rocks, being cut, deformation value in the neighbourhood of a mine working decreases by 18%. The above is followed by the decreased deformations in the rock layer one of the immediate roof of the mine working.

Fig. 5. Total deformations of rock mass in front of the stope face in the process of backfilling with the help of packs if height of the rocks being cut is 0.7 m

Fig. 6. Total deformations of rock mass in front of the stope face in the process of complete backfilling if height of the rocks being cut is 0.7 m

To compare with the calculation results concerning packing (see Fig. 5), in terms of complete backfilling, changes in height of rocks being cut factor into the increased deformations of rock mass in the neighbourhood of a mine working. If height of the rocks being cut is 0.5 m then roof rock deformations are comparable for packs and complete backfilling. If the heights are 0.6 and 0.7 m then the deformations experience 12-15% increase. Thus, mine working support takes up the increased wall pressure which worsens its operational characteristics [10, 11].

Deformation gradient area is in the wall of a mine working from a stope. The area width increases according to an exponential law with the increase in the height of rocks being cut. Rock layer two of the immediate roof of a stope reflects the changes at the most. Increase in the deformation gradient area achieves 370% with its shift towards middle plane of the stope. Thus, there is a possibility to form multilevel block system to break up the stratified rock mass of the stope roof [10, 12]. In this context, height of the blocks and their width are determined by means of combination between a height of rock layers of the stope roof and absolute value of a gradient of total deformations [7, 11, 13].

Analyze deformation development of rock mass within a mine working roof relying upon curves, represented in Fig. 7, concerning changes for packs (*a*) and complete backfilling (*b*).

Periodical variations in the deformation graph during packing illustrate basic feature of the method. Actually, SSS conditions, typical for the complete backfilling for the whole length of the stope, are

formed for each pack. The graph is formed on the basis of deformation development superposition along the whole length of stope as well as totality of areas experiencing effect of packs. By means of the above mentioned, decrease in absolute value of total deformations takes place as well as concentration of potential energy within bend points of the deformation graph. In this context, deformation increase along the length of a stope is 57 %.

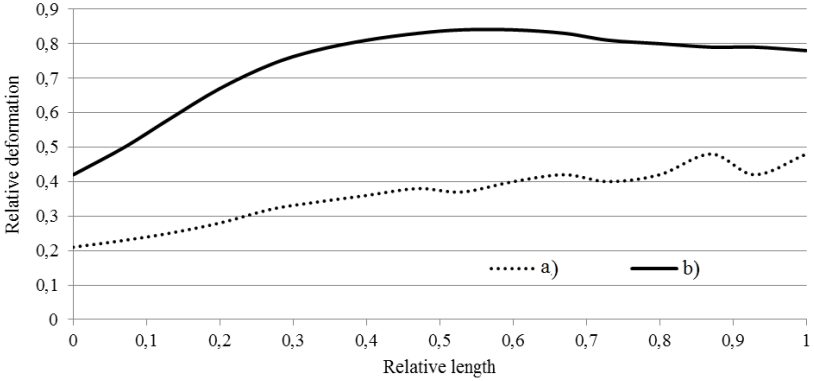

Fig. 7. Curves of changes in relative deformations across the stope in rock layer two when height of rocks being cut is 0.6 m in the context of: *a* - packing; and *b* - complete backfilling

Thus, while comparing total deformation change in the process of pack use, and in the process of complete backfilling of a stope, we obtain that in terms of alternative one, dissipation energy of rock layer deformation is almost 11% higher. If optimum width of empty space between packs is selected, smooth lowering of immediate roof of a stope may be achieved with no uncontrolled dynamic processes.

Findings. Assume a stope face-its central vertical section junction as the area to be analyzed. Consider compressive stresses (Fig. 8) and tensile stresses (Fig. 9), arising in certain rock layers, separately and compared together. Graphs in Fig. 8, represented qualitatively, differ slightly. It is understood that in terms of the alternatives, rock layer two experiences maximum stresses. Levels one and three take up stresses with a wider scatter but degrees differ. Such a specific feature of the graphs denotes effect of rock deformation characteristics on the stress distribution within the rock mass substantiating indirectly the adequacy of the calculations.

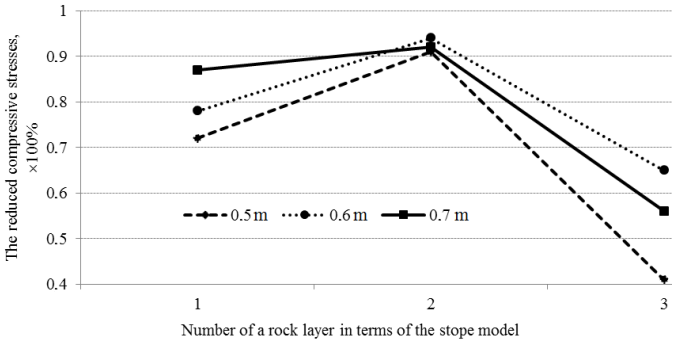

Fig. 8. Changes in the reduced maximum compressive stresses in accordance with rock layers on the stope face within the central share of the mine working in the process of complete backfilling in terms of different heights of rocks being cut

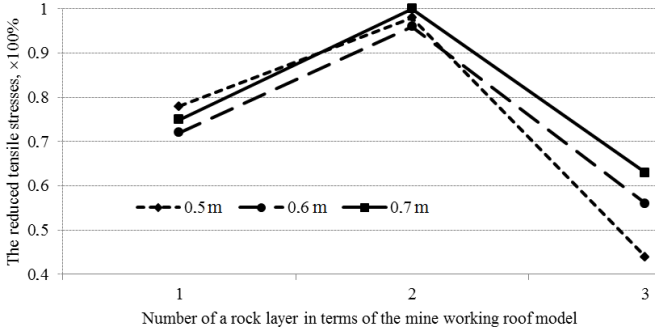

Fig. 9. Changes in the reduced maximum tensile horizontal vertical stresses on the stope face within the central share of the mine working in the process of complete backfilling in terms of different heights of rocks being cut

Analysis of graphs of tensile stresses (see Fig. 9) demonstrates a pattern opposing the graphs of compressive stresses.

If height is 0.5 m, then changes in maximum stresses in terms of rock layers of the immediate roof differ markedly from 0.6 and 0.7 m heights of rocks being cut; layer one is loaded greater and load, taken up by layer three, is quite lesser. On the whole, calculation alternative for 0.6 m height demonstrates indices of the limit efficiency state as for the provision of a stope immediate roof in the context of complete backfilling.

Furthermore, effect of compressive stresses on the stable state of a mine working immediate roof is greater to compare with the effect by tensile stresses.

The research is carried out within the framework of scientific topics GP-497 "Resource-saving geotechnical and hydrodynamic parametrization of the extraction of low-capacity mineral raw materials in an technogenically loaded environment", financed by the state budget of Ukraine.

The publication contains the results of studies conducted by President's of Ukraine grant for competitive projects F-82 "Resource-saving parameterization of the waste-free technology of backfilling the produced space in coal mines".

Conclusions. 1. The analysis of geomechanical model of rock mass, and a mine working, driven in it and propped up by the powered support section has shown that, if block caving of roof takes place, dynamic changes in stress-strain state of rock mass depend upon height and location of the roof layers within which stress concentration arises with up to 80% values of stresses arising in front of the stope. In this context, geometry of the blocks varies as well as mechanical nature of rock layer failure.

2. The powered support section, being designed, makes it possible to overcome structural features of the support, used during partial backfilling owing to up to 0.12 increase in safety margin of components supporting a reverse console which is achieved at the expense of introduction of additional rigid structural elements. In this context, stress concentration level within the junctions of the support design decreases.

Nevertheless, the effect results in the redistribution of the section pressure on a mine working floor. In terms of certain strength characteristics of enclosing rocks, that will cause uniform forcing of a base plate in the neighbouring rock layer.

3. Concentration of horizontal stresses, oriented along a stope face above the powered support inside a mine working roof is the key factor effecting a mode of progress of the main fissures within a stope roof while backfilling.

4. In the context of selective coal mining, height of rocks being cut determines optimum parameters of the mine working roof deformation irrespective of the structure of fine-grained rock mass in terms of the selected backfilling operation schedule.

References

1. **Sotskov, V., Demchenko, Yu., Salli S., Dereviahina N**. Optimization of parameters of overworked mining gallery support while carrying out long-wall face workings. Naukovyi Visnyk Natsionalnoho Hirnychoho Universytetu, №6, (2017). 34–40.

2. **Fomychov, V.V.** (2012). Bases of calculation models plotting of bolt-frame support considering non-linear characteristics of physical environment behavior. Scientific herald of National Mining Ukraine, 4, 54-58.

3. **O. Inkin, V. Tishkov, N. Dereviahina and V. Sotskov**. (2018). Integrated analysis of geofiltrational parameters in the context of underground coal gasification relying upon calculations and modeling// Ukrainian School of Mining Engineering, Volume 60, 1-9 https://doi.org/10.1051/e3sconf/20186000035

4. **Huang, Y.L., Zhang, J.X., Zhang, Q., Nie, S.J., and An, B.F**. (2012). Strata movement control due to bulk factor of backfilling body in fully mechanized backfilling mining face. J. Min. Saf. Eng., 29, 126–167.

5. **Kiyashko, YU.I.** (2001). Scientific and technical principles for creating high-performance technologies for coal seam mining. Dnepropetrovsk.

6. **Kovalevs'ka, I., Symanovych, G., Fomychov, V**. (2013). Research of stress-strain state of cracked coalcontaining massif near-the-working area using finite elements technique. Mining of Mineral Deposits, 159 - 163.

7. **Bondarenko, V.I., Kovalevskaya, I.A., Simanovich, G.A., Fomichev, V.V**. (2010). Trends in the stress state of weak rocks of a formation overburden roof. Materials of the International Conference «Forum Hirnikiv», 183 - 188.

9. **Glamheden, R., Hökmark, H.** (2010). Creep in jointed rock masses. State of knowledge. Stockholm: Svensk Kärnbränslehantering AB, 51.

10. **Ma, C., Yao, W., Yao, Y., Li, J**. (2018). Simulating Strength Parameters andSize Effect of Stochastic Jointed Rock Mass using DEM Method. KSCE Journal of Civil Engineering, 22(12), 4872-4881.

11. **Fomychov, V., Sotskov, V.** (2018). Determination of parameters of non-uniform fractured rock massif in computing experiment. Journal of Geology, Geography and Geoecology, 26, 26-32.

12. **Fomichev, V.V., Sotskov, V.A., Malykhin, A.V**. (2014) Definition and analysis of changes in acceptable indicators of the stress-strain state of the elements of the frame-anchor lining of the dismantling drift when approaching the face. Naukoviy vísnik NGU, 1, 22 - 25.

13**. Sadovenko I., Inkin O., Dereviahina N., Hriplivec Y.** Analyzing the parameters influencing the efficiency of undereground coal gasification. Dniprop. Univer. bulletin, Geology, geography, 27 (2), p. 332 – 336.

ELABORATION OF GEOLOGICAL AND TECHNOLOGICAL MODELS FOR RATIONAL DEVELOPMENT OF TITANIUM DEPOSITS

Remezova O.
D(Sc), associate professor, chief of mineral resources geology department Mineral Resources Geology Department Institute of Geological Sciences of the National Academy of Sciences of Ukraine (IGS NAS Ukraine), Kyiv, Ukraine

Vasylenko S.
PhD, senior researcher Mineral Resources Geology Department Institute of Geological Sciences of the National Academy of Sciences of Ukraine (IGS NAS Ukraine), Kyiv, Ukraine

Okholina T.
PhD, senior researcher Mineral Resources Geology Department Institute of Geological Sciences of the National Academy of Sciences of Ukraine (IGS NAS Ukraine), Kyiv, Ukraine

Yaremenko O.
junior research scientist
Mineral Resources Geology Department
Institute of Geological Sciences of the National Academy of Sciences of Ukraine (IGS NAS Ukraine), Kyiv, Ukraine

The article deals with approaches to the rational and complex development of titanium deposits of different genetic types: primary, residual and placers. The task was to select the most rational way of working out prospective fields for which the modeling of deposits using GIS was made. For the primary deposits, the geological section was detailed by geochemical methods, with allocation within each unitthe layers with different mineralization; the distribution of minerals was studied, and the existence of latent layering was proved. These researches improve the ore enrichment schemes. An open cast-underground mining method has been proposed for the Stremyhorod deposit, which allows reducing by 15-18 hectares the area of the extracted lands and by 25-28 million m^3 of the amount of overburden. For the residual Torchyn deposit it is proposed to use a vertical reserve index to construct the geological-technological model, which allowed the selecting the most profitable blocks for mining. On the example of the Tarasovka placer it is shown a model where an integral indicator is applied, which includes the sale value of all useful components in two productive horizons and the cost of their extraction. Such approaches allow the development of a rational scheme for field exploration, providing complex extraction of useful components.

Introduction. Ukraine has a powerful industrial base of titanium. The level of potential titanium resources and productioncapacity of ilmenite concentrates in Ukraine is currently estimated at 20% of the world balance. The mineral and resource base of titaniun in Ukraine is represented by deposits of different size and genesis, which are at different stages of geological study.

The major resources of Ukraine's titanium are concentrated in large ilmenite and ilmenite-rutile-zircon alluvial andbeach-submarine placers[1]. It should be noted that in the development of them there were problems:

1. The decline of the quality of concentrates. This is concerned to both the Irsha group placers, from where the concentrate is sent for the production of titanium dioxide pigment, and to beach-submarine deposits, where the size of ilmenite grains is reduced (for sands of the Poltava series).

2. Complication of technology of extraction and dressing of ore sands. This is due to the fact that the ilmenite reserve deposits are often associated to fine-grained and clay-bearing rocks.

3. The complex nature of the placers (ilmenite, rutile, zircon, leucoxen, disthene, sillimanite and other minerals) requires a revision of traditional technology.

It is also impeded the opening of primary and residual deposits, due to lack of technology for their development.

2. Literature review and problem statement. Previous studies have revealed the main features of the structure of titanium deposits, mineralogy, and their genesis [2-5]. Concerning the Stremyhorod deposit, its genesis was considered from the point of view of the metasomatic-zonal structure[2], which led to wrong decisions for its development.

The IGS NAS Ukraine is developing a method of structural-lithological modeling, which has been tested for a number of placers[6]. However, it should be complemented by geological and technological models aimed at identifying areas with the most favorable extraction conditions.

Our team of researchers was tasked with selecting the most rational way of working out promising fields of different genetic types, including placers, residual and primary ones, and allocation of priority areas. For this purpose, we carried out geological-technological

modeling by means of GIS and conducted mineral-geochemical researches[7-9].

3. Exploration data and methods. Exploration data(mineralogical, lithological, geochemical, geophysical research data) were used to develop the models of the deposits, which are summarized in databases. For the identification of stratification in the massifs of gabbroids, the geochemical methods described in[7] Based on the exploration data, the project of open-underground exploitation of the Stremyhorod primary deposit was elaborated, using the own methodology by Dr(Sc)O.Chernyh, the former employee of the IGS NAS Ukraine[10,11].

4. The results obtained in the study of titanium deposits of different genetic types.

1.*Primary deposits*.

Having a significant potential of titanium deposits, in recent years Ukraine has gradually moved to the development of titanium deposits with more complex geological conditions. Promising titanium deposits in the world are primary ores associated with layered intrusions. The primary titanium ores reserves stand at more than 50% of all balance reserves in Ukraine.

Within Ukraine, the most important titanium deposit is the unique Stremihorod primary phosphorus-titanium deposit, confined to the eponymous layered intrusion.The productive stratum is dense primary ores of the mafics composition of the Korosten intrusive complex (leucogabbro, olivine - pyroxene gabbro, troctolite, gabbro-peridotite) and the weathering crust of the Mesozoic-Cenozoic age.

The primary ores form a single steeply dipping body of a rod-like shape with a zonal structure - rich ores of the central part, which gradually change to endocontacts with poor ones. The carrier of titanium mineralization is ilmenite. The richest ores are melanotroctolites and peridotites in the central part of the intrusion. The mineral resources of the Stremyhorod deposit are the gabbroids with a TiO_2 and P_2O_5 content of 4.5-5 to 7-8% and 0.7-4%, respectively. Theyare represented by ore body 2.4 km long and 1.0 km wide in the center and 100-150 m on the flanks.

According to our methodology, within each of the above described gabbroid varieties, 3-4 interlayers with different levels of Fe-Ti mineralization were identified[7]. This geological and genetic

model was adopted to develop the rational development of this deposit. Stremyhorod intrusion is characterized by changes in the composition of Fe-Ti oxide minerals, which are a sign of latent layering in the massif. In melanocratic variations, along with the homogeneous ilmenite, it is occurred also ilmenite with relatively wide plate-like inclusions of magnetite, which together form the primary ilmenite - titanomagnetite aggregates.In mesocratic rocks in the structure of the decomposition of ilmenite, thin-walled hematite separations prevails, and in leucogabbrothe ilmenite is primarily homogeneous. Only titanium magnetite growths are occasionally observed.

Apatite in the Stremyhorod massif tends to accumulate with increasing of iron. It is represented by two generations: early and late magmatic, which form scattered inclusions of larger crystals.The first generation is characteristic of melano- and mesocratic varieties, and the second is characteristic of leukocratic differentiates. In the first case, apatite forms idiomorphic small hexagonal crystals (0.1-0.2 mm) in the joints with ilmenite and olivine, cemented with uralite. It is usually grouped into nested clusters or chains, consisting of hexagonal individuals. The content of apatite tends to increase due to the increase of the ferruginosity of the rocks, accumulating mainly in the central more melanocratic part of the massif. Apatite content decreases with the depth in intrusion.

The chemical composition of ilmenite in unconsolidated rocks and in primary ores is almost identical. The content of TiO_2 in ilmenite from the weathering crust is 51.4%, from primary ores - 48.93%. The content of harmful impurities: P_2O_5-0.05-0.22% (average for samples 0.1%), Cr_2O_3-0.03-0.05%.According to these indicators, ilmenite concentrate can be used in the production of pigment titanium dioxide. The content of P_2O_5 in apatites is 40.5%, and fluorine content is 1.3-2.9% (2.22% on average).

Improving the crushing process, as well as the dressing scheme for ores of such type as a whole, and the selection of flotation reagents will make it possible to obtain a number of ore processing products (ilmenite, apatite concentrates, vanadium cast iron, etc.).

With the purpose of the rational exploitation of this object the open cast - underground mining method of exploitations developed in IGS NAS Ukraine[10].

Taking into account the significant depths to which mineralization extends, it is advisable to develop this deposit in a complex open cast-underground method to a depth of 1200m: the upper part of the deposit is taped with a spiral internal trench with the development of open-cut mining to a depth of 380 m (-190 m), the under-quarry part to a depth of 935m (-745m) - by vertical trunks: ore-lifting and auxiliary drainage and ventilation[10].

Open-cast works are carried out by a 380m deep quarry, developing the thickest part of the deposit. Considering the high hardness of ores and host rocks, the overall slope angle of the pit side is 55 °(Fig.1). The areal size of the open pit: width 1600m, length 1800m. The formation of non-working sides of the quarry is carried out without leaving safety berms. In the process of open-cast works, the special wall control is carried out - non-working opencast bench with a height of 15 m are built without berms, forming 45 meter benches without berms. This will reduce by 15-18 hectares the area of extracted lands on the surface and reduce the development of rock overburden by 25-28 million m^3. When developing an open pit, "loading shovel" excavators with a struck bucket capacity of 12 m^3 and mining trucks with a loading capacity of 100-120 tons are used. The annual capacity of the quarry will be 12 million tons of ore. When the quarry reaches a depth of 280-300 m and transportation costs increase, an option is provided for ore delivery from deep horizons of the quarry (300-380 m) according to the scheme: transport adit from the quarry - rock shaft.

Underground work between elevations of 380-935 m (-190: -745m) is carried out by a floor-and-chamber development system. Underground work is carried out simultaneously with the work of the quarry.The initial mark of underground work (410 m) is below the mark of the temporary under-quarry ceiling, with a thickness of 30m. The ground floor at elevations of 410-530m is practiced by chambers 120m high and 40 m wide. The length of the chambers corresponds to the thickness of the ore body.The height of the chamber was adopted on the basis of practical experience in underground mining of quartzites similar in properties to the mine named after Ordzhonikidze. The second lower floor at elevations of 560-680 m is practiced similarly. An ore ceiling of 30m of thickness is left between the first and second underground floors. This system has been widely tested

in the world practice of open-underground mining of iron ore deposits and has shown high technical and economic indicators.

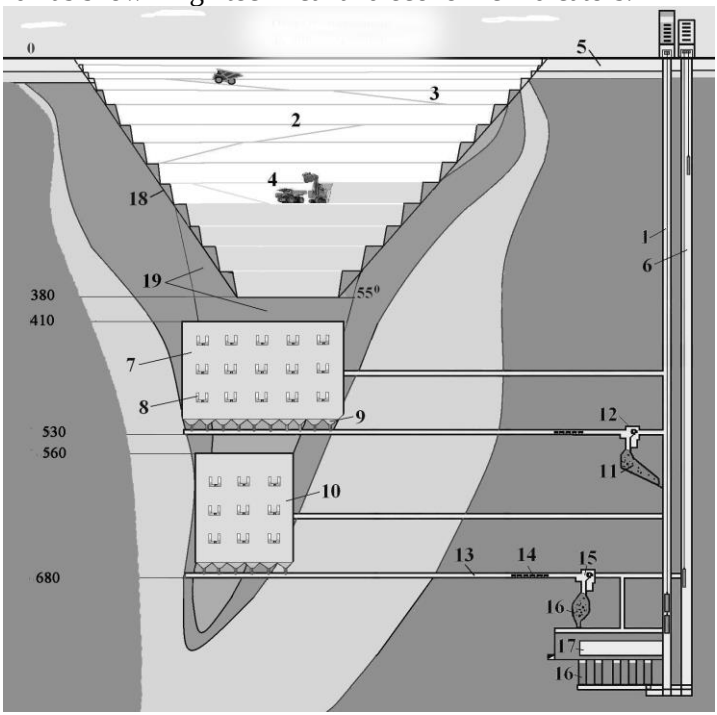

Fig.1. Recommended option for simultaneous open and underground mining of the Stremyhorod deposit using a floor-and-chamber development system for underground work: *1* - ore-lifting trunk; *2* - quarry; *3* - spiral automobile exit; *4* - mining quarry according to the scheme: excavator-dump truck; *5* - sediment and weathering crust; *6* - auxiliary shaft for the delivery of people, overall equipment and ventilation; *7* - underground chambers practiced at elevations: 410-530 m; *8* - vertical concentrated charges; *9* - horizon for the release of broken ore; *10* - floor-chamber development system between elevations 560-680 m with a height of chambers 120 m; *11* - underground storage hopper for crushed ore with its subsequent loading into mine skips; *12* - crusher of the first underground floor; 13 - transport crossdrift; *14* - mine trolleys; *15* - crusher of the II underground floor; *16* - storage pocket; *17* - sorting; *18* - the general angle of slope of the non-working side of the quarry - 55°; *19* - instrument and sub-quarry ore reserves mined by the open-underground method at the time of completion of open work

For loading and transport operations, vibratory feeders are used in combination with mine cars with side or bottom unloading, depend-

ing on the chosen scheme for unloading cars in transport skips. The annual capacity of underground work is 8 million tons.

Using this method will reduce by 15-18 hectares the area of extracted fertile land and reduce the development of rock overburden by 25-28 million m^3.

2. *Residual deposits*

Ukraine is provided with explored titanium ores reserves for at least half a millennium at the current rate of extraction.

Torchyn ilmenite deposit is located in Zhytomyr region within three administrative districts (Radomyshl, Korostyshiv and Chernyakhiv).

The ore body is traced from the northwest to the southeast for 12 km, at a width of 9 km. In geostructural terms, the deposit is located within the north-western part of the Ukrainian Shield, the south-eastern part of the Volodarsk-Volyn massif of basic rocks.

The large inner part of the massif is composed of leucocratic rocks, and its endocontact part - weakly and moderately ore-bearing marginal facies gabbronorites, which are rhythmically stratified into melanocratic ores, mesocratic ore and leucocratic pure layers and packs.

The Lower Proterozoic crystalline rocks of the basement, the Meso-Cenozoic weathering crust, and Cenozoic sedimentary deposits take place in the geological structure of the deposit. The residual type deposit was formed in the hypergenesis zone due to the removal of lithophilic components. The average thickness of the ore bed is 11 meters. The thickness of the overburden rocks is 16 m.

Kaolins contain about 65% of reserves, in hard 20-25%, in weathered gabbroids about 10%. The Torchyn field was planned to develop a huge quarry with an area of about 10 km^2, which negatively affects the hydrogeology and ecology of the area.

The company profitability was only 8%. Payback period is 12 years. Taking into account these characteristics, the feasibility of development remained questionable for 30 years.

For the commissioning of this deposit, it is necessary the new, modern approaches and complex mining of the deposit. Except apatite and ilmenite the vanadium and scandium it is possible to obtain from the ores of Torchyn deposit, as well as kaolin as raw materials for the building.

In order to develop a rational approach for the development of this facility, we have elaborated geological-technological models using GIS technologies.

One of the model elements is the distribution of the vertical reserves of ilmenite on the deposit. The vertical stock of ilmenite shows its quantity per 1 m^2 of the deposit area.

This parameter determines the spatial distribution of the field reserves. The values of this indicator are distributed unevenly: maximum values of 1621-3843 kg/m^2 are within the north-western part of the deposit and in the eastern part of the deposit (30-40 kg/t).

The thickness of the productive layer is an important parameter, which tends to decrease from east to west. Another indicator is the overburden thickness the highest indicators are in the northwest of the deposit.

The total thickness of both parameters varies from the first centimeters to 39 m within the deposit.

An integral index was calculated for blocks selection with optimal economic and geological parameters.

This parameter was calculated as the difference between the conditional cost of ilmenite concentrate and the cost of performing overburden and processing of the productive layer.

The allocation of blocks by queue is carried out in accordance with the value of the development profitability, determined by the integral indicator.

Blocks with maximum profitability of ilmenite ore extraction (first stage) are located in the western part of the deposit (Fig. 2).

One of the problems, connected with development of the Torchyn field, which has a large area, in the case of a single quarry development are significant decrease of groundwater (more than 10 m).

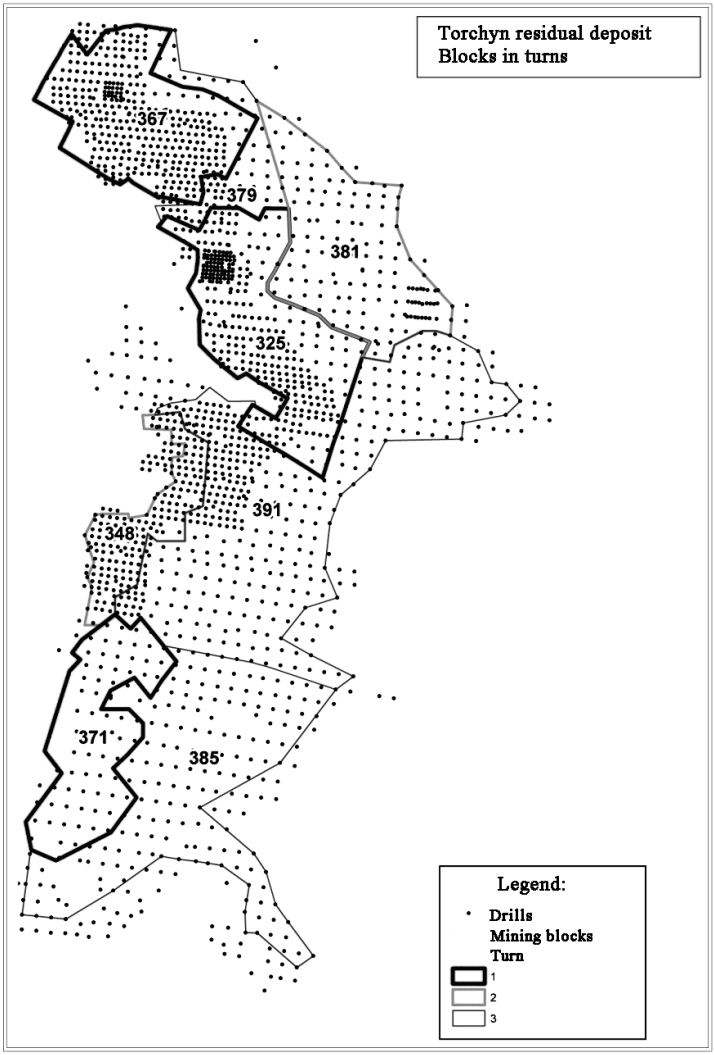

Fig. 2. Torchyn deposit. The proposed scheme of mining

As a result of conducted modeling have been selected perspective sections, which will be worked out in turn. The picture changes significantly in the case of mining within the proposed sites. The

model of groundwater reductions due to the open-pit drainage system for Block # 367 as one of the most promising, have been constructed. The reduction of the development area and the gradual movement of the recess along the block reduce the area of influence of the depressing funnel to 500m.

In addition, the funnel is constantly moving as the open-pit develops, without delaying in a constant range more than 1 year. Due to its smaller area, water inflows in such a quarry are not significant in this case and will not affect the water supply of settlements near the quarry.

3. *Placers*

Alluvial deposits contain varying degrees of modified ilmenite, as well as a number of related components (zircon, disthene, sillimanite, etc.). Ukraine takes the third place in the world on the ilmenite concentrate production (its share is about 12%); in the world export of titanium concentrates - 8%, sponge titanium - 7,4%.

Within the Eastern European alluvial province there is a Ukrainian sub-province, which is the most promising for titanium-zirconium mineralization. There are four alluvial zones - Prydneprovskaia, Pryazovskaia, Azovo-Chernomorskaia and Kharkovsko-Sumskaia are part of the Ukrainian sub-province [4]. The mineralization of alluvial deposits is represented by leukoxenization ilmenite, zircon, rutile, disthene, sillimanite, staurolite, monazite. It has a stable composition and varies insignificantly. Placer deposits are ore base of titanium of Ukraine. This type of deposits are gradually exhausted, the new ones are hardly explored. Further direction of exploration for titanium and zirconium of the Ukrainian alluvial sub-province is hampered by the lack data on the composition, facial and genetic conditions of distribution of ore-bearing deposits. Promising alluvial deposits are: Volyn group of placers (Zlobychskoe, Valky-Hatskovskoe, Trostianetskoe, Paromovskoe), Tarasovskoe, Zelenoiarskoe, Samotkanskaia group of placers (Malyshevskoye, Motrono-Annovskoye, Volchanskoye).

The Tarasovskoe rutile-zircon-ilmenite placer deposit is considered to be the most promising after the Motronovsko-Annivsky [12] located in the Middle Dnieper region. This object is similar to placers of samotkansky type, which have been successfully developed for more than 50 years.

The purpose of the work is to develop geological and technological models for the rational development of titanium deposits, to study the conditions of the formation and evaluation of titanium-zirconium ore potential [12].

Tarasovskoye rutile-ilmenite-zircon deposit is located in the southwestern part of the Kiev region, Ukraine.

Stratigraphically the industrial concentrations of titanium and zirconium minerals are confined to the lower-middle Miocene sandy depositions. A productive layer up to 25 km long with a width of 10-12 km has a sub-latitudinal extension. This placer is divided into two layers, which are joining into one in the southwestern part.

The upper layer is the main industrial ore body. It contains up to 90% of the heavy fraction minerals. The layer thickness is 2,0-20,7 m, the distribution area is about 78,5 km^2. The thickness of overburden is 1,5-52,4 m.

The lower layer is located 0,2-11 m deeper than the upper one. Its capacity ranges from 0,1 to 8 m, an average of 5,69 m, and the power of intermediate overburden to 11,0 m. The nature of regular shape, sorted and roundness of grains, the presence of mineral-enriched layers of ore minerals indicate that the accumulation of ore-bearing sands occurred in a weakly flowing shallow basin of the lake type, under conditions of constant movement of the coastline.

Natural gravitational separation and concentration of minerals took place along the shoreline in separate sections, based on their specific gravity. The source of the crystalline rock material was rocks of elevated sections of the crystalline foundation, which from the southwest limited the sedimentary basin.

For the first time, the working group from Institute of Geological Sciences constructed and analyzed the distribution maps of zircon, rutile, ilmenite and leucoxene, disthene and sillimanite. Also were constructed the distribution map of the integral indicator, with a real reference to the coordinate system. A map of the integral indicator is shown on Fig. 3. This parameter includes the sale value of all useful components in both productive horizons and the costs of their removal.

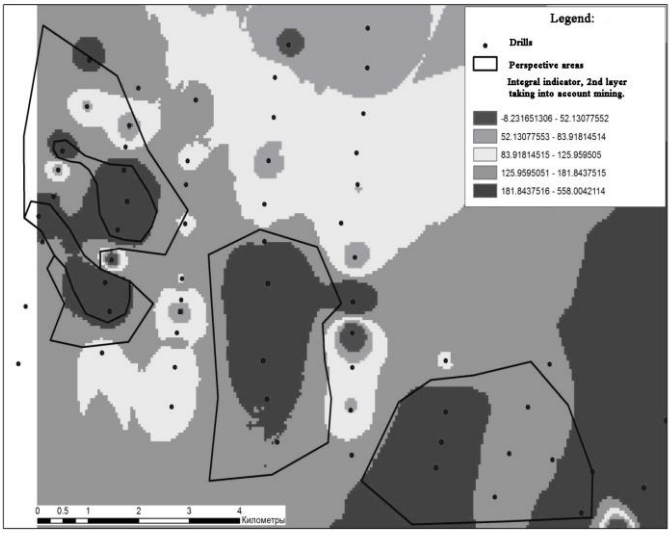

Fig.3. Tarasovskoe deposit. Distribution of the total integral indicator

Using this map, we identified promising areas with high content of heavy fraction *(dark colored on the map)* and acceptable economic indicators for development, which allows us to rationally and comprehensively develop this field.

In addition to the problem of the gradual depletion of titanium deposits, the ores of which are suitable for metallurgy, the actual question about the deficit of non-leukoxenized ilmenite. Such unchanged ilmenite is in sufficient quantities at the Torchyn residual deposit. Ilmenite concentrate with the TiO_2 content of up to 55%, (unchanged), is used for pigment titanium dioxide obtaining using the sulfate technology.

Conclusions:

- Primary phosphorus-titanium deposits in Ukraine are associated to layered intrusions of gabbro. Among them are known various geological bodies - bosses, lopolithes, cup-shaped intrusions. For layered massifs, gabbro is characterized by latent layering, which is manifested in the distribution of main ore minerals and chemical composition. The most enriched by ore minerals melanocratic macrhythms are, within which owing to the manifestation of acid-base differentia-

tion and other processes, layers are found in magmatic chambers, more enriched and less enriched in titanium and phosphorus (micro-rhythms). These peculiarities must be taking into account during elaboration of project of mining and ore dressing scheme.

The largest in reserves is the Stremyhorod deposit, associated to the gabbroid boss. The geological structure of a steeply declining field contributes to the greatest degree to the effectiveness of open and underground operations.

The quarry fits into the configuration of the reservoir, which can significantly reduce the volume of stripping operations. The angle of inclination of the deposit (84-87 °) allows to reduce to a minimum the volume of sinking of permanent mine opening in underground operations, to reduce ore losses and to prevent unwanted collapse due to geomechanical conditions.

-The feasibility study of the selected blocks on Torchyn deposit will significantly increase the previously identified profitability by almost three times from 8% to 30% and reduce the return from 12 to 3 years.

This guarantees a long and successful open pit and provides for the subsequent consistent development of the entire area under the proposed scheme.

- Environmental impact is minimal. Depression funnels that have a significant impact on landscapes and the quality of life of the population do not go beyond the 500-meter radius of influence and exist in the territories for no more than a year.

Their relocation is due to the fact that the reclamation of quarries occurs in parallel with the extraction.

- Thus, the development of the quarry field should be carried out in small areas, starting with the proposed Blocks: 325, 367, 371, which will provide high productivity, minimal impact on the environment and the development of mineral resources for titanium industry in Ukraine.

- The elaboration of geological-technological models for Tarasovskoe deposit helps to organize project of complex extraction of heavy minerals on the most prospective areas.

References

1. **Ghalecjkyj L.S., Remezova** O.O.(2011)Strateghija rozvytku mineraljno-syrovynnoji bazy tytanu Ukrajiny. Gheologhichnyj zhurnal, 3, 66-72.

2. **Proskurin G.P**. (1984). Ob"emnaya zonal'nost' apatit-il'menitovogo orudeneniya v gabbroidakh Korostenskogo plutona. Vertikal'naya zonal'nost' magmatogennykh rudnykh mestorozhdeniy, Moskva: Nauka, 45-67.

3. **Shvajberov S.K., Metalidi V.S., Prykhodjko V.L**. et al. (2003) Mineraljno-syrovynna baza fosfor-tytanovykh rud pivnochi Ukrajiny. Naukovyj visnyk NGhU, 9, 23-24.

4. **Tsymbal S.N., Polkanov Yu.A.** (1975). Mineralogiya titano-tsirkonievykh rossypey Ukrainy, Kiev : Nauk. dumka, 248p.

5. **Mitrokhin A.V., Mitrokhina T.V.** (2006).Petrologiya i rudonosnost' Fedorovskogo apatit-il'menitovogo mestorozhdeniya. Mineralogichniy zhurnal, 28, 4, 43-52.

6. **Khrushchev D.P., Kovalchuk M.S., Remezova E.A.,Lalomov A.V., Tsymbal S.N., Lobasov A.P., Ganzha E.A.,DudchenkoYu.V., KroshkoYu.V**.(2017). Structurallithologic modeling of sedimentary formations. Kiev: Interservice, 352 p.

7. **Ghalecjkyj L.S., Komsjkyj N.M., Marynovych B.A., Remezova O.O.** (2009). Gheologho-ghenetychna modelj Fedorivsjkogho tytanonosnogho intruzyvu. Gheokhimija ta rudoutvorennja, 27, 15-20.

8. **VasylenkoS.P., OkholinaT.V., RemezovaO.O., YaremenkoO.V**. (2016).The analysis of ilmenite distributing in titaniumdeposits by GIS-modeling (on the example of Torchyn apatite-ilmenite deposit).Teoretychni ta prykladni aspekty gheoinformatyky, 13, 4-13.

9. **Vasylenko S.P., Okholina T.V., Tkachenko P. Gh**. (2016).Gheologho-ghenetychna modelj ob'jekta "Tarasivka skhidna". Aktualjni problemy ta perspektyvy rozvytku gheologhiji: nauka j vyrobnyctvo. Materialy Mizhnarodnogho gheologhichnogho forumu (15-20 serpnja 2016 r., s. Kobleve, Mykolajivsjka obl.,Ukrajina). – Kyiv: UkrDGhRI, 10-14.

10. **Galetskiy L.S., Chernykh A.D., Remezova E.A**. (2013). Ratsional'nyy sposob otrabotki unikal'nogo Stremigorodskogo apatit-il'menitovogo mestorozhdeniya v Zhitomirskoy oblasti Ukrainy . Sb. tr. Mezhdunar. konf. "Ti-2013 v SNG" (Donetsk, 26-29 maya 2013 g.). Kiev, 77-82.

11**. Chernykh A.D., KolosovV.A., Bryukhovetskiy O.S., Galetskiy L.S., Gozhik P.F**.(2005).Kompleksnaya razrabotka rudnykh mestorozhdeniy :Kyiv: Tekhnika, 376.

12. **Remezova E.A., Vasylenko S.P., Svivalneva T.V., Yaremenko O.V**., 2014. Conditions of zircon accumulation in titanium-zirconium deposits in the Dnieper alluvial zone of Ukraine. Vestnik Voronezhskogo Universiteta. Ser. Geologiya, iss. 3, p. 79-84

MEASUREMENT OF FRACTURE VOLUMETRIC RATIO BY ELECTRICAL METHOD

Didenko M.
Candidate of Science, associate professor of Mining sub faculty
of Volodymyr Dahl East Ukrainian National University, Ukraine

The subject of the experimental research was the analysis of the distribution of the electric field in a massif of dry fractured rocks around the probe of an electric capacitive introscope. The study was carried out to determine the dependence of the readings of the device on the fracture volumetric ratio of the rocks, the fracturing of which is caused by a pattern of small randomly directed cracks. The determining of this dependence is necessary for the subsequent calculation of the deformations of the rock mass around the mining. The research methodology based on numerical computer simulation of the distribution of the electric field. It was carried out using a specially designed computer program. Its calculation algorithm ensures the adaptation of the finite element method to the solution of a problem. By the results of simulation, it was found that the coefficient of disturbance of the rock mass, calculated from the readings of the electric capacitive introscope, changes almost proportionally to the fracture volumetric ratio. Moreover, the lithological character of the rocks has a significant effect on the numerical values of the coefficients of the obtained dependence. The conducted studies are part of a concept for monitoring of current geomechanical processes.

Introduction

Mine instrumental observations during the exploitation of preparatory workings, despite their laboriousness, are the main method for studying the effects of mining pressure. In geomechanics, certain experience has been accumulated in the creation and use of methods and equipment for monitoring geomechanical processes, which highlighted significant difficulties in solving this problem. First of all, they are associated with the variety of information received, which is characterized by a large number of controlled parameters that are different in their physical nature, and the technical methods for obtaining them. Among the many methods for determining the state of a rock mass, the most advanced is the electric capacitive method [1]. The method is based on the dependence of the current frequency produced by the measuring generator on the capacitance of the capacitor sensor, which, in turn, is determined by the dielectric constant and fracturing of the rocks that present the massif. As mine measurements and laboratory studies have shown, the diameter of the

hole, the displacement of the axis of the probe relative to the axis of the hole, resulting from transverse movements of layered rocks or the deformation of stabilizers of the position of the probe in the hole, and other factors have a significant influence on the readings of the device. Therefore, the real readings of the introscope have a clearly expressed random character, and the coefficient of disturbance [2], proposed by the authors of the method for estimating fracturing in a rock mass, can only be used as a qualitative characteristic of disturbance at the sampling site. Through laboratory studies, the dependence of the instrument readings on the main influencing factors was previously determined [3] (including the influence of a single or group of cracks that have a sufficiently large opening). However, until now, the response of the device to the presence of a fracture pattern formed by small cracks and the relationship of its readings with the fracture volumetric ratio of the rock mass, which is understood as the ratio of the volume of voids formed by cracks to the volume of rock, has remained undetermined.

The purpose of the studies described in this article is to determine quantitative parameters that allow us to calculate the fracture volumetric ratio depending on the readings of the electric capacitive introscope. Such dependence is necessary for the subsequent calculation of the displacements of the rock contour of the mine [3], the prediction of the aftereffects of rock pressure on it, and the selection of rational support parameters [4]. This goal was achieved through experimental studies, since analytical studies without significant simplifications are extremely complex, but the introduction of simplifications reduces the value and practical significance of the results. Since in order to obtain reliable results of experimental studies, it is necessary to accumulate a statistically significant number of experimental results, but varying over a wide range or even maintaining a certain value of the fracture volumetric ratio of the medium does not seem possible not only in natural conditions, but even in laboratory, it was decided to simulate the operation of the electro-capacitive probe of the introscope using a mathematical model. The most suitable and most developed method of mathematical modeling of such problems is the finite element method. There is a variety of computer software that allows you to simulate electric fields using the finite element method. Such programs include, for example, ANSYS,

COMSOL-MultiPhysics, ELCUT, etc. However, all these programs are foreign and, for various reasons, inaccessible to Ukrainian researchers. Usually, an obstacle to widespread use of such software in Ukraine is its high cost. Among the mentioned programs, the ELCUT program is shareware; however, it was developed in the Russian Federation, Ukraine's relations with which have been complicated in recent years. So this program cannot be used for political reasons. Meanwhile, it is relatively not difficult to algorithmize the calculation by the finite element method and implement it in an application program. Thus, to achieve the intended goal it is necessary to solve the following tasks: to develop a method for simulation of electric field based on the finite element method; to develop an application program that implements such method; to carry out with this program a series of calculations with varying over a wide range of the fracture volumetric ratio of the medium of models that represent a rock mass with different lithological character; to process the results of numeric simulation and to obtain a relationship that allows to determine the fracture volumetric ratio from the readings of an electric capacitive introscope. Further content of the article is presented in order to solve the tasks.

Methods of numerical simulation

The essence of the finite element method [6] is that the domain in which the solution to the system of differential equations is sought is divided into a finite number of subdomains (elements). In each such subdomain, the type of the approximating function is arbitrarily selected. To find its coefficients, a system of linear algebraic equations is compiled. The total number of nodes in the element should provide an unambiguous determination of the coefficients, and the number of nodes located on the boundary of the element should ensure the coupling of the approximating functions of neighboring elements without a gap. The simplest flat finite element satisfying these conditions is a triangular element. The number of nodes in it, equal to three, provides the determination of the coefficients of a linear approximating function of the form

$$u(x,y) = a_0 + a_1 \cdot x + a_2 \cdot y = \begin{bmatrix} 1 & x & y \end{bmatrix} \cdot \begin{bmatrix} a_0 \\ a_1 \\ a_2 \end{bmatrix}, \qquad (1)$$

the surface described by this function is an inclined plane, which along the boundary of the element can be represented by a straight line. The straight line position is uniquely determined by two points. Thus, to pair adjacent elements without a gap, two nodes are sufficient. And in fact they are available at each of the boundaries of a triangular element.

The system of equations for finding the values of the coefficients of the approximating function has the form

$$\begin{bmatrix} 1 & x_1 & y_1 \\ 1 & x_2 & y_2 \\ 1 & x_3 & y_3 \end{bmatrix} \cdot \begin{bmatrix} a_0 \\ a_1 \\ a_2 \end{bmatrix} = \begin{bmatrix} u_1 \\ u_2 \\ u_3 \end{bmatrix}, \qquad (2)$$

u_1, u_2, u_3 are nodal potentials of the electric field.

After substituting the solution of system (2) into function (1), we obtain

$$u(x,y) = \begin{bmatrix} 1 & x & y \end{bmatrix} \cdot \begin{bmatrix} 1 & x_1 & y_1 \\ 1 & x_2 & y_2 \\ 1 & x_3 & y_3 \end{bmatrix}^{-1} \cdot \begin{bmatrix} u_1 \\ u_2 \\ u_3 \end{bmatrix} = \alpha(x,y) \cdot \begin{bmatrix} u_1 \\ u_2 \\ u_3 \end{bmatrix}, \qquad (3)$$

$\alpha(x, y)$ is the so-called element shape function

$$\alpha(x,y) = \begin{bmatrix} 1 & x & y \end{bmatrix} \cdot \begin{bmatrix} 1 & x_1 & y_1 \\ 1 & x_2 & y_2 \\ 1 & x_3 & y_3 \end{bmatrix}^{-1}. \qquad (4)$$

The electric field strength vector in the element can be calculated through the gradient of the field potential

$$\vec{E} = -\nabla_{x,y} u(x,y). \qquad (5)$$

The potential energy of electric field is related to its strength as follows

$$W = \tfrac{1}{2} \cdot \varepsilon_0 \cdot \varepsilon \cdot E^2 = \tfrac{1}{2} \cdot \varepsilon_0 \cdot \varepsilon \cdot (\vec{E} \cdot \vec{E}), \qquad (6)$$

ε_0 is the electric constant (previously called the dielectric constant of vacuum);

ε is the relative dielectric constant of the medium (within the finite element is considered constant).

The scalar product of electric field strength vectors included in expression (6) taking into account expressions (5) and (3) can be represented in the form

$$\overset{\rho}{E}\cdot\overset{\rho}{E}=\begin{bmatrix}u_1 & u_2 & u_3\end{bmatrix}\cdot Z\cdot\begin{bmatrix}u_1\\ u_2\\ u_3\end{bmatrix}. \quad (7)$$

Z is a certain matrix composed of partial derivatives of an element shape function (4), which in turn can be represented as a product of matrices

$$Z=B^T\cdot B, \quad (8)$$

B is the so-called element shape matrix, which can be calculated as follows

$$B=\begin{bmatrix}\frac{\partial}{\partial x}\left(\frac{\partial}{\partial u_1}u(x,y)\right) & \frac{\partial}{\partial x}\left(\frac{\partial}{\partial u_2}u(x,y)\right) & \frac{\partial}{\partial x}\left(\frac{\partial}{\partial u_3}u(x,y)\right)\\ \frac{\partial}{\partial y}\left(\frac{\partial}{\partial u_1}u(x,y)\right) & \frac{\partial}{\partial y}\left(\frac{\partial}{\partial u_2}u(x,y)\right) & \frac{\partial}{\partial y}\left(\frac{\partial}{\partial u_3}u(x,y)\right)\end{bmatrix}. \quad (9)$$

After simplification, the elements of the element shape matrix (9), as well as the coefficients of the element shape function (4), are expressed only through the coordinates of the nodes of the finite element

$$B=\left|\begin{bmatrix}1 & x_1 & y_1\\ 1 & x_2 & y_2\\ 1 & x_3 & y_3\end{bmatrix}\right|^{-1}\cdot\begin{bmatrix}y_2-y_3 & y_3-y_1 & y_1-y_2\\ x_3-x_2 & x_1-x_3 & x_2-x_1\end{bmatrix}. \quad (10)$$

Hereinafter, with the operator $|M|$ the operation of calculating the determinant of the matrix is denoted.

The energy of an electric field enclosed within a finite element

$$W=\frac{\varepsilon_0\cdot\varepsilon}{2}\cdot\int E^2\,ds. \quad (11)$$

The natural distribution of electric field potentials over the studied domain provides a minimum of field energy. So the solution of the original problem is reduced to finding the minimum of energy functional. Based on the variational principle, the following relation should be satisfied within the finite element

$$\begin{bmatrix} \frac{d}{du_1} W \\ \frac{d}{du_2} W \\ \frac{d}{du_3} W \end{bmatrix} = 0 . \tag{12}$$

In view of the previously derived relations (7) and (8), for an isotropic finite element, the equality holds

$$\begin{bmatrix} \frac{d}{du_1} W \\ \frac{d}{du_2} W \\ \frac{d}{du_3} W \end{bmatrix} = \frac{\varepsilon_0 \cdot \varepsilon}{2} \cdot \int \begin{bmatrix} \frac{\partial}{\partial u_1} E^2 \\ \frac{\partial}{\partial u_2} E^2 \\ \frac{\partial}{\partial u_3} E^2 \end{bmatrix} ds = \varepsilon_0 \cdot \varepsilon \cdot B^T \cdot B \cdot \begin{bmatrix} u_1 \\ u_2 \\ u_3 \end{bmatrix} \cdot \Delta s , \tag{13}$$

Δs is the area of the finite element, which for a triangular element can be calculated as follows

$$\Delta s = \frac{1}{2} \cdot abs\left(\left| \begin{bmatrix} 1 & x_1 & y_1 \\ 1 & x_2 & y_2 \\ 1 & x_3 & y_3 \end{bmatrix} \right| \right), \tag{14}$$

Taking into account (10) and (14), expression (13) takes the form

$$\begin{bmatrix} \frac{d}{du_1} W \\ \frac{d}{du_2} W \\ \frac{d}{du_3} W \end{bmatrix} = \frac{\varepsilon_0 \cdot \varepsilon \cdot L^T \cdot L}{2 \cdot abs\left(\left| \begin{bmatrix} 1 & x_1 & y_1 \\ 1 & x_2 & y_2 \\ 1 & x_3 & y_3 \end{bmatrix} \right| \right)} \cdot \begin{bmatrix} u_1 \\ u_2 \\ u_3 \end{bmatrix}, \tag{15}$$

L is matrix calculated as follows

$$L = \begin{bmatrix} y_2 - y_3 & y_3 - y_1 & y_1 - y_2 \\ x_3 - x_2 & x_1 - x_3 & x_2 - x_1 \end{bmatrix}. \tag{16}$$

For the anisotropic finite element, the same relations are true, but instead of the scalar value of the dielectric constant, the product of anisotropy and rotation matrices is involved in them. Thus, expression (15) for the anisotropic element takes the form

$$\begin{bmatrix} \frac{d}{du_1}W \\ \frac{d}{du_2}W \\ \frac{d}{du_3}W \end{bmatrix} = \frac{\varepsilon_0 \cdot C^T \cdot \theta^T \cdot D \cdot \theta \cdot C}{2 \cdot abs\left(\left\|\begin{bmatrix} 1 & x_1 & y_1 \\ 1 & x_2 & y_2 \\ 1 & x_3 & y_3 \end{bmatrix}\right\|\right)} \cdot \begin{bmatrix} u_1 \\ u_2 \\ u_3 \end{bmatrix}, \quad (17)$$

$D = \begin{bmatrix} \varepsilon_x & 0 \\ 0 & \varepsilon_y \end{bmatrix}$ is an anisotropy matrix in which ε_x and ε_y are relative dielectric constant in two mutually perpendicular directions;

$\theta = \begin{bmatrix} \cos\varphi & \sin\varphi \\ -\sin\varphi & \cos\varphi \end{bmatrix}$ is the rotation matrix, in which φ is the angle of rotation of the finite element anisotropy direction relative to the coordinate axes.

For an axisymmetric volumetric problem (in which the central axis is the *Y* axis) for an isotropic finite element the following expression will be true

$$\begin{bmatrix} \frac{d}{du_1}W \\ \frac{d}{du_2}W \\ \frac{d}{du_3}W \end{bmatrix} = \varepsilon_0 \cdot \varepsilon \cdot B^T \cdot B \cdot \begin{bmatrix} u_1 \\ u_2 \\ u_3 \end{bmatrix} \cdot \left(\Delta s \cdot 2\pi \cdot \frac{x_1 + x_2 + x_3}{3} \right) =$$

$$= \frac{\pi \cdot \varepsilon_0 \cdot \varepsilon \cdot L^T \cdot L}{abs\left(\left\|\begin{bmatrix} 1 & x_1 & y_1 \\ 1 & x_2 & y_2 \\ 1 & x_3 & y_3 \end{bmatrix}\right\|\right)} \cdot \frac{x_1 + x_2 + x_3}{3} \cdot \begin{bmatrix} u_1 \\ u_2 \\ u_3 \end{bmatrix}. \quad (18)$$

Similarly, an expression is obtained for an anisotropic element.

When compiling a general system of equations for the entire studied domain a global matrix is formed from the factors that stand in front of the node potential vector in (15), (17) or (18). The number of rows and columns in global matrix corresponds to the total number of nodes of all finite elements into which the studied domain is divided. In this case, the local terms corresponding to the common nodes of adjacent elements are added when writing to the rows and columns of the global matrix. From the vectors of the node potentials

of the elements, a global vector of unknowns is formed. If at some node the potential is given, then the elements of the entire global matrix row corresponding to this node are zeroed, except for the element standing on the main diagonal of the matrix, which is equal to unity. In this case, the specified value of the nodal potential is written into the product vector. The remaining elements of the product vector are equal to zero in accordance with the expression (12).

After solving the resulting global linear system of equations (the least number of computational operations provides the Gauss method), the potentials of all nodes located in the studied area will become known. Then it will be possible to calculate the field energy of each individual element

$$W = \frac{\varepsilon_0 \cdot \varepsilon}{2} \cdot \begin{bmatrix} u_1 & u_2 & u_3 \end{bmatrix} \cdot B^T \cdot B \cdot \begin{bmatrix} u_1 \\ u_2 \\ u_3 \end{bmatrix} \quad (19)$$

and field energy in the entire studied domain by summing the energies of all elements. Next, you can calculate the electrical capacitance of the probe of the introscope using the expression

$$W = \frac{C \cdot U^2}{2}, \quad (20)$$

U is the preset potential difference of the electrodes of the device;

C is the electric capacity of the probe.

The readings of the advanced introscope [5] are inversely proportional to the electric capacitance of its probe, which makes it easy to determine them from the results of numerical simulation.

To implement the described methodology, a computer program in C++ was developed, with which a series of calculations was performed.

Research

The distribution of the electric field in the rock mass surrounding the introscope probe was simulated by solving the axisymmetric volumetric problem. The axis of the probe was aligned with the axis of the model. The diameter of the model was taken equal to 10 probe diameters. The computational domain was divided into annular finite elements with a triangular cross section. The number of finite elements in the model was 5416, the number of nodes 2905. The differ-

ence of electric potentials on the probe electrodes was set equal to 1 Volt. Around the probe electrodes, a 2 mm thick polyethylene layer was simulated on the model, which corresponds to the wall thickness of the plastic pipe in which the sensitive element of the probe is enclosed [5]. The outer diameter of the probe is taken equal to the outer diameter of the pipe (20 mm). The geometric length of the probe was 150 mm; the length of the model along the axis of the probe was taken equal to 600 mm. The ratio of the diameter of the hole to the outer diameter of the probe of the introscope was taken equal to 1.1.

The relative dielectric constant of air was assumed to be approximately equal to 1. The relative dielectric constant of polyethylene was taken equal to 2.35 [7]. During the calculations, side rocks represented by mudstone, sandstone and limestone were simulated. The dielectric constant of these rocks (without the presence of fracturing) was specified as follows [8]: mudstone - 5.5, sandstone - 4.35, limestone - 8. A fractured medium was considered as a two-component heterogeneous system in which the cracks are filled with air. Wet fractured rocks at this stage were not the subject of research, since their dielectric constant substantially depends on filling not only the cracks, but also the pore space [9], the volumes of which, usually, are not known in practice. To calculate the dielectric constant of dry fractured rock, the mathematical model of Maxwell-Wagner was used [10]

$$\varepsilon = \varepsilon_1 \frac{2\varepsilon_1 + \varepsilon_2 + 2V \cdot (\varepsilon_2 - \varepsilon_1)}{2\varepsilon_1 + \varepsilon_2 - V \cdot (\varepsilon_2 - \varepsilon_1)}, \quad (21)$$

ε_1 is the relative dielectric constant of the rock without cracks;

ε_2 is the relative dielectric constant of crack filler (air);

V is the ratio of the volume of voids formed by cracks to the volume of the rock (which is identical to the fracture volumetric ratio).

When performing calculations, the fracture volumetric ratio varied in the range from 0 to 0.15. The frequency of generation of the device in air was taken equal to A_{air}=2385 kHz. According to the results of the first calculation, with a fracture void ratio of 0, the readings of the device in the undisturbed A_r rock mass were determined. According to the results of subsequent calculations (with a fracture volumetric ratio different from zero), the readings of instrument A

were determined, then the coefficient of disturbance P_d [2] was calculated by the formula

$$P_d = (A - A_r)/(A_{air} - A_r). \quad (22)$$

The dependences of the fracture volumetric ratio k_f, which is equivalent to the relative volume of cracks V in formula (21), on the coefficient of disturbance P_d are presented in fig. 1.

The analysis of dependencies showed that with a change in one of these parameters, the second changes almost proportionally.

Moreover, the numerical parameters of this proportion significantly depend on the lithological character of the rocks that formed the massif.

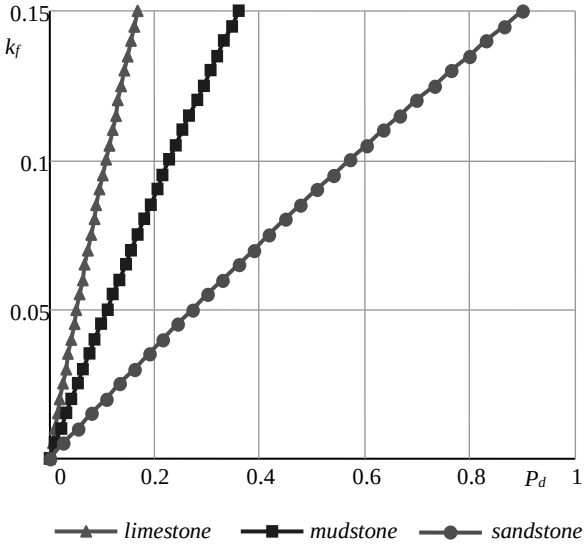

Figure 1. Dependence of the fracture volumetric k_f on the coefficient of disturbance P_d of massif when measured in rocks with different lithological character

The selection of empirical dependences and the calculation of their coefficients by the least squares method showed that, with a relative error not exceeding 0.5% in the entire studied range, the dependences can be represented as

-sandstone $k_f = 0.191 \cdot P_d - 0.027 \cdot P_d^2$; (23)

- mudstone $k_f = 0.477 \cdot P_d - 0.167 \cdot P_d^2$; (24)

- limestone $k_f = 1.013 \cdot P_d - 0.718 \cdot P_d^2$. (25)

With larger, but not exceeding 5%, relative error, the dependences can be approximated by a linear function, since dependent parameters correlate with the correlation coefficient not less than $r = 0.98$ for rock with any lithological character

- sandstone $k_f = 0.17 \cdot P_d$; (26)

- mudstone $k_f = 0.43 \cdot P_d$; (27)

- limestone $k_f = 0.91 \cdot P_d$. (28)

The obtained dependences are true when the ratio of the diameters of the hole and the probe of the device is 1.1. For other values of this ratio the readings of the device should be corrected in accordance with the results of previous laboratory studies [3].

Conclusions

Based on experimental studies of the electric-capacitive method of estimation of the disturbance in a rock mass, dependences are determined that allow calculating the fracture volumetric ratio of the surrounding rock mass by the readings of the introscope (by its signal frequency).

These dependencies are needed to determine the deformations of the rock mass and predict the aftereffects of rock pressure in the coal mine.

The conducted studies are part of the concept being developed for the current control of geomechanical processes and their effects.

In the future, this concept can form the basis of an automated system of geomechanical control in coal mines, the development of which will be launched in the foreseeable future.

References

1. **Litvinsky, G.G.**, Kasyanov, V.A. (1990). *Certificate of authorship of USSR No. 1794253*. Retrieved from http://patents.su/4-1794253-sposob-opredeleniya-neodnorodnostejj-massiva-gornykh-porod.html

2. **Litvinsky, G.G.**, Kasyanov, V.A. (1988). Izmereniye strukturnykh neodnorodnostey massiva pri sooruzhenii vyrabotok. *Tekhnologiya, mekhanizatsiya i organizatsiya stroitelstva gornykh vyrabotok*, 100-107.

3. **Babiyuk, G.V.**, Puntus, V.F., Didenko, M.A. (2012). Issledovaniye, sovershenstvovaniye i ispolzovaniye elektroyemkostnogo metoda dlya otsenivaniya proyavleniy gornogo davleniya vokrug vyrabotok. *Problemy girskogo tysku, 20/21*, 10-56. Retrieved from http://pgd.donntu.org/images/archive/20-21/02_g.v.babnjuk.pdf

4. **Babiyuk, G.V.**, Didenko, M.A. (2011). Dvukhetapnoye prognozirovaniye proyavleniy gornogo davleniya pri provedenii vyrabotok. *Sbornik nauchnykh trudov DonGTU, 34*(1), 24-34. Retrieved from http://sbornik.dstu.education/articles/RU/314.pdf

5. **Didenko, M.O.**, Babiiuk, H.V., Puntus, V.F. (2010). *Patent of Ukraine No. 57376.* Retrieved from http://uapatents.com/3-57376-elektroehmnisnijj-introskop-dlya-masivu-girskikh-porid.html?do=download

6. **Gallagher, R.H.** (1974). *Finite element analysis: fundamentals*. Upper Saddle River, New Jersey: Prentice Hall.

7. **Babichev, A.P.**, Babushkina, A.N., Bratkovskiy, A.M. (1991). *Fizicheskiye velichiny. Spravochnik*. Moscow, Russian Federation: Energoatomizdat.

8. **Brylkin, Yu.L.**, Dubman, L.I. (1972). O dielektricheskoy pronitsayemosti gornykh porod osadochnogo proiskhozhdeniya. *Geologiya i geofizika*, *1*, 117-121.

9. **Brylkin, Yu.L.**, Dubman, L.I. (1979). O dielektricheskoy pronitsayemosti vlazhnykh peschanykh porod. *Elektromagnitnyye metody issledovaniya skvazhin*, 233-242. Retrieved from http://www.emf.ru/mpg/geoelectrycs/works/ems/ems13.pdf

10. **Chelidze, T.L.** (1977). *Elektricheskaya spektroskopiya geterogennykh sistem*. Kyiv, Ukraine: Naukova dumka.

IMPROVE THE EFFICIENCY OF GAS HYDRATE TECHNOLOGY FOR GAS OFFSHORE DEPOSITS TRANSPORTATION

N.M. Pedchenko
Postgraduate, Poltava National Technical Yuri Kondratuk University Poltava, Ukraine

T.M. Nesterenko
Ph.D, Associate Prof. Poltava National Technical Yuri Kondratuk University Poltava, Ukraine

L.A. Pedchenko
Ph.D, Associate Prof.Poltava National Technical Yuri Kondratuk University Poltava, Ukraine

M.M. Pedchenko
Ph.D, Associate Prof. Poltava National Technical Yuri Kondratuk University Poltava, Ukraine

Reducing the reserves of extracted hydrocarbons activates the search for new energy sources, new technologies for its transmission and storage. The natural tendency of increasing the part of offshore fields, including gas, has been observed in recent years. However, traditional technologies for transporting produced gas are often ineffective. The work is devoted to improving the system of preparation well products based on gas hydrate technology in the development of offshore gas fields. The thermodynamic parameters of the «gas – water – gas hydrate» system in a vertical pipeline under non-adiabatic conditions were the object of research. A method to increase the competitive of offshore gas transportation in gas hydrate form has been proposed. It provides for the implementation of the most energy-intensive operation – hydrate formation at the expense of alternative energy sources. The presence of the required thermobaric conditions during the passage of gas by the pipeline through the sea layer and the expediency of the rational use of reservoir energy is shown. The pipeline connecting the well and the production platform was considered as a reactor. Thermobaric conditions for the formation of gas hydrates were studied in it. A mathematical model for describing the process of hydrate formation with an water excess in non-adiabatic conditions in a vertical pipe has been proposed. Vertical pipe is washed with water. The finite difference method is applied for its numerical solution, and the calculation of the hydrate formation process is performed in the Matlab environment. It has established that the process of hydrate formation as result of the gas complete incorporation into the composition of the hydrate is completed at the point along the length of the pipe-reactor with the maximum temperature. The temperature in the pipe-reactor gradually decreases further after this point. For these conditions, the length of the pipe-reactor under the

condition of complete binding of the stream produced gas in gas hydrate was about 300 meters. The proposed gas hydrate technology creates important precondition for the development of small and medium-sized remote gas fields, improving the efficiency and competitive of the of offshore transportation technology of natural gas in gas hydrate form.

Keywords: gas hydrates, production platform, heat exchange.

1. Introduction

Growing global energy demands brought about the necessity to develop new oil and gas fields (Giavarini & Hester, 2011; Lu, 2016) unconventional hydrocarbon deposits (Mykhailov, 2016) as well as conventional primary energy resources. Consequently, the technologies of transportation and storage of extracted minerals are constantly improving (Dychkovskyi et al., 2018).

In view of this, natural gas is definitely the most acceptable resource in terms of environmental impact and technological use. According to the British Petroleum report of 2015, global natural gas reserves constitute approximately 6607 billion m^3. However, nearly half of that amount is assumed to be stranded and associated gas that is not economical for market delivery because of its remoteness from potential markets and lack of transportation infrastructure. First of all it concerns offshore deposits, though their share is growing rapidly with each passing year. But the demand for natural gas from offshore fields is continuously increasing. Despite this, traditional technologies for its transportation often turn ineffective, especially in the case of remote offshore deposits with small gas reserves. Construction of pipelines to such deposits is unprofitable. Especially it concerns LNG technology.

In recent years, liquefied natural gas (LNG) has become the preferred method of natural gas transportation for large distances, particularly across the ocean. However, LNG projects will be profitable only for sufficiently large volumes of gas and a considerable transport distance (Economides, Sun, & Subero, 2006). At present, there are several alternative gas transportation technologies at the various stages of implementation: compressed natural gas (CNG), gas in natural gas hydrate form (NGH), gas-to-liquids (GTL), and gas to electricity (GTW). Each of these technologies, with all its advantages and disadvantages, can be applied for the transportation of gas from offshore deposits. Though

NGH technology has been around for a long time (Gudmundsson, Parlaktuna, & Khokhar, 1994; Gudmundsson & Børrehaug 1996), it has not been fully appreciated yet, since it is still at the stage of technological processes development and improvement.

2. Development the technology of the conversion of extracted natural gas of marine deposits into gas hydrate form

The technology based on the ability of gas and water molecules to form gas hydrates has been actively developing in recent years. Methane clathrates, known as methane hydrates or gas hydrates, are crystalline solid hydrocarbon compounds formed when methane gas is trapped within the crystalline water structure at low temperatures (5 – 15°C) and high pressures (2 – 3 MPa) (Sloan, 2003). One cubic meter of hydrate can store approximately 150 – 170 cubic meters of natural gas depending on thermobaric conditions and the gas composition (Makogon, 2010).

Enormous amounts of natural gas can be extracted from NGH reserves available worldwide. Approximately 98% of them are concentrated in the World Ocean at depths ranging from 200 to 700 m, and in the bottom sediments with thickness of 400 – 800 m. Hence, their development does not require drilling of the ultra-deep wells. Gas hydrate reserves in the world are reported to vary widely within the range between 10^{15}-10^{18} m^3 (Birchwood et al., 2010; Maksymova, 2018). The amount of methane gas within these NGHs is estimated to be $2.1 \cdot 10^{16}$ m^3, which is more than all carbonaceous fuel reserves of the planet (Boswell & Collett, 2011).

Studies have shown that gas hydrates in the appropriate conditions remain stable for a sufficiently long time and can be used to transport gas at considerable distances (Gudmundsson, Parlaktuna, & Khokhar, 1994). Therefore, hydrates are a feasible way to transport and store natural gas in large quantities (Gudmundsson, Graff, & Kvaerner, 2003; Kanda, 2006).

The storage of natural gas in the gas hydrate form was first proposed by Benesh (1938) (produced at 283 K and the pressure of 35 MPa, stored at 241 K, i.e. in conditions close to the equilibrium) (Khokhar, 1998). The fact that natural gas hydrate contains not only gas but also water makes NGH technology the safest. In addition, the processes of formation, storage and melting of the gas hydrate take

place in rather mild thermobaric conditions, in comparison with compression pressure (25 MPa) for CNG or with the temperature of 111 K for LNG. Hydrates are usually stable at moderate temperatures and pressures when compared to the conditions required for LNG and CNG (Bondarenko, Svietkina, & Sai, 2017). The scheme incorporating natural gas hydrates can be an economically preferable solution for the production, storage, and transportation of natural gas from deep water reserves to the shore.

Since Gudmundsson & Børrehaug (1996) proposed the first concept of hydrates utilization in natural gas transportation, some companies and organizations got engaged in the research into this issue. Through these investigations, it was established that NGH could be transported under atmospheric pressure at the temperature around 253 K because NGH has a self-preservation effect. A Japanese consortium, led by Mitsui Shipbuilding Co., managed to commercialize natural gas distribution via a supply chain incorporating NGH (Satoo, 2012). The comparison of capital expenditures incurred during realization of LNG and NGH projects is given in (Gudmundsson, Graff, & Kvaerner, 2003). The latter techno-logy was 23 – 27% more efficient. In addition, the capacity of the gas hydrate production lines can be 4 times lower compared to the LNG production line, without increasing its cost. This allows for smooth adjustment of production to the change in demand for natural gas (Gudmundsson, Parlaktuna, & Khokhar, 1994). Research has identified a number of advantages inherent to the techno-logy of gas transportation in gas hydrate form (NGH).

But the arguments in favor of this technology were not convincing enough to stimulate significant investments in its refinement and practical implementation. The research was based on the fact that processes involved in the gas hydrate production and its melting were carried out at the expense of traditional energy sources (for example, a part of the gas). Therefore, calculation of transportation costs included the cost of the energy used. At the same time, in the case of NGH-technology, these operations are the most energy consuming.

Besides, the granulated gas hydrate was considered the main form for this technology (Gudmundsson, 1996), though it has a number of disadvantages (Dawe, Thomas, & Kromah, 2003). As a rule, granular

hydrates tend to freeze into a monolith which complicates unloading. Consequently, they fill only 78% of the volume of vehicles or storages (Gudmundsson, Graff, & Kvaerner, 2003). Furthermore, much of the total granules surface area and the system of open channels between granule channels induce the process of volumetric dissociation in the gas hydrate mass. Preserving stability at the atmospheric pressure needs additional costs for cooling to temperatures below 258 K. Here, large monolithic blocks become a good solution.

For industrial implementation of gas transportation technology in gas hydrate form, it is necessary to enhance its commercial attractiveness and improve its economic efficiency. This can be achieved by sharply reducing energy costs related to the technological process. As noted above, the main part of energy in NGH-technology is consumed by phase transitions (processes of production and melting of gas hydrate) (Bondarenko & Sai, 2018). Therefore, it is impossible to reduce these costs without violating the fundamental laws. Considering the properties of gas hydrates and specifics of gas extraction from offshore deposits, it is possible to carry out the technological processes at the expense of the environment energy (Bondarenko, Ganushevych, Sai, & Tyshchenko, 2011).

A method of producing a gas hydrate in the form of large size blocks, preserved in the ice layer, is proposed in the patent (Pedchenko & Pedchenko, 2013). Suitability of such gas hydrate blocks for long-term storage at atmospheric pressure and slightly subzero temperature (270 K) is discussed in Pedchenko & Pedchenko (2012) and Pedchenko & Pedchenko (2016).

The technology of transportation and storage of gas hydrate blocks is substantiated, its economic advantages are also defined. In addition, the authors developed a design for mobile land storages and the technology of their maintenance. To increase the efficiency of technology, it is proposed to melt gas hydrate using solar energy.

In the case of offshore gas fields development, the NGH technology efficiency can be increased by optimizing gas hydrates production. Intensive gas hydrate formation requires creation of a maximum phases interface area (gas – water) and the removal of heat produced during the exothermic process. The extracted gas exiting

the well has a certain reserve of the reservoir energy. On the way to the consumer, this energy is quickly spent on gas preparation and friction in the pipeline during transportation. Additionally, in offshore deposits, the process of well products transfer above sea bottom level is accompanied by heat transfer with seawater through the walls of the pipeline. All the mixture is cooled at the average seawater temperature of 278 K. Cooling of gas during the extraction process may also occur because of its throttling (Joule-Thomson effect). As a result, thermobaric parameters in the flowline can reach the conditions of hydrates formation which will start in the presence of condensed water. Although hydrates formation is accompanied by heat release, the temperature in the pipeline does not achieve the equilibrium value due to heat transfer with seawater. Thus, the process of hydrates formation will continue, which is undesirable under the existing technology because it leads to the formation of hydrate cork and requires significant costs for its prevention (gas drying, introduction of process inhibitors, heating of the products).

However, in the case of the NGH technology implementation, it would be logical to use the existing sea body potential (high pressure, relatively low temperature, source of water) and gas (reservoir energy) for gas hydrate production. The optimal configuration takes advantage of conditions ensuring NGH formation in situ. The proposed method generates NGH in such ocean region where the combination of pressure and temperature inherently contributes to their formation, kinetics and thermodynamics. The scheme of the technological process is presented in Figure 1. It combines the method for the conversion of gas extracted from the well into the gas hydrate form using the energy of the sea and gas flow. The final product of the process is the cooled blocks, covered with an ice layer.

Based on these considerations, the authors of (Pedchenko & Pedchenko, 2016) proposed a method of joint development and transportation of products from gas and gas hydrate offshore deposits in gas hydrated form.

In accordance with this method (Fig. 1), the gas from the production well *1* being in contact with the water flow in the pipe-reactor *2*, gives the heat to the surround-ding seawater, binds into the gas hydrate and forms a mixture of water and gas hydrate (gas

hydrate pulp). Gas hydrate in the pulp (flow *I*) is fed onto FPU platform, where it is concentrated and formed into the gas hydrate blocks. Gas-hydrated blocks are transported by sea and stored in gas hydrate storages until the time of consumption.

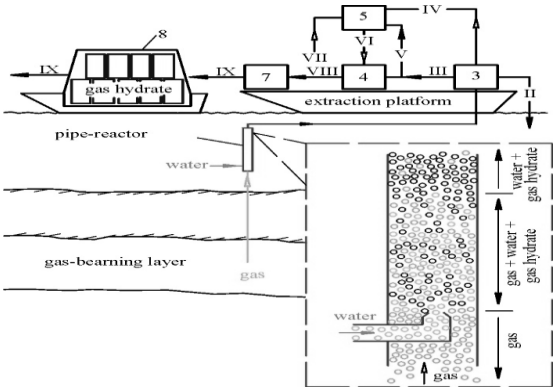

Fig. 1. Schematic diagram of technology for the conversion of extracted natural gas from offshore deposits into the gas hydrate form: *1* – well; 2 – pipe-reactor; 3 – elements of the system for gas hydrate mass preparation; 4 – formation of gas hydrates blocks; 5 – gas hydrate compression; 6 – preservation of gas hydrate blocks in ice layer; 7 – transportation of gas hydrate; flows: I – gas hydrate pulp; II – water discharge; III, V – moist gas hydrate; IV, VII – low pressure gas; VI – compressed gas; VIII – gas hydrate blocks; IX – gas hydrate blocks covered with ice

Thus, the purpose of the work is to estimate the principle possibility of binding gas from offshore deposits (during the contact of gas and water in a vertical pipe) into the gas hydrate using alternative energy sources (energy of the productive reservoir and low potential energy of sea water), as well as to determine the main parameters of the technological process.

Since experimental research and field tests involve significant material and financial costs, the authors have developed a mathematical model of this process and the corresponding software product for its realization which are discussed further on in this paper.

3. Analytical and experimental study of gas hydrate formation

Let us consider the vertical pipe of diameter $d = 0.3$ m (Fig. 1), which connects the offshore gas well and the FPU platform (i.e., the pipe passes through the thickness of water). The gas extracted from

the well moves through the pipe. At some distance (depth) from the platform, the gas is throttled to the pressure of 5 MPa and cooled as a result of the Joule-Thomson effect. Immediately next to the place of throttling, the jet pump injects sea water into the pipe proportionally to the gas volume 1/1.15 (1/56 in normal conditions) at the pressure of 5 MPa. Taking into account the ratio of phases volume under this pressure, the mixture of sea water and gas moves further along the pipe with a considerable area of the phase contact. However, thermobaric parameters of this section of the pipeline will meet the conditions for the gas hydrates formation. Therefore, the solid phase of the gas hydrate will appear in the flow.

Since the gas hydrate formation takes place with the release of thermal energy, the intensity of the solid phase formation (and, consequently, the ratio of the phases volumes in the flow) will depend on the intensity of the heat transfer between the mixture (water, gas and gas hydrate) in the pipe and seawater. The section of the pipeline, where all the gas will be bound into the gas hydrate, can be considered a hydrate formation reactor. This reactor uses local energy of the gas flow and a low-potential energy of seawater to sustain the process. So, the problem is to determine the minimum length of the reactor and, consequently, the optimum depth for the placement of the gas throttling node and input of sea water.

Curve *1* in Figure 2 (obtained experimentally) corresponds to the equilibrium thermobaric parameters of the hydrate formation process for fresh water and gas (CH_4 - 92.8%, C_2H_6 - 5.1%, C_3H_8 - 2.1%).

This curve is described by the dependence

$$\ln P = 37.21 - \frac{9582.62}{T}. \qquad (1)$$

The enthalpy of hydrate formation ΔH_1 for the gas of this composition was determined by the formula given in (Mork, 2002):

$$\ln P = \frac{-\Delta H_1}{zR \cdot T_{equil}} + const,$$

or

$$\ln P = \frac{-\Delta H_1}{zR^*} \cdot \frac{1}{T_{equil}} + const, \qquad (2)$$

where ΔH_1 - heat released during formation of 1 mol of hydrate from water, J/mol; z - coefficient of gas compressibility; R^* - universal gas constant, J/(mol·K); T_{equil} - equilibrium temperature for pressure P, K; const - a constant.

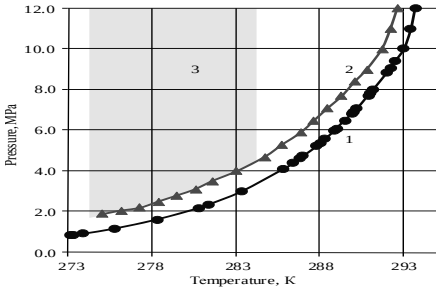

Fig. 2. Equilibrium hydrate formation curves for systems "fresh water - natural gas" (curve 1) and "sea water of variable mineralization in the pipe-reactor – natural gas" (curve 2); 3 – region of hydrate formation parameters for sea water and natural gas mixture in the pipe-reactor

The value of ΔH_1 for the temperature T_{equil} is determined graphically (Fig. 3) with respect to the value of the line inclination $\ln P = f(1/T)$ (dependence of the equilibrium pressure on the temperature in the system "gas – water – gas hydrate" in logarithmic coordinates)

$$\Delta H_1 = -zR^* \cdot \frac{d(\ln P)}{d\left(\frac{1}{T_{equil}}\right)} = -zR^* B, \qquad (3)$$

where B - coefficient of the line inclination.

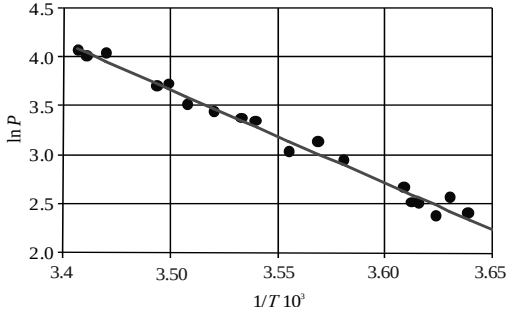

Fig. 3. Dependence of equilibrium pressure on temperature in the system "gas – water – gas hydrate"

To obtain the formula for the gas hydrate of this composition, the hydration number n was calculated by the Forkran's method (for the lower quadrupole point) (Degtyarev & Bukhgalter, 1976)

$$n = \frac{\Delta H_1 - \Delta H_2}{\Delta H_3} = 6.81, \quad (4)$$

where ΔH_2 - heat released during formation of 1 mol of hydrate from ice, J/mol; ΔH_3 - the energy of melting 1 mol of ice, J/mole (at T = 273.1 K, it is 6008 J/mol).

According to the results of experimental data processing for the temperature range 273.1 - 289.3 K and the pressure range 0.77 - 5.82 MPa, the studied gas hydrate mass had the following parameters: hydration number (n) - 6.81 mol H_2O/mol of gas, the heat of hydrate formation - 78.04 kJ/mol.

Sea water enters the pipe-reactor. The content of soluble salts in the water of the Black Sea, for example, is 2%. However, there are no salt ions and other admixtures in the composition of gas hydrate. As a result, their concentration in water gradually increases during the whole process of hydrate formation. According to the preliminary calculation, it has increased to 4.2%. Due to such concentration, the equilibrium curve for the system "fresh water – natural gas" has shifted to the left by 1.07 - 2.31 K (Fig. 4).

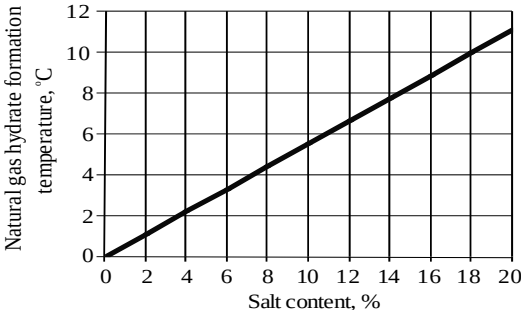

Fig. 4. Relationship between the decrease of the natural gas hydrate formation temperature and the salt content in water (Smirnov, 1990)

This fact has been taken into account in the calculations. The equilibrium curve of hydrate formation for the "sea water - natural gas" system was plotted taking into account the process of salt ions concentration in the pipe-reactor (Fig. 2, curve *2*). Based on the data obtained, we determined the thermobaric parameters of hydrate formation in the pipe-reactor: the pressure at the bottom of the pipe (P_{init}) was 5 MPa, at the top (P_{fin}) - 3 MPa, the temperature of the mixture at the bottom of the pipe (T_{init}) - 278 K, at the top (T_{fin}) - 280 K. The area delineated by these parameters is shown in Figure 2.

The temperature along the length of the pipe-reactor will change. Since gas hydrates can form throughout its length, and the volume of the gas phase will depend on the pressure in the corresponding section of the pipe, the mixture density will vary with height (depth) but it will reach the maximum after complete exhaustion of the gas phase. Concentration of gas hydrate in the water-hydrated mixture, according to (Pedchenko, 2013) was taken to be 33%. This is necessary to prevent formation of hydrate plugs in the pipeline. Hence, the maximum density of the mixture $\rho_{\max}$ was 1004.5 kg/m^3.

It was assumed that the liquid-gas mixture moved in a slug (plug) regime, when the gas bubbles plug the pipe section and intersperse with the liquid and hydrate particles. The flow velocity v was 0.35 m/s. Reynolds number in this case was 103.960. Thus, the movement of the mixture in the pipe-reactor is turbulent. The flow velocities in the near-wall area and in the center are approximately equal. Therefore, it is not reasonable to study the temperature change along the pipe diameter. The size of the bubbles affects the velocity of their movement and homogeneity of the mixture. At the same time, the rate of gas hydrate formation depends on the interface area. That is, for intensification of the gas hydrates formation, gas bubbles should be the smallest in size.

Since the mixture flow velocity is 0.35 m/s, the maximum radius of bubbles is determined by the formula

$$v = (1+1.05)\cdot(9.8_{bubbl})^{0.5}. \quad (5)$$

Then the bubbles radius will be 0.001 - 0.002 m.

Let us consider the processes in the system "seawater – natural gas – gas hydrates" which occurs during the flow motion along the

pipe-reactor. The temperature of the sea water (T_{sea}) is 278 K, while the initial temperature of the mixture ($T_{mix\ init}$) is 273.3 K (taking into account the temperature of throttled gas and sea water and their mass ratio). So $T_{sea}>T_{mix\ init}$. Therefore, in the initial section of the pipe-reactor, thermal energy will flow from the outside through its wall and heat the mixture. The process will continue until the mixture temperature in the pipe reaches 278 K and will comprise:

a - heat transfer between the mixture and seawater through the wall, which is described by the equation:

$$Q_{sea} = \alpha\left(T_{sea} - \bar{T}_{inside}\right) S_{surface}\tau_1 = \\ = 2\alpha\left(T_{sea} - \frac{T_{278} + T_{init}}{2}\right)\pi r\varpi\tau_1^2, \quad (6)$$

where α - heat transfer coefficient, W/(m^2·K); T_{278} - time, s; ω - mixture flow velocity in the pipe, m/s; *r* - radius of the pipeline, m; *b* - heat radiation during the gas hydrate formation

$$Q_{gh_1} = Hm_{278} = HV\rho_{gh} = H\pi r^2\omega\tau_1\rho_{gh}, \quad (7)$$

where *H* - enthalpy of hydrate formation, J/kg; m_{278} - mass of the formed gas hydrate, kg.

The total temperature change over time τ_{278} in the sector of volume $S_{sect}\,\omega\tau$ corresponds to the sum $Q_{sea} + Q_{gh}$, and is determined by

$$Q_{fin_1} = c\rho_1 S_{\mathrm{sec}t}\omega\tau_1\left(T_{init} - T_{fin}\right) = \\ = c\left(\rho_0 + ...\ln\omega\tau_1\right)\pi r^2\omega\tau_1\left(T_{init} - T_{fin}\right), \quad (8)$$

where *c* - specific thermal conductivity, J/(kg·K); ρ_0, ρ_1 - density of the mixture at the beginning and at the end of the process, kg/m^3.

Since $Q_{sea} + Q_{gh} = Q_{fin}$, then

$$2\alpha\left(T_{sea} - \frac{T_{278} + T_{init}}{2}\right)\pi r\varpi\tau_1^2 + H\pi r^2\omega\tau_1\rho_{gh} = \\ = c\left(\rho_0 + ...\ln\left(\omega\tau_1\right)\right)\pi r^2\omega\tau_1\left(T_{init} - T_{fin}\right). \quad (9)$$

The mixture in the pipe-reactor will quickly heat to the sea water temperature. When $T_{sea} \le T_{sum_1}$, the thermal energy of hydrate formation process will be released through the pipe wall. Then the sea water will cool the mixture that moves along the pipe. Since the diameter of the pipe-reactor (d) is much smaller than the length (L) ($d<<L$), we will treat it as a rod. The peculiarities of heat transfer in such a rod are considered below.

The rod (Fig. 5) is in thermal equilibrium with sea water whose temperature (T_{sea}) is 278 K. The initial temperature of the rod is assumed to be equal to the temperature of water and is described by the function $T_r(x, 0)=f(x)$.

Gas hydrates can form all the time along the length of the rod. This process is accompanied by the release of energy, mixture heating and changing of the rod density according to the law

$$\Delta\rho = a\ln(x-b), \tag{10}$$

where x - length of the rod (pipe-reactor), m; b - constant.

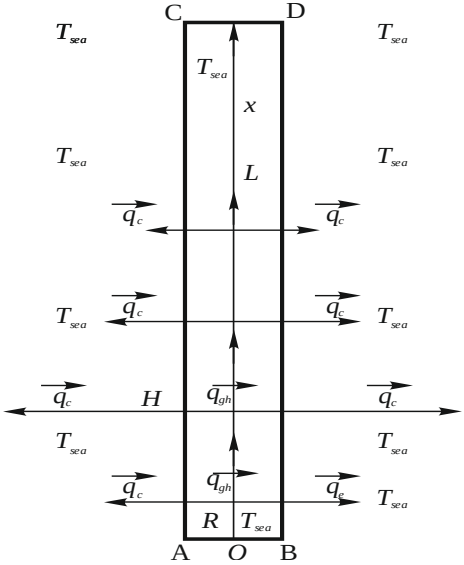

Fig. 5. Physical model of temperature distribution in the rod (pipe-reactor) without heat insulation of the lateral surface

The accumulated heat of gas hydrate formation in the rod was taken as its source. Since the lateral surface of the rod was not insulated, heat transfer with seawater was always governed by the Newton's law. The heat transfer from the lateral surface to the environment was taken into account in the differential equation as a source of thermal energy with a negative sign. It is vital that the temperature distribution along the length of the rod be detected at any time. On the basis of the obtained dependence, it is necessary to determine the length of the pipe-reactor section, where the gas will completely bind into the gas hydrate.

The length value can be established when the mixture temperature drops to 276 - 278 K. To derive an equation that describes this process, let us define the rod volume (pipe-reactor) $dxdS$. Then, thermal energy $qxdSd_\tau$ will have penetrated inside through the dS_{AB} wall with the area dS_{CD} - $qx + d_x dSd\tau$ during a certain period of time. The amount of energy released through the uninsulated side wall per unit of time is:

$$q_{S_{surf}} dS_{surf} d\tau = \alpha \left(T_{rod} - T_{sea}\right) 2\pi r dx d\tau . \quad (11)$$

Gas hydrate is formed along the length of the rod with heat release. The mixture density in the allocated volume varies with height

$$Hdm = Hd\rho dSdx . \quad (12)$$

The allocated rod's volume accumulates the energy

$$\left(q_{x+dx} - q_x\right) dSd\tau - q_{S_{surf}} dS_{surf} d\tau + Hd\rho dSdx . \quad (13)$$

This will cause the temperature change in the allocated volume $c\rho(T_{fin} - T_{init})\, dSdx$. The energy change in the allocated volume per time unit is

$$\left(q_{x+dx} - q_x\right) dS - q_{S_{surf}} dS_{surf} + \frac{Hd\rho dSdx}{d\tau} =$$

$$= c\rho\left(T_{fin} - T_{init}\right) \frac{dSdx}{d\tau} . \quad (14)$$

Then the energy change per unit of volume will be

$$\frac{\partial q}{\partial x} - \frac{2\alpha}{r}\left(T_{rod} - T_{sea}\right) + \frac{Hd\rho}{d\tau} = \frac{c\rho\partial T}{d\tau}. \qquad (15)$$

The final equation describing temperature change in the rod (pipe-reactor) looks

$$\lambda\frac{\partial^2 T}{\partial x^2} - \frac{2\alpha}{R}\left(T_{rod} - T_{sea}\right) + \frac{Hd\rho}{d\tau} = \frac{c\rho\partial T}{d\tau}. \qquad (16)$$

The function $T_{rod}(x, \tau)$ describes the temperature change in the rod and the initial conditions

$$T_{rod}\left(x,0\right) = T_{mix_1} \text{ for } 0 < \tau \text{ ; } 0 < x < \infty;$$

$$T_{sea} = T_{mix_1}. \qquad (17)$$

Boundary conditions for the rod bottom end

$$T_{rod}\left(0,\tau\right) = T_{mix_1} \text{ for } 0 < \tau. \qquad (18)$$

The point in the pipe-reactor, where the thermal energy is not released any more (the internal source will stop working), will correspond to the point of gas hydration process completion. Therefore, after a certain period of time, the rod temperature will drop and become stable, at the value approximately equal to the temperature of sea water T_{sea}. Since the rod is semi-limited, the boundary condition for its other end will be

$$T_{rod}\left(\infty,\tau\right) = T_{sea} \text{ for } 0 < \tau. \qquad (19)$$

In some point of the rod, the temperature of flow will become stable during τ time and close to the temperature of seawater (T_{sea}). Completion of the gas hydrate formation process corresponds to the maximum temperature of the rod (and mixture in the pipe-reactor, point *H*) (Fig. 6).

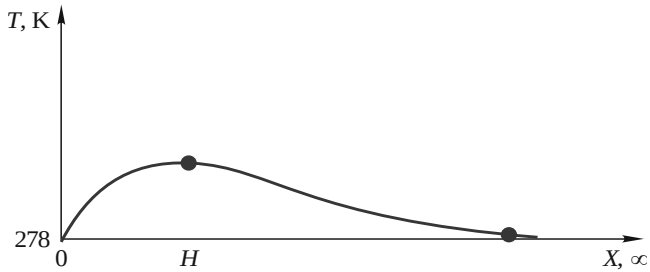

Fig. 6. Scheme of heat transfer process between the pipe and seawater

In order to obtain the numerical solution of the problem, we applied the finite-difference method (mesh method). The calculation of the gas hydrate formation process was performed in Matlab environment. The resulting graph is shown in Figures 7, 8.

As an example, we considered the dynamics of the heat transfer process in a vertical pipe-reactor for 7 days (168 hours). Analysis of the obtained graphs showed that the gas flow will completely become a part of gas hydrate composition in the pipe-reactor section 305 m long.

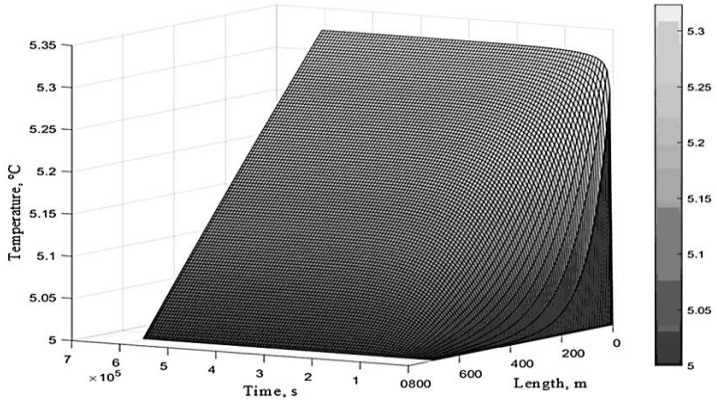

Fig. 7. Heat transfer in a vertical pipe during gas hydrate formation (T, L, τ)

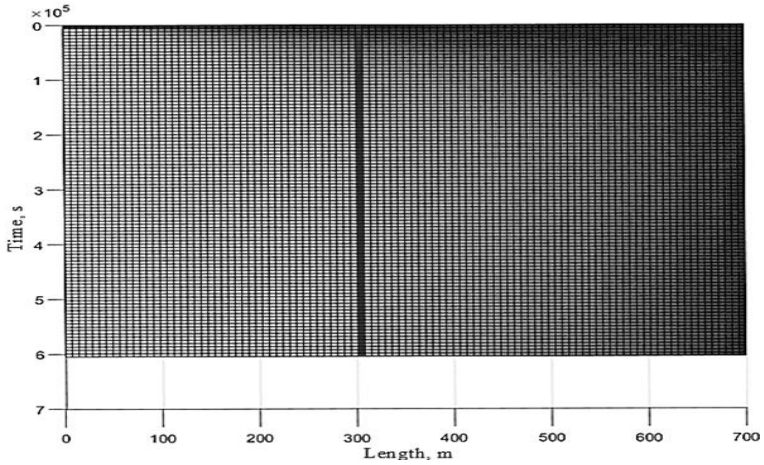

Fig. 8. Heat transfer dynamics in the pipe-reactor during 168 hours (7 days)

The dynamics of the heat transfer process in the pipe section 305 m long is shown in Figure 9. The temperature was observed to stabilize since the second day.

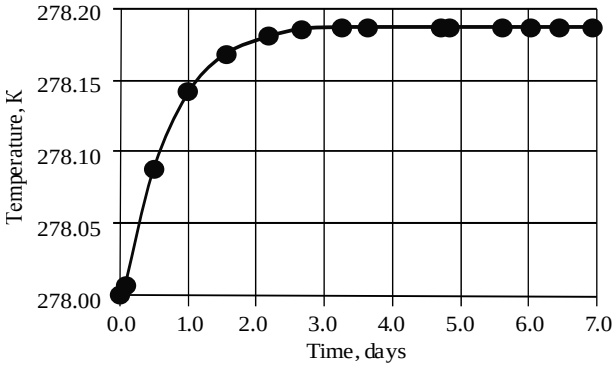

Fig. 9. Graph of the mixture temperature change (stabilization) for 7 days in 305 m long pipe-reactor

4. Conclusions

The technology of gas transportation in gas hydrate form is promising because it is necessary to diversify natural gas supplies to Ukraine and develop offshore hydrocarbon deposits.

As a result of the mathematical modelling of hydration process in a vertical pipe-reactor immersed in the sea, the following conclusions were made:

1. Taking into account that $x \to \infty$, the rod (mixture) is observed to cool to the temperature of sea water $T(x,\tau) \approx T_{sea}$.

2. Testing of the model during 7 days has confirmed its adequacy.

3. The process of gas hydrate formation was completed in the point with the maximum temperature along the pipe-reactor, which is the result of the gas full bin-ding into the gas hydrate. After that, the temperature starts decreasing.

4. Under these conditions, the length of the pipe-reactor ensuring the entire binding of the gas flow into the gas hydrate will be 305 m.

5. The density of the obtained 33% mixture of water and gas hydrate will be 1004.5 kg/m^3. The initial density of the water-gas mixture ($\rho_{mix\ init}$) in the interface was 722.6 kg/m^3.

References

1. **Birchwood, R., Dai, J., Shelander, D., Boswell, R., Collett, T., Cook, A., Dallimore, S., Fujii, K., Imasato, Y., Fukuhara, M., Kusaka, K., Murray, D., & Saeki, T**. (2010) Deve-lopments in Gas Hydrates. Oilfield Review, (22), 18-33.

2. **Bondarenko, V., Ganushevych, K., Sai, K., & Tyshchenko, A.** (2011). Development of Gas Hydrates in the Black Sea. Technical and Geoinformational Systems in Mining, 55-59. https://doi.org/10.1201/b11586-11

3. **Bondarenko, V., Svietkina, O., & Sai, K.** (2017). Study of the Formation Mechanism of Gas Hydrates of Methane in the Presence of Surface-Active Substances. Eastern-European Journal of Enterprise Technologies, 5(6(89)), 48-55. https://doi.org/10.15587/1729-4061.2017.112313

4. **Bondarenko, V., & Sai, K**. (2018). Process Pattern of Heterogeneous Gas Hydrate Deposits Dissociation. Naukovyi Visnyk Natsionalnoho Hirnychoho Universytetu, (2), 21-28.

5. **Boswell, R., & Collett, T.S.** (2011). Current Perspectives on Gas Hydrate Resources. Energy & Environmental Science, 4(4), 1206-1215. 6. https://doi.org/10.1039/c0ee00203h

6. **Dawe, R., Thomas, M., & Kromah, M.** (2003). Hydrate Technology for Transporting Natural Gas. Engineering Journal of the University of Qatar, (16), 11-18.

7. **Degtyarev, B.V., & Bukhgalter, E.B.** (1976). Bor'ba s hidratami pri ekspluatatsii gazovykh skvazhin v severnykh ra-yonakh. Moskva, Russian Federation: Nedra.

8 **Dychkovskyi, R.O., Lozynskyi, V.H., Saik, P.B., Petlovanyi, M.V., Malanchuk, Ye.Z., & Malanchuk, Z.R.** (2018). Modeling of the Disjunctive Geological Fault Influence on the Exploitation Wells Stability During Underground Coal Gasification. Archives of Civil and Mechanical Engineering, 18(4), 1183-1197. https://doi.org/10.1016/j.acme.2018.01.012

9. **Economides, M.J., Sun, K., & Subero, G.** (2006). Compressed Natural Gas (CNG): An Alternative to Liquefied Natural Gas (LNG). SPE Production & Operations, 21(2), 318-324. https://doi.org/10.2118/92047-pa

10. **Giavarini, C., & Hester, K.** (2011). Hydrates as an Energy Source. Green Energy and Technology, 117-140. https://doi.org/10.1007/978-0-85729-956-7_8

11. **Gudmundsson, J.-S., Parlaktuna, M., & Khokhar, A.A.** (1994). Storage of Natural Gas as Frozen Hydrate. SPE Production & Facilities, 9(1), 69-73. https://doi.org/10.2118/24924-pa

12. **Gudmundsson, J.** (1996). Method for Production of Gas Hydrates for Transportation and Storage. Patent US 5536893. United States.

13. **Gudmundsson, J.S., & Børrehaug, A.** (1996). Frozen Hydrate for Transport of Natural Gas. Proceeding of the 2nd International Conference Natural Gas Hydrates, 415-422.

14. **Gudmundsson, J., Graff, O., & Kvaerner, A**. (2003). Hydrate Non-Pipeline Technology for Transport of Natural Gas. In Proceeding of the 22nd World Gas Conference Tokyo (pp. 1-5). Tokyo, Japan: International Gas Union.

15. **Kanda, H.** (2006) Economics Study on Natural Gas Transportation with Natural Gas Hydrate Pellets. In Proceedings of the 23rd World Gas Conference (pp. 1-11). Amsterdam, Netherlands: International Gas Union.

16. **Khokhar, A.A.** (1998) Storage Properties of Natural Gas Hydrates. PhD Thesis. Trondheim.

17. **Lu, S.M**. (2016). Retraction Notice to: "A Global Survey of Gas Hydrate Development and Reserves: Specifically in the Marine Field". Renewable and Sustainable Energy Reviews, (64), 1-856. https://doi.org/10.1016/j.rser.2016.07.005

22. **Makogon, Y.F**. (2010). Natural Gas Hydrates – A Promising Source of Energy. Journal of Natural Gas Science and Engineering, 2(1), 49-59. https://doi.org/10.1016/j.jngse.2009.12.004

24. **Maksymova, E**. (2018). Selecting the Method of Gas Hydrate Deposits Development in Terms of the Regularities of Their Formation. Mining of Mineral Deposits, 12(1), 103-108. https://doi.org/10.15407/mining12.01.103

25. **Mork, M**. (2002). Formation Rate of Natural Gas Hydrate. Reactor Experiments and Models. PhD Thesis. Trondheim, Norway: Norwegian University of Science and Technology.

26. **Mykhailov, V**. (2016). Prospection and Estimation of Unconventional Hydrocarbon Deposits in Ukraine. Visnyk of Taras Shevchenko National University of Kyiv. Geology, 2(73), 38-45. https://doi.org/10.17721/1728-2713.73.06

27. **Pedchenko, L., & Pedchenko, M**. (2012). Substantiation of Method of Formation of Ice Hydrate Blocks with the Purpose of Transporting and Storage of Hydrate Gas. Naukovyi Visnyk Natsionalnoho Hirnychoho Universytetu, (1), 28-34.

28. **Pedchenko, L., & Pedchenko, M**. (2013). Method of Production of Associated Oil Gas Hydrates for the Purpose of Transportation and Storage. Patent No.101882. Ukraine.

29. **Pedchenko, M.M.** (2013) Theoretical and Experimental Researches of Process of Hydration of Hydrocarbon Gases in the Reactors of Jet Type. PhD Thesis. Kharkiv, Ukraine: Kharkiv Polytechnic Institute.

30. **Pedchenko, M., & Pedchenko, L**. (2016). Technological Complex for Production, Transportation and Storage of Gas from the Offshore Gas and Gas Hydrates Fields. Mining of Mineral Deposits, 10(3), 20-30. https://doi.org/10.15407/mining10.03.020

31. **Petlovanyi, M.V., Lozynskyi, V.H., Saik, P.B., & Sai, K.S.** (2018). Modern Experience of Low-Coal Seams Underground Mining in Ukraine. International Journal of Mining Science and Technology. Article in press. https://doi.org/10.1016/j.ijmst.2018.05.014

32. **Satoo, N.** (2012). Development of Natural Gas Hydrate (NGH) Supply Chain. In Proceedings of the 25th World Gas Conference (pp. 1-10). Kuala Lumpur, Malaysia: International Gas Union.

33. **Sloan, E.D**. (2003). Fundamental Principles and Applications of Natural Gas Hydrates. Nature, 426(6964), 353-359. https://doi.org/10.1038/nature02135

34. **Smirnov, L.F.** (1990). Tekhnologicheskoe ispolzovanie gazo-vykh gidratov. Moskva, Russian Federation: VNIIGAZ.

Scientific edition

MODERNIZATION AND ENGINEERING DEVELOPMENT OF RESOURCE-SAVING TECHNOLOGIES IN MINERAL MINING AND PROCESSING

Multi-authored monograph

First publication

Chief editor **Vsevolod KALINICHENKO**,
Full Member of the Academy of Mining Sciences of Ukraine,
DSc (Engineering), Professor, Kryvyi Rih National University, Ukraine.

Co-editor . **Ronald MORARU**
Ph.D.Habil.Eng., Professor, Research
Vice-Rector UNIVERSITY OF PETROSANI, Romania.

Deputy chief editor **Serhii CHUKHAREV**,
PhD (Engineering), Associate Professor.

Technical editor **Elena SAMOILUK**

Signed to print 01.11.19. Format A5.
29 conventional printed sheets.
The printing run is 300 copies.

UNIVERSITAS Publishing, Petroșani,
University of Petroșani
Str. Universității nr. 20, 332006, Petroșani, jud. Hunedoara, Romania